Mechanochemistry

Edited by José G. Hernández

Imprint

Mechanochemistry

José G. Hernández

Editorial

Address:
Institute of Organic Chemistry, RWTH Aachen University,
Landoltweg 1, D-52074 Aachen, Germany

Email:
José G. Hernández - jose.hernandez@oc.rwth-aachen.de

The scientific community's general interest in using mechanical energy to trigger or facilitate chemical reactivity has been growing at a speedy pace. In particular, in recent years, organic chemistry has witnessed a constant flow of examples where the use of mechanochemical techniques proved not only to outperform traditional solution-based methodologies, but also enabled access to otherwise impossible chemical reactivity in many cases. From a green chemistry perspective, mechanochemical activation conducted by milling, shearing, pulling or ultrasonic irradiation allows for the possibility to drastically reduce the amount of solvent needed during chemical reactions, even to the point of achieving chemical reactivity under solvent-free conditions. Additionally, the utilization of mechanochemical technology can often further simplify the posterior work-up procedures, having a deeper impact on the sustainability of the global synthetic process (reduction of waste, lower energy consumption, absence of external heating, fast reactivity, etc.).

When compared with other, more established alternatives to carry out chemical transformations, mechanochemistry can still be considered as a nascent approach. Therefore, Thematic Series like this one gathers works from experts on the topic to encourage the chemistry community to adopt the concepts of mechanochemistry, and secondly, it strengthens the field. In addition to the previous special issues dedicated to mechanochem-

istry published in other peer-reviewed scientific journals [1,2], the *Beilstein Journal of Organic Chemistry* sought to host a Thematic Series specifically covering the field of organic mechanochemistry. Altogether, this Thematic Series contains more than two dozen papers from colleagues working in at least fifteen different countries across America, Asia, Africa and Europe. As a consequence, the fantastic job by the *Beilstein Journal of Organic Chemistry* editorial and production teams, authors and reviewers will definitely help in the consolidation of mechanochemistry worldwide.

While exploring this Thematic Series, the reader will find a substantial collection of papers where the advantages of mechanosynthesis are demonstrated throughout the numerous full research papers and highlighted in the review articles that complement this Thematic Series. These contributions are set to become the background knowledge for future applications in the field, which are anticipated to continue to push the boundaries of mechanochemistry further and beyond.

José G. Hernández

Aachen, September 2017

ORCID® iDs

José G. Hernández - https://orcid.org/0000-0001-9064-4456

References

1. James, S. L.; Friščić, T. *Chem. Commun.* **2013,** *49,* 5349–5350. doi:10.1039/C3CC90136J
2. Komatsu, K.; Bolm, C., Eds. Mechanochemistry. *Molecules* http://www.mdpi.com/journal/molecules/special_issues/Mechanochemistry

Kinetic analysis of mechanoradical formation during the mechanolysis of dextran and glycogen

Naoki Doi[1], Yasushi Sasai[1], Yukinori Yamauchi[2], Tetsuo Adachi[3], Masayuki Kuzuya[4] and Shin-ichi Kondo[*1]

Address:
[1]Laboratory of Pharmaceutical Physical Chemistry, Gifu Pharmaceutical University, 1-25-4 Daigaku-Nishi, Gifu 501-1196, Japan, [2]Department of Pharmaceutical Physical Chemistry, Faculty of Pharmaceutical Sciences, Matsuyama University, 4-2 Bunkyo-cho, Matsuyama, Ehime 790-8578, Japan, [3]Laboratory of Clinical Pharmaceutics, Gifu Pharmaceutical University, 1-25-4 Daigaku-Nishi, Gifu 501-1196, Japan and [4]Department of Health and Welfare, Faculty of Human Welfare, Chubu Gakuin University, 2-1 Kirigaoka, Seki-shi, Gifu 501-3993, Japan

Email:
Shin-ichi Kondo[*] - skondo@gifu-pu.ac.jp

* Corresponding author

Keywords:
dextran; electron spin resonance (ESR); glycogen; mechanoradical; polysaccharide

Abstract

A detailed electron spin resonance (ESR) analysis of mechanically induced free radicals (mechanoradicals) formation of glucose-based polysaccharides, dextran (Dx) and glycogen (Gly) was performed in comparison with amylose mechanoradicals. The ESR spectra of the samples mechanically fractured at room temperature were multicomponent. The radical concentration of Dx and Gly mechanoradicals gradually decreased during vibratory milling after reaching the maximum value. Although the molecular weight of Dx or the particle diameter of Gly steeply diminished until reaching the each maximum value of radical concentration, after that the molecular weight or the particle diameter slowly decreased. These results suggested that Dx and Gly mechanoradicals might be more unstable than amylose radicals possessing an intramolecular helical structure due to the branched structure.

Introduction

There are many reports on the mechanolysis of synthetic and natural polymers. It is well-known that mechanically induced radicals, so-called mechanoradicals, are produced by the mechanolysis of a polymer at a temperature below its glass-transition temperature (T_g) due to the disruption of the polymer main chain [1]. Although most pulverization operations for a practical use are carried out at room temperature, electron spin resonance (ESR) spectroscopy analyses of mechanoradical formation have generally been conducted at low temperature (77 K) [2]. In previous papers we discussed the mechanoradical formation through mechanolysis of synthetic polymers [3,4] and polysaccharides such as amylose and cellulose [5] at room tem-

perature under strictly anaerobic conditions. ESR spectral analysis and the progressive changes in the physicochemical properties were also studied in detail. As a representative example, Figure 1 shows the radical structures observed following mechanolysis of cellulose and summarizes the possible reaction sequence.

The cellulose mechanoradicals, which were generated by subsequent radical reactions such as hydrogen abstraction and/or recombination after polymer main-chain scission, could be assigned to alkoxylalkyl-type radicals at the C1 and acylalkyl-type radicals at the C2 and/or C3 positions. Therefore, these observed mechanoradicals were mid-chain radicals.

Great attention has been paid to graft polymerization of synthetic polymers onto polysaccharides, because this method easily produces a polymer combining the advantages of both natural and synthetic macromolecules [6]. A polysaccharide possessing functional group on its backbone that allows to initiate the polymerization is frequently used to synthesize such a graft polymer [7]. Dextran (Dx), a biodegradable polysaccharide, has been

utilized as a graft copolymer backbone. The glycosidic linkages between the α-glucose units of Dx synthesized from *Leuconostoc mesenteroides* are composed of approximately 95% α-D-1,6-linkages, which form a straight chain, and 5% α-1,3-linkages, from which branches begin, as shown in Figure 2 [8-10].

The grafting of synthetic polymers onto Dx has generally been carried out using oxygen-based radicals produced via a hydrogen abstraction method (e.g., radical initiation, γ-irradiation) from hydroxy groups [11-14]. However, as the polysaccharide backbone is unstable under these harsh and high temperature conditions, these compounds are not suitable for condensation polymerizations to synthesize graft copolymers [15]. In general a radical polymerization can be used for the synthesis of graft polymers consisting of vinyl monomers and polysaccharides [16]. Mid-chain radicals can also be formed by mechanolysis of hydroxyethylcellulose (HEC), so that it was hoped that the mechanolysis of HEC in the presence of vinyl monomers would produce graft copolymers possessing synthetic polymers as branches. Sakaguchi et al. reported a diblock copolymer forma-
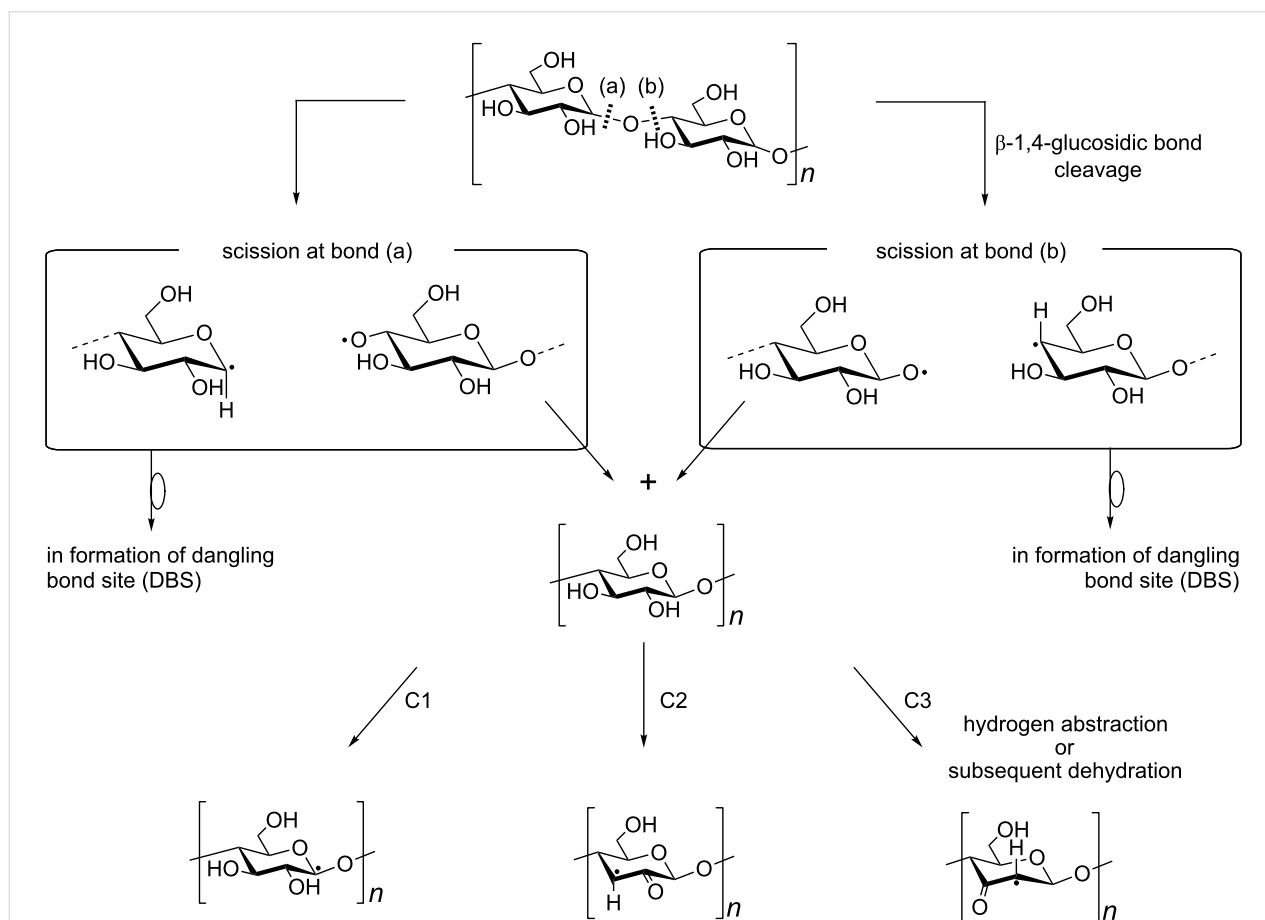
Figure 1: Structures of discrete mechanoradicals and the reaction sequence for their formation from cellulose [5].

**Figure 2:** Schematic structure of amylose, dextran and glycogen.
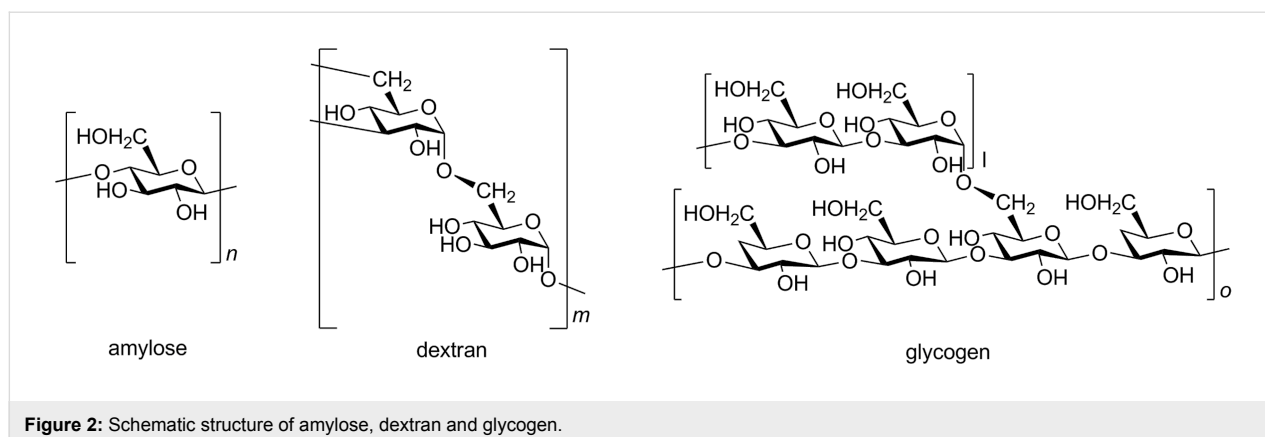
tion through the mechanochemical reaction of bacterial cellulose and methyl methacrylate in vacuum at 77 K [17]. Solala et al. studied the mechanochemical reaction of cotton in the presence of styrene and disclosed the formation of polystyrene on the cotton [18]. In a previous paper, we reported the synthesis of water-soluble graft polymeric prodrugs through the mechanochemical reaction of HEC and methacryloyl derivatives of 5-fluorouracil [19]. We also discussed the nature of drug release from the polymeric prodrugs produced as a prototype [19]. However, HEC is not metabolized by humans. Therefore if one could use a polymer metabolized by humans, such as Dx or glycogen (Gly), a promising graft polymeric prodrug could be obtained through a mechanochemical reaction in a totally dry process. It is necessary to elucidate the structure and stability of mechanoradicals of Dx and Gly as a pre-screening test for the development of such a graft polymeric prodrug. However, to our knowledge, there are no reports describing the formation of Dx or Gly mechanoradicals at room temperature.

In this paper we discuss the mechanoradical formation from Dx and Gly at room temperature in detail. To obtain fundamental insights into the mechanolysis of Dx and Gly, we conducted detailed ESR spectra analyses of the Dx and Gly mechanoradicals in comparison with those of amylose. Because amylose is an α-glucose-based polysaccharide and its detailed analysis of ESR spectra of mechanoradicals has been studied [5], we selected it as a reference sample.

In a previous paper [5], we studied the radical formation by plasma-irradiation and mechanolysis of amylose and the β-glucose-based linear polysaccharide, cellulose, in view of the difference of bonding type. The present paper focused on the polymer structure, such as helical (amylose), branched (Dx) and hyper-branched structure (Gly), to clarify the stability of component radicals depending on the polymer structure. Progressive changes in Dx molecular weight and Gly particle diameter were also investigated.

Results and Discussion

Figure 3 shows the progressive changes in the ESR spectra of amylose [5], Dx, and Gly mechanically fractured by vibratory ball milling at 60 Hz at room temperature for various periods of time under anaerobic conditions, together with the corresponding simulated spectra (shown as dotted lines).
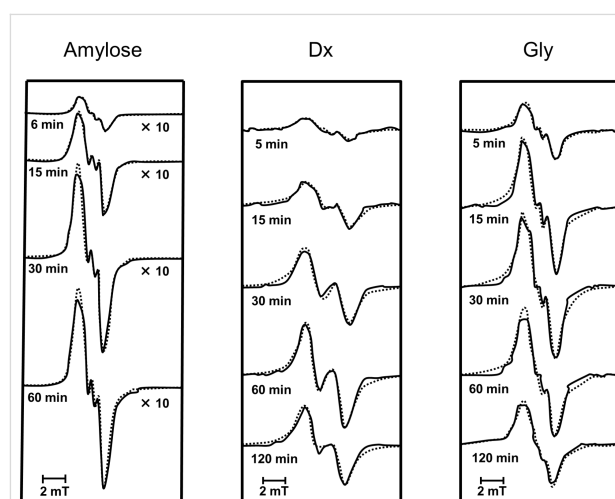
Figure 3: Progressive changes in observed ESR spectra of fractured amylose [5], Dx, and Gly, together with simulated spectra (shown as dotted lines).

It can be seen from Figure 3 that spectra of amylose, Dx, and Gly appreciably differ from one another, but the individual spectra remained nearly unchanged during the course of vibratory milling.

As mentioned above, amylose is a linear poly-D-glucose connected by α-1,4-bonds, and Dx is also a linear poly-D-glucose connected by α-1,6-bonds and possessing branches through α-1,3-bonds. It is also known that the average length of Dx branched chains is less than three glucose units [20,21]. Previously we have performed the mechanolysis of various types

of polymers and found that the limiting molecular weight was more than 10,000 g/mol under our experimental conditions [5], thus the scission of Dx branched chains could not occur during mechanolysis. Instead, an α-1,6-glucosidic bond cleavage is expected to preferentially take place in the mechanolysis of Dx. As shown in Figure 4, four types of mechanoradicals could be produced by bond cleavage at α-1,4- and α-1,6-bond in each case. It has been reported that these end-chain radicals mechanically produced from polysaccharides, such as cellulose, HEC, amylose and so on, might be unstable at room temperature. Therefore these radicals could steeply abstract hydrogen from the surrounding glucose units to produce mid-chain alkyl radicals [5].

On the other hand, Gly is a hyperbranched poly-D-glucose connected through α-1,4-bonds with branches through α-1,6-bonds every 24 to 30 residues [22]. So, Gly mechanoradicals

would be initially generated by α-1,4- and/or α-1,6-bond cleavage in the course of vibratory milling. Subsequently the mechanoradicals could undergo a following reaction, such as hydrogen abstraction to generate other types of radicals. Thus, the differences in the spectral patterns of amylose, Dx, and Gly could be due to the degree of hydrogen abstraction from the surrounding glucose units giving rise to glucose-derived mid-chain alkyl-type radicals and/or radical–radical coupling yielding non-radical species, followed by main-chain scission (Figure 4).

Sakaguchi et al. reported that not only a homogeneous scission (mechanoradical formation) but also heterogeneous bond cleavage (mechanoanion formation) took place in the course of mechanochemical reaction of bacterial cellulose in a glass ball mill in vacuum in the dark at 77 K [23]. The same authors also demonstrated the modification of microcrystalline cellulose powder through mechanocation polymerization with isobutyl

Figure 4: Schematic representation of bond cleavage at α-1,4- and α-1,6-bonds.
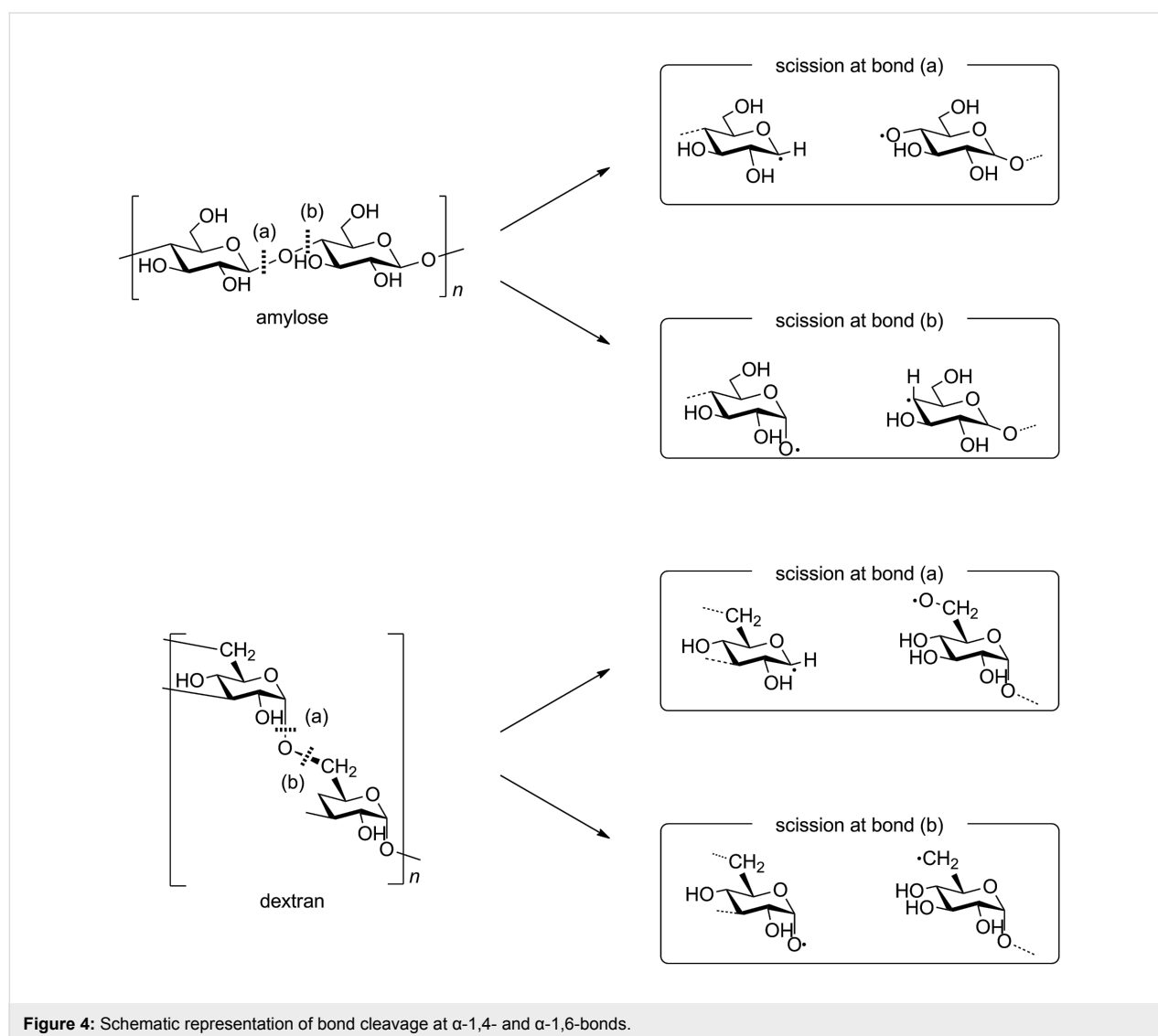
vinyl ether in vacuum at 77 K [24]. The aforementioned mecha-noanion was confirmed through tetracyanoethylene (TCNE) radical anion formation. The latter radical is produced by a single-electron transfer from the mechanoanion to TCNE under visible-light irradiation. We adopted this method by Sakaguchi et al for the detection of mechanoanions (see Experimental). Figure 5 shows the observed ESR spectrum before and after visible-light irradiation of the fractured sample of Dx and TCNE.
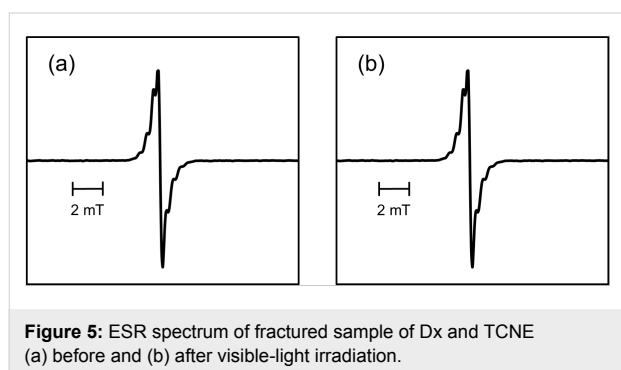

Figure 5: ESR spectrum of fractured sample of Dx and TCNE (a) before and (b) after visible-light irradiation.

As no ESR spectrum was observed after the mechanochemical reaction of pure TCNE, it was assumed that the ESR spectrum depicted in Figure 5a might be ascribed to the radical produced by the reaction of Dx mechanoradical and TCNE. As the characteristics of the spectrum and the intensity before and after visible-light irradiation remained unaffected, there was no mechanoanion in the fractured sample to a detectable extent. It was considered that a mechanoanion might promptly dissipate in the course of the mechanochemical reaction performed in a metallic vessel at room temperature.

To gain an insight into the component radicals a systematic computer simulation was performed for the ESR spectra of Dx and Gly and the results are shown in Figure 3 in an interrelated manner. The simulated spectra shown in Figure 3, represented as dotted lines, satisfactorily reproduced the observed.

Figure 6 shows the spectral components of the simulated spectra: one doublet (I) and a singlet (II). The simulated spectra of Dx and Gly were obtained from I and II, similar to those of amylose [5]. In addition, all of the simulated spectra were reproduced with the different ratios of the component spectra.

The singlet spectrum (II) was the major component in the simulated Dx and Gly spectra and is assigned to a carbon-centered radical; an oxygen-centered radical has been excluded based on the *g*-value (ca. 2.0047 for Dx and Gly). This radical might have been formed through ring-opening and/or conjugating reactions after α-1,4- and/or α-1,6-glucosidic-bond cleavage and
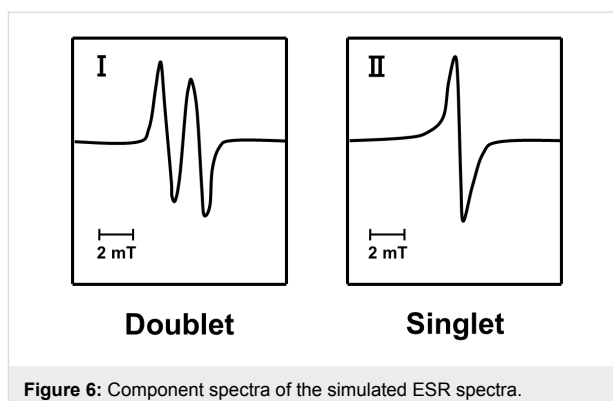
Figure 6: Component spectra of the simulated ESR spectra.

subsequent transformation and has no defined structure. On the other hand, we assigned the nearly isotropic doublet (I) to an alkoxylalkyl-type radical formed by hydrogen abstraction at the C1 position of the glucose unit, as assigned in the case of amylose. The ESR spectroscopic parameters for these Dx and Gly component spectra were consistent with those of amylose, and the associated parameters are shown in Table 1.

Table 1: ESR spectral data for component radicals in simulated spectra of amylose, Dx, and Gly.[a]

I	II	
	$\bar{g}$ = 2.0047	g_1 = 1.9999
g = 2.0052		g_2 = 2.0067
		g_3 = 2.0074
Aβ(1) = 1.70		

[a]HSC values are given in mT.

The values for principal anisotropic parameters are only of semiquantitative significance, because these values slightly differed with the spectra. The progressive changes in the spectral intensity of the component radicals are shown in Figure 7, together with those of amylose for comparison.

For amylose, the total radical concentration did not decrease after 60 min of vibratory milling and also the ratio of amylose component radicals remained constant over time [5]. It was considered that the amylose mechanoradicals were more stable due to their intramolecular helical structure (rigid conformation). The maximum total radical concentration of Dx and Gly, however, was observed at 60 and 30 min, respectively. Afterwards the radical concentration gradually decreased. Kondo et al. and Solala et al. have also reported a similar behaviour of total radical concentration for polymethylmethacrylate and cotton, respectively [18,25]. These results suggested that the mechanoradicals produced during milling underwent radical–radical coupling and/or disproportionation reactions
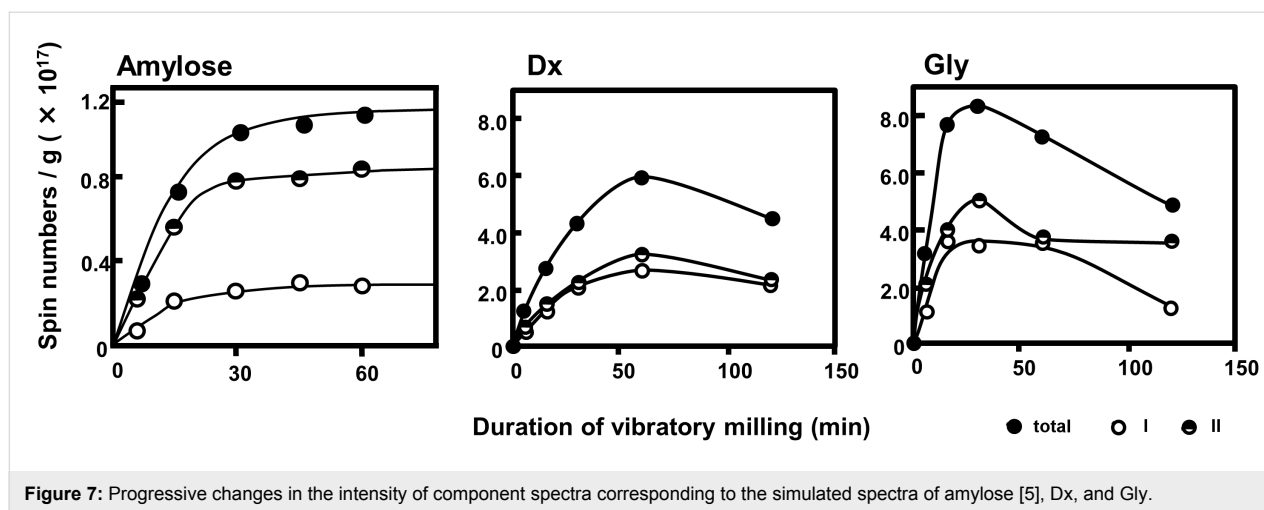
Figure 7: Progressive changes in the intensity of component spectra corresponding to the simulated spectra of amylose [5], Dx, and Gly.

such as hydrogen abstraction to give non-radical species. We also reported the decrease of the total radical concentration in the mechanolysis of cellulose derivatives after achieving the maximum concentration. Here, an abstraction of hydrogen atoms from a substituted group of a cellulose derivative has been suggested and the resulting radicals disappeared rapidly due to radical recombination and/or disproportionation reactions [5]. As described above amylose has a rigid conformation due to a helical structure. On the other hand, Dx and Gly are more flexible due to their branched structures and it is assumed that the main and branched-chains of Dx and Gly move easier than the main-chain of amylose. This difference of the polymer structures might affect the elimination rate of mechanoradicals.

Furthermore, as shown in Figure 7, the spectral intensity ratio of each component radical of Dx did not change appreciably with the duration of vibratory milling. Although the spectral intensity of each Gly component radical increased within the first 30 min of reaction and gradually decreased thereafter, the progressive changes for the two components' spectral intensity differed after 60 min. The spectral intensity of the doublet (I) assigned to an alkoxylalkyl-type radical decreased after 60 min, and that of the singlet (II) almost remained unchanged. The singlet (II) was assigned as a dangling bond site (DBS) that arose from ring-opened and/or conjugated polysaccharide structures. A DBS is a radical formed in a cross-linking region without defined structure (structureless). We compared the spectral intensities of the singlet (II) in Dx and Gly. In Dx the spectral intensity of II reached the maximum value at 60 min of vibratory milling, and then tended to decrease gradually. On the other hand, the spectral intensity of singlet II in Gly decreased after reaching the maximum value (30 min), but remained constant after 60 min. It was also shown that the spectral intensity of doublet I in Gly continued to decrease beyond 60 min, so that

the total spectral intensity decreased. It was presumed that the DBS of Gly might be more stabilized than that of Dx due to higher cross-linking in the hyper-branched structure of Gly.

As mechanoradicals are formed by polymer main-chain scission [3-5], the quantity of mechanoradicals formed in the course of mechanolysis is associated with a change in molecular weight. To gain further insights into mechanoradical formation, we examined the progressive changes in the molecular weight of Dx using GPC analysis.

Figure 8 shows the changes in molecular-weight distribution (MWD) during the course of vibratory milling of Dx. A single broad MWD was observed regardless of milling duration, suggesting that polymer main-chain scission occurred randomly.
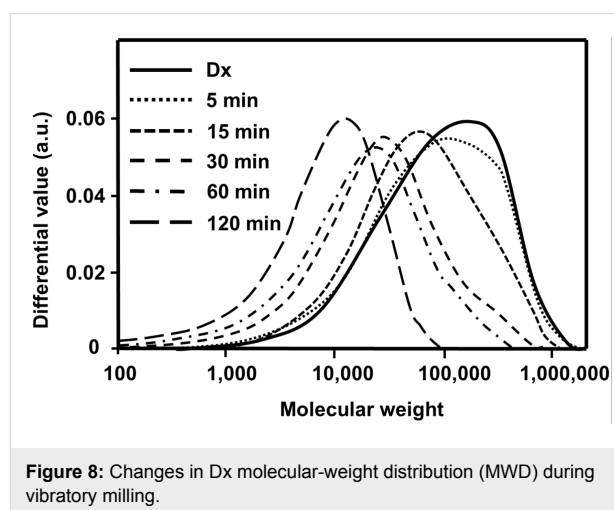
Figure 8: Changes in Dx molecular-weight distribution (MWD) during vibratory milling.

The changes in the weight-average molecular weight (M_w) over time of fractured Dx are shown in Figure 9.
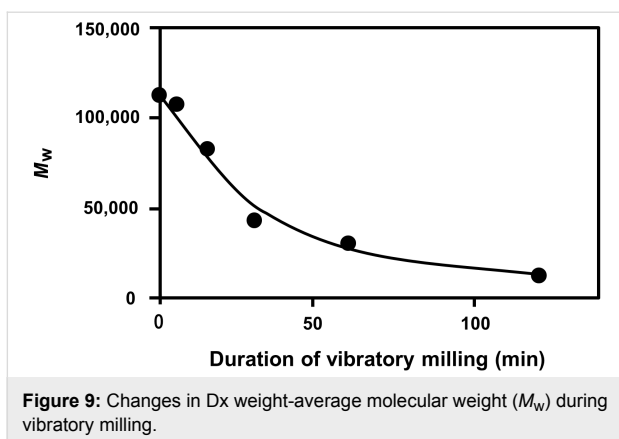
Figure 9: Changes in Dx weight-average molecular weight (M_w) during vibratory milling.

As can be seen from Figure 9, the M_w of Dx decreased exponentially toward the limiting molecular weight ($M_{w,\infty}$) under the experimental conditions. As described above, the maximum Dx spectral intensity was observed at 60 min and the decrease in the molecular weight after 60 min was smaller than that before 60 min. This indicates that the mechanoradical formation is suppressed after 60 min. Thus, the changes in molecular weight are in good agreement with the change in radical concentration over time.

It is known from vibratory milling of several kinds of polymers that the M_w exponentially decreases toward $M_{w,\infty}$ which can be expressed as follows:

$$M_{w,t} = M_{w,\infty} + (M_{w,0} - M_{w,\infty}) \cdot e^{-kt} \qquad (1)$$

where $M_{w,t}$ represents the molecular weight at a given mechanolysis time t, $M_{w,0}$ indicates the molecular weight at $t = 0$, and k denotes the proportionality constant comprising system-dependent parameters [26,27]. The time-dependent changes in M_w depicted in Figure 9 fit the above Equation 1:

$$M_{w,t} = 11,100 + 107,000 \cdot e^{-0.0320t} \quad (r = 0.9884) \qquad (2)$$

The $M_{w,\infty}$ of Dx was determined as 11,000 g/mol under the experimental conditions, similar to that of cellulose [5].

The concept of molecular weight is not suitable for a hyper-branched polysaccharide such as Gly. As Gly is a spherical polymer, it is considered that the particle diameter of Gly might decrease during the mechanolysis. Although a particle diameter of a hyper-branched polysaccharide could be measured by dynamic light scattering (DLS), it is difficult to precisely detect a particle with a diameter of less than 10 nm with our experimental setup.

The hydrodynamic radius (R_h) is utilized as an index of the spread of a polymer. It is well-known that the R_h of a spherical polymer dissolved in a solvent is correlated with its weight-average molecular weight. GPC is a size-exclusion technique in which molecules in solution are separated based on their size, and in some cases, based on their molecular weight. Pullulan, a linear polysaccharide, is a standard sample used in GPC analyses of polymers including polysaccharides. Rolland-Sabate et al. reported that the R_h of pullulan measured by DLS is proportional to the square of the weight average molecular weight determined by GPC [28]. Based on this result, we estimated the R_h of Gly by comparing its GPC elution time with that of pullulan as the standard. Figure 10 shows the time-dependent changes in the particle diameter (R_h) of Gly during vibratory milling.
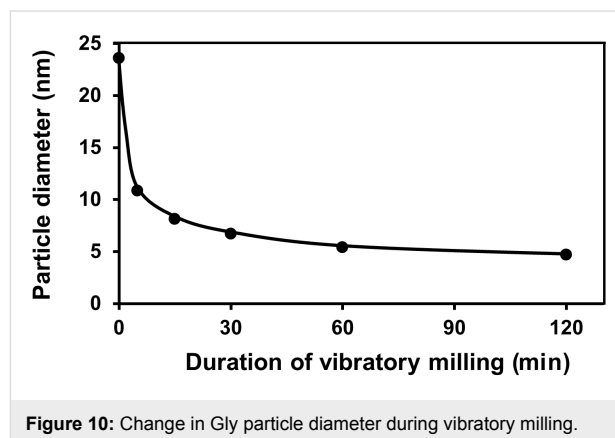
Figure 10: Change in Gly particle diameter during vibratory milling.

It can be seen from Figure 10 that the Gly particle diameter decreased rapidly up to 30 min of milling time and thereafter gradually decreased toward the limiting value. This result was consistent with the total radical concentration of Gly, which exhibited a maximum at 30 min (see Figure 7).

In both cases of Dx and Gly, the molecular weight of Dx or the particle diameter of Gly steeply decreased until reaching the maximum value of total radical concentration. Thereafter, the molecular weight or particle diameter gradually decreased toward the limiting value (Figure 9 and Figure 10). Thus, decreases in each component radical concentrations of Dx and Gly were due to intra- and/or intermolecular flexibility associated with their characteristic branched chains, different from amylose. Figure 7 also shows that the DBS in Gly was considerably more stable than that in Dx due to the higher cross-linking present in the hyper-branched structure of Gly.

Conclusion

We discussed here the nature of mechanoradical formation during mechanolysis of Dx and Gly, based on ESR spectra

coupled with systematic computer simulations, in comparison with the mechanolysis of amylose.

The component spectra of Dx and Gly were essentially identical to those of amylose and remained nearly unchanged in the course of vibratory milling. Simulated Dx, Gly, and amylose spectra were also obtained from admixtures of the component spectra at different ratios. Computer simulations revealed that a singlet spectrum (II) assignable to the immobilized DBS was a major component of milled Dx and Gly.

The generated Dx and Gly mechanoradicals dissipated more readily than amylose mechanoradicals in the course of vibratory milling. Amylose has a helical structure, and Dx and Gly exhibit branched structures and it was speculated that the difference of polymer structure among them could affect the dissipation of mechanoradicals. Thus, hydrogen atoms on the main and branched chains of Dx and Gly could be abstracted, so that the resulting mechanoradicals could rapidly disappear by radical recombination and/or disproportionation reactions due to the flexible structure. Additionally, the hyperbranched structure of Gly might be responsible for the greater stability of the DBS in Gly than that in Dx. The other component spectrum of milled Dx and Gly was a nearly isotropic doublet (I), which could be assigned to an alkoxylalkyl-type radical formed by hydrogen abstraction at the C1 position of the glucose unit, indicating the generation of glucose-based mid-chain alkyl-type radicals. The total radical concentration of both Dx and Gly decreased after reaching the maximum concentration, suggesting that the resulting mechanoradicals underwent radical–radical coupling and/or disproportionation reactions to produce non-radical species.

Systematic analyses of various physicochemical properties showed that the molecular weight of Dx and the particle diameter of Gly exponentially decreased toward the respective limiting value under the experimental conditions examined. This finding was consistent with the progressive changes in the respective radical concentrations. These results demonstrated that the quantity of the mechanoradicals generated during mechanolysis is correlated with the changes in molecular weight or particle diameter. The molecular weight of Dx and particle diameter of Gly approached to the limiting value after reaching the maximum value of total radical concentration (after 60 and 30 min for Dx and Gly, respectively). The disappearance of the Dx and Gly mechanoradicals began due to the presence of flexible branched chains. This phenomenon differed from the case of amylose, which possesses a helical intramolecular structure. The DBS in Gly was found to be more stable than that in Dx due to its hyperbranched structure. The present results also indicated that the mechanolysis of Dx at room temperature not only afforded lower molecular weight polymers but

also led to partial decomposition of the Dx structure by ring-opening and/or conjugating reaction to emerge the cross-linking region. If one performs the mechanolysis of Dx open to air, such structural decomposition of Dx might have occurred and some oxidized functional groups could be incorporated in Dx. The present findings are expected to facilitate graft polymerization of vinyl or acryl monomers onto Dx and Gly.

Experimental
Materials
Powdered Dx (clinical grade), was purchased from Wako Co., Ltd., passed through a 200–235 mesh sieve, and then dried at 60 °C for 12 h in vacuo. Powdered Gly (from Oyster, reagent for molecular biology) was purchased from Nacalai Tesque Co., Ltd. and treated in a similar way to Dx.

Mechanolysis methods
Analogous to the description in [19], powdered samples (100 mg) were mechanically fractured under a nitrogen atmosphere in a vibratory ball-milling apparatus (Shofu Co., Ltd., Kyoto, Japan) equipped with a stainless steel twin-shell blender (7.8 mm diameter, 24 mm length) and a stainless steel ball (6.0 mm diameter, 890 mg) at room temperature for a prescribed period of time at 60 Hz. Residual oxygen was removed using a Model 1000 Oxygen Trap (Chromatography Research Supplies Inc., Louisville, US) and the oxygen concentration was monitored using an oxygen analyser (LC750/PC-120, Toray Engineering Co., Ltd., Shiga, Japan) and kept below 0.01 ppm. The fractured samples were transferred to an ESR tube, which was then sealed and subjected to ESR analysis. All sample manipulations were carried out in a vacuum glove box (Sanplatec Corp., Osaka, Japan). The mechanolysis was carried out for the experimental time points to obtain the fractured sample.

ESR spectral measurements
Similarly as described in [19], ESR spectra were recorded on a JES-RE1X (JEOL Ltd., Japan) spectrometer with X-band and 100 kHz field modulation. Special care was taken to ensure that no saturation occurred and that the line shape was not distorted by excessive modulation amplitude. The square root of the microwave power versus the signal peak height was plotted, so that a microwave power level of 0.04 mW was chosen. The ESR spectral intensity was determined by double integration. The radical concentration (spin numbers per gram of sample) was calculated from the spectral intensity of a poly(methyl methacrylate) sample and impregnating with 2,2-diphenyl-picrylhydrazyl. ESR spectra were measured for all experimental time points. The observed ESR spectra were unchanged for at least several hours at room temperature in the intensity and shape within a detectable extent.

Procedure to detect mechanoanions

Dx was fractured in a metallic vessel at room temperature. The fractured Dx and TCNE were mixed in the dark to avoid the decomposition of mechanoanion and exposed to visible light to induce electron release. After vigorously shaking of the mixture it was transferred to an ESR tube in the dark. ESR spectra were taken before and after visible-light irradiation.

Molecular weight measurements

Similarly as described in [19], the molecular weight of each resulting polymer was measured by gel-permeation chromatography (GPC) using a PU 610 HPLC pump (GL Sciences Inc., Tokyo, Japan) equipped with an RI 504R refractive index detector (GL Sciences Inc.), a model 556 LC column oven (GL Sciences Inc.), gel column (GF-1G 7B and GF-7M HQ, Shodex, Kawasaki, Japan), and a data analyser (Runtime Instruments Chromato-PRO, Runtime Instruments Ltd., Tokyo, Japan). The following conditions were applied: elution solvent, distilled water containing 0.05 wt/vol % NaCl; flow rate, 0.7 mL/min; column temperature, 40 °C. Calibration was carried out with pullulan standards (peak top molecular weight $[M_{peak}]$ = 5,900, 9,600, 21,100, 47,100, 109,000, 200,000, 344,000, and 708,000 g/mol).

Dynamic light scattering measurements

Analogous to the description in [29], dynamic light scattering was measured using a DLS-5500G Photal dynamic light scattering spectrophotometer (Otsuka Electronics Co., Ltd., Osaka, Japan) equipped with a He/Ne laser. A scattering angle of 90° was used in this study. The hydrodynamic diameter and the polydispersity factor of the polymers, represented as μ_2/Γ^2, were calculated using the Stokes–Einstein equation and the cumulant method. The number-average particle diameter and weight-average particle diameter were determined by the histogram method with the Marquardt calculation.

Computer simulations of ESR spectra

Analogous to the description in [5], computational simulations were performed on a personal computer (DELL Inspiron 545S) using a simulation program developed in our laboratory. The simulated spectra were obtained from Lorentzian functions by iterative fitting of the spectroscopic parameters (*g*-value, line width at half-height, hyperfine splitting constant [HSC], and relative intensity) with the observed digitized spectra using a non-linear least-squares method [30-36]. The simulation program included the effect of anisotropy in the *g*-factor and/or α-hydrogen hyperfine tensor on the line shape of powder spectra, according to Kneubuhl's [37] and Cochran's [38] equations, respectively. An anisotropic interaction of β-hydrogens is usually small (less than 0.3 mT), so that such an effect is easily blurred due to broadening of the width of the individual peak

and was therefore not considered in the spectral simulations. To assist the simulation procedure, we also enhanced the program for obtaining the difference spectra by subtracting one observed spectrum from another.

References

1. Haward, R. N. Papers of the international conference on physics and non-crystalline solids. In *Amorphous Materials;* Douglas, R. W.; Ellis, G., Eds.; John Wiley: London, United Kingdom, 1972; Vol. 3, pp 513–521.
2. Sohma, J.; Sakaguchi, M. *Adv. Polym. Sci.* **1976,** *20,* 109–158. doi:10.1007/BFb0023970
3. Kuzuya, M.; Kondo, S.; Noguchi, A. *Macromolecules* **1991,** *24,* 4047–4053. doi:10.1021/ma00014a013
4. Kuzuya, M.; Kondo, S.-I.; Noguchi, A.; Noda, N. *J. Polym. Sci., Part B: Polym. Phys.* **1992,** *30,* 97–103. doi:10.1002/polb.1992.090300110
5. Kuzuya, M.; Yamauchi, Y.; Kondo, S.-i. *J. Phys. Chem. B* **1999,** *103,* 8051–8059. doi:10.1021/jp984278d
6. Dhaneshwar, S. S.; Kandpal, M.; Gairola, N.; Kandam, S. S. *Indian J. Pharm. Sci.* **2006,** *68,* 705–714. doi:10.4103/0250-474X.31000
7. Mahdavania, G. R.; Zohuriaan-Mehr, M. J.; Pourjavadi, A. *Polym. Adv. Technol.* **2004,** *15,* 173–180. doi:10.1002/pat.408
8. Jeanes, A.; Haynes, W. C.; Wilham, C. A.; Rankin, J. C.; Melvin, E. H.; Austin, M. J.; Cluskey, J. E.; Fisher, B. E.; Tsuchiya, H. M.; Rist, C. E. *J. Am. Chem. Soc.* **1954,** *76,* 5041–5052. doi:10.1021/ja01649a011
9. Dimlerl, R. J.; Wolff, A.; Sloan, J. W.; Rist, C. E. *J. Am. Chem. Soc.* **1955,** *77,* 6568–6573. doi:10.1021/ja01629a044
10. Van Cleve, J. W.; Schaefer, W. C.; Rist, C. E. *J. Am. Chem. Soc.* **1956,** *78,* 4435–4438. doi:10.1021/ja01598a064
11. Ricketts, C. R.; Rowe, C. E. *J. Chem. Soc.* **1955,** 3809–3813. doi:10.1039/jr9550003809
12. Price, F. P.; Bellamy, W. D.; Lawton, E. J. *J. Phys. Chem.* **1954,** *58,* 821–824. doi:10.1021/j150520a005
13. Flynn, J. H.; Wall, L. A.; Morrow, W. L. *J. Res. Natl. Bur. Stand., Sect. A* **1967,** *71A,* 25–31.
14. Phillips, G. O.; Moody, G. J. *J. Chem. Soc.* **1958,** *711,* 3534–3539. doi:10.1039/jr9580003534
15. Zohuriaan-Mehr, M. J. *Iran. Polym. J.* **2005,** *14,* 235–265.
16. Maiti, S.; Ranjit, S.; Sa, B. *Int. J. PharmTech Res.* **2010,** *2,* 1350–1358.
17. Sakaguchi, M.; Ohura, T.; Iwata, T.; Takahashi, S.; Akai, S.; Kan, T.; Murai, H.; Fujiwara, M.; Watanabe, O.; Narita, M. *Biomacromolecules* **2010,** *11,* 3059–3066. doi:10.1021/bm100879v
18. Solala, I.; Henniges, U.; Pirker, K. F.; Rosenau, T.; Potthast, A.; Vuorinen, T. *Cellulose* **2015,** *22,* 3217–3224. doi:10.1007/s10570-015-0724-x
19. Doi, N.; Sasai, Y.; Yamauchi, Y.; Adachi, T.; Kuzuya, M.; Kondo, S.-i. *Chem. Pharm. Bull.* **2015,** *63,* 992–997. doi:10.1248/cpb.c15-00497
20. Lindberg, B.; Svensson, S. *Acta Chem. Scand.* **1968,** *22,* 1907–1912. doi:10.3891/acta.chem.scand.22-1907
21. Larm, O.; Lindberg, B.; Svensson, S. *Carbohydr. Res.* **1971,** *20,* 39–48. doi:10.1016/S0008-6215(00)84947-2
22. Voet, D.; Voet, J. G. *Biochemistry,* 4th ed.; John Wiley & Sons: New York City, NY, U.S.A..
23. Sakaguchi, M.; Makino, M.; Ohura, T.; Iwata, T. *J. Phys. Chem. A* **2012,** *116,* 9872–9877. doi:10.1021/jp306261k

24. Motokawa, T.; Makino, M.; Enomoto-Rogers, Y.; Kawaguchi, T.; Ohura, T.; Iwata, T.; Sakaguchi, M. *Adv. Powder Technol.* **2015,** *26,* 1383–1390. doi:10.1016/j.apt.2015.07.012

25. Kondo, S.-i.; Sasai, Y.; Hosaka, S.; Ishikawa, T.; Kuzuya, M. *J. Polym. Sci., Part A: Polym. Chem.* **2004,** *42,* 4161–4167. doi:10.1002/pola.20245

26. Harrington, R. E.; Zimm, B. H. *J. Phys. Chem.* **1965,** *69,* 161–175. doi:10.1021/j100885a025

27. Kanamaru, K. *Kolloid Z. Z. Polym.* **1966,** *209,* 151–162. doi:10.1007/BF01500633

28. Rolland-Sabaté, A.; Mendez-Monteaalvo, M. G.; Colonna, P.; Planchot, V. *Biomacromolecules* **2008,** *9,* 1719–17301. doi:10.1021/bm7013119

29. Kondo, S.-i.; Asano, Y.; Koizumi, N.; Tatematsu, K.; Sawama, Y.; Sasai, Y.; Yamauchi, Y.; Kuzuya, M.; Kurosawa, S. *Chem. Pharm. Bull.* **2015,** *63,* 489–494. doi:10.1248/cpb.c14-00869

30. Kuzuya, M.; Morisaki, K.; Niwa, J.; Yamauchi, Y.; Xu, K. *J. Phys. Chem.* **1994,** *98,* 11301–11307. doi:10.1021/j100095a011

31. Kuzuya, M.; Yamauchi, Y.; Niwa, J.; Kondo, S.-i.; Sakai, Y. *Chem. Pharm. Bull.* **1995,** *43,* 2037–2041. doi:10.1248/cpb.43.2037

32. Kuzuya, M.; Noguchi, A.; Ishikawa, M.; Koide, A.; Sawada, K.; Ito, A.; Noda, N. *J. Phys. Chem.* **1991,** *95,* 2398–2403. doi:10.1021/j100159a052

33. Kuzuya, M.; Ito, H.; Kondo, S.; Noda, N.; Noguchi, A. *Macromolecules* **1991,** *24,* 6612–6617. doi:10.1021/ma00025a010

34. Kuzuya, M.; Niwa, J.; Ito, H. *Macromolecules* **1993,** *26,* 1990–1995. doi:10.1021/ma00060a030

35. Kuzuya, M.; Yamashiro, T.; Kondo, S.-i.; Sugito, M.; Mouri, M. *Macromolecules* **1998,** *31,* 3225–3229. doi:10.1021/ma9709361

36. Kuzuya, M.; Kondo, S.-i.; Sugito, M.; Yamashiro, T. *Macromolecules* **1998,** *31,* 3230–3234. doi:10.1021/ma970937t

37. Kneubühl, F. K. *J. Chem. Phys.* **1960,** *33,* 1074–1078. doi:10.1063/1.1731336

38. Cochran, E. L.; Adrian, F. J.; Bowers, V. A. *J. Chem. Phys.* **1961,** *34,* 1161–1175. doi:10.1063/1.1731715

Mechanochemistry-assisted synthesis of hierarchical porous carbons applied as supercapacitors

Desirée Leistenschneider[1], Nicolas Jäckel[2,3], Felix Hippauf[4], Volker Presser[2,3] and Lars Borchardt[*1,§]

Address:
[1]Institute of Inorganic Chemistry, Technische Universität Dresden, Dresden, Germany, [2]INM - Leibniz Institute for New Materials & Saarland University, Saarbrücken, Germany, [3]Department of Materials Science and Engineering, Saarland University, Saarbrücken, Germany and [4]Fraunhofer Institute for Material and Beam Technology IWS, Dresden, Germany

Email:
Lars Borchardt[*] - lars.borchardt@tu-dresden.de

* Corresponding author
§ Tel: +49 35146334960

Abstract

A solvent-free synthesis of hierarchical porous carbons is conducted by a facile and fast mechanochemical reaction in a ball mill. By means of a mechanochemical ball-milling approach, we obtained titanium(IV) citrate-based polymers, which have been processed via high temperature chlorine treatment to hierarchical porous carbons with a high specific surface area of up to 1814 m^2 g^{-1} and well-defined pore structures. The carbons are applied as electrode materials in electric double-layer capacitors showing high specific capacitances with 98 F g^{-1} in organic and 138 F g^{-1} in an ionic liquid electrolyte as well as good rate capabilities, maintaining 87% of the initial capacitance with 1 M TEA-BF$_4$ in acetonitrile (ACN) and 81% at 10 A g^{-1} in EMIM-BF$_4$.

Introduction

Porous carbons are key components in many energy and environmentally-relevant applications, such as catalysis [1], gas storage and separation [2,3], and electrochemical energy storage [4-6]. Among them, activated carbons derived from natural precursors such as coconut shells are widely used in industrial applications [7]. Due to their high specific surface area, predominantly provided by micropores, they can physisorb large quantities of molecules. They are also particularly suitable as electrode materials for supercapacitors, in which the energy storage is based on the electrosorption of electrolyte ions on the electrode surface [8-10]. These micropores are usually introduced by physical or chemical activation, often leading to broad pore-size distributions and non-uniform pore structures [11]. However, for size-selective applications [12], non-uniform broad pore-

size distributions lead to lower performance metrics [13,14]; they are also detrimental to derive clear statements about structure–performance relationships for fundamental research, such as the influence of the pore size and the pore structure on (electro)sorption in energy storage devices [15-17]. Moreover, purely microporous carbons suffer from diffusion limitations resulting in low electrochemical performances at high charge/discharge rates [4,18,19]. Larger pores, like mesopores, or hierarchical micro-meso-macroporous pore systems, facilitate fast ion transport through the carbon pore network [20,21]. Therefore, synthesis approaches leading to such pore systems are highly desirable to improve the electrochemical performance of carbon supercapacitors.

A well-established strategy for designing the porosity of carbon materials involves hard or soft templates [22-24]. Hard-templating utilizes metal oxide nanoparticles [25] and salts [26-28], which have to be synthesized in advance. Soft-templating employs surfactants or other structure-directing molecules, which self-assemble to form the desired template [29,30]. A severe disadvantage of both routes is the need of large amounts of solvents, eventually accumulating as waste during the process. Moreover, these approaches require multiple synthesis steps, including template synthesis, calcination, impregnation, pyrolysis, and template removal. Therefore, the preparation of porous carbons with a tailored pore structure by conventional templating processes is often time and cost-intensive and environmentally unfavorable. For a more sustainable carbon production, especially in industrial scale, it is necessary to reduce the number of synthesis steps and to minimize waste accumulation, at best by avoiding any solvents [7,31].

Lately, mechanochemistry has gained momentum in organic chemistry [32-34]. The initiation of chemical reactions by mechanical forces enables organic and inorganic syntheses without the use of any solvent within short reaction times of only few minutes [32,35]. A mechanochemical synthesis also enables high yields, making it a promising approach to obtain carbons and carbon precursors [36,37]. So far, mechanochemical reactions for the synthesis of porous carbon materials have rarely been used [38]. For example, the preparation of nanocarbon structures such as graphene sheets or fullerenes [39-41] as well as porous carbonaceous polymers [42,43] have been conducted mechanochemically. Our work demonstrates that a templating approach can be transferred into the solvent-free environment of a ball mill, and thus simplify the synthesis of hierarchical porous carbons drastically. Moreover, it is the first proof that even well-defined carbon pore structures can be derived making use of solid-state conditions like ball-milling. In detail, we apply the Pechini method, an approach commonly used for the synthesis of uniform metal oxide nanoparticles to synthesize a titanium(IV) citrate-based polymer [44,45]. The Pechini method is applicable to synthesize templated mesoporous carbons [46-49], but has never been utilized for a solvent-free and rapid process based on mechanochemistry.

The combination of this approach with a high temperature chlorine treatment enabled us to simultaneously carbonize the polymer and selectively remove the titania. By this way, we obtained a hierarchical carbon with a high pore volume, high specific surface area, tunable mesopore volume, and a well-defined pore-size distribution. The material was further investigated as supercapacitor electrode using organic and ionic liquid electrolytes (Figure 1).

Figure 1: Synthesis of hierarchical porous carbons by mechanochemical polymerization of ethylene glycol (EG) with citric acid (CA) and Ti(IV) isopropoxide as a porogen, resulting in CA-EG polymers. After carbochlorination at 900 °C hierarchical carbons are obtained. The byproduct TiCl$_4$ can be recycled to be used as Ti(IV) isopropoxide, and acts as porogen in further syntheses.

Results and Discussion
Mechanochemical synthesis of the polymeric precursor

For a typical synthesis, ethylene glycol (EG), citric acid (CA), and titanium isopropoxide (TIPP) were ground with a molar ratio of 3:1:1 in a ZrO_2 milling cup for 5 min. A practical indicator for a successful mechanochemical reaction is a color change. The white and colorless educts turn to a yellow polymer with a honey-like texture. We first characterized the polymerization of the educts induced by mechanochemical forces by IR spectroscopy (Figure 2). Two bands at 1703 cm^{-1} and 1136 cm^{-1} appear, indicating the formation of the polyester (EG-CA). Likewise, the characteristic bands of the educts (CA: 1210 cm^{-1}; EG: 1418 cm^{-1}) become less pronounced and much broader as they are gradually consumed by the mechanically-induced polymerization. The spectrum of the Ti-containing polymer (Polymer-SF-3) displays the appearance of a band at 1558 cm^{-1}, which corresponds to titanium, bidentate to a carboxylic group [50]. Additionally, the blue-shift of the vibration at 1703 cm^{-1} indicates complexation [51]. The sample Polymer-SF-3 was investigated by matrix-assisted laser desorption/ionization with a time-of-flight mass spectrometer (MALDI–TOF) revealing a weight-averaged molar mass (M_w) of 2015.6 g mol^{-1}, which is equivalent to 6 monomeric units.
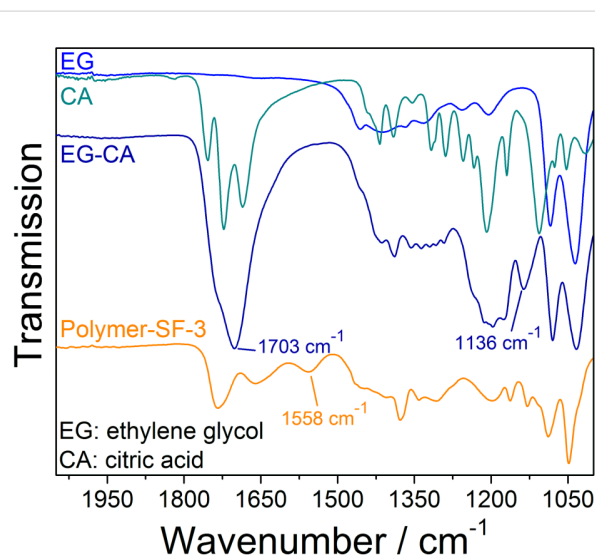

Figure 2: Infrared spectra of the monomers ethylene glycol (EG, blue) and citric acid (CA, green blue), the metal-free polymer achieved by 5 min ball milling with ZrO_2 balls (*d* = 15 mm) (EG-CA, dark blue) and the polymeric precursor after adding titanium(IV) isopropoxide (Polymer-SF-3, orange).

Synthesis of the hierarchical porous carbons

After the mechanochemical synthesis, we conducted a carbochlorination reaction, leading to the carbonization of the precursor and the removal of the dispersed titanium species

(Equation 1). This process is comparable to the industrial Kroll process and responsible for the generation of mesopores that correspond to the size of the former titania nanostructures [25]. While titanium is removed as gaseous $TiCl_4$, oxygen is extracted as CO, whereby carbon is being partially consumed as well. This partial carbon removal leads to an etching of the carbon framework and an in situ formation of micropores, surrounding the formed mesopores. Consequently, a hierarchical porous carbon material is formed [52]. The resulting byproduct $TiCl_4$ is a valuable precursor for Ti-containing [53] chemicals like Ti(IV) isopropoxide, other Ti-alkoxides, or can directly be applied in the presented synthesis approach once again [52].

$$TiO_2 + (2+x)C + 2Cl_2 \rightarrow TiCl_4 + 2CO + xC \qquad (1)$$
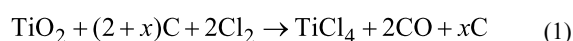
Scanning and transmission electron micrographs indicate that the carbon material exhibits spherically shaped mesopores (Figure 3), corresponding to the removal of TiO_2 particles which have been formed during the pyrolysis (Figure 4). The pores are homogenously distributed, resulting in a well-connected pore system of the carbon material (Figure 3A,B).
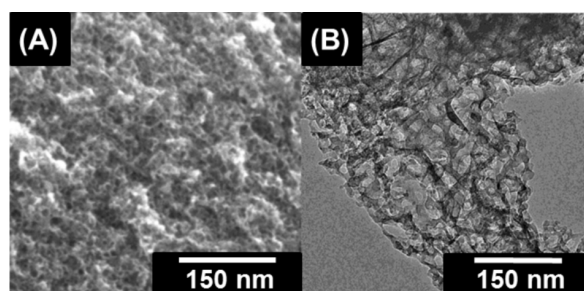

Figure 3: SEM (A) and TEM (B) images of the Carb-SF-3 sample.

To display the complete removal of the porogenous TiO_2, we compared the XRD pattern (Figure 4) of the material at different synthesis steps: after mechanochemical polymerization (Polymer-SF-3), after temperature treatment but before Cl_2 addition (Comp-SF-3), and after the carbochlorination reaction (Carb-SF-3).

The absence of X-ray reflections confirms the amorphous nature of the polymeric precursor. Titanium is atomically coordinated and distributed within the polymer and does not form crystalline TiO_2 nanoparticle domains. After carbonization broadened reflections occur due to the conversion of the bidenated Ti atoms to TiO_2 nanoparticles of the rutile and anatase modification. We calculated the average domain size of crystalline TiO_2 from the reflections at 25.4°, 48.0°, and 54.5° 2θ to be 6–9 nm after background adjustment using the Scherrer equation. Carbochlorination will remove these nanoparticles,
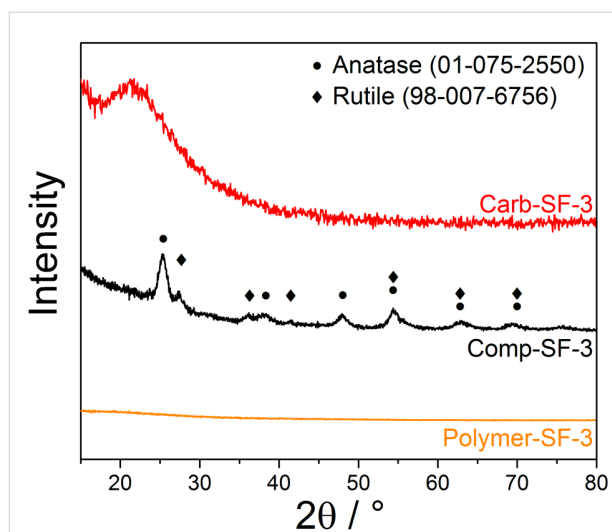
Figure 4: XRD-pattern of the polymeric precursor (Polymer-SF-3, orange), the carbonized composite (Comp-SF-3, black) and the carbon received by chlorine treatment (Carb-SF-3, red).

The low specific surface area of 298 m^2 g^{-1} for the composite arises from chemical activation processes of volatile functional groups such as carboxylic acids, which form micropores during pyrolysis.

After carbochlorination at 900 °C, the obtained carbon (Carb-SF-3) shows a well-developed micro- and mesoporosity, obvious due to a type IV isotherm and a high nitrogen uptake at low relative pressure, which is attributed to the amount of micropores in the samples. The obtained material has a high specific surface area of up to 1814 m^2 g^{-1} and a pore volume of 1.83 cm^3 g^{-1}. The contributions of the individual pore-size increments are shown in Table 1 and Figure 6. The carbons possess narrowly distributed micropores with an average size of 0.96 nm (due to the in situ activation process), as well as mesopores with an average diameter of 8 nm (due to the removal of TiO$_2$ nanodomains) (Figure 6, Equation 1). The mesopore diameter (Table 1 and Figure 6) aligns very well with the calculated domain size of TiO$_2$ nanocrystals derived from the Scherrer equation. A more precisely evaluation of the hierarchical pore structure is given in Table S1 in Supporting Information File 1.

leading to mesopores of comparable size. The XRD pattern of the carbon shows the broad (002) reflection of nanocrystalline carbon, but all signals related to titania have disappeared. This assumption was further supported by EDX measurements (Table 1), showing a Ti content below the detection limit.

The pore structure of the materials was analyzed by nitrogen physisorption (Figure 5A). Neither the polymer (Polymer-SF-3) nor the carbonized composite material (Comp-SF-3) show a significant porosity (Table 1). This was expected since the porogens have not been removed during this step in the synthesis.

We further investigated the influence of the EG to CA ratio on the porosity of the material, while keeping the TIPP to CA ratio constant (1:1). The pore volume increased with a higher content of ethylene glycol from 1.34 cm^3 g^{-1} for a ratio of 1:1 to 1.83 cm^3 g^{-1} for a ratio of 3:1. This is mainly attributed to the increased mesopore volume, while the micropore volume stayed nearly the same (0.20 cm^3 g^{-1}, Table 1). The higher mesopore content originates from the higher amount of ethylene glycol,

**Table 1:** Porosity and composition data summary for the different samples.

Samples[a]	SSA$_{BET}$[b] / m^2 g^{-1}	SSA$_{DFT,microc}$ / m^2 g^{-1}	V$_{total}$[d] / cm^3 g^{-1}	V$_{meso}$[e] / cm^3 g^{-1}	V$_{micro}$[f] / cm^3 g^{-1}	d$_{mesopore}$[g] / nm	Ti content[h] / %
Polymer-SF-3[i]	–	–	–	–	–	–	15.7[j]
Comp-SF-3	298	185	0.17	0.10	0.07	–	45.8 ± 13.4
Carb-SF-1	1442	623	1.34	1.11	0.23	4–14	<d.l.
Carb-SF-2	1532	480	1.62	1.43	0.19	4; 6–12	<d.l.
Carb-SF-3	1814	558	1.83	1.62	0.23	4; 6–14	<d.l.
Carb$_{HF}$-SF-3	291	144	0.20	0.14	0.06	–	n.d.
Comp-LA-3	312	173	0.18	0.14	0.04	–	62.8 ± 16.7
Carb-LA-3	1590	445	1.59	1.41	0.18	4; 6–13	<d.l.
Carb$_{HF}$-LA-3	706	123	0.62	0.48	0.14	4–12	11.1

[a]Sample code x−y−z as follows, x describes the material after polymerization (Polymer), after heat treatment (Comp) and after carbochlorination (Carbon), the indices HF notices that the template was removed by HF instead of Cl$_2$, y describes the reaction conducted solvent-free (SF) or liquid-assisted (LA), z describes the ratio of EG to CA. [b]Specific surface area (SSA) determined in a pressure range of 0.05 < p/p_0 < 0.2. [c]Specific surface area of the mesopores determined by QSDFT below 2 nm. [d]Total pore volume determined at p/p_0 = 0.99. [e]Mesopore volume = $V_{total} - V_{micro}$. [f]Micropore volume determined by QSDFT below 2 nm. [g]Mesopore size determined by QSDFT kernel for slit-shaped, cylindrical, spherical pores using the adsorption branch. [h]Ti content determined by EDX measurement, <d.l. = below detection limit. [i]The polymer is non-porous. [j]The polymer is not stable in the electron beam; therefore, the composition must be determined from thermogravimetric analysis (TG) rather than from EDX.
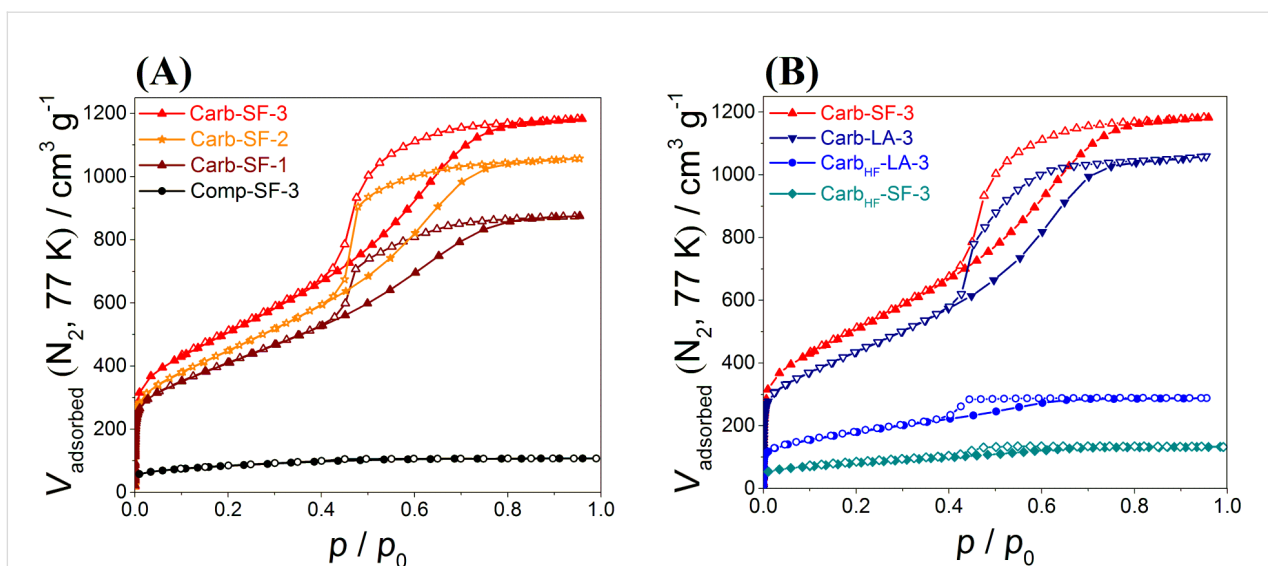
Figure 5: Nitrogen physisorption isotherms for carbon samples achieved from (A) different amounts of ethylene glycol and (B) different syntheses.
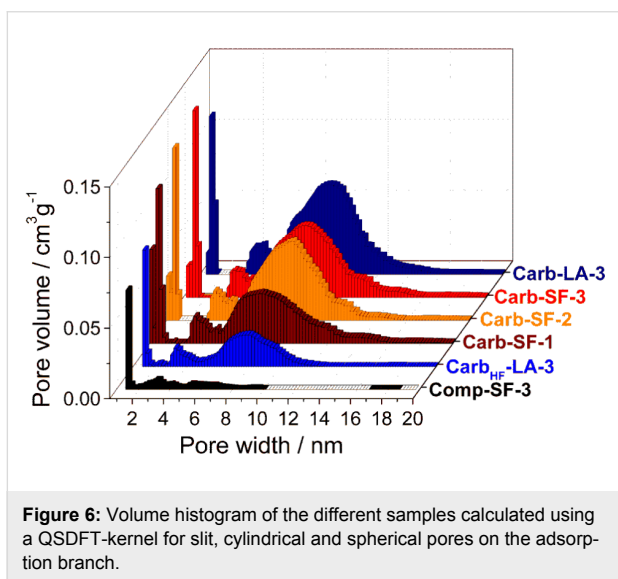
Figure 6: Volume histogram of the different samples calculated using a QSDFT-kernel for slit, cylindrical and spherical pores on the adsorption branch.

which promotes the formation of more slightly larger pores. This process finally leads to a higher mesopore volume at the expense of a narrower pore-size distribution (Figure 6). The EG ratio does not impact the particle size of the TiO_2 nanostructures and thus the pore-size distributions are similar for all investigated materials (average diameter of 8 nm). The reaction in total absence of EG yields white powder next to purely black carbon phases (see Figure S2, Supporting Information File 1). This indicates that the carbon content was insufficient and demonstrates the inevitable role of EG.

To further investigate the mechanochemical polymerization and the carbochlorination step, we conducted the synthesis under liquid-assisted conditions while adding ethanol as a solvent to see if there is a difference in the polymerization and investigated an alternative template removal approach based on etching with hydrofluoric acid (HF) as well [54]. The latter is a common process used in industry [55]. However, by doing so, it is impossible to remove the porogenous TiO_2 completely from the carbon matrix (sample $Carb_{HF}$-SF-3). The resulting material still contained 11.1 wt % of Ti and did not show a high porosity (Figure 5B and Table 1) with a pore volume of 0.20 cm^3 g^{-1} and a surface area of 291 m^2 g^{-1}. Indeed, the high temperature chlorination reaction is essential to obtain the full porosity of the desired carbon. However, when we conducted the mechanochemical polymerization in the presence of small amounts of ethanol (liquid-assisted grinding, LA), the porogens could be partially removed by HF ($Carb_{HF}$-LA-3). We assume that the carbon matrix obtained from a solvent-free approach is possibly denser and thus the diffusion of HF to the particles is inhibited (incomplete removal). This aligns with the assumption that the energy-input and accordingly the embedding of the particles are higher in case of solvent-free syntheses. When we compare SF and LA samples (both received by carbochlorination), we observe full template removal and obtain hierarchical porous carbons with high surface area and pore volume (Table 1 and Figure 5B). The addition of a solvent during the mechanochemical synthesis does not influence the porosity of the composite materials, since both composites (Comp-SF-3 and Comp-LA-3) provide the same pore volume (0.2 cm^3 g^{-1}) and SSA (300 m^2 g^{-1}, Table 1). However, the carbons derived after carbochlorination differ in their porosities. The solvent-free synthesis results in a higher specific surface area and pore volume as compared to the liquid-assisted approach. We

suggest that this is also attributed to more homogenously distributed particles while conducting the polymerization solvent-free. In the presence of solvents, a phase-separation phenomena might be induced, which results in a lower pore volume of the received carbon material (Table 1). Although chlorine gas is widely used in many industrial processes such as the Kroll process, it should be the attempt of future research to substitute chlorine gas by a green alternative to advance this mechanochemical process to an even more sustainable synthesis.

Application as supercapacitor electrodes

We selected Carb-SF-3 as electrode material in a symmetrical supercapacitor because of its high specific surface area and pore volume (Table 1). The electrochemical characterization was done in 1 M TEA-BF$_4$ in acetonitrile (ACN) and neat EMIM-BF$_4$ as an ionic liquid. Since ionic liquids show a lower ion mobility as compared to aqueous or organic electrolytes, a well-connected transport pore system is of particular importance to guarantee a fast ion transport and should result in better power performance [21,56]. Hierarchical pore systems provide enhanced ion transport in meso-/macropores in combination with high energy density due to accessible surface area in micropores [21].

The energy storage is accomplished by ion electrosorption as can be inferred from the rectangular shaped cyclic voltammograms (CVs) in both electrolytes (Figure 7A,B) [53]. At low current rates, the material shows good specific capacitance (Table 2) of 138 F g^{-1} in neat EMIM-BF$_4$ and 98 F g^{-1} in 1 M TEA-BF$_4$ (ACN) determined by galvanostatic cycling with potential limitation at 0.1 A g^{-1}. These values are comparable to other known Kroll carbons [52] and non-doped mesoporous carbons [57].
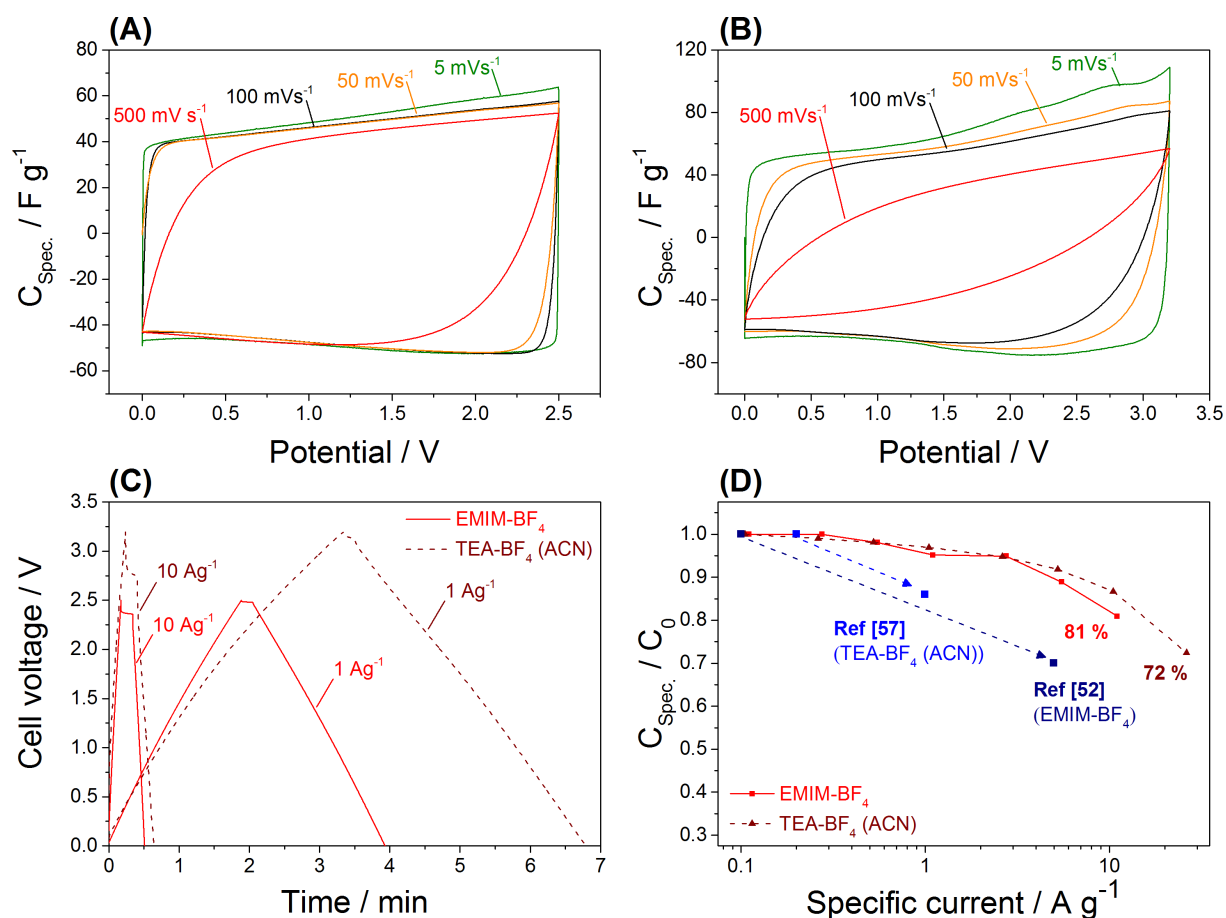
Figure 7: Cyclic voltammograms performed with different scan rates in (A) 1 M TEA-BF$_4$ (ACN) and (B) EMIM-BF$_4$; galvanostatic charge/discharge curves in two different electrolytes at different specific currents (C); normalized rate capability test with different specific currents (D) in comparison to another Kroll carbon (from [52]) and a mesoporous template carbon (from [57]) with comparable mesopore sizes and surface areas.

Table 2: Electrochemical data summary for sample Carb-SF-3 measured in two different electrolytes.

Sample	Electrolyte[a]	C_0[b] / F g^{-1}	C_0[c] / F m^{-2}	Capacitance loss / %	Specific energy[d] / Wh kg^{-1}	Energy efficiency[e] / %
Carb-SF-3	O	98	0.054	13[f]	18.99	95.0
Carb-SF-3	IL	138	0.076	19[f]	41.30	83.5
Ref [52][g]	IL	135	0.072	30[f]	n. d.	n. d.
Ref [57][h]	O	93	0.062	14[i]	n. d.	n. d.

[a]Electrolyte is abbreviated as followed: O = 1 M TEA-BF$_4$, IL = EMIM-BF$_4$. [b]Weigth normalized capacitance at 0.1 A g^{-1}. [c]BET-surface area normalized capacitance at 0.1 A g^{-1}, [d]Specific energy obtained from discharge at 1 A g^{-1} measured in 1 M TEA-BF$_4$ (ACN) and at 1 A g^{-1} in EMIM-BF$_4$. [e]Energy efficiency calculated as quotient of the specific energy obtained from discharge and charge at 1 A g^{-1} loss of specific capacitance, calculated as 1 − quotient of C_{spec} at 1 A g^{-1} and C_0. [f]Loss of specific capacitance, calculated as 1 − quotient of C_{spec} at 10 A g^{-1} and C_0. [g]Reference Kroll carbon. [h]Reference mesoporous carbon. [i]Loss of specific capacitance, calculated as 1 − quotient of C_{spec} at 1 A g^{-1} and C_0 reference non-doped mesoporous carbon.

At a high sweep rate of 500 mV s^{-1}, the shape of the CV, recorded in the organic electrolyte (Figure 7A) remains nearly rectangular, which indicated a high power handling ability. The ion mobility of ionic liquids is lower compared to organic electrolytes, as can be seen from the stronger deformation of the CV at high scan rates (Figure 7B). The different rate handling is also quantified by galvanostatic cycling with potential limitation (GCPL) conducted at different specific currents as presented in Figure 7C. At a high current rate of 10 A g^{-1}, the specific capacitance was 87% in the organic electrolyte and 81% in EMIM-BF$_4$ compared to the specific capacitance at 0.1 A g^{-1}. The ability of the carbon to enable a fast charge and discharge is superior compared to other mesoporous non-doped carbon electrodes (Figure 7D). The material also exhibited excellent performance stability, as seen from 92% and 95% after 100 h of floating at 2.7 V for TEA-BF$_4$ in ACN and 3.2 V in EMIM-BF$_4$, respectively.

Conclusion

Our work presents a novel, solvent-free approach to receive hierarchical porous carbons with tailorable mesopore volume involving two synthesis steps: firstly, the mechanochemical synthesis of a polymeric composite, received by ball-milling within five minutes only, and secondly, the conversion of this precursor to a hierarchical carbon by a carbochlorination reaction. The received carbons exhibit specific surface areas of up to 1800 m^2 g^{-1} and high mesopore volumes up to 1.8 cm^3 g^{-1}, making them very attractive for energy applications. When benchmarked as supercapacitor electrode material, Carb-SF-3 shows good specific capacitances with 98 F g^{-1} in 1 M TEA-BF$_4$ (ACN) and 138 F g^{-1} in EMIM-BF$_4$. Even with high specific currents of 10 A g^{-1} the carbon shows 87% in organic and 91% in ionic liquid electrolyte of its specific capacitance. Moreover, the carbon enables a stable electrochemical performance in both surveyed electrolytes with over 92% capacitance retention after 100 h of voltage floating. Due to the ability to design

the mesopore volumes and their relatively narrow pore size distribution, the carbons are also interesting as model carbons for the investigation of different adsorption phenomena.

Experimental
Synthesis

Citric acid monohydrate (CA, purity: 95.5%) and titanium isopropoxide (TIPP, purity: 97%) were purchased from Sigma-Aldrich. Ethylene glycol (EG, purity 99.5%) was purchased from Fluka Analytics.

For the solvent-free synthesis of hierarchical porous carbons, 5.25 g CA were ground with 7.10 g TIPP in a molar ratio of 1:1 in a 45 mL ZrO$_2$ milling cup for 1 min with 700 rpm. Seven grinding balls out of ZrO$_2$ with a diameter of 15 mm were used. Afterwards, different amounts of EG are added and the mixture was ball-milled for another 5 min with 700 rpm. The molar ratio of CA and EG was varied from 1:3 to 1:1. For the liquid-assisted synthesis, 5 mL EtOH were added to the first grinding step.

The resulting polymer was heated to 900 °C at a heating rate of 300 °C h^{-1} in a horizontal tubular furnace under argon atmosphere with a flowrate of 150 mL min^{-1}. After 1 h at 900 °C, the gas atmosphere was changed to a mixture of argon (flowrate: 70 mL min^{-1}) and chlorine gas (flowrate: 80 mL min^{-1}) while the temperature was held for additional 2 h at 900 °C. After cooling to 600 °C under argon, remaining chlorine was removed by hydrogen treatment (flowrate: 80 mL min^{-1}) for 1 h.

Characterization

Nitrogen physisorption experiments were carried out with an AUTOSORB-iQ-C-XR from Quantachrome at −196 °C. Prior to the measurements, the samples were degassed for at least 24 h at 150 °C under vacuum. The specific surface area was

calculated in a relative pressure range of 0.05–0.2 per the Brunauer–Emmett–Teller (BET) theory. Values for the total pore volume were determined at a relative pressure of 0.99. Pore size distributions were achieved by applying the hybrid QSDFT model for slit-shaped, cylindrical and spherical pores at −196 °C. The micropore volume was calculated from the cumulative QSDFT pore volume data at 2 nm. Energy dispersive X-ray (EDX) analyses were performed with a SU8020 from Hitachi at an acceleration voltage of 20 kV. Transmission electron microscopy (TEM) was executed with a TEM Libra 200 system from Carl Zeiss Microscopy GmbH with an acceleration voltage of 200 kV. For the TEM, the sample powder was sonicated in acetone for 5 s. A lacey-carbon film on copper net (300 mesh) from Plano was used as TEM grid. Afterward, 5 µL were dropped on the grid and evaporated. IR spectra were conducted with the use of ATR technique, as well as with the DRIFTS technique with a Bruker Vertex 70 in the range of 4000–400 cm^{-1}. The hierarchical porous carbon was prepared as free standing electrodes. The carbon material was dispersed in ethanol and we added 10 wt % polytetrafluoroethylene (PTFE, 60 wt % solution in water) as the polymer binder. By crushing the mixture in an agate mortar until the ethanol is evaporated, a dough-like mass was obtained, which was further rolled out until the electrode had a thickness of about 150 µm. The electrode was dried in a vacuum oven at 120 °C for 24 h and we used a disc cutter to obtain electrodes with a diameter of 12 mm. The measurement was done in custom-built cells in a symmetrical two-electrode setup with a quasi-reference electrode out of YP-50F bound with PTFE [58,59]. A 13 mm diameter Whatmann GF/D was used as a separator and 12 mm diameter carbon-coated aluminum discs from MTI Corporation was used as a current collector.

The electrochemical measurements were performed with a Biologic VMP-300 potentiostat/galvanostat. The specific capacitances were calculated with Equation 2 from galvanostatic cycling with potential limitation (GCPL). To compare the electrodes with other materials, they were normalized to their active mass, which is equivalent to the carbon mass in the electrodes, as well as to their specific surface area obtained by the BET method. For the graphical representation of the cyclic voltammograms, the specific capacitances were calculated with Equation 3.

$$C_{spec.} = \frac{4Q(\text{discharge})}{U \cdot m} \tag{2}$$

$$C_{spec.} = \frac{I(t)}{\left(\dfrac{dU(t)}{dt}\right)m} \tag{3}$$

For the calculation of the specific energy of the carbon electrodes in two different electrolytes, Equation 4 was applied with discharge data after the iR drop.

$$E = \frac{I}{m}\int U dt \tag{4}$$

Supporting Information

Supporting Information File 1
Additional data.
[http://www.beilstein-journals.org/bjoc/content/supplementary/1860-5397-13-130-S1.pdf]

Acknowledgements

References

1. Rodríguez-reinoso, F. *Carbon* **1998,** *36,* 159–175. doi:10.1016/S0008-6223(97)00173-5
2. Suda, H.; Haraya, K. *Chem. Commun.* **1997,** 93–94. doi:10.1039/a606385c
3. Suda, H.; Haraya, K. *J. Phys. Chem. B* **1997,** *101,* 3988–3994. doi:10.1021/jp963997u
4. Rose, M.; Korenblit, Y.; Kockrick, E.; Borchardt, L.; Oschatz, M.; Kaskel, S.; Yushin, G. *Small* **2011,** *7,* 1108–1117. doi:10.1002/smll.201001898
5. Simon, P.; Taberna, P.-L.; Béguin, F. Electrical Double-Layer Capacitors and Carbons for EDLCs. In *Supercapacitors: Materials, Systems, and Applications;* Béguin, F.; Frackowiak, E., Eds.; Wiley-VCH: Weinheim, 2013; pp 131–165.
6. Oschatz, M.; Boukhalfa, S.; Nickel, W.; Hofmann, J. P.; Fischer, C.; Yushin, G.; Kaskel, S. *Carbon* **2017,** *113,* 283–291. doi:10.1016/j.carbon.2016.11.050
7. Titirici, M.-M.; White, R. J.; Brun, N.; Budarin, V. L.; Su, D. S.; del Monte, F.; Clark, J. H.; MacLachlan, M. J. *Chem. Soc. Rev.* **2015,** *44,* 250–290. doi:10.1039/C4CS00232F
8. Simon, P.; Gogotsi, Y. *Nat. Mater.* **2008,** *7,* 845–854. doi:10.1038/nmat2297
9. Merlet, C.; Rotenberg, B.; Madden, P. A.; Taberna, P.-L.; Simon, P.; Gogotsi, Y.; Salanne, M. *Nat. Mater.* **2012,** *11,* 306–310. doi:10.1038/nmat3260
10. Piwek, J.; Platek, A.; Fic, K.; Frackowiak, E. *Electrochim. Acta* **2016,** *215,* 179–186. doi:10.1016/j.electacta.2016.08.061
11. Borchardt, L.; Oschatz, M.; Kaskel, S. *Mater. Horiz.* **2014,** *1,* 157–168. doi:10.1039/C3MH00112A

12. Hippauf, F.; Lunow, D.; Huettner, C.; Nickel, W.; Borchardt, L.; Henle, T.; Kaskel, S. *Carbon* **2015,** *87,* 309–316. doi:10.1016/j.carbon.2015.02.023

13. Kyotani, T. *Carbon* **2000,** *38,* 269–286. doi:10.1016/S0008-6223(99)00142-6

14. Jäckel, N.; Simon, P.; Gogotsi, Y.; Presser, V. *ACS Energy Lett.* **2016,** *1,* 1262–1265. doi:10.1021/acsenergylett.6b00516

15. Borchardt, L.; Nickel, W.; Casco, M.; Senkovska, I.; Bon, V.; Wallacher, D.; Grimm, N.; Krause, S.; Silvestre-Albero, J. *Phys. Chem. Chem. Phys.* **2016,** *18,* 20607–20614. doi:10.1039/C6CP03993F

16. Oschatz, M.; Hoffmann, H. C.; Pallmann, J.; Schaber, J.; Borchardt, L.; Nickel, W.; Senkovska, I.; Rico-Francés, S.; Silvestre-Albero, J.; Kaskel, S.; Brunner, E. *Chem. Mater.* **2014,** *26,* 3280–3288. doi:10.1021/cm501102y

17. Oschatz, M.; Borchardt, L.; Hippauf, F.; Nickel, W.; Kaskel, S.; Brunner, E. *Annu. Rep. NMR Spectrosc.* **2016,** *87,* 237–318. doi:10.1016/bs.arnmr.2015.08.003

18. Péan, C.; Merlet, C.; Rotenberg, B.; Madden, P. A.; Taberna, P.-L.; Daffos, B.; Salanne, M.; Simon, P. *ACS Nano* **2014,** *8,* 1576–1583. doi:10.1021/nn4058243

19. Oschatz, M.; Kockrick, E.; Rose, M.; Borchardt, L.; Klein, N.; Senkovska, I.; Freudenberg, T.; Korenblit, Y.; Yushin, G.; Kaskel, S. *Carbon* **2010,** *48,* 3987–3992. doi:10.1016/j.carbon.2010.06.058

20. Fuertes, A. B.; Pico, F.; Rojo, J. M. *J. Power Sources* **2004,** *133,* 329–336. doi:10.1016/j.jpowsour.2004.02.013

21. Wang, D.-W.; Li, F.; Liu, M.; Lu, G. Q.; Cheng, H.-M. *Angew. Chem., Int. Ed.* **2007,** *47,* 373–376. doi:10.1002/anie.200702721

22. Meng, Y.; Gu, D.; Zhang, F.; Shi, Y.; Yang, H.; Li, Z.; Yu, C.; Tu, B.; Zhao, D. *Angew. Chem., Int. Ed.* **2005,** *44,* 7053–7059. doi:10.1002/anie.200501561

23. Ryoo, R.; Joo, S. H.; Jun, S. *J. Phys. Chem. B* **1999,** *103,* 7743–7746. doi:10.1021/jp991673a

24. Wang, Y.; Wang, F.; Chen, Y.; Li, B.; Zhang, C.; Cui, L.; Kang, S.; Li, X. *Int. J. Electrochem. Sci.* **2013,** *8,* 7868–7874.

25. Oschatz, M.; Thieme, S.; Borchardt, L.; Lohe, M. R.; Biemelt, T.; Brückner, J.; Althues, H.; Kaskel, S. *Chem. Commun.* **2013,** *49,* 5832–5834. doi:10.1039/c3cc42841a

26. Fechler, N.; Fellinger, T.-P.; Antonietti, M. *Adv. Mater.* **2013,** *25,* 75–79. doi:10.1002/adma.201203422

27. Yang, C.-M.; Weidenthaler, C.; Spliethoff, B.; Mayanna, M.; Schüth, F. *Chem. Mater.* **2005,** *10,* 355–358. doi:10.1021/cm049164v

28. Zhu, H.; Liu, Z.; Wang, Y.; Kong, D.; Yuan, X.; Xie, Z. *Chem. Mater.* **2008,** *20,* 1134–1139. doi:10.1021/cm071385o

29. Chuenchom, L.; Kraehnert, R.; Smarsly, B. M. *Soft Matter* **2012,** *8,* 10801–10812. doi:10.1039/c2sm07448f

30. Sakintuna, B.; Yürüm, Y. *Ind. Eng. Chem. Res.* **2005,** *44,* 2893–2902. doi:10.1021/ie049080w

31. Gawande, M. B.; Bonifácio, V. D. B.; Luque, R.; Branco, P. S.; Varma, R. S. *ChemSusChem* **2014,** *7,* 24–44. doi:10.1002/cssc.201300485

32. Tojo, T.; Zhang, Q.; Saito, F. *J. Solid State Chem.* **2006,** *179,* 433–437. doi:10.1016/j.jssc.2005.11.002

33. Stolle, A.; Szuppa, T.; Leonhardt, S. E. S.; Ondruschka, B. *Chem. Soc. Rev.* **2011,** *40,* 2317–2329. doi:10.1039/c0cs00195c

34. James, S. L.; Adams, C. J.; Bolm, C.; Braga, D.; Collier, P.; Friščić, T.; Grepioni, F.; Harris, K. D. M.; Hyett, G.; Jones, W.; Krebs, A.; Mack, J.; Maini, L.; Orpen, A. G.; Parkin, I. P.; Shearouse, W. C.; Steed, J. W.; Waddell, D. C. *Chem. Soc. Rev.* **2012,** *41,* 413–447. doi:10.1039/C1CS15171A

35. Jörres, M.; Aceña, J. L.; Soloshonok, V. A.; Bolm, C. *ChemCatChem* **2015,** *7,* 1265–1269. doi:10.1002/cctc.201500102

36. Wang, Y.-F.; Chen, R.-X.; Wang, K.; Zhang, B.-B.; Li, Z.-B.; Xu, D.-Q. *Green Chem.* **2012,** *14,* 893–895. doi:10.1039/c2gc16521j

37. Grätz, S.; Borchardt, L. *RSC Adv.* **2016,** *6,* 64799–64802. doi:10.1039/C6RA15677K

38. Schneidermann, C.; Jäckel, N.; Oswald, S.; Giebeler, L.; Presser, V.; Borchardt, L. *ChemSusChem* **2017,** *10,* 2416–2424. doi:10.1002/cssc.201700459

39. Wang, G.-W.; Komatsu, K.; Murata, Y.; Shiro, M. *Nature* **1997,** *387,* 583–586. doi:10.1038/42439

40. Kabbani, M. A.; Tiwary, C. S.; Autreto, P. A. S.; Brunetto, G.; Som, A.; Krishnadas, K. R.; Ozden, S.; Hackenberg, K. P.; Gong, Y.; Galvao, D. S.; Vajtai, R.; Kabbani, A. T.; Pradeep, T.; Ajayan, P. M. *Nat. Commun.* **2015,** *6,* No. 7291. doi:10.1038/ncomms8291

41. Kunitake, M.; Uemura, S.; Ito, O.; Fujiwara, K.; Murata, Y.; Komatsu, K. *Angew. Chem., Int. Ed.* **2002,** *41,* 969–972. doi:10.1002/1521-3773(20020315)41:6<969::AID-ANIE969>3.0.CO;2-I

42. Troschke, E.; Grätz, S.; Lübken, T.; Borchardt, L. *Angew. Chem., Int. Ed.* **2017,** *56,* 6859–6863. doi:10.1002/anie.201702303

43. Grätz, S.; Wolfrum, B.; Borchardt, L. *Green Chem.* **2017,** in press. doi:10.1039/C7GC00693D

44. Ribeiro, P. C.; de Melo da Costa, A. C. F.; Kiminami, R. H. G. A.; Sasaki, J. M.; Lira, H. L. *Mater. Res. (Sao Carlos, Braz.)* **2013,** *16,* 468–472. doi:10.1590/S1516-14392012005000176

45. Pechini, M. P. Method of Preparing Lead and Alkaline Earth Titanates and Niobates and Coating Method Using the Same To Form a Capacitor. U.S. Patent US3330697 A, July 11, 1967.

46. Strubel, P.; Althues, H.; Kaskel, S. *Carbon* **2016,** *107,* 705–710. doi:10.1016/j.carbon.2016.06.075

47. Sevilla, M.; Fuertes, A. B. *ACS Nano* **2014,** *8,* 5069–5078. doi:10.1021/nn501124h

48. Ferrero, G. A.; Sevilla, M.; Fuertes, A. B. *Carbon* **2015,** *88,* 239–251. doi:10.1016/j.carbon.2015.03.014

49. Tao, X.; Chen, X.; Xia, Y.; Huang, H.; Gan, Y.; Wu, R.; Chen, F.; Zhang, W. *J. Mater. Chem. A* **2013,** *1,* 3295–3303. doi:10.1039/c2ta01213h

50. Vasconcelos, D. C. L.; Costa, V. C.; Nunes, E. H. M.; Sabioni, A. C. S.; Gasparon, M.; Vasconcelos, W. L. *Mater. Sci. Appl.* **2011,** *2,* 1375–1382. doi:10.4236/msa.2011.210186

51. Hočevar, M.; Berginc, M.; Topič, M.; Krašovec, U. O. *J. Sol-Gel Sci. Technol.* **2010,** *53,* 647–654. doi:10.1007/s10971-009-2144-6

52. Oschatz, M.; Boukhalfa, S.; Nickel, W.; Lee, J. T.; Klosz, S.; Borchardt, L.; Eychmüller, A.; Yushin, G.; Kaskel, S. *J. Mater. Chem. A* **2014,** *2,* 5131–5139. doi:10.1039/c3ta14815g

53. Nelles, J. Preparation of Titanium Alcoholates and Phenolates. U.S. Patent US2187821 A, Jan 23, 1940.

54. Hernández, J. G.; Friščić, T. *Tetrahedron Lett.* **2015,** *56,* 4253–4265. doi:10.1016/j.tetlet.2015.03.135

55. Kim, K.; Choi, M.; Ryoo, R. *Carbon* **2013,** *60,* 175–185. doi:10.1016/j.carbon.2013.04.011

56. Frackowiak, E. *Phys. Chem. Chem. Phys.* **2007,** *9,* 1774–1785. doi:10.1039/b618139m

57. Fuertes, A. B.; Lota, G.; Centeno, T. A.; Frackowiak, E. *Electrochim. Acta* **2005,** *50,* 2799–2805. doi:10.1016/j.electacta.2004.11.027

58. Weingarth, D.; Foelske-Schmitz, A.; Wokaun, A.; Kötz, R. *Electrochem. Commun.* **2012,** *18,* 116–118. doi:10.1016/j.elecom.2012.02.040

59. Ruch, P. W.; Cericola, D.; Hahn, M.; Kötz, R.; Wokaun, A. *J. Electroanal. Chem.* **2009,** *636,* 128–131. doi:10.1016/j.jelechem.2009.09.007

Mechanochemical borylation of aryldiazonium salts; merging light and ball milling

José G. Hernández

Abstract

Merging of photo- and mechanochemical activation permitted studying the role of eosin Y in the borylation of aryldiazonium salts in a ball mill. Simultaneous neat grinding/irradiation of the reactants and the photocatalyst led to the formation of boronates in a molten state. On the other hand, the catalyst-free liquid-assisted grinding/irradiation reaction also led to product formation, featuring a direct photolysis pathway facilitated by substrate–solvent charge-transfer complex formation.

Introduction

The use of mechanical force to process materials or to induce chemical transformations is perhaps as old as the history of mankind itself [1]. Similarly, from time immemorial light has also been present on earth, being perhaps photosynthesis and visions the most fundamental connections between light and living organisms [2]. However, combining synergistically photo- and mechanical activations in organic synthesis is still challenging despite the enormous potential of having both activation modes acting simultaneously.

In recent years, mechanochemistry, which encompasses the use of mechanical means by milling, grinding, shearing, cavitation or pulling to induce chemical transformations [3] has become fundamental for discovering new chemical reactivity [4,5] and

to develop more sustainable syntheses. Typically, mechanochemical reactions by milling are conducted in non-translucent containers (e.g., agate, ceramics, steels, and tungsten carbide). While this diversity of milling media materials enables controlling, for example, the energy input during the mechanical process, it becomes an obstacle for in situ characterization of mechanochemical reactions, or to facilitate synergistic activation types involving, for example, light and mechanical energy. Recently, however, the in situ study of mechanochemical transformations has been accomplished by combining translucent milling vessels made of poly(methyl methacrylate) (PMMA) with powder X-ray diffraction (PXRD) [6,7], Raman spectroscopy [8], or a combination of both techniques [9]. On the other hand, attempts to combine photo- and mechanical activation to

favor chemical processes have been mainly explored in the photodimerizations of olefins by manual grinding of the reactants followed by long UV-light exposure [10], or by vortex grinding [11]. However, until now, studies of photocatalyzed mechanochemical reactions involving, for example, metal complexes [12] or organic photocatalysts (PC) [13] has been underexplored [14], despite photocatalysis could clearly benefit from the excellent mixing under neat or liquid-assisted grinding (LAG) [15] conditions. Additionally, in contrast to solution-based methods, reactions by milling do not suffer from solubility restrictions due to the possibility to bring reactants and catalysts of very different solubility, into close proximity for achieving chemical reactivity. This last aspect is foreseen as highly valuable in transformations using low-soluble PCs (e.g., porphyrins) [16] or during the photochemical synthesis or modification of polymers [17].
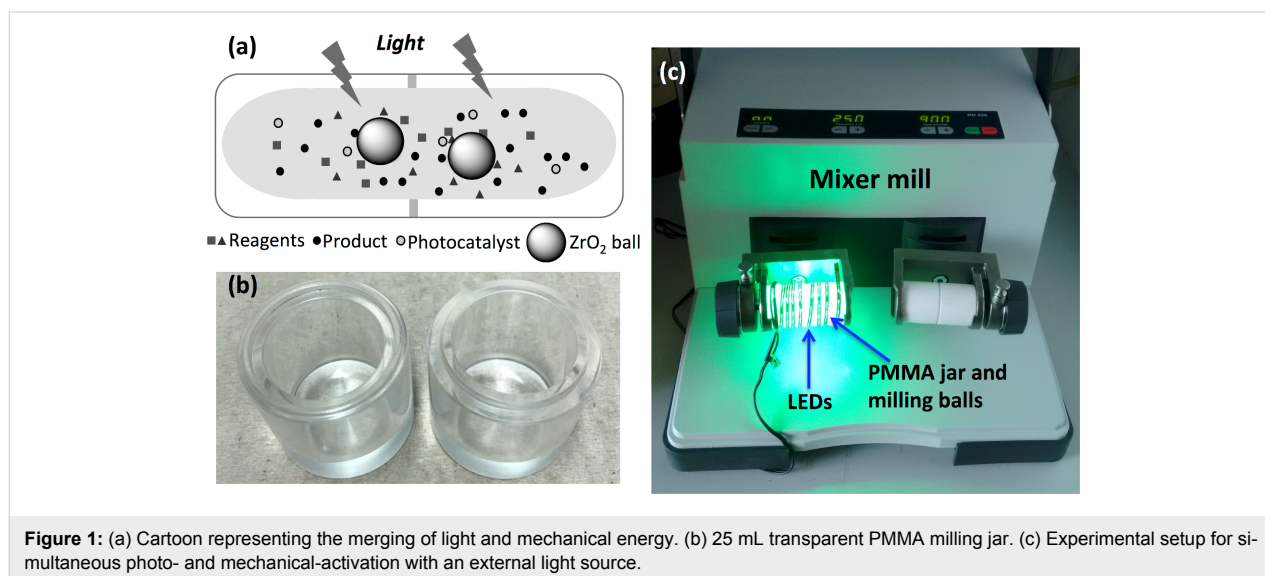
The aforementioned context makes one wonder about the potential for conducting chemical reactions under simultaneous photo- and mechanical activation. To test this idea, the photocatalyzed borylation of aryldiazonium salts, first reported in solution by Yan and co-workers was selected as a model reaction [18]. In the original study, irradiation for 18 h of a MeCN solution of aryldiazonium salts, bis(pinacolato)diboron (B$_2$pin$_2$, **2**) and eosin Y with a 25 W visible light lamp led to the corresponding arylboronates in moderate to good yields [18].
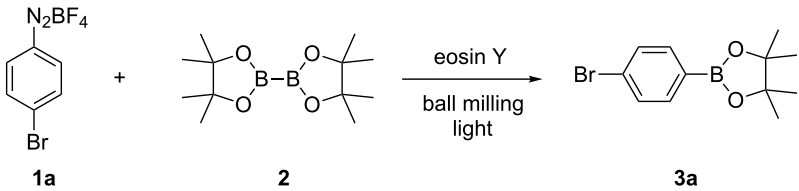
Results and Discussion

To commence, a PMMA milling jar was designed to enable external light irradiation of the reaction mixture while having simultaneously the high-speed ball milling acting on the mixture of reactants and PC (Figure 1; for details, see Supporting Information File 1).

Subsequently, with the aim to determine the role of the light, PC and the mechanical milling in the borylation of the aryldiazonium salts, and especially to exclude a potential background borylation reaction triggered by either thermal, mechanical or light-induced heterolytic cleavage of aryldiazonium salts, various control reactions were conducted. First, an equimolar mixture of the diazonium salt **1a** and B$_2$pin$_2$ (**2**) was milled for 2 h at 25 Hz in a mixer mill, using a Teflon milling jar and ZrO$_2$ ball bearings. The safe use of diazonium salt under ball milling conditions has been previously reported in the literature [19]. The analysis of the reaction mixture by ^{1}H NMR spectroscopy revealed just the presence of both reactants, both in the presence or absence of the organic photocatalyst eosin Y (5.0 mol %). Ruling out a sole mechanochemical activation pathway (Table 1, entries 1 and 2).

Repeating the reaction in the presence of the PC in the transparent PPMA milling jar yielded the same negative result proving that ambient light did not mediate the photoredox catalytic borylation reaction under mechanochemical conditions (Table 1, entry 3). Furthermore, neat grinding of a catalyst-free mixture of **1a** and **2** under blue LEDs (light-emitting diodes) light did not afford the borylated product **3a**. In addition to the ^{1}H NMR analysis in solution, this result was confirmed by immediate ex situ analysis using IR spectroscopy of the solid reaction mixture, which revealed only the presence of both starting materials. Thereby, excluding a direct thermal [20,21] or photolysis pathway operating under solventless conditions (Table 1, entry 4). Then, a premilled mixture of **1a**, B$_2$pin$_2$, and eosin Y was subjected to irradiation with blue LEDs for 2 h in the absence of milling (Table 1, entry 5). After the irradiation was halted, the reaction mixture was immediately analyzed by ^{1}H NMR spectroscopy. This time trace quantities of product **3a**

Figure 1: (a) Cartoon representing the merging of light and mechanical energy. (b) 25 mL transparent PMMA milling jar. (c) Experimental setup for simultaneous photo- and mechanical-activation with an external light source.

Table 1: Screening of the reaction conditions.[a]

Entry	Eosin Y (mol %)	Time (h)	Light	**1a**:**3a** (%)[b]
1[c]	–	2	–	100:0
2[c]	(5)	2	–	100:0
3	(5)	2	ambient	100:0
4	–	2	blue LEDs	100:0
5[d]	(5)	2	blue LEDs	94:6
6	(5)	0.5	blue LEDs	83:17
7	(5)	1	blue LEDs	54:46
8	(5)	1.5	blue LEDs	27:73
9	(5)	2	blue LEDs	15:85
10[e]	(5)	2	blue LEDs	59:41
11[f]	(5)	2	blue LEDs	51:49
12	**(5)**	**1**	**green LEDs**	**6:94**
13	(0.5)	1.5	green LEDs	63:37

[a]Reaction conditions: a mixture of **1a** (0.369 mmol), **2** (0.369 mmol) and eosin Y was mixed in a 25 mL PMMA milling jar with 15 ZrO$_2$ balls of 5 mm in diameter at 25 Hz. [b]Determined by ^{1}H NMR spectroscopy. [c]A 25 mL Teflon milling jar was used. [d]**1a**, **2** and the PC were mixed for 30 s in the PMMA jar, then the mixing was stopped and the milling jar was exposed to the light irradiation for 2 h. [e]The irradiation was stopped after 1 h of reaction. [f]The milling was stopped after 1 h of reaction.

were detected (Table 1, entry 5). This interesting result under solvent-free conditions encouraged performing the light irradiation accompanied by milling to improve mixing and to increase the surface exposure of the reaction mixture. In a following set of experiments, milling of the reactants and PC was carried out for a time in the range of 15 min to 2 h. The analysis of the composition of the reaction mixture showed significant formation of the product after 30 min of milling/irradiation (Table 1, entry 6). Monitoring the progress of a mixture of the reactants and PC in CD$_3$CN at room temperature by ^{1}H NMR spectroscopy over a period of time of 20 h showed a composition (98:2; **1a**:**3a**), ruling out the formation of the **3a** during the standard analysis time. Furthermore, the presence of **3a** in the mixture coincided with the observation of an initial molten state of the mixture inside the milling jar [22]. This more homogeneous mixture could have increased the mobility of the reactants favoring the SET process. Reaching the molten state clearly required having both activation modes acting simultaneously, since only milling of **1a** (mp 138–141 °C), **2** (mp 139–140 °C) and eosin Y (mp 305–307 °C), or just irradiation of the mixture did not lead to an observable melting of the solids (Table 1, entries 2–4 and 5). Besides, propagation of this molten state could have been favored by the gradual rise in concentration of the lower-melting product **3a** (mp 69–70 °C) in the mixture.

Indeed, milling the product **3a** under the standard milling conditions using the LEDs led to its melt. Similarly, milling a mixture of **1a**, **2** and **3a** for 1 h under light irradiation reached a eutectic melt phase. The need for simultaneous light and mechanical milling was also confirmed after conducting experiments for 2 h where either the milling or the irradiation was stopped after the first hour. In both cases the outcome of the reaction gave similar results compared to having both energy sources acting together for 1 h (Table 1, entries 7, 10, and 11).

Next, further tuning of the reaction conditions revealed green LEDs to be a more efficient light source for the reaction with eosin Y (for details, see Table S1 in Supporting Information File 1). This change permitted the transformation to take place after 1 h of milling/irradiation. Under these conditions, the ratio **1a**:**3a** in the reaction mixture reached 6:94 (entry 12 in Table 1). Alternatively, longer reaction times allowed reducing the amount of the organic photocatalyst to 1.0 mol % and 0.5 mol % (entry 13 in Table 1; for more details, see Table S1 in Supporting Information File 1). Then, using the green LEDs an experiment in the presence of 1,1-diphenylethene (**4**) as a radical inhibitor was conducted. After the standard 1 h of milling, the formation of **3a** was slowed down and the analysis of the reaction mixture by gas chromatography–mass spectrom-

etry showed the presence of the phenyl radical trapping adduct **5** (Scheme 1).

With the optimized reaction conditions in hand, we explored the photomechanochemical borylation of the halogenated aryldiazonium salts **1a–d** (Table 2).

Analogously to the case of **1a**, the fluoro and chloro substituted aryldiazonium salts **1b** and **1c** did react affording the boronates **3b** and **3c** (Table 2, entries 1 and 2). It was noticed, however, that the milling/irradiation time required for these substrates to react varied in comparison with the reaction of **1a**. Furthermore, attempts to react the 4-iodobenzenediazonium tetrafluoroborate
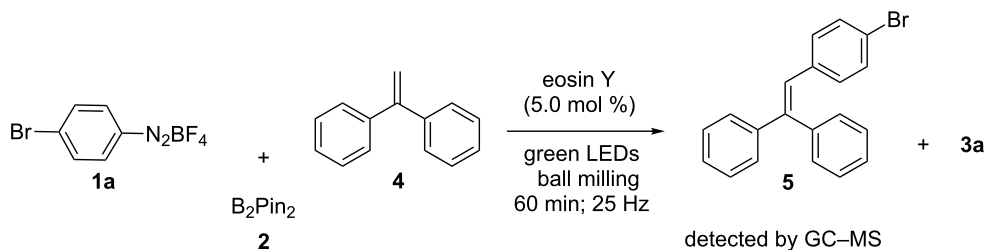
Scheme 1: Borylation of **1a** in the presence of 1,1-diphenylethene (**4**).

Table 2: Borylation of aryl diazonium salts **1** with **2**.[a]

Entry	Aryldiazonium salt	Product	Time (min)	Yield (%)[b]
1	**1b**	**3b**	90	60
2	**1c**	**3c**	45	55
3	**1a**	**3a**	60	68
4	**1d**	**3d**	120	41
5	**1e**	**3e**	120	49

[a]Reaction conditions: a mixture of **1** (0.369 mmol), **2** (140.6 mg; 0.554 mmol) and photocatalyst (5 mol %) was mixed in a 25 mL PMMA milling jar with 15 ZrO$_2$ balls of 5 mm in diameter at 25 Hz. [b]After column chromatography.

(**1d**) with **2** were made with low success even after 2 h of reaction time (Table 2, entry 4). As indicated above, the development of a molten state upon irradiation and milling appears to be a key prerequisite for the photomechanochemical borylation to occur [14,22]. Reaching that molten state in the reaction with the iodo derivative **1d** proved challenging, only a part of the reaction mixture seemed homogeneous. Differential scanning calorimetry (DSC) analysis of the aryldiazonium salts **1a–d** revealed that **1a–c** melt followed by decomposition of the samples. However, the DSC profile of the iodobenzenediazonium salt **1d** showed a direct thermal decomposition upon heating. NMR analysis of the molten **1d** revealed the presence of 1-fluoro-4-iodobenzene (for details, see Supporting Information File 1). Therefore, the difference in melting point temperatures of the substrates and their thermal stability could have a direct correlation with the observed reactivity in the ball mill (Table 2). Control experiments by stirring/heating **1a–d** and **2** in an oil bath until the melting of the mixture was reached, showed predominantly thermal decomposition of the aryldiazonium salts **1a–d** into the 1-halo-4-fluorobenzene derivatives [23] and only in some cases trace quantities of **3a–d** were detected. Meaning that the external light contributes to both, heating the reaction mixture to its eutectic and it also initiated the photoredox process. Similarly, a photocatalyzed reaction between **2** and 4-nitrobenzenediazonium tetrafluoroborate (**1e**), a salt found also to undergo decomposition at 423 K, turned out difficult (for the DSC traces of **1a–e** see Supporting Information File 1).

After 2 h of milling/irradiation the corresponding product **3e** was obtained in moderate yield. In general, after the milling/irradiation experiments no aryldiazonium salt was observed in the reaction mixture, however, the moderate yields for the products **3a–e**, even in the presence of 1.5 equiv of **2**, could have been the result of background reactions undergone by **1a–e** under the reaction conditions, especially due to the rise in temperature observed upon light irradiation.

As mentioned above, LAG, an alternative to the standard neat grinding, has become an useful parameter in mechanochemistry to control chemical selectivity and product composition by having catalytic volumes of organic solvent during the milling [24]. Here, a change in the milling approach from neat to LAG was anticipated to have the potential for switching the activation mode from a SET process to a direct heterolytic photolysis. Jacobi von Wangelin et al. noticed that the borylation product **3a** could also occurred in the absence of eosin Y, upon irradiation of a MeCN solution of the reactants with white LEDs [23,25]. Pleasingly, LAG (MeCN or DMSO η = 0.25) of **1a** and **2** under blue LEDs, and in the absence of eosin Y did also generate the product **3a**. In contrast, LAG experiments using *n*-heptane failed at producing **3a** (Scheme 2; for details, see Table S2 in Supporting Information File 1).

Similarly, control LAG/irradiation experiments conducted in a Teflon milling jar, only formed trace quantities of the product **3a**, ruling out a sole thermal activation of the system by the light source. These results not only illustrates the versatility of mechanochemistry to control the chemical reaction pathway operating in the process, but also sheds light on the role of the photocatalyst in the borylation of the aryldiazonium salts.

Under non-catalyzed LAG/irradiation conditions, charge-transfer complexes between **1a** and appropriate organic solvents could be responsible for the fast generation of the aryl cations in the ball mill, leading to the direct formation of **3a** [26,27]. This observation is in agreement with the findings by Jacobi von Wangelin et al., who described that upon irradiation of a solution of **1a** in MeCN direct heterolytic cleavage of the aryldiazonium salt occurred [23,25]. However, the formation of **3a** under solvent-free milling conditions (vide supra) could have been indeed the result of a photoredox transformation where the organic photocatalyst eosin Y played a key role in triggering the SET process.

Conclusion

In summary, simultaneous activation of an organic system by light and ball milling techniques has been successfully accomplished for the first time. The utilization of translucent milling vessels permitted the study of the photoborylation of aryldiazonium salts in the presence and in the absence of the organic photocatalyst eosin Y. The results of this proof-of-concept demonstration revealed that under neat grinding conditions the PC does play a role in initiating a SET borylation. Furthermore, the implementation of a LAG/irradiation approach allowed the borylation reaction to occur under catalyst-free conditions. This

LAG	(%)[a]
n-C$_7$H$_{16}$	–
CH$_3$CN	39
DMSO	82 (65)[b]
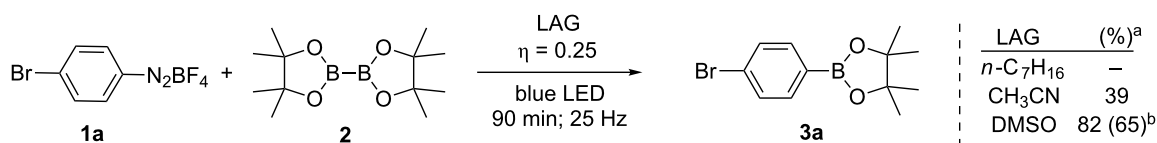
Scheme 2: Light-mediated LAG borylation of **1a**. [a]Determined by ^{1}H NMR spectroscopy using internal standard. [b]After column chromatography.

observation is supported by the tendency of the electrophilic aryldiazonium salts to undergo direct heterolytic photolysis facilitated by organic solvents, upon exposure to near-UV or blue light. In addition to this, the contribution from the increase in temperature experienced during the light exposure and mechanical milling was observed to be vital for the neat grinding, facilitating the formation of molten reaction mixtures.

Despite the still existing technical challenges for merging light and mechanical energy, the positive cooperative synergism between light and mechanical activation reported here, will certainly stimulate the design of more innovative experimental setups [28] and, more important, the exploration of new photomechanochemical organic reactions, where solubility constrains caused by working with low-soluble photocatalysts, substrates or products can be bypassed by mechanochemical means.

Supporting Information

Supporting Information File 1

Experimental procedures, experimental set-ups and characterization data, NMR spectra, and DSC traces.
[http://www.beilstein-journals.org/bjoc/content/supplementary/1860-5397-13-144-S1.pdf]

Acknowledgements

References

1. Takacs, L. *Chem. Soc. Rev.* **2013,** *42,* 7649–7659. doi:10.1039/C2CS35442J
2. Valentini, A.; Rivero, D.; Zapata, F.; García-Iriepa, C.; Marazzi, M.; Palmeiro, R.; Galván, I. F.; Sampedro, D.; Olivucci, M.; Frutos, L. M. *Angew. Chem., Int. Ed.* **2017,** *56,* 3842–3846. doi:10.1002/anie.201611265
3. James, S. L.; Adams, C. J.; Bolm, C.; Braga, D.; Collier, P.; Friščić, T.; Grepioni, F.; Harris, K. D. M.; Hyett, G.; Jones, W.; Krebs, A.; Mack, J.; Maini, L.; Orpen, A. G.; Parkin, I. P.; Shearouse, W. C.; Steed, J. W.; Waddell, D. C. *Chem. Soc. Rev.* **2012,** *41,* 413–447. doi:10.1039/C1CS15171A
4. Hernández, J. G.; Bolm, C. *J. Org. Chem.* **2017,** *82,* 4007–4019. doi:10.1021/acs.joc.6b02887
5. Do, J.-L.; Friščić, T. *ACS Cent. Sci.* **2017,** *3,* 13–19. doi:10.1021/acscentsci.6b00277
6. Friščić, T.; Halasz, I.; Beldon, P. J.; Belenguer, A. M.; Adams, F.; Kimber, S. A. J.; Honkimäki, V.; Dinnebier, R. E. *Nat. Chem.* **2013,** *5,* 66–73. doi:10.1038/nchem.1505
7. Užarević, K.; Halasz, I.; Friščić, T. *J. Phys. Chem. Lett.* **2015,** *6,* 4129–4140. doi:10.1021/acs.jpclett.5b01837
8. Gracin, D.; Štrukil, V.; Friščić, T.; Halasz, I.; Užarević, K. *Angew. Chem., Int. Ed.* **2014,** *53,* 6193–6197. doi:10.1002/anie.201402334
9. Batzdorf, L.; Fischer, F.; Wilke, M.; Wenzel, K.-J.; Emmerling, F. *Angew. Chem., Int. Ed.* **2015,** *54,* 1799–1802. doi:10.1002/anie.201409834
10. Sokolov, A. N.; Bučar, D.-K.; Baltrusaitis, J.; Gu, S. X.; MacGillivray, L. R. *Angew. Chem., Int. Ed.* **2010,** *49,* 4273–4277. doi:10.1002/anie.201000874
11. Stojaković, J.; Farris, B. S.; MacGillivray, L. R. *Faraday Discuss.* **2014,** *170,* 35–40. doi:10.1039/C4FD00006D
12. Teegardin, K.; Day, J. I.; Chan, J.; Weaver, J. *Org. Process Res. Dev.* **2016,** *20,* 1156–1163. doi:10.1021/acs.oprd.6b00101
13. Hari, D. P.; König, B. *Chem. Commun.* **2014,** *50,* 6688–6699. doi:10.1039/C4CC00751D
14. Obst, M.; König, B. *Beilstein J. Org. Chem.* **2016,** *12,* 2358–2363. doi:10.3762/bjoc.12.229
15. Friščić, T.; Childs, S. L.; Rizvi, S. A. A.; Jones, W. *CrystEngComm* **2009,** *11,* 418–426. doi:10.1039/B815174A
16. Rybicka-Jasińska, K.; König, B.; Gryko, D. *Eur. J. Org. Chem.* **2017,** 2104–2107. doi:10.1002/ejoc.201601518
17. Corrigan, N.; Shanmugam, S.; Xu, J.; Boyer, C. *Chem. Soc. Rev.* **2016,** *45,* 6165–6212. doi:10.1039/C6CS00185H
18. Yu, J.; Zhang, L.; Yan, G. *Adv. Synth. Catal.* **2012,** *354,* 2625–2628. doi:10.1002/adsc.201200416
19. Mukherjee, N.; Chatterjee, T.; Ranu, B. C. *J. Org. Chem.* **2013,** *78,* 11110–11114. doi:10.1021/jo402071b
20. Kulla, H.; Wilke, M.; Fischer, F.; Rölling, M.; Maierhofer, C.; Emmerling, F. *Chem. Commun.* **2017,** *53,* 1664–1667. doi:10.1039/C6CC08950J
21. Zhu, C.; Yamane, M. *Org. Lett.* **2012,** *14,* 4560–4563. doi:10.1021/ol302024m
22. Rothenberg, G.; Downie, A. P.; Raston, C. L.; Scott, J. L. *J. Am. Chem. Soc.* **2001,** *123,* 8701–8708. doi:10.1021/ja0034388
23. Majek, M.; Jacobi von Wangelin, A. *Acc. Chem. Res.* **2016,** *49,* 2316–2327. doi:10.1021/acs.accounts.6b00293
24. Hasa, D.; Miniussi, E.; Jones, W. *Cryst. Growth Des.* **2016,** *16,* 4582–4588. doi:10.1021/acs.cgd.6b00682
25. Majek, M.; Filace, F.; Jacobi von Wangelin, A. *Beilstein J. Org. Chem.* **2014,** *10,* 981–989. doi:10.3762/bjoc.10.97
26. Hirose, Y.; Wahl, G. H., Jr.; Zollinger, H. *Helv. Chim. Acta* **1976,** *59,* 1427–1437. doi:10.1002/hlca.19760590504
27. Szele, I.; Zollinger, H. *Helv. Chim. Acta* **1978,** *61,* 1721–1729. doi:10.1002/hlca.19780610520
28. Obst, M.; Shaikh, R. S.; König, B. *React. Chem. Eng.* **2017.** doi:10.1039/C6RE00220J

Encaging palladium(0) in layered double hydroxide: A sustainable catalyst for solvent-free and ligand-free Heck reaction in a ball mill

Wei Shi, Jingbo Yu, Zhijiang Jiang, Qiaoling Shao and Weike Su[*]

Abstract

In this paper, the synthesis of a cheap, reusable and ligand-free Pd catalyst supported on MgAl layered double hydroxides (Pd/MgAl-LDHs) by co-precipitation and reduction methods is described. The catalyst was used in Heck reactions under high-speed ball milling (HSBM) conditions at room temperature. The effects of milling-ball size, milling-ball filling degree, reaction time, rotation speed and grinding auxiliary category, which would influence the yields of mechanochemical Heck reactions, were investigated in detail. The characterization results of XRD, ICP–MS and XPS suggest that Pd/MgAl-LDHs have excellent textural properties with zero-valence Pd on its layers. The reaction results indicate that the catalyst could be utilized in HSBM systems to afford a wide range of Heck coupling products in satisfactory yields. Furthermore, this catalyst could be easily recovered and reused for at least five times without significant loss of catalytic activity.

Introduction

High-speed ball milling (HSBM)-assisted transition metal-catalyzed cross-coupling reactions such as Heck, Suzuki, Sonogashira and Glaser reactions are still unusual methods for the formation of C–C bonds [1-7], but the method arouse considerable attention because of an environmentally benign and solvent-free synthesis approach as well as high efficiency and good atom economy, which is desirable in the fields of chemistry, materials science, biology, pharmaceutical, dyestuff, agriculture and so forth [8-12].

The homogeneous palladium salts along with phosphine- or nitrogen-based ligands were employed as the traditional catalyst systems not only in solution-based C–C cross coupling [13-16] reactions but also in mechanically activated Heck [4,17-22], Suzuki [23-26], and Sonogashira [5,27,28] coupling reactions. The limitations of which are obviously unstable ligands and expensive Pd catalysts. Furthermore, the contamination of the coupled products with unacceptable Pd species led to a hard separation and recycling of homogeneous catalyst systems. In

our previous study [4] we reported a ball-milling Heck reaction catalyzed by Pd(OAc)₂. Although the catalyst showed the satisfactory reactivity, it was difficult to recover. Thus, Pd catalysts anchored on heterogeneous solid support materials such as MCM-41 [29], alumina [30], silica [31], carbon nanotubes [32], microporous polymers [33], SBA-15 [34], or some dendrimers [35] were preferred to develop a ligandless and recyclable catalyst system. However, to the best of our knowledge, only a few of supported Pd catalysts were used in mechanochemically assisted coupling reactions because of the low mechanical strength of the catalysts, the active component of which is easy to leach and deactivate under HSBM conditions. Mack and co-workers [36] reported a kind of polymer supported Pd(PPh₃)₄ catalyst with high activity in a Glaser reaction (Scheme 1). They found that the catalyst could only be recycled twice without the addition of the PPh₃ ligand and the Pd component was significantly leached from polymer support after each run. Cravotto et al. [37] used an ultrasound-assisted method to prepare Pd catalysts immobilized on modified chitosan (Scheme 1). Although these catalysts were found to be effective in the Suzuki reaction after three cycles, the modification conditions of chitosan were rigorous.

As catalyst-supported material, layered double hydroxides (LDHs) have received much attention in the organic catalysis for its excellent properties such as low costs, high specific surface area, double-layered structure, anion exchange capacity, high mechanical stability and chemical stability [38-43]. Our previous studies have proved that LDH catalysts could be successfully applied in the degradation of organic pollutants [44,45]. Bai and co-worker [46] synthesized Pd/SDS–LDHs by using an ultrasonic method, which exhibited excellent activity

in Suzuki reactions. Jiang et al. [47] demonstrated that LDH-supported on alkaline materials performed higher catalytic activity in coupling reactions than that on acidic-supported materials. In the present work, co-precipitation was used for fabricating MgAl-LDHs with nitrate anions, followed by introducing disodium tetrachloropalladate (Na₂PdCl₄) into the LDH interlayer by the ion exchange method. The prepared hybrid LDHs were then reduced by hydrazine hydrate (N₂H₄·H₂O) to obtain the Pd catalyst supported on MgAl-LDHs (Pd/MgAl-LDHs). The as-prepared Pd/MgAl-LDH catalyst was further applied in representative cross-coupling Heck reactions under HSBM conditions (Scheme 1) by using a planetary ball mill (Pulverisette 7, Fritsch, Germany). The influence of milling-ball filling degree (Φ_{MB}), reaction time (t), milling-ball size (d_{MB}) and rotation speed (n), along with catalyst loading, alkaline type and grinding auxiliary category were further investigated in detail.

Results and Discussion
Characteristics of prepared materials
We initially prepared the Pd/MgAl-LDHs catalyst as described in the Experimental section (see Supporting Information File 1). Figure 1 shows the powder XRD patterns of MgAl-LDHs, MgAl-LDHs-PdCl₄²⁻ and Pd/MgAl-LDHs at 2θ = 5–80°. All samples have diffraction peaks located around 10°, 20°, 33°, 38°, 60°, indexing to (003), (006), (009), (015), (110) reflections, which indicates the highly neat degree and well-crystallinity structure of LDH materials without phase impurities apparent. Moreover, the MgAl-LDHs presents an interlayer distance of 0.82 nm from the basal spacing of d_{003}, which matches the results well for the intercalation of nitrate (NO₃⁻) into MgAl-LDHs in literature [48]. In the MgAl-LDHs-PdCl₄²⁻
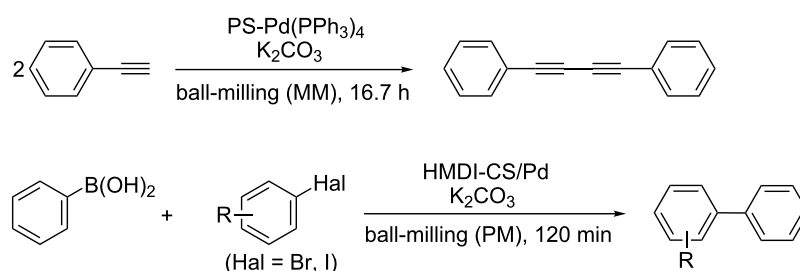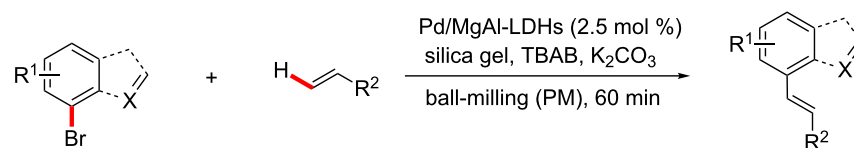

Scheme 1: Supported catalysts in cross-coupling reactions. MM represents mixer mill; PM represents planetary mill.

sample, the (003) plane shifted to the lower position of 8.8°, resulting to an expansion of interlayer spacing of 1.01 nm from 0.82 nm. These phenomena suggest that $PdCl_4^{2-}$ successfully intercalated into the MgAl-LDHs interlayers. As compared with MgAl-LDHs and MgAl-LDHs-$PdCl_4^{2-}$, the catalyst of Pd/MgAl-LDHs exhibited a lower intensity pattern except for the diffraction peaks at 38° and 44°, which was due to the random dispersion of the Pd component on the Pd/MgAl-LDHs surface. The Pd loading of catalyst was 8.5 wt %, and the molar ratio of Mg and Al in LDH layers were 2.97, which is in accordance with the ratio of 3.00 employed in the synthesis step (see Table S1 in the Supporting Information File 1). Furthermore, the binding energy of Pd $3d_{5/2}$ and Pd $3d_{3/2}$ in LDH layers approximately centered at 334.7 eV and 340.2 eV, respectively, assigning to the existence zero oxidation state of Pd bulk (around 335.0 eV and 341.0 eV [49,50]), verified that $PdCl_4^{2-}$ had been reduced to zero-valence Pd from interlayers and loaded on MgAl-LDH surface successfully (see Figure S1 in Supporting Information File 1).
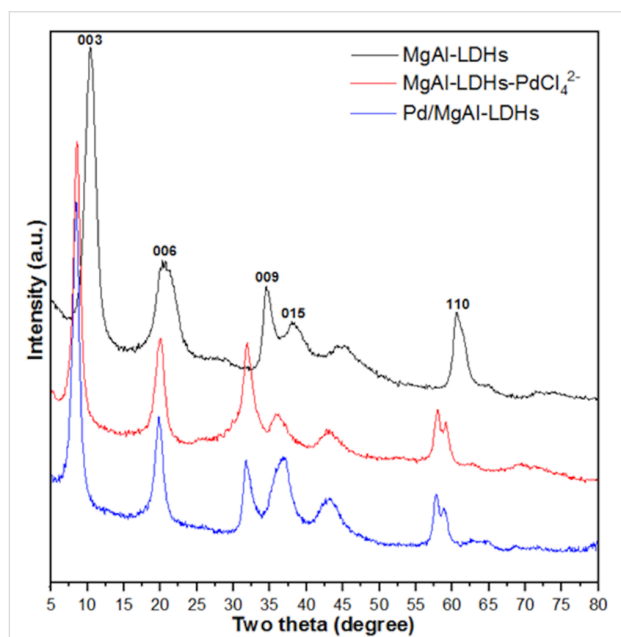
Figure 1: The XRD patterns for the samples of MgAl-LDHs, MgAl-LDHs-$PdCl_4^{2-}$ and Pd/MgAl-LDHs.

## The Heck coupling reaction under HSBM conditions

m-Bromoacetophenone (**1a**) and styrene (**2a**) were chosen as the model reactants (Scheme 2), catalyzed by Pd/MgAl-LDHs under ball-milling conditions with silica gel (5 g) and stainless-steel balls ($\Phi_{MB} = 0.2$, $d_{MB} = 14$ mm) at 800 rpm.

Based on our previous researches [4,51], it is found that the bases used have a significant influence on the yields of the reaction. Thus, several bases such as NaOH, KOH, Cs_2CO_3, K_2CO_3, *t*-BuOK, Et_3N and DBU were investigated and the results are shown in Table 1. It is notable that both inorganic and organic bases could facilitate the reaction successfully. K_2CO_3 exhibited the best yield of 72% (Table 1, entries 1–7) as compared with other bases for the reaction. In further tests, different loadings of Pd/MgAl-LDHs were employed in the model reaction (Table 1, entries 8–10) in order to optimize the usage of catalyst. The results show that the reaction yield kept unchanged when the Pd/MgAl-LDHs loading was reduced to 2.5 mol % (Table 1, entry 9).

After getting access to the optimal reactant system, we shifted our focus on the mechanochemistry parameters of mill-ball size and its filling degree. The milling-ball filling degree (Φ_{MB}) represents the volume of the milling balls relative to the beaker volume, which is calculated as the ratio of the overall milling ball volume (V_{MB}) to the total beaker volume (V_{BV}):

$$\Phi_{MB} = \frac{\sum V_{MB}}{V_{BV}}$$

This parameter is proved to be the essential factor not only on the occurrence of collision and friction, but also on the energy distribution and product yield [52]. In Figure 2, we chose four types of milling-balls with diameters of 5 mm, 8 mm, 10 mm and 14 mm in the model reaction under four kinds of filling degrees ($\Phi_{MB} = 0.15, 0.2, 0.25, 0.3$). It could be found that no matter which kind of the milling-ball diameter is, the tendency of the product yield is similar under different filling degrees. A maximum yield (84%) was obtained by using 5 mm milling balls at 0.25 filling degree. In addition, the 14 mm milling balls
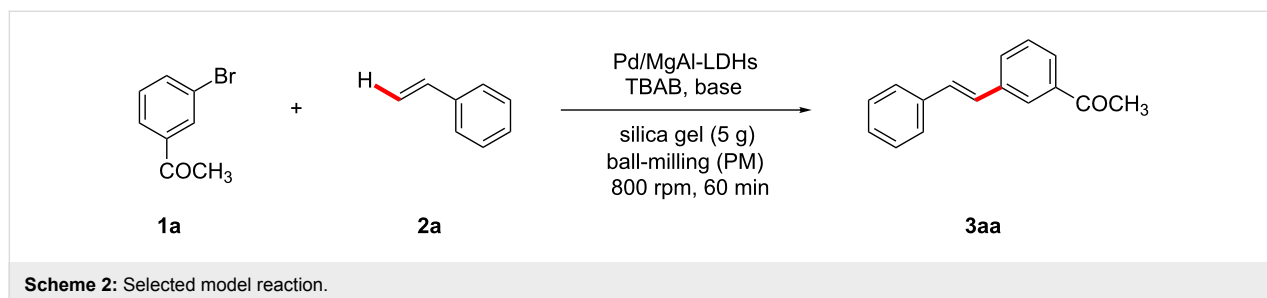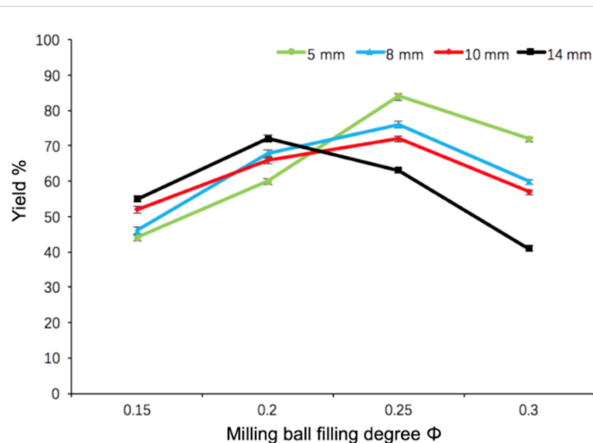

Scheme 2: Selected model reaction.

Table 1: Optimization of Heck reaction conditions.[a]

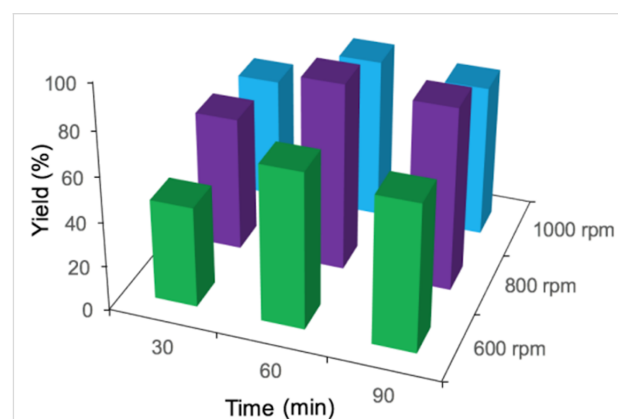| Entry	Base	Pd (mol %)	Yield (%)[b]
1	NaOH	10	56
2	KOH	10	64
3	*t*-BuOK	10	59
4	Et$_3$N	10	54
5	Cs$_2$CO$_3$	10	60
6	K$_2$CO$_3$	10	72
7	DBU	10	43
8	K$_2$CO$_3$	5	71
9	K$_2$CO$_3$	2.5	71
10	K$_2$CO$_3$	1.25	54

[a]Reaction conditions unless otherwise noted: **1a** (1.5 mmol), **2a** (2.1 mmol), Pd/MgAl-LDHs, TBAB (1.5 mmol), base (3.6 mmol), and 5 g silica gel were placed in a 80 mL stainless-steel vessel (Φ_{MB} = 0.2, d_{MB} = 14 mm). HSBM conditions: 60 min at 800 rpm. [b]Isolated yield.

Because the ball-milling time and the rotation speed have a strong influence on the energy input, which directly regulates the product structure and yield during the mechanochemical process, the combined effect of ball-milling time and rotation speed was investigated systematically. The results are summarized in Figure 3. It can be seen that with increasing rotation speed, the yield of **3aa** increased first, but decreased at the highest speed of 1000 rpm. This is mainly due to the overabundant energy input resulting in side products. Furthermore, prolonging the reaction time over 60 min did not help improving the product yield, the reactants had all been consumed after 60 min. Therefore, 800 rpm together with 60 min is regarded as the optimum condition for the maximum yield.

Figure 2: Examination of the milling-ball filling degree (Φ_{MB}) and milling-ball sizes on the yield of **3aa**. Reaction conditions: **1a** (1.5 mmol), **2a** (2.1 mmol), Pd/MgAl-LDHs (2.5 mol %), TBAB (1.5 mmol), K$_2$CO$_3$ (3.6 mmol), 5 g silica gel were placed in a 80 mL stainless-steel vessel. HSBM conditions: 60 min at 800 rpm.

Figure 3: Examination of ball-milling time and rotation speed on the yield of **3aa**. Reaction conditions: **1a** (1.5 mmol), **2a** (2.1 mmol), Pd/ MgAl-LDHs (2.5 mol %), TBAB (1.5 mmol), K$_2$CO$_3$ (3.6 mmol), and 5 g silica gel were placed in a 80 mL stainless-steel vessel (Φ_{MB} = 0.25, d_{MB} = 5 mm). HSBM conditions: 60 min at 800 rpm.

exhibited the higher yields than 5 mm, 8 mm and 10 mm milling balls under the low filling degrees (Φ_{MB} = 0.15, 0.2). And then, with the filling degree increased to the value of 0.25, the movement space for 14 mm milling balls was hindered in the ball-milling jar, resulting in the apparent decrease in the yield of **3aa**. On the contrary, 5 mm, 8 mm and 10 mm milling balls had sufficient collision to produce enough energy under the filling degree of 0.25, leading to the high yields. Furthermore, the sharp decrease in the yield could be also observed in 5 mm, 8 mm and 10 mm milling-ball systems with a filling degree over 0.25, which might be due to the overfull ball-milling jar and the overabundant energy input. These results mentioned above are consistent with the previous studies reported by us [53] and the others [52,54].

In the ball-milling process, the grinding auxiliary is found to be an efficient transfer medium between energy and reactant [1,2,55,56]. Additional investigations on the effects of the grinding auxiliaries were carried out. The results shown in Table 2 indicate that 5 g silica gel is considered as the most effective choice for the reaction (Table 2, entry 1), but MgAl-LDHs gave also a good result (Table 2, entry 5). With NaCl, α-Al$_2$O$_3$ and γ-Al$_2$O$_3$, the yields were unsatisfactory (Table 2, entries 2–4). Increasing or decreasing the amount of silica gel would led to a reduction of the yield of **3aa** (Table 2, entries 6 and 7), which might be due to the uneven distribution of the reactants.

After having the optimum reaction conditions in hand, the Pd/ MgAl-LDH catalyst was evaluated to expand the generality and substrate scope in Heck reactions, the results are presented in Figure 4 and Scheme 3. As we expected, both with electron-withdrawing and electron-donating groups substituted bromobenzenes (**1a–l**) and styrenes (**2a–e**) react with each other

Table 2: Examination of grinding auxiliaries on yield of **3aa**.[a]

Entry	Grinding auxiliary	Weight (g)	Yield (%)
1	silica-gel	5	84 (n.r.)[b]
2	NaCl	5	54
3	α-Al$_2$O$_3$ (base)	5	68
4	γ-Al$_2$O$_3$(neutral)	5	61
5	MgAl-LDHs	5	72 (n.r.)[c]
6	silica-gel	3	74
7	silica-gel	7	70

[a]Reaction conditions unless otherwise noted: **1a** (1.5 mmol), **2a** (2.1 mmol), Pd/MgAl-LDHs (2.5 mol %), TBAB (1.5 mmol), K$_2$CO$_3$ (3.6 mmol), grinding auxiliary were placed in a 80 mL stainless-steel vessel (Φ_{MB} = 0.25, d_{MB} = 5 mm). HSBM conditions: 60 min at 800 rpm. [b]Silica gel used as grinding auxiliary without Pd/MgAl-LDHs catalyst. [c]MgAl-LDHs used as grinding auxiliary without Pd/MgAl-LDHs catalyst.
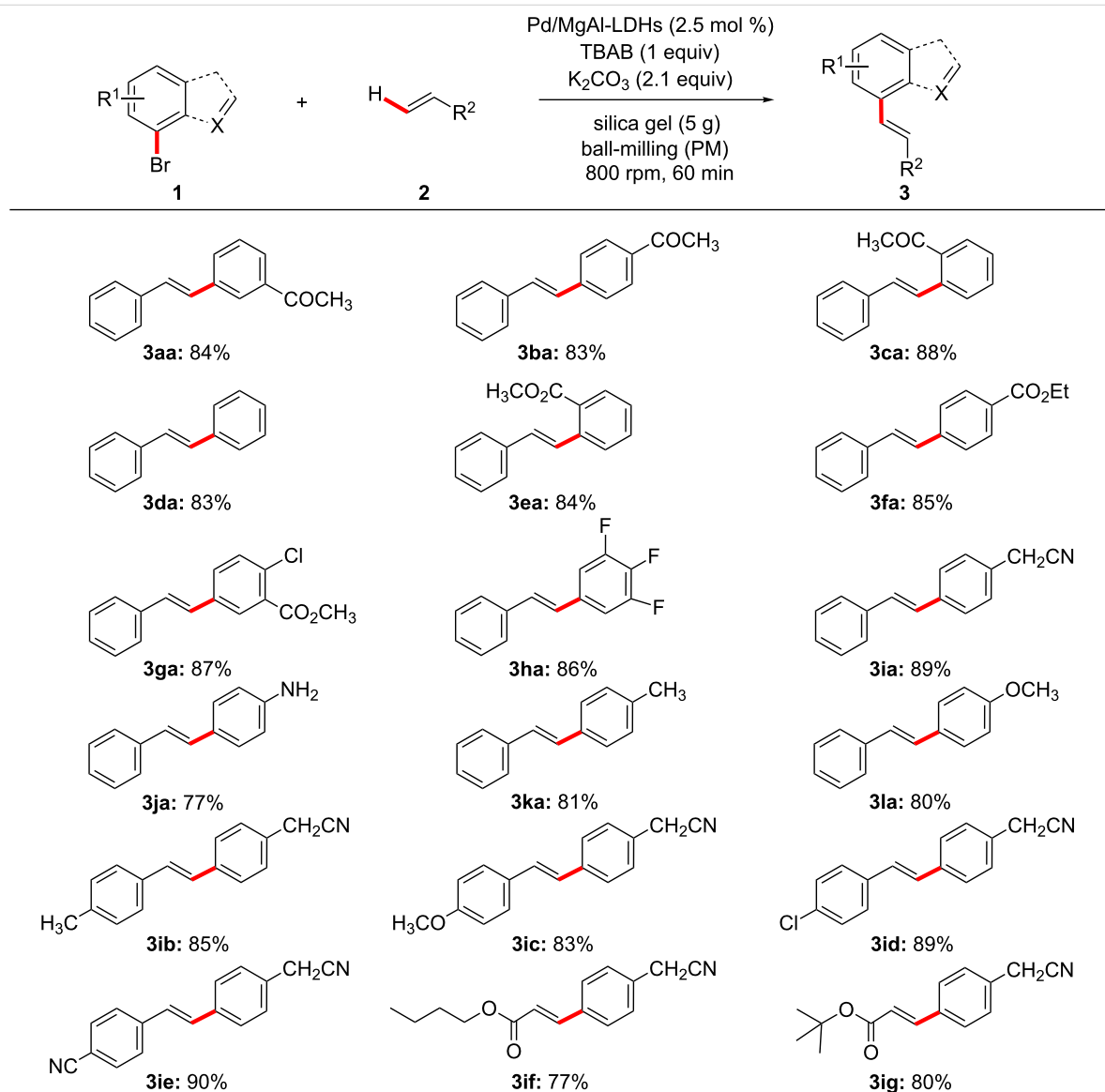

Figure 4: Substrate scope of Pd/MgAl-LDHs catalyzed Heck reactions. Reaction conditions unless otherwise noted: **1a** (1.5 mmol), **2a** (2.1 mmol), Pd/MgAl-LDHs (2.5 mol %), TBAB (1.5 mmol), K$_2$CO$_3$ (3.6 mmol), and 5 g silica gel were placed in a 80 mL stainless-steel vessel (Φ_{MB} = 0.25, d_{MB} = 5 mm). HSBM conditions: 60 min at 800 rpm.

Scheme 3: Pd/MgAl-LDHs catalyzed Heck reactions of heteroaryl bromides. Reaction conditions unless otherwise noted: **1a** (1.5 mmol), **2a** (2.1 mmol), Pd/MgAl-LDHs (2.5 mol %), TBAB (1.5 mmol), K_2CO_3 (3.6 mmol), and 5 g silica gel were placed in a 80 mL stainless-steel vessel (Φ_{MB} = 0.25, d_{MB} = 5 mm). HSBM conditions: 60 min at 800 rpm.
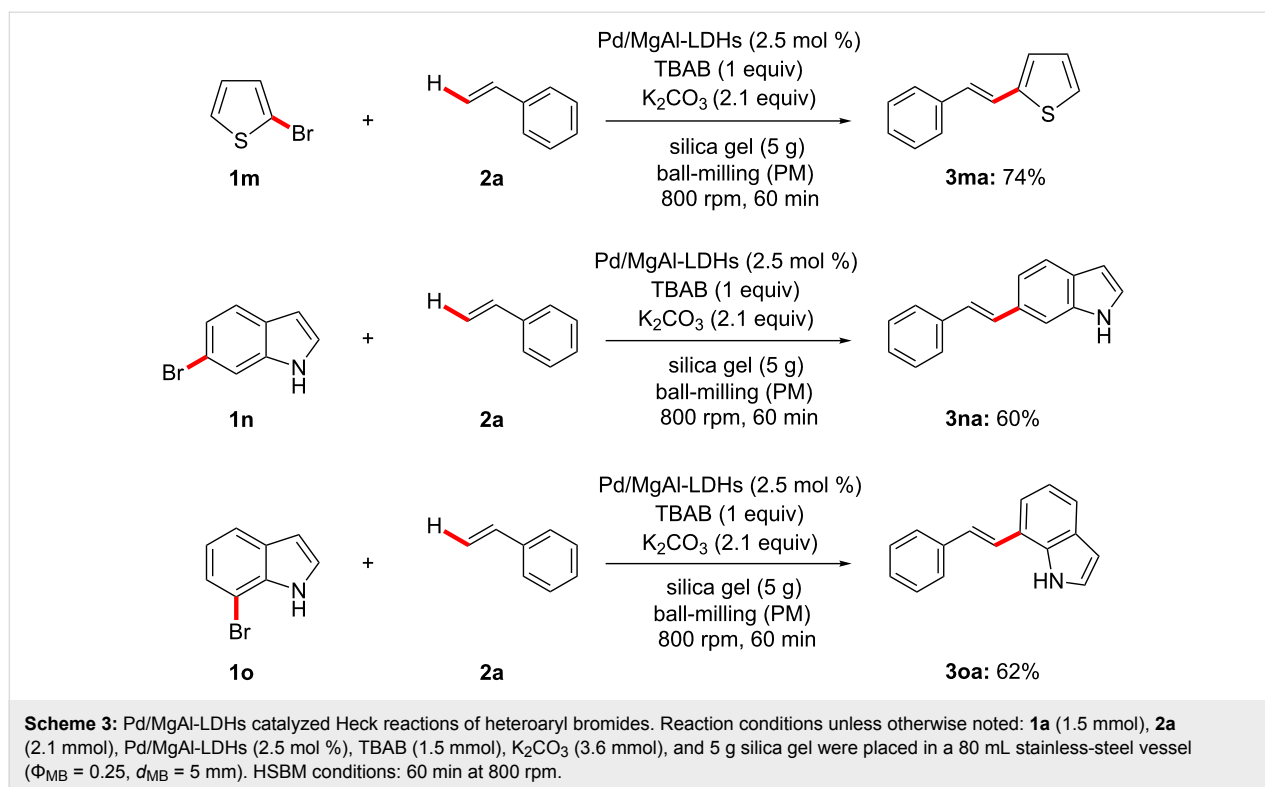
successfully to afford the coupling products in satisfactory yields. The electron-deficient bromobenzenes (**1a–c**, **1e–i**) or styrenes (**2d**, **2e**) show slightly higher yields than the electron-rich substrates. The ketone group at *ortho-*, *meta-* and *para-*positions (**1a–c**) were chosen to examine the steric hindrance for this reaction. To our surprise, the position of the ketone group had a little effect on the yields and the larger sterically hindered substrate **1c** led to a higher yield as compared with **1a** and **1b**, which is contrary to Li's study [57] in solution-based Heck reactions. This might be because of the lone pairs of the oxygen atom in the keto group at the *ortho-*position could coordinate with Pd/MgAl-LDHs under HSBM conditions and promote the reaction efficiently. Furthermore, the couplings of heteroaryl bromides (**1m–o**) and styrene (**2a**) as well as substituted bromobenzene (**1i**) and butyl acrylate (**2f**, **2g**) were investigated to extend the scope and generality of the reaction. The results clearly demonstrate that all the substrates are well tolerated to give the corresponding coupling products smoothly with yields of 60–80%.

Finally, the coupling reactions of aryl bromide **1i** and styrene (**2a**) as well as heterocyclic bromide **1m** and styrene (**2a**) were chosen as the model reactions under the optimized conditions to investigate the reusability of the Pd/MgAl-LDH catalyst. The catalyst together with the grinding auxiliary are recovered by a simple rinse after each run, which is more convenient compared to other methods [36,37]. As can be seen in Figure 5,

regardless of the substrate type, the catalyst system could be reused at least five times efficiently without significant loss in catalytic activity, resulting in almost no change in the yields. Hence, the reusability of Pd/MgAl-LDHs is one of the major advantages for Heck reactions under HSBM conditions.
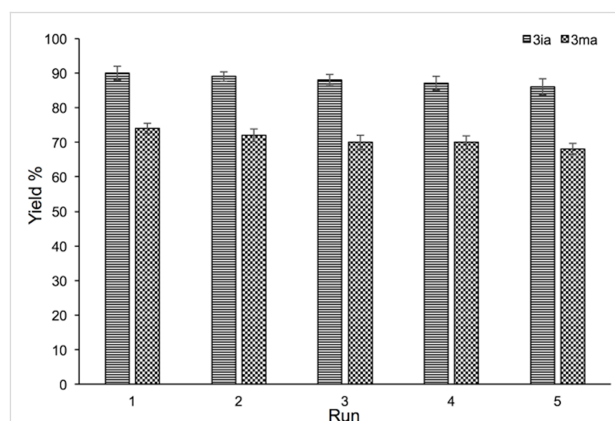
Figure 5: Recycling studies of the Pd/MgAl-LDH catalyst for Heck reactions. Reaction conditions: **1i** or **1m** (1.5 mmol), **2a** (2.1 mmol), Pd/MgAl-LDHs (2.5 mol %), TBAB (1.5 mmol), K_2CO_3 (3.6 mmol), and silica gel 5 g were placed in a 80 mL stainless-steel vessel (Φ_{MB} = 0.25, d_{MB} = 5 mm). HSBM conditions: 60 min at 800 rpm.

Conclusion

In summary, a supported and recyclable Pd catalyst (Pd/MgAl-LDHs) was designed and synthesized by co-precipi-

tation and reduction methods. The catlyst was further applied to Heck reactions under HSBM conditions. The results indicate that the Pd is successfully dispersed on the surface of Pd/MgAl-LDHs, and a small quantity of Pd/MgAl-LDHs (2.5 mol % of Pd) shows the remarkable activity in Heck reactions with a wide range of aryl bromides and olefins under mild conditions. In these cases, toxic solvents, expensive ligands and inert atmosphere were efficiently avoided. Furthermore, the Pd/MgAl-LDH catalyst can be recycled for at least five times without significant loss in coupling product yields.

Supporting Information

Supporting Information File 1

Details of experimental procedures and characterization data of prepared compounds, ^{1}H, ^{13}C NMR, and MS spectra of all coupling compounds.
[http://www.beilstein-journals.org/bjoc/content/supplementary/1860-5397-13-160-S1.pdf]

Acknowledgement

References

1. Stolle, A.; Szuppa, T.; Leonhardt, S. E. S.; Ondruschka, B. *Chem. Soc. Rev.* **2011,** *40,* 2317–2329. doi:10.1039/c0cs00195c
2. Hermann, G. N.; Becker, P.; Bolm, C. *Angew. Chem., Int. Ed.* **2015,** *54,* 7414–7417. doi:10.1002/anie.201502536
3. Jiang, Z.-J.; Li, Z.-H.; Yu, J.-B.; Su, W.-K. *J. Org. Chem.* **2016,** *81,* 10049–10055. doi:10.1021/acs.joc.6b01938
4. Zhu, X.; Liu, J.; Chen, T.; Su, W. *Appl. Organomet. Chem.* **2012,** *26,* 145–147. doi:10.1002/aoc.2827
5. Thorwirth, R.; Stolle, A.; Ondruschka, B. *Green Chem.* **2010,** *12,* 985–991. doi:10.1039/c000674b
6. Bernhardt, F.; Trotzki, R.; Szuppa, T.; Stolle, A.; Ondruschka, B. *Beilstein J. Org. Chem.* **2010,** *6,* No. 7. doi:10.3762/bjoc.6.7
7. Hernández, J. G.; Bolm, C. *J. Org. Chem.* **2017,** *82,* 4007–4019. doi:10.1021/acs.joc.6b02887
8. Wang, G.-W. *Chem. Soc. Rev.* **2013,** *42,* 7668–7700. doi:10.1039/c3cs35526h
9. Hernández, J. G.; Friščić, T. *Tetrahedron Lett.* **2015,** *56,* 4253–4265. doi:10.1016/j.tetlet.2015.03.135
10. Lou, S.-J.; Mao, Y.-J.; Xu, D.-Q.; He, J.-Q.; Chen, Q.; Xu, Z.-Y. *ACS Catal.* **2016,** *6,* 3890–3894. doi:10.1021/acscatal.6b00861
11. Li, L.; Wang, J.-J.; Wang, G.-W. *J. Org. Chem.* **2016,** *81,* 5433–5439. doi:10.1021/acs.joc.6b00786
12. Do, J.-L.; Friščić, T. *ACS Cent. Sci.* **2017,** *3,* 13–19. doi:10.1021/acscentsci.6b00277
13. Phan, N. T. S.; Van Der Sluys, M.; Jones, C. W. *Adv. Synth. Catal.* **2006,** *348,* 609–679. doi:10.1002/adsc.200505473
14. Amatore, C.; Jutand, A. *Acc. Chem. Res.* **2000,** *33,* 314–321. doi:10.1021/ar980063a
15. Littke, A. F.; Dai, C.; Fu, G. C. *J. Am. Chem. Soc.* **2000,** *122,* 4020–4028. doi:10.1021/ja0002058
16. Chinchilla, R.; Nájera, C. *Chem. Soc. Rev.* **2011,** *40,* 5084–5121. doi:10.1039/c1cs15071e
17. Tullberg, E.; Peters, D.; Frejd, T. *J. Organomet. Chem.* **2004,** *689,* 3778–3781. doi:10.1016/j.jorganchem.2004.06.045
18. Tullberg, E.; Schacher, F.; Peters, D.; Frejd, T. *Synthesis* **2006,** 1183–1189. doi:10.1055/s-2006-926371
19. Alonso, F.; Beletskaya, I. P.; Yus, M. *Tetrahedron* **2005,** *61,* 11771–11835. doi:10.1016/j.tet.2005.08.054
20. Declerck, V.; Colacino, E.; Bantreil, X.; Martinez, J.; Lamaty, F. *Chem. Commun.* **2012,** *48,* 11778–11780. doi:10.1039/c2cc36286d
21. Chen, X.; Engle, K. M.; Wang, D.-H.; Yu, J.-Q. *Angew. Chem., Int. Ed.* **2009,** *48,* 5094–5115. doi:10.1002/anie.200806273
22. Kantchev, E. A. B.; O'Brien, C. J.; Organ, M. G. *Angew. Chem., Int. Ed.* **2007,** *46,* 2768–2813. doi:10.1002/anie.200601663
23. Schneider, F.; Szuppa, T.; Stolle, A.; Ondruschka, B.; Hopf, H. *Green Chem.* **2009,** *11,* 1894–1899. doi:10.1039/b915744c
24. Schneider, F.; Ondruschka, B. *ChemSusChem* **2008,** *1,* 622–625. doi:10.1002/cssc.200800086
25. Schneider, F.; Stolle, A.; Ondruschka, B.; Hopf, H. *Org. Process Res. Dev.* **2009,** *13,* 44–48. doi:10.1021/op800148y
26. Lai, Y.; Zong, Z.; Tang, Y.; Mo, W.; Sun, N.; Hu, B.; Shen, Z.; Jin, L.; Sun, W.-h.; Hu, X. *Beilstein J. Org. Chem.* **2017,** *13,* 213–221. doi:10.3762/bjoc.13.24
27. Fulmer, D. A.; Shearouse, W. C.; Medonza, S. T.; Mack, J. *Green Chem.* **2009,** *11,* 1821–1825. doi:10.1039/b915669k
28. Stolle, A.; Ondruschka, B. *Pure Appl. Chem.* **2011,** *83,* 1343–1349. doi:10.1351/PAC-CON-10-09-26
29. Noori, N.; Nikoorazm, M.; Ghorbani-Choghamarani, A. *J. Porous Mater.* **2016,** *23,* 1467–1481. doi:10.1007/s10934-016-0207-y
30. Gniewek, A. *J. Organomet. Chem.* **2016,** *823,* 90–96. doi:10.1016/j.jorganchem.2016.09.018
31. Ghasemi, S.; Farjadian, F.; Tamami, B. *Appl. Organomet. Chem.* **2016,** *30,* 818–822. doi:10.1002/aoc.3508
32. Hajighorbani, M.; Hekmati, M. *RSC Adv.* **2016,** *6,* 88916–88924. doi:10.1039/C6RA19934H
33. Wang, C.-A.; Li, Y.-W.; Hou, X.-M.; Han, Y.-F.; Nie, K.; Zhang, J.-P. *ChemistrySelect* **2016,** *1,* 1371–1376. doi:10.1002/slct.201600174
34. Satapathy, A.; Gadge, S. T.; Kusumawati, E. N.; Harada, K.; Sasaki, T.; Nishio-Hamane, D.; Bhanage, B. M. *Catal. Lett.* **2015,** *145,* 824–833. doi:10.1007/s10562-015-1489-4
35. Lu, F.; Astruc, D. *Eur. J. Inorg. Chem.* **2015,** 5595–5600. doi:10.1002/ejic.201501103
36. Chen, L.; Lemma, B. E.; Rich, J. S.; Mack, J. *Green Chem.* **2014,** *16,* 1101–1103. doi:10.1039/C3GC41847B
37. Cravotto, G.; Garella, D.; Tagliapietra, S.; Stolle, A.; Schüßler, S.; Leonhardt, S. E. S.; Ondruschka, B. *New J. Chem.* **2012,** *36,* 1304–1307. doi:10.1039/c2nj40064b
38. Alexandre, M.; Dubois, P. *Mater. Sci. Eng., R* **2000,** *28,* 1–63. doi:10.1016/S0927-796X(00)00012-7
39. Parlett, C. M. A.; Wilson, K.; Lee, A. F. *Chem. Soc. Rev.* **2013,** *42,* 3876–3893. doi:10.1039/C2CS35378D
40. Fan, G.; Li, F.; Evans, D. G.; Duan, X. *Chem. Soc. Rev.* **2014,** *43,* 7040–7066. doi:10.1039/C4CS00160E
41. Li, C.; Wei, M.; Evans, D. G.; Duan, X. *Catal. Today* **2015,** *247,* 163–169. doi:10.1016/j.cattod.2014.05.032

42. Gómez-Avilés, A.; Aranda, P.; Ruiz-Hitzky, E. *Appl. Clay Sci.* **2016,** *130,* 83–92. doi:10.1016/j.clay.2015.12.011

43. Takehira, K. *Appl. Clay Sci.* **2017,** *136,* 112–141. doi:10.1016/j.clay.2016.11.012

44. Xia, S.-J.; Liu, F.-X.; Ni, Z.-M.; Shi, W.; Xue, J.-L.; Qian, P.-P. *Appl. Catal., B* **2014,** *144,* 570–579. doi:10.1016/j.apcatb.2013.07.060

45. Xia, S.-j.; Zhou, X.-b.; Shi, W.; Pan, G.-x.; Ni, Z.-m. *J. Mol. Catal. A: Chem.* **2014,** *392,* 270–277. doi:10.1016/j.molcata.2014.05.028

46. Li, J. Z.; Bai, X. F. *J. Mater. Sci.* **2016,** *51,* 9108–9122. doi:10.1007/s10853-016-0164-5

47. Zhou, H.; Zhuo, G. L.; Jiang, X. Z. *J. Mol. Catal. A: Chem.* **2006,** *248,* 26–31. doi:10.1016/j.molcata.2005.12.007

48. Li, J.; Cui, H.; Song, X.; Zhang, G.; Wang, X.; Song, Q.; Wei, N.; Tian, J. *RSC Adv.* **2016,** *6,* 92402–92410. doi:10.1039/C6RA18783H

49. Cao, Y.; Ran, R.; Wu, X.; Zhao, B.; Wan, J.; Weng, D. *Appl. Catal., A* **2013,** *457,* 52–61. doi:10.1016/j.apcata.2013.03.002

50. Hosseini-Sarvari, M.; Razmi, Z.; Doroodmand, M. M. *Appl. Catal., A* **2014,** *475,* 477–486. doi:10.1016/j.apcata.2014.02.002

51. Zhu, X.; Zhang, Q.; Su, W. *RSC Adv.* **2014,** *4,* 22775–22778. doi:10.1039/c4ra02952f

52. Schmidt, R.; Burmeister, C. F.; Baláž, M.; Kwade, A.; Stolle, A. *Org. Process Res. Dev.* **2015,** *19,* 427–436. doi:10.1021/op5003787

53. Yu, J.-B.; Peng, G.; Jiang, Z.-J.; Hong, Z.-K.; Su, W.-K. *Eur. J. Org. Chem.* **2016,** 5340–5344. doi:10.1002/ejoc.201600987

54. Stolle, A.; Schmidt, R.; Jacob, K. *Faraday Discuss.* **2014,** *170,* 267–286. doi:10.1039/C3FD00144J

55. Hernández, J. G.; Turberg, M.; Schiffers, I.; Bolm, C. *Chem. – Eur. J.* **2016,** *22,* 14513–14517. doi:10.1002/chem.201603057

56. Zou, Y.; Chen, C.; Chen, X.; Zhang, X.; Rao, W. *Eur. J. Org. Chem.* **2017,** 2266–2271. doi:10.1002/ejoc.201700088

57. Jiang, Z.-j.; Wang, W.; Zhou, R.; Zhang, L.; Fu, H.-y.; Zheng, X.-l.; Chen, H.; Li, R.-x. *Catal. Commun.* **2014,** *57,* 14–18. doi:10.1016/j.catcom.2014.07.031

License and Terms

Theoretical simulation of the infrared signature of mechanically stressed polymer solids

Matthew S. Sammon, Milan Ončák[*] and Martin K. Beyer[*]

Abstract

Mechanical stress leads to deformation of strands in polymer solids, including elongation of covalent bonds and widening of bond angles, which changes the infrared spectrum. Here, the infrared spectrum of solid polymer samples exposed to mechanical stress is simulated by density functional theory calculations. Mechanical stress is described with the external force explicitly included (EFEI) method. The uneven distribution of the external stress on individual polymer strands is accounted for by a convolution of simulated spectra with a realistic force distribution. *N*-Propylpropanamide and propyl propanoate are chosen as model molecules for polyamide and polyester, respectively. The effect of a specific force on the polymer backbone is a redshift of vibrational modes involving the C–N and C–O bonds in the backbone, while the free C–O stretching mode perpendicular to the backbone is largely unaffected. The convolution with a realistic force distribution shows that the dominant effect on the strongest infrared bands is not a shift of the peak position, but rather peak broadening and a characteristic change in the relative intensities of the strongest bands, which may serve for the identification and quantification of mechanical stress in polymer solids.

Introduction

Mechanical stress on polymer solids leads to conformational changes, bond elongation and widening of bond angles on the molecular level [1-4]. If the local force on an individual polymer strand reaches values in the range of nN, rupture of covalent bonds becomes possible, leading to irreversible changes and the destruction of the molecule [5-8]. In addition, new minima on the potential energy surface (PES) might become available through relaxation due to the applied force [9]. Covalent bond rupture plays an important role in stress-induced aging of polymeric materials [1,10]. On the other hand, elegant routes have been established to harness this effect for the design of self-healing and stress-responsive materials [11-15]. The influence of an external force on the molecular structure of a polymer can be followed by recording infrared spectra

[16-29]. External force modifies the force constants of vibrational modes [30]. Since structural deformation changes the charge distribution in the molecule, the transition dipole moment and thus the infrared intensity is influenced as well [30], resulting in the observed force-dependent shift of the infrared bands and changes in the intensity.

Computational chemistry has proven to be an indispensable tool in the analysis of mechanochemical phenomena of organic molecules, polymers and mechanophores [5,6,31-74]. A variety of theoretical approaches have been developed to model external force using methods of quantum chemistry [9,75,76], including constrained geometries simulate external force (COGEF) [4], external force is explicitly included (EFEI) [61,77] and force modified potential energy surface (FMPES) [45]. Within the EFEI method, force is applied along the direction defined by two atoms in the molecule, which modifies the potential energy surface, closely resembling FMPES. With EFEI, standard quantum chemical tasks like geometry optimization, reaction path following [54,56,68] and frequency calculations can be performed with minor modifications of standard packages. UV–vis, Raman and IR spectra of small model molecules exposed to mechanical stress have been calculated in this way [30,78,79]. Calculated vibrational frequencies have been employed in the theoretical modeling of force-dependent silyl ester hydrolysis rates [33]. The judgement of energy distribution (JEDI) tool developed by Stauch and Dreuw relies on the Hessian matrix in redundant internal coordinates under the influence of an external mechanical force [75,80].
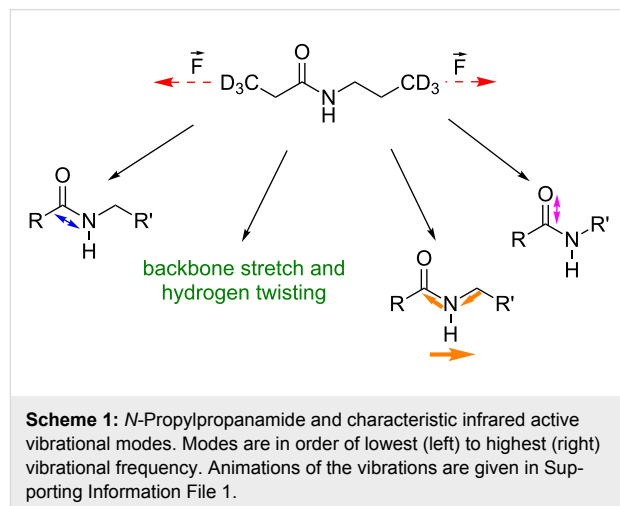
So far, most studies on infrared spectroscopy of stressed polymers focused on polypropylene [30]. Lacking a pronounced infrared chromophore, however, the spectrum is relatively complicated, especially since a large number of C–H stretching, bending and wagging modes are more or less strongly coupled [30]. In the present study, we therefore focus on molecules with strong infrared chromophores, such as C–N and C–O groups. In particular, we choose *N*-propylpropanamide and propyl propanoate as model molecules for polyamide and polyester, respectively. To facilitate a comparison with future experimental studies, we convolute simulated infrared spectra with the exponential force distribution recently derived by Adhikari and Makarov for elastomeric polymer networks [81].

Results and Discussion
Amide
We investigate force-induced changes on an *N*-propylpropanamide molecule. By applying an external force to the terminal C-atoms of *N*-propylpropanamide, Scheme 1, the calculated distance between them increases from 7.43 to 8.33 Å when the force is increased from 0 nN to 4 nN in steps of

0.1 nN. Due to the vector property of the applied force, the change of the vibrational modes with increasing force depends on the orientation of the normal mode displacement of each atom relative to the force vector.

Scheme 1: *N*-Propylpropanamide and characteristic infrared active vibrational modes. Modes are in order of lowest (left) to highest (right) vibrational frequency. Animations of the vibrations are given in Supporting Information File 1.

To illustrate the molecular origin of the changes in the calculated infrared spectrum due to force, the four characteristic vibrational modes illustrated in Scheme 1 were chosen. Figure 1 shows their vibrational frequency as a function of force. The C–N stretching mode in the backbone, in which the carbon atom from the amide bond is involved, shows a significant redshift when external force is applied, shifting from 1212 cm^{-1} at 0 nN to 1080 cm^{-1} at 4 nN. This is explained by the elongation of the molecule, which weakens the bond and reduces the force constant. Since the influence of the external force is most pronounced in the backbone, the C–N stretching mode shows the strongest shift among the four characteristic vibrational modes. A weak backbone stretch coupled with twisting of the CH$_2$ groups occurs between 1251 cm^{-1} and 1230 cm^{-1} and will be discussed exemplarily for the force influence on weaker C–H vibrations. It changes monotonically over the entire force range and experiences a moderate shift of −21 cm^{-1}, compared to −132 cm^{-1} for the C–N stretching vibration. With increasing external force the coupling with neighboring CH$_2$ groups decreases significantly (see animations in Supporting Information File 1). A second C–N stretching mode in the backbone, which is accompanied by an N–H wagging mode, again exhibits a strong negative force dependence, with the frequency shifting from 1549 to 1447 cm^{-1}. The dominant motion of the free C–O stretching mode at 1793–1800 cm^{-1} is perpendicular to the external force, which explains the absence of a significant shift.

As shown before, vibrational modes involving the backbone exhibit a strong force dependence [30]. What is surprising, how-
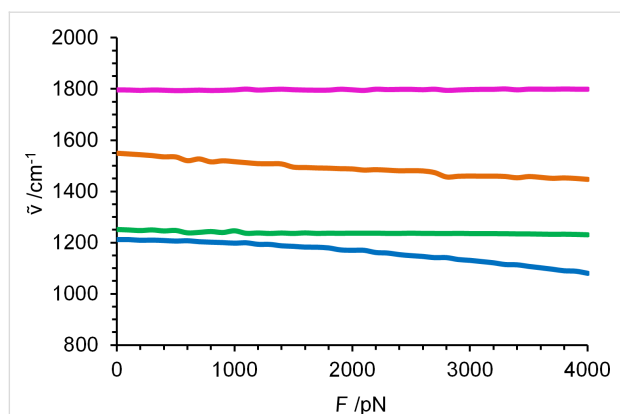
Figure 1: Force dependence of the modes shown in Scheme 1 in the fingerprint region from 800 to 2000 cm^{-1}. C–N stretch of the amide bond (blue); backbone stretch combined with C–H$_2$ twisting (green); N–H wagging (orange); free C–O stretch (purple).
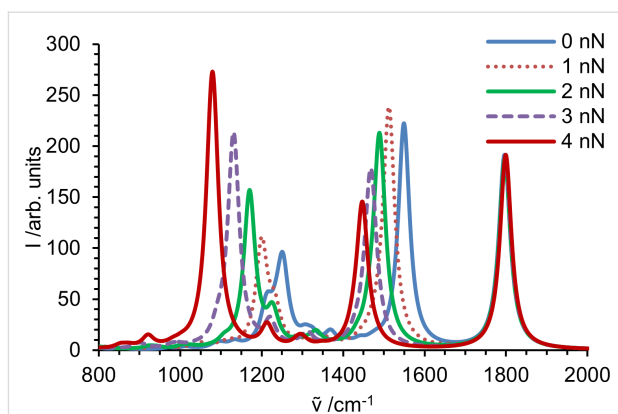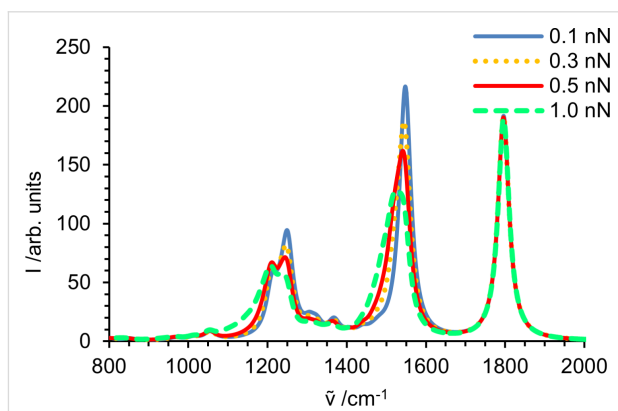

Figure 2: Intensities in fingerprint region of the infrared spectrum obtained for *N*-propylpropanamide. Spectral lines are broadened with a Lorentzian (34 cm^{-1} at FWHM) and summed up, yielding the spectrum of a stretched molecule.

ever, is the almost complete insensitivity of the free C–O stretch. One might expect that the deformation of the amide bond in the backbone changes the electron distribution, and that the weakening of the C–N bond in the backbone is compensated by a strengthening of the free C–O bond. This is obviously not the case as the bond seems to be completely unaffected by the external force, which is in line with a negligible change of the C–O bond length, from 1.22 to 1.21 Å.

The calculated spectra in the fingerprint area are given in Figure 2. Since the modes show different force dependences, spectral overlap and coupling of different modes can significantly influence the peak intensities. This leads to the significant change of the overall shape of the spectrum. While an external force does not influence the C–O stretching vibration, IR bands mainly attributed to modes including backbone vibrations show a considerable change in intensities. The intensity of the C–N stretching vibration in the range of 1000–1220 cm^{-1} continuously increases with increasing force due to a stronger dipole moment change resulting from interatomic bond elongation in the backbone.

However, the spectra of molecules exposed to a specific force, shown in Figure 2, cannot be compared with experimental data. In a polymer solid, the individual polymer strands experience a broad distribution of forces. Adhikari and Makarov have recently shown for elastomeric polymer networks that an exponential distribution is an excellent approximation [81]. It is straightforward to calculate spectra as a convolution of the spectra at specific forces with the exponential force distribution. The result of this convolution is displayed in Figure 3 for mean forces of 0.1 to 1 nN. Since the most probable force is close to zero, the peak position does not change dramatically. The bands originating from strongly red shifting modes are only slightly

red shifted, but significantly broadened. Moreover, the broadening leads to a significantly decreased peak height of the band around 1550 cm^{-1}. The band around 1250 cm^{-1} is composed of several vibrational modes, and their different force dependence leads to seemingly erratic changes in peak shape. Interestingly, the change in the peak shape with increasing force resembles the experimentally observed difference between bulk and surface spectra reported by Vettegren and co-workers [27].

Figure 3: Fingerprint region of a simulated spectrum of an *N*-propylpropanamide solid sample at 0.1, 0.3, 0.5 and 1.0 nN mean force per polymer strand.

Since the peak of the C–O stretching vibration does not change with force, the relative intensity of the two strong bands around 1550 cm^{-1} and 1800 cm^{-1} may actually serve as a direct measurement of the mechanical stress experienced locally in a polymer solid.
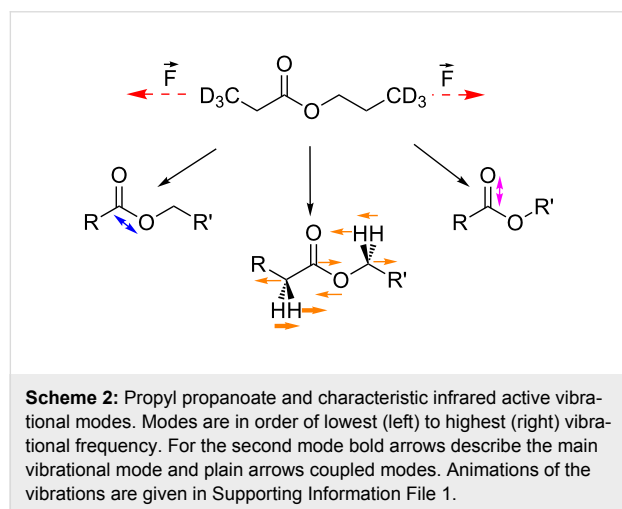
Ester

Another technically relevant polymer is polyester, for which propyl pronanoate was chosen as model molecule. According to

our EFEI geometry optimizations, the distance between terminal C-atoms in propyl propanoate increases from 7.42 to 8.19 Å when an external force of 4 nN is applied. This elongation of 0.77 Å is significantly smaller than for the previously discussed *N*-propylpropanamide with 0.90 Å.
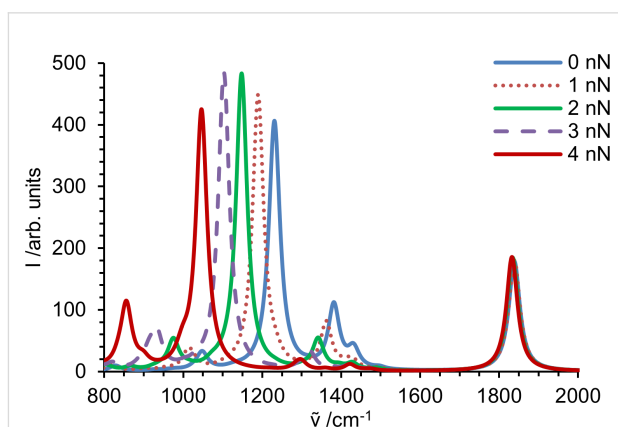
For propyl propanoate, the three representative vibrational modes shown in Scheme 2 were selected in the fingerprint region and followed over the calculated force range of 0–4 nN, Figure 4. The C–O backbone-stretching mode exhibits the strongest negative force dependence, shifting from 1231 to 1046 cm^{-1}, due to its strong alignment with the external force vector. If no force is applied, a CH$_2$ wagging mode next to the ester group, combined with a stretching vibration in the backbone (orange) is present at 1381 cm^{-1}. Upon increasing the external force to 4 nN, it shifts to 1298 cm^{-1}. Again, the vibrational modes involving motion of atoms along the backbone experience a strong redshift. The C–O stretching vibration (pink) perpendicular to the applied force occurs at slightly higher wavenumbers than for the amide bond, in the range of 1830–1846 cm^{-1}. It is basically independent of the force applied to the molecule.

Figure 4: Force dependence of the modes shown in Scheme 2 in the fingerprint region from 800 to 2000 cm^{-1}. C–O backbone stretch of the ester bond (blue); backbone stretch combined with C–H$_2$ wagging (orange); free C-O stretch (purple).

Scheme 2: Propyl propanoate and characteristic infrared active vibrational modes. Modes are in order of lowest (left) to highest (right) vibrational frequency. For the second mode bold arrows describe the main vibrational mode and plain arrows coupled modes. Animations of the vibrations are given in Supporting Information File 1.

Simulated spectra in the fingerprint region of individual molecules exposed to a specific force are presented in Figure 5. As discussed above for *N*-propylpropanamide, the intensity of the stretching vibration of the C–O double bond of propyl propanoate is not affected by external force applied at the terminal C-atoms. Modes containing vibrations along the backbone, however, experience significant changes in intensity. The wagging mode of hydrogen adjacent to the ester bond decreases in intensity and almost vanishes at 4 nN. For the C–O-stretching mode in the backbone the intensity first increases similar to the C–N vibration in the amide, reaches a maximum around 2.2 nN and then decreases again. Peaks propagating from 1047 cm^{-1} at
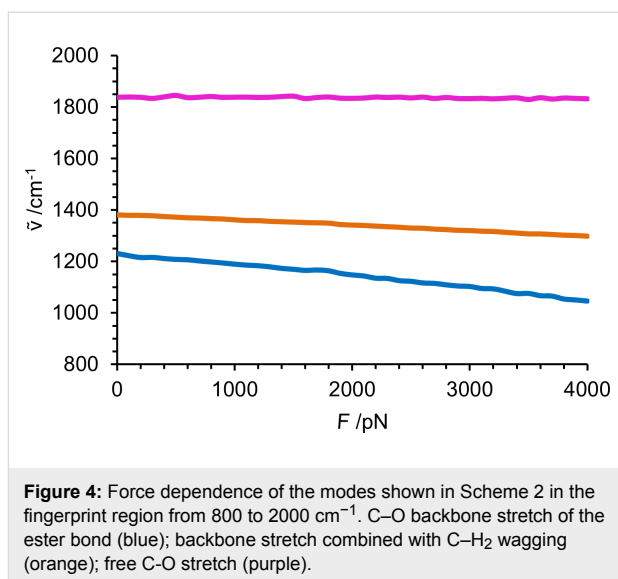
0 nN to 858 cm^{-1} at 4 nN result from numerous overlapping C–H and backbone vibrations. Due to their complexity, as described in detail before for polypropylene [30], as well as the lower intensity compared to vibrations from strongly IR active functional groups, they do not seem to be a valuable reference for force-dependent evaluation of the resulting spectra. Moreover, the complex interplay of different modes generating these broad absorptions may be strongly affected by the limited length of the model molecule, while the behavior of the lines originating from the ester moiety should be robust.

Figure 5: Intensities in fingerprint region of the infrared spectrum obtained for propyl propanoate. Spectral lines are broadened with a Lorentzian (34 cm^{-1} at FWHM) and summed up, yielding the spectrum of a stretched molecule.

The weighted spectra, obtained again by convolution with an exponential force distribution [81], are given in Figure 6. As for the amide, the bands dominated by backbone vibrations show a significant decrease in intensity accompanied by a broadening

towards smaller wavenumbers, while the free C–O stretching vibration remains unaffected.
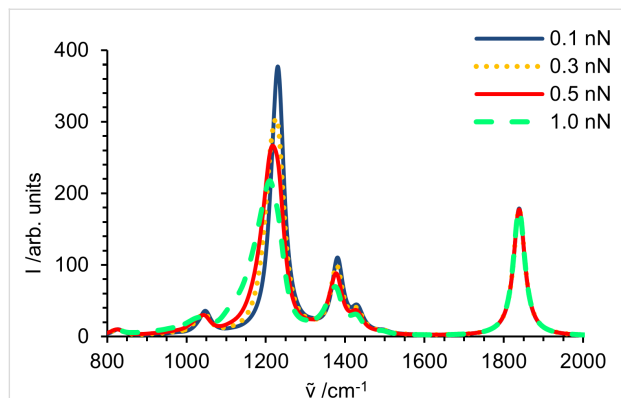
Figure 6: Fingerprint region of a simulated spectrum of a propyl propanoate solid sample at 0.1, 0.3, 0.5 and 1.0 nN mean force per polymer strand.

Conclusion

Experimental studies on the IR spectra of mechanically stressed polymers mostly focused on possible shifts in the peak position of bands around 1000 cm^{-1}. These shifts, however, are due to a complex interplay of overlapping backbone modes involving CH$_2$ groups, and are difficult to interpret. For polymers with strong IR active modes, like polyamides or polyesters, we have shown here that the peak positions of real samples do not shift strongly. This is due to the exponential force distribution used for the modeling, which means that most functional polymer strands are exposed to very small forces, but a small number of groups experiences very high forces. This results in a significant broadening combined with a small redshift of bands involving backbone vibrations. The peak broadening also leads to a decrease of the absorption maximum. In contrast, both peak position and intensity of the free C–O stretching mode are completely unaffected in both studied molecules. Thus, for comparison with experimental results we propose using the free C–O stretching mode as a reference band to quantify the influence of external force on the remaining strong infrared modes.

Methods

DFT calculations were performed using the B3LYP functional along with Ahlrich's SVP basis set. For computations, TURBO-MOLE 7.0.2 was used [82,83] with a script implementing EFEI using numerical calculation of the second derivative after geometry optimization, as described by Pill et al. [30]. Initial optimization leads to a fairly consistent increase in the distance between pulling points, but includes structures with imaginary vibrational modes and abrupt conformational changes. Respective structures were re-calculated using the geometry obtained for the next higher force as starting structure (see Figure S3,

Supporting Information File 1). All calculated structures represent local minima. No frequency scaling factor was applied. To validate the sufficiency of Ahlrich's SVP basis set, calculations without applying external force were performed using the TZVP basis set. Furthermore, computations were carried out for 0 nN using numerical calculations as implemented in TURBO-MOLE. See Supporting Information File 1 for details.

N-Propylpropanamide and propyl propanoate were used as model molecules for polyamides and polyesters, respectively. Since polymers consist of multiple repetition units, any vibrational modes specific to the polymer ends would be very weak. Therefore, hydrogen atoms from the terminal methyl groups were substituted with deuterium. The spectral lines originating from these CD$_3$ groups were removed from the simulated spectra. To simulate the intensities of infrared bands in the fingerprint region at a given force, the remaining spectral lines were broadened using a Lorentzian with a full width at half maximum of 34 cm^{-1}. To simulate spectra of polymer solids, the broadened spectra were convoluted with the probability distribution $P(F)$ derived by Adhikari and Makarov [81], Equation 1, with the actual force acting on the polymer strand F and the mean force $<F>$.

$$P(F) = e^{-F/\langle F \rangle} / \langle F \rangle \qquad (1)$$

Supporting Information

The Supporting information comprises a short description of steps taken to validate the accuracy of the methods used, the elongation of the respective model structures, animations of the vibrational modes in the fingerprint region, calculated infrared spectra and convoluted spectra over the entire frequency range. Additionally, the atomic coordinates calculated for the model molecules without external force are given.

Supporting Information File 1

Additional material.
[http://www.beilstein-journals.org/bjoc/content/supplementary/1860-5397-13-165-S1.docx]

Acknowledgements

References

1. Dubinskaya, A. M. *Russ. Chem. Rev.* **1999,** *68,* 637–652. doi:10.1070/RC1999v068n08ABEH000435
2. Beyer, M. K.; Clausen-Schaumann, H. *Chem. Rev.* **2005,** *105,* 2921–2948. doi:10.1021/cr030697h
3. Caruso, M. M.; Davis, D. A.; Shen, Q.; Odom, S. A.; Sottos, N. R.; White, S. R.; Moore, J. S. *Chem. Rev.* **2009,** *109,* 5755–5798. doi:10.1021/cr9001353
4. Beyer, M. K. Mechanochemical Reactions of Polymers. In *Encyclopedia Of Polymer Science and Technology;* Mark, H. F., Ed.; John Wiley and Sons: Inc.: Hoboken, NJ, USA, 2014; pp 1–20. doi:10.1002/0471440264.pst630
5. Grandbois, M.; Beyer, M.; Rief, M.; Clausen-Schaumann, H.; Gaub, H. E. *Science* **1999,** *283,* 1727–1730. doi:10.1126/science.283.5408.1727
6. Beyer, M. K. *J. Chem. Phys.* **2000,** *112,* 7307–7312. doi:10.1063/1.481330
7. Zhurkov, S. N.; Korsukov, V. E. *J. Polym. Sci., Polym. Phys. Ed.* **1974,** *12,* 385–398. doi:10.1002/pol.1974.180120211
8. Zhurkov, S. N. *Int. J. Fract.* **1984,** *26,* 295–307. doi:10.1007/BF00962961
9. Ribas-Arino, J.; Marx, D. *Chem. Rev.* **2012,** *112,* 5412–5487. doi:10.1021/cr200399q
10. Popov, A. A.; Zaikov, G. E.; Semeriov, N. N. *Int. J. Polym. Mater.* **1992,** *17,* 143–149. doi:10.1080/00914039208041109
11. Groote, R.; Jakobs, R. T. M.; Sijbesma, R. P. *Polym. Chem.* **2013,** *4,* 4846–4859. doi:10.1039/c3py00071k
12. Blaiszik, B.; Kramer, S. L. B.; Olugebefola, S. C.; Moore, J. S.; Sottos, N. R.; White, S. R. *Annu. Rev. Mater. Res.* **2010,** *40,* 179–211. doi:10.1146/annurev-matsci-070909-104532
13. Kean, Z. S.; Craig, S. L. *Polymer* **2012,** *53,* 1035–1048. doi:10.1016/j.polymer.2012.01.018
14. Wilson, G. O.; Andersson, H. M.; White, S. R.; Sottos, N. R.; Moore, J. S.; Braun, P. V. Self-Healing Polymers. In *Encyclopedia Of Polymer Science and Technology;* Mark, H. F., Ed.; John Wiley and Sons: Inc.: Hoboken, NJ, USA, 2010. doi:10.1002/0471440264.pst469
15. Black, A. L.; Lenhardt, J. M.; Craig, S. L. *J. Mater. Chem.* **2011,** *21,* 1655–1663. doi:10.1039/C0JM02636K
16. Bretzlaff, R. S.; Wool, R. P. *Macromolecules* **1983,** *16,* 1907–1917. doi:10.1021/ma00246a019
17. Wool, R. P. *J. Polym. Sci., Polym. Phys. Ed.* **1981,** *19,* 449–457. doi:10.1002/pol.1981.180190305
18. Wool, R. P.; Boyd, R. H. *J. Appl. Phys.* **1980,** *51,* 5116–5124. doi:10.1063/1.327429
19. Wool, R. P.; Statton, W. O. *J. Polym. Sci., Polym. Phys. Ed.* **1974,** *12,* 1575–1586. doi:10.1002/pol.1974.180120806
20. Chalmers, J.; Mackenzie, M. W.; Willis, H. A.; Edwards, H. G. M.; Lees, J. S.; Long, D. A. *Spectrochim. Acta, Part A* **1991,** *47,* 1677–1683. doi:10.1016/0584-8539(91)80005-4
21. Young, R. J. *J. Text. Inst.* **1995,** *86,* 360–381. doi:10.1080/00405009508631340
22. Brownlow, S. R.; Moravsky, A. P.; Kalugin, N. G.; Majumdar, B. S. *Compos. Sci. Technol.* **2010,** *70,* 1460–1468. doi:10.1016/j.compscitech.2010.04.025
23. Eichhorn, S. J.; Young, R. J. *Compos. Sci. Technol.* **2003,** *63,* 1225–1230. doi:10.1016/S0266-3538(03)00091-5
24. Huang, Y.; Young, R. J. *Carbon* **1995,** *33,* 97–107. doi:10.1016/0008-6223(94)00109-D
25. Vettegren, V. I.; Novak, I. I. *J. Polym. Sci., Part A-2* **1973,** *11,* 2135–2142. doi:10.1002/pol.1973.180111105
26. Vettegren, V. I.; Novak, I. I.; Friedland, K. J. *Int. J. Fract.* **1975,** *11,* 789–801. doi:10.1007/BF00012897
27. Vettegren, V. I.; Novak, I. I.; Kulik, V. B. *Phys. Solid State* **2005,** *47,* 920–926. doi:10.1134/1.1924856
28. Roylance, D. K.; DeVries, K. L. *J. Polym. Sci., Part C: Polym. Lett.* **1971,** *9,* 443–447. doi:10.1002/pol.1971.110090607
29. Reynolds, J.; Sternstein, S. S. *J. Chem. Phys.* **1964,** *41,* 47–50. doi:10.1063/1.1725646
30. Pill, M. F.; Kersch, A.; Clausen-Schaumann, H.; Beyer, M. K. *Polym. Degrad. Stab.* **2016,** *128,* 294–299. doi:10.1016/j.polymdegradstab.2016.03.025
31. Beyer, M. K. *Angew. Chem., Int. Ed.* **2003,** *42,* 4913–4915. doi:10.1002/anie.200351748
32. Pill, M. F.; Holz, K.; Preußke, N.; Berger, F.; Clausen-Schaumann, H.; Lüning, U.; Beyer, M. K. *Chem. – Eur. J.* **2016,** *22,* 12034–12039. doi:10.1002/chem.201600866
33. Pill, M. F.; Schmidt, S. W.; Beyer, M. K.; Clausen-Schaumann, H.; Kersch, A. *J. Chem. Phys.* **2014,** *140,* 044321. doi:10.1063/1.4862827
34. Schütze, D.; Holz, K.; Müller, J.; Beyer, M. K.; Lüning, U.; Hartke, B. *Angew. Chem., Int. Ed.* **2015,** *54,* 2556–2559. doi:10.1002/anie.201409691
35. Ainavarapu, S. R. K.; Wiita, A. P.; Dougan, L.; Uggerud, E.; Fernández, J. M. *J. Am. Chem. Soc.* **2008,** *130,* 6479–6487. doi:10.1021/ja800180u
36. Iozzi, M. F.; Helgaker, T.; Uggerud, E. *Mol. Phys.* **2009,** *107,* 2537–2546. doi:10.1080/00268970903401041
37. Iozzi, M. F.; Helgaker, T.; Uggerud, E. *J. Phys. Chem. A* **2011,** *115,* 2308–2315. doi:10.1021/jp109428g
38. Smalø, H. S.; Rybkin, V. V.; Klopper, W.; Helgaker, T.; Uggerud, E. *J. Phys. Chem. A* **2014,** *118,* 7683–7694. doi:10.1021/jp504959z
39. Smalø, H. S.; Uggerud, E. *Chem. Commun.* **2012,** *48,* 10443–10445. doi:10.1039/c2cc34056a
40. Smalø, H. S.; Uggerud, E. *Mol. Phys.* **2013,** *111,* 1563–1573. doi:10.1080/00268976.2013.811554
41. Davis, D. A.; Hamilton, A.; Yang, J.; Cremar, L. D.; van Gough, D.; Potisek, S. L.; Ong, M. T.; Braun, P. V.; Martínez, T. J.; White, S. R.; Moore, J. S.; Sottos, N. R. *Nature* **2009,** *459,* 68–72. doi:10.1038/nature07970
42. Kryger, M. J.; Ong, M. T.; Odom, S. A.; Sottos, N. R.; White, S. R.; Martínez, T. J.; Moore, J. S. *J. Am. Chem. Soc.* **2010,** *132,* 4558–4559. doi:10.1021/ja1008932
43. Lenhardt, J. M.; Ogle, J. W.; Ong, M. T.; Choe, R.; Martínez, T. J.; Craig, S. L. *J. Am. Chem. Soc.* **2011,** *133,* 3222–3225. doi:10.1021/ja107645c
44. Lenhardt, J. M.; Ong, M. T.; Choe, R.; Evenhuis, C. R.; Martínez, T. J.; Craig, S. L. *Science* **2010,** *329,* 1057–1060. doi:10.1126/science.1193412
45. Ong, M. T.; Leiding, J.; Tao, H.; Virshup, A. M.; Martínez, T. J. *J. Am. Chem. Soc.* **2009,** *131,* 6377–6379. doi:10.1021/ja8095834
46. Silberstein, M. N.; Min, K.; Cremar, L. D.; Degen, C. M.; Martínez, T. J.; Aluru, N. R.; White, S. R.; Sottos, N. R. *J. Appl. Phys.* **2013,** *114,* 023504. doi:10.1063/1.4812581
47. Wang, J.; Kouznetsova, T. B.; Niu, Z.; Ong, M. T.; Klukovich, H. M.; Rheingold, A. L.; Martínez, T. J.; Craig, S. L. *Nat. Chem.* **2015,** *7,* 323–327. doi:10.1038/nchem.2185
48. Wang, J.; Kouznetsova, T. B.; Kean, Z. S.; Fan, L.; Mar, B. D.; Martínez, T. J.; Craig, S. L. *J. Am. Chem. Soc.* **2014,** *136,* 15162–15165. doi:10.1021/ja509585g

49. Kean, Z. S.; Akbulatov, S.; Tian, Y.; Widenhoefer, R. A.; Boulatov, R.; Craig, S. L. *Angew. Chem., Int. Ed.* **2014,** *53,* 14508–14511. doi:10.1002/anie.201407494

50. Kucharski, T. J.; Boulatov, R. *J. Mater. Chem.* **2011,** *21,* 8237–8255. doi:10.1039/c0jm04079g

51. Kucharski, T. J.; Huang, Z.; Yang, Q.-Z.; Tian, Y.; Rubin, N. C.; Concepcion, C. D.; Boulatov, R. *Angew. Chem., Int. Ed.* **2009,** *48,* 7040–7043. doi:10.1002/anie.200901511

52. Dopieralski, P.; Anjukandi, P.; Rückert, M.; Shiga, M.; Ribas-Arino, J.; Marx, D. *J. Mater. Chem.* **2011,** *21,* 8309–8316. doi:10.1039/c0jm03698f

53. Dopieralski, P.; Ribas-Arino, J.; Marx, D. *Angew. Chem., Int. Ed.* **2011,** *50,* 7105–7108. doi:10.1002/anie.201100399

54. Dopieralski, P.; Ribas-Arino, J.; Anjukandi, P.; Krupicka, M.; Kiss, J.; Marx, D. *Nat. Chem.* **2013,** *5,* 685–691. doi:10.1038/nchem.1676

55. Dopieralski, P.; Ribas-Arino, J.; Anjukandi, P.; Krupicka, M.; Marx, D. *Angew. Chem., Int. Ed.* **2016,** *55,* 1304–1308. doi:10.1002/anie.201508005

56. Dopieralski, P.; Ribas-Arino, J.; Anjukandi, P.; Krupicka, M.; Marx, D. *Nat. Chem.* **2017,** *9,* 164–170. doi:10.1038/nchem.2632

57. Konôpka, M.; Rousseau, R.; Štich, I.; Marx, D. *J. Am. Chem. Soc.* **2004,** *126,* 12103–12111. doi:10.1021/ja047946j

58. Konôpka, M.; Turanský, R.; Reichert, J.; Fuchs, H.; Marx, D.; Štich, I. *Phys. Rev. Lett.* **2008,** *100,* 115503. doi:10.1103/PhysRevLett.100.115503

59. Konôpka, M.; Turanský, R.; Dubecký, M.; Marx, D.; Štich, I. *J. Phys. Chem. C* **2009,** *113,* 8878–8887. doi:10.1021/jp9017025

60. Krüger, D.; Fuchs, H.; Rousseau, R.; Marx, D.; Parrinello, M. *Phys. Rev. Lett.* **2002,** *89,* 186402. doi:10.1103/PhysRevLett.89.186402

61. Ribas-Arino, J.; Shiga, M.; Marx, D. *Angew. Chem., Int. Ed.* **2009,** *48,* 4190–4193. doi:10.1002/anie.200900673

62. Ribas-Arino, J.; Shiga, M.; Marx, D. *Chem. – Eur. J.* **2009,** *15,* 13331–13335. doi:10.1002/chem.200902573

63. Ribas-Arino, J.; Shiga, M.; Marx, D. *J. Am. Chem. Soc.* **2010,** *132,* 10609–10614. doi:10.1021/ja104958e

64. Seema, P.; Behler, J.; Marx, D. *Phys. Chem. Chem. Phys.* **2013,** *15,* 16001–16011. doi:10.1039/c3cp52181h

65. Turanský, R.; Konôpka, M.; Doltsinis, N. L.; Štich, I.; Marx, D. *ChemPhysChem* **2010,** *11,* 345–348. doi:10.1002/cphc.200900690

66. Zoloff Michoff, M. E.; Ribas-Arino, J.; Marx, D. *Phys. Rev. Lett.* **2015,** *114,* 075501. doi:10.1103/PhysRevLett.114.075501

67. Avdoshenko, S. M.; Konda, S. S. M.; Makarov, D. E. *J. Chem. Phys.* **2014,** *141,* 134115. doi:10.1063/1.4896944

68. Avdoshenko, S. M.; Makarov, D. E. *J. Phys. Chem. B* **2016,** *120,* 1537–1545. doi:10.1021/acs.jpcb.5b07613

69. Brantley, J. N.; Konda, S. S. M.; Makarov, D. E.; Bielawski, C. W. *J. Am. Chem. Soc.* **2012,** *134,* 9882–9885. doi:10.1021/ja303147a

70. Konda, S. S. M.; Brantley, J. N.; Bielawski, C. W.; Makarov, D. E. *J. Chem. Phys.* **2011,** *135,* 164103. doi:10.1063/1.3656367

71. Konda, S. S. M.; Brantley, J. N.; Varghese, B. T.; Wiggins, K. M.; Bielawski, C. W.; Makarov, D. E. *J. Am. Chem. Soc.* **2013,** *135,* 12722–12729. doi:10.1021/ja4051108

72. Makarov, D. E. *J. Chem. Phys.* **2016,** *144,* 030901. doi:10.1063/1.4939791

73. Bailey, A.; Mosey, N. J. *J. Chem. Phys.* **2012,** *136,* 044102. doi:10.1063/1.3678010

74. Kochhar, G. S.; Mosey, N. J. *Sci. Rep.* **2016,** *6,* No. 23059. doi:10.1038/srep23059

75. Stauch, T.; Dreuw, A. *Chem. Rev.* **2016,** *116,* 14137–14180. doi:10.1021/acs.chemrev.6b00458

76. Stauch, T.; Dreuw, A. *Acc. Chem. Res.* **2017,** *50,* 1041–1048. doi:10.1021/acs.accounts.7b00038

77. Wolinski, K.; Baker, J. *Mol. Phys.* **2009,** *107,* 2403–2417. doi:10.1080/00268970903321348

78. Stauch, T.; Dreuw, A. *Angew. Chem., Int. Ed.* **2014,** *53,* 2759–2761. doi:10.1002/anie.201309794

79. Stauch, T.; Hoffmann, M. T.; Dreuw, A. *ChemPhysChem* **2016,** *17,* 1486–1492. doi:10.1002/cphc.201600016

80. Stauch, T.; Dreuw, A. *J. Chem. Phys.* **2014,** *140,* 134107. doi:10.1063/1.4870334

81. Adhikari, R.; Makarov, D. E. *J. Phys. Chem. B* **2017,** *121,* 2359–2365. doi:10.1021/acs.jpcb.6b12758

82. Ahlrichs, R.; Bär, M.; Häser, M.; Horn, H.; Kölmel, C. *Chem. Phys. Lett.* **1989,** *162,* 165–169. doi:10.1016/0009-2614(89)85118-8

83. *TURBOMOLE,* V7.0.2; University of Karlsruhe and Forschungszentrum Karlsruhe GmbH, 2015.

Mechanochemical enzymatic resolution of *N*-benzylated-β^3-amino esters

Mario Pérez-Venegas[1], Gloria Reyes-Rangel[1], Adrián Neri[2], Jaime Escalante[*2]
and Eusebio Juaristi[*1,3]

Address:
[1]Departamento de Química, Centro de Investigación y de Estudios Avanzados, Avenida I.P.N. 2508, Ciudad de México, 07360, Mexico, [2]Centro de Investigaciones Químicas, Universidad Autónoma del Estado de Morelos, Av. Universidad 1001, Cuernavaca, Morelos, 62210, Mexico and [3]El Colegio Nacional, Luis Gonzáles Obregón 23, Centro Histórico, Ciudad de México, 06020, Mexico

Email:
Jaime Escalante[*] - jaime@uaem.mx; Eusebio Juaristi[*] - juaristi@relaq.mx

* Corresponding author

Abstract

The use of mechanochemistry to carry out enantioselective reactions has been explored in the last ten years with excellent results. Several chiral organocatalysts and even enzymes have proved to be resistant to milling conditions, which allows for rather efficient enantioselective transformations under ball-milling conditions. The present article reports the first example of a liquid-assisted grinding (LAG) mechanochemical enzymatic resolution of racemic β^3-amino esters employing *Candida antarctica* lipase B (CALB) to afford highly valuable enantioenriched *N*-benzylated-β^3-amino acids in good yields. Furthermore the present protocol is readily scalable.

Introduction

β-Amino acids are rather interesting molecules that frequently exhibit exceptional biological properties [1-3]; for instance, some of them are efficient inhibitors of several enzymes [4,5]. Furthermore, β-amino acid residues can be used to protect peptides and proteins against the activity of proteolytic enzymes [6,7], or are precursors of numerous active compounds such as β-lactams [8,9]. Finally, β-amino acids are present in numerous natural products [10]. These properties have generated great interest in the development of synthetic methods for the preparation of β-amino acids, especially protocols leading to products with high enantiomeric excess (ee), which are required to test the pharmacological activity of each enantiomer [11-13]. In this regard, several methods for the asymmetric synthesis of β-amino acids have been documented [14-22] includ-

ing strategies based on organocatalysis [23-26] and kinetic resolution using enzymes such as *Candida antarctica* lipase B, which was shown to be efficient in the resolution of racemic β-amino acids under various conditions [27-30].

Among recent developments in instrumentation for synthetic chemistry, mechanochemistry has proved a rather attractive and useful technique [31-37]. In particular, it has been demonstrated that mechanochemistry allows for the generation of products through catalysts that can be recovered and reused [38-44], so this converts mechanochemistry into a green technique, whose field of application is still very wide.

In this context, the use of a minimal amount of solvent (LAG) enable the development of convenient ball-milling protocols. In particular, LAG facilitates mechanochemical applications on a large scale [45,46].

Very recently, Hernández, Frings, and Bolm developed a method to carry out the kinetic resolution of secondary alcohols through selective acylation using *Candida antarctica* lipase B, under solvent-free ball-milling conditions [47,48]. Inspired by this ground-breaking report, which is in line with our continuous interest in developing new sustainable organocatalytic protocols [39,49-51], and taking advantage of previous experience with the enzymatic hydrolysis of a racemic mixture of *N*-protected-β³-amino acid methyl esters [52], we decided to examine the use of CALB enzyme under high-speed ball-milling (HSBM) conditions as a method to obtain enantiopure *N*-benzylated-β³-amino acids (Scheme 1).

Results and Discussion

A racemic mixture of substrate *rac*-**1a** (82 mg, 1 equiv) was milled in an Agate jar (12 mm of diameter, 4.6 mL) with an Agate ball (6 mm of diameter, 480 mg weight) using water (3.6 μL, 0.5 equiv), 0.2 mL of 2-methyl-2-butanol (2M2B) as a LAG additive (η = 1.63) and 40 mg of CALB (Novozym 435, Novozymes, recombinant, expressed in Aspergillus niger, immobilized in acrylic resin, >10000 U/g) at 25 Hz during 30 min. Gratifyingly, 55% conversion to the enantioenriched (*R*)-*N*-benzylated-β³-amino acid (*R*)-**2a** was observed, recovering 51% of enantioenriched starting material. It could be established by chiral HPLC that the ee of the product amounted 80% (Table 1, entry 1). This assay demonstrated that enzymatic hydrolysis can indeed be carried out under HSBM conditions. A second reaction was carried out under the same conditions but in the absence of the enzyme, which did not proceed and the starting material was recovered in its totality. This result shows that the observed hydrolysis is induced by CALB and not by the milling process per se. Furthermore, it could be established that the CALB enzyme and *N*-benzylated-β³-amino esters are stable to the mechanical force caused by HSBM. We then focused our attention on the search of the best conditions for this enzymatic mechanochemical resolution.

First of all, we examined the effect of the milling frequency, 15 Hz (Table 1, entry 2). Both yield and ee decreased substantially in comparison with the initial approach carried out at 25 Hz (Table 1, entry 1). Nevertheless, when the reaction time was increased from 30 min to 1 h at 15 Hz (Table 1, entry 3) the yield of the *N*-benzylated-β³-amino acid reached 49%, and presented high ee (95%, *E* > 200). These data represent an improvement both in ee and yield compared with the data recorded in solution [52]. Motivated by this result, we investigated the effect of other LAG additives in the reaction (see Supporting Information File 1, Table S1, entries 4–10). When 2M2B was replaced with other LAG additives a lower yield was observed (Table 1, entries 4–6). Nevertheless, the enantioselectivity of the process is maintained (95% ee), except when hexane was used (Table 1, entry 7), where a higher yield was observed (60%) although with a lower enantiomeric excess (86% ee). In the absence of a LAG additive and using
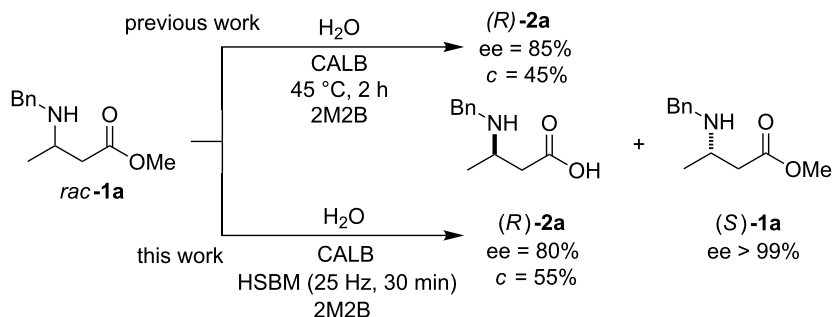
Scheme 1: Enantioselective enzymatic hydrolysis of racemic β³-amino ester *rac*-**1a** using CALB in solution [52] (top) and under HSBM conditions (button). 2M2B: 2-methyl-2-butanol.

Table 1: Search of the best parameters in the enzymatic enantioselective hydrolysis of *rac*-**1a** under ball milling.

entry[a]	LAG additive[b]	yield (%)[c] (S)-1a/(R)-2a	time (h)	ee (S)-1a (%)[d]	ee (R)-2a (%)[d]	c[e] (%)	E[f]
1[g]	2M2B	51/49	0.5	99	80	55	46
2	2M2B	70/30	0.5	89	77	54	23
3	**2M2B**	**51/49**	**1**	**99**	**95**	**51**	**>200**
4	AcOEt	86/13	1	69	95	42	81
5	IPA	82/21	1	48	95	34	63
6	CH₃CN	65/29	1	65	95	41	77
7	hexane	40/60	1	97	86	53	55
8	–	58/41	1	95	92	51	89
9[g]	–	58/42	1	93	86	52	45
10[h]	–	68/31	1	74	80	48	20

[a]Reactions were carried out with 0.5 equivalents of water and 15 Hz of frequency. [b]0.2 mL of LAG additive was used. [c]Determined after purification by flash chromatography. [d]Determined by HPLC with chiral stationary phase. [e]Calculated from $c = ee_s/(ee_s + ee_p)$. [f]$E = \ln[1 − c(1 + ee_p)]/\ln[1 − c(1 − ee_p)]$. [g]25 Hz of frequency was used. [h]0.25 equivalents of water were used.

0.25 equivalents of water (Table 1, entries 8–10) both yield and ee were lower.

Water plays an important role in the reaction controlling the activity of the enzyme; for example, the use of 0.5 equivalents of water yielded 49% of product **2a** (Table 1, entry 3). However, when 1 equivalent of water was employed the yield of the product increased to 92%. By contrast, when the reaction was

carried out in the absence of water only traces of product were detected (see Supporting Information File 1 Table S1).

To determine the substrate scope, the conditions that led to the best results in the enzymatic resolution of substrate *rac*-**1a** (Table 1, entry 3) were employed with other racemic *N*-benzylated-β³-amino esters as substrates (Table 2). It can be appreciated that reaction yields decrease when longer aliphatic chains

Table 2: Substrate scope for the enzymatic resolution of *N*-benzylated-β³-amino esters.

entry[a]	rac	R	yield (%)[b] (S)-1/(R)-2	ee[c] (S)-1 (%)	$[\alpha]_D^{25}$[d]	ee[c] (R)-2 (%)	$[\alpha]_D^{25}$[e]	c[f] (%)	E[g]	absolute configuration[h]
1	1b	CH₃-(CH₂)-	51/49	91	4.5	97	−36.5	48	>200	R
2	1c	CH₃-(CH₂)₂-	53/43	84	2.1	98	−45.2	46	>200	R
3	1d	CH₃-(CH₂)₃-	68/29	23	2.0	94	−35.3	20	40	R
4	1e	CH₃-(CH₂)₄-	74/24	57	0.2	94	−40.0	15	38	R
5	1f	CH₃-(CH₂)₅-	79/18	13	0.8	91	−39.7	13	24	R
6[i]	1g	Ph	92/10	18	3.4	83	−35.0	18	13	S
7[i]	1h	4-MeO-Ph	89/10	1	−0.5	80	−31.7	1	9	S
8	1i	t-Bu	89/4	4	−0.6	94	12.8	4	34	S

[a]Reactions were carried out with 0.5 equivalents of water and 0.2 mL of 2M2B at 15 Hz during 1 h. [b]Determined after purification by flash chromatography. [c]Determined by HPLC with chiral stationary phase. [d]$c = 0.33$ in CH₃Cl. [e]$c = 0.33$ in MeOH. [f]Calculated from $c = ee_s/(ee_s + ee_p)$. [g]$E = \ln[1 − c(1 + ee_p)]/\ln[1 − c(1 − ee_p)]$. [h]Assigned by chemical correlation and by HPLC with chiral stationary phase. [i]0.75 equivalents of water were used.

are present in the substrate (Table 2, entries 1–5), although the ee in products **2b–f** remained rather high (>90%). Notably, this aliphatic chain-length effect has been studied in other systems with similar results [53].

The introduction of an aromatic ring (either unsubstituted or *para*-substituted) in the substrate resulted in diminished yields (Table 2, entries 6 and 7) but good ee (≥80%). With bulky groups, such as *tert*-butyl, the experimentally observed low yield was accompanied nevertheless by high ee (Table 2, entry 8). Other reaction conditions were tested aiming of increasing both yield and ee (see Supporting Information File 1); however, the best results continued to be obtained by using the conditions indicated in Table 1, entry 3.

To establish the absolute configuration of product **2a**, a sample was crystallized to give a suitable single-crystal for X-ray diffraction analysis. The resulting structure showed the *R* configuration (Flack parameter = 0.154) in the stereocenter delimited by the atoms marked as C1, N1 and C3 (Figure 1). The *R* configuration in hydrolyzed product **2a** was confirmed by comparison with literature data [52]. The configuration of products **2b**, **2g** to **2i** was also assigned by comparison with literature data [52,54,55]. Finally, in the case of products **2c–f**, comparison of the elution order for both enantiomers with the tendency found in **2a** and **2b** suggested that the configuration is the same in all of them (see Supporting Information File 1) [56,57].

The enzyme employed in these experiments was recovered by centrifugation of the reaction crude followed by drying under vacuum (90% of recovered enzyme; we will call it rCALB). This recovered material was reused to evaluate the enzyme recyclability after the mechanochemical protocol. When the reaction was carried out using the recovered enzyme the yield was
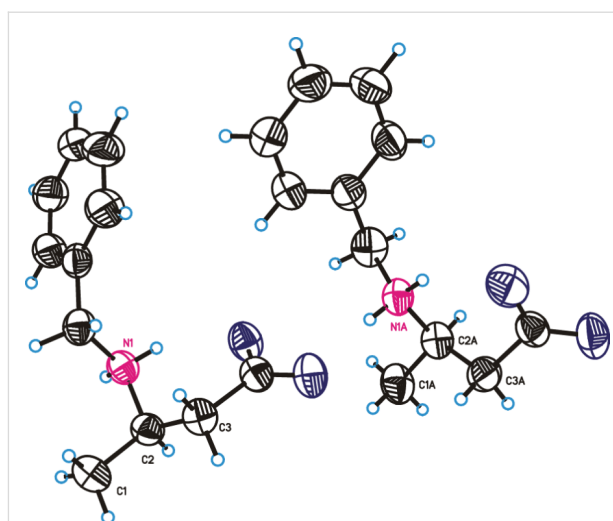
Figure 1: X-ray crystallographic structure of product (*R*)-**2a** (50% of probability ellipsoids). CCDC registry number 1552645.

not as good as the obtained with fresh catalyst (compare entries 1 and 2 in Table 3). This might suggest that the enzyme undergoes partial denaturation and/or partial destruction of the support, within each cycle (Table 3, entry 3). Interestingly, however, ee values of the isolated β-amino acid still resulted quite acceptable. On the other hand, no product was detected after the third cycle. To evaluate the denaturalization of the enzyme provoked by the milling process, a sample of fresh catalyst was milled for 1 h at 15 Hz under solvent-free conditions and in the presence of a LAG additive, finding that both reaction yield (38%) and ee (>90%) are higher (see Supporting Information File 1, Table S3, entries 5 and 6), compared with results from the hydrolysis using the catalyst recovered after the first cycle (Table 4, entry 2). The milling process carried out using the catalyst milled with 2M2B presents a slight decrease in ee compared with the resolution reaction using the milled en-

Table 3: Recycling capacity of immobilized CALB under HSBM conditions.

entry[a]	recycling cycle	yield (%)[b] (*S*)-**1a**/(*R*)-**2a**	ee[c] (*S*)-**1a** (%)	ee[c] (*R*)-**2a** (%)	c^d (%)	E^e
1	–	51/49	49	95	51	>200
2	1	65/37	35	88	59	22
3	2	80/20	6	80	51	10
4	3	100/0	0	–	–	–

[a]Reactions were carried out with 0.5 equivalents of water and 0.2 mL of 2M2B at 15 Hz during 1 h. [b]Determined after purification by flash chromatography. [c]Determined by HPLC with chiral stationary phase. [d]Calculated from $c = ee_s/(ee_s + ee_p)$. [e]$E = \ln[1 - c(1 + ee_p)]/\ln[1 - c(1 - ee_p)]$.

Table 4: Scaling-up of the enzymatic hydrolysis reaction under ball-milling using substrate *rac*-**1a**.

entry[a]	catalyst/substrate (equiv) [b]	yield (%)[c] (S)-**1a**/(R)-**2a**	ee[d] (S)-**1a** (%)	ee[d] (R)-**2a** (%)	c^e (%)	E^f
1[g]	1/1	51/49	>99	95	51	>200
2	1/3	52/48	62	93	40	52
3	1/6	61/42	53	93	36	47
4	1/9	59/40	49	94	34	53

[a]Reactions were carried out with 0.5 equivalents of water at 15 Hz during 1 h. [b]1 equivalent of enzyme = 40 mg; 1 equivalent of susbtrate = 82 mg. [c]Determined after purification by flash chromatography. [d]Determined by HPLC with chiral stationary phase. [e]Calculated from $c = ee_s/(ee_s + ee_p)$. [f]$E = \ln[1 - c(1 + ee_p)]/\ln[1 - c(1 - ee_p)]$. [g]0.2 mL of LAG additive were used.

zyme under solvent-free conditions. This observation suggests that the LAG additive increases to some extent the degree of denaturation of the enzyme, reducing the enantiodiscrimination (ee = 91%) although maintaining significant catalytic activity (yield = 38%).

Finally, to test the scalability of the process, a set of reactions was carried out increasing the amount of substrate *rac*-**1a** under the optimized reaction parameters. (Table 4).

Relative to the results obtained with 1 equivalent of *rac*-**1a** in the presence of LAG additive (Table 4, entry 1) a slight decrease in yield was observed when 3 equivalents of substrate (and no LAG additive) were used to carry out the reaction (Table 4, entry 2). Nevertheless, the hydrolysis still proceeds with excellent ee (93%). This result confirms that under solvent-free conditions a particular amount of enzyme can catalyze a larger amount of substrate, even up to nine equivalents, without loss of enantiodiscrimination (Table 4, entry 4). It appears that this high efficiency is a consequence of the highly-concentrated medium that is generated under solvent-free mechanochemical conditions, an effect that is not possible to reach in solution [52]. This effect also allows for an increase in the amount of product per cycle of the enzymatic reaction.

Conclusion

The capacity of immobilized CALB to carry out the enzymatic hydrolytic resolution of *N*-benzylated-β³-amino esters under mechanochemical conditions was demonstrated. The reaction proceeds with an excellent yield (up to 49% of the theoretical 50% maximum) and high enantioselectivity (up to 98% ee). The method proved to be efficient in the resolution of racemic mixtures of β³-amino esters with aliphatic chains of different lengths, affording high ees of the resulting β-amino acids in spite of a decrease in yield in the case of long aliphatic chains. This efficiency of the enzymatic process is also observed in substrates with bulky aromatic groups (ee ≥ 80%). The reaction is best carried out in the presence of the LAG additive 2-methyl-2-butanol when the concentration of the substrate is low. The enzymatic process could be scaled-up to 9-fold affording the hydrolyzed product with high ee (≥93%) and an excellent yield (40% out of a 50% theoretical maximum). Finally, the enzyme catalyst could be recovered and reused several times affording the desired amino acids with good ee although with a decrease in conversion due to a partial denaturation process and partial destruction of the enzyme support.

Supporting Information

Supporting Information File 1

Experimental section, NMR spectra, chromatograms and X-ray diffraction data.
[http://www.beilstein-journals.org/bjoc/content/supplementary/1860-5397-13-167-S1.pdf]

References

1. Seebach, D.; Beck, A. K.; Capone, S.; Deniau, G.; Grošelj, U.; Zass, E. *Synthesis* **2009,** 1–32. doi:10.1055/s-0028-1087490
2. Steer, D. L.; Lew, R. A.; Perlmutter, P.; Smith, A. I.; Aguilar, M.-I. *Curr. Med. Chem.* **2002,** *9,* 811–822. doi:10.2174/0929867024606759
3. Ton, J.; Mauch-Mani, B. *Plant J.* **2004,** *38,* 119–130. doi:10.1111/j.1365-313X.2004.02028.x

4. Farmer, L. J.; Clark, M. P.; Boyd, M. J.; Perola, E.; Jones, S. M.; Tsai, A.; Jacobs, M. D.; Bandarage, U. K.; Ledeboer, M. W.; Wang, T.; Deng, H.; Ledford, B.; Gu, W.; Duffy, J. P.; Bethiel, R. S.; Shannon, D.; Byrn, R. A.; Leeman, J. R.; Rijnbrand, R.; Bennett, H. B.; O'Brien, C.; Memmott, C.; Nti-Addae, K.; Bennani, Y. L.; Charifson, P. S. *ACS Med. Chem. Lett.* **2017,** *8,* 256–260. doi:10.1021/acsmedchemlett.6b00486

5. Seebach, D.; Beck, A. K.; Bierbaum, D. J. *Chem. Biodiversity* **2004,** *1,* 1111–1239. doi:10.1002/cbdv.200490087

6. Gentilucci, L.; De Marco, R.; Cerisoli, L. *Curr. Pharm. Des.* **2010,** *16,* 3185–3203. doi:10.2174/138161210793292555

7. Zubrzak, P.; Williams, H.; Coast, G. M.; Issac, R. E.; Reyes-Rangel, G.; Juaristi, E.; Zabrocki, J.; Nachman, R. J. *Pept. Sci.* **2007,** *88,* 76–82. doi:10.1002/bip.20638

8. Magriotis, P. A. *Angew. Chem., Int. Ed.* **2001,** *40,* 4377–4379. doi:10.1002/1521-3773(20011203)40:23<4377::AID-ANIE4377>3.0.CO;2-J

9. Escalante, J.; González-Tototzin, M. A.; Aviña, J.; Muñoz-Muñiz, O.; Juaristi, E. *Tetrahedron* **2001,** *57,* 1883–1890. doi:10.1016/S0040-4020(00)01169-8

10. Spiteller, P.; von Nussbaum, F. β-Amino Acids in Natural Products. In *Enantioselective Synthesis of β-Amino acids,* 2nd ed.; Juaristi, E.; Soloshonok, V. A., Eds.; Wiley-VCH: New York, 2005; pp 19–91. doi:10.1002/0471698482.ch2

11. Hoekstra,, W. J.; Maryanoff, B. E.; Damiano, B. P.; Andrade-Gordon, P.; Cohen, J. H.; Costanzo, M. J.; Haertlein, B. J.; Hecker, L. R.; Hulshizer, B. L.; Kauffman, J. A.; Keane, P.; McComsey, D. F.; Mitchell, J. A.; Scott, L.; Shah, R. D.; Yabut, S. C. *J. Med. Chem.* **1999,** *42,* 5254–5265. doi:10.1021/jm990418b

12. *Synthesis of Non-Natural Amino Acids.* In *Handbook of Chiral Chemicals,* 2nd ed.; Ager, D. J., Ed.; DSM Pharma Chemicals: Raleigh, NC, 2006.

13. Bandala, Y.; Juaristi, E. Recent Developments in the Synthesis of b-Amino Acids. In *Amino Acids, Peptides and Proteins in Organic Chemistry;* Hughes, A. B., Ed.; Wiley-VCH: Weinheim, 2009; pp 291–365. doi:10.1002/9783527631766.ch7

14. Juaristi, E.; Soloshonok, V. A., Eds *Enantioselective Synthesis of β-Amino Acids,* 2nd ed.; John Wiley and Sons: Hoboken, NJ, 2005.

15. Weiner, B.; Szymański, W.; Janssen, D. B.; Minnaard, A. J.; Feringa, B. L. *Chem. Soc. Rev.* **2010,** *39,* 1656–1691. doi:10.1039/b919599h

16. Gedey, S.; Liljeblad, A.; Lázár, L.; Fülöp, F.; Kanerva, L. T. *Tetrahedron: Asymmetry* **2001,** *12,* 105–110. doi:10.1016/S0957-4166(01)00002-7

17. Juaristi, E.; Quintana, D.; Escalante, J. *Aldrichimica Acta* **1994,** *27,* 3–11.

18. Juaristi, E.; López-Ruiz, H. *Curr. Med. Chem.* **1999,** *6,* 983–1004.

19. Abele, S.; Seebach, D. *Eur. J. Org. Chem.* **2000,** 1–15. doi:10.1002/(SICI)1099-0690(200001)2000:1<1::AID-EJOC1>3.0.CO;2-6

20. Fülöp, F. *Chem. Rev.* **2001,** *101,* 2181–2204. doi:10.1021/cr000456z

21. Liu, M.; Sibi, M. P. *Tetrahedron* **2002,** *58,* 7991–8035. doi:10.1016/S0040-4020(02)00991-2

22. Ma, J.-A. *Angew. Chem., Int. Ed.* **2003,** *42,* 4290–4299. doi:10.1002/anie.200301600

23. Wenzel, A. G.; Jacobsen, E. N. *J. Am. Chem. Soc.* **2002,** *124,* 12964–12965. doi:10.1021/ja028353g

24. Ting, A.; Schaus, S. E. *Eur. J. Org. Chem.* **2007,** *35,* 5797–5815. doi:10.1002/ejoc.200700409

25. Wilson, J. E.; Casarez, A. D.; MacMillan, D. W. C. *J. Am. Chem. Soc.* **2009,** *131,* 11332–11334. doi:10.1021/ja904504j

26. Meyer, D.; Marti, R.; Seebach, D. *Eur. J. Org. Chem.* **2015,** *2015,* 4883–4891. doi:10.1002/ejoc.201500636

27. Forró, E.; Fülöp, F. *Chem. – Eur. J.* **2007,** *13,* 6397–6401. doi:10.1002/chem.200700257

28. Fitz, M.; Forró, E.; Vigóczki, E.; Lázár, L.; Fülöp, F. *Tetrahedron: Asymmetry* **2008,** *19,* 1114–1119. doi:10.1016/j.tetasy.2008.04.002

29. Heck, T.; Seebach, D.; Steffen, O.; ter Wiel, M. K. J.; Kohler, H.-P. E.; Geueke, B. *ChemBioChem* **2009,** *10,* 1558–1561. doi:10.1002/cbic.200900184

30. Weise, N. J.; Ahmed, S. T.; Parmeggiani, F.; Turner, N. J. *Adv. Synth. Catal.* **2017,** *359,* 1570–1576. doi:10.1002/adsc.201600894

31. Hernández, J. G.; Bolm, C. *J. Org. Chem.* **2017,** *82,* 4007–4019. doi:10.1021/acs.joc.6b02887

32. Rodríguez, B.; Rantanen, T.; Bolm, C. *Angew. Chem., Int. Ed.* **2006,** *45,* 6924–6926. doi:10.1002/anie.200602820

33. Declerck, V.; Nun, P.; Martinez, J.; Lamaty, F. *Angew. Chem., Int. Ed.* **2009,** *48,* 9318–9321. doi:10.1002/anie.200903510

34. Bonnamour, J.; Métro, T.-X.; Martinez, J.; Lamaty, F. *Green Chem.* **2013,** *15,* 1116–1120. doi:10.1039/c3gc40302e

35. Baig, R. B. N.; Varma, R. S. *Chem. Soc. Rev.* **2012,** *41,* 1559–1584. doi:10.1039/C1CS15204A

36. Jones, W.; Eddleston, M. D. *Faraday Discuss.* **2014,** *170,* 9–34. doi:10.1039/C4FD00162A

37. Hernández, J. G.; Friščić, T. *Tetrahedron Lett.* **2015,** *56,* 4253–4265. doi:10.1016/j.tetlet.2015.03.135

38. Lawrenson, S. B.; Arav, R.; North, M. *Green Chem.* **2017,** *19,* 1685–1691. doi:10.1039/C7GC00247E

39. Hernández, J. G.; Juaristi, E. *Chem. Commun.* **2012,** *48,* 5396–5409. doi:10.1039/c2cc30951c

40. Schmidt, R.; Stolle, A.; Ondruschka, B. *Green Chem.* **2012,** *14,* 1673–1679. doi:10.1039/c2gc16508b

41. Hernández, J. G.; Macdonald, N. A. J.; Mottillo, C.; Butler, I. S.; Friščić, T. *Green Chem.* **2014,** *16,* 1087–1092. doi:10.1039/C3GC42104J

42. Machuca, E.; Juaristi, E. Asymmetric Organocatalytic Reactions Under Ball Milling. In *Ball Milling Towards Green Synthesis: Applications, Projects, Challenges;* Ranu, B.; Stolle, A., Eds.; Royal Society of Chemistry: Cambridge, UK, 2015; pp 81–95.

43. McKissic, K. S.; Caruso, J. T.; Blair, R. G.; Mack, J. *Green Chem.* **2014,** *16,* 1628–1632. doi:10.1039/c3gc41496e

44. Schmidt, R.; Burmeister, C. F.; Baláž, M.; Kwade, A.; Stolle, A. *Org. Process Res. Dev.* **2015,** *19,* 427–436. doi:10.1021/op5003787

45. Friščić, T.; Trask, A. V.; Jones, W.; Motherwell, W. D. S. *Angew. Chem., Int. Ed.* **2006,** *45,* 7546–7550. doi:10.1002/anie.200603235

46. Friščić, T.; Jones, W. *Cryst. Growth Des.* **2009,** *9,* 1621–1637. doi:10.1021/cg800764n

47. Hernández, J. G.; Frings, M.; Bolm, C. *ChemCatChem* **2016,** *8,* 1769–1772. doi:10.1002/cctc.201600455

48. Hernández, J. G.; Ardila-Fierro, K. J.; Crawford, D.; James, S. L.; Bolm, C. *Green Chem.* **2017,** *19,* 2620–2625. doi:10.1039/C7GC00615B

49. Hernández, J. G.; Juaristi, E. *J. Org. Chem.* **2010,** *75,* 7107–7111. doi:10.1021/jo101159a

50. Polindara-García, L. A.; Juaristi, E. *Eur. J. Org. Chem.* **2016,** 1095–1102. doi:10.1002/ejoc.201501371

51. Landeros, J. M.; Juaristi, E. *Eur. J. Org. Chem.* **2017,** 687–694. doi:10.1002/ejoc.201601276
52. Rangel, H.; Carrillo-Morales, M.; Galindo, J. M.; Castillo, E.; Obregón-Zúñiga, A.; Juaristi, E.; Escalante, J. *Tetrahedron: Asymmetry* **2015,** *26,* 325–332. doi:10.1016/j.tetasy.2015.02.007
53. Vaysse, L.; Ly, A.; Moulin, G.; Dubreucq, E. *Enzyme Microb. Technol.* **2002,** *31,* 648–655. doi:10.1016/S0141-0229(02)00166-7
54. Guizzetti, S.; Benaglia, M.; Bonsignore, M.; Raimondi, L. *Org. Biomol. Chem.* **2011,** *9,* 739–743. doi:10.1039/C0OB00570C
55. Bonsignore, M.; Benaglia, M.; Annunziata, R.; Celentano, G. *Synlett* **2011,** 1085–1088. doi:10.1055/s-0030-1259941
56. Péter, A.; Lázár, L.; Fülöp, F.; Armstrong, D. W. *J. Chromatogr. A* **2001,** *926,* 229–238. doi:10.1016/S0021-9673(01)01078-0
57. Enders, D.; Wahl, H.; Bettray, W. *Angew. Chem., Int. Ed. Engl.* **1995,** *34,* 455–457. doi:10.1002/anie.199504551

Mechanochemical *N*-alkylation of imides

Anamarija Briš, Mateja Đud and Davor Margetić*§

Abstract

The mechanochemical *N*-alkylation of imide derivatives was studied. Reactions under solvent-free conditions in a ball mill gave good yields and could be put in place of the classical solution conditions. The method is general and can be applied to various imides and alkyl halides. Phthalimides prepared under ball milling conditions were used in a mechanochemical Gabriel synthesis of amines by their reaction with 1,2-diaminoethane.

Introduction

The development of environmentally friendly organic reactions is a growing area of interest [1]. The reduction of the impact of chemical reactions on the environment could be achieved by the minimization of waste produced in the process, the employment of the more efficient reagents and catalysts and by the application of microwave [2], photochemical [3] or high pressure conditions [4], thus reducing reaction time and energy consumption. In recent time, important progress was made in the development of various solvent-free organic reactions [5], especially by the use of the ball milling technique [6-8]. In continuation of our interest in eco-friendly organic syntheses [9-14], we studied mechanochemical *N*-alkylation reactions of imides with alkyl halogenides, and the results are presented in this paper. Until now, ball milling *N*-alkylations of ureas [15], hydrazones [16], imines [17,18], pyridines [19], pyrimidines [20], imidazoles [21], secondary amines [22], as well as allylic

alkylation reactions [23] were reported in the literature. The aim of this study was to establish simple and effective imide alkylation mechanochemical protocols. Imides are usually alkylated with alkyl halides in solution (DMF, acetone, DMSO) and the reactions were heated for several hours in the presence of a base [24].

Results and Discussion

The reaction of the norbornene *endo*-succinimide **1** [25] with 1,3-dibromopropane (**2**) was used as a model system for the optimization of the reaction conditions [26]. Here, imide **1** is a solid, while dibromopropane is a liquid reagent. It was found that during the ball-milling process (Retsch MM400 mill at 30 Hz, stainless steel 10 mL vial, one 12 mm steel ball) of this solid/liquid system, mono-alkylation and formation of imide **3** was accompanied by the bisalkylated product **4** (Scheme 1).
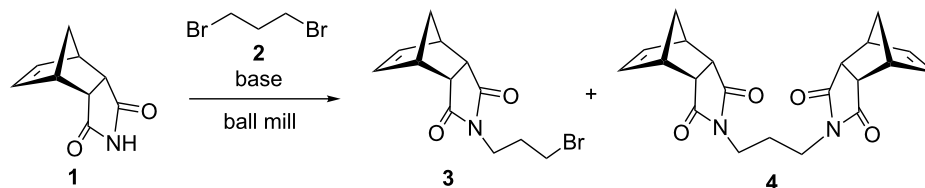
Scheme 1: *N*-Alkylation of imide **1** with 1,3-dibromopropane (**2**) in a ball mill.

To optimize the reaction conditions, the molar ratio of reagents, the reaction time and bases were varied. The addition of a small amount of solvent for LAG (liquid-assisted grinding) [27] was tested as well. The results are collected in Table 1. The best results were achieved by the use of K₂CO₃ as base, with large excess of dibromide and carbonate. Within one hour of milling, **1** was quantitatively converted to the mono-alkylated product **3** which was and isolated in 88% yield by simple work-up consisting of dissolving the reaction mixture in dichloromethane and washing with water (Table 1, entry 8). Under these milling conditions, an excess of inorganic base may have helped by acting as a grinding auxiliary. A comparison with the synthesis carried out in solution (acetone, 60 °C) showed a significant reduction in time (Table 1, entry 11). Also less efficient was the use of acetone under LAG conditions (Table 1, entry 9). It was found that the outcome of the reaction could be efficiently con-

trolled by variation of molar ratios of reagents. When 0.3 equivalents of dibromide **2** were used, bisalkylation was the sole reaction and imide **4** was isolated in 52% yield (Table 1, entry 5). Other inorganic and organic bases employed were less reactive than K₂CO₃, whereas Cs₂CO₃ showed a higher reactivity, which, due to the inevitable formation of **4**, prevented clean mono-alkylation.

The optimized reaction conditions were used to establish the scope of this reaction. Firstly, other alkyl halides were employed (Scheme 2). These experiments revealed that the solvent-free *N*-alkylation could be effectively carried out with different alkyl halides, however, the conditions had to be optimized for each substrate. In particular, reactions carried out by a one-pot, two-step process [28] of **1** with K₂CO₃ (producing in situ the potassium imide salt), followed by the addition of the

Table 1: *N*-Alkylation of imide **1** with **2**.[a]

Entry	Base	Ratio **1:2**:base	Time [h]	Ratio **1:3:4**	Yield [%][b]
1	K₂CO₃	1:1:5	0.5	68:28:4	
2		1:1:5	1	0:82:18	
3		1:1:5	2	0:80:20	
4		1:0.5:5	2	0:45:55	
5		1:0.3:5	2	43:0:57	**4**; 52
6		1:3:5	1	0:93:7	
7		1:3:5	1[c]	14:83:3	
8		1:12:5	1	0:100:0	**3**; 88
9		1:3:5	1[d]	16:65:19	
10		1:3:5	24[d]	0:0:100	**4**; >95
11		1:20:5	24[e]	0:100:0	**3**; >95
12		1:2:2	1 + 1[f]		**3**; 54, **4**; 6
13	Na₂CO₃	1:12:5	2	89:11:0	
14	Cs₂CO₃	1:12:5	2	0:97:3	
15	Cs₂CO₃	1:12:3	1	0:97:3	
16	NaHCO₃	1:1:5	1	48:38:12	
17	DBU	1:1:5	1	24:58:18	
18	DMAP	1:1:5	1	35:61:14	

[a]Retsch MM400 ball mill, 10 mL stainless steel vial, 1 × 12 mm stainless steel ball, 30 Hz; [b]isolated yields, ratio determined by ¹H NMR spectroscopy; [c]2 × 6 mm balls; [d]LAG acetone (η = 0.25 µL mg⁻¹); [e]acetone, 60 °C; [f]milling of **1** with K₂CO₃ for 1 h, followed by the addition of **2** and LAG DMF (η = 2 µL mg⁻¹) and ball milling for another 1 h.
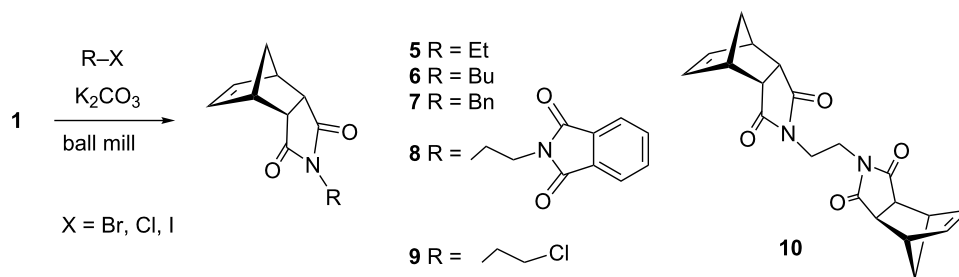
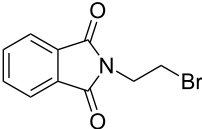**Scheme 2:** Mechanochemical *N*-alkylation of imide **1**.

halide and further milling in conjunction with LAG (DMF) proved useful. Ball milling of **1** with alkyl halides afforded after 2 h the corresponding *N*-alkylated products in high yields, with exception of butyl chloride (Table 2, entry 4). The sequential milling procedure is advantageous in terms of the use of smaller amounts of reagents and a significant reduction of the reaction time was achieved in comparison with the reaction in DMF. In contrast to the milling of imide **1** with 1,3-dibromopropane (**2**), the reaction with 1,2-dichloroethane gave products **9** and **10**, where bis-product **10** was the major, despite of large excess of reagent (Table 2, entry 9). The physical state of the halide reagents (either liquid or solid alkyl halides) did not influence the reaction outcome (see Supporting Information File 1, Table S1).

Further alkylation experiments were carried out with selected imides **11–17** (Figure 1, Table 3). The sequential mechanochemical alkylation was found to be often advantageous over the reaction carried out by standard procedure in sol-

vent, either by shorter reaction time, less vigorous conditions or better yields. Another advantage of solvent-free conditions is the circumvention of the problematic low solubility of some of the substrates employed. By conducting the reaction in a ball mill, solubility problems and the issues associated with the selection of the most suitable solvent could be avoided. In addition, solid-state reaction diminishes the heterogeneous character of alkylation, since inorganic bases in general are not soluble in organic solvents.

Ex situ IR spectroscopy (ATR) of milling of imides **11–17** with K_2CO_3 was used for monitoring the reaction progress, which showed for instance, that potassium phthalimide [29] was formed after one hour of grinding (Figure 2). This salt was, without isolation, subjected to further milling with benzyl bromide with LAG (DMF) to obtain alkylated products in high yields. Formation of potassium salts of other imides listed in Table 3 by K_2CO_3 has been also proven by ex situ IR monitoring (see Supporting Information File 1). It indicates that potas-

Table 2: Mechanochemical *N*-alkylation of imide **1**.

Entry	Halide	Product	Ratio **1**:RX:K_2CO_3	Time, conditions	Ratio **1**:product[a]	Yield [%][b]
1	EtBr	**5**	1:10:5	2 h	0:100	>95
2		**5**	1:2:2	1 + 1 h[c]		87
3	EtI	**5**	1:10:5	2 h	10:90	
4	BuCl	**6**	1:6:2	1 + 1 h[c]	97:3	
5	BnBr	**7**	1:2:2	1 + 1 h[c]		81
6		**8**	1:1:5	2 h	65:35	
7		**8**	1:2:4	1 + 1 h[c]		63
8		**8**	1:1:5	72 h[d]		59
9	ClCH₂CH₂Cl	**9,10**	1:12:5	2 h	51:6:43	

[a]Ratio determined by ^{1}H NMR spectroscopy; [b]isolated yields; [c]milling of **1** with K_2CO_3 for 1 h, followed by the addition of RX and LAG (DMF, η = 2 μL mg⁻¹) and ball milling for another 1 h; [d]DMF, 50 °C, 3d.
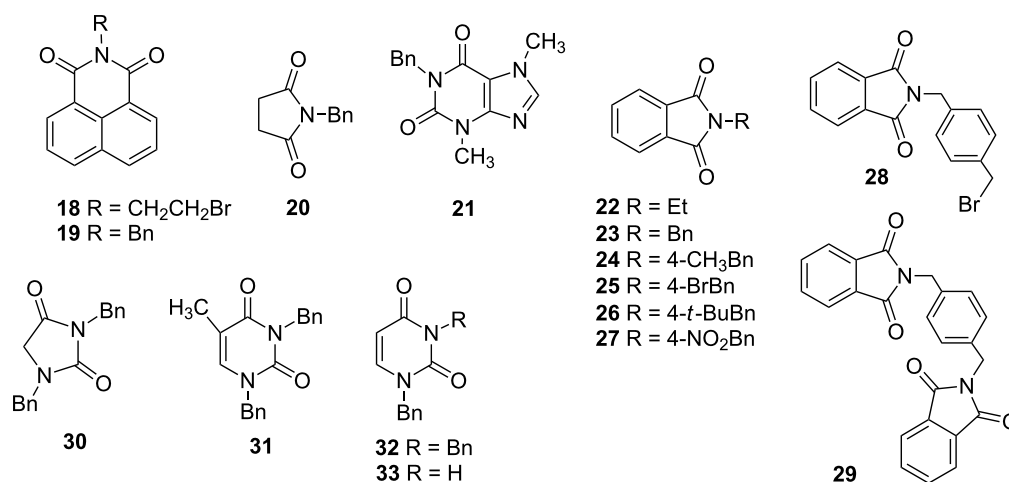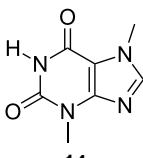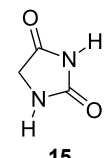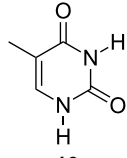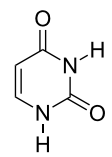
Figure 1: Products of alkylation of imides **11–17**.

Table 3: Mechanochemical *N*-alkylation of imides **11–17**.[a]

Entry	Substrate	Bromide	Ratio imide:RX:K$_2$CO$_3$	Product, yield [%][b]
1	**11**	**2**	1:2:4	**18**, 73
2		BnBr	1:2:2	**19**, 98
3	**12**	EtBr	1:2:2	**22, 75**
4		BnBr	1:2:2	**23, 97**
5		H$_3$C—⬡—CH$_2$Br	1:2:2	**24**, 94
6		Br—⬡—CH$_2$Br	1:2:2	**25**, 95
7		*t*-Bu—⬡—CH$_2$Br	1:2:2	**26**, 90
8		O$_2$N—⬡—CH$_2$Br	1:2:2	**27**, 98
9		BrCH$_2$—⬡—CH$_2$Br	1:2:2	**28**, 32; **29**, 4
10	**13**	BnBr	1:2:2	**20**, 89

Table 3: Mechanochemical *N*-alkylation of imides **11–17**.[a] (continued)

11	**14**	BnBr	1:2:2	**21**, 67
12	**15**	BnBr	1:4:4	**30**, 93
13	**16**	BnBr	1:4:4	**31**, 99
14 15	**17**	BnBr	1:2:2 1:1:2	**32**, 98 **32**, 37; **33**, 17

[a]Milling of imides with K_2CO_3 for 1 h, followed by the addition of RX and LAG (DMF, η = 2 µL mg⁻¹) and ball milling for another 1 h; [b]isolated yields.
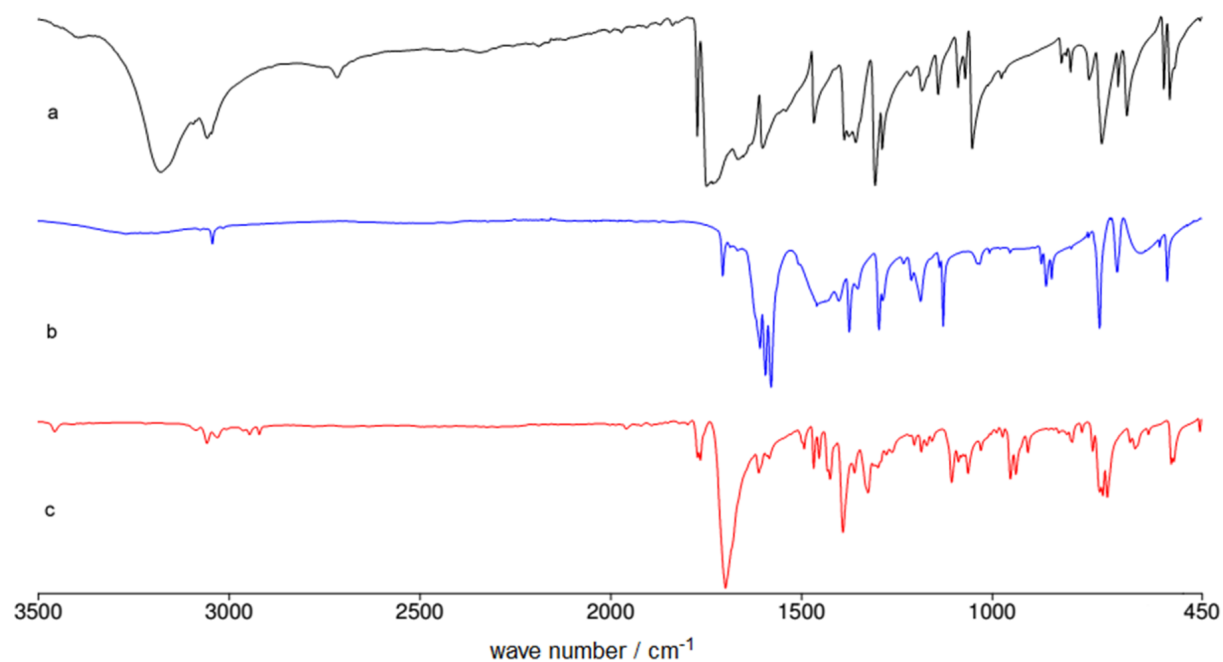
Figure 2: Ex situ IR spectroscopy of the reaction of **12** and benzyl bromide in the ball mill: a) phthalimide **12**; b) first step: phthalimide + K_2CO_3, 1 h milling; c) second step: addition of benzyl bromide, LAG DMF and further 1 h milling.

sium carbonate is capable of the deprotonation of the imides with pK_a values at least within the range of 8.3–9.9 units [30] under ball milling conditions.

Deprotonation of phthalimide in solution is usually carried out with the use of bases stronger than K_2CO_3 [31] and this difference in reactivity in comparison to solvent free conditions has a precedence in the application of weaker base in mechanochemical synthesis of triphenylphosphoranes [32]. Often DMF is used as solvent in imide alkylation reactions, which promotes S_N2 reactions [33] and its low volatility is advantageous over more environmentally friendly solvents which might be considered for LAG in mechanosynthesis.

A comparison of results with literature values demonstrates the benefits of mechanosynthesis. For instance, alkylation of theobromine (**14**) [34] in a microwave reactor in solution gives two side-products, an *O*-alkylated and a uracil ring-opened product (induced by base). The reaction selectivity is highly influenced by the solvent. The formation of the ring-opened product could be fully suppressed under mechanochemical conditions, due to the mild conditions and the absence of solvent. An additional advantage of the solvent-free milling procedure is that there is no need for tetrabutylammonium iodide as phase-transfer catalyst to increase the limited solubility of **14**.

The selectivity was observed for certain substrates. For example, the alkylation of phthalimide **12** with 1,4-bis(bromomethyl)benzene led to the formation of two products, namely **28** and **29**. By keeping the ratio of the alkyl halide reagent at two equivalents, ball milling afforded mainly the targeted monoalkylated product **28** (Table 3, entry 9). The regioselectivity of substrates with two nitrogen-sites available for alkylation could be also controlled by reagent ratio or choice of the alkyl halide. For instance in the reaction of uracil (**17**) or 7,8-dimethylallox-

azine (**36**). The required substrate **36** was prepared by mechanochemical condensation [35] of alloxane (**34**) and 4,5-dimethyl-1,2-phenylenediamine (**35**) in the presence of *p*-toluenesulfonic acid [36,37] (Scheme 3). The α-dione/α-diamine reaction proceeds in a similar manner and yield to the condensation reaction carried out under classical reaction conditions (1 M HCl, 60 °C, 30 min) [38]. Mechanochemical one-pot, two-step solid-state *N*-alkylation of **36** with benzyl bromide yielded 1,3-dibenzylalloxazine **39** in quantitative yield, whereas the reaction of **36** with less reactive ethyl bromide (four equivalents) under LAG conditions afforded bis- and mono-alkylated products **37** and **38** (in 62% overall yield), with 1,3-diethylalloxazine **37** as the major component (4:1 ratio). A change of the stoichiometry of reagents by milling with an equimolar amount of ethyl bromide resulted in the dominant formation of the mono-alkylated 1-ethyl product **38**.

The *N*-alkylated phthalimides **23** and **24**, which were prepared in the previous section were employed in solvent-free Gabriel synthesis of primary amines (Scheme 4). In these milling reactions, the hazardous hydrazine hydrate was replaced by 1,2-diaminoethane [39] and conversion to the corresponding benzylamines was quantitative within 1 h. As a proof of concept of reaction, *p*-methylbenzylamine was isolated in 41% yield in the form of acetamide **42**. In this way, a three-step, two-pot (A and B, Scheme 5) Gabriel synthesis of amines was carried out in a ball mill. The synthetically desired development of a three-step, one-pot mechanochemical Gabriel synthesis of amines could not be accomplished, as the complex reaction mixtures containing considerable amounts of various side products such as bisamide **43**.
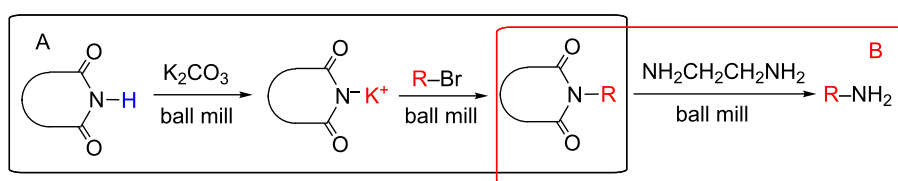
Computational section

To elucidate reasons for the observed regioselectivities, the reactions of uracil and 7,8-dimethylalloxazine with benzyl-
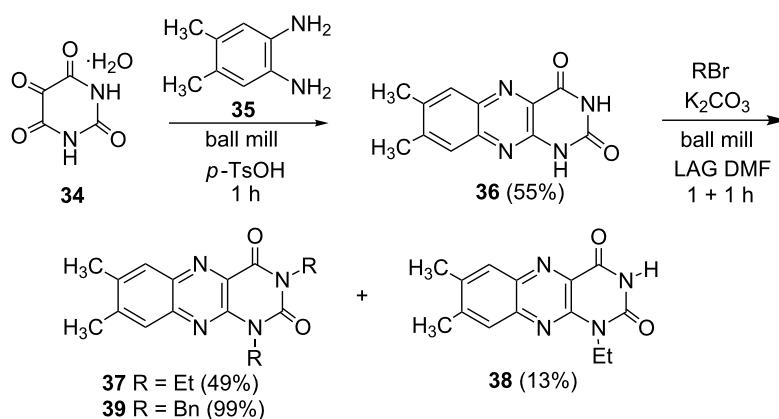
Scheme 3: Mechanosynthesis of 7,8-dimethylalloxazine (**36**) and its *N*-alkylation.
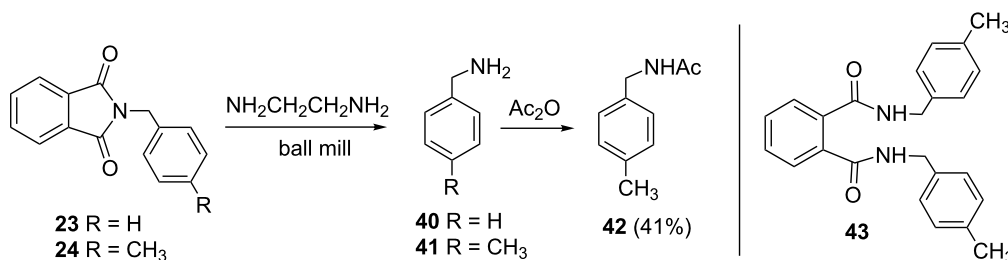
Scheme 4: Gabriel synthesis of amines in ball mill.

Scheme 5: Three-step, two-pot Gabriel synthesis of amines in ball mill.

amine and ethyl bromide were studied by DFT calculations using the B3LYP/6-311+G**//B3LYP/6-31G*+ZPVE method. The transition-state calculations of the S_N2 reaction of imides and bromides were used to determine the activation energies. It was found that for benzyl and ethyl bromides the activation energy differences are 2–3 kcal mol^{-1} in favor of the N1 positions in uracil and 7,8-dimethylalloxazine. These calculations are in good accordance with the experimentally observed results and could be further rationalized by the more nucleophilic character of these two imide N1 positions in comparison to the N3 positions.

Conclusion

We have shown that *N*-alkylation of imides could be effectively carried out by ball milling, affording the products in high yields. Effective in situ preparation of potassium phthalimide and its alkylation has a potential for the application in mechanochemical Gabriel synthesis of amines. This account illustrates that organic chemists should explore the advantages of mechanosynthesis and apply this method routinely for screening of the best conditions for various organic reactions.

Supporting Information

Supporting Information File 1

Additional experimental details, ^{1}H, ^{13}C NMR and IR spectra.
[http://www.beilstein-journals.org/bjoc/content/supplementary/1860-5397-13-169-S1.pdf]

Acknowledgements

References

1. Ballini, R. *Eco-Friendly Synthesis of Fine Chemicals;* RSC Green Chemistry Series; RSC: Cambridge, 2009.
2. Margetić, D. *Microwave Assisted Cycloaddition Reactions;* Nova Science Publishers: New York, 2011.
3. Albini, A.; Fagnoni, M.; Mella, M. *Pure Appl. Chem.* **2000,** *72,* 1321–1326. doi:10.1351/pac200072071321
4. Matsumoto, K.; Acheson, R. M., Eds. *Organic Synthesis at high pressures;* Wiley: New York, 1991.
5. Tanaka, K. *Solvent-free Organic Synthesis;* Wiley-VCH: Weinheim, 2003.
6. Margetić, D.; Štrukil, V. *Mechanochemical Organic Synthesis;* Elsevier: Amsterdam, 2016.
7. James, S. L.; Adams, C. J.; Bolm, C.; Braga, D.; Collier, P.; Friščić, T.; Grepioni, F.; Harris, K. D. M.; Hyett, G.; Jones, W.; Krebs, A.; Mack, J.; Maini, L.; Orpen, A. G.; Parkin, I. P.; Shearouse, W. C.; Steed, J. W.; Waddell, D. C. *Chem. Soc. Rev.* **2012,** *41,* 413–447. doi:10.1039/C1CS15171A
8. Margetić, D. *Kem. Ind.* **2005,** *54,* 351–358.
9. Glasovac, Z.; Trošelj, P.; Jušinski, I.; Margetić, D.; Eckert-Maksić, M. *Synlett* **2013,** *24,* 2540–2544. doi:10.1055/s-0033-1339876
10. Margetić, D.; Warrener, R. N. *J. Heterocycl. Chem.* **2014,** *51,* 1369–1379. doi:10.1002/jhet.2015
11. Margetić, D.; Trošelj, P.; Murata, Y. *Synth. Commun.* **2011,** *41,* 1239–1246. doi:10.1080/00397911.2010.481744

12. Margetić, D.; Butler, D. N.; Warrener, R. N. *Aust. J. Chem.* **2000,** *53,* 959–963. doi:10.1071/CH00129

13. Štrukil, V.; Margetić, D.; Igrc, M. D.; Eckert-Maksić, M.; Friščić, T. *Chem. Commun.* **2012,** *48,* 9705–9707. doi:10.1039/C2CC34013E

14. Đud, M.; Magdysyuk, O. V.; Margetić, D.; Štrukil, V. *Green Chem.* **2016,** *18,* 2666–2674. doi:10.1039/C6GC00089D

15. Waddell, D. C.; Thiel, I.; Bunger, A.; Nkata, D.; Maloney, A.; Clark, T.; Smith, B.; Mack, J. *Green Chem.* **2011,** *13,* 3156–3161. doi:10.1039/c1gc15594f

16. Nun, P.; Martin, C.; Martinez, J.; Lamaty, F. *Tetrahedron* **2011,** *67,* 8187–8194. doi:10.1016/j.tet.2011.07.056

17. Kaupp, G.; Schmeyers, J.; Boy, J. *J. Prakt. Chem.* **2000,** *342,* 269–280. doi:10.1002/(SICI)1521-3897(200003)342:3<269::AID-PRAC269>3.0. CO;2-0

18. Nun, P.; Pérez, V.; Calmés, M.; Martinez, J.; Lamaty, F. *Chem. – Eur. J.* **2012,** *18,* 3773–3779. doi:10.1002/chem.201102885

19. Swinburne, A. N.; Steed, J. W. *CrystEngComm* **2009,** *11,* 433–438. doi:10.1039/b817067c

20. Im, J.; Kim, J.; Kim, S.; Hahn, B.; Toda, F. *Tetrahedron Lett.* **1997,** *38,* 451–452. doi:10.1016/S0040-4039(96)02323-4

21. Beillard, A.; Golliard, E.; Gillet, V.; Bantreil, X.; Métro, T.-X.; Martinez, J.; Lamaty, F. *Chem. – Eur. J.* **2015,** *21,* 17614–17617. doi:10.1002/chem.201503472

22. Métro, T.-X.; Salom-Roig, X. J.; Reverte, M.; Martinez, J.; Lamaty, F. *Green Chem.* **2015,** *17,* 204–208. doi:10.1039/C4GC01416B

23. Fan, G.-P.; Liu, Z.; Wang, G.-W. *Green Chem.* **2013,** *15,* 1659–1664. doi:10.1039/C3GC40262B

24. Jaśkowska, J.; Kowalski, P. *J. Heterocycl. Chem.* **2008,** *45,* 1371–1375. doi:10.1002/jhet.5570450519

25. Morgan, M. S.; Tipson, R. S.; Lowy, A.; Baldwin, W. E. *J. Am. Chem. Soc.* **1944,** *66,* 404–407. doi:10.1021/ja01231a028

26. Briš, A.; Trošelj, P.; Margetić, D.; Flamigni, L.; Ventura, B. *ChemPlusChem* **2016,** *81,* 985–994. doi:10.1002/cplu.201600231

27. Friščić, T.; Trask, A. V.; Jones, W.; Motherwell, W. D. S. *Angew. Chem., Int. Ed.* **2006,** *45,* 7546–7550. doi:10.1002/anie.200603235

28. Tan, D.; Štrukil, V.; Mottillo, C.; Friščić, T. *Chem. Commun.* **2014,** *50,* 5248–5250. doi:10.1039/C3CC47905F

29. Salzberg, P. L.; Supniewski, J. V. *Org. Synth.* Wiley: New York, 1927; Vol. 7, pp 8–10. doi:10.15227/orgsyn.007.0008

30. http://www.chem.wisc.edu/areas/reich/pkatable/pKa_compilation-1-Willi ams.pdf.

31. Salzberg, P. L.; Supniewski, J. V. *Org. Synth.* Wiley: New York, 1941; Vol. Coll. Vol. 1, pp 119–121.

32. Balema, V. P.; Wiench, J. W.; Pruski, M.; Pecharsky, V. K. *J. Am. Chem. Soc.* **2002,** *124,* 6244–6245. doi:10.1021/ja017908p

33. Kurti, L.; Czako, B. *Strategic Applications of Named Reactions in Organic Synthesis,* 1st ed.; Elsevier: Oxford, 2005; pp 182–183.

34. MW reactor, K_2CO_3, TBAI, DMF, 80-100 °C: Skwierawska, A.; Pazik, A. *J. Inclusion Phenom. Macrocyclic Chem.* **2012,** *74,* 145–155. doi:10.1007/s10847-011-0093-5

35. Margetić, D.; Mann, D. A.; Warrener, R. N. *ARKIVOC* **2014,** *15,* 210–224. doi:10.3998/ark.5550190.0015.500

36. Berezovskii, V. M.; Eremenko, T. V. *Russ. Chem. Rev.* **1963,** *32,* 290–307. doi:10.1070/RC1963v032n06ABEH001343

37. Kuhn, R.; Rudy, H. *Ber. Dtsch. Chem. Ges. B* **1934,** *67,* 1826–1829. doi:10.1002/cber.19340671112

38. Rong, D.; Ye, H.; Boehlow, T. R.; D'Souza, V. T. *J. Org. Chem.* **1992,** *57,* 163–167. doi:10.1021/jo00027a031

39. Kanie, O.; Crawley, S. C.; Palcic, M. M.; Hindsgaul, O. *Carbohydr. Res.* **1993,** *243,* 139–164. doi:10.1016/0008-6215(93)84087-M

License and Terms

Selective enzymatic esterification of lignin model compounds in the ball mill

Ulla Weißbach, Saumya Dabral, Laure Konnert, Carsten Bolm[*] and José G. Hernández[*]

Abstract

A lipase-catalyzed esterification of lignin model compounds in the ball mill was developed combining the advantages of enzyme catalysis and mechanochemistry. Under the described conditions, the primary aliphatic hydroxy groups present in the substrates were selectively modified by the biocatalyst to afford monoesterified products. Amongst the tested lipases, CALB proved to be the most effective biocatalyst for these transformations. Noteworthy, various acyl donors of different chain lengths were tolerated under the mechanochemical conditions.

Introduction

Mechanochemical reactions, particularly those carried out by ball milling, have recently attracted attention of a wider scientific community, owing to the many advantages the excellent mixing inside the ball mill can offer [1]. Besides avoiding or minimizing the use of organic solvents as reaction media, chemical transformations by ball milling very often take place more rapidly than their solution-based counterparts. Furthermore, mechanochemical reactions are known to afford products in higher yields with minimal formation of byproducts. In addition to this, mechanochemical activation has resulted in the discovery of otherwise inaccessible products or materials [2,3].
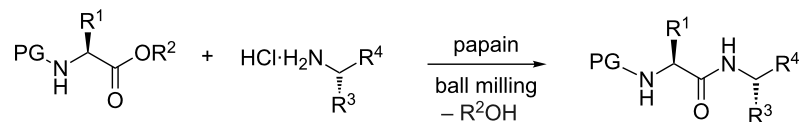
In organic chemistry, amino acids and short peptides are not only known for being stable under automated ball milling

conditions during their preparation [4], but also when applied as catalysts to perform stereoselective transformations [5-7]. Encouraged by these facts, we recently investigated the resilience of enzymes under ball milling conditions. The results from these studies have shown that biocatalysts such as cysteine and serine proteases tolerated the milling conditions and catalyzed the mechanoenzymatic peptide and amide bond formation after short milling times (Scheme 1a) [8].
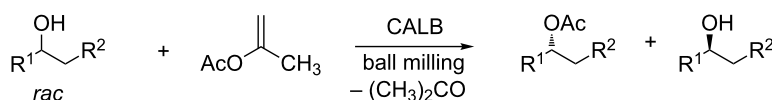
Similarly, immobilized lipases (triglycerol acylhydrolases EC 3.1.1.3) such as Amano lipase PS-IM from *Burkholderia cepacia* immobilized on diatomaceous earth and lipase B from *Candida antarctica* (expressed *in Aspergillus niger*) adsorbed on polymethacrylate beads (ca. 400 μm–600 μm in diameter)

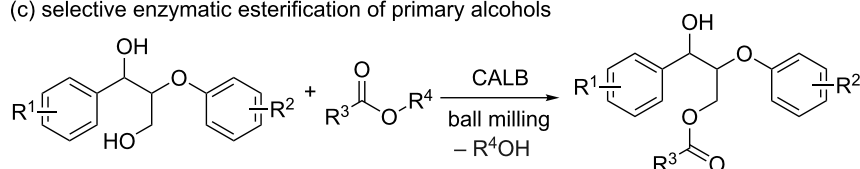**Scheme 1:** Enzymatic reactions under ball milling conditions.

[9], demonstrated to efficiently mediate the enzymatic kinetic resolution of secondary alcohols under solvent-free conditions in both mixer and planetary ball mills (Scheme 1b) [10]. Interestingly, this latter lipase (a commercial preparation known as Novozyme 345, hereinafter referred as CALB), showed the highest selectivity and could also be recycled by centrifugation and reused with little loss in stereoselectivity after four consecutive cycles [10].

Besides the above stated, one additional advantage of mechanochemistry includes the possibility to overcome solubility restrictions in chemical reactions involving reactants of poor solubility. This characteristic feature of mechanochemistry has proven fundamental while dealing with chemically induced cleavage of biomaterials such as lignin [11,12], cellulose [13-15] or chitin [16]. In regard to lignin chemistry, solution-based lignin depolymerization approaches or new applications of lignocellulose materials [17] often encounter solubility obstacles, forcing the alternate use of highly polar organic solvents, which thereby pose problems during metal-catalyzed transformations in the presence of strongly Lewis basic or donor solvents. In addition to this, miscibility and solubility of lignin samples in apolar matrices during the blending of lignin with polymeric materials is always a challenge.

To mitigate such solubility problems and to facilitate the utilization of lignin for various applications, efforts have been devoted to improve its lipophilicity, for instance through sulfation [18], silylation or esterification [19] of the aliphatic hydroxy and phenolic groups found in lignin. Chemical esterification of lignin [19-21] or its model compounds [22], using acetic anhydride in organic solvents such as DCM or pyridine have previously been reported to be effective in yielding new molecules and materials with higher hydrophobicity. However, controlling the degree of acetylation has not been an easy task, with the esterification process often resulting in a mixture of esters or fully esterified samples.

In this regard, enzymatic esterification thus can be an attractive alternative to specifically address one type of hydroxy groups in the complex lignin structure. This could not only allow a selective control over the degree of hydrophilicity in lignin samples, but would also help tailoring their potential applications. One interesting approach in this field of study involves the modification of lignins by selectively esterifying the primary alcohols present in the biopolymer (Figure 1a), leaving untouched the phenolic and secondary alcohol functionalities, given that these functional groups have been associated with the biopolymer's antioxidant, antibacterial and sun protection properties [17,23,24]. Motivated by the aforementioned scenario and in line with our research interest on studying the compatibility of biocatalysts and mechanochemical milling, we decided to investigate the enzymatic esterification of lignin model compounds in the ball mill (Scheme 1c). The results of this proof-of-concept study are presented here.

Figure 1: (a) Molecular representation of lignin. (b) Lignin model compound *erythro*-**1a**.
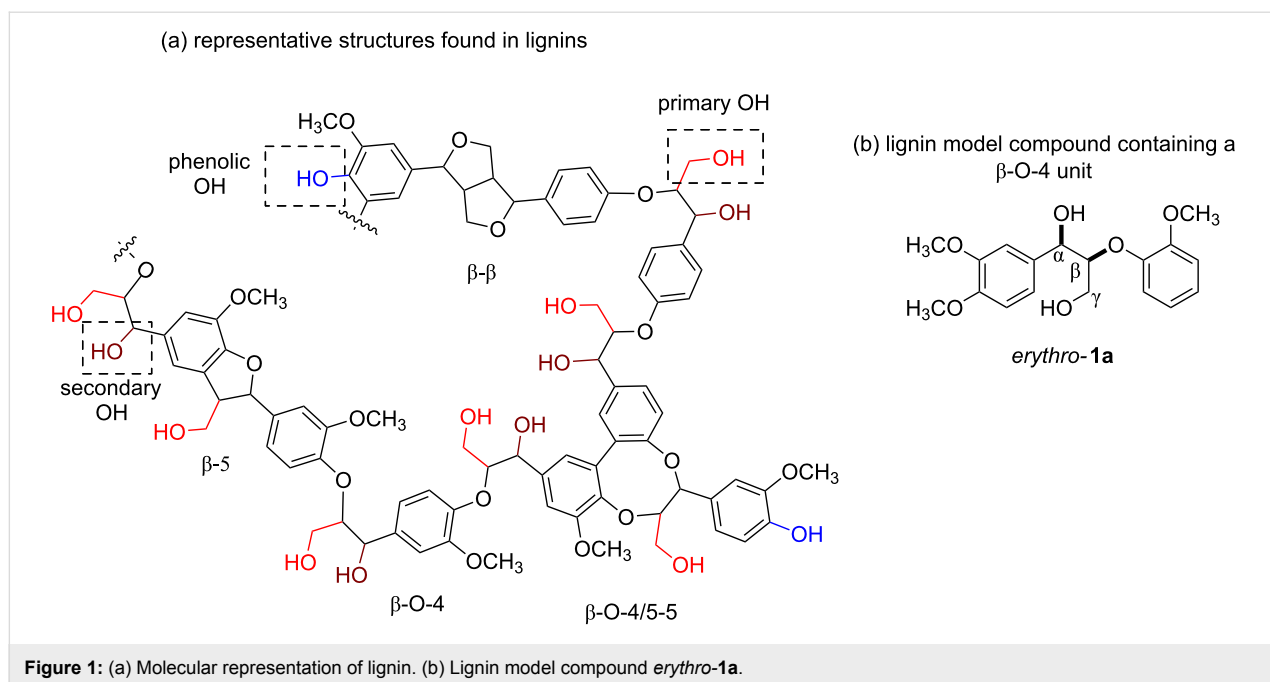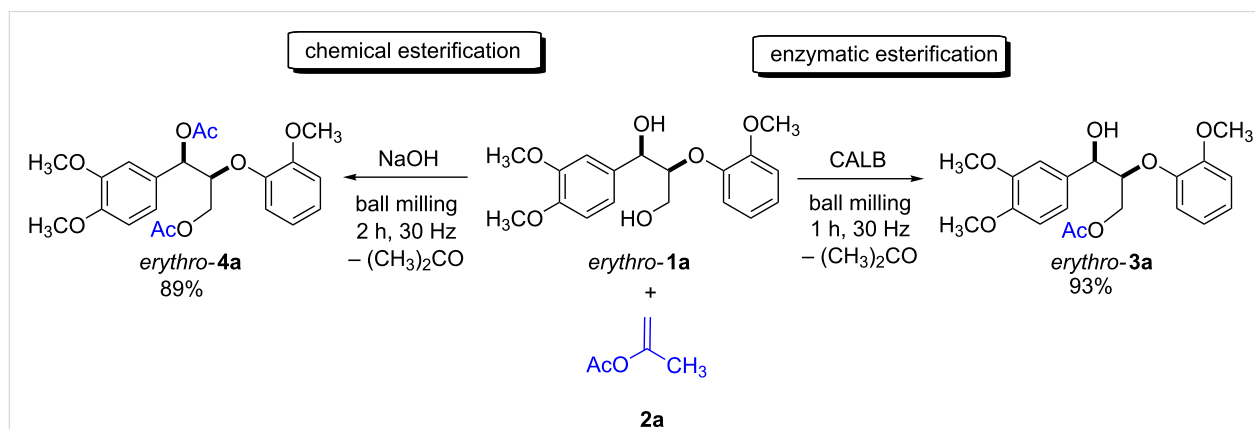
Results and Discussion

Due to the high complexity of the lignin structure, which often presents a challenge during the product composition analysis, the use of lignin model compounds to monitor preliminary research advancements is a common practice [25-29]. Thus, for this investigation various dimeric compounds containing the β-O-4 linkage, primary and secondary hydroxy groups as well as several methoxy/phenolic moieties, were used. To begin with, we selected *erythro*-**1a** as a model compound to study the enzymatic esterification reactions in the ball mill (Scheme 2).

Based on our previous work [10], isopropenyl acetate (**2a**), a non-reversible acyl donor, was chosen as the acetylating agent.

Milling a mixture of *erythro*-**1a** and **2a** for 2 h at 30 Hz did not afford any product, and only the reactants were observed by ^{1}H NMR spectroscopy. Repeating the experiment in the presence of 30 mg of the immobilized lipase CALB led to a total conversion of the *erythro*-**1a** after just 1 h. Purification of the product by column chromatography afforded the monoacetylated *erythro*-**3a** in 93% yield (Scheme 2; right). To corroborate the role of the biocatalyst in the esterification, the experiment was repeated with sodium hydroxide in place of CALB. Consequently, after 2 h of milling the reaction only generated the diacetylated product *erythro*-**4a** (Scheme 2; left). These results reflect the high selectivity of the biocatalyst for primary hydroxy groups. In nature, lipases catalyze the hydrolysis of

Scheme 2: Chemical and enzymatic esterification of *erythro*-**1a** with isopropenyl acetate (**2a**) in the ball mill. Reaction conditions: *erythro*-**1a** (50 mg, 0.15 mmol), **2a** (0.60 mmol), CALB (30 mg of immobilized enzyme) or NaOH (12 mg, 0.30 mmol), 10 mL ZrO$_2$ milling jar, 6 ZrO$_2$ milling balls (5 mm in diameter).

triglycerides, and are known for acting preferentially at the terminal position of triacylglycerol derivatives [30]. It is worth mentioning here that, even when *erythro*-**1a** was milled with an excess of acyl donor for longer time, CALB yielded exclusively the monoacetylated product *erythro*-**3a**.

Further screening of the reaction parameters revealed that lowering the amount of acyl donor was doable, although longer milling times were required. Similarly, the effect of the number of milling balls, frequency of milling, reaction time and additives was also investigated (Table S1 in Supporting Information File 1). In addition to this, the catalytic activity of a number of other lipases was studied (Table 1).

Table 1: Influence of various enzymes on the esterification of *erythro*-**1a** with isopropenyl acetate (**2a**) in the ball mill.[a]

Entry	Enzyme	1a:3a (%)[b]
1[c]	CALB	0:100
2	CALA	90:10
3	PS-IM	90:10
4	lipase A	100:0

[a]Reaction conditions: *erythro*-**1a** (50 mg, 0.15 mmol), enzyme (30 mg), **2a** (0.6 mmol), 10 mL ZrO$_2$ milling jar, 6 ZrO$_2$ milling balls (5 mm in diameter), milling time 2 h, milling frequency 30 Hz. [b]Determined by ^{1}H NMR spectroscopy. [c]Milling time 1 h. CALB (lipase B from *Candida antarctica* (expressed in *Aspergillus niger*) adsorbed on polymethacrylate beads, known also as Novozyme 345); CALA (lipase A from *Candida antarctica,* immobilized on Immobead 150, recombinant from *Aspergillus oryzae*); PS-IM (Amano lipase from *Burkholderia cepacia* immobilized on diatomaceous earth); Lipase A (Amano lipase A from *Aspergillus niger*).

Amongst the commercially available lipases, CALA (lipase A from *Candida antarctica*, immobilized on Immobead), immobilized lipase from *Burkholderia cepacia* (PS-IM) and lipase A from *Aspergillus niger* were tested. Firstly, hoping to find differences between the two hydrolases derived from *Candida antarctica*, an experiment using CALA was conducted. Despite CALB and CALA being produced by the same yeast, the latter proved less active at catalyzing the esterification of *erythro*-**1a** (Table 1, entry 2). This difference in reactivity between both of the lipases has been documented previously in the literature [31]. Comparably, lipase PS-IM, which has been reported to facilitate the acetylation of secondary β-nitro alcohols [32], and proved to be stable under ball milling conditions [10] exhibited lower catalytic activity than CALB (Table 1, entry 3). However, in both cases the alternative biocatalysts also afforded the monoacetylated dilignol derivative *erythro*-**3a**. Finally, lipase A showed no conversion of the substrate, which could be explained by its poor recognition of **1a** (Table 1, entry 4). Furthermore, a possible reason could be the reduced stability of the non-immobilized lipase when subjected to mechanochemical stress.

In the preliminary results, isopropenyl acetate (**2a**) proved highly efficient for the enzyme-catalyzed selective esterification of the model compound *erythro*-**1a**, partly due to the non-reversibility of the reaction. However, isopropenyl esters of carboxylic acids are, in general, not readily available. Therefore, in order to find alternative acyl donors for the biocatalyst in the ball mill, a series of acylating agents was screened (Table 2) [33].

Table 2: Screening of acyl donors for the selective monoacetylation of dilignol *erythro*-**1a**.[a]

Entry	R	Milling time (min)	1a:3a (%)[b]
1	isopropenyl (**2a**)	120	0:100
2	vinyl (**2b**)	120	6:94
3	phenyl (**2c**)	120	7:93
4	ethyl (**2d**)	120	70:30
5	isopropyl (**2e**)	120	66:34
6	allyl (**2f**)	120	63:37
7	*tert*-butyl (**2g**)	120	98:2
8[c]	H (**2h**)	90	100:0

[a]Reaction conditions: *erythro*-**1a** (50 mg, 0.15 mmol), CALB (30 mg of immobilized enzyme), acyl donor (0.60 mmol), 10 mL ZrO$_2$ milling jar, 6 ZrO$_2$ milling balls (5 mm in diameter). [b]Determined by ^{1}H NMR spectroscopy. [c]10 equiv of **2h** were used.

Out of all the acyl donors tested, vinyl acetate (**2b**) and phenyl acetate (**2c**) were recognized and transferred by the lipase CALB to the acceptor *erythro*-**1a**, affording selectively the product *erythro*-**3a** (Table 2, entries 2 and 3). Notably, ethyl acetate (**2d**), isopropyl acetate (**2e**) and allyl acetate (**2f**) were suitable for the enzymatic esterification of *erythro*-**1a** as well, although to a lesser extent (Table 2, entries 4–6). Finally, lower and no reactivity was observed using *tert*-butyl acetate (**2g**) and acetic acid (**2h**) as acyl donor, respectively (Table 2, entries 7 and 8).

Having determined the best reaction conditions for the selective enzymatic acetylation of the *erythro*-**1a** in the ball mill, the protocol was applied to other β-O-4 model compounds (Scheme 3).

In general, all the substrates **1a–h** generated the monoacetylated derivatives, and the reactions occurred regioselectively at the primary hydroxy group of the model compounds. The regioselectivity of the reaction was further confirmed after the milling of isopropenyl acetate (**2a**) and the monolignol **1i**, only containing a benzylic alcohol. After the standard milling time, analysis of the reaction mixture by ¹H NMR spectroscopy showed no product formation.

Moreover, under the standard reaction conditions, it was observed that the model compound *threo*-**1b** reacted slower in comparison to its diastereomer *erythro*-**1a**. After 2 h of milling, the product *threo*-**3b** was isolated in 45% yield (Scheme 3). These results highlight the importance of the stereochemistry of the substrates when interacting with the chiral biocatalyst. The reaction of the *erythro*-diastereoisomer **1c** showed comparable reactivity to *erythro*-**1a**, and the corresponding monoacetylated product *erythro*-**3c** could be isolated in 89% yield (Scheme 3). On the other hand, its diastereomer *threo*-**1d** was much less reactive and only trace quantities of *threo*-**3d** could be isolated. This difference in reactivity, which follows the trend previously observed for the pair *erythro*-**1a** and *threo*-**1b**, could have stemmed from matched/mismatched interactions of the diastereomeric diols and the chiral biocatalyst. Similarly, the unsubstituted model compound **1e** reacted smoothly to give **3e** in 92% yield. Purification of **3e** was done by filtration through a pad of celite, since it proved unstable towards standard purification procedures by column chromatography on silica gel.

Noteworthy is the low reactivity of the substrate **1f** bearing a phenolic group in its structure. In this case, only trace quantities of the monoacetylated product **3f** were observed after 2 h of milling and no esterification was seen to occur in the phenolic group. Initially, it was hypothesized that the presence of a phenolic functionality present in **1f** could have inhibited the

lipase activity or perhaps caused some degree of denaturation in the enzyme. To test this hypothesis, control experiments using *erythro*-**1a**, **2a** and CALB in the presence of phenol (1.0 equiv) and phenol derivatives (guaiacol, 3-methoxyphenol, etc.) were carried out. In most cases, the presence of the additives had no negative effect on the performance of CALB (for details see Table S2 in Supporting Information File 1). Only the presence of 2,2'-biphenol seemed to have slowed down the acetylation of *erythro*-**1a**. A plausible explanation could be the nature of the 2,2'-biphenol moiety, which could have acted as a ligand interfering with the enzyme.

The resilience of CALB to phenols is in agreement with the high reactivity observed when phenyl acetate (**2c**), *erythro*-**1a** and CALB were milled (Table 2, entry 3), and formation of phenol was expected as a byproduct of the reaction. Hence, the lower reactivity of **1f** could have been a consequence of aggregation of the substrate or possible changes in its conformation. This could have reduced the affinity of CALB for **1f** compared to the non-phenolic counterparts. Additionally, milling experiments between **1f** and **2a**, where twice the amount of the enzyme was added in small portions, afforded the same negative result. Finally, the screening of the more hindered lignin model compounds **1g** and **1h** revealed that these substrates also reacted well in the ball mill, generating the monoacetylated derivatives **3g** and **3h** in 68% and 82% yield, respectively (Scheme 3).

To test the catalytic efficiency of CALB in the ball mill, we decided to evaluate the performance of the biocatalyst in the esterification of *erythro*-**1a** using saturated fatty esters as acyl donors (Scheme 4).

Because of the excellent affinity of CALB for vinyl acetate (**2b**, Table 2, entry 2), and due to the commercial availability of vinyl esters in contrast to their isopropenyl analogues [33], vinyl esters **5a–c** were chosen. Pleasingly, under the optimized milling reaction conditions (2 h, 30 Hz), *erythro*-**1a** and **5a** afforded the monoacetylated dilignol derivative **6a** in 74% yield (Scheme 4). On the other hand, lengthening the carbon chain of the acyl donor (e.g., **5b** and **5c**) resulted in slowing down the reaction speed. However, an increase in the milling time from 2 h to 6 h proved beneficial and both the long-chain fatty ester dilignol derivatives **6b,c** were isolated in good yields (Scheme 4).

Conclusion

In summary, the lipase-catalyzed esterification of lignin model compounds under mechanochemical conditions was investigated. Experimental parameters such as milling time, milling frequency, presence of additives and different acyl donors were studied in detail. Amongst the various biocatalysts tested, the
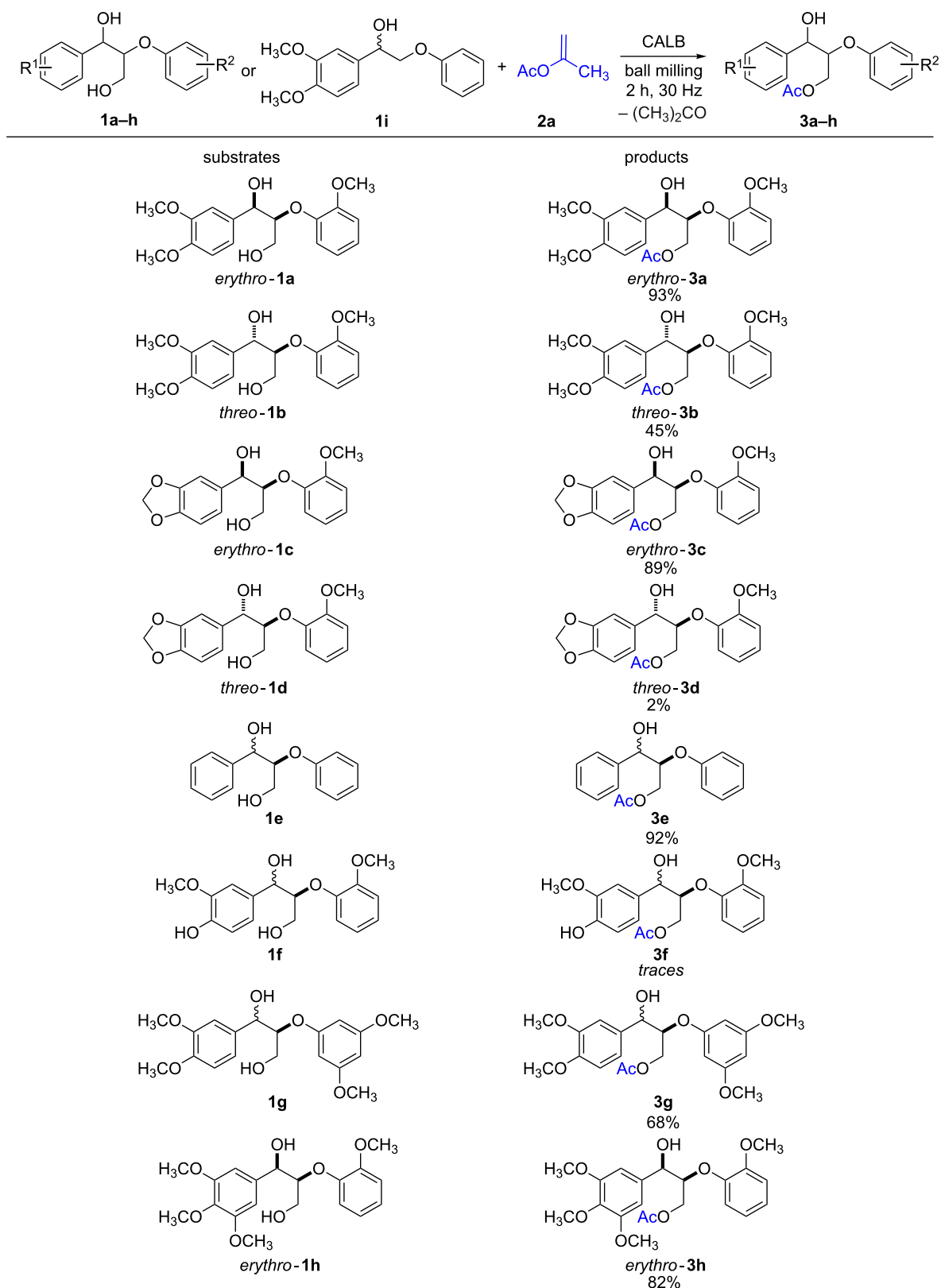
Scheme 3: CALB-catalyzed esterification of lignin model compounds in the ball mill.
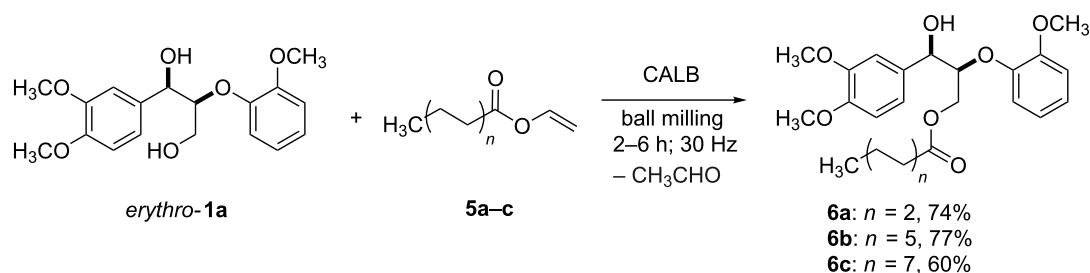
Scheme 4: Selective esterification of *erythro*-**1a** using long-chain vinyl esters as acyl donors in the ball mill.

lipase CALB proved superior in terms of catalytic activity and stability in the ball mill. The high catalytic activity of the enzyme facilitated the monoacetylation of β-O-4 lignin model compounds in good to high yields. Additionally, the biocatalyst exhibited higher preference for the aliphatic primary hydroxy group at the γ-position of the substrates. The enzymatic acetylation protocol was easily transferred to the esterification of the model substrate using long-chain fatty esters. This result is of high importance for introducing, in a controlled manner, various degrees of hydrophobicity to the substrates. This possibility is anticipated to be beneficial for future research initiatives employing lignin samples. Along these lines, it is important to comment on the lower reactivity towards the esterification of the substrate containing a phenolic substituent **1f**. Although it is known that lignin samples contain units bearing aromatic phenols, these phenolic fragments are mostly located at the terminal sides of the biopolymer. Therefore, enzymatically addressing the centrally-located primary aliphatic hydroxyl content of lignins is still highly possible. This strategy is expected to allow the preservation of the phenolic and benzylic alcohol contents in modified lignins, in order to keep the antibacterial and antioxidant activities of this biopolymer.

Experimental

All reagents were obtained from commercial suppliers and used without further purification. All lignin model compounds were prepared following the reported procedures [25,34].

Analytical TLC was performed on silica gel plates, and the products were visualized by UV detection (wavelength 254 nm). Ball milling experiments were conducted using a Fritsch Mini-mill PULVERISETTE 23. NMR measurements were performed on Bruker AV 400 or AV 600 instruments. High-resolution mass spectra (HRMS) were measured using a Thermo Scientific LTQ Orbitrap XL with positive ion mode.

Enzymatic acetylation of *erythro*-**1a** with CALB in the ball mill

A mixture of *erythro*-**1a** (50 mg, 0.15 mmol), acyl donor **2** (0.60 mmol) and CALB (30 mg of the immobilized enzyme) was milled for 2 h to 6 h at 30 Hz in a 10 mL ZrO_2 milling jar loaded with 6 ZrO_2 milling balls (5 mm in diameter). After the milling was stopped, the reaction mixture was recovered from the milling jar, supported on silica gel and the product was purified by silica column chromatography.

Supporting Information

Supporting Information File 1

Experimental procedures, optimization tables, characterization data and NMR spectra.
[http://www.beilstein-journals.org/bjoc/content/supplementary/1860-5397-13-173-S1.pdf]

Acknowledgements

References

1. James, S. L.; Adams, C. J.; Bolm, C.; Braga, D.; Collier, P.; Friščić, T.; Grepioni, F.; Harris, K. D. M.; Hyett, G.; Jones, W.; Krebs, A.; Mack, J.; Maini, L.; Orpen, A. G.; Parkin, I. P.; Shearouse, W. C.; Steed, J. W.; Waddell, D. C. *Chem. Soc. Rev.* **2012,** *41,* 413–447. doi:10.1039/C1CS15171A
2. Hernández, J. G.; Bolm, C. *J. Org. Chem.* **2017,** *82,* 4007–4019. doi:10.1021/acs.joc.6b02887

3. Do, J.-L.; Friščić, T. *ACS Cent. Sci.* **2017,** *3,* 13–19. doi:10.1021/acscentsci.6b00277

4. Métro, T.-X.; Colacino, E.; Martinez, J.; Lamaty, F. Amino Acids and Peptides in Ball Milling. *Ball Milling Towards Green Synthesis: Applications, Projects, Challenges;* The Royal Society of Chemistry: Cambridge, 2015; pp 114–150. doi:10.1039/9781782621980-00114

5. Rodríguez, B.; Bruckmann, A.; Bolm, C. *Chem. – Eur. J.* **2007,** *13,* 4710–4722. doi:10.1002/chem.200700188

6. Hernández, J. G.; Juaristi, E. *J. Org. Chem.* **2011,** *76,* 1464–1467. doi:10.1021/jo1022469

7. Hernández, J. G.; Avila-Ortiz, C. G.; Juaristi, E. Useful Chemical Activation Alternatives in Solvent-Free Organic Reactions. In *Comprehensive Organic Synthesis,* 2nd ed.; Molander, G. A.; Knochel, P., Eds.; Elsevier BV, 2014; pp 287–314. doi:10.1016/B978-0-08-097742-3.00935-6

8. Hernández, J. G.; Ardila-Fierro, K. J.; Crawford, D.; James, S. L.; Bolm, C. *Green Chem.* **2017,** *19,* 2620–2625. doi:10.1039/C7gc00615b

9. Wiemann, L. O.; Nieguth, R.; Eckstein, M.; Naumann, M.; Thum, O.; Ansorge-Schumacher, M. B. *ChemCatChem* **2009,** *1,* 455–462. doi:10.1002/cctc.200900199

10. Hernández, J. G.; Frings, M.; Bolm, C. *ChemCatChem* **2016,** *8,* 1769–1772. doi:10.1002/cctc.201600455

11. Kleine, T.; Buendia, J.; Bolm, C. *Green Chem.* **2013,** *15,* 160–166. doi:10.1039/C2GC36456E

12. Calvaruso, G.; Clough, M. T.; Rinaldi, R. *Green Chem.* **2017,** *19,* 2803–2811. doi:10.1039/c6gc03191a

13. Hick, S. M.; Griebel, C.; Restrepo, D. T.; Truitt, J. H.; Buker, E. J.; Bylda, C.; Blair, R. G. *Green Chem.* **2010,** *12,* 468–474. doi:10.1039/B923079C

14. Boissou, F.; Sayoud, N.; De Oliveira Vigier, K.; Barakat, A.; Marinkovic, S.; Estrine, B.; Jérôme, F. *ChemSusChem* **2015,** *8,* 3263–3269. doi:10.1002/cssc.201500700

15. Rechulski, M. D. K.; Käldström, M.; Richter, U.; Schüth, F.; Rinaldi, R. *Ind. Eng. Chem. Res.* **2015,** *54,* 4581–4592. doi:10.1021/acs.iecr.5b00224

16. Chen, X.; Yang, H.; Zhong, Z.; Yan, N. *Green Chem.* **2017,** *19,* 2783–2792. doi:10.1039/c7gc00089h

17. Qian, Y.; Qiu, X.; Zhu, S. *ACS Sustainable Chem. Eng.* **2016,** *4,* 4029–4035. doi:10.1021/acssuschemeng.6b00934

18. Prinsen, P.; Narani, A.; Hartog, A. F.; Wever, R.; Rothenberg, G. *ChemSusChem* **2017,** *10,* 2267–2273. doi:10.1002/cssc.201700376

19. Buono, P.; Duval, A.; Verge, P.; Averous, L.; Habibi, Y. *ACS Sustainable Chem. Eng.* **2016,** *4,* 5212–5222. doi:10.1021/acssuschemeng.6b00903

20. Zhao, X.; Huang, A.; Zhang, Y.; Yang, M.; Chen, D.; Huang, K.; Hu, H.; Huang, A.; Qin, X.; Feng, Z. *J. Appl. Polym. Sci.* **2017,** *134,* 44276–44289. doi:10.1002/app.44276

21. Hulin, L.; Husson, E.; Bonnet, J.-P.; Stevanovic, T.; Sarazin, C. *Molecules* **2015,** *20,* 16334–16353. doi:10.3390/molecules200916334

22. Lohr, T. L.; Li, Z.; Marks, T. J. *ACS Catal.* **2015,** *5,* 7004–7007. doi:10.1021/acscatal.5b01972

23. Pan, X.; Kadla, J. F.; Ehara, K.; Gilkes, N.; Saddler, J. N. *J. Agric. Food Chem.* **2006,** *54,* 5806–5813. doi:10.1021/jf0605392

24. Qian, Y.; Qiu, X.; Zhu, S. *Green Chem.* **2015,** *17,* 320–324. doi:10.1039/c4gc01333f

25. Buendia, J.; Mottweiler, J.; Bolm, C. *Chem. – Eur. J.* **2011,** *17,* 13877–13882. doi:10.1002/chem.201101579

26. Dabral, S.; Mottweiler, J.; Rinesch, T.; Bolm, C. *Green Chem.* **2015,** *17,* 4908–4912. doi:10.1039/C5GC00186B

27. Mottweiler, J.; Puche, M.; Räuber, C.; Schmidt, T.; Concepción, P.; Corma, A.; Bolm, C. *ChemSusChem* **2015,** *8,* 2106–2113. doi:10.1002/cssc.201500131

28. Mottweiler, J.; Rinesch, T.; Besson, C.; Buendia, J.; Bolm, C. *Green Chem.* **2015,** *17,* 5001–5008. doi:10.1039/C5GC01306B

29. Dabral, S.; Hernández, J. G.; Kamer, P. C. J.; Bolm, C. *ChemSusChem* **2017,** *10,* 2707–2713. doi:10.1002/cssc.201700703

30. Stergiou, P.-Y.; Foukis, A.; Filippou, M.; Koukouritaki, M.; Parapouli, M.; Theodorou, L. G.; Hatziloukas, E.; Afendra, A.; Pandey, A.; Papamichael, E. M. *Biotechnol. Adv.* **2013,** *31,* 1846–1859. doi:10.1016/j.biotechadv.2013.08.006

31. Kirk, O.; Christensen, M. W. *Org. Process Res. Dev.* **2002,** *6,* 446–451. doi:10.1021/op0200165

32. Xu, F.; Wang, J.; Liu, B.; Wu, Q.; Lin, X. *Green Chem.* **2011,** *13,* 2359–2361. doi:10.1039/C1GC15417F

33. Paravidino, M.; Hanefeld, U. *Green Chem.* **2011,** *13,* 2651–2657. doi:10.1039/c1gc15576h

34. Rahimi, A.; Azarpira, A.; Kim, H.; Ralph, J.; Stahl, S. S. *J. Am. Chem. Soc.* **2013,** *135,* 6415–6418. doi:10.1021/ja401793n

Mechanochemical synthesis of thioureas, ureas and guanidines
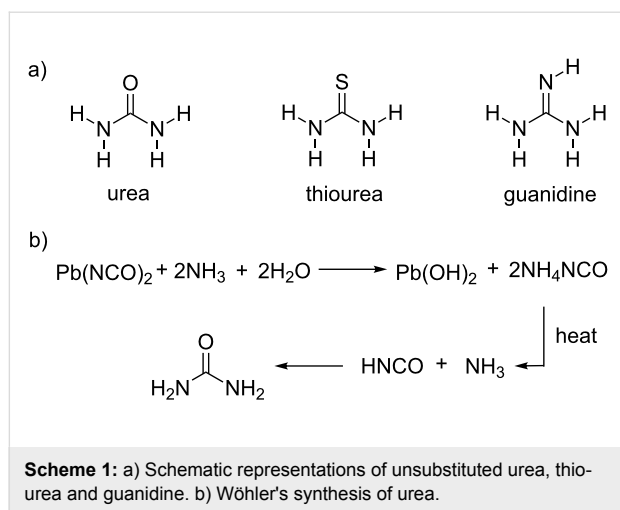
Vjekoslav Štrukil

Abstract

In this review, the recent progress in the synthesis of ureas, thioureas and guanidines by solid-state mechanochemical ball milling is highlighted. While the literature is abundant on their preparation in conventional solution environment, it was not until the advent of solvent-free manual grinding using a mortar and pestle and automated ball milling that new synthetic opportunities have opened. The mechanochemical approach not only has enabled the quantitative synthesis of (thio)ureas and guanidines without using bulk solvents and the generation of byproducts, but it has also been established as a means to develop "click-type" chemistry for these classes of compounds and the concept of small molecule desymmetrization. Moreover, mechanochemistry has been demonstrated as an effective tool in reaction discovery, with emphasis on the reactivity differences in solution and in the solid state. These three classes of organic compounds share some structural features which are reflected in their physical and chemical properties, important for application as organocatalysts and sensors. On the other hand, the specific and unique nature of each of these functionalities render (thio)ureas and guanidines as the key constituents of pharmaceuticals and other biologically active compounds.

Introduction

The urea molecule played the central role in the development of organic chemistry since its first documented synthesis in 1828 when the German chemist Friedrich Wöhler prepared it starting from ammonium cyanate (Scheme 1) [1]. This simple, yet intriguing transformation of an inorganic chemical into an organic product, at that time only available from living organisms, was in contradiction with the prevailing doctrine of vitalism, which was in the years to come abandoned enabling a rapid evolution of organic chemistry in the 19th century.
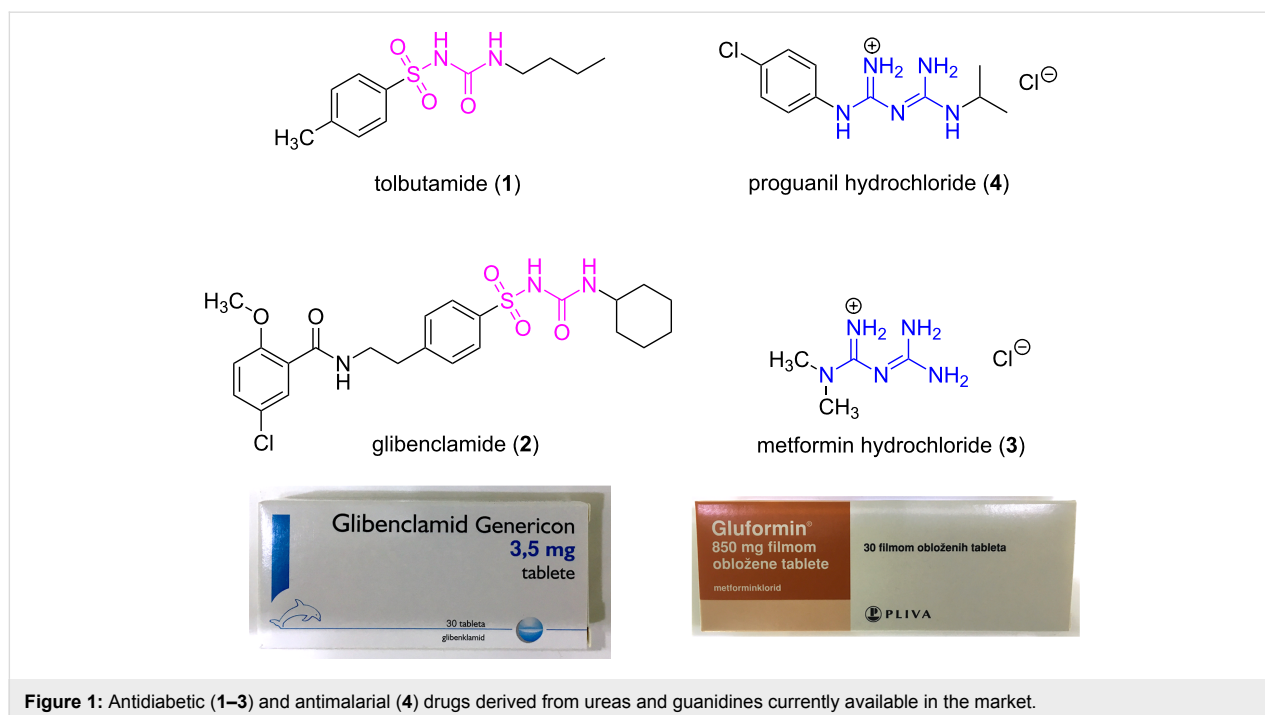
During the 20th century, synthetic routes to (thio)ureas and guanidines and their properties were extensively investigated, especially in terms of biological activity [2-5]. Most notable examples of pharmaceutically relevant ureas and guanidines avail-

Scheme 1: a) Schematic representations of unsubstituted urea, thiourea and guanidine. b) Wöhler's synthesis of urea.

Green Chemistry, which aims at turning chemical reactions into more effective and sustainable processes with high conversions of the starting materials and no byproduct formation, has emerged as a mainstream paradigm in chemical research in the past 25 years. Anastas and Warner have proposed 12 Principles of Green Chemistry as a guide to help making chemical processes more environmentally friendly [13,14]. Many of the requirements contained in these principles (e.g., prevention, atom economy, energy efficiency, catalysis, safe synthesis) can be met if the reactions are transferred from the solution into the solid state. In a typical solid state organic synthesis, reactants are simply ground together in a mortar using a pestle, where the mechanical force is exerted by a hand (manual grinding) [15]. Whereas mechanochemistry [16], at least on the laboratory scale, is usually associated with mortar and pestle processing, this approach suffers from several issues, such as non-constant energy input leading to inhomogeneous mixing and transfer of mechanical energy, irreproducibility, exposure to air/humidity (unless the experiment is carried out in a glovebox) and finally the compromised safety for the researcher. These drawbacks can be eliminated or substantially reduced by the application of automated ball mills. The precise control of parameters such as reaction time, milling frequency, number and size of milling balls, type of milling media (stainless steel, zirconia, teflon, plastic) and even milling atmosphere allows reproducible solid state syntheses in such instruments. The progress made over the past 15 years has transformed grinding or milling from a purely physical tool for mechanical processing into a synthetic method of choice when one wishes to conduct chemical reactions in an
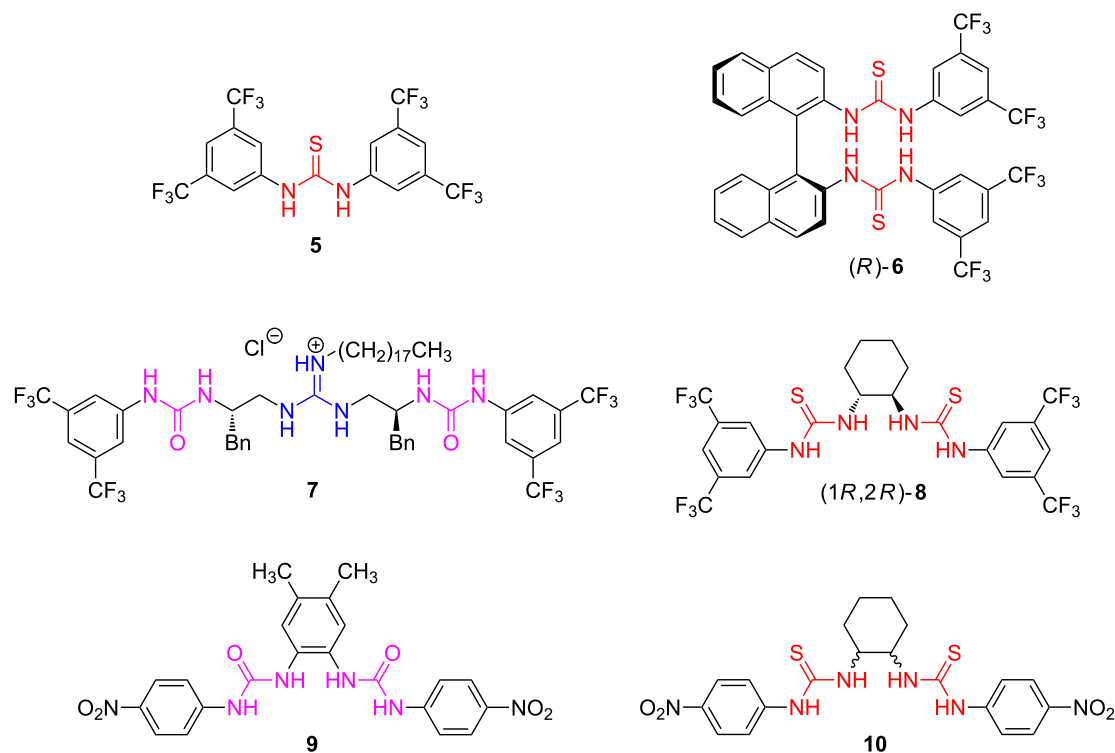
able on the market are shown in Figure 1. The antidiabetic drugs tolbutamide (**1**) and glibenclamide (**2**), which belong to the class of sulfonylureas, and guanidine-derived metformin (**3**) are among the top selling oral hypoglycemics globally. Proguanil (**4**), a biguanide derivative, is widely prescribed to treat malaria, a disease that took over 430 000 lives in 2015 [6].

In the past 20 years, molecules with incorporated (thio)urea and guanidine subunits, due to their ability to coordinate other molecules and ions via N–H hydrogen bonding, have also been considered as organocatalysts and anion sensors [7-12]. In Scheme 2, several examples of (thio)urea- and guanidine-based organocatalysts are shown.

Figure 1: Antidiabetic (**1–3**) and antimalarial (**4**) drugs derived from ureas and guanidines currently available in the market.

Scheme 2: The structures of some representative (thio)urea and guanidine organocatalysts **5**–**8** and anion sensors **9** and **10**.

environmentally-friendly fashion [17,18]. In this respect, there have been several turning points in the development of solid-state mechanochemistry. The first key discovery was made by Jones et al. who discovered the rate-accelerating effect of adding small catalytic quantities of a liquid phase to a mixture treated by manual grinding or ball milling [19]. What was in the beginning termed as "solvent-drop grinding" (SDG) eventually became "liquid-assisted grinding" or LAG, now a well-established method for improving the outcome of mechanochemical reactions [20]. In continuation of this research, Friščić et al. introduced the so called "ion and liquid-assisted grinding" or ILAG by recognizing the effect of cations such as Na⁺, K⁺ or NH₄⁺ or anions like Cl⁻, NO₃⁻ and SO₄²⁻ on the formation of polymorphs during LAG synthesis of metal-organic frameworks [21]. Recently, Jones et al. employed polymeric macromolecular catalysts, e.g., PEG 200 and PEG 10000 as solid auxiliaries to enhance crystallization under LAG mechanochemical conditions in "polymer and liquid-assisted grinding" or POLAG [22,23]. While the focus in these investigations has been on the improvement of the macroscopic parameters such as the reaction yield, another aspect of mechanochemical reactions that is becoming important for further development in the field is the mechanism of solid-state reactions. To be able to see beyond the usual ex situ analyses of mechanochemical reactions, modifications of the milling equip-

ment had to be made. Since these are solid-state reactions, powder X-ray diffraction (PXRD) using synchrotron radiation was suitable as the analytical tool to monitor the changes during ball milling on a microscopic level in real time [24]. In this way, the first in situ observations of mechanochemical reactions were performed which has led to the discovery of reactive intermediates, new phases and novel topologies in systems previously studied only by ex situ analyses [25,26]. To overcome the inability of PXRD to provide structural information on amorphous materials, a method based on real time in situ Raman spectroscopy was devised [27]. Finally, these two in situ techniques have been successfully merged to allow simultaneous monitoring of mechanochemical reactions by PXRD and Raman spectroscopy [28,29].

Review
Mechanochemical synthesis of (thio)ureas
Thioureas
In a paper by Kaupp et al. a study on the reactivity of gaseous and solid amines with solid isothiocyanates was described [30]. The authors carried out gas–solid reactions via vapour digestion and solid–solid reactions by means of ball milling. To ensure that the investigated reactions were genuine solid-state processes, in some cases the milling was performed at low temperatures (−30 °C) using an in-house ball mill equipped with a

cooling jacket. As isothiocyanate component, liquid phenyl iso-thiocyanate and solid methyl, 1-naphthyl, 4-bromophenyl and 4-nitrophenyl isothiocyanates were screened. While ammonia, methylamine and dimethylamine were selected as gaseous amines and quantitatively afforded thioureas at pressures of 0.4–1 bar and reaction temperatures of −30 °C to rt , solid anilines such as 4-methoxy, 4-chloro and 4-bromoaniline were reacted in the solid-state under ball milling conditions at rt. In all three cases the authors reported 100% yields (Scheme 3a).

Starting from solid phenylene-1,4-diisothiocyanate and methyl-amine or dimethylamine, bis-thioureas **12a** and **12b** were quan-titatively prepared by gas–solid reactions. When phenylene-1,2-diisothiocyanate was used in solid-state reactions with 4-hydroxyaniline, 4-chloroaniline and 1,2-phenylenediamine, benzimidazolidine-2-thiones **14a–c** were isolated in 100% yields via cyclization of an unstable intermediate **13** (Scheme 3b,c). Compared to the solvent-free synthesis, the cor-responding solution reactions resulted in lower yields (81–95%). Li and co-workers conducted a mortar-and-pestle synthesis of 14 diarylthioureas by reacting 4-ethoxy-, 4-chloro- and 4-bromophenyl isothiocyanates with several anilines. After manual grinding for 5–40 min, the crude products were recrys-tallized from ethanol or acetone, and dried under vacuum to afford the thioureas in 89–98% yield [31].

Inspired by these findings, our group decided to explore the re-activity pattern of aromatic and aliphatic amines and aromatic isothiocyanates during mechanochemical synthesis of 49 sym-metrical and non-symmetrical *N,N′*-disubstituted thioureas [32]. For this purpose, a range of amines and isothiocyanates were screened with electron-donating and electron-withdrawing groups attached to aromatic rings. The reactions were per-formed in a 1:1 stoichiometry by manual grinding in a mortar and by automated ball milling in a laboratory mixer mill. Also, the performance of solvent-free or neat grinding was compared to liquid-assisted grinding, as well as the effect of the physical state of the reactants (liquid or solid) on the isolated yields. In general, manual grinding for 5–45 min (typically 15–20 min to ensure quantitative conversion) worked well with ≥99% yields in all cases regardless of the electronic effects exerted by differ-ent substituents, or liquid or solid character of the starting mate-rials. Interestingly, in most cases a simple manual mechanical agitation of the reaction mixtures in a mortar provided products after only a few minutes of grinding. However, the combina-tion of an electron-withdrawing group in the amine (lower nucleophilicity) and an electron-donating group in the isothio-cyanate component (lower electrophilicity) led to prolonged grinding times necessary to achieve quantitative conversion. The reaction time in these cases was successfully reduced by LAG, providing *N,N′*-disubstituted thioureas in quantitative
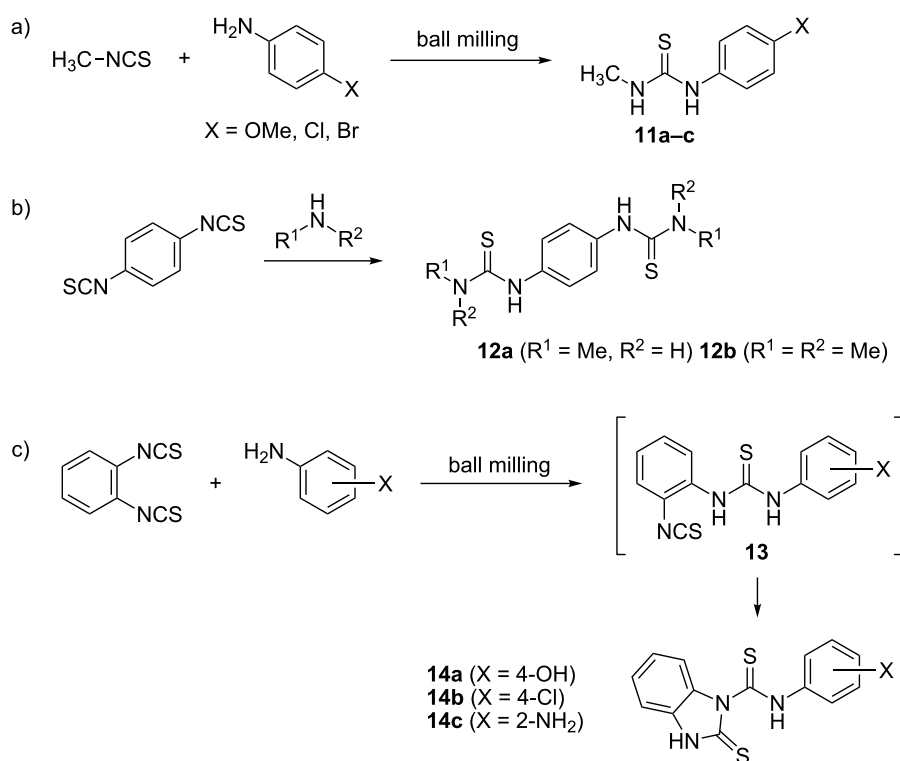

Scheme 3: Solid-state reactivity of isothiocyanates reported by Kaupp [30].

yields. In contrast to mortar-and-pestle synthesis, automated ball milling at 30 Hz using a single 12 mm stainless steel ball afforded the desired products quantitatively in 10 minutes, demonstrating its efficiency for a rapid and general synthesis of thioureas via click-type amine–isothiocyanate coupling reaction (Scheme 4).

In the case of secondary amines (piperidine, morpholine and thiomorpholine) and sterically hindered amines (2,4- and 2,6-dimethylanilines), ball milling again resulted in ≥99% yields in 10 minutes, except for the reactions involving 4-methoxyphenyl isothiocyanate, which required 45 minutes of manual grinding and 15 or 45 minutes of milling, due to its diminished electrophilicity.

In the context of these results, it is reasonable to assume that the solvent-free microwave synthesis of diarylthioureas described by Li et al. actually proceeded in the solid-state before having been exposed to microwave irradiation for 1.5–4.5 minutes. In their paper, the authors state: "Aryl isothiocyanate (1 mmol) and aromatic primary amine (1 mmol) were mixed thoroughly in an agate mortar" [33]. Considering the established reactivity pattern of electron-withdrawing aryl isothiocyanates with anilines used for the synthesis of *N*,*N*′-disubstituted thioureas, thorough mixing in an agate mortar typically leads to the formation of the products in a couple of minutes.

As an extension of the mechanochemical click-coupling of amines with isothiocyanates, the thiourea products were struc-
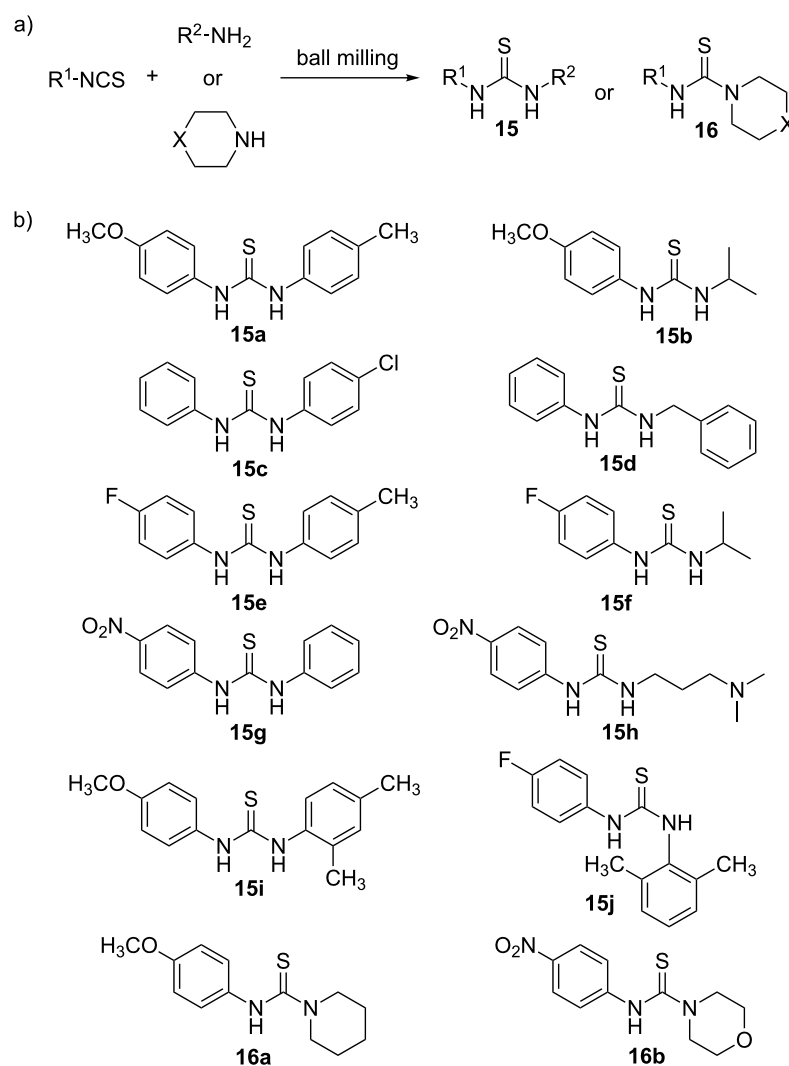
Scheme 4: a) Mechanochemical synthesis of aromatic and aliphatic di- and trisubstituted thioureas by click-coupling of amines with aromatic isothiocyanates. b) Selected examples of thioureas synthesized in quantitative yields.

turally characterized by solid-state analytical methods such as powder X-ray diffraction (PXRD) and solid-state NMR (ssNMR) spectroscopy. In this way, mechanochemical organic synthesis and solid-state analysis are incorporated into the paradigm of solvent-free synthetic organic research laboratory, where all the steps from synthesis to structural characterization are carried out without using bulk solvents. The systematic PXRD analyses of 49 thioureas revealed that thioureas, on a supramolecular level, organize into three types of self-assembly motifs based on N–H···S hydrogen bonds: corrugated chains of head-to-head or head-to-tail aligned molecules and discrete centrosymmetric dimers based on the $R_2^2(8)$ supramolecular synthon in the case of sterically hindered thioureas (Figure 2).

The crystal structures of *N,N′*-diarylthioureas linked in chains via N–H···S hydrogen bonds can further be subdivided into two structural families. The chains in the family I are stacked in a parallel fashion with a width of the supramolecular stack corresponding to the Bragg diffraction angle range 5–7° and the (200) reflection, intensity of which is a result of diffraction from the sulfur atoms in neighbouring stacks.
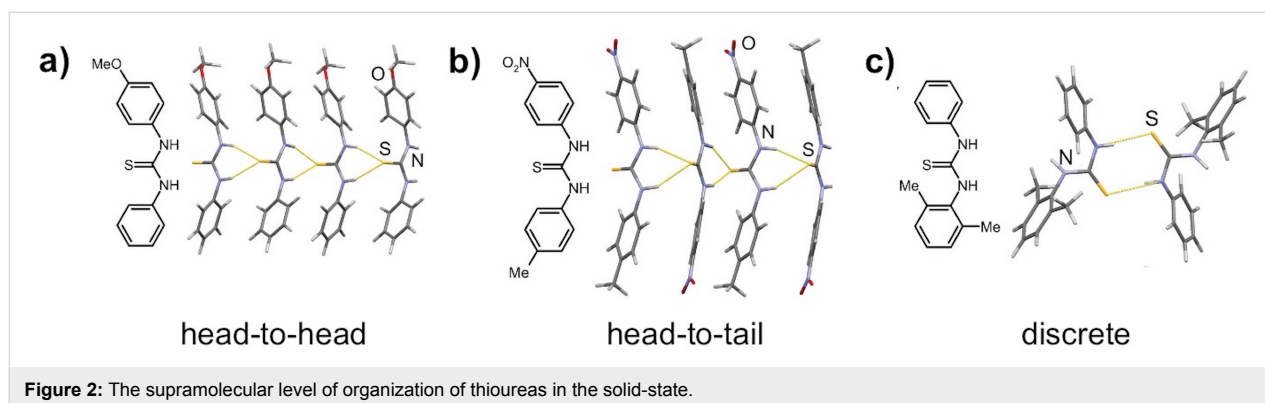
In the structural family II, the characteristic (110) reflection is slightly shifted and appears at the Bragg diffraction angle range 8–10°. The infinite hydrogen-bonded chains are arranged in a herringbone pattern with an angle of 44° between neighbouring stacks (Figure 3).
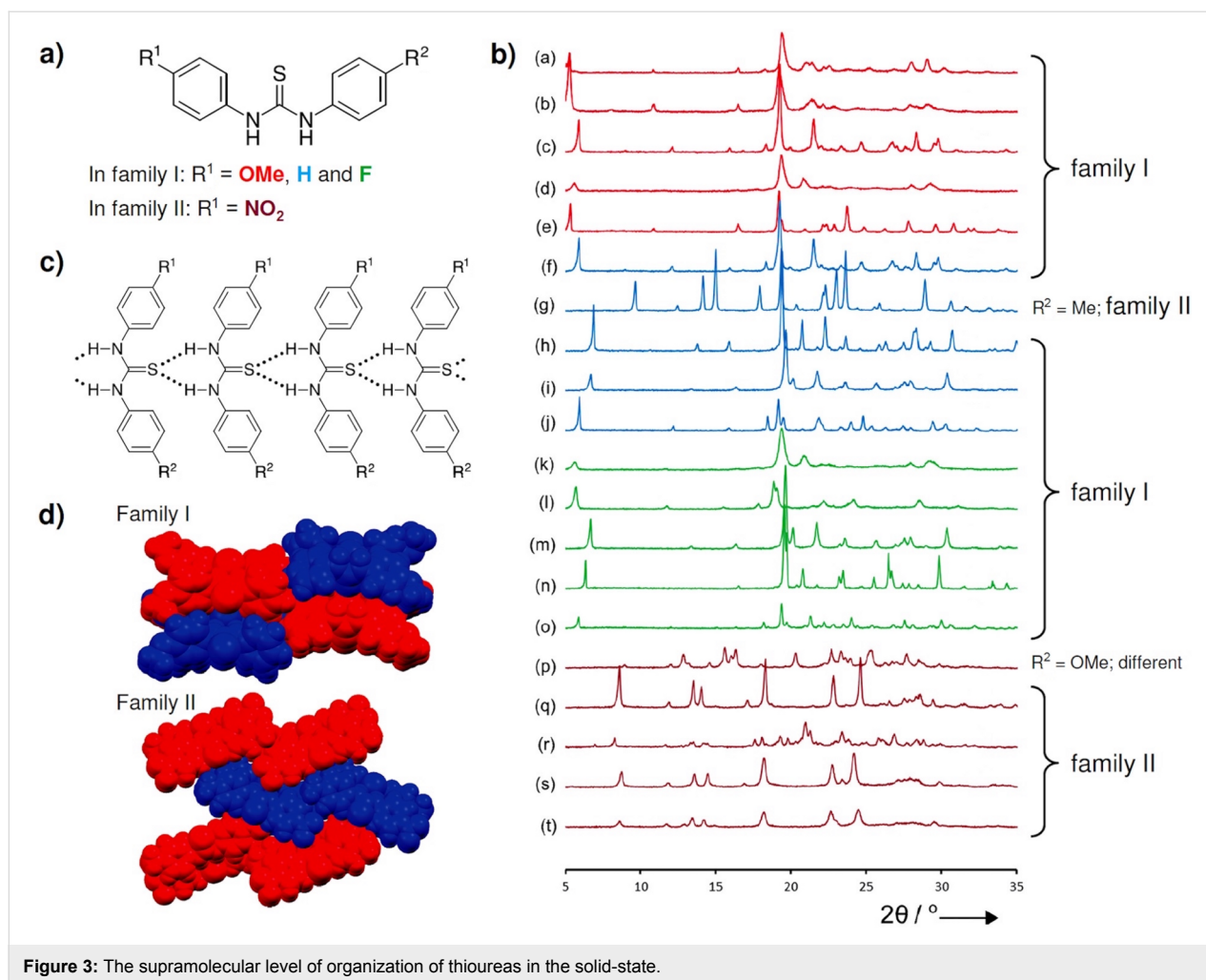
In the follow-up paper, the ball milling approach was then applied for a quantitative click-mechanosynthesis of thiourea-based organocatalysts and anion sensors (Scheme 5) [34]. The demonstrated efficiency of mechanochemical milling synthesis of thioureas was exploited for a quantitative transformation of enantiomerically-pure chiral reagents, availability of which in a laboratory is dictated by their high costs. For that reason, we looked into the possibility to convert these reagents into functional chiral molecules with the highest synthetic efficiency. The privileged 3,5-di(trifluoromethyl)phenyl motif in

organocatalyst design was first introduced by reacting 3,5-di(trifluoromethyl)phenyl isothiocyanate with 3,5-di(trifluoromethyl)aniline and 4-chloroaniline in a 1:1 ratio under LAG conditions using methanol as the grinding liquid. This led to quantitative formation of the Schreiner's catalyst **5** and thiourea **17** as evidenced by the disappearance of the characteristic –N=C=S stretching band between 2000 and 2200 cm^{-1} in the FTIR-ATR spectra.

The isothiocyanate was then coupled with other chiral diamines such as enantiomers of *trans*-1,2-diaminocyclohexane, (1*R*,2*R*)-(+)-1,2-diphenylethylenediamine and (*R*)-(+)-1,1′-binaphthyl-2,2′-diamine in a stoichiometric ratio. The corresponding chiral bis-thiourea organocatalysts were isolated in ≥99% yields after only 20 minutes (60 min in the case of binaphthylthiourea) of neat grinding or LAG. Interestingly, while the solution synthesis of (1*R*,2*R*)-**8** in THF followed by recrystallization from a hexane/ethyl acetate mixture gave previously unrecognized but highly stable 1:1 ethyl acetate solvate, the mechanochemical synthesis led to the pure non-solvated catalyst. The mechanochemically prepared achiral thiourea **5** as well as enantiomers (1*R*,2*R*)-**8** and (1*S*,2*S*)-**8** were next screened as catalysts in Morita–Baylis–Hillman reaction, and their performance matched the previously published catalytic activity. An analogous click-type reaction between 4-nitrophenyl isothiocyanate and *trans*-1,2-diaminocyclohexane quantitatively afforded enantiomeric (1*R*,2*R*)-**10** and (1*S*,2*S*)-**10** bis-thioureas which were tested as cyanide anion sensors in DMSO solution.

Our group continued the research on the solid-state synthesis of thioureas focusing now on the reactivity of sterically hindered *ortho*-phenylenediamine (*o*-pda) with isothiocyanates [35]. Whereas Kaupp's approach to prepare a bis-thiourea derivative by milling 1,2-diisothiocyanate with two equivalents of an amine failed and resulted in the formation of benzimidazolidine-2-thiones **14a–c** by cyclization of the mono-thiourea intermediate **13** (Scheme 3), our reaction design was based on the click-coupling of *o*-pda with either one or two equivalents of

Figure 2: The supramolecular level of organization of thioureas in the solid-state.

a) head-to-head   b) head-to-tail   c) discrete

Figure 3: The supramolecular level of organization of thioureas in the solid-state.

phenyl, 4-methoxyphenyl, 4-chlorophenyl or 4-nitrophenyl isothiocyanate.

In the 1:1 reaction, solvent-free mechanosynthesis selectively provided stable mono-thioureas **19a–d** in ≥95% after 30 minutes (Scheme 6a). When the reactants were milled in a 1:2 ratio for 3 hours (9 hours for 4-methoxy derivative), the symmetrical bis-thioureas **20a–d** were isolated in excellent ≥95% yields (Scheme 6b). Such a selective transformation of *o*-pda into mono-thioureas enabled the synthesis of non-symmetrical bis-thioureas **20e–h** by a one-pot two-step mechanochemical reaction, without the need to isolate and purify the mono-thiourea intermediates. For example, the reaction of 4-methoxy **19a**, phenyl **19b** and 4-nitro mono-thiourea **19d**, with the second equivalent of an isothiocyanate furnished the non-symmetrical products in ≥99% after 3 hours of LAG using methanol (Scheme 6c). In the case of *para*-phenylenediamine (*p*-pda) where steric hindrance is absent, the desymmetrization was more challenging. It was only achieved in 97% **21a** in the reaction with less reactive 4-methoxyphenyl isothio-

cyanate under NaCl dilution and LAG using ethyl acetate. When highly reactive 4-nitrophenyl isothiocyanate was utilized, a mixture of mono- **21b** and bis-thioureas **22b** was isolated (Scheme 7).

However, the corresponding 1:2 reactions quantitatively gave symmetrical bis-thioureas **22a** and **22b** after only 30 minutes of LAG. Also, the non-symmetrical thioureas **22c** and **22d** were prepared by coupling mono-thiourea **21a** with 4-chloro- and 4-nitrophenyl isothiocyanates. This study demonstrated that solid-state ball milling can efficiently be employed for desymmetrization of *ortho*- and *para*-phenylenediamines, enabling selective functionalization of small symmetrical molecules through the extension of molecular structure in a one-pot two-step mechanochemical sequence.

Another typical synthetic method for the preparation of thioureas, particularly if the desired isothiocyanate is not available, is the condensation of an amine with carbon disulfide [36]. This reaction proceeds through the formation of a dithiocarba-
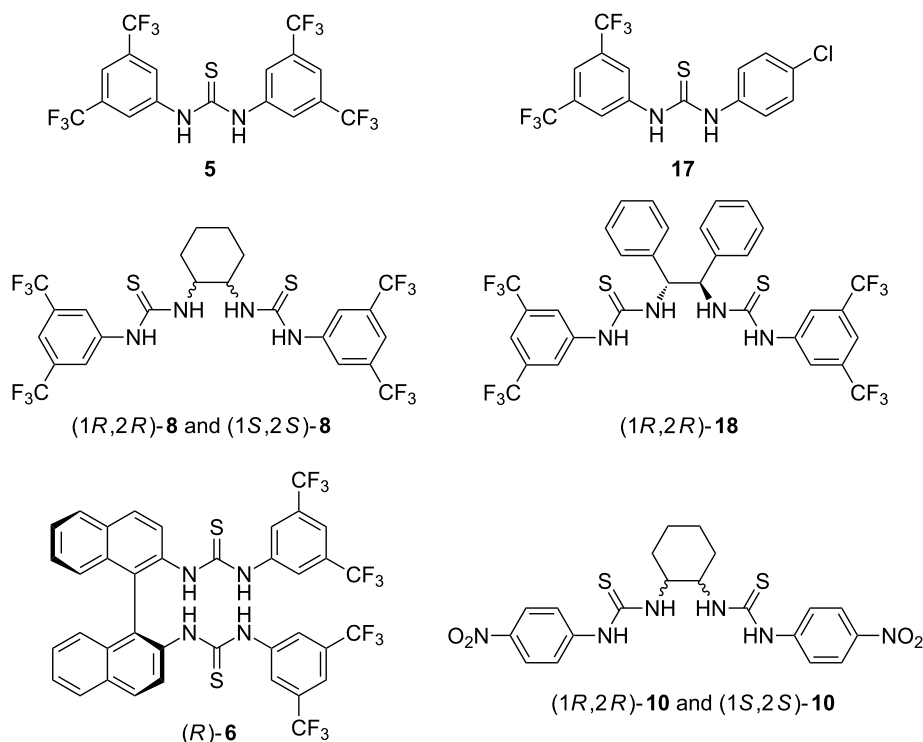
Scheme 5: Thiourea-based organocatalysts and anion sensors obtained by click-mechanochemical synthesis.
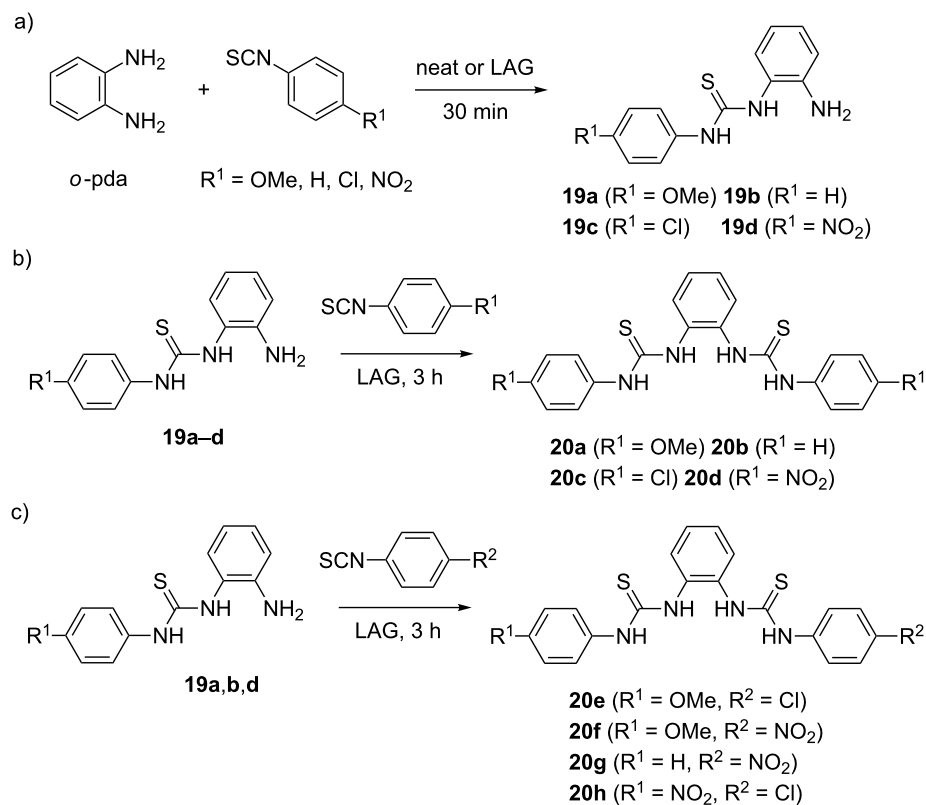

Scheme 6: Mechanochemical desymmetrization of *ortho*-phenylenediamine.
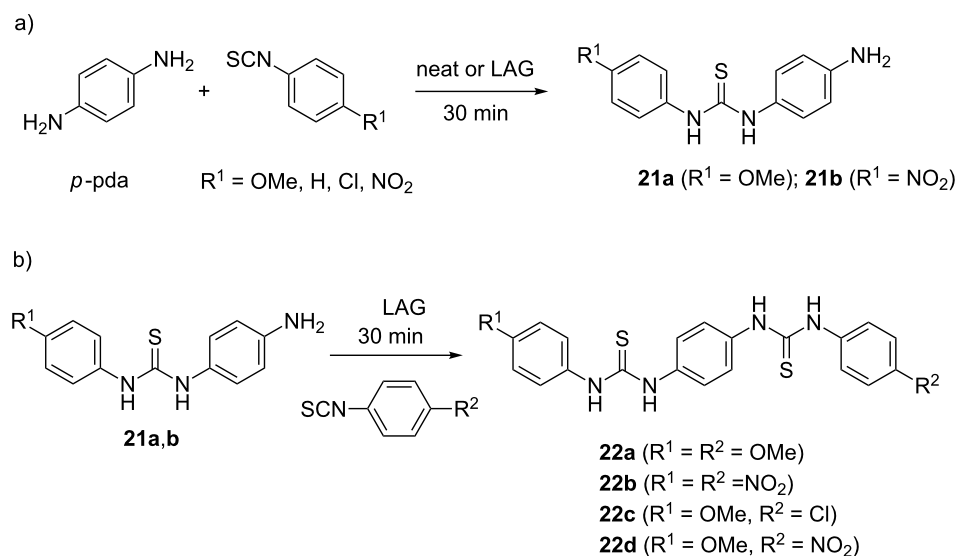
Scheme 7: Mechanochemical desymmetrization of *para*-phenylenediamine.

mate salt in the first step, which can be isolated or desulfurized in situ to provide the isothiocyanate reagent. Without isolation, the isothiocyanate undergoes a reaction with the amine and produces the thiourea product. Such an approach for thiourea synthesis under mechanochemical ball milling conditions was investigated by Zhang et al. [37]. In their procedure, anilines were mechanochemically transformed into isothiocyanates **24** in

the presence of 5.0 equivalents of CS_2 or symmetrical thioureas (in the presence of 1.0 equiv CS_2) by potassium hydroxide-promoted decomposition of the intermediate dithiocarbamate salt **23** (Scheme 8a). In comparison with 24 h reactions carried out in solvents (CH_2Cl_2, THF, acetone, methanol, DMF, DMSO or neat CS_2), the mechanochemical synthesis was rapid and furnished electron-rich isothiocyanates in high yields in
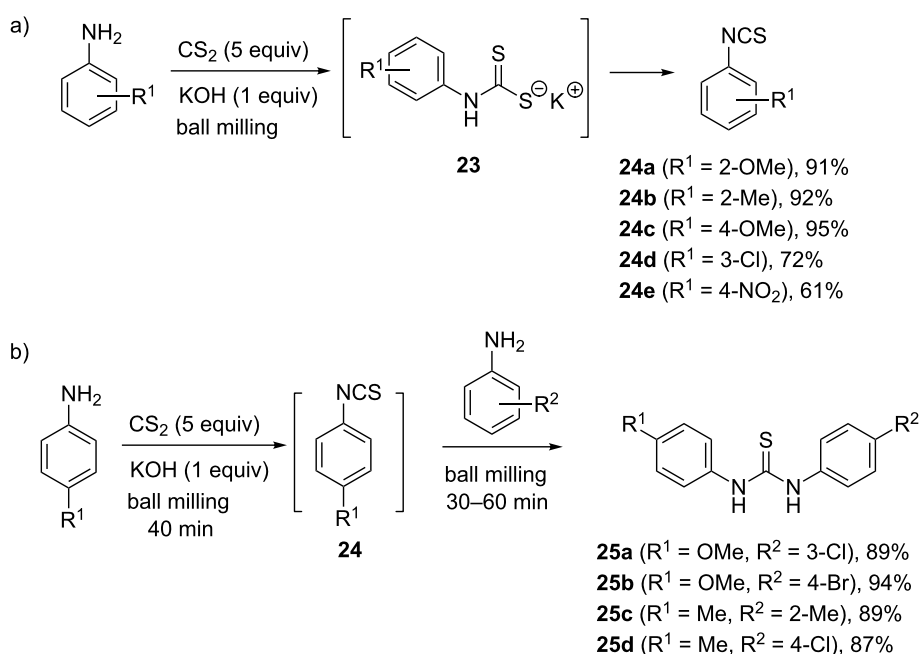
Scheme 8: a) Selected examples of a mechanochemical synthesis of aromatic isothiocyanates from anilines. b) One-pot two-step synthesis of some non-symmetrical thioureas **25a–d**.
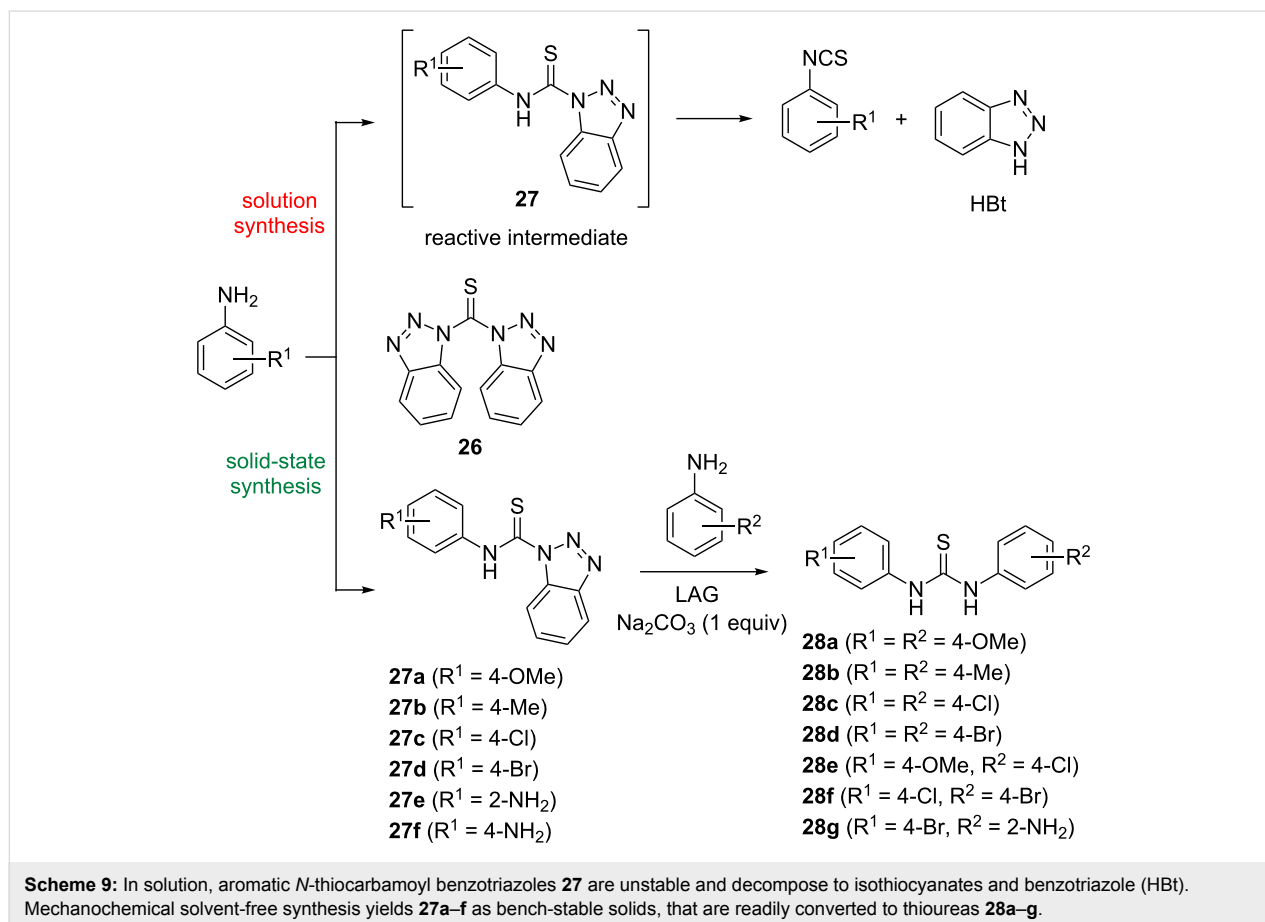
40–45 minutes (e.g., **24a–c**). On the other hand, anilines bearing electron-withdrawing substituents were less reactive, resulting in prolonged milling (90 minutes) and only moderate yields of the isothiocyanate products **24d**,**e**.

The observation that isothiocyanates were major products when excess CS$_2$ (5.0 equiv) was employed, while the stoichiometric reaction with 1.0 equiv of CS$_2$ switched the reactivity and afforded symmetrical thioureas in good to excellent yields, prompted the authors to conduct a two-step synthesis of non-symmetrical thioureas **25** (Scheme 8b). In the first step, electron-rich 4-methoxyaniline or 4-methylaniline were ball milled with CS$_2$ (5.0 equiv) for 40 minutes, followed by the click-coupling reaction of the second equivalent of an aniline with the intermediate isothiocyanate. In this way, non-symmetrical thioureas **25a–d** were synthesized and isolated in high 87–94% yields.

Instead of using thiophosgene and CS$_2$ as corrosive and hazardous liquid reactants that require special handling, solid thioacylating reagents such as 1,1'-thiocarbonyldiimidazole and bis(1-benzotriazolyl)methanethione (**26**) are air-stable and easier to work with during thiourea synthesis. While their solu-

tion chemistry in thioacylation and thiocarbamoylation reactions has been documented [38-40], the reactivity of these compounds in the solid-state mechanochemical transformations remained unexplored. Our attention was also caught by the fact that thiocarbamoylation in solution using **26**, provided only alkyl derivatives in 60–98% yield. For aromatic derivatives **27**, it has been explicitly stated in the literature that these compounds are very reactive intermediates and immediately decompose to isothiocyanates and 1*H*-benzotriazole (HBt). With this in mind, we investigated the possibility to run the thiocarbamoylation reaction of *para*-substituted anilines as nucleophilic aromatic substrates with bis(1-benzotriazolyl)-methanethione (**26**) under ball-milling conditions (Scheme 9) [41]. The application of in situ Raman spectroscopy monitoring of mechanochemical reactions, in combination with solid-state characterization through FTIR-ATR, PXRD and ssNMR analyses, confirmed that mechanochemistry afforded the elusive aromatic *N*-thiocarbamoyl benzotriazoles **27** in quantitative yields after only 10 minutes of LAG and a simple aqueous work-up.

Furthermore, conducting the reaction in two steps, where the thiocarbamoyl benzotriazole was prepared in the first step fol-

Scheme 9: In solution, aromatic *N*-thiocarbamoyl benzotriazoles **27** are unstable and decompose to isothiocyanates and benzotriazole (HBt). Mechanochemical solvent-free synthesis yields **27a–f** as bench-stable solids, that are readily converted to thioureas **28a–g**.

lowed by the addition of the second equivalent of aniline, led to non-symmetrical thioureas **28e–g** in ≥97% yields (Scheme 9).

Treating *p*-pda with two equivalents of **26** gave 99% of bis-thiocarbamoyl benzotriazole **29**, a masked 1,4-phenylene diisothiocyanate equivalent. In contrast, the analogous reaction of *o*-pda failed to give the desired *ortho*-bis-thiocarbamoyl benzotriazole **30** after 2 hours of LAG. The isolated product was identified as benzimidazole thione **31**, formed presumably by an intramolecular cyclization of the unstable bis-derivative **30** (Scheme 10a and b).

Since *N*-thiocarbamoyl benzotriazoles can be regarded as synthetic equivalents of isothiocyanate reagents, they were utilized
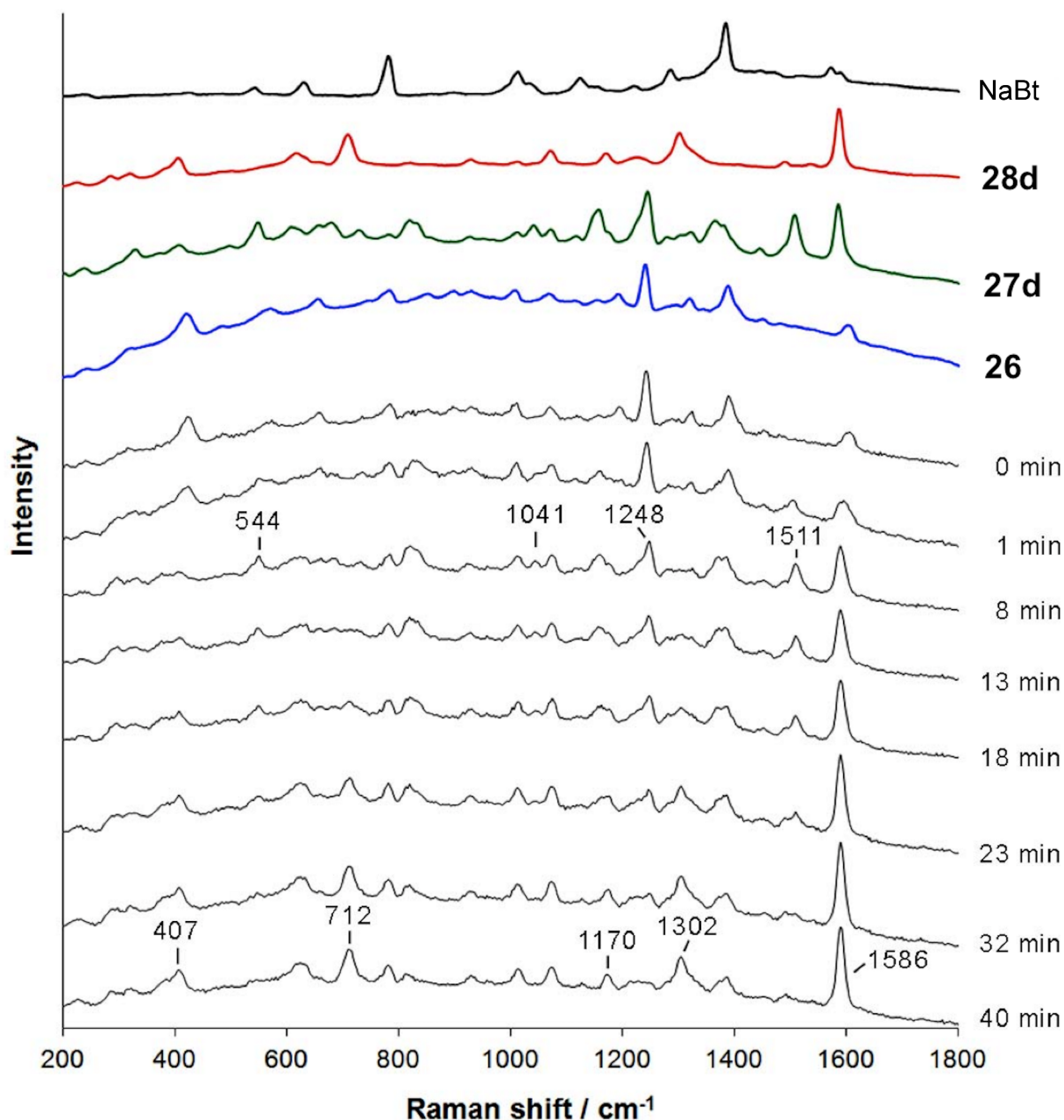
for the solid-state synthesis of thioureas by milling **26** with two equivalents of aniline in the presence of sodium carbonate as the base. After 10 minutes, symmetrical aromatic thioureas **28a–d** were obtained in almost quantitative yields. The in situ Raman monitoring of a 1:2 mixture of **26** and 4-bromoaniline, which results in the formation of symmetrical bis(4-bromophenyl)thiourea **28d** revealed thiocarbamoyl benzotriazole **27d** as the reactive intermediate (Figure 4).

Starting from **27a** or **29**, bis-thiourea **22a** can be quantitatively accessed by controlling the aniline to thiocarbamoyl benzotriazole stoichiometry (Scheme 10c).

Apart from providing another example of stoichiometry-controlled synthesis under mechanochemical conditions, these
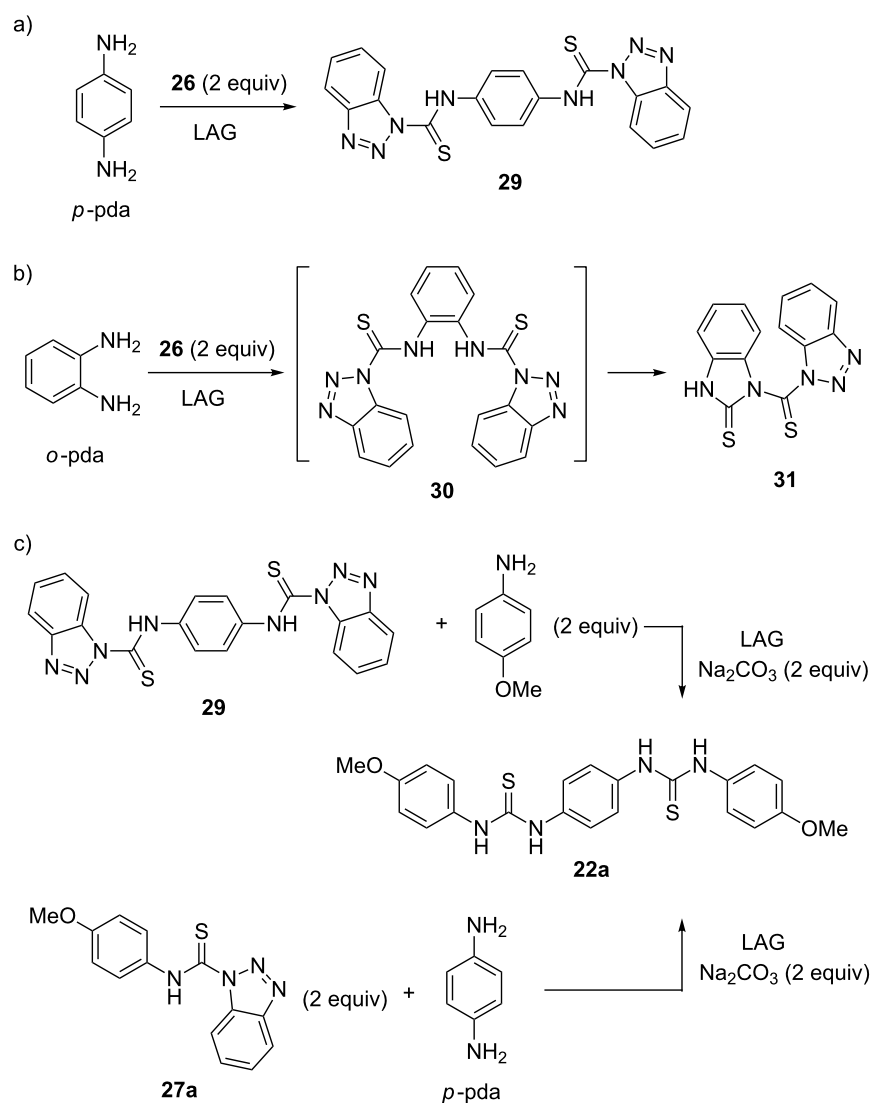
Scheme 10: Mechanosynthesis of a) bis-thiocarbamoyl benzotriazole **29** and b) benzimidazole thione **31**. c) Synthesis of bis-thiourea **22a** from mono- (**27a**) and bis- (**29**) *N*-thiocarbamoyl benzotriazoles.

Figure 4: In situ Raman spectroscopy monitoring the synthesis of thiourea **28d** in the solid-state. *N*-Thiocarbamoyl benzotriazole **27d** was identified as the intermediate, with the characteristic bands at 544, 1041, 1248, and 1511 cm^{-1} appearing ca. 2 min into milling and disappearing with the formation of **28d**.

results have also demonstrated the power of solid-state milling as a synthetic tool that enables the synthesis and isolation of molecular species as bench-stable chemicals, that are normally considered as reactive intermediates in solution environment.

The observed reactivity of thiocarbamoyl benzotriazoles prompted us to examine their reaction with ammonia, as a potential route to primary monosubstituted thioureas **32** [42]. Primary thioureas are typically prepared in solution from

benzoyl chloride and ammonium thiocyanate or by condensation of amine hydrochlorides and potassium thiocyanate [43,44]. Our strategy was to synthesize the desired thiocarbamoyl benzotriazole in the first step, and then carry out the amination reaction in the second step using the appropriate ammonia source (Scheme 11a). As a test reaction, the amination of 1-[(4-bromophenyl)thiocarbamoyl]benzotriazole (**27d**) in ammonia vapours by the so called aging or vapour digestion was selected. It was evident by the colour change of the sample
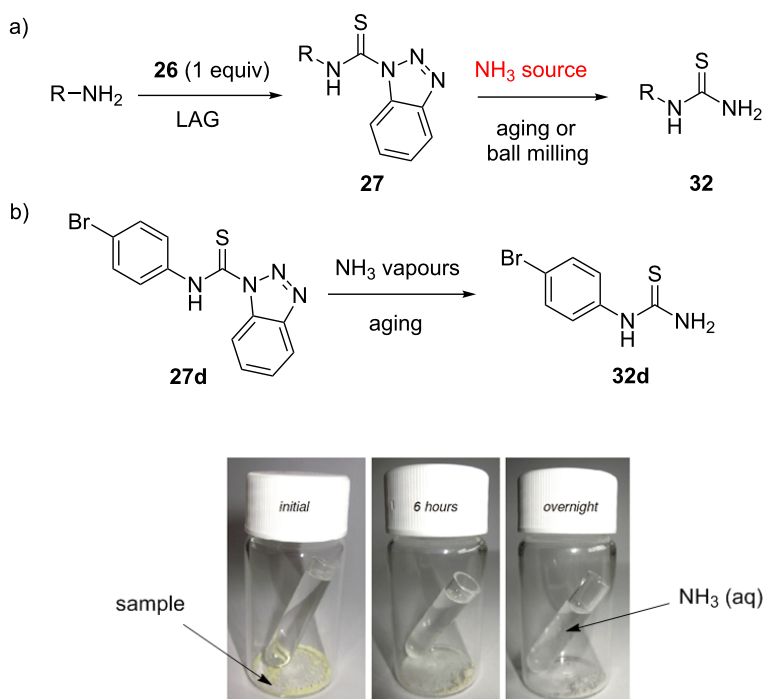
Scheme 11: a) The proposed synthesis of monosubstituted thioureas **32**. b) Conversion of *N*-thiocarbamoyl benzotriazole **27d** to thiourea **32d** by aging in ammonia vapours.

that the chemical reaction occured which was also confirmed by FTIR-ATR analysis (Scheme 11b). The decrease of band intensities of thiocarbamoyl benzotriazole **27d** at 1588, 1520, 1157, 1143, 968, 924 and 494 cm^{-1} was accompanied by the appearance of characteristic absorption bands of *N*-(4-bromophenyl)thiourea (**32d**) at 1617 and 509 cm^{-1}. Several other thiocarbamoyl benzotriazoles were also quantitatively transformed to primary thioureas by this method.

For the purpose of performing the amination reaction in a ball mill, ammonia gas was generated in situ by milling the thiocarbamoyl substrate with a mixture of sodium carbonate and ammonium chloride. This mixture released ammonia gas during milling and allowed the amination reaction to take place under solvent-free mechanochemical conditions. Following a simple aqueous work-up and filtration, the desired primary thioureas **32** were isolated in quantitative yields. The amination reaction was then performed on a number of substrates, ranging from simple mono- and disubstituted anilines, benzylamines and polyaromatic amines such as anthracene-, phenanthrene-, pyrene- and crysenamine (Scheme 12).

An interesting feature of LAG synthesis of monosubstituted thioureas was that water as the grinding liquid, or aqueous solutions of organic solvents where $x(H_2O) > 0.8$, significantly affected the conversion of thiocarbamoyl benzotriazole **27d**. In

the case of LAG with water, the quantitative IR analysis revealed only 3% conversion to thiourea **32d**, whereas LAG with aqueous ammonia solution as a source of NH$_3$ (instead of Na$_2$CO$_3$/NH$_4$Cl mixture) gave a poor yield of 24%. The phenomenon of LAG inhibition was explained by strong hydrogen-bonding solvation of NH$_3$ molecules in water which are likely to form cluster species NH$_4^+$(H$_2$O)$_n$, not reactive in the amination reaction.
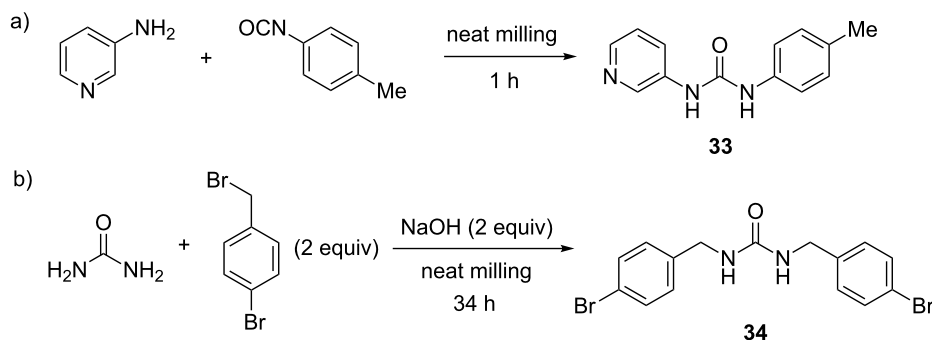
Ureas
Just as thioureas are typically synthesized by coupling reaction between amines and isothiocyanates, ureas as oxygen analogues are prepared from the corresponding isocyanates. This approach was employed in the synthesis of anion binding 1-(pyridin-3-yl)-3-*p*-tolylurea (**33**) reported by Swinburne and Steed in 2009 [45]. This compound was found to bind anions individually and as part of a tripodal anion receptor. In contrast to solution synthesis in dichloromethane for 12 hours, the mechanochemical solvent-free coupling of 3-aminopyridine and 4-methylphenyl isocyanate provided the target urea sensor after milling for 60 minutes at 18 Hz (Scheme 13a). Monitoring the progress of the reaction by ex situ ^{1}H NMR spectroscopy in DMSO-d_6 revealed that the reaction reached completion after only 30 minutes of ball milling with a conversion greater than 90%. Although the purity of the sample was satisfactory enough to be further used as-synthesized, an analytically pure sample
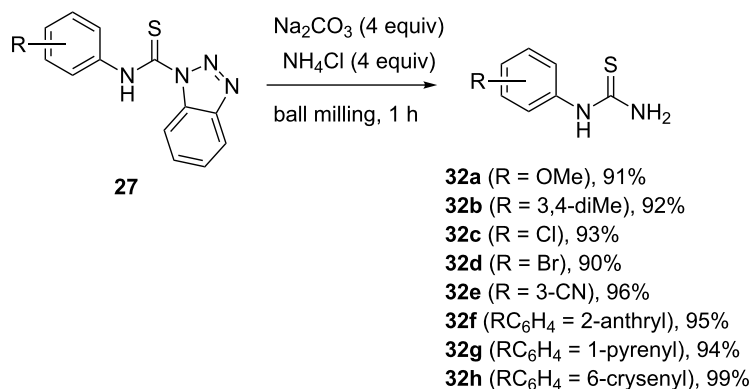
Scheme 12: A few examples of mechanochemical amination of thiocarbamoyl benzotriazoles by in situ generated ammonia.

32a (R = OMe), 91%
32b (R = 3,4-diMe), 92%
32c (R = Cl), 93%
32d (R = Br), 90%
32e (R = 3-CN), 96%
32f (RC$_6$H$_4$ = 2-anthryl), 95%
32g (RC$_6$H$_4$ = 1-pyrenyl), 94%
32h (RC$_6$H$_4$ = 6-crysenyl), 99%

Scheme 13: Mechanochemical synthesis of a) anion binding urea **33** by amine-isocyanate coupling and b) dialkylurea **34** by alkylation of unsubstituted urea.

could easily be obtained by simple washing with CH$_2$Cl$_2$. The mechanochemically prepared urea **33** was next used in the synthesis of tri- and tetrapodal anion receptors, again by exploiting the solid-state LAG ball milling approach.

Mack et al. looked into the formation of a dialkylurea from the parent urea in the context of the mechanochemical formation of dialkyl carbonates from metal carbonates [46]. Whereas urea is normally considered as unreactive compound, the authors succeeded to activate it under ball-milling conditions by using two equivalents of sodium hydroxide. Deprotonation of the N–H group increased the nucleophilicity of the nitrogen atoms, enabling the nucleophilic displacement reaction with two equivalents of 4-bromobenzyl bromide to yield di(4-bromobenzyl)urea **34** in 41%, after a total of 34 hours of milling (Scheme 13b). This transformation showed that ball milling could potentially be applied to increase the nucleophilicity of an otherwise poorly reactive compound.

In the course of our studies on mechanochemical desymmetrization, we also investigated the reaction of *o*-pda and mono-urea **36** with phenyl isocyanate under the milling conditions used for

the synthesis of bis-thioureas [35]. A known bis-urea anion sensor **35** was prepared in quantitative yield in 30 minutes by milling *o*-pda with phenyl isocyanate in a 1:2 molar ratio. However, in the 1:1 reaction, a mixture of mono-urea **36** (78%), bisurea **35** (12%) and *o*-pda (10%) was isolated, thus contrasting the reactions involving isothiocyanates (Scheme 14a,b). On the other hand, milling mono-urea **36** with one equivalent of *p*-nitrophenyl isothiocyanate for 30 minutes quantitatively yielded the mixed urea–thiourea **37d**. When mono-thiourea **19b** was used under these conditions, the conversion to bis-thiourea **20g** was 68% due to lower reactivity of mono-thioureas in comparison with mono-ureas (Scheme 14c).

Quantum mechanical frontier molecular orbital (FMO) analysis of mono-(thio)ureas allowed us to rationalize different reactivity patterns observed experimentally. The FMO analysis of **19b** showed more electron density on the sulfur atom compared to the nitrogen of the amino group in the highest occupied molecular orbital (HOMO−1). In contrast, the coefficient was larger on the NH$_2$ nitrogen atom in HOMO−1 of mono-urea **36** thus making it more nucleophilic in the addition reaction to isocyanates (Scheme 15a). The ability to selectively convert
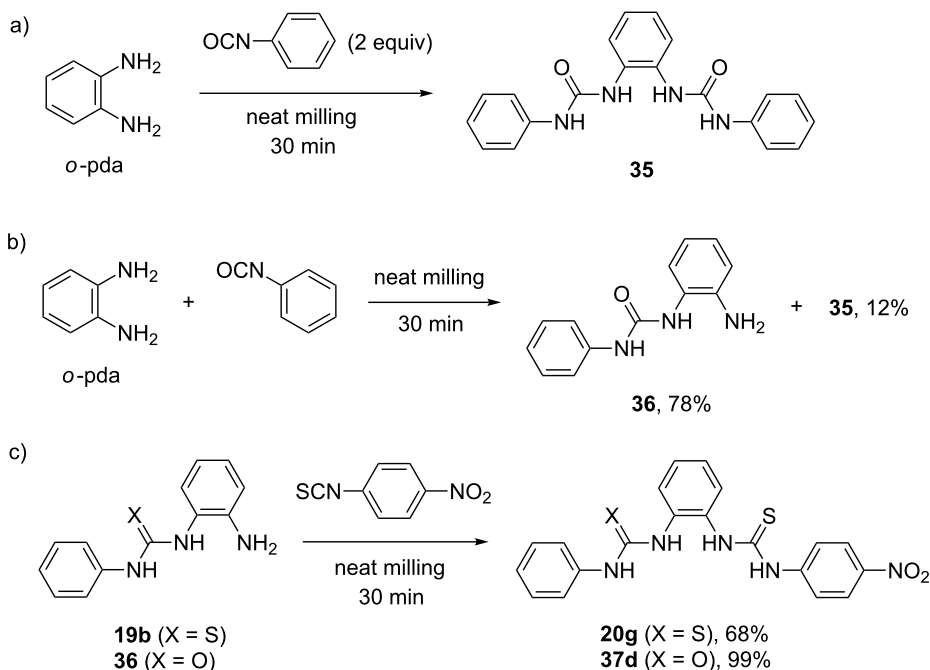
Scheme 14: a) Solvent-free milling synthesis of the bis-urea anion sensor **35**. b) Non-selective desymmetrization of *o*-pda with phenyl isocyanate. c) Different reactivity of mono-thiourea **19b** and mono-urea **36** under mechanochemical conditions.

o-pda into non-symmetrical mono-thioureas provided an opportunity to synthesize hybrid urea–thiourea derivatives **37a–d** in a one-pot, two-step mechanochemical solvent-free process. After

ball milling for three hours, the addition of phenyl isocyanate (1 equiv) to mono-thioureas **19a–d** quantitatively yielded the mixed urea–thioureas **37a–d** (Scheme 15b), which could also be
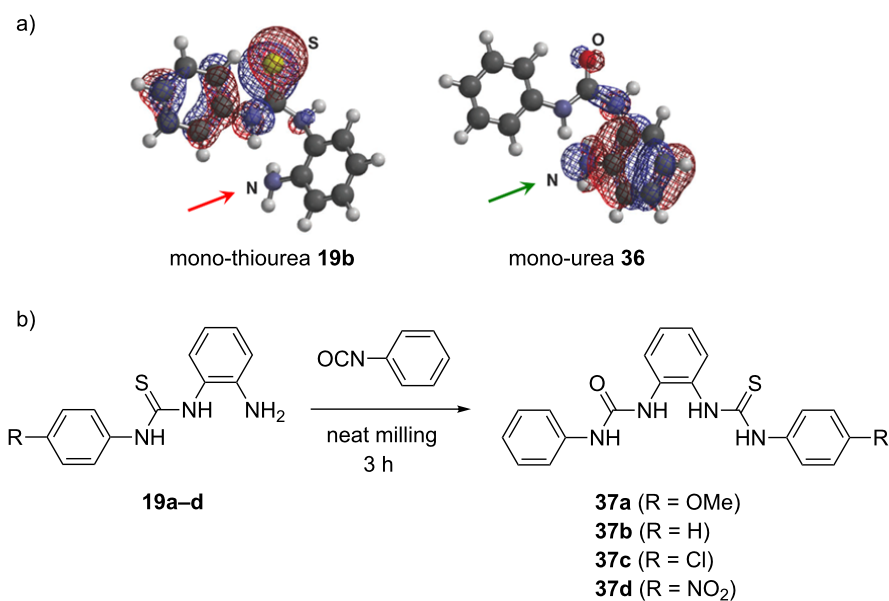
Scheme 15: a) HOMO−1 contours of mono-thiourea **19b** and mono-urea **36**. b) Mechanochemical synthesis of hybrid urea-thioureas **37a–d**.

prepared by a ''reverse'' mechanosynthesis starting from the mono-urea **36**.

An interesting approach, published by Colacino et al., to introducing urea functionality in amino acid methyl esters by mechanochemically reacting them with potassium cyanate (KOCN) was described [47]. The ureido products arising from this reaction are intermediates in what is known in the literature as the Urech synthesis of 1,3-unsubstituted hydantoins. The in situ basic conditions, necessary for the deprotonation of the amino acid methyl ester hydrochloride salts in order to make the amino group nucleophilic, were generated by the hydrolysis of KOCN. Following the addition reaction with KOCN starting from hydrochloride salts of L-phenylalanine or L-(*tert*-butyl)threonine methyl esters, ureido derivatives **38** and **39** were isolated in high yields (96 and 97%, respectively; Scheme 16a,b). A number of other α-amino methyl esters, quaternary amino methyl esters or β-amino methyl esters were also successfully converted to intermediate ureas (without isolation) and cyclized in the presence of a base to 5-substituted hydantoins in good to excellent yields.

Then the ball milling methodology was applied to the synthesis of phenytoin (**41**), a known antiepileptic drug. In this case, KOCN had to be replaced with trimethylsilyl isocyanate (TMS-NCO) which generated the strong hexamethyldisilazane (HMDS) base upon hydrolysis. Deprotonation of sterically
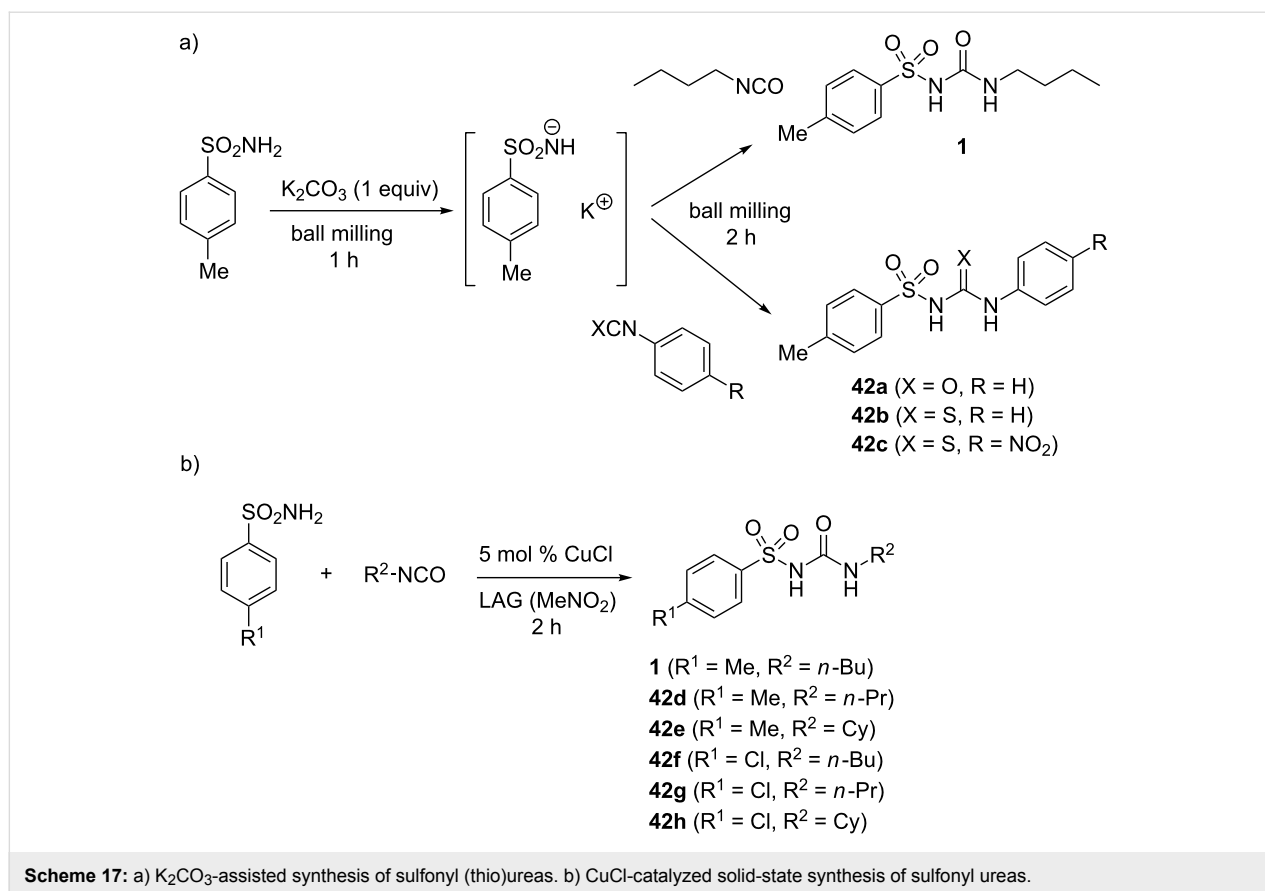
hindered diphenylglycine methyl ester hydrochloride followed by the hydrolysis of the TMS group provided the ureido-intermediate **40** after 8 hours of milling at 450 rpm. The cyclization of **40** with Cs_2CO_3 for 3 hours finally afforded phenytoin in an excellent 84% isolated yield (Scheme 16c).

The introduction of a sulfonyl group on the urea framework has been found to be the crucial structural modification in the development of the 1st generation antidiabetic drugs such as tolbutamide and chlorpropamide or the 2nd generation drugs like glibenclamide (Figure 1). These molecules were interesting synthetic targets for our mechanochemical approach which is based on a stoichiometric base-assisted or copper-catalyzed coupling of sulfonamides and iso(thio)cyanates [48].

For that purpose, 0.5–1 equiv of potassium carbonate as the base was necessary to deprotonate the sulfonamide and thus increase its reactivity. After milling for 2 hours with the corresponding iso(thio)cyanate, the sulfonyl (thio)ureas **42a–c** were isolated in excellent yields, for example the drug tolbutamide (**1**) in 92% (Scheme 17a). Sulfonylureas could also be obtained by coupling of sulfonyl isocyanates with amines which was demonstrated by an efficient solvent-, base- and catalyst-free synthesis of tolbutamide (93%) starting from *p*-toluenesulfonyl isocyanate and *n*-butylamine. However, this approach was not further pursued due to the air-sensitivity and corrosive nature of the sulfonyl isocyanate reagent. In addition, these reagents are
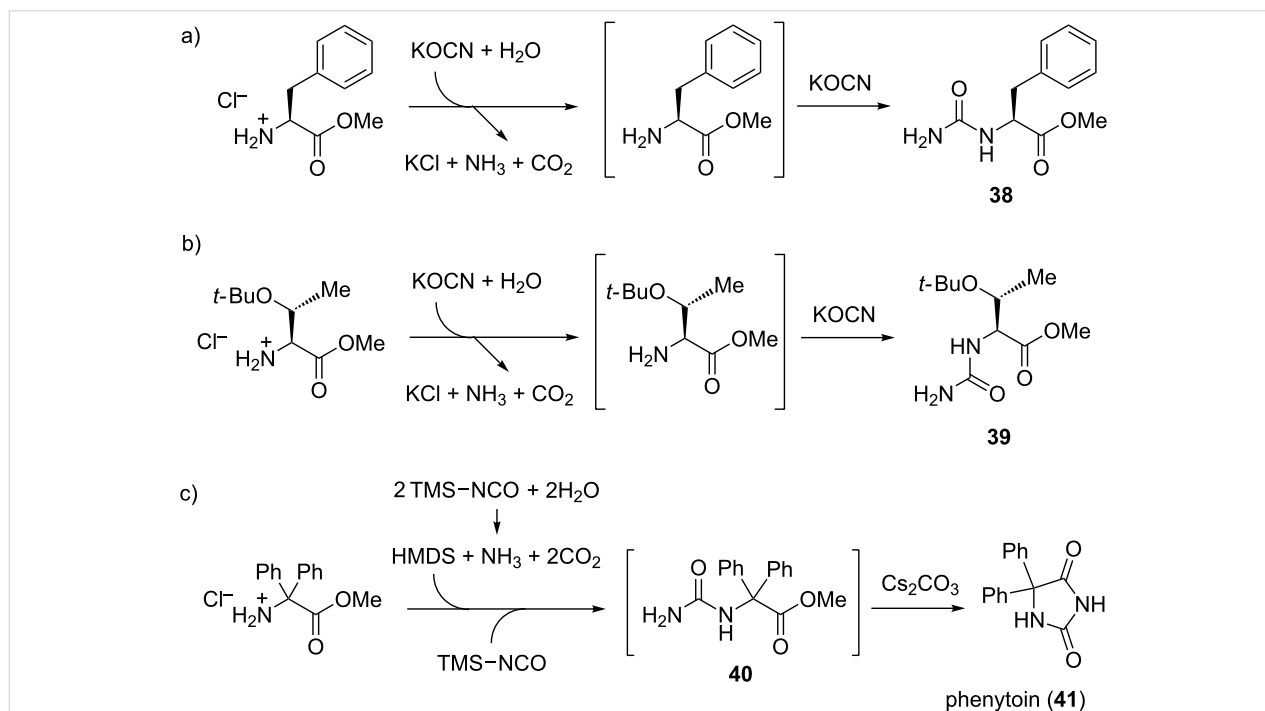
Scheme 16: Synthesis of ureido derivatives **38** and **39** from KOCN and hydrochloride salts of a) L-phenylalanine methyl ester and b) L-threonine(O*t*-Bu) methyl ester. c) Mechanochemical synthesis of the anti-epileptic drug phenytoin (**41**).

Scheme 17: a) K$_2$CO$_3$-assisted synthesis of sulfonyl (thio)ureas. b) CuCl-catalyzed solid-state synthesis of sulfonyl ureas.

generally unavailable in comparison with sulfonamides, many of which are air-stable commercial chemicals [49].

In order to avoid using stoichiometric quantities of a base, a mechanochemical catalytic approach to tolbutamide with CuCl as the catalyst was explored (Scheme 17b). Two hours of neat grinding of an equimolar mixture of *p*-toluenesulfonamide and *n*-butyl isocyanate in the presence of 5 mol % of CuCl resulted in 68% of the desired product **1**. Increasing the catalyst loading to 20 mol % improved the yield to 91%. Conducting the ball milling under LAG conditions enabled the CuCl loading to be kept as low as 5 mol %. Using nitromethane as the most effective grinding liquid, tolbutamide (**1**) was isolated in 90% yield. The optimization study also revealed that other sources of copper such as Cu(II) salts and Cu(0) in the powder form catalyzed the reaction. Most notably, the reaction proceeded in an excellent 87% yield even without external copper catalyst, only by using a brass milling ball. The catalyst was removed from the crude reaction mixture by briefly milling it with aqueous sodium ethylenediaminetetraacetate.

Glibenclamide (**2**) as our next target was more complex as it also posesses the additional amide functionality. We envisaged a two-step mechanochemical synthesis of glibenclamide, where
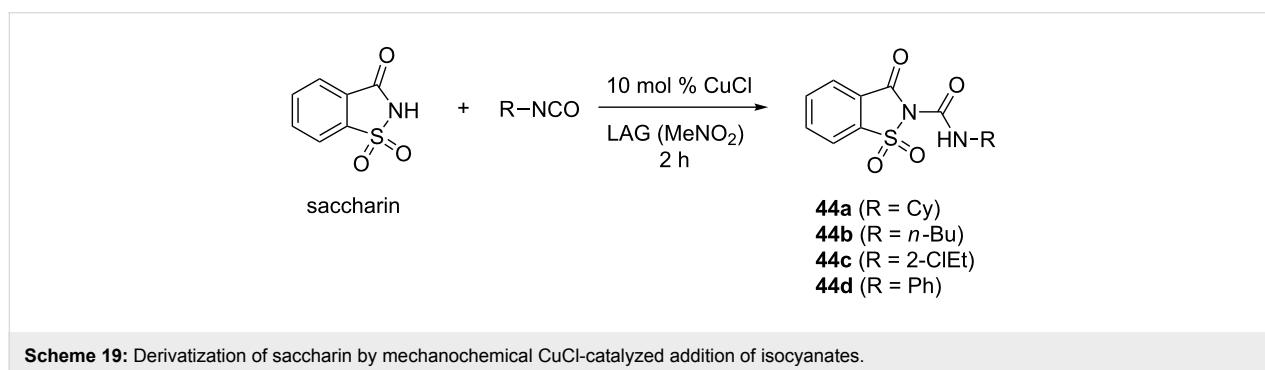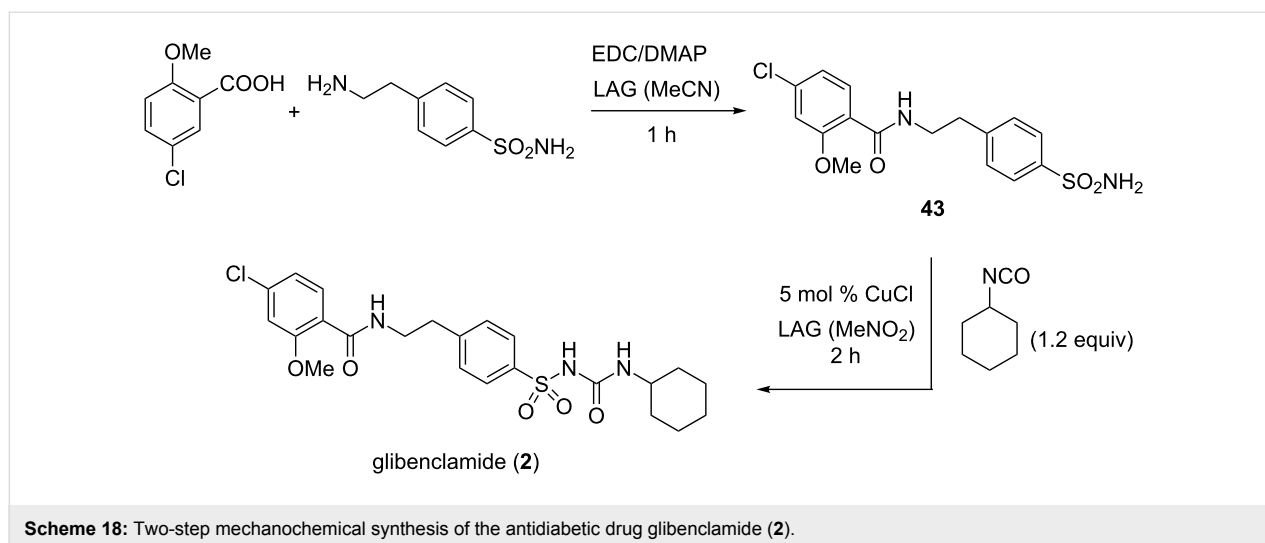
in the first step the amide bond would be constructed by amine–carboxylic acid coupling, followed by catalytic sulfonamide–isocyanate coupling. The mechanochemical EDC-mediated amide bond formation [50] was successful and provided the intermediate **43** in 74% yield. In the second step, coupling of the sulfonamide intermediate **43** with 1.2 equivalents of cyclohexyl isocyanate in the presence of 5 mol % of CuCl and nitromethane as the grinding liquid in LAG ($\eta = 0.25$ μL mg^{-1}), quantitatively yielded glibenclamide (**2**, Scheme 18).

The same group reported on the use of the famous artificial sweetener saccharin in the mechanochemical coupling with cyclohexyl, *n*-butyl, 2-chloroethyl and phenyl isocyanates [51]. The corresponding saccharyl ureas **44a–d** were isolated in high yields after CuCl-catalyzed (10 mol %) LAG for 2 hours (Scheme 19). These several examples of sulfonylureas nicely demonstrate that ball milling is also a very powerful environmentally-friendly synthetic tool in medicinal chemistry.

Mechanochemical synthesis of guanidines
Guanidines
The success of mechanochemical synthesis of sulfonylureas by the coupling of sulfonamides with isocyanates led us to investigate the reactivity of sulfonamides with carbodiimides as

Scheme 18: Two-step mechanochemical synthesis of the antidiabetic drug glibenclamide (**2**).

Scheme 19: Derivatization of saccharin by mechanochemical CuCl-catalyzed addition of isocyanates.

another example of the heterocumulene system [52]. The attempted addition of *p*-toluenesulfonamide to *N,N'*-dicyclo-hexylcarbodiimdie (DCC) failed in solution, but also under solvent-free and LAG mechanochemical conditions (Scheme 20a). However, when this mixture was milled for 2 hours neat in the presence of 5 mol % of CuCl, the product **45a** was obtained in 81%, while LAG (nitromethane, η = 0.25 μL mg^{-1}) resulted in almost quantitative yield. Interestingly, the catalysis in solution did not work, hence representing the first example of carbon–nitrogen coupling reaction that was accessible only by mechanochemistry. This discovery suggests that milling not only enhances the previously known reactivity, but it also has the potential for reaction discovery and development.

Applying the standard milling conditions, a series of sulfonyl-guanidines was synthesised in ≥90% yields from alkyl or aromatic carbodiimides and aromatic sulfonamides (Scheme 20b). Sterically hindered carbodiimides such as *tert*-butyl and trimethylsilyl derivatives displayed no reactivity. With 2-naphthyl and *p*-nitrophenylsulfonamides as poorly reactive compounds, additional LAG screening experiments were required to

establish the optimal reaction conditions by switching to acetone as the grinding liquid, prolonging the milling time to 4 hours and increasing the catalyst loading to 10–20 mol %. In general, there was no reactivity without CuCl, in solution or in the presence of a base instead of CuCl, implying that CuCl activated the carbodiimide component during this catalytic reaction.

Tan and Friščić further developed this mechanochemical synthetic strategy and applied it to a previously unknown carbodiimide insertion into sulfonimides, resulting in two-atom ring expansion and chain extension reactions [51]. Saccharin was selected as a model cyclic sulfonimide substrate, while 4-methyl-*N*-tosylbenzamide was employed as an acyclic analogue. Single crystal X-ray diffraction analyses of the products obtained by firstly reacting saccharin with several carbodiimides in solution (ethyl acetate, acetone or acetonitrile) revealed the formation of the 7-membered benzo[1,2,4]thiadiazepine ring in all cases. For example, the product **46b** (Scheme 21), which was previously characterized as a simple guanidine adduct between saccharin and DCC, arose from the DCC insertion into the 5-membered saccharin ring.
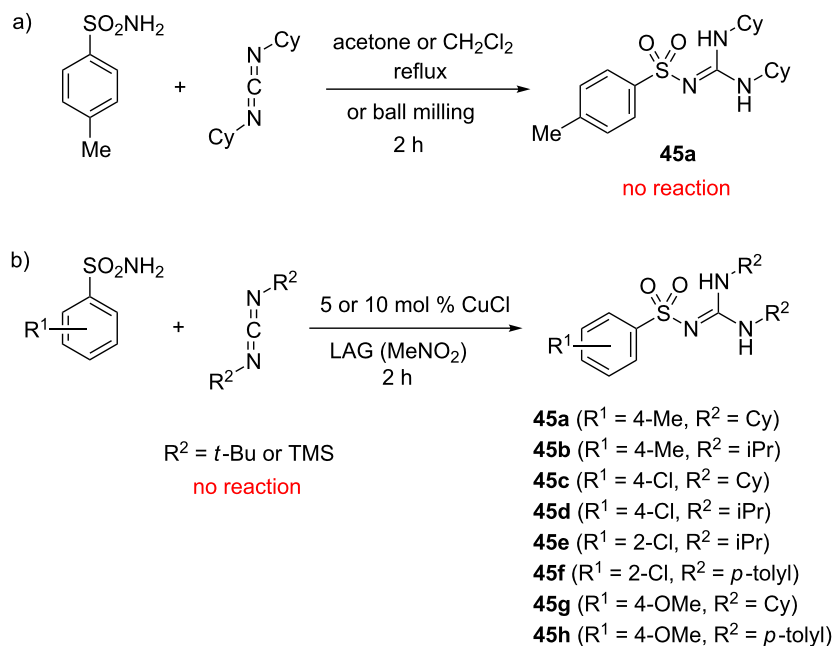
Scheme 20: a) Unsuccessful coupling of *p*-toluenesulfonamide and DCC in solution and by neat/LAG ball milling. b) CuCl-catalyzed synthesis of some sulfonyl guanidines under LAG milling conditions.

Under mechanochemical conditions, solvent-free or LAG milling of saccharin with *N,N'*-diisopropylcarbodiimide (DIC) failed to afford the desired product. However, the addition of 10 mol % of CuCl catalyst led to the quantitative formation of benzo[1,2,4]thiadiazepine **46a** after 2 hours, as evidenced by FTIR-ATR and PXRD analyses of the crude reaction mixture.

Other carbodiimides also smoothly underwent the mechanochemical insertion, e.g., DCC (78%), *N*-ethyl-*N'*-*tert*-butylcarbodiimide (85%) and di-*p*-tolylcarbodiimide (80%, Scheme 21a). The performance of the reaction was not affected even on >1 g scale. Milling 4-methyl-*N*-tosylbenzamide (**47**) with DIC and CuCl (10 mol %) for 2 hours resulted in the inser-
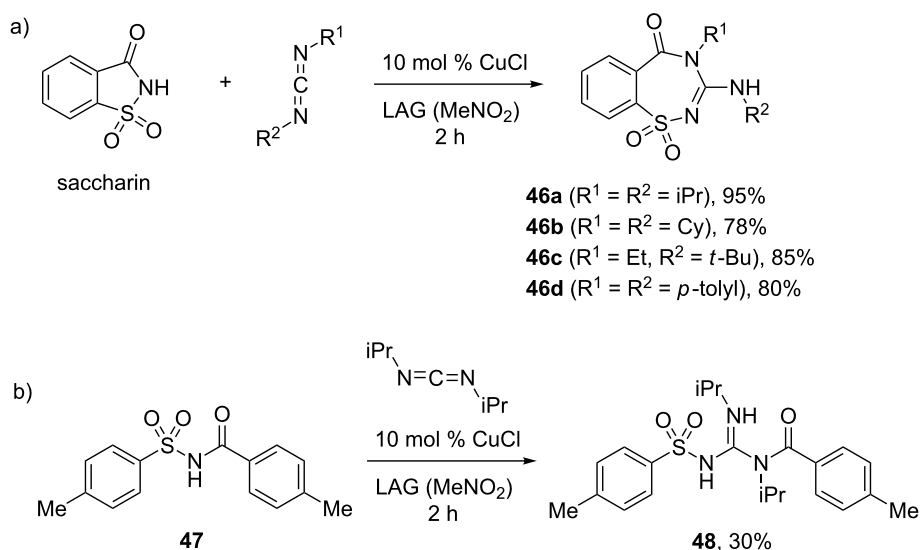
Scheme 21: a) Expansion of the saccharin ring by mechanochemical insertion of carbodiimides. b) Insertion of DIC into the linear analogue **47**.

tion of the carbodiimide into the C–N bond of benzamide and the formation of *N*-acylsulfonylguanidine **48** extended by two atoms (Scheme 21b).

Biguanides

The attachment of an amidine subunit onto the guanidine core, which is typically accomplished by the addition of a carbodiimide molecule, leads to a biguanide framework. In a paper by Margetić and Eckert-Maksić, several non-classical preparative methods were evaluated for the synthesis of highly basic hexasubstituted biguanides **49a–g** (Scheme 22) [53]. One of the techniques employed was mechanochemical ball milling in a mixer mill and a planetary mill. In the case of the mixer mill, the reaction conditions were 2 hours at 30 Hz frequency using a 12 mm stainless steel ball, while in the planetary mill 50 × 3 mm balls were used at 500 rpm. Sodium chloride was added as the solid auxiliary to facilitate the mass transfer during milling. Under these conditions, 1,1,3,3-tetramethylguanidine as the nucleophile was reacted with 1.3 equiv of dialkyl- and alkylaromatic carbodiimides.

With less reactive dialkyl carbodiimides the yields were poor, however, the introduction of an aromatic substituent (phenyl or 4-methoxyphenyl) in the carbodiimide component significantly increased the reactivity resulting in >90% conversion and >80% isolated yields of biguanides **49f** and **49g** (Table 1).
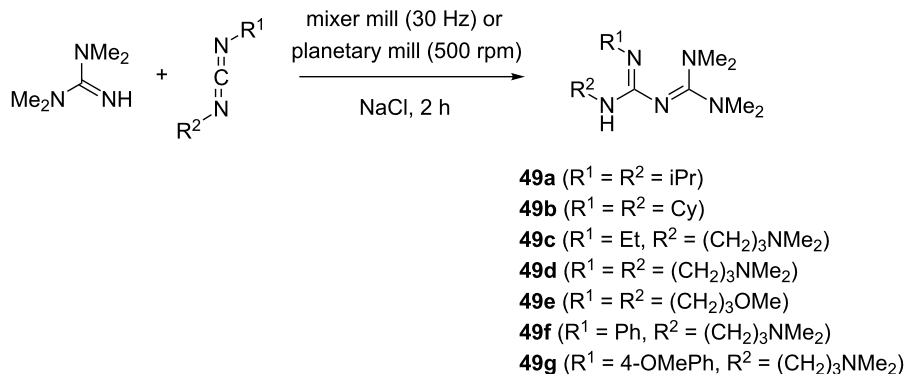
Conclusion

Mechanochemical solid-state ball milling has enabled the efficient, high-yielding, rapid and operationally-simple syntheses of (thio)ureas and guanidines. The utility of these compounds as synthetic intermediates, organocatalysts and anion sensors, in combination with specific reactivity of iso(thio)cyanates or carbodiimides with amines as suggested by the experimental and theoretical observations, has kept the focus of mechanochemical synthesis primarily on thioureas. Still, the

Table 1: The efficiency of mixer and planetary ball milling in the synthesis of biguanides **49a–g**.[a]

biguanide	conversion [%]	
	mixer mill	planetary mill
49a	15	40
49b	–	5
49c	traces	–
49d	<5[b]	–
49e	44[b]	–
49f	95[b] (82)	–
49g	94[b] (86)	–

[a]Mixer mill: 12 mm ball, 30 Hz, 2 h; planetary mill: 50 × 3 mm balls, 500 rpm; NaCl (Na_2SO_4 for **49f** and **49g**) as the solid auxiliary. [b]Milling time 1 h.

structural diversity of the molecules presented herein testify that mechanochemistry can be utilized to successfully cope with the challenges of modern synthetic organic chemistry, in terms of quantitative conversion of chiral substrates, desymmetrization of small molecules, metal-catalyzed reactions and molecular rearrangements. Many examples demonstrate that the mechanochemical approach to synthesis enhances the already described reactivity patterns, but also allows the development and discovery of novel reactions under milling conditions. The possibility to conduct mechanochemical reactions in near-quantitative yields has eliminated the need for excess reagents, transforming them into stoichiometric, or even catalytic processes. Finally, as an inherently solvent-free methodology, mechanochemistry has made the usage of bulk solvents obsolete in the synthesis steps, thus simplifying the isolation procedures as well. With the principal synthetic routes to (thio)ureas and guanidines in the solid-state now established, the next challenge of incorporation of these simple structural units into more complex molecular systems by mechanochemistry is expected.

49a (R^1 = R^2 = iPr)
49b (R^1 = R^2 = Cy)
49c (R^1 = Et, R^2 = (CH$_2$)$_3$NMe$_2$)
49d (R^1 = R^2 = (CH$_2$)$_3$NMe$_2$)
49e (R^1 = R^2 = (CH$_2$)$_3$OMe)
49f (R^1 = Ph, R^2 = (CH$_2$)$_3$NMe$_2$)
49g (R^1 = 4-OMePh, R^2 = (CH$_2$)$_3$NMe$_2$)

Scheme 22: Synthesis of highly basic biguanides by ball milling.

References

1. Wöhler, F. *Ann. Phys.* **1828,** *88,* 253–256.
   doi:10.1002/andp.18280880206

2. Van Daele, I.; Munier-Lehmann, H.; Froeyen, M.; Balzarini, J.;
   Van Calenbergh, S. *J. Med. Chem.* **2007,** *50,* 5281–5292.
   doi:10.1021/jm0706158

3. Bukvić Krajačić, M.; Novak, P.; Dumić, M.; Cindrić, M.;
   Čipčić Paljetak, H.; Kujundžić, N. *Eur. J. Med. Chem.* **2009,** *44,*
   3459–3470. doi:10.1016/j.ejmech.2009.02.001

4. Bloom, J. D.; DiGrandi, M. J.; Dushin, R. G.; Curran, K. J.; Ross, A. A.;
   Norton, E. B.; Terefenko, E.; Jones, T. R.; Feld, B.; Lang, S. A.
   Bioorg. Med. Chem. Lett. **2003,** *13,* 2929–2932.
   doi:10.1016/S0960-894X(03)00586-9

5. Sharma, S. K.; Wu, Y.; Steinbergs, N.; Crowley, M. L.; Hanson, A. S.;
   Casero, R. A., Jr.; Woster, P. M. *J. Med. Chem.* **2010,** *53,* 5197–5212.
   doi:10.1021/jm100217a

6. *World Malaria Report 2016: Summary;* World Health Organization:
   Geneva, 2017.

7. Selig, P. *Synthesis* **2013,** *45,* 703–718. doi:10.1055/s-0032-1318154

8. Sohtome, Y.; Takemura, N.; Takagi, R.; Hashimoto, Y.; Nagasawa, K.
   Tetrahedron **2008,** *64,* 9423–9429. doi:10.1016/j.tet.2008.07.087

9. Kotke, M.; Schreiner, P. R. *Tetrahedron* **2006,** *62,* 434–439.
   doi:10.1016/j.tet.2005.09.079

10. Herrera, R. P.; Sgarzani, V.; Bernardi, L.; Ricci, A.
    Angew. Chem., Int. Ed. **2005,** *44,* 6576–6579.
    doi:10.1002/anie.200500227

11. Gale, P. A. *Acc. Chem. Res.* **2011,** *44,* 216–226.
    doi:10.1021/ar100134p

12. Caltagirone, C.; Gale, P. A. *Chem. Soc. Rev.* **2009,** *38,* 520–563.
    doi:10.1039/B806422A

13. Anastas, P. T.; Warner, J. C. *Green Chemistry: Theory and Practice;*
    Oxford University Press: New York, 1998; pp 30 ff.

14. Tang, S. Y.; Bourne, R. A.; Smith, R. L.; Poliakoff, M. *Green Chem.*
    2008, *10,* 268–269. doi:10.1039/b719469m

15. Wang, G.-W. *Chem. Soc. Rev.* **2013,** *42,* 7668–7700.
    doi:10.1039/c3cs35526h

16. Margetić, D.; Štrukil, V. *Mechanochemical Organic Synthesis;* Elsevier:
    Amsterdam, 2016.

17. James, S. L.; Adams, C. J.; Bolm, C.; Braga, D.; Collier, P.; Friščić, T.;
    Grepioni, F.; Harris, K. D. M.; Hyett, G.; Jones, W.; Krebs, A.; Mack, J.;
    Maini, L.; Orpen, A. G.; Parkin, I. P.; Shearouse, W. C.; Steed, J. W.;
    Waddell, D. C. *Chem. Soc. Rev.* **2012,** *41,* 413–447.
    doi:10.1039/C1CS15171A

18. Tan, D.; Loots, L.; Friščić, T. *Chem. Commun.* **2016,** *52,* 7760–7781.
    doi:10.1039/C6CC02015A

19. Shan, N.; Toda, F.; Jones, W. *Chem. Commun.* **2002,** 2372–2373.
    doi:10.1039/b207369m

20. Friščić, T.; Trask, A. V.; Jones, W.; Motherwell, W. D. S.
    Angew. Chem., Int. Ed. **2006,** *45,* 7546–7550.
    doi:10.1002/anie.200603235

21. Friščić, T.; Reid, D. G.; Halasz, I.; Stein, R. S.; Dinnebier, R. E.;
    Duer, M. J. *Angew. Chem., Int. Ed.* **2010,** *49,* 712–715.
    doi:10.1002/anie.200906583

22. Hasa, D.; Schneider Rauber, G.; Voinovich, D.; Jones, W.
    Angew. Chem., Int. Ed. **2015,** *54,* 7371–7375.
    doi:10.1002/anie.201501638

23. Hasa, D.; Carlino, E.; Jones, W. *Cryst. Growth Des.* **2016,** *16,*
    1772–1779. doi:10.1021/acs.cgd.6b00084

24. Friščić, T.; Halasz, I.; Beldon, P. J.; Belenguer, A. M.; Adams, F.;
    Kimber, S. A. J.; Honkimäki, V.; Dinnebier, R. E. *Nat. Chem.* **2013,** *5,*
    66–73. doi:10.1038/nchem.1505

25. Halasz, I.; Puškarić, A.; Kimber, S. A. J.; Beldon, P. J.;
    Belenguer, A. M.; Adams, F.; Honkimäki, V.; Dinnebier, R. E.; Patel, B.;
    Jones, W.; Štrukil, V.; Friščić, T. *Angew. Chem., Int. Ed.* **2013,** *52,*
    11538–11541. doi:10.1002/anie.201305928

26. Katsenis, A. D.; Puškarić, A.; Štrukil, V.; Mottillo, C.; Julien, P. A.;
    Užarević, K.; Pham, M.-H.; Do, T.-O.; Kimber, S. A. J.; Lazić, P.;
    Magdysyuk, O.; Dinnebier, R. E.; Halasz, I.; Friščić, T. *Nat. Commun.*
    2015, *6,* No. 6662. doi:10.1038/ncomms7662

27. Gracin, D.; Štrukil, V.; Friščić, T.; Halasz, I.; Užarević, K.
    Angew. Chem., Int. Ed. **2014,** *53,* 6193–6197.
    doi:10.1002/anie.201402334

28. Batzdorf, L.; Fischer, F.; Wilke, M.; Wenzel, K.-J.; Emmerling, F.
    Angew. Chem., Int. Ed. **2015,** *54,* 1799–1802.
    doi:10.1002/anie.201409834

29. Užarević, K.; Halasz, I.; Friščić, T. *J. Phys. Chem. Lett.* **2015,** *6,*
    4129–4140. doi:10.1021/acs.jpclett.5b01837

30. Kaupp, G.; Schmeyers, J.; Boy, J. *Tetrahedron* **2000,** *56,* 6899–6911.
    doi:10.1016/S0040-4020(00)00511-1

31. Li, J.-P.; Wang, Y.-L.; Wang, H.; Luo, Q.-F.; Wang, X.-Y.
    Synth. Commun. **2001,** *31,* 781–785. doi:10.1081/SCC-100103270

32. Štrukil, V.; Igrc, M. D.; Fábián, L.; Eckert-Maksić, M.; Childs, S. L.;
    Reid, D. G.; Duer, M. J.; Halasz, I.; Mottillo, C.; Friščić, T. *Green Chem.*
    2012, *14,* 2462–2473. doi:10.1039/c2gc35799b

33. Li, J. P.; Luo, Q. F.; Song, Y. M.; Wang, Y. L. *Chin. Chem. Lett.* **2001,**
    12, 383–386.

34. Štrukil, V.; Igrc, M. D.; Eckert-Maksić, M.; Friščić, T. *Chem. – Eur. J.*
    2012, *18,* 8464–8473. doi:10.1002/chem.201200632

35. Štrukil, V.; Margetić, D.; Igrc, M. D.; Eckert-Maksić, M.; Friščić, T.
    Chem. Commun. **2012,** *48,* 9705–9707. doi:10.1039/c2cc34013e

36. Rudorf, W.-D. *J. Sulfur Chem.* **2007,** *28,* 295–339.
    doi:10.1080/17415990701245107

37. Zhang, Z.; Wu, H.-H.; Tan, Y.-J. *RSC Adv.* **2013,** *3,* 16940–16944.
    doi:10.1039/c3ra43252a

38. Katritzky, A. R.; Witek, R. M.; Rodriguez-Garcia, V.; Mohapatra, P. P.;
    Rogers, J. W.; Cusido, J.; Abdel-Fattah, A. A. A.; Steel, P. J.
    J. Org. Chem. **2005,** *70,* 7866–7881. doi:10.1021/jo050670t

39. Katritzky, A. R.; Ledoux, S.; Witek, R. M.; Nair, S. K. *J. Org. Chem.*
    2004, *69,* 2976–2982. doi:10.1021/jo035680d

40. Katritzky, A. R.; Rogovoy, B. V. *Chem. – Eur. J.* **2003,** *9,* 4586–4593.
    doi:10.1002/chem.200304990

41. Štrukil, V.; Gracin, D.; Magdysyuk, O. V.; Dinnebier, R. E.; Friščić, T.
    Angew. Chem., Int. Ed. **2015,** *54,* 8440–8443.
    doi:10.1002/anie.201502026

42. Đud, M.; Magdysyuk, O. V.; Margetić, D.; Štrukil, V. *Green Chem.*
    2016, *18,* 2666–2674. doi:10.1039/C6GC00089D

43. Douglass, I. B.; Dains, F. B. *J. Am. Chem. Soc.* **1934,** *56,* 1408–1409.
    doi:10.1021/ja01321a061

44. Herr, R. J.; Kuhler, J. L.; Meckler, H.; Opalka, C. J. *Synthesis* **2000,**
    1569–1574. doi:10.1055/s-2000-7607

45. Swinburne, A. N.; Steed, J. W. *CrystEngComm* **2009,** *11,* 433–438.
    doi:10.1039/b817067c

46. Waddell, D. C.; Thiel, I.; Bunger, A.; Nkata, D.; Maloney, A.; Clark, T.;
    Smith, B.; Mack, J. *Green Chem.* **2011,** *13,* 3156–3161.
    doi:10.1039/c1gc15594f

47. Konnert, L.; Reneaud, B.; de Figueiredo, R. M.; Campagne, J.-M.;
    Lamaty, F.; Martinez, J.; Colacino, E. *J. Org. Chem.* **2014,** *79,*
    10132–10142. doi:10.1021/jo5017629

48. Tan, D.; Štrukil, V.; Mottillo, C.; Friščić, T. *Chem. Commun.* **2014,** *50,* 5248–5250. doi:10.1039/C3CC47905F

49. Commercial sulfonyl isocyanates, available from Sigma-Aldrich (May 2017) include only 7 compounds: chlorosulfonyl, benzenesulfonyl, *p*-toluenesulfonyl, *o*-toluenesulfonyl, 4-chlorobenzenesulfonyl, 2-chlorobenzenesulfonyl and 4-fluorobenzenesulfonyl derivatives.

50. Štrukil, V.; Bartolec, B.; Portada, T.; Đilović, I.; Halasz, I.; Margetić, D. *Chem. Commun.* **2012,** *48,* 12100–12102. doi:10.1039/c2cc36613d

51. Tan, D.; Friščić, T. *Chem. Commun.* **2017,** *53,* 901–904. doi:10.1039/C6CC07331J

52. Tan, D.; Mottillo, C.; Katsenis, A. D.; Štrukil, V.; Friščić, T. *Angew. Chem., Int. Ed.* **2014,** *53,* 9321–9324. doi:10.1002/anie.201404120

53. Glasovac, Z.; Trošelj, P.; Jušinski, I.; Margetić, D.; Eckert-Maksić, M. *Synlett* **2013,** *24,* 2540–2544. doi:10.1055/s-0033-1339876

Solvent-free sonochemistry: Sonochemical organic synthesis in the absence of a liquid medium

Deborah E. Crawford

Full Research Paper

Address:
School of Chemistry and Chemical Engineering, Queen's University Belfast, David Keir Building, 39–123 Stranmillis Road, Belfast, BT9 5AG, Northern Ireland, UK

Email:
Deborah E. Crawford - d.crawford@qub.ac.uk

Abstract

Sonochemistry, i.e., the application of mechanical energy in the form of sound waves, has recently been recognised for its similarity to mechanochemistry and is now included under the umbrella term of mechanochemistry. Typically, due to the hypothesised cavitation mechanism, a liquid medium is considered as a necessity for a process to take place as a result of ultrasonic irradiation. In view of this, condensation reactions between solid reagents in the complete absence of solvent were carried out successfully by ultrasonic irradiation with the importance of particle size being highlighted. This work increases the potential of sonochemistry in the drive towards a sustainable future.

Introduction

Mechanochemistry is typically regarded as the grinding of solid reagents in a ball mill (or mortar and pestle), to instigate and accelerate chemical reactions [1]. In recent years, mechanochemistry has evolved to include techniques such as shearing [2], microfluidics [3] and twin screw extrusion [4-6]. More recently, sonochemistry has been included under the umbrella term of mechanochemistry [7] as it has demonstrated excellent potential when instigating chemical activity in solutions by applying mechanical energy (Figure 1) [8,9].

Sonochemistry is hypothesised to originate from acoustic cavitation and bubble collapse as a result of the mechanical effects of sounds on liquids [8,9]. Bubble collapse in particular results in intense compressional heating, thereby creating hot spots, a phenomenon currently employed to explain the processes occurring in ball milling [7]. It must also be noted that there is a similar technology available to sonochemistry, that is considered to be less harsh than mechanochemistry, and this is resonant acoustic mixing (RAM). The RAM mixes by controlling
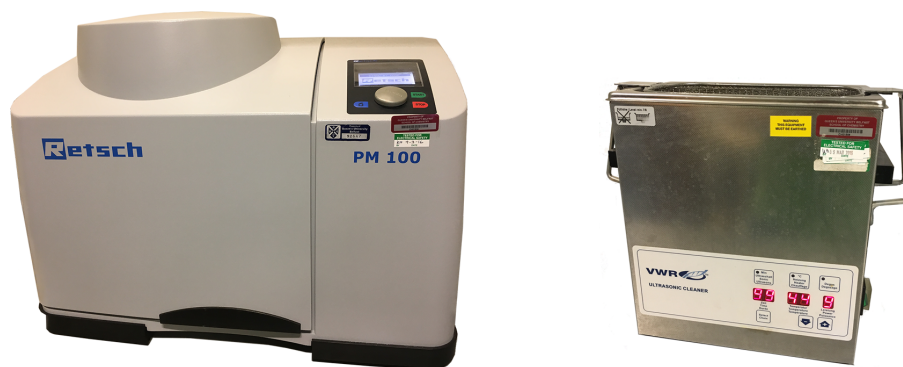
Figure 1: Typical laboratory employed planetary ball mill and ultrasonic bath.

the vibration applied to the material through acceleration and frequency, and therefore is actually mechanistically different from sonochemical mixing [8,9]. Other effects that have been found to be common for both sonochemistry and mechanochemistry include: local heating, crystal deformation and phase transitions amongst others [7].

Ultrasonic irradiation is commonly carried out on liquid/gas mixtures (for gas removal), liquid/liquid mixtures and liquid/solid mixtures. The technique is used extensively in materials chemistry, for example, it has been demonstrated to be one of the most efficient methods to exfoliate layered materials such as graphite (to form graphene) [10], but it has also been employed in the formation of organometallic [11] and organic compounds [12]. Great success has been found in the treatment of waste water by ultrasonic irradiation, to remove heavy metals or degrade aromatic constituents [13].

Metal catalysts are prepared by the sonication of metal halides (e.g., Pt and Pd – reduction of metal) in the presence of Li and THF [14,15]. Furthermore, the catalytic behaviour of catalysts such as Raney Nickel, has reportedly been increased solely due to the effect of using ultrasound [16]. Catalyst coatings, such as metal oxide, can be broken up and removed as a result of ultrasonic cavitation, therefore this technology overcomes the drawbacks of reacting a solid and a liquid in a heterogeneous system, allowing the reaction to proceed further [16].

The reaction of toluene with benzyl bromide in the presence of KCN/Al_2O_3, is an example of organic synthesis employing ultrasound [17]. Interestingly, the conventional solution method results in the alkylation of the toluene aromatic ring, however, when sonication is employed, a reaction between benzyl bromide and KCN occurs producing $PhCH_2CN$, indicating that alternative products can be formed using this technique, as with ball milling.

The Knoevenagel condensation [18], Michael addition [19] and Biginelli reactions [20] amongst others have been instigated by ultrasonic irradiation in the presence of solvents such as pyridine and methanol, resulting in a decrease of their reaction times from >10 hours to 1–2 hours. Also, in some cases sonication greatly improved the yield, for example in a Vilsmeier–Haack reaction [21]; in addition selectivity can also be improved as demonstrated in a Pinacol coupling whereby a *meso*-isomer was the dominant product, a result only observed when the reaction is sonicated [22].

Results and Discussion

The presence of a liquid medium in a system undergoing ultrasonic irradiation is greatly important to facilitate the cavitation process and a consequence of this is that there has not been any research into sonochemical reactions being carried out in the absence of solvent, or a liquid reagent [8,9]. Herein, we report two condensation reactions (investigated extensively by ball milling), one to form salen ligand **1** by sonicating *o*-vanillin and 1,2-phenylenediamine, and the second to form 1,3-indandione **2** from ninhydrin and dimedone. Both systems were investigated in the complete absence of solvent and without the presence of any grinding media (such as inert silica beads) to help mediate the reaction. The aldol reaction was successfully carried out by twin screw extrusion, as I have reported previously [6]. The success of both of these reactions by ultrasound irradiation in the absence of solvent creates potential for organic synthesis to be carried out by applying a milder form of mechanical energy, i.e., sound waves. As a result, it may be possible that reactions which are particularly sensitive to intense mechanical energy (and may undergo degradation) may be successful by ultrasonic irradiation.

It must be noted that the conventional reaction between *o*-vanillin and 1,2-phenylenediamine requires refluxing for 9 hours in ethanol for a complete conversion to the product. For

the initial sonochemistry experiments (Scheme 1), both reagents were used as received, *o*-vanillin came in the form of small flakes and 1,2-phenylenediamine was received as large crystalline beads (Figure 2).

Upon sonication of the mixed reagents (using a standard ultrasonication bath with a frequency of 35 kHz) for 60 minutes, it was observed that the temperature of the ultrasonic bath increased to 70–75 °C, causing both reagents to form a melt (*o*-vanillin has a melting point of 42 °C, 1,2-phenylenediamine has a melting point of 104 °C), which is likely to be the result of an eutectic melt forming. This was quite surprising as the melting point of 1,2-phenylenediamine is greater than that of the observed temperature of the ultrasonic bath. The molten substance then changed to a hard solid form and not the preferred free flowing solid. It was expected that because the reagents melted then they would have reacted completely to form the product, aided by the help of heating. However, ^{1}H NMR spectroscopy showed that the conversion to the product was only 36%, therefore, the reaction did not proceed significantly as a result of the high temperature, and the reaction was potentially hindered as a result of the hard solid formed.

Stopping the reaction to grind this solid form into a free flowing solid would lead to inaccurate results as mechanical energy in the form of grinding could have a significant effect on the outcome of the reaction. Therefore, as the application of heat may have an effect on the conversion to product and the mixture needed to remain as a free slowing solid, sonication was carried out for 10 minute intervals, preventing an increase in temperature and melting of the reagents (alternatively a cooling fluid could be used). After 60 minutes of sonicating, a colour change was observed (Figure 3 – to bright orange) but there was a clear separation between the two solids, indicating that the variation of particle size and morphology was too great for the reaction to proceed quantitatively.

Therefore, both reagents were ground and sieved to both be fine powders of particle size <500 μm. A ca. 0.2 g mixture was sonicated for 60 minutes (keeping the temperature of the bath at ambient temperature) and it was clear to see that a more successful reaction had taken place. A homogeneous orange solid was produced; however, there was an increase in the pressure of the system that was too great to be withheld in the 2 mL vial employed. This was presumably due to the production of the
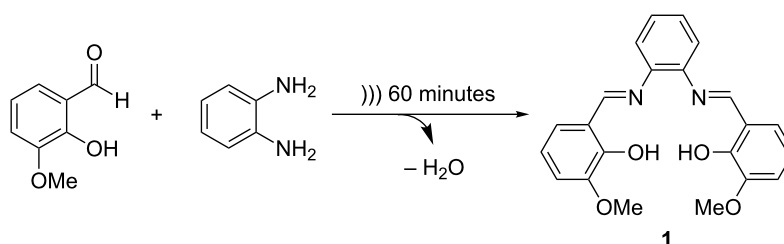
Scheme 1: Reaction between *o*-vanillin and 1,2-phenylenediamine by ultrasonic irradiation for 60 minutes.

**Figure 2:** *o*-Vanillin in its flake form and 1,2-phenylenediamine in its bead form.

Figure 3: Clear separation of the reagents observed, with orange coated beads of 1,2-phenylenediamine residing at the bottom of the mixture.

byproduct – water, which was seen to be in its vapour form, most likely due to the heat produced from the exothermic reaction of the aldehyde and the diamine. This indicated that a greater free volume (also known as 'headspace') in the vial was required to accommodate this increase in pressure.

A larger vial (25 mL) was then employed, which was able to sustain the pressure of the water vapour produced in the system, and with that there was a 5-fold scale-up of the reaction mixture from ca. 0.2 g to ca. 1.0 g. After 60 minutes of ultrasonic irradiation a bright orange free flowing solid was produced indicating that a reaction had occurred. ^{1}H NMR spectroscopy showed that indeed a reaction had taken place to form the desired imine; however, a conversion to product of only 69% was determined. The experiment was repeated but ultrasonic irradiation was carried out for 90 minutes, leading to a marginally higher conversion to product of 73%.

In order to improve the rate of conversion to product, a mild base, anhydrous Na_2CO_3 (0.1 equiv) was added to the reaction. *o*-Vanillin, 1,2-phenylenediamine and Na_2CO_3 were then sonicated for 60 minutes to produce a dark red solid (similar to that obtained from solution). ^{1}H NMR spectroscopy indicated that the reagents had almost all been consumed; however, it was noted that the ^{1}H NMR spectrum was more complicated than expected with two peaks representing imine protons. It was determined that the desired product had formed along with the product from the 1:1 reaction of the aldehyde and the diamine, **1'** (Figure 4). Excess aldehyde was expected to be present; however, this was not the case (<1% present), indicating that the reaction mixture was still not completely homogeneous.

In order to overcome this problem, the particle size of both starting materials was reduced further to <200 μm and soni-
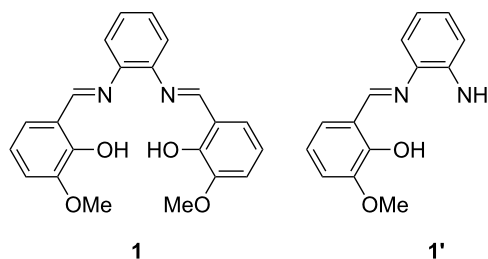

Figure 4: Chemical structures of the products obtained from the reaction between *o*-vanillin and 1,2-phenylenediamine.

cated for 60 minutes, resulting in a dark red powder (Figure 5). ^{1}H NMR spectroscopy showed that the reaction had fully converted to the desired product – the desired diimine, **1** (Figure 6). Powder X-ray diffraction (PXRD) analysis shows that the powder patterns of both the sonochemical product and the solu-
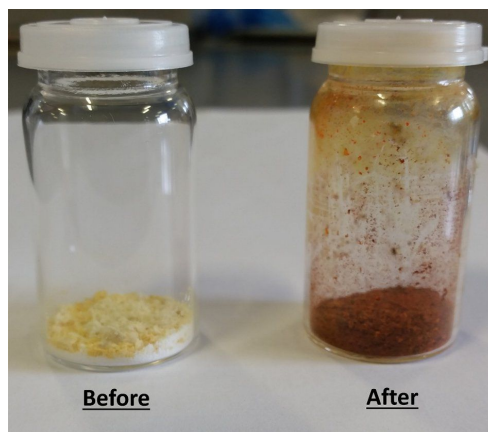
**Figure 5:** Reaction mixture before and after ultrasonic irradiation for 60 minutes.
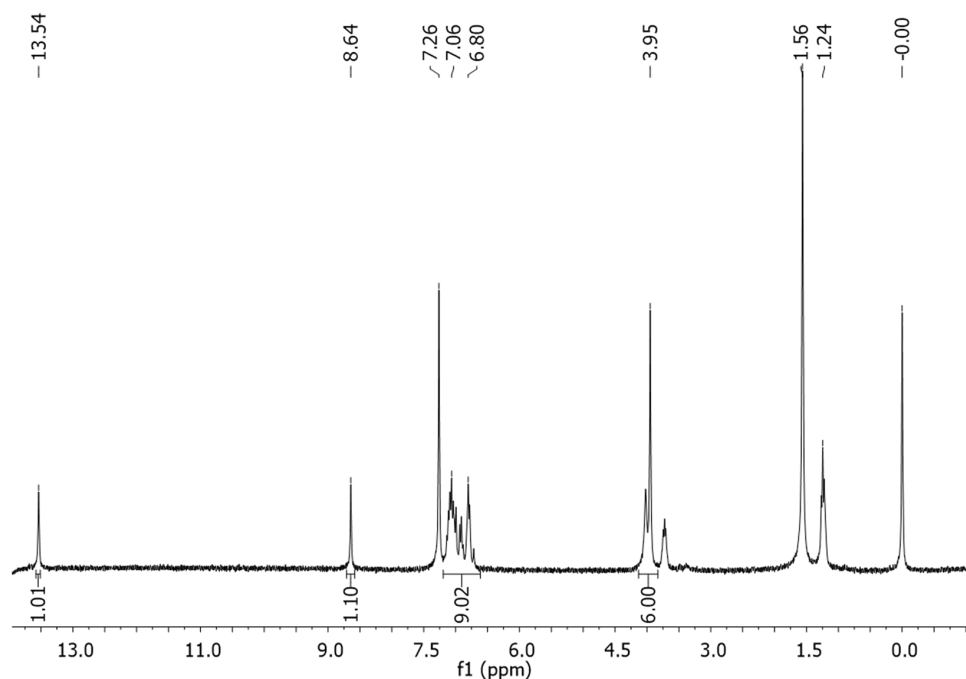
Figure 6: ^{1}H NMR spectrum of diimine **1** in CDCl$_3$/EtOD.

tion product are the same and IR spectroscopy confirmed that an imine bond was present in the product, with no indication of an aldehyde functionality being present (see Supporting Information File 1).

Sonochemical reactions are reportedly irreproducible [11] and to determine if this was the case in the reaction between *o*-vanillin and 1,2-phenylenediamine, the experiment was repeated under the optimised conditions three times. In each case, the reaction was reproducible showing a complete conversion to the product (as determined by ^{1}H NMR spectroscopy). In addition, a control reaction was carried out whereby the reagents (in the same concentrations) were mixed manually and left for several days without being agitated. Although there was some colour change in the mixture, the reaction had not proceeded significantly (after 3 days, <5% conversion to product was observed). Furthermore, the reaction was monitored in

CDCl$_3$ to ensure that the reactions were not proceeding as a result of exposure to the NMR spectroscopy solvent, which was found to be the case. Therefore, it is ultrasonic irradiation at room temperature that is instigating and accelerating this chemical reaction.

Further confirmation that sonochemistry is a viable method to carry out solid state organic synthesis was obtained by carrying out an aldol reaction between ninhydrin and dimedone (Scheme 2). The optimised parameters from the previous system were applied, i.e., the particle size of the reagents was reduced (to <200 µm) and ultrasonic irradiation was carried out in 10 minute intervals to prevent melting of the reagents. After 90 minutes of sonicating, a pink solid was produced with ^{1}H NMR spectroscopy indicating that a complete reaction had taken place between a hydroxy group of ninhydrin and the activated methylene of dimedone (Figure 7). This reaction has pre-
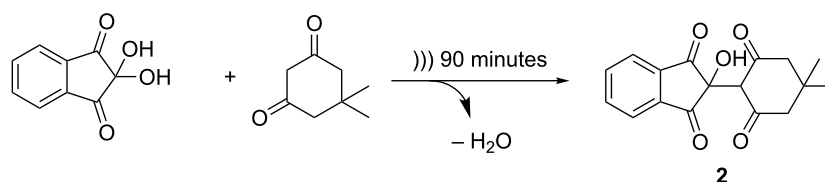
Scheme 2: Aldol reaction between ninhydrin and dimedone to form **2**.
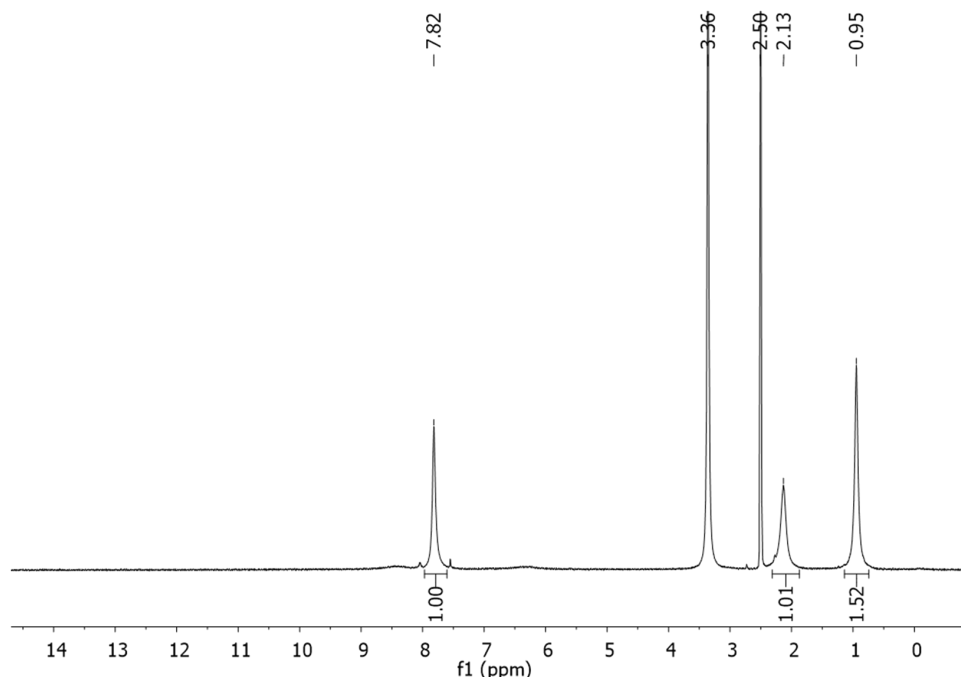
Figure 7: ¹H NMR spectrum of 1,3-indandione **2** in DMSO-*d*₆.

viously been carried out by twin screw extrusion in the absence of solvent [6], and it was confirmed that the same product was obtained by both synthetic methods (see Supporting Information File 1). A control experiment was carried out, whereby the reagents were mixed as two solids and left under ambient temperature and pressure for several weeks, after three weeks, a conversion of 72% to the desired product was observed, confirming the advantage of employing sonochemistry.

Conclusion

In conclusion, the first examples of ultrasound induced solvent-free condensation reactions are reported, forming a Schiff base **1** (which has significant applications in catalysis) and a 1,3-indandione **2**. It was concluded that one of the key parameters in these reactions was the particle size of the starting materials, with a reduced particle size of <200 µm resulting in a homogeneous mixture leading to complete conversion to the product. This provides an excellent foundation for further investigations into solvent-free or solid-state sonochemistry, including studying a larger scope of chemical reactions and the mechanism behind which the liquid/solvent-free reactions occur. It also provides a means of applying a gentler form of mechanical energy to a system which may increase the range of organic and inorganic mechanochemical transformations that can be carried out (where grinding results in degradation of the material). Finally, as with ball milling, there is potential for the scale-up

of sonochemical reactions, therefore aiding in the drive towards sustainable chemistry.

Supporting Information

Supporting Information File 1

Experimental part.
[http://www.beilstein-journals.org/bjoc/content/
supplementary/1860-5397-13-179-S1.pdf]

Acknowledgements

References

1. James, S. L.; Adams, C. J.; Bolm, C.; Braga, D.; Collier, P.; Friščić, T.; Grepioni, F.; Harris, K. D. M.; Hyett, G.; Jones, W.; Krebs, A.; Mack, J.; Maini, L.; Orpen, A. G.; Parkin, I. P.; Shearouse, W. C.; Steed, J. W.; Waddelli, D. C. *Chem. Soc. Rev.* **2012**, *41*, 413–447. doi:10.1039/C1CS15171A
2. Kaupp, G. *CrystEngComm* **2009**, *11*, 388–403. doi:10.1039/B810822F
3. Rivas, D. F.; Cintas, P.; Gardeniers, H. J. G. E. *Chem. Commun.* **2012**, *48*, 10935–10947. doi:10.1039/c2cc33920j

4. Crawford, D. E.; Casaban, J.; Haydon, R.; Giri, N.; McNally, T.; James, S. L. *Chem. Sci.* **2015,** *6,* 1645–1649. doi:10.1039/C4SC03217A

5. Crawford, D. E.; Wright, L. A.; James, S. L.; Abbott, A. P. *Chem. Commun.* **2016,** *52,* 4215–4218. doi:10.1039/C5CC09685E

6. Crawford, D. E.; Miskimmin, C. K. G.; Albadarin, A. B.; Walker, G.; James, S. L. *Green Chem.* **2017,** *19,* 1507–1518. doi:10.1039/C6GC03413F

7. Suslick, K. S. *Faraday Discuss.* **2014,** *170,* 411–422. doi:10.1039/C4FD00148F

8. Margulis, M. A. *Ultrason. Sonochem.* **1994,** *1,* S87–S90. doi:10.1016/1350-4177(94)90003-5

9. Tanaka, R.; Takahashi, N.; Nakamura, Y.; Hattori, Y.; Ashizawa, K.; Otsuka, M. *RSC Adv.* **2016,** *6,* 87049–87057. doi:10.1039/C6RA16209F

10. Notley, S. M. *Langmuir* **2012,** *28,* 14110–14113. doi:10.1021/la302750e

11. Suslick, K. S. *Adv. Organomet. Chem.* **1986,** *25,* 73–119. doi:10.1016/S0065-3055(08)60573-0

12. Li, J.-T.; Wang, S.-X.; Chen, G.-F.; Li, T.-S. *Curr. Org. Synth.* **2005,** *2,* 415–436. doi:10.2174/1570179054368509

13. Jamali, M. K.; Kazi, T. G.; Arain, M. B.; Afridi, H. I.; Jalbani, N.; Memon, A. R. *J. Agron. Crop Sci.* **2007,** *193,* 218–228. doi:10.1111/j.1439-037X.2007.00261.x

14. Wen-Chou, L.; Maltsev, A. N.; Kobosev, N. I. *Russ. J. Phys. Chem.* **1964,** *38,* 41–46.

15. Maltsev, A. N. *Russ. J. Phys. Chem.* **1976,** *50,* 995–998.

16. Kowalska, E.; Dziegielewska, M. *Ultrasonics* **1976,** *14,* 73–75. doi:10.1016/0041-624X(76)90102-5

17. Doan, T. L. H.; Le, T. N. *Synth. Commun.* **2012,** *42,* 337–340. doi:10.1080/00397911.2010.524338

18. Li, J.-T.; Li, T.-S.; Li, L.-J.; Cheng, X. *Ultrason. Sonochem.* **1999,** *6,* 199–201. doi:10.1016/S1350-4177(99)00014-0

19. Li, J.-T.; Cui, Y.; Chen, G.-F.; Cheng, Z.-L.; Li, T.-S. *Synth. Commun.* **2003,** *33,* 353–359. doi:10.1081/SCC-120015762

20. Yadav, J. S.; Reddy, B. V. S.; Reddy, K. B.; Raj, K. R.; Prasad, A. R. *J. Chem. Soc., Perkin Trans. 1* **2001,** 1939–1941. doi:10.1039/b102565c

21. Ali, M. M.; Sana, S.; Tasneem; Rajanna, K. C.; Saiprakash, P. K. *Synth. Commun.* **2002,** *32,* 1351–1356. doi:10.1081/SCC-120003631

22. Rieke, R. D.; Kim, S.-H. *J. Org. Chem.* **1998,** *63,* 5235–5239. doi:10.1021/jo971942y

Influence of the milling parameters on the nucleophilic substitution reaction of activated β-cyclodextrins

László Jicsinszky[*1], Kata Tuza[2], Giancarlo Cravotto[1], Andrea Porcheddu[3], Francesco Delogu[4] and Evelina Colacino[*1,5]

Abstract

The present work focuses on the mechanochemical preparation of industrially important β-cyclodextrin (CD) derivatives. Activated CDs have been reacted with nitrogen and sulfur nucleophiles using a planetary mill equipped with stainless steel, zirconia and glass milling tools of different sizes. It is shown that the milling frequency and the number as well as the size of the milling balls have an effect on the nucleophilic reaction.

Introduction

Their hollow structures make cyclodextrins (CDs) a class of carbohydrates that can form inclusion complexes with organic molecules, inorganic salts and complex metal ions [1]. Such a unique capacity makes CD derivatives crucial in a number of every-day sectors, ranging from paintings [2] to food [3]. The

availability of convenient methods for their large-scale production has made CDs all but ubiquitous, including their use in a variety of investigations at the cutting edge of biological [4] and chemical science research [5]. However, there is still considerable room for the synthesis of specific CDs on the laboratory

scale. This is the case, for instance, with 6^I-monoamino-6^I-monodeoxy-β-CD, which is easily prepared via the reduction of the parent mono-azido derivative and is used in analytical chemistry as chiral stationary phase [6]. CDs functionalized with triazole substituents can be similarly prepared through click reactions involving the azido group as a dipolarophile [7], and utilized as suitable starting material to access hydroxy functionality after derivatization [8]. Although the preparation of carbohydrate-based complexes in a ball mill has been already reported [9-11], the use of mechanical activation for the chemical derivatization of CDs has been rather sporadic [12-15]. In this respect, it is worth noting that CDs exhibit a characteristic reactivity profile. Neither traditional synthetic routes nor a conventional carbohydrate activation methodology allow for CD derivatization. The major issues stem from the differing solubility of the reagents in organic solvents, meaning that high boiling polar solvents, such as DMF or DMSO, need to be used. However, these solvents are difficult to remove and usually have considerable energy contribution. Under these circumstances, the promise shown by the mechanical processing of solids of enabling chemical transformations in the absence of solvent phases renders mechanical activation extremely appealing. This is particularly true in light of the well-known capability of mechanical treatment to induce significant enhancements in chemical reactivity.

Despite the vast amount of literature on the mechanically activated synthesis of organic molecules [16-23], CD mechanochemistry offers significant challenges. For instance, the molecular weight negatively affects the reaction design and is almost one order of magnitude higher here than for common organic molecules. The laborious preparation of the starting CD-tosylate [24,25], and the considerable reactant molecular mass differences are also elements of complexity. The mechanical processing of CDs in the absence of solvent therefore promises to simplify the work-up and allows the almost complete utilization of the CD key-intermediate [13], in comparison with the classic method [6]. Moreover, the absence of a solvent, high-boiling-point ones in particular, could prevent the undesired side-reactions, that would be caused by the decomposition of DMF (formation of dimethylamine), by hydrolysis (from residual crystal water), and by alkylation and/or oxidation (DMSO) [13], leading to cleaner reaction profiles under mechanochemical conditions. Previous work on mechanically activated substitutions on tosyl ester-activated CDs resulted in high yields of the targeted 6-monoderivatized CDs, but also in complex isolation procedures due to the large number of small balls used (50 of ø 5 mm + 1500 of ø 1 mm steel balls) [13]. Despite the longer milling times, using less balls allow outcomes to be improved [14]. This work takes the above-mentioned results as a base from which to address the

mechanochemical synthesis of 6^I-monoazido-6^I-monodeoxy-β-CD and 6^I-*S*-monodeoxy-6^I-monothiouronium-β-CD tosylate (TU-β-CD), an important CD intermediate for the preparation of 6^I-*S*-monodeoxy-6^I-monothio-β-CD [26]. Having selected the 6^I-*O*-monotosyl-β-CD (Ts-β-CD) as the benchmark, the nucleophilic displacement of the tosylate group in the presence of azido or thiourea (TU) nucleophiles was chosen for the study under different milling conditions. The reaction was performed in a planetary ball mill and the processing parameters were systematically varied with the aim of pointing out their influence on the nucleophilic substitution reactions in terms of rate and yield. Specifically systematic variation involved rotation speed, milling tool materials, ball number and size, ball-to-powder mass ratio, the fraction of reactor volume occupied by balls and the reactor volume itself.

Results and Discussion

We previously reported [13] a successful scale-up monoazidation reaction of Ts-β-CD (the reaction scale was 6.5 g, 5 mmol) in a ball-mill (Supporting Information File 1, Table S1, entries 1–4). Considering that the preparation of Ts-β-CD is laborious [24,25], its commercial availability is restricted by high costs and limited number of producers, the systematic investigation on the influence of the milling parameters on the reaction outcome was investigated using a reaction scale of dominantly 1 mmol of substrate, in the presence of 3 equivalents of NaN$_3$ or thiourea (TU) as nucleophiles (Scheme 1). Being the removal of the starting Ts-β-CD from the 6-monoazido-β-CD complicated due to the solubility similarities, the time to reach complete conversion (> 99.5%, defined as milling time) of the starting material had been targeted as main control parameter (see details in Supporting Information File 1).

No significant role can be ascribed to the temperature, since systematic measurements under different processing conditions indicated that it never exceeded 72 °C. Further, no degradation of the activated Ts-β-CD was observed.

The yield of the mechanically induced azidation is invariably higher than the one observed in our previous work [13]. However, the rate of the reaction involving the more nucleophilic TU is considerably lower. Chemical conversion data regarding the reactions performed under different milling conditions are summarized in Table S1 (Supporting Information File 1). It can be seen that the reaction yield shows significant scatter. No definite relationship between the set of processing parameters and the yield can be identified. Nevertheless, sets of balls with different size seemingly assure the best performances in terms of yield and reaction rate, enabling full substrate conversion in shorter reaction times (Supporting Information File 1, Table S1, entries 2, 6, 11, and 12).
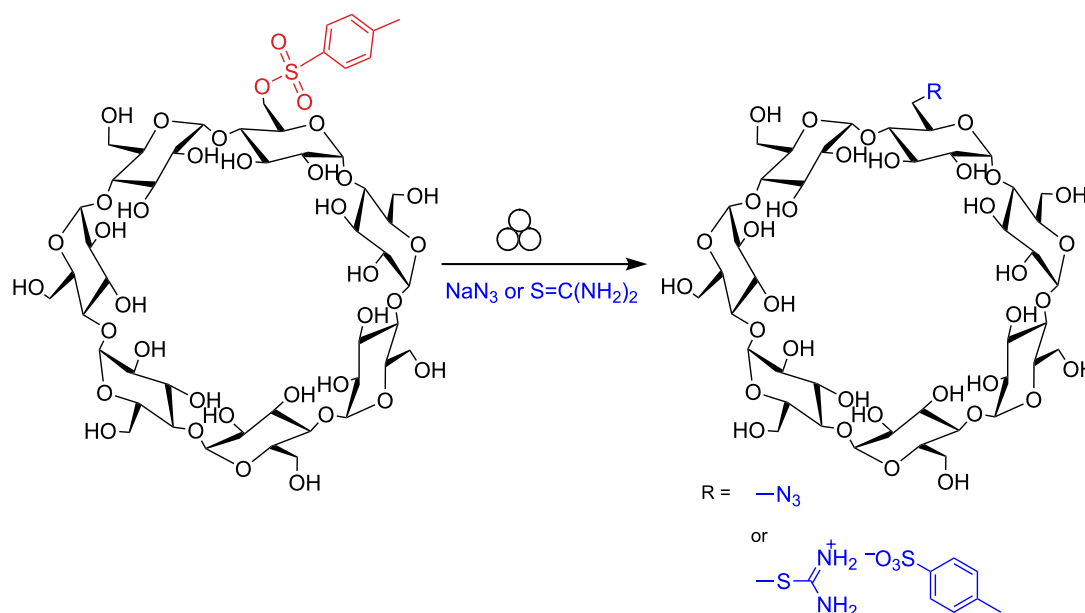
Scheme 1: Nucleophilic substitution of the 4-toluenesulfonyl group. The formalism for the mechanochemical activation was suggested by Rightmire [27].

The observed yield enhancement can be tentatively related to the effectiveness of energy transfer, which can be expected to increase as the volume occupied by balls inside the reactor increases, thus allowing milling conditions to approach frictional regimes.

In the attempt of clarifying the role of the volume fraction occupied by balls inside the reactor, the nucleophilic substitution with NaN_3 was performed using glass reactors 2 and 25 mL in volume and the same number of balls of equal size (30 balls of 1 mm in diameter). The experimental findings are summarized in Figure 1 and Supporting Information File 1, Table S1 entries 18 and 19. The reaction rate definitely increases as the volume fraction occupied by balls inside the reactor increases. Therefore, it would appear that an increasing ball contact density shortens milling time.

Further support for the hypothesis that the higher number of impacts among balls per unit of time enhances the outcome of the reaction comes from data shown in Figure 2a and Supporting Information File 1, Table S1 entries 6 and 7. The data in Figure 2 refer to experiments performed varying the ball size while keeping the total volume occupied by balls approximately constant. Under these circumstances, the number of contacts between balls increases as the ball size decreases. Based on the above-mentioned hypothesis, reaction rate should be expected to increase. In line with expectations [18], the experimental findings indicate that the smaller the ball size, the shorter the reaction time for both nucleophiles.

Most experiments were performed at a planetary mill sun wheel speed of 550 min^{-1}. Under these conditions, the reaction involving NaN_3 as the nucleophile was investigated using the same weight of balls (ca. 45 g), but varying the ratio of balls with different size. The data in Figure 2a and Supporting Information File 1, Table S1 entries 6–8 and 13 show no dramatic change in reaction rate. TU exhibits a slower kinetics than NaN_3 under the same milling conditions (Supporting Information File 1, Table S1, entry 13 vs. 16), which hints at substrate-dependent reactivity (Figure 3b and Supporting Information File 1, Table S1, entries 9, 11, 13 and 14 for NaN_3 vs. 10, 12, 16 and 17 for TU, respectively).

However, from the experiments the highest sun wheel speed at 650 min^{-1} resulted in faster reaction (Figure 2a) and the number of balls seemed to have less influence on the investigated reaction. It is assumed that a combination of the kinetic energies of the individual balls and the number of impacts can play an important role in the reaction rate.

The material constituting milling tools affects the outcomes of the substitution reaction. Data in Figure 2b (Supporting Information File 1, Table S1, entries 13 and 14 vs. 16 and 17, respectively) shows that, as far as NaN_3 was used in combination with 12 mm balls, the best reaction yield and rate were obtained in stainless steel reactors (Supporting Information File 1, Table S1, entries 13 and 14). By contrast, under the same processing conditions, ZrO_2 gave the best performances in reactions involving TU (Supporting Information File 1, Table S1, entries 16
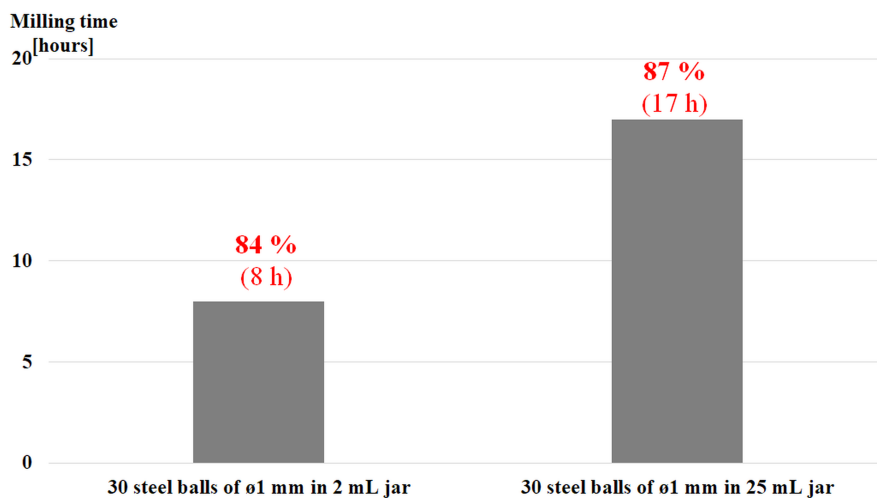
Figure 1: Effect of jar size on the reaction time using an equal number (30) of steel balls (ø 1 mm) for the Ts → N$_3$ exchange reaction in glass vials at 550 min^{-1} sun wheel speed.
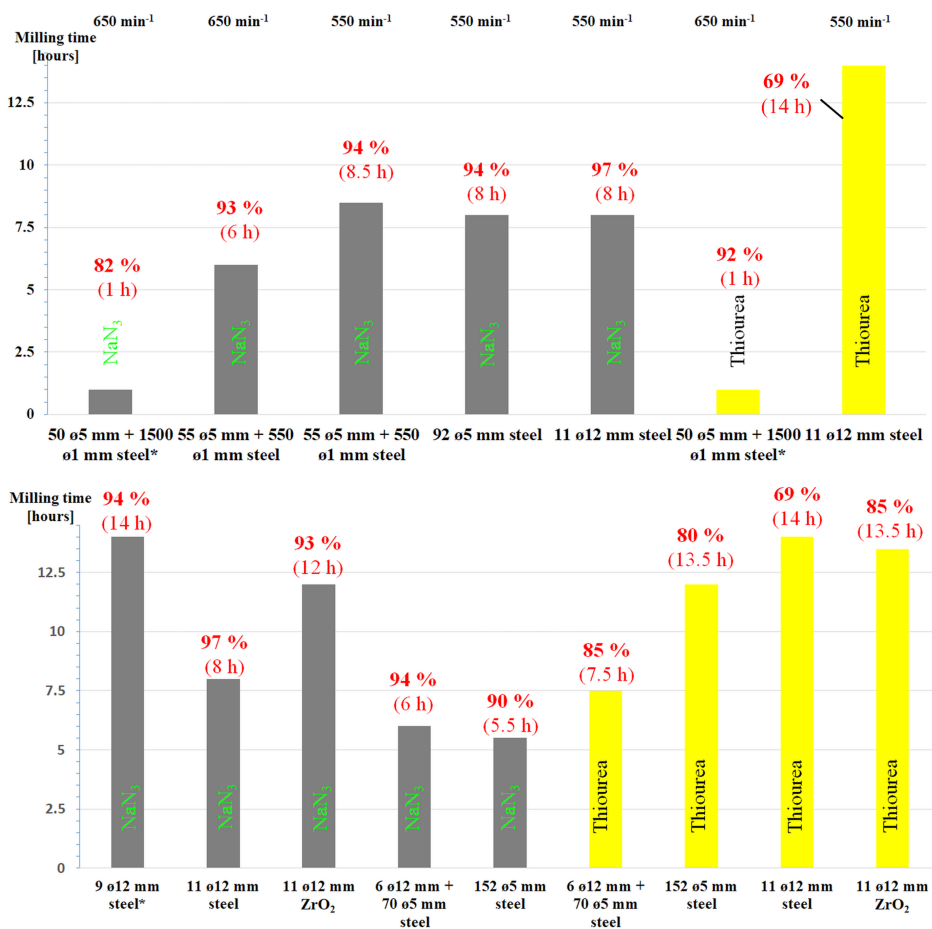
Figure 2: Effect of ball size on the reaction time to a full conversion of Ts-β-CD: a) reactions performed at constant total steel ball weight of ca. 45 g (*weight of steel balls ca. 70 g for comparison with [13]); b) the number (and size) of balls were combined to be equal to the volume occupied by 11 balls of ø 12 mm (ca. 10 mL) at 550 min^{-1} (*weight of steel balls ca. 40 g kept similar to 11 zirconia balls of 12 mm in diameter (ø) for comparison). Values given on the graph bars indicate, respectively, the yield and the reaction time to achieve full conversion of the starting Ts-β-CD.
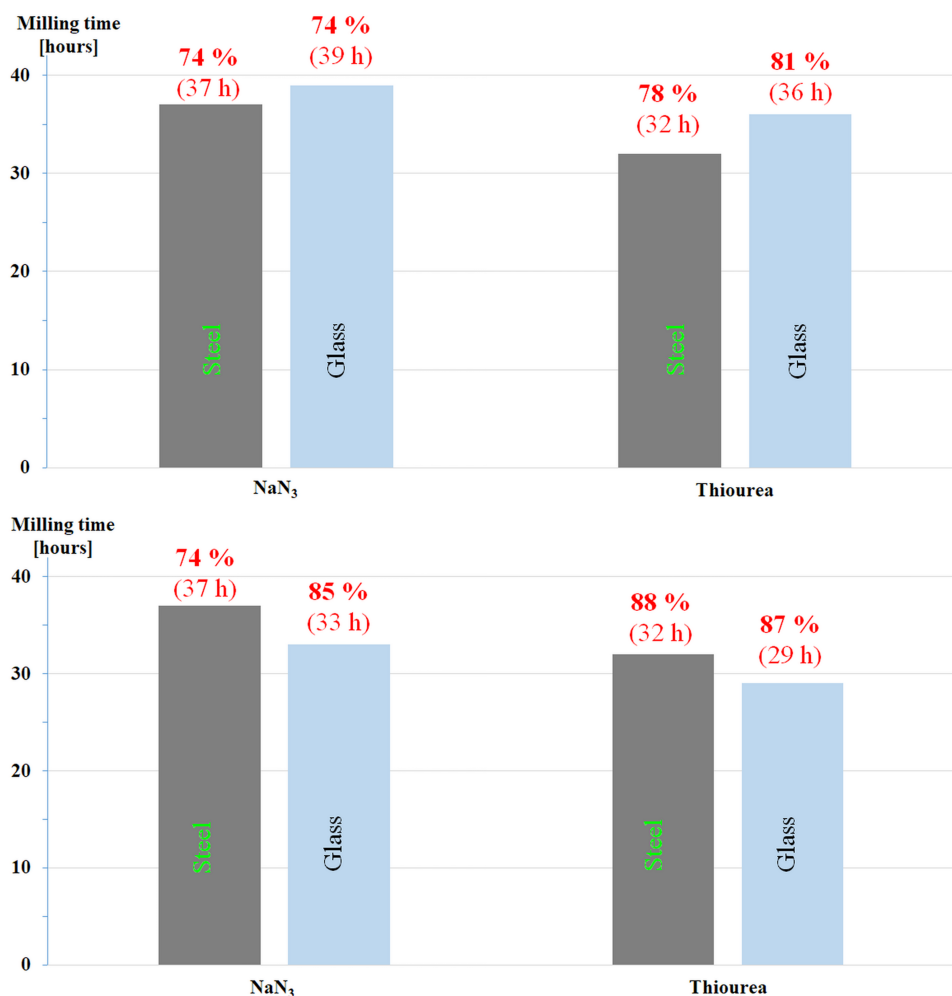
Figure 3: Reaction time as a function of ball materials at 550 min^{-1} in glass vials of 25 mL: a) equal weight: 60 steel balls of ø 1 mm (1.8 g) vs. 20 glass balls of ø 3 mm (1.8 g); b) 60 steel balls of ø 1 mm (m_B = 1.8 g, m_B/m_R ca. 12, $\Phi_{MB,packing}$ = 0.003) vs. 60 glass balls of ø 3 mm (m_B = 5.4 g, m_B/m_R ca. 35, $\Phi_{MB,packing}$ = 0.077). Values given on the graphic bars indicate, respectively, the yield and the reaction time to achieve full conversion of the starting Ts-β-CD.

and 17). Thus, NaN$_3$ seemingly displayed stronger nucleophilicity than TU when stainless steel milling tools were utilized and vice versa for ZrO$_2$ milling tools.

In another set of experiments, for the same nucleophile, comparative experiments were performed using a total number of glass balls having the same weight (1.8 g) of 60 steel balls of 1 mm ø (Figure 3a and Supporting Information File 1, Table S1, entries 20/22 for NaN$_3$ and 21/23 for TU).

The less hard glass balls (and jars) are in general less effective in terms of energy transfer as compared to steel. This was confirmed in the case of TU (Figure 3a and Supporting Information File 1, Table S1 entries 21 vs. 23), while milling times did not considerably change as expected [17] in the case of NaN$_3$

(Figure 3a and Supporting Information File 1, Table S1 entry 20 vs. 22). However, an increase of the number of glass balls, led to somehow better yields after slightly shorter reaction times for both nucleophiles (Figure 3a vs. 3b), even at an improved m_B/m_R ratio and $\Phi_{MB,packing}$ values (Figure 3b and Supporting Information File 1, Table S1, entries 20, 21 vs. 24, 25).

Finally, the experimental findings collected in Supporting Information File 1, Table S1 show that for a larger volume occupied by balls inside the reactor, faster reactions were observed, independent of the material that the milling tools were made from.

Conclusion

Mechanical activation in a planetary ball mill allows the studied reactions to take place at a rate higher than the corresponding

reactions in solution. Indeed, the nucleophilic substitution of tosyl groups is very slow at $T < 80$ °C (in DMF), while in water (at 50–70 °C) the most competitive side reaction is the hydrolysis of the starting material. Moreover, mechanochemical activation allowed solve one of the major problems for cyclodextrin derivatization in solution. This is usually related to the very different solubilities of the reagents, thus requiring energy transfer by heating to induce reactions. Although it is difficult to reach a compromise between the reaction and side reactions, without a massive energy transfer the derivatizations are rarely successful in solution. By mechanochemistry, the reactivity is mainly affected by the sun wheel speed and the number and size of balls for both nitrogen and sulfur nucleophiles. In general, reaction rates reach a maximum as the volume fraction occupied by balls inside the reactor increases and the ball size decreases but no simple correlation was found. Consequently, it seems reasonable to connect reaction yield and rate with the total number of contact between balls. Unlike the reactivity in solution, under mechanochemical conditions the sulfur nucleophile (thiourea, TU) was less effective than the azide ion in the substitution reaction. A similar reversal of reactivity has been already observed for halogens [12,13,28]. The experimental findings lend support to the idea that mechanical activation can induce chemical reactivity [29] and selectivity [30] which is different to that observed in solution, which can be further complicated by the inclusion complex formation property of cyclodextrins.

How exactly the milling parameters influence the kinetics and the mechanisms of organic reactions is still question of investigation in the scientific community. Even though our contribution tries to delineate some trends, additional investigations and experiments need to be performed for a fully understanding of this still understudied and poorly understood aspect of mechanochemistry.

Supporting Information

Supporting Information File 1
Experimental procedures and technical details.
[http://www.beilstein-journals.org/bjoc/content/
supplementary/1860-5397-13-184-S1.pdf]

Acknowledgements

References

1. Cyclodextrins. In *Comprehensive Supramolecular Chemistry;* Szejtli, J.; Osa, T., Eds.; Pergamon: New York, 1996; Vol. 3, pp 1–693.
2. Hashidzume, A.; Takashima, Y.; Yamaguchi, H.; Harada, A. Cyclodextrin. In *Comprehensive Supramolecular Chemistry II;* Atwood, J. L., Ed.; Elsevier: Oxford, 2017; pp 269–316. doi:10.1016/B978-0-12-409547-2.13829-6
3. Martina, K.; Binello, A.; Lawson, D.; Jicsinszky, L.; Cravotto, G. *Curr. Nutr. Food Sci.* **2013,** *9,* 167–179. doi:10.2174/1573401311309030001
4. Adeoye, O.; Cabral-Marques, H. *Int. J. Pharm.* **2017,** in press. doi:10.1016/j.ijpharm.2017.04.050
5. Zhu, G.; Yi, Y.; Chen, J. *TrAC, Trends Anal. Chem.* **2016,** *80,* 232–241. doi:10.1016/j.trac.2016.03.022
6. Jicsinszky, L.; Iványi, R. *Carbohydr. Polym.* **2001,** *45,* 139–145. doi:10.1016/S0144-8617(00)00319-2
7. Earla, A.; Braslau, R. *Macromol. Rapid Commun.* **2014,** *35,* 666–671. doi:10.1002/marc.201300865
8. Jicsinszky, L.; Ivanyi, R. In *Proceedings of the 10th International Symposium on Cyclodextrins,* Ann Harbor, Michigan, USA, May 21–24, 2000; pp 46–52.
9. Rinaldi, L.; Binello, A.; Stolle, A.; Curini, M.; Cravotto, G. *Steroids* **2015,** *98,* 58–62. doi:10.1016/j.steroids.2015.02.016
10. Hedges, A.; Tenbarge, F. Cyclodextrin complexing method. U.S. Pat. Appl. 5,007,966 A, April 16, 1991.
11. Czugler, M.; Pintér, I. *Carbohydr. Res.* **2011,** *346,* 1610–1616. doi:10.1016/j.carres.2011.03.014
12. Jicsinszky, L.; Caporaso, M.; Martina, K.; Gaudino, E. C.; Cravotto, G. *Beilstein J. Org. Chem.* **2016,** *12,* 2364–2371. doi:10.3762/bjoc.12.230
13. Jicsinszky, L.; Caporaso, M.; Tuza, K.; Martina, K.; Gaudino, E. C.; Cravotto, G. *ACS Sustainable Chem. Eng.* **2016,** *4,* 919–929. doi:10.1021/acssuschemeng.5b01006
14. Jicsinszky, L.; Caporaso, M.; Gaudino, E. C.; Giovannoli, C.; Cravotto, G. *Molecules* **2017,** *22,* 485. doi:10.3390/molecules22030485
15. Menuel, S.; Doumert, B.; Saitzek, S.; Ponchel, A.; Delevoye, L.; Monflier, E.; Hapiot, F. *J. Org. Chem.* **2015,** *80,* 6259–6266. doi:10.1021/acs.joc.5b00697
16. Sánchez-Jiménez, P. E.; Valverde, J. M.; Perejón, A.; de la Calle, A.; Medina, S.; Pérez-Maqueda, L. A. *Cryst. Growth Des.* **2016,** *16,* 7025–7036. doi:10.1021/acs.cgd.6b01228
17. Stolle, A.; Szuppa, T.; Leonhardt, S. E. S.; Ondruschka, B. *Chem. Soc. Rev.* **2011,** *40,* 2317–2329. doi:10.1039/c0cs00195c
18. Stolle, A.; Schmidt, R.; Jacob, K. *Faraday Discuss.* **2014,** *170,* 267–286. doi:10.1039/C3FD00144J
19. Ball Milling Towards Green Synthesis: Applications, Projects, Challenges. In *RSC Green Chemistry;* Ranu, B.; Stolle, A., Eds.; Royal Society of Chemistry, 2015; pp 1–303. doi:10.1039/9781782621980
20. Wang, G.-W. *Chem. Soc. Rev.* **2013,** *42,* 7668–7700. doi:10.1039/c3cs35526h
21. James, S. L.; Adams, C. J.; Bolm, C.; Braga, D.; Collier, P.; Friščić, T.; Grepioni, F.; Harris, K. D. M.; Hyett, G.; Jones, W.; Krebs, A.; Mack, J.; Maini, L.; Orpen, A. G.; Parkin, I. P.; Shearouse, W. C.; Steed, J. W.; Waddell, D. C. *Chem. Soc. Rev.* **2012,** *41,* 413–447. doi:10.1039/C1CS15171A
22. Tan, D.; Loots, L.; Friščić, T. *Chem. Commun.* **2016,** *52,* 7760–7781. doi:10.1039/C6CC02015A
23. Do, J.-L.; Friščić, T. *ACS Cent. Sci.* **2017,** *3,* 13–19. doi:10.1021/acscentsci.6b00277

24. Law, H.; Benito, J. M.; Garcia Fernandez, J. M.; Jicsinszky, L.; Crouzy, S.; Defaye, J. *J. Phys. Chem. B* **2011,** *115,* 7524–7532. doi:10.1021/jp2035345

25. Brady, B.; Lynam, N.; O'Sullivan, T.; Ahern, C.; Darcy, R. *Org. Synth.* **2000,** *77,* 220. doi:10.15227/orgsyn.077.0220

26. Liu, A.; Zhao, Q.; Guan, X. *Anal. Chim. Acta* **2010,** *675,* 106–115. doi:10.1016/j.aca.2010.07.001

27. Rightmire, N. R.; Hanusa, T. P. *Dalton Trans.* **2016,** *45,* 2352–2362. doi:10.1039/C5DT03866A

28. Konnert, L.; Dimassi, M.; Gonnet, L.; Lamaty, F.; Martinez, J.; Colacino, E. *RSC Adv.* **2016,** *6,* 36978–36986. doi:10.1039/C6RA03222B

29. Konnert, L.; Reneaud, B.; de Figueiredo, R. M.; Campagne, J.-M.; Lamaty, F.; Martinez, J.; Colacino, E. *J. Org. Chem.* **2014,** *79,* 10132–10142. doi:10.1021/jo5017629

30. Hernández, J. G.; Bolm, C. *J. Org. Chem.* **2017,** *82,* 4007–4019. doi:10.1021/acs.joc.6b02887

Mechanochemical synthesis of small organic molecules

Tapas Kumar Achar, Anima Bose and Prasenjit Mal[*]

Abstract

With the growing interest in renewable energy and global warming, it is important to minimize the usage of hazardous chemicals in both academic and industrial research, elimination of waste, and possibly recycle them to obtain better results in greener fashion. The studies under the area of mechanochemistry which cover the grinding chemistry to ball milling, sonication, etc. are certainly of interest to the researchers working on the development of green methodologies. In this review, a collection of examples on recent developments in organic bond formation reactions like carbon–carbon (C–C), carbon–nitrogen (C–N), carbon–oxygen (C–O), carbon–halogen (C–X), etc. is documented. Mechanochemical syntheses of heterocyclic rings, multicomponent reactions and organometallic molecules including their catalytic applications are also highlighted.

Introduction

The field of organic synthesis has experienced recently significant changes towards achieving the goal of more efficient and sustainable processes [1]. Thus, a new branch of chemistry termed as "Green Chemistry" has become a part of research interest by the chemists [2-4]. Green chemistry covers a wide range of research areas and generally deals with 12 principles [5,6] and few of them are: avoiding the use of volatile and toxic solvents, reducing the quantity of catalyst and reagents, using environmentally benign chemicals, atom-economical synthesis, minimization of chemical-waste/energy, etc. Non-conventional energy sources for chemical reactions such as microwave, mechanical mixing, visible-light and ultrasound are becoming surge of interest to the chemist as alternative energy sources in

laboratories [7]. By imposing these techniques innumerable chemical transformations have been documented and thereby developing many existing protocols with superior results are further anticipated [8,9].

To address one of the major issues of green chemistry, i.e., minimizing chemical-waste/energy, solvent-free syntheses have become a popular research topic [8]. The mechanochemical techniques like ball-milling or hand grinding are considered to be promising candidates in solvent-free synthesis [10,11]. Mechanochemical methods deal with chemical transformations induced by mechanical energy, such as compression, shear, or friction [12]. Wilhelm Ostwald, a Russian-German chemist who

received the Nobel Prize in 1909, mentioned the term "Mechanochemistry" as, like a branch of physical chemistry, i.e., thermochemistry, photochemistry and electrochemistry [13,14]. He defined the subject as "Mechanochemistry is a branch of chemistry which is concerned with chemical and physio-chemical changes of substances of all states of aggregation due to the influence of mechanical energy". Moreover, according to IUPAC, a mechano-chemical reaction is a 'Chemical reaction that is induced by the direct absorption of mechanical energy' and with a note 'Shearing, stretching, and grinding are typical methods for the mechano-chemical generation of reactive sites, usually macroradicals, in polymer chains that undergo mechano-chemical reactions' [15].

The mechanistic understanding of mechanochemical reactions is still unclear [16]. A single idea could not be conceived because of the diversified nature of the reactions being practiced under mechanochemistry. Among the proposed models "hot spot" and "magma–plasma model" are mostly acceptable [17,18]. Other models like spherical model, dislocation and phonon theory, short-live-active center theory, kinetic and impulse model are also well known [19,20]. Nevertheless, this subject needs more attention to the both experimental and theoretical chemists [21].

The sophisticated technique of ball-milling or mechanomilling is the adaptation from the traditional grinding methods using a mortar and pestle. These mechanomillings methods are generally conducted in vibration mills or planetary mills at frequencies of 5–60 Hz [22,23]. The extensively used mechanomilling technique has limitations in controlling the reactions for air- and moisture-sensitive substances. In mechanomilling methods generally, the reactions are carried out in sealed vessels or jars of materials like stainless steel, tungsten carbide, zirconia, agate, etc. [24].

In the past decade, mechanochemical reactions were developed under the areas of chemistry like supramolecular chemistry [25,26], organic synthesis [27,28], nanoparticle synthesis, etc. [29,30]. The historical development of mechanochemistry [31], mechanistic aspects [32], mechanochemical synthesis of inorganic material [33], co-crystals [34], metal–ligand complexes [35], metal organic frameworks [36], polymers [37], etc. are well documented in seminal reviews and will not be discussed here. The organic mechanochemistry has remained undeveloped until the pioneering work reported by Toda in the 1980s [38] and Kaupp [24]. Due to several advantages, the area mechanochemistry has received significant attention over solution-based chemical methods and process developments [12,27,29]. The mechanochemical formation of carbon–carbon [39,40], carbon–heteroatom [41,42], metal–ligand coordination

bonds [43], non-covalent interactions such as hydrogen bonds or π–π arene stacking interactions [44], etc. are popularly known in literature. In this review the efforts are given towards documentation of various mechanochemical reactions like organic bond formation reactions, multicomponent reactions, heterocyclic ring synthesis, synthesis of organometallic complexes and their catalytic applications, and so on.

Review
Mechanochemical organic synthesis
Famous philosopher Aristotle's statement *"No Coopora nisi Fluida"* means 'no reaction is possible in the absence of solvent' and that was a common belief till last few decades. However, during the 1980s the pioneering works of Toda and co-workers proved that many organic reactions of solution chemistry would be reproducible in solid state too [22,23]. In the solid state reactions the ingredients are mixed to finely powdered form for better mixing. The ball-milling chemistry can better be conceived as the updated and sophisticated version of traditional grinding chemistry [38].

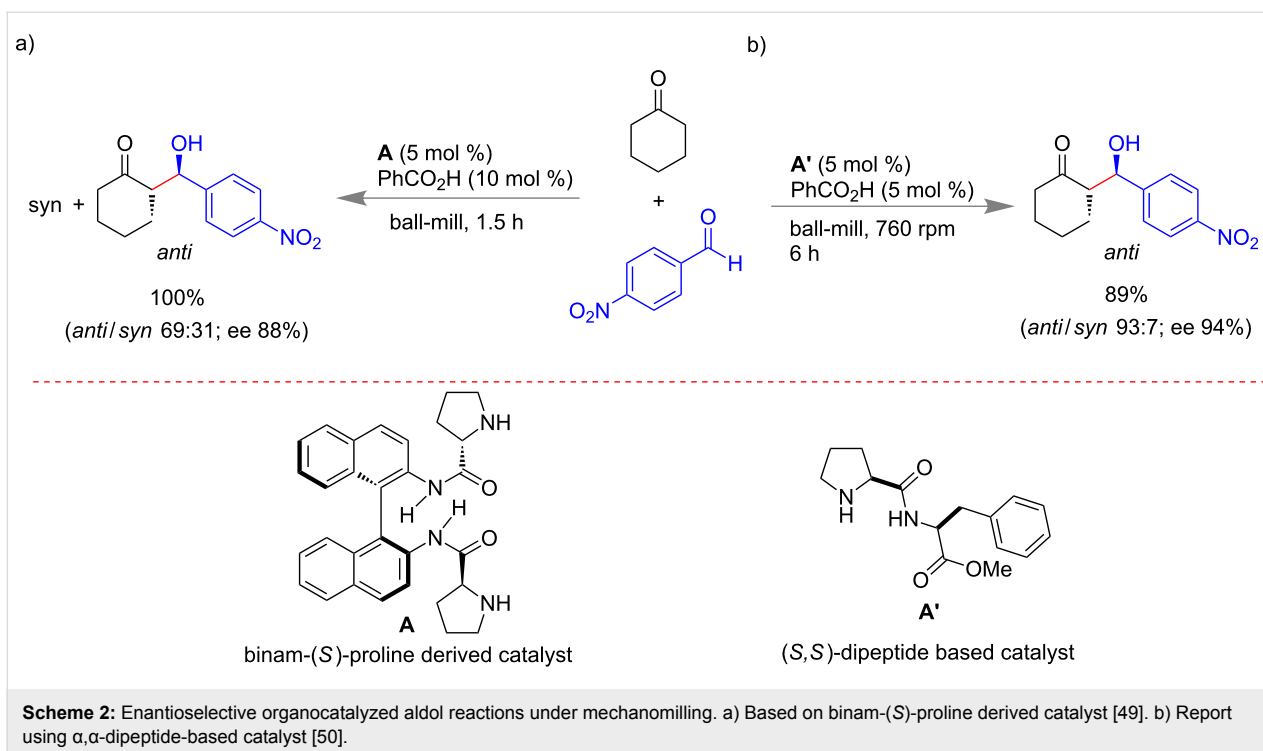## Mechanochemical synthesis of C–C bond
More atom economic, energy efficient, time efficient and mild syntheses of C–C bonds are always desired. The solvent-free mechanomilling technique can also be an important alternative to replace traditional hand grinding methods [45]. Many solution-based C–C bond synthesis methods are reproducible under mechanomilling conditions with improved time and energy efficiency [46,47]. In this section some of the most important C–C bond forming reactions and their advantages are discussed.

Aldol reaction
In 2000, Raston and Scott first reported the aldol condensation reaction using veratraldehyde, 4-phenylcyclohexanone and 1-indanone in the presence of NaOH in a vibrating ball mill and the products were obtained in the yield up to 98% within 10 min (Scheme 1) [48].

Scheme 1: Mechanochemical aldol condensation reactions [48].
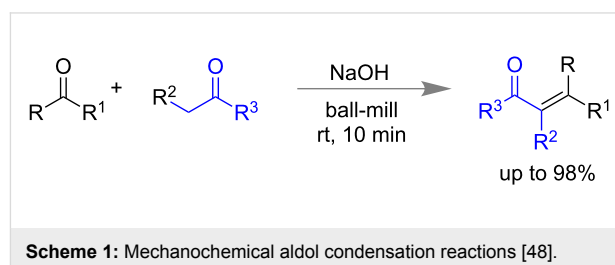
However, the asymmetric version of a mechanochemical aldol condensation reaction was reported by Guillena and Nájera with co-workers (Scheme 2a) in 2008. Reactions between various ketones and aldehydes under solvent-free conditions were per-

Scheme 2: Enantioselective organocatalyzed aldol reactions under mechanomilling. a) Based on binam-(*S*)-proline derived catalyst [49]. b) Report using α,α-dipeptide-based catalyst [50].

formed using a combination of (*S*)-binam-L-Pro (**A**, 5 mol %) and benzoic acid (10 mol %) as organocatalyst [49].

Juaristi and co-workers investigated the mechanistic aspects of α,α-dipeptide derivatives of a (*S*)-proline- (**A′**)-catalyzed asymmetric aldol reaction (Scheme 2b) under solvent-free mechanomilling [50]. By varying the electron density on the aromatic aldehydes, it was observed that electron deficient aldehydes provided a better yield with excellent stereo selectivity over electron rich systems. The observed result suggests that a π–π stacking interaction between electron-poor aromatic aldehydes and aromatic ring of the organocatalyst plays a crucial role for excellent yield and selectivity. Apparently the solvent-free system enhances the rigidity of the transition state for more selective reactions under mechanochemical activation.

Michael addition

Generally strong bases like NaOH, KOH, NaOEt etc. have been used as catalyst for the Michael addition of 1,3-dicarbonyl

compounds to α,β-unsaturated ketones. In 2004, Wang and co-workers first reported a mechanochemical Michael reaction of 1,3-dicarbonyl compounds with chalcones and azachalcones using the mild base K_2CO_3 (Scheme 3). Michael adducts were isolated with good to excellent yield (76–99%) in a high-speed vibration mill (HSVM) within 10–60 min [51].

Bolm and co-workers reported an organocatalytic asymmetric version of Michael addition reaction under planetary-milling (PM) conditions. Differently substituted thiourea-based organocatalysts were screened for the reaction to achieve stereoselective adducts through hydrogen bonding. Only with 2.5 mol % of thiourea-based catalyst **B**, α-nitrocyclohexanone and nitroalkene derivatives could undergo a Michael addition to yield up to 95% of the desired product within 30 min (Scheme 4). Excellent stereoselectivity was also achieved with a diastereomeric ratio of 98:2 and enantiomeric ratio up to 99:1. Simple flash column chromatographic purification methods, low catalyst loading,

Scheme 3: Mechanochemical Michael reaction [51].
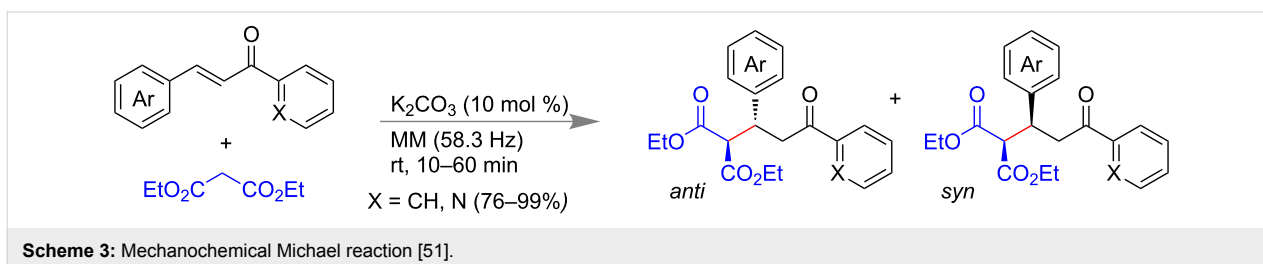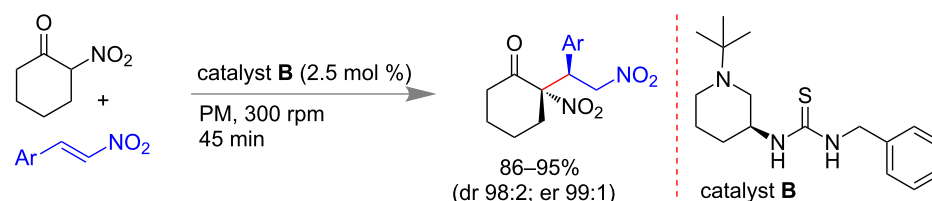
Scheme 4: Mechanochemical organocatalytic asymmetric Michael reaction [52].

gram scale synthesis, etc. were advantageous for the reaction [52].

Morita–Baylis–Hillman reaction

The Morita–Baylis–Hillman reaction (MBH) employs olefins, tertiary amine catalysts and electrophile aldehydes to produce multifunctional products. Mack et al., found a significant enhancement in the rate of a Morita–Baylis–Hillman (MBH) reaction under ball milling conditions (Scheme 5) compared to the conventional method that generally takes days to a week for completion. The reaction of methyl acrylate with different *para*-substituted aryl aldehydes in the presence of 20 mol % 1,4-

diazabicyclo[2.2.2]octane (DABCO) catalyst at 0.5–45 h yielded the MBH products in 28–98% yield [53].
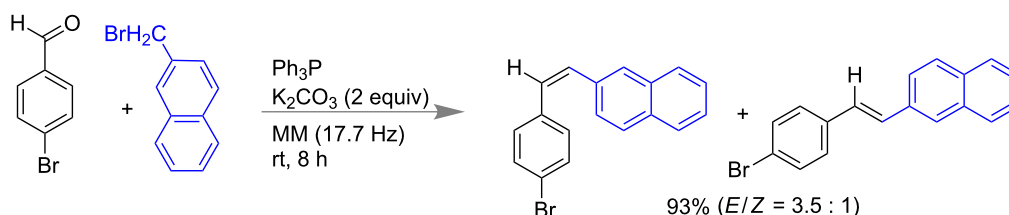
Wittig Reaction

Pecharsky and co-workers reported the solvent-free mechanochemical synthesis of phosphonium salts [54] and phosphorus ylides [55] in the presence of the weak base K_2CO_3. Mechanochemically prepared phosphorous ylide from triphenylphosphine in presence of K_2CO_3 was utilized for a one-pot solvent-free Wittig reaction of organic halides with aldehydes or ketones (Scheme 6) [55].

Suzuki Coupling

In 2000, Peters and co-workers first reported the palladium-catalyzed Suzuki coupling reaction under ball-milling conditions [56]. In a planetary mill for 30–60 min, the mixture of aryl halide (1.0 equiv), phenylboronic acid (2.0 equiv), K_2CO_3 (3.0 equiv) and $Pd(PPh_3)_4$ (5 mol %) resulted in coupled products with 96% yield (Scheme 7). The NaCl was used as an additive to make the reaction mixture sufficiently powdery for uniform mixing.
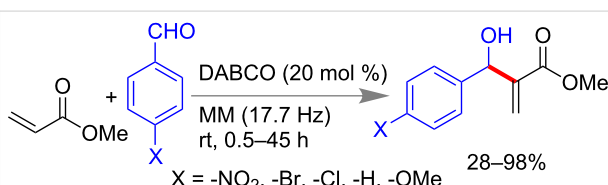
Scheme 5: Mechanochemical Morita–Baylis–Hillman (MBH) reaction [53].

Scheme 6: Mechanochemical Wittig reactions [55].
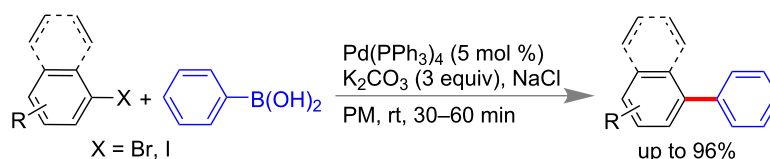
Scheme 7: Mechanochemical Suzuki reaction [56].

The use of aryl chlorides is generally restricted in Suzuki reactions because of their low reactivity. Recently, Li and Su with co-workers have developed a liquid-assisted grinding (LAG) method for the Suzuki–Miyaura coupling between aryl chlorides and boronic acids to synthesize the biaryls in nearly quantitative yield. Under optimized conditions 2 mol % Pd(OAc)$_2$ and 4 mol % of PCy$_3$·HBF$_4$ along with an excess K$_2$CO$_3$–MeOH led to biaryls within 99 min and with a yield up to 97% (Scheme 8) [57].

Heck reaction

Frejd and co-workers reported the first mechanochemical Heck reaction [58]. Su and co-workers demonstrated that (*E*)-stilbene derivatives were synthesized by the coupling of styrenes with aryl bromides or aryl chlorides (Scheme 9) [59].
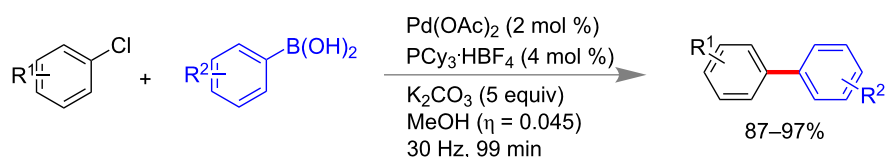
Sonogashira reaction

Stolle and co-workers have reported a Sonogashira coupling reaction under ball milling conditions in which the reactions were done in absence of any copper catalyst or any additional ligands [60]. In presence of palladium salts (Pd(OAc)$_2$ or Pd(PPh$_3$)$_4$) and DABCO (1,4-diazabicyclo[2.2.2]octane) various acetylenes and aryl halides were coupled to obtain the Sonogashira coupling products in excellent yields (near quantitative, Scheme 10a). The reactions were reported for aliphatic alkynes as well. In Scheme 10b, an example of a double Sonogashira reaction is shown [60].

Oxidative cross-dehydrogenative coupling

Copper-catalyzed mechanochemical oxidative cross-dehydrogenative coupling (CDC) reactions [61-66] of tetrahydroisoquinolines with alkynes and indoles was reported by Su and co-workers (Scheme 11) using 2,3-dichloro-5,6-dicyanoquinone (DDQ) as an efficient oxidant [67].

Su and co-workers have also reported an asymmetric version of the CDC reaction between terminal alkynes and sp^3 C–H bonds under high speed ball milling conditions [68]. Several optically

Scheme 8: Mechanochemical Suzuki–Miyaura coupling by LAG [57].
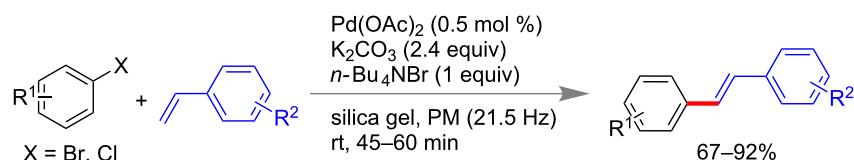
Scheme 9: Mechanochemical Heck reaction [59].
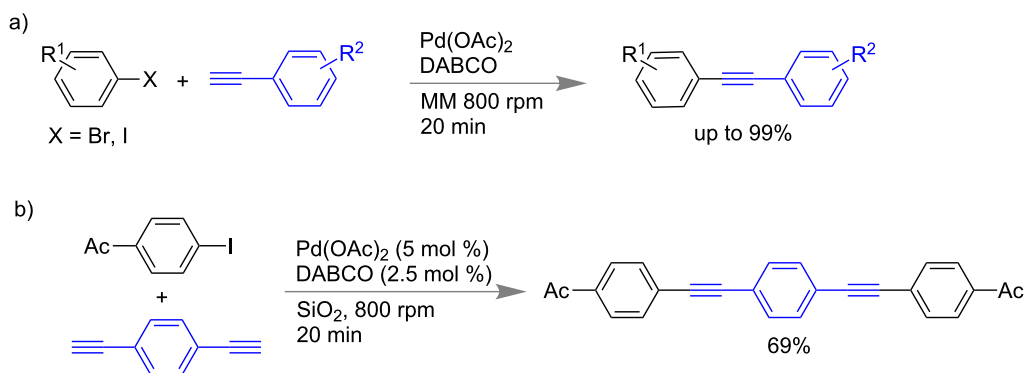
Scheme 10: a) Sonogashira coupling under milling conditions. b) The representative example of a double Sonogashira reaction of *p*-iodoacetophenone with 1,4-bis-ethynyl benzene.

Scheme 11: Copper-catalyzed CDC reaction under mechanomilling [67].

active 1-alkynyl tetrahydroisoquinoline derivatives were synthesized using a pyridine-based chiral ligand (PyBox, Scheme 12) in the presence of DDQ (2,3-dichloro-5,6-dicyano-1,4-benzoquinone). The coupling products were isolated in fair yields with ee's (enantiomeric excesses) up to 79%. The milling copper balls were also identified as reacting catalyst.
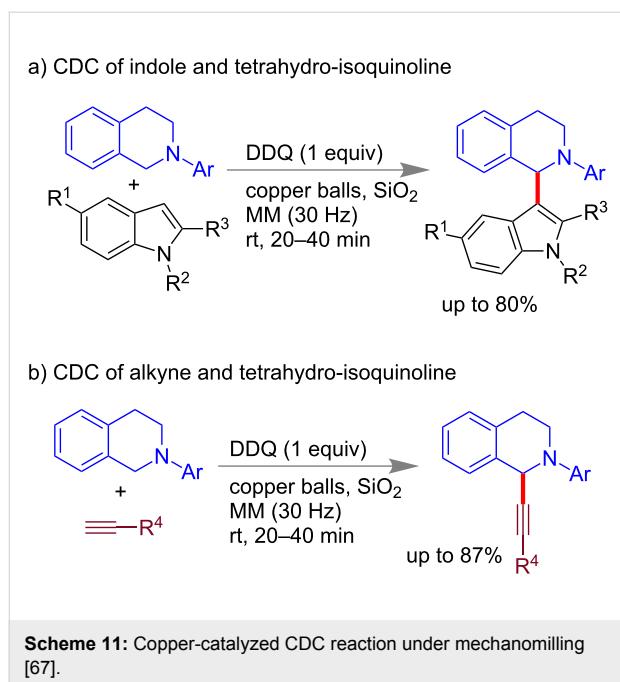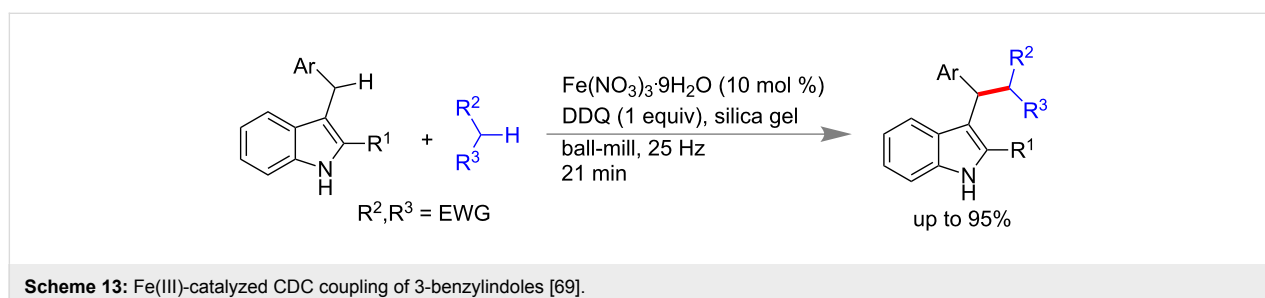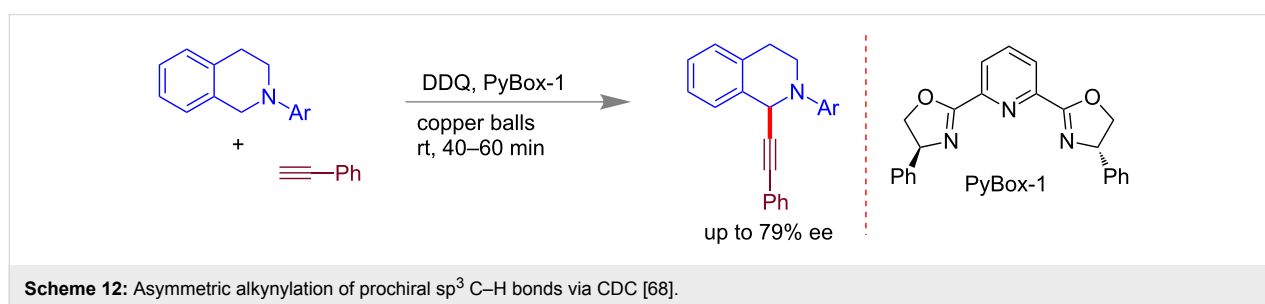
Su and co-workers reported an Fe(III)-catalyzed coupling of 3-benzyl indoles with molecules having active methylene group under s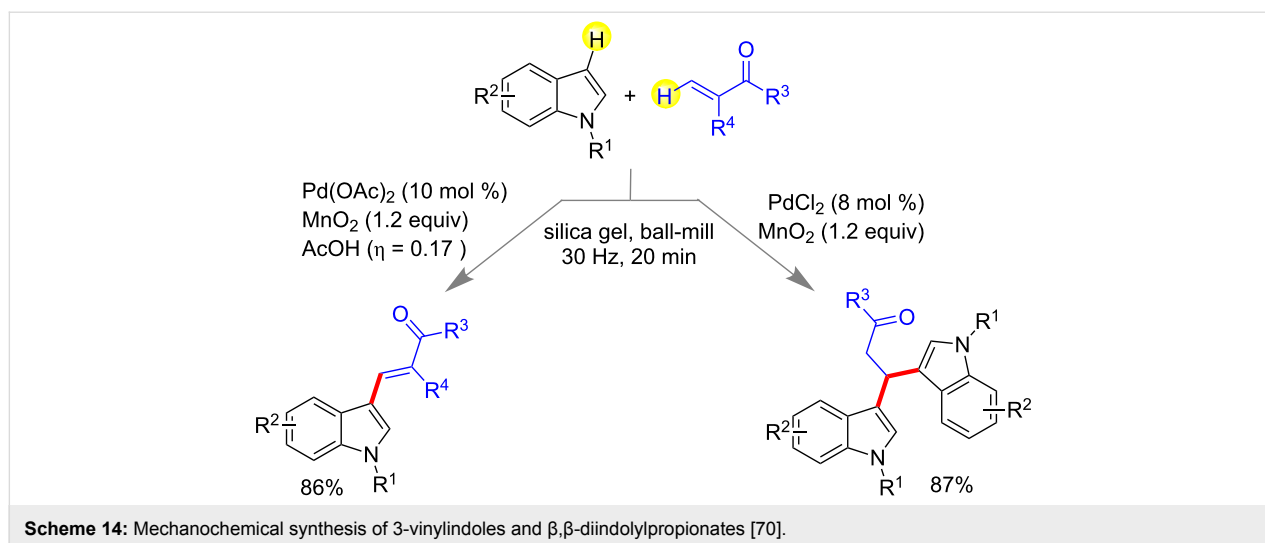olvent-free ball-mill in presence of silica gel as milling auxiliary. Using 10 mol % $Fe(NO_3)_3 \cdot 9H_2O$ as catalyst and 1.0 equiv of DDQ afforded good yield of desired product at 25 Hz within 30 min (Scheme 13) [69]. The oxidant DDQ was added in portions at 7 min intervals to get better yields. Different active methylene compounds like diethylmalonate, dibenzylmalonate, malonitrile, and unsymmetrical 1,3-dicarbonyl compounds were explored for the CDC reaction.

They have also demonstrated a mechanochemical synthesis of 3-vinylindoles and β,β-diindolylpropionates by C–H activation. Substituted indoles and ethyl acrylates were reacted in presence of 10 mol % of $Pd(OAc)_2$ and 1.2 equiv of MnO_2 to afford highly substituted 3-vinylindoles using silica gel and acetic acid (LAG). Contrastingly, when acrylic esters were treated with 8 mol % of $PdCl_2$ and in absence of acetic acid, β,β-diindolylpropionates were obtained as the major product (Scheme 14) [70].

C–N bond synthesis

Amongst C–N bonds the amide bonds are most abundant and important too [71]. According to the American Chemical Society (ACS) and the Green Chemistry Institute (GCI), the "amide bond formation avoiding poor atom economy reagent" is one of the top challenges for organic chemists [72]. Easy, economical, selective and convenient approaches on C–N bond syntheses are of great importance [73-76]. In view of this, chemists have introduced alternative energy sources like, microwave, sonication, mechanomilling, etc. [12,27,77]. Su and co-workers reported a copper-catalyzed arylation of anilines using arylboronic acid under high speed ball-milling conditions. Using 1.0 equiv of $Cu(OAc)_2$ and 2.5 equiv of K_2CO_3 and in

Scheme 12: Asymmetric alkynylation of prochiral sp³ C–H bonds via CDC [68].

Scheme 13: Fe(III)-catalyzed CDC coupling of 3-benzylindoles [69].

Scheme 14: Mechanochemical synthesis of 3-vinylindoles and β,β-diindolylpropionates [70].
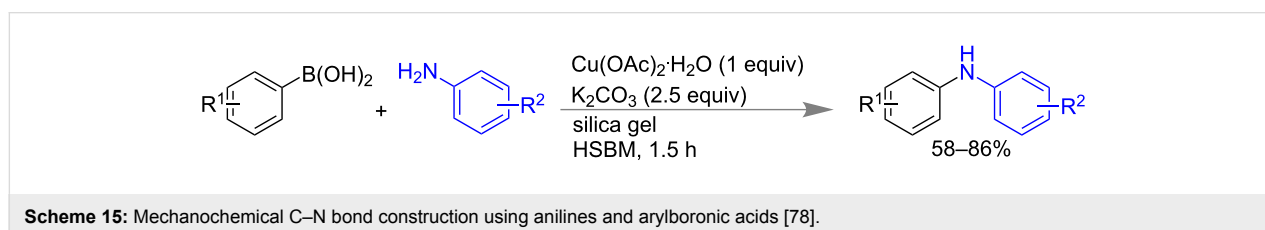
the presence of milling auxiliary silica gel, differently substituted arylboronic acid and anilines led to *N*-arylated products in 58–86% yield (Scheme 15) [78]. They have also explored the reactivity of other amines like alkyl, primary, secondary, heterocyclic, etc.
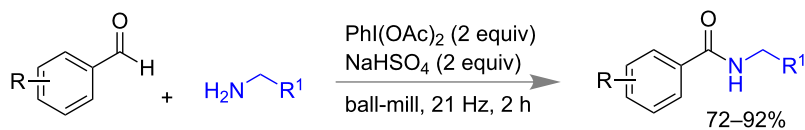
Mal and co-workers reported a metal free, solvent-free and room temperature synthesis of amide bonds at 62–75% yield under ball-milling (21 Hz) from aromatic aldehydes and *N*-chloramine in presence of 20 mol % of tetrabutylammonium iodide (TBAI) and 2.0 equiv of TBHP (Scheme 16) [79]. Aromatic aldehydes having electron-donating or -withdrawing substituents and different *N*-chloramines were well tolerated for this moderately yielding reaction.

They have also reported a method of controlling the chemical reactivity of contact explosives by exploiting weak interactions or soft force [80] during amide bond synthesis under ball-milling conditions. Cross dehydrogenative coupling reactions between benzaldehydes and benzylamines were performed in presence of phenyliodine diacetate (PIDA) using the acid salt NaHSO₄ [81]. The highly exergonic reaction (contact explosive) of acidic iodine(III) and basic amines were safely controlled at maximum contacts (solvent-free) by the acid salt NaHSO₄. Using 2.0 equiv of both NaHSO₄ and PIDA, 72–92% of amides were isolated within 2 h (Scheme 17) [81].

Scheme 16: Mechanochemical amidation reaction from aromatic aldehydes and *N*-chloramine [79].
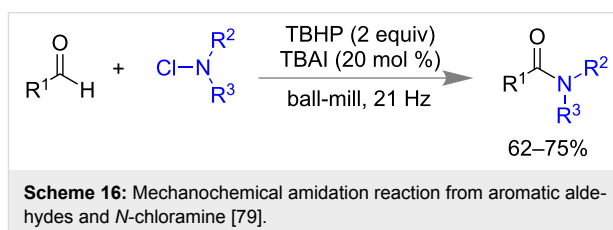
Amino acids are one of the important biomolecules for example as building block of peptides and proteins [75,82-84]. During the synthetic application of these molecules protection of -NH₂ and -COOH group are needed. The traditional protection chemistry involves hazardous solvents, direct handling of corrosive reagents, longer reaction time, and tedious purification processes, etc. Therefore, methodologies involving mild reaction conditions, simple purification processes are always desirable. In 2014, Colacino and co-workers reported the protection of -NH₂ and -COOH groups of amino acids by solvent-free milling methods using two different conditions [85]: 1) carbamoylation of amino esters using Fmoc-Cl and NaHCO₃ (base); 2) esterification of *N*-protected amino acid using different dialkyl dicarbonate or alkyl chloroformate in the presence of DMAP as catalyst and followed by acidic workup. For *N*-terminal protection, different precursors like Fmoc-Cl, benzoyl chloride and Boc₂O were used successfully to get nearly 90% yields for α-amino esters in 90–120 min (Scheme 18).

Scheme 15: Mechanochemical C–N bond construction using anilines and arylboronic acids [78].

Scheme 17: Mechanochemical CDC between benzaldehydes and benzyl amines [81].

Scheme 18: Mechanochemical protection of -NH₂ and -COOH group of amino acids [85].

The Ritter reaction is another significant carbon–nitrogen (C–N) bond forming reaction in the synthesis of amides [86]. Generally, a nitrile and a tertiary alcohol in presence of a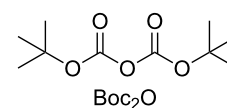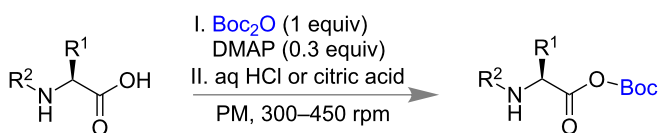 strong acid react to create amides. Major drawbacks associated with this method are the requirement of stoichiometric amounts of strong acid, higher temperature, narrower substrate scope, etc. In 2015, Gredičak and co-workers developed a milder version of the Ritter reaction under mechanomilling conditions. Using 0.5 equivalents of H_2SO_4, amides were isolated in good yields within 30 min of reaction time (Scheme 19) [87]. Various aromatic and aliphatic nitriles including acetonitrile, alcohols like *tert*-butanol and other secondary alcohols were used for this reaction. In case of solid nitriles 1.0 equiv of nitromethane was added during the grinding process to stabilize the carbocation species. This method was proved to be efficient by performing the reaction at 9.7 mmol scale to obtain 84% yield of the product.
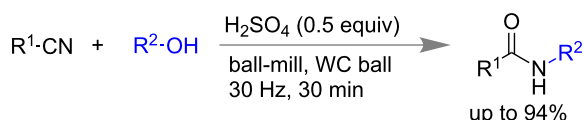
Scheme 19: Mechanochemical Ritter reaction [87].

C–O bond formation reaction

Carbon–oxygen (C–O) bonds are widely present in molecules containing ester, carbamate and amino acid, etc. [88]. Tradi-

tional solution-based C–O bond synthesis generally needs large amount of solvents, excess chlorinating agent, harsh reaction conditions, a tedious isolation process, etc. compared to solvent-less grinding or mechanomilling [89]. In 2011, Mack and co-workers applied the high-speed ball milling (HSBM) technique for the synthesis of dialkyl carbonates [90]. Using potassium carbonate, alkyl halide and 2 equiv of phase-transfer catalyst 18-crown-6 yielded dialkyl carbonate in 74%. However, in absence of 18-crown-6 the yield was only 2% at 17 h (Scheme 20).
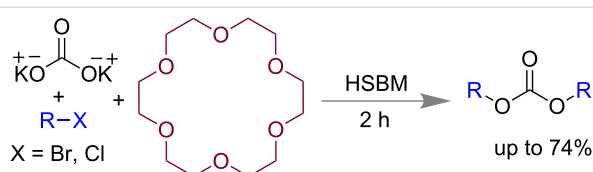
Scheme 20: Mechanochemical synthesis of dialkyl carbonates [90].

Transesterification is a synthetic approach mostly being used for making higher homologous esters from the simpler ones. Ranu and co-workers developed simple method for transesterification under mechanomilling [91]. The mixture of ester and alcohols were adsorbed on the surface of basic alumina and followed by milling of the materials for 2–3 h led to 65–81% of trans-esterified product (Scheme 21). Differently substituted benzene rings including hetero-aromatics were also well tolerated under the similar condition.
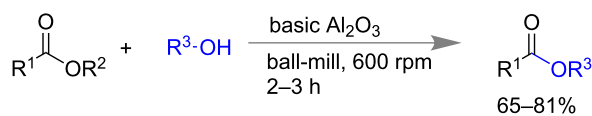
Scheme 21: Mechanochemical transesterification reaction using basic Al$_2$O$_3$ [91].

Colacino and co-workers reported the preparation of carbamates by using 1,1'-carbonyldiimidazole (CDI) and in presence of either alcohols or amines as nucleophile [92]. When 2 equiv of CDI was treated with alcohol in a mixer mill at 30 Hz, within 15 min imidazolecarboxylic acid derivatives were isolated with a new C–O bond formation (Scheme 22).
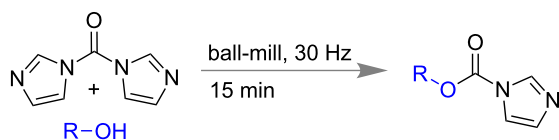
Scheme 22: Mechanochemical carbamate synthesis [92].

C–X bond forming reactions

Carbon–halogen (C–X) bond forming reactions are also significant in organic synthesis because aryl halides are important synthons for the synthesis of many natural and non-natural products [93,94]. In 2005, Rahman and co-workers reported a pioneering solid state benzylic bromination of diquinoline derivatives via *N*-bromosuccinimide (NBS) [95]. In 2012, Wang and co-workers reported bromination of phenol derivatives, chalcones, 1,3-dicarbonyl compounds using NaBr as bromine source and oxone as oxidant under ball-milling conditions [96]. Within 1 h they could isolate more than 90% of mono or polybrominated products of phenol and 1,3-dicarbonyl compounds (Scheme 23). α,β-Unsaturated carbonyl compounds could also undergo a *trans*-bromination reaction efficiently within 40 min.

Following to Wang's report, Stolle and co-workers also reported a similar method of aryl bromination and chlorination using NaBr and NaCl, respectively, in the presence of oxidizing agent oxone (Scheme 24) [97].

Carbon–carbon double (C=C) and triple (C≡C) bonds-containing compounds are also reported to undergo dihalogenation reactions under mec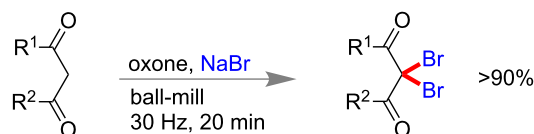hanochemical conditions. In 2014, Mal and co-workers reported a mild aryl halogenation reaction using respective *N*-halosuccinimide (NXS) under solvent-free ball milling condition [88]. Aryl rings containing electron donating groups worked efficiently to yield 70–98% of mono or dibromo derivatives within 2 h. Similarly, NIS led to aryl iodination in

Scheme 23: Mechanochemical bromination reaction using NaBr and oxone [96].
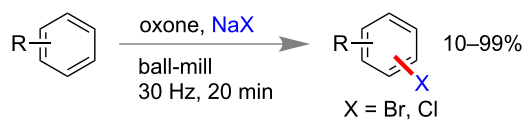
Scheme 24: Mechanochemical aryl halogenation reactions using NaX and oxone [97].

near quantitative yield and NCS failed to produce any chlorination product (Scheme 25). However, NCS-cericammonium nitrate (CAN) successfully yielded mono-chlorinated products [88]. Consecutively, the same group reported metal-free oxidative iodination of electron rich aromatic rings with molecular iodine and oxone (Scheme 25) [98]. This method proved to be highly chemoselective and no benzylic iodination could be observed in case of alkyl benzenes. Interestingly, benzaldehyde derivatives did not lead to any over-oxidation to acids in presence of oxone.

Trihaloisocyanuric acids are also used effectively for halogenations of arenes and 1,3-dicarbonyl compounds and double bond-containing systems [99]. Moorthy and co-workers investigated the potential of tribromoisocyanuric acid (TBCA) and trichloroisocyanuric acid (TCCA) under a solvent-free mechanomilling system for halogenations of electron rich arenes. The reactions were found to have yields above 80% for most of the cases but with poor selectivity in mono- or polybrominations (Scheme 26). They have also explored halogena-
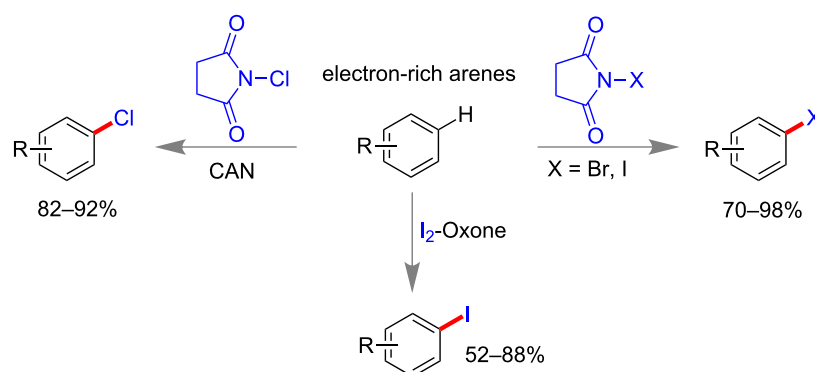
Scheme 25: Mechanochemical halogenation reaction of electron-rich arenes [88,98].

tions of 1,3-dicarbonyl compounds to obtain dihalo derivatives in excellent yield [100].
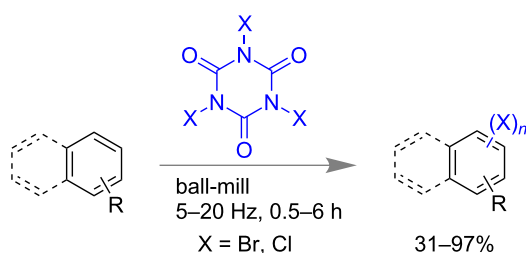
Scheme 26: Mechanochemical aryl halogenation reaction using trihaloisocyanuric acids [100].

In 2016, Browne and co-workers reported selective mechanochemical fluorination of 1,3-dicarbonyl compounds using selectfluor [101,102]. They could control the selectivity of the reaction through LAG using ACN (≈10% v/v of total materials) to get predominantly mono-fluorinated product over difluorinated derivatives (Scheme 27). Contrastingly, addition of 1.0 equiv of Na$_2$CO$_3$ led to switching of the selectivity predominantly towards di-fluorinated product [102].

Multi-component reactions

Multi-component reactions are one of the most powerful tools for the one pot synthesis of complex molecular structures with various functional groups [103-108]. Starting from the development of the Strecker synthesis of amino acids, many variations have been made till date. In solution these reactions generally proceed via a series of equilibrium processes and finally leading to the product through thermodynamic control [109,110]. However, in mechanochemical methods reactions are kinetically controlled [111]. Mechanochemical methods of the Mannich reaction, Paal–Knorr synthesis, Bigineli reaction, Hantzsch reaction, and syntheses of substituted pyran, thiophene, isoquinoline derivatives, etc. are also reported [104,107,112,113]. Isocyanide-based multi-component reactions are also well known [114,115]. Recently, in 2016 Juaristi and co-workers have reported Ugi 4-component reactions (4-CR) by liquid-assisted grinding (LAG) using MeOH. Equimolar amounts of benzaldehyde, chloroacetic acid, *tert*-butyl isocyanide, and propargylamine in the presence of 2 mol % InCl$_3$, under ball-mill yielded the desired Ugi product in 74% yield (Scheme 28) [116].

Juaristi and co-workers have also reported a mechanochemical Passerine 3-component reaction (3-CR). *tert*-Butyl isocyanide,
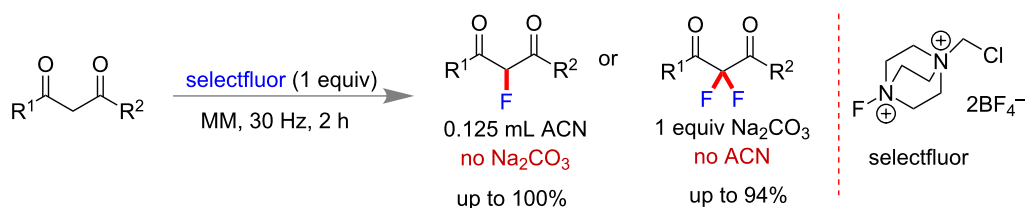
Scheme 27: Mechanochemical fluorination reaction by LAG method [102].
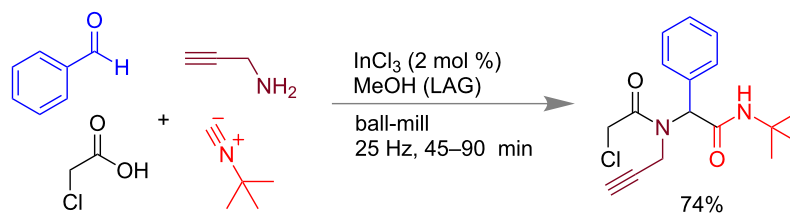
Scheme 28: Mechanochemical Ugi reaction [116].

benzaldehyde and benzoic acid in equimolar proportion under milling conditions for 90 min led to 73% of Passerine product (Scheme 29). Both electron-donating and -withdrawing substitutions on benzaldehydes or in benzoic acids have worked well under the mechano-chemical conditions [116].

In a multicomponent Strecker reaction the syntheses of α-aminonitriles are generally done by condensation of aldehydes, ammonia and hydrogen cyanide [117,118]. The aminonitriles are important synthons for the preparation of nitrogen-containing heterocycles and amino acids [119]. In 2016, Bolm and co-workers reported a mechanochemical synthesis of α-aminonitriles using benzaldehyde, benzyl amine, KCN and the milling auxiliary SiO$_2$ to isolate 70–97% of α-aminonitriles as the sole products. Contrastingly, in the solution of acetonitrile imines of benzaldehyde and amines were formed prefer-

ably. Different aromatic or heteroaromatic aldehydes including thiophene carboxaldehyde, pyridine carboxaldehyde and cyclohexyl carboxaldehyde as well as various amines like morpholine, aliphatic amines and sulfonamides worked smoothly under these conditions to obtain the desired product in 3 h. They have also extended the methodology for the synthesis of tetrahydroisoquinoline by using *o*-formyl phenethyl bromide with amine and KCN (Scheme 30) [120].

Since the discovery in 1890, the Hantzsch pyrrole synthesis is well known for the construction of poly substituted pyrroles [121,122]. In 1998, Jung and co-workers reported polymer supported solid phase synthesis of *N*-substituted pyrroles [123]. In 2013, Menendez and co-workers reported a ceric ammonium nitrate (CAN) and silver-nitrate-promoted three-component Hantzsch pyrrole synthesis under ball-milling conditions [121].
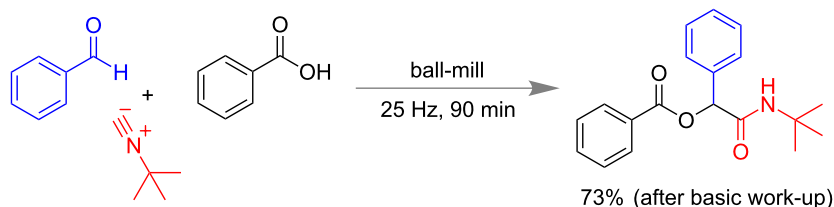
Scheme 29: Mechanochemical Passerine reaction [116].
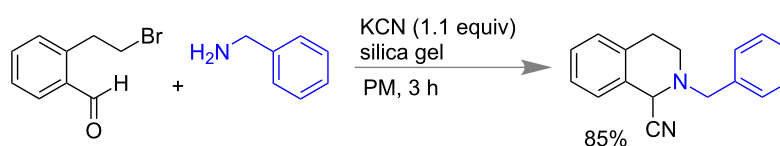
Scheme 30: Mechanochemical synthesis of α-aminonitriles [120].

A ketone in presence of *N*-iodosuccinimide (NIS) and *p*-toluenesulfonic acid led to α-iodoketone in 1 h. Subsequent addition of the primary amine, β-dicarbonyl compound, 5 mol % CAN and 1 equiv silver nitrate led to the intermediate β-enaminone which further reacted with α-iodoketone following by a cyclo-condensation which resulted in the substituted pyrroles shown in Scheme 31.

The Biginelli reaction is a well-known 3-component reaction for the synthesis of dihydropyrimidinones [124,125]. During the last few decades many variations are adopted to improve the efficiency of this reaction for practical application towards drug discovery [126-128]. Modifications have been done in substrates by replacing urea with substituted ureas and thio urea, use of various 1,3-dicarbonyl compounds etc. Reactions using ionic liquids as reaction medium, solvent-free synthesis, microwave synthesis, use of different Lewis acids $FeCl_3$, $NiCl_2$, $BiCl_3$, $InBr_3$, use of Brønsted acids PTSA, etc. are also reported [129,130]. Recently, Mal and co-workers reported a mechanochemical Biginelli reaction by a subcomponent synthesis approach [131-133] in which the component aldehyde and catalytic amount of acid were generated in situ for the final step

of dihydropyrimidinone synthesis. Benzyl alcohols were oxidized by a reagent combination of oxone (0.6 equiv), KBr (10 mol %) and 2,2,6,6-tetramethylpiperidin-1-yloxy radical (TEMPO, 1 mol %) to give benzaldehydes and H^+ under solvent-free mechanochemical conditions within 30 min. Further, addition of 1,3-dicarbonyl compounds and urea derivatives within the same milling jar led to the desired products in 78–95% yield at 3 h (Scheme 32). Benzaldehydes with electron-donating or -withdrawing groups, heteroaromatic aldehydes, *N*-methyl urea and thio urea also resulted in good to excellent yield with high regioselectivity. It is interesting to note that the reaction was irreproducible in the solution of ethyl acetate at room temperature even after 24 h [133].

A mechanochemical asymmetric three component reaction is recently reported by Su and co-workers in the synthesis of propargyl amines using aldehyde, alkyne and amine under high vibration ball milling (HVBM) condition. Using 10 mol % of $Cu(OTf)_2$ as catalyst, 10 mol % of Ph-PyBox ligand **C** and silica gel as milling auxiliary they could achieve near quantitative synthesis with >95% ee at 60 min (Scheme 33) [134]. However, aldehydes having strong electron-withdrawing or -donat-
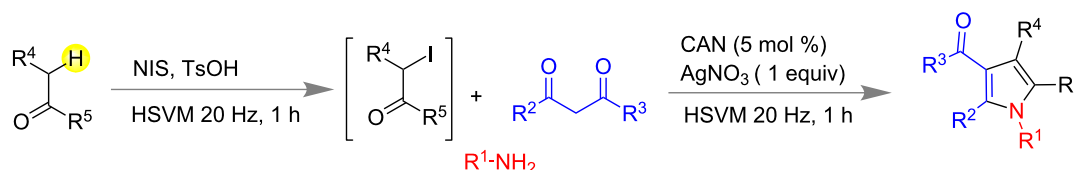
Scheme 31: Mechanochemical Hantzsch pyrrole synthesis [121].
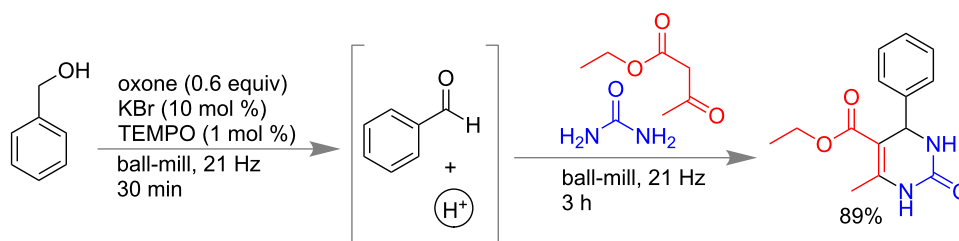
Scheme 32: Mechanochemical Biginelli reaction by subcomponent synthesis approach [133].
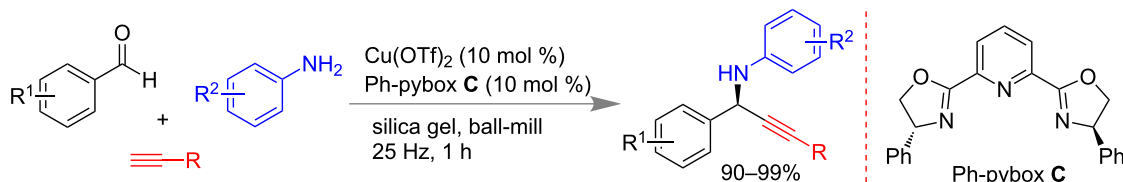
Scheme 33: Mechanochemical asymmetric multicomponent reaction [134].

ing groups yielded the product with lesser enantioselectivity. The silica-supported catalyst could be recovered from the reaction mixture by washing with DCM. They have also observed that an oven-dried catalyst worked effectively to give 99% of product with 99% ee up to few cycles.

Heterocycle synthesis

Multicomponent reactions [135], cyclo-condensations and cascaded transformations are common strategies to make heterocyclic ring [113] systems like pyrroles, pyrans, benzimidazoles, pyrimidines, indoles, etc. [114,136-139]. Further improvements are in demand for the development of synthesis with solvent-less, time efficient, less byproducts, energy saving, easy handling procedures, etc. [112,140,141]. In 2016, Rousseau and co-workers reported a solvent-free mechanochemical Paal–Knorr pyrrole synthesis using a solid bio-sourced acid like citric acid. Using substituted aniline, benzyl or aliphatic amine and 1,4-diketo compounds in presence of 1 mol % citric acid under ball-milling afforded the desired *N*-substituted pyrrole with quantitative yield (Scheme 34) [142].

Scheme 34: Mechanochemical Paal–Knorr pyrrole synthesis [142].
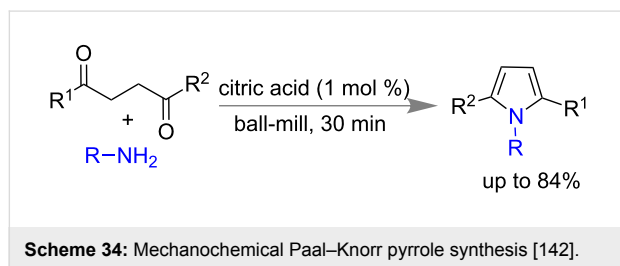
Jang and co-workers reported a mechanochemical synthesis of benzimidazoles [143,144], benzoxazole [145] and benzothiazole derivatives in presence of ZnO nano particles as catalyst [146]. Using 0.5 mol % of ZnO nano particles which were grown on aromatic imine **D** as capping agent, resulted in the best yield within 30 min at 600 rpm. Differently substituted diamines, 2-aminothiophenol and 2-aminophenols reacted with benzaldehyde or aliphatic aldehyde derivatives to give 79–94% of the desired product (Scheme 35). Major advantage of this method was the regeneration of catalyst by filtration and washing with methanol. Secondly, the method was also applic-

able up to 10 g of 2-aminothiophenol and avoided the use of toxic metals which are common in benzimidazole synthesis [147,148].

Scheme 35: Mechanochemical synthesis of benzothiazole using ZnO nano particles [146].
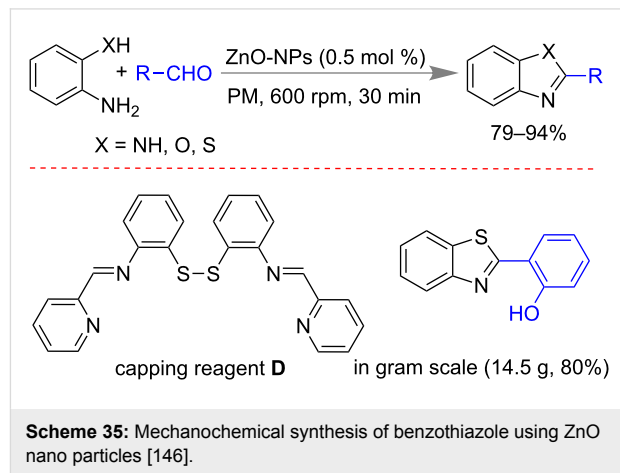
Subsequently, the same group reported the preparation of 1,2-disubstituted benzimidazoles via mechanochemical activation using carboxymethylimidazole-based ionic-liquid-coated ZnO nano particles as catalyst (Scheme 36) [149]. The catalyst worked efficiently till to the fifth cycle after regeneration by filtration of product and washing with methanol. The method was scalable up to using of 8 g of *o*-phenylene diamine.

1,2,3-Triazoles have important applications in pharmaceutical chemistry [150] and traditionally they are prepared by 1,3-dipolar cycloaddition reactions at high temperature, long reaction times and produce low yield with multiple products [151]. In 2013, Ranu and co-workers reported mechanochemical synthesis of triazole moiety (Scheme 37a) using benzyl halides, sodium azide and a terminal alkyne via an alumina-supported copper catalyst. Using 10 mol % of Cu/Al$_2$O$_3$, differently substituted phenyl acetylenes and aliphatic alkynes led to 70–96% yield of triazoles [152]. Phenyl boronic acids were also used to synthesize the triazole rings with additional 1 equiv of K$_2$CO$_3$ which resulted in >85% of product (Scheme 37b).

Mack and co-workers reported another mechanochemical variation of "click" reaction [153,154] where they could isolate

Scheme 36: Mechanochemical synthesis of 1,2-di-substituted benzimidazoles [149].

Scheme 37: Mechanochemical click reaction using an alumina-supported Cu-catalyst [152].

Scheme 39: Mechanochemical indole synthesis [157].
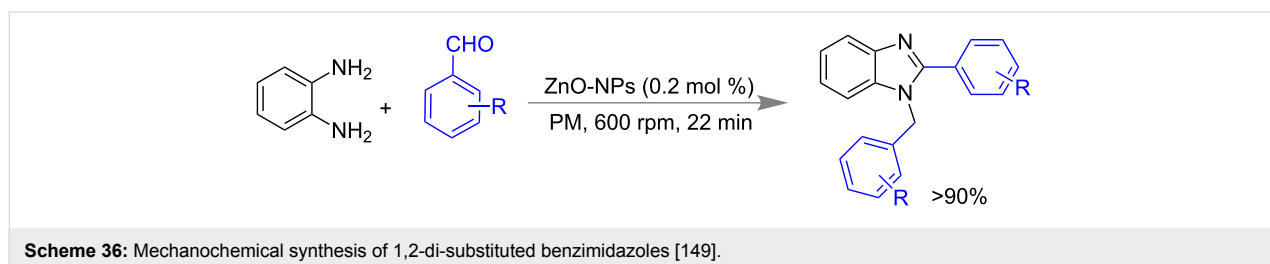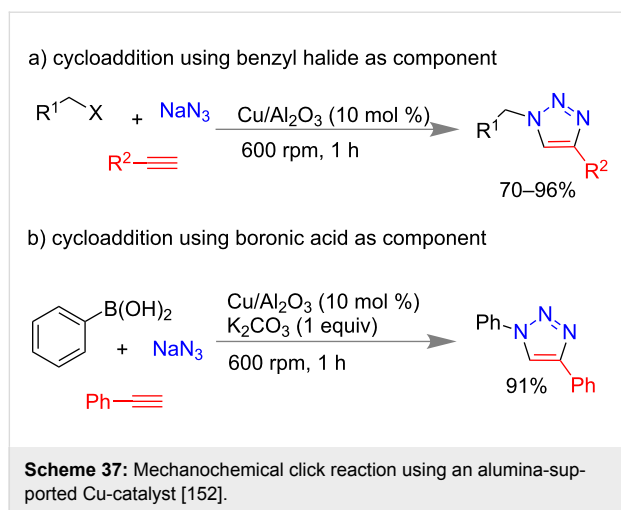
33–90% of triazole derivatives using copper reaction vial in ball mill for 16 h (Scheme 38). The same method was easily applicable to the synthesis using alkyl azide in 15 min [155].

Scheme 38: Mechanochemical click reaction using copper vial [155].
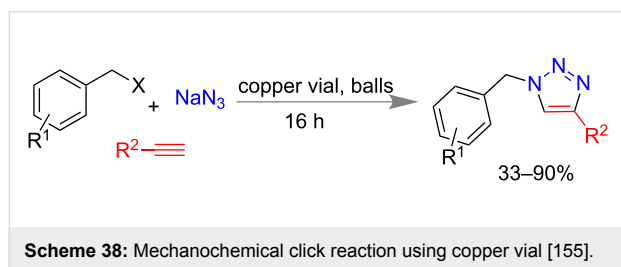
Among various synthetic routes of indoles synthesis, Larock method [156] possibly be the important one which utilizes 2-alkynylaniline as intermediate towards intra-molecular cyclization. Stolle and co-workers also demonstrated mechanochemical synthesis of indoles using stoichiometric amounts of ZnBr$_2$ and NaCl as milling auxiliary starting from 2-alkynylaniline derivatives (Scheme 39) [157]. They have correlated the milling frequency and time of reaction to the product yields and selectivity. For example, a) at higher frequency (800 min^{-1}) for 45 min lower yield with less selectivity was observed and b) using lower frequency, 200 min^{-1} for 8 h led to 82% of yield with high selectivity.
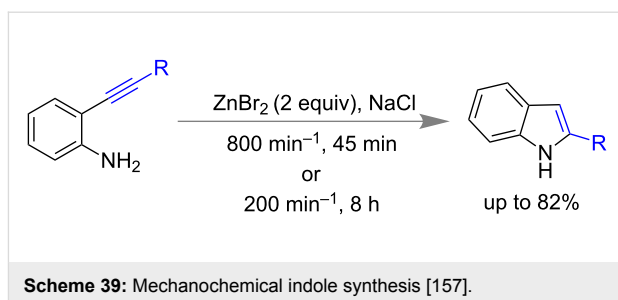
In the traditional method of pyran synthesis the use of transition metal catalyst, corrosive acid, longer reaction time, hazardous organic solvent, and tedious isolation procedure are implemented. Dekamin and co-workers have demonstrated the synthesis of pyrans using potassium phthalimide (POPI) as a catalyst under ball-milling which is found to be advantageous over solution phase synthesis [158]. Malonitrile, benzaldehydes and electron-rich phenols in presence of 5 mol % of POPI, afforded near quantitative yield of chromene derivatives within 20 min (Scheme 40). Similarly, various benzaldehydes with electron-withdrawing groups at the *o/p*-position accelerated the reaction and electron-donating groups slowed that down. Hetero aromatic aldehydes also worked efficiently to give the products in 96–98% yield [158].

Acenes and hetero-acenes have important applications in material development such as semiconductors, photovoltaic cells, field effect transistors, organic light emitting diodes, etc. [159-165]. Moreover, the literature known methods adopted mainly harsh reaction condition and they are generally found to be low yielding [166-168]. Recently, Mal and co-workers reported mechanochemical synthesis of hetero-acenes from 1,2-dicarbonyl compounds and 1,2-diaminoarenes using 10 mol % *p*-toluenesulfonic acid as catalyst. Using this process they could isolate 72–96% of pyrazaacene, phenazine, bis(phenazine), bis(quinoxaine) derivatives (Scheme 41). Major advantages of this mechanomilling methods were time efficient (2–4 h), simple purification procedure (washing with polar solvent), high yielding, room temperature conditions, etc. Previously reported solvent-based synthesis required reflux for 3 days to get 30–40% yield [169].

Scheme 40: Mechanochemical synthesis of chromene [158].
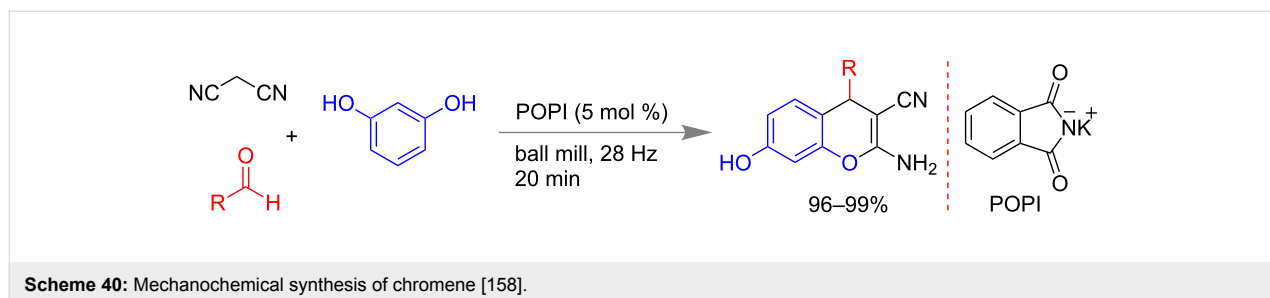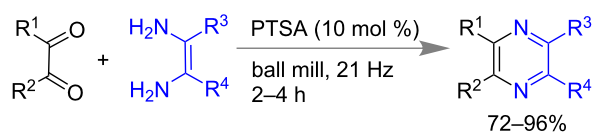
Scheme 41: Mechanochemical synthesis of azacenes [169].

Scheme 43: Mechanochemical C–chalcogen bond formation [171].

Miscellaneous bond formation reaction
Carbon–phosphorus bond synthesis

Recently, Wang and co-workers reported the first carbon–phosphorous (C–P) bond synthesis under mechanochemical conditions. Phosphonylation of benzothiazole and thiazole derivatives were done with organophosphorus compounds using 3 equiv of $Mn(OAc)_3 \cdot 2H_2O$ in a mixer mill for 1.5 h. Benzothiazole or thiazole rings having electron-donating or -withdrawing groups worked efficiently under this protocol. Different organophosphorus compounds including phosphine oxides, phosphinate ester, and phosphonate diester underwent C–P bond formation to give 22–94% of yield (Scheme 42). This method was also found to be applicable in gram scale synthesis with excellent yield. Mechanistically they have shown that the reaction followed a radical pathway [170].

C–Chalcogen bond formation

Ranu and co-workers reported carbon–chalcogen (C–S, C–Se, C–Te) bond formation from aryldiazonium tetrafluoroborate (1 equiv), diaryl chalocogenide (0.5 equiv) in a stainless steel jar at 600 rpm for 15 min. They have used KOH as base, neutral alumina as milling auxiliary. Both electron-donating and -withdrawing diazonium salts worked efficiently to give 70–90% of the products (Scheme 43) [171]. This solvent-free mechanomilling strategy reported to be superior to any solution phase synthesis because it avoids transition metals, could be performed in shorter reaction time and uses stable dichalcogenides rather than toxic thiols and selenols.

Organometallic synthesis and catalytic application
Mechano-synthesis of organometallic compounds

The last decade has witnessed a rapid growth of mechanochemistry in organic synthesis as well as in inorganic coordination chemistry [172]. However, the mechanochemical organometallic synthesis is still in its infancy due to certain difficulties under solvent-free synthesis. Recently the solid state syntheses of organometallic compounds have become popular. In their pioneering work Coville and co-workers presented solvent-free organometallic transformations (e.g., migratory insertion and ligand substitution reactions) at elevated temperature (Scheme 44) which have close resemblance to mechanochemistry [173].
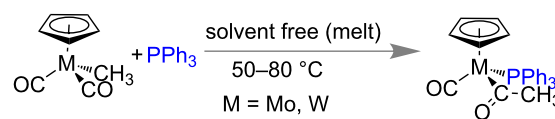
Scheme 44: Solvent-free synthesis of an organometallic complex.

The examples of mechanochemical organometallic complex synthesis are relatively small, but experienced significant growth in recent times. In the early 1990s, the first examples of mechanochemical organometallic reactions were discovered, included the synthesis of various indenyl, cyclopentadienyl and metallocarborane complexes [174]. In Scheme 45, few exam-
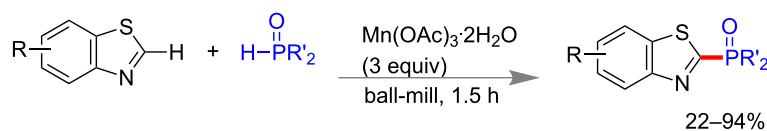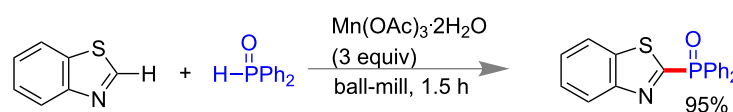
Scheme 42: Mechanochemical oxidative C-P bond formation [170].

a) halogenation of organometallic Re(I) complex
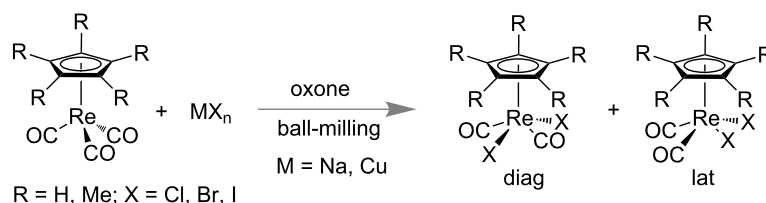
b) multistep and multicomponent organometallic synthesis
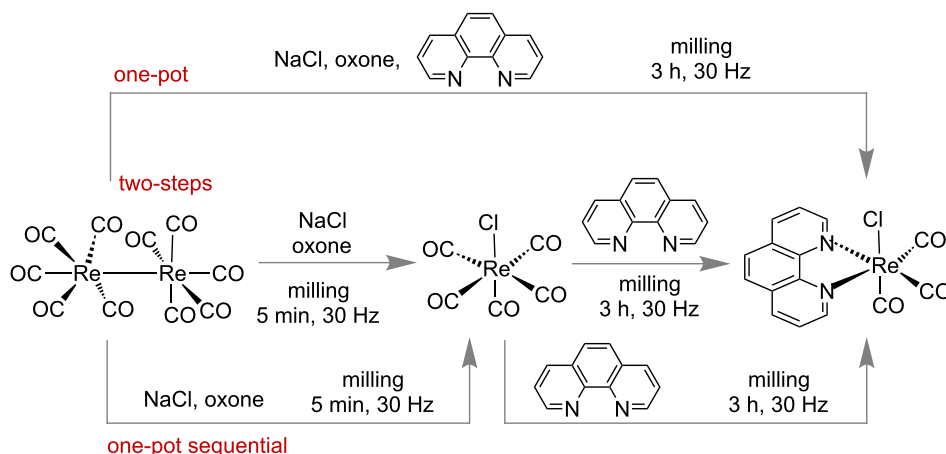
c) mechanosynthesis of *N*-heterocyclic carbene–gold complexes
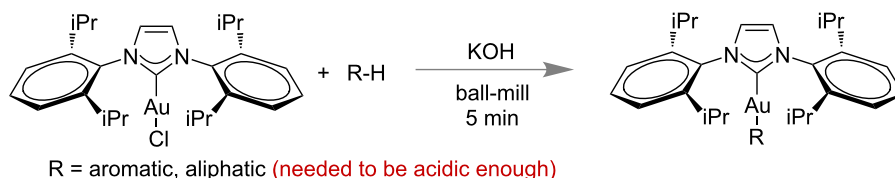
Scheme 45: Selective examples of mechano-synthesis of organometallic complexes. a) Halogenation reaction of Re-complexes [175]. b) Multistep and multicomponent synthesis of Re-complexes [176]. c) Mechano-synthesis of NHC-Au complex [177].

ples of mechanosynthesis of organometallic complexes are shown.

Ćurić and co-workers reported the first mechanochemical activation of a C–H bond of unsymmetrical azobenzene with Pd(OAc)$_2$ [178]. The cyclopalladation process was highly regioselective and the rate of palladation was also faster than traditional solution phase processes. 4'-(*N,N*-dimethylamino)-4-nitroazobenzene with an equimolar amount of Pd(OAc)$_2$ and 25 μL of glacial acetic acid (for LAG) resulted in regioselective C–H activation to give cyclopalladated complex **E** in 4.5 h where two Pd- and two azobenzene groups were involved. Treating this complex with another 1 equiv of Pd(OAc)$_2$ resulted in a second C–H activation to give dicyclopalladated complex **F** in 7.5 h (Scheme 46). It is notable that the monocy-

clopalladated complexation generally takes 3 days in solution and dicyclopalladated complex in solution was never been identified [178].

Recently Aleksanyan and co-workers reported the first gram-scale synthesis of a Pd^{II} organometallic pincer complex under mechanomilling via C–H bond activation. After successful isolation of the Pd^{II} pincer complex by grinding of bis(thiocarbamate) and PdCl$_2$(NCPh)$_2$ they could scale up the reaction up to 1.76 mmol. Using a stainless steel jar they could isolate 95% of the pure pincer complex within 2 min (Scheme 47) [179].

Hanusa and co-workers developed a base-free mechanochemical synthesis of a tris(allyl)aluminum complex. Importantly, unsolvated tris(allyl)aluminum was never been isolated from
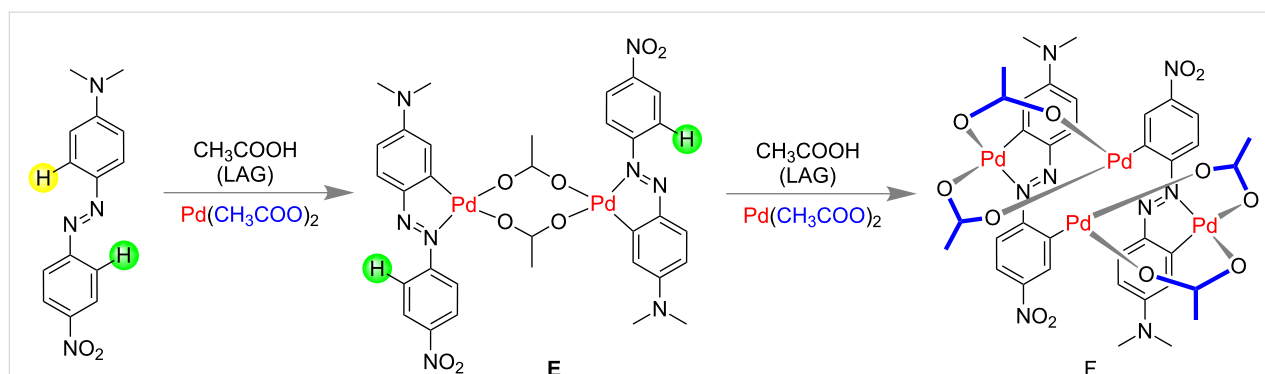
Scheme 46: Mechanochemical activation of C–H bond of unsymmetrical azobenzene [178].
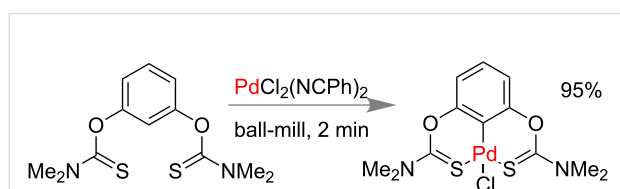
Scheme 47: Mechanochemical synthesis of organometallic pincer complex [179].

solution, but mechanochemically found to be a high yielding reaction when bulky 1,3-bis(trimethylsilyl)allyl anion (Scheme 48) was reacted with aluminum iodide [180].
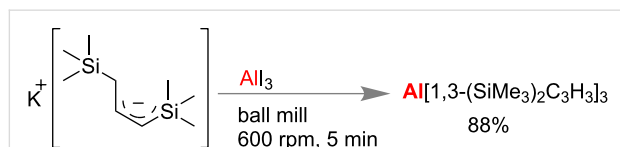
Scheme 48: Mechanochemical synthesis of tris(allyl)aluminum complex [180].

Catalytic application

The success of the mechanochemical synthesis over traditional solvent-based synthesis in different areas has been recognized over the decades. Importantly catalytic application of these mechano-synthesized complexes are also explored. Friščić and

co-workers recently reported an efficient mechanochemical approach towards Ru-based Hoveyda–Grubbs catalyzed olefin metathesis, cross-metathesis and ring-closing metathesis reactions (Scheme 49) [181]. Advantageously this methodology was applicable for both solid and liquid olefins.

Mechanochemical C–H functionalization

Transition-metal-catalyzed activation and functionalization of inert C–H bonds of organic molecules provides a broad avenue in the synthesis of wide range of compounds. In 2015, Bolm and co-workers have successfully demonstrated rhodium(III)-catalyzed C–H bond functionalization under mechanochemical conditions [182]. Advantageously, the developed method adopted mild reaction conditions, i.e., in solvent-free medium and at room temperature. It required a minimum amount of toxic metal salt of Rh, $Cu(OAc)_2$ as a redox modulator and dioxygen as a terminal oxidant (Scheme 50). This efficient technique was turned out to be a greener alternative to the common and mechanistically similar solution based method.

They have also extended mechanochemical C–H functionalization methodology by varying the metal catalyst from rhodium to iridium. In 2016, using an Ir(III) catalyst an unprecedented *ortho*-selective Csp^2–H bond amidation of benzamides with sulfonyl azides as the amide source was done under solvent-free ball mill conditions (Scheme 51) [183]. They could also isolate cyclic iridium complex **H** in ball-milling conditions.
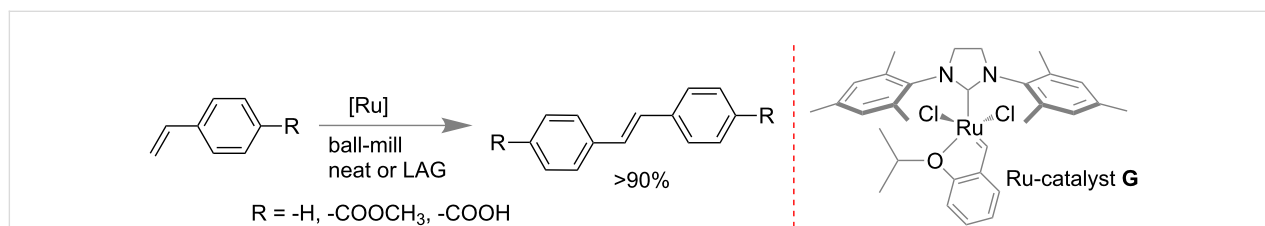
Scheme 49: Mechanochemical Ru-catalyzed olefin metathesis reaction [181].
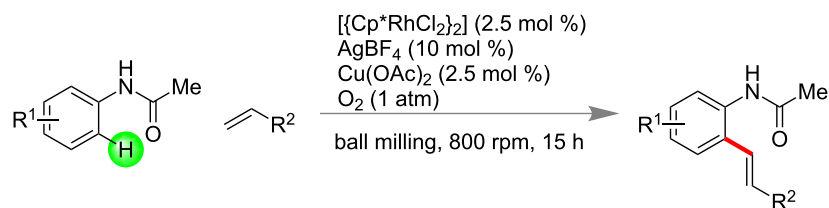
Scheme 50: Rhodium(III)-catalyzed C–H bond functionalization under mechanochemical conditions [182].
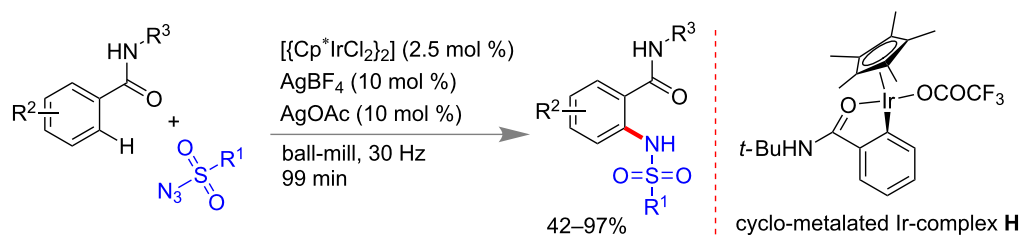
Scheme 51: Mechanochemical Csp^2–H bond amidation using Ir(III) catalyst [183].

In 2015, the Bolm group reported the synthesis of [Cp*RhCl$_2$]$_2$ under LAG from rhodium(III) chloride hydrate and pentamethylcyclopentadiene (Cp*H) at lesser reaction time than solution-based protocols. Subsequently, they utilized the [Cp*RhCl$_2$]$_2$ for the solvent-free mechanochemical C–H bond functionalization of 2-phenylpyridine (Scheme 52). With 2.2 equiv of NXS (X = Br, I) and 5 mol % of [Cp*RhCl$_2$]$_2$ catalyst in a mixer mill, 74% and 84% of dibromo- and diiodo derivatives of 2-phenylpyridine, respectively, were isolated within 3 h [184].

Xu and co-workers developed a palladium-catalyzed site selective mechanochemical dehydrogenative C–H/C–H arylation between oxime and arene moiety for the construction of C$_{sp2}$–C$_{sp2}$ bond with high *para*-selectivity of arene component via LAG. Using 10 mol % of Pd(OAc)$_2$, 2.0 equiv of Na$_2$S$_2$O$_8$ and 1.0 equiv TfOH the biaryls were synthesized in good to excellent yield within 1 h. Dimethyl formamide (DMF) acted as ligand during the activation process (Scheme 53). The protocol was also equally applicable to electron deficient oximes and electron rich anilides [185].
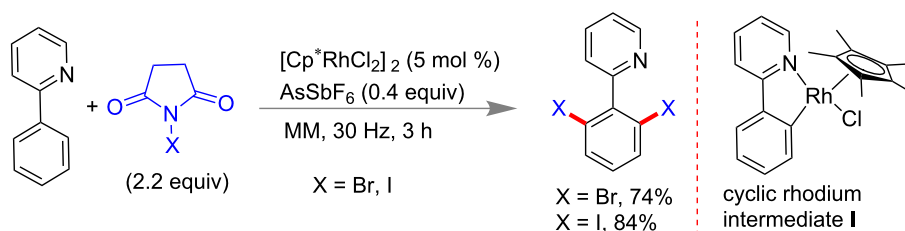
Scheme 52: Mechanochemical Rh-catalyzed C$_{sp2}$–X bond formation [184].
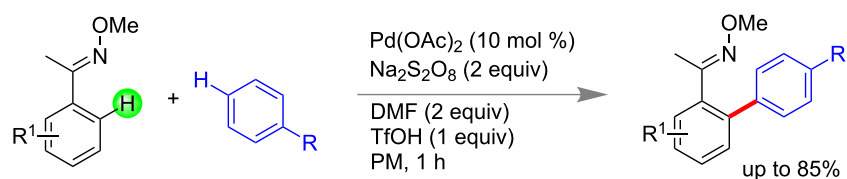
Scheme 53: Mechanochemical Pd-catalyzed C–H activation [185].

Bolm and co-workers reported a Rh-catalyzed amidation of Csp^2–H bonds using dioxazolone as the amide source under ball milling conditions (Scheme 54). Using 5 mol % of Rh catalyst, 20 mol % of AgSbF$_6$ and 20 mol % of AgOAc they have successfully achieved up to 99% of *ortho*-amidation product with diversely substituted arene moiety [186].

Recently Bolm and co-workers developed a mechanochemical synthesis of an indole moiety via a Rh-catalyzed C–H functionalization strategy under planetary ball mill [187]. Using acetanilide and diphenylacetylene as the alkyne component in presence of 5 mol % Rh catalyst and 2.5 mol % Cu(OAc)$_2$ and 1 atm O$_2$ as terminal oxidant they could isolate up to 77% of differently substituted indole derivatives (Scheme 55).

Advantages and limitations

Over a couple of decades the area of mechanochemistry considered to be one of the best solvent-free synthetic methods. This area has become significantly interesting to chemists due to its benefits over conventional solution-based protocols. Importantly in mechanochemistry, avoiding traditional work-up might be considered as one of the major beneficial aspects. This benefit also leading to a significant development to green processes, turned out to be economical, time-efficient and environmentally benign. Easy purification procedures, towards quantitative conversion and minimum byproducts are additionally considered to be major significance to this method. Tullberg et al. investigated the Mizoroki–Heck reaction between iodobenzene and the methyl ester of *N*-Boc-protected aminoacylate under different conditions of energy (Scheme 56) and showed that efficiency under mechanomilling is far better over other methods [58].

Scheme 56: Mizoroki–Heck reaction of aminoacrylates with aryl halide in a ball-mill [58].
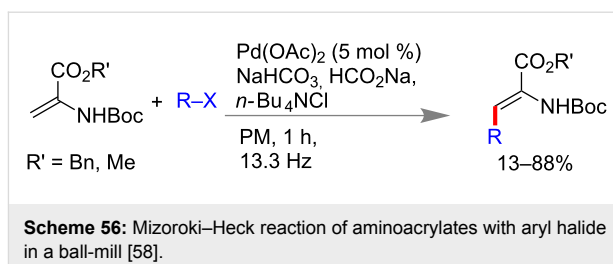
Mal and co-workers have addressed the efficiency of 2-iodoxybenzoic acid (IBX) under mechanomilling conditions (Scheme 57) [8]. Generally the major drawback of IBX is its insolubility in common organic solvents except DMSO and also its explosive nature at higher temperature [188]. They could overcome these limitations by using IBX under solvent-free mechanomilling conditions. They have demonstrated various oxidation reactions, synthesis of benzimidazoles, deprotection of dithianes, etc. The byproduct iodosobenzoic acid (IBA) was recycled over 15 cycles with the help of the oxidant oxone. The economic benefits of IBX under ball milling was also discussed by comparing the literature-known DMSO mediated procedure [8].

The bis(benzotriazolyl)methanethione-assisted thiocarbamoylation of anilines proceed through the formation of unisolable reactive intermediate, aryl *N*-thiocarbamoylbenzotriazole, which rapidly decomposes to the corresponding isothiocyanate in organic solvent [189]. The Štrukil and Friščić group successfully demonstrated the formation of aryl-*N*-thiocarbamoylbenzotriazole under the LAG (liquid-assisted grinding) synthesis (Scheme 58) [190]. Initially, in situ monitoring of mechanochemical thiocarbamoylation suggests the formation of

Scheme 54: Mechanochemical Csp^2–H bond amidation using Rh catalyst.

Scheme 55: Mechanochemical synthesis of indoles using Rh catalyst [187].

Scheme 57: IBX under mechanomilling conditions [8].

Scheme 58: Thiocarbamoylation of anilines; trapping of reactive aryl-*N*-thiocarbamoylbenzotriazole intermediate in mechanochemical synthesis while not isolable in solution-based synthesis [190].

reactive intermediate which gradually disappears with the formation of thiocarbamoylated product. Furthermore isolation and spectroscopic characterization of aryl-*N*-thiocarbamoylbenzotriazole intermediate clearly established the advantage of mechanochemistry over traditional solution-based synthesis and unwraps a new avenue for the mechanistic study as a promising technique.

Recently, the field of C–H activation has gained huge attention of chemists. It allows selective functionalization of C–H bonds

to C–hetero atoms as discussed herein. Moreover, the major drawbacks are involvement of harsh reaction conditions like high temperature, longer reaction time, and huge amount of toxic organic solvents and handling of sensitive metal catalyst. But fortunately, mechanochemistry has overcome all these limitations and proved to be advantageous since it uses minimum amount of solvents, shorter reaction time, and easy handling of reagents and room temperature conditions. Despite the advantages of ball milling in chemical synthesis still there are some limitations to be noted. Mechanochemical methods are general-

ly uncontrollable to temperature controlled reactions, time controlled reactions, in handling low boiling liquids, moisture sensitive systems, heterogeneous reactions, pressure controlled reactions, etc. The mechanochemistry is focused on making the known solution-based synthetic procedures more environmentally friendly by avoiding the solvent which is also one of the major drawbacks. So development of innovative bond formation reactions under mechanomilling should be highly appreciated that are inaccessible from solution phase chemistry.

Conclusion

Significant progress has been made under the area of mechanochemistry during the last few decades owing to their improvement of environmentally sustainable and more selective processes. The major focus of this review is to cover the application of mechanochemistry in the synthesis of small organic molecules including heterocycles. In addition, the mechanosynthesis of organometallics as well as their selective applications in catalysis are also discussed. The understanding of the mechanism of mechanochemical reactions is still unclear and requires significant advancement in this research area. Improvement in new synthetic methodologies under mechanomilling conditions with better results are always demanding, rather than "greening" the solution phase synthesis.

Acknowledgements

References

1. Kulla, H.; Wilke, M.; Fischer, F.; Röllig, M.; Maierhofer, C.; Emmerling, F. *Chem. Commun.* **2017,** *53,* 1664–1667. doi:10.1039/c6cc08950j

2. Ravelli, D.; Dondi, D.; Fagnoni, M.; Albini, A. *Chem. Soc. Rev.* **2009,** *38,* 1999–2011. doi:10.1039/b714786b

3. Walsh, P. J.; Li, H.; de Parrodi, C. A. *Chem. Rev.* **2007,** *107,* 2503–2545. doi:10.1021/cr0509556

4. Constable, D. J. C.; Dunn, P. J.; Hayler, J. D.; Humphrey, G. R.; Leazer, J. L., Jr.; Linderman, R. J.; Lorenz, K.; Manley, J.; Pearlman, B. A.; Wells, A.; Zaks, A.; Zhang, T. Y. *Green Chem.* **2007,** *9,* 411–420. doi:10.1039/B703488C

5. DeVierno Kreuder, A.; House-Knight, T.; Whitford, J.; Ponnusamy, E.; Miller, P.; Jesse, N.; Rodenborn, R.; Sayag, S.; Gebel, M.; Aped, I.; Sharfstein, I.; Manaster, E.; Ergaz, I.; Harris, A.; Nelowet Grice, L. *ACS Sustainable Chem. Eng.* **2017,** *5,* 2927–2935. doi:10.1021/acssuschemeng.6b02399

6. Tobiszewski, M.; Mechlińska, A.; Namieśnik, J. *Chem. Soc. Rev.* **2010,** *39,* 2869–2878. doi:10.1039/b926439f

7. O'Brien, M.; Denton, R.; Ley, S. V. *Synthesis* **2011,** 1157–1192. doi:10.1055/s-0030-1259979

8. Achar, T. K.; Maiti, S.; Mal, P. *RSC Adv.* **2014,** *4,* 12834–12839. doi:10.1039/C4RA00415A

9. Margetić, D.; Štrukil, V. *Mechanochemical Organic Synthesis;* Elsevier: Boston, 2016; pp 1–54. doi:10.1016/B978-0-12-802184-2.00001-7

10. Bhutia, Z. T.; Prasannakumar, G.; Das, A.; Biswas, M.; Chatterjee, A.; Banerjee, M. *ChemistrySelect* **2017,** *2,* 1183–1187. doi:10.1002/slct.201601672

11. Margetić, D.; Štrukil, V. *Mechanochemical Organic Synthesis;* Elsevier: Boston, 2016; pp 351–360. doi:10.1016/B978-0-12-802184-2.00009-1

12. Baig, R. B. N.; Varma, R. S. *Chem. Soc. Rev.* **2012,** *41,* 1559–1584. doi:10.1039/c1cs15204a

13. Do, J.-L.; Friščić, T. *ACS Cent. Sci.* **2017,** *3,* 13–19. doi:10.1021/acscentsci.6b00277

14. Stauch, T.; Dreuw, A. *Chem. Rev.* **2016,** *116,* 14137–14180. doi:10.1021/acs.chemrev.6b00458

15. IUPAC. Compendium of Chemical Terminology, 2nd ed. (the "Gold Book"). Compiled by A. D. McNaught and A. Wilkinson. Blackwell Scientific Publications, Oxford (1997).

16. Kajdas, C. General Approach to Mechanochemistry and Its Relation to Tribochemistry. *Tribology in Engineering;* InTech, 2013; pp 209–240. doi:10.5772/50507

17. Cintas, P.; Tagliapietra, S.; Caporaso, M.; Tabasso, S.; Cravotto, G. *Ultrason. Sonochem.* **2015,** *25,* 8–16. doi:10.1016/j.ultsonch.2014.12.004

18. Baláž, P.; Achimovičová, M.; Baláž, M.; Billik, P.; Cherkezova-Zheleva, Z.; Criado, J. M.; Delogu, F.; Dutková, E.; Gaffet, E.; Gotor, F. J.; Kumar, R.; Mitov, I.; Rojac, T.; Senna, M.; Streletskii, A.; Wieczorek-Ciurowa, K. *Chem. Soc. Rev.* **2013,** *42,* 7571–7637. doi:10.1039/C3CS35468G

19. Zhang, H.; Lin, Y.; Xu, Y.; Weng, W. *Top. Curr. Chem.* **2015,** *369,* 135–207. doi:10.1007/128_2014_617

20. Cintas, P.; Cravotto, G.; Barge, A.; Martina, K. *Top. Curr. Chem.* **2015,** *369,* 239–284. doi:10.1007/128_2014_623

21. Smalø, H. S.; Rybkin, V. V.; Klopper, W.; Helgaker, T.; Uggerud, E. *J. Phys. Chem. A* **2014,** *118,* 7683–7694. doi:10.1021/jp504959z

22. Toda, F. *Acc. Chem. Res.* **1995,** *28,* 480–486. doi:10.1021/ar00060a003

23. Tanaka, K.; Toda, F. *Chem. Rev.* **2000,** *100,* 1025–1074. doi:10.1021/cr940089p

24. Kaupp, G. *Kirk-Othmer Encyclopedia of Chemical Technology;* John Wiley & Sons, Inc., 2012. doi:10.1002/0471238961.solvkaup.a01

25. Friščić, T. *Chem. Soc. Rev.* **2012,** *41,* 3493–3510. doi:10.1039/c2cs15332g

26. Margetić, D.; Štrukil, V. *Mechanochemical Organic Synthesis;* Elsevier: Boston, 2016; pp 343–350. doi:10.1016/B978-0-12-802184-2.00008-X

27. Wang, G.-W. *Chem. Soc. Rev.* **2013,** *42,* 7668–7700. doi:10.1039/C3CS35526H

28. Hernández, J. G.; Friščić, T. *Tetrahedron Lett.* **2015,** *56,* 4253–4265. doi:10.1016/j.tetlet.2015.03.135

29. James, S. L.; Adams, C. J.; Bolm, C.; Braga, D.; Collier, P.; Friščić, T.; Grepioni, F.; Harris, K. D. M.; Hyett, G.; Jones, W.; Krebs, A.; Mack, J.; Maini, L.; Orpen, A. G.; Parkin, I. P.; Shearouse, W. C.; Steed, J. W.; Waddell, D. C. *Chem. Soc. Rev.* **2012,** *41,* 413–447. doi:10.1039/C1CS15171A

30. Margetić, D.; Štrukil, V. *Mechanochemical Organic Synthesis;* Elsevier: Boston, 2016; pp 323–342. doi:10.1016/B978-0-12-802184-2.00007-8

31. Takacs, L. *Chem. Soc. Rev.* **2013,** *42,* 7649–7659. doi:10.1039/c2cs35442j

32. Ribas-Arino, J.; Marx, D. *Chem. Rev.* **2012,** *112,* 5412–5487. doi:10.1021/cr200399q

33. Šepelák, V.; Düvel, A.; Wilkening, M.; Becker, K.-D.; Heitjans, P. *Chem. Soc. Rev.* **2013,** *42,* 7507–7520. doi:10.1039/c2cs35462d

34. Braga, D.; Maini, L.; Grepioni, F. *Chem. Soc. Rev.* **2013,** *42,* 7638–7648. doi:10.1039/c3cs60014a

35. Groote, R.; van Haandel, L.; Sijbesma, R. P. *J. Polym. Sci., Part A: Polym. Chem.* **2012,** *50,* 4929–4935. doi:10.1002/pola.26323

36. Friščić, T. *J. Mater. Chem.* **2010,** *20,* 7599–7605. doi:10.1039/c0jm00872a

37. Haehnel, A. P.; Sagara, Y.; Simon, Y. C.; Weder, C. *Top. Curr. Chem.* **2015,** *369,* 345–375. doi:10.1007/128_2015_640

38. Toda, F.; Tanaka, K.; Iwata, S. *J. Org. Chem.* **1989,** *54,* 3007–3009. doi:10.1021/jo00274a007

39. Jörres, M.; Aceña, J. L.; Soloshonok, V. A.; Bolm, C. *ChemCatChem* **2015,** *7,* 1265–1269. doi:10.1002/cctc.201500102

40. Jacob, K.; Schmidt, R.; Stolle, A. *Ball Milling Towards Green Synthesis: Applications, Projects, Challenges;* The Royal Society of Chemistry, 2015; pp 34–57. doi:10.1039/9781782621980-00034

41. Tan, D.; Mottillo, C.; Katsenis, A. D.; Štrukil, V.; Friščić, T. *Angew. Chem., Int. Ed.* **2014,** *53,* 9321–9324. doi:10.1002/anie.201404120

42. Ranu, B. C.; Chatterjee, T.; Mukherjee, N. *Ball Milling Towards Green Synthesis: Applications, Projects, Challenges;* The Royal Society of Chemistry, 2015; pp 1–33. doi:10.1039/9781782621980-00001

43. Friščić, T. *Ball Milling Towards Green Synthesis: Applications, Projects, Challenges;* The Royal Society of Chemistry, 2015; pp 151–189. doi:10.1039/9781782621980-00151

44. Saunders, G. C.; Wehr-Candler, T. T. *J. Fluorine Chem.* **2013,** *153,* 162–164. doi:10.1016/j.jfluchem.2013.05.030

45. Margetić, D.; Štrukil, V. *Mechanochemical Organic Synthesis;* Elsevier: Boston, 2016; pp 55–139. doi:10.1016/B978-0-12-802184-2.00002-9

46. Margetić, D.; Štrukil, V. *Mechanochemical Organic Synthesis;* Elsevier: Boston, 2016; pp 293–321. doi:10.1016/B978-0-12-802184-2.00006-6

47. Margetić, D.; Štrukil, V. *Mechanochemical Organic Synthesis;* Elsevier: Boston, 2016; pp 283–292. doi:10.1016/B978-0-12-802184-2.00005-4

48. Raston, C. L.; Scott, J. L. *Green Chem.* **2000,** *2,* 49–52. doi:10.1039/A907688C

49. Guillena, G.; Hita, M. d. C.; Nájera, C.; Viózquez, S. F. *J. Org. Chem.* **2008,** *73,* 5933–5943. doi:10.1021/jo800773q

50. Machuca, E.; Juaristi, E. *Tetrahedron Lett.* **2015,** *56,* 1144–1148. doi:10.1016/j.tetlet.2015.01.079

51. Zhang, Z.; Dong, Y.-W.; Wang, G.-W.; Komatsu, K. *Chem. Lett.* **2004,** *33,* 168–169. doi:10.1246/cl.2004.168

52. Jörres, M.; Mersmann, S.; Raabe, G.; Bolm, C. *Green Chem.* **2013,** *15,* 612–616. doi:10.1039/c2gc36906k

53. Mack, J.; Shumba, M. *Green Chem.* **2007,** *9,* 328–330. doi:10.1039/B612983H

54. Balema, V. P.; Wiench, J. W.; Pruski, M.; Pecharsky, V. K. *Chem. Commun.* **2002,** 724–725. doi:10.1039/B111515D

55. Balema, V. P.; Wiench, J. W.; Pruski, M.; Pecharsky, V. K. *J. Am. Chem. Soc.* **2002,** *124,* 6244–6245. doi:10.1021/ja017908p

56. Nielsen, S. F.; Peters, D.; Axelsson, O. *Synth. Commun.* **2000,** *30,* 3501–3509. doi:10.1080/00397910008087262

57. Jiang, Z.-J.; Li, Z.-H.; Yu, J.-B.; Su, W.-K. *J. Org. Chem.* **2016,** *81,* 10049–10055. doi:10.1021/acs.joc.6b01938

58. Tullberg, E.; Schacher, F.; Peters, D.; Frejd, T. *Synthesis* **2006,** 1183–1189. doi:10.1055/s-2006-926371

59. Zhu, X.; Liu, J.; Chen, T.; Su, W. *Appl. Organomet. Chem.* **2012,** *26,* 145–147. doi:10.1002/aoc.2827

60. Thorwirth, R.; Stolle, A.; Ondruschka, B. *Green Chem.* **2010,** *12,* 985–991. doi:10.1039/c000674b

61. Maiti, S.; Mal, P. *Org. Lett.* **2017,** *19,* 2454–2457. doi:10.1021/acs.orglett.7b01117

62. Maiti, S.; Achar, T. K.; Mal, P. *Org. Lett.* **2017,** *19,* 2006–2009. doi:10.1021/acs.orglett.7b00562

63. Girard, S. A.; Knauber, T.; Li, C.-J. *From C-H to C-C Bonds: Cross-Dehydrogenative-Coupling;* The Royal Society of Chemistry, 2015; pp 1–32. doi:10.1039/9781782620082-00001

64. Yeung, C. S.; Dong, V. M. *Chem. Rev.* **2011,** *111,* 1215–1292. doi:10.1021/cr100280d

65. Yoo, W.-J.; Li, C.-J. *Top. Curr. Chem.* **2010,** *292,* 281–302. doi:10.1007/128_2009_17

66. Li, C.-J. *Acc. Chem. Res.* **2009,** *42,* 335–344. doi:10.1021/ar800164n

67. Su, W.; Yu, J.; Li, Z.; Jiang, Z. *J. Org. Chem.* **2011,** *76,* 9144–9150. doi:10.1021/jo2015533

68. Yu, J.; Li, Z.; Jia, K.; Jiang, Z.; Liu, M.; Su, W. *Tetrahedron Lett.* **2013,** *54,* 2006–2009. doi:10.1016/j.tetlet.2013.02.007

69. Yu, J.-B.; Zhang, Y.; Jiang, Z.-J.; Su, W.-K. *J. Org. Chem.* **2016,** *81,* 11514–11520. doi:10.1021/acs.joc.6b02197

70. Jia, K.-Y.; Yu, J.-B.; Jiang, Z.-J.; Su, W.-K. *J. Org. Chem.* **2016,** *81,* 6049–6055. doi:10.1021/acs.joc.6b01138

71. Ruiz-Castillo, P.; Buchwald, S. L. *Chem. Rev.* **2016,** *116,* 12564–12649. doi:10.1021/acs.chemrev.6b00512

72. Fennie, M. W.; Roth, J. M. *J. Chem. Educ.* **2016,** *93,* 1788–1793. doi:10.1021/acs.jchemed.6b00090

73. Muñiz, K. *Top. Curr. Chem.* **2016,** *373,* 105–133. doi:10.1007/128_2015_663

74. Louillat, M.-L.; Patureau, F. W. *Chem. Soc. Rev.* **2014,** *43,* 901–910. doi:10.1039/C3CS60318K

75. Bariwal, J.; Van der Eycken, E. *Chem. Soc. Rev.* **2013,** *42,* 9283–9303. doi:10.1039/C3CS60228A

76. Schmidt, A. W.; Reddy, K. R.; Knölker, H.-J. *Chem. Rev.* **2012,** *112,* 3193–3328. doi:10.1021/cr200447s

77. Margetić, D.; Štrukil, V. *Mechanochemical Organic Synthesis;* Elsevier: Boston, 2016; pp 141–233. doi:10.1016/B978-0-12-802184-2.00003-0

78. Zhu, X.; Zhang, Q.; Su, W. *RSC Adv.* **2014,** *4,* 22775–22778. doi:10.1039/c4ra02952f

79. Achar, T. K.; Mal, P. *J. Org. Chem.* **2015,** *80,* 666–672. doi:10.1021/jo502464n

80. Achar, T. K.; Sahoo, P. K.; Mal, P. *ChemistrySelect* **2017,** *2,* 1944–1949. doi:10.1002/slct.201700210

81. Achar, T. K.; Mal, P. *Adv. Synth. Catal.* **2015,** *357,* 3977–3985. doi:10.1002/adsc.201500914

82. Alt, I. T.; Plietker, B. *Angew. Chem., Int. Ed.* **2016,** *55,* 1519–1522. doi:10.1002/anie.201510045

83. Antonchick, A. P.; Samanta, R.; Kulikov, K.; Lategahn, J. *Angew. Chem., Int. Ed.* **2011,** *50,* 8605–8608. doi:10.1002/anie.201102984

84. Camasso, N. M.; Sanford, M. S. *Science* **2015,** *347,* 1218–1220. doi:10.1126/science.aaa4526

85. Konnert, L.; Lamaty, F.; Martinez, J.; Colacino, E. *J. Org. Chem.* **2014,** *79,* 4008–4017. doi:10.1021/jo500463y

86. Jiang, D.; He, T.; Ma, L.; Wang, Z. *RSC Adv.* **2014,** *4,* 64936–64946. doi:10.1039/C4RA10784E

87. Dokli, I.; Gredičak, M. *Eur. J. Org. Chem.* **2015,** 2727–2732. doi:10.1002/ejoc.201500051

88. Bose, A.; Mal, P. *Tetrahedron Lett.* **2014,** *55,* 2154–2156. doi:10.1016/j.tetlet.2014.02.064

89. Margetić, D.; Štrukil, V. *Mechanochemical Organic Synthesis;* Elsevier: Boston, 2016; pp 235–282. doi:10.1016/B978-0-12-802184-2.00004-2

90. Waddell, D. C.; Thiel, I.; Bunger, A.; Nkata, D.; Maloney, A.; Clark, T.; Smith, B.; Mack, J. *Green Chem.* **2011,** *13,* 3156–3161. doi:10.1039/c1gc15594f

91. Chatterjee, T.; Saha, D.; Ranu, B. C. *Tetrahedron Lett.* **2012,** *53,* 4142–4144. doi:10.1016/j.tetlet.2012.05.127

92. Lanzillotto, M.; Konnert, L.; Lamaty, F.; Martinez, J.; Colacino, E. *ACS Sustainable Chem. Eng.* **2015,** *3,* 2882–2889. doi:10.1021/acssuschemeng.5b00819

93. Gribble, G. W. *Acc. Chem. Res.* **1998,** *31,* 141–152. doi:10.1021/ar9701777

94. Gribble, G. W. *Chem. Soc. Rev.* **1999,** *28,* 335–346. doi:10.1039/A900201D

95. Rahman, A. N. M. M.; Bishop, R.; Tan, R.; Shan, N. *Green Chem.* **2005,** *7,* 207–209. doi:10.1039/B416275G

96. Wang, G.-W.; Gao, J. *Green Chem.* **2012,** *14,* 1125–1131. doi:10.1039/c2gc16606b

97. Schmidt, R.; Stolle, A.; Ondruschka, B. *Green Chem.* **2012,** *14,* 1673–1679. doi:10.1039/c2gc16508b

98. Maiti, S.; Mal, P. *Synth. Commun.* **2014,** *44,* 3461–3469. doi:10.1080/00397911.2014.946995

99. Mendonça, G. F.; de Almeida, L. S.; de Mattos, M. C. S.; Esteves, P. M.; Ribeiro, R. S. *Curr. Org. Synth.* **2015,** *12,* 603–617. doi:10.2174/1570179412051508211130712

100. Mishra, A. K.; Nagarajaiah, H.; Moorthy, J. N. *Eur. J. Org. Chem.* **2015,** 2733–2738. doi:10.1002/ejoc.201403463

101. Nyffeler, P. T.; Durón, S. G.; Burkart, M. D.; Vincent, S. P.; Wong, C.-H. *Angew. Chem., Int. Ed.* **2004,** *44,* 192–212. doi:10.1002/anie.200400648

102. Howard, J. L.; Sagatov, Y.; Repusseau, L.; Schotten, C.; Browne, D. L. *Green Chem.* **2017,** *19,* 2798–2802. doi:10.1039/c6gc03139k

103. Brauch, S.; van Berkel, S. S.; Westermann, B. *Chem. Soc. Rev.* **2013,** *42,* 4948–4962. doi:10.1039/C3CS35505E

104. Eberlin, L.; Tripoteau, F.; Carreaux, F.; Whiting, A.; Carboni, B. *Beilstein J. Org. Chem.* **2014,** *10,* 237–250. doi:10.3762/bjoc.10.19

105. De, M. F.; Banfi, L.; Riva, R.; Basso, A. *Comb. Chem. High Throughput Screening* **2011,** *14,* 782–810. doi:10.2174/138620711796957099

106. Cho, H. Y.; Morken, J. P. *Chem. Soc. Rev.* **2014,** *43,* 4368–4380. doi:10.1039/c3cs60482a

107. Cores, A.; Carbajales, C.; Coelho, A. *Curr. Top. Med. Chem.* **2014,** *14,* 2209–2230. doi:10.2174/1568026614666141127115130

108. Ahmadi, T.; Ziarani, G. M.; Gholamzadeh, P.; Mollabagher, H. *Tetrahedron: Asymmetry* **2017,** *28,* 708–724. doi:10.1016/j.tetasy.2017.04.002

109. Dichtel, W. R.; Miljanić, O. Š.; Zhang, W.; Spruell, J. M.; Patel, K.; Aprahamian, I.; Heath, J. R.; Stoddart, J. F. *Acc. Chem. Res.* **2008,** *41,* 1750–1761. doi:10.1021/ar800067h

110. Miljanić, O. Š. *Chem* **2017,** *2,* 502–524. doi:10.1016/j.chempr.2017.03.002

111. Giri, C.; Sahoo, P. K.; Puttreddy, R.; Rissanen, K.; Mal, P. *Chem. – Eur. J.* **2015,** *21,* 6390–6393. doi:10.1002/chem.201500734

112. Haji, M. *Beilstein J. Org. Chem.* **2016,** *12,* 1269–1301. doi:10.3762/bjoc.12.121

113. Rotstein, B. H.; Zaretsky, S.; Rai, V.; Yudin, A. K. *Chem. Rev.* **2014,** *114,* 8323–8359. doi:10.1021/cr400615v

114. Koopmanschap, G.; Ruijter, E.; Orru, R. V. A. *Beilstein J. Org. Chem.* **2014,** *10,* 544–598. doi:10.3762/bjoc.10.50

115. Kruithof, A.; Ruijter, E.; Orru, R. V. A. *Chem. – Asian J.* **2015,** *10,* 508–520. doi:10.1002/asia.201403207

116. Polindara-García, L. A.; Juaristi, E. *Eur. J. Org. Chem.* **2016,** 1095–1102. doi:10.1002/ejoc.201501371

117. Liu, Y.-L.; Zhou, J. *Synthesis* **2015,** *47,* 1210–1226. doi:10.1055/s-0034-1380117

118. Cai, X.-H.; Xie, B. *ARKIVOC* **2014,** 205–248. doi:10.3998/ark.5550190.p008.487

119. Sun, X.; Sun, Y.; Rao, Y. *Curr. Org. Chem.* **2016,** *20,* 1878–1901. doi:10.2174/1385272820666160331235519

120. Hernández, J. G.; Turberg, M.; Schiffers, I.; Bolm, C. *Chem. – Eur. J.* **2016,** *22,* 14513–14517. doi:10.1002/chem.201603057

121. Estévez, V.; Villacampa, M.; Menéndez, J. C. *Chem. Commun.* **2013,** *49,* 591–593. doi:10.1039/C2CC38099D

122. Tamaddon, F.; Moradi, S. *J. Mol. Catal. A: Chem.* **2013,** *370,* 117–122. doi:10.1016/j.molcata.2012.12.005

123. Trautwein, A. W.; Süßmuth, R. D.; Jung, G. *Bioorg. Med. Chem. Lett.* **1998,** *8,* 2381–2384. doi:10.1016/S0960-894X(98)00430-2

124. Suresh; Sandhu, J. S. *ARKIVOC* **2012,** 66–133. doi:10.3998/ark.5550190.0013.103

125. Kappe, C. O. *Acc. Chem. Res.* **2000,** *33,* 879–888. doi:10.1021/ar000048h

126. Kaur, R.; Chaudhary, S.; Kumar, K.; Gupta, M. K.; Rawal, R. K. *Eur. J. Med. Chem.* **2017,** *132,* 108–134. doi:10.1016/j.ejmech.2017.03.025

127. Andraos, J. *Beilstein J. Org. Chem.* **2016,** *12,* 2420–2442. doi:10.3762/bjoc.12.236

128. de Fátima, Â.; Braga, T. C.; Neto, L. d. S.; Terra, B. S.; Oliveira, B. G. F.; da Silva, D. L.; Modolo, L. V. *J. Adv. Res.* **2015,** *6,* 363–373. doi:10.1016/j.jare.2014.10.006

129. Kappe, C. O. *Tetrahedron* **1993,** *49,* 6937–6963. doi:10.1016/S0040-4020(01)87971-0

130. Nagarajaiah, H.; Mukhopadhyay, A.; Moorthy, J. N. *Tetrahedron Lett.* **2016,** *57,* 5135–5149. doi:10.1016/j.tetlet.2016.09.047

131. Castilla, A. M.; Ramsay, W. J.; Nitschke, J. R. *Acc. Chem. Res.* **2014,** *47,* 2063–2073. doi:10.1021/ar5000924

132. Nitschke, J. R. *Acc. Chem. Res.* **2007,** *40,* 103–112. doi:10.1021/ar068185n

133. Sahoo, P. K.; Bose, A.; Mal, P. *Eur. J. Org. Chem.* **2015,** 6994–6998. doi:10.1002/ejoc.201501039

134. Li, Z.; Jiang, Z.; Su, W. *Green Chem.* **2015,** *17,* 2330–2334. doi:10.1039/c5gc00079c

135. Khan, M. M.; Khan, S.; Saigal; Iqbal, S. *RSC Adv.* **2016,** *6,* 42045–42061. doi:10.1039/c6ra06767k

136. Ruijter, E.; Scheffelaar, R.; Orru, R. V. A. *Angew. Chem., Int. Ed.* **2011,** *50,* 6234–6246. doi:10.1002/anie.201006515

137. Jiang, B.; Rajale, T.; Wever, W.; Tu, S.-J.; Li, G. *Chem. – Asian J.* **2010,** *5,* 2318–2335. doi:10.1002/asia.201000310

138. Estévez, V.; Villacampa, M.; Menéndez, J. C. *Chem. Soc. Rev.* **2014,** *43,* 4633–4657. doi:10.1039/C3CS60015G

139. Estévez, V.; Villacampa, M.; Menéndez, J. C. *Chem. Soc. Rev.* **2010,** *39,* 4402–4421. doi:10.1039/B917644F

140. Garbarino, S.; Ravelli, D.; Protti, S.; Basso, A. *Angew. Chem., Int. Ed.* **2016,** *55,* 15476–15484. doi:10.1002/anie.201605288

141. Hügel, H. M. *Molecules* **2009,** *14,* 4936–4972.
doi:10.3390/molecules14124936

142. Akelis, L.; Rousseau, J.; Juskenas, R.; Dodonova, J.; Rousseau, C.;
Menuel, S.; Prevost, D.; Tumkevičius, S.; Monflier, E.; Hapiot, F.
Eur. J. Org. Chem. **2016,** 31–35. doi:10.1002/ejoc.201501223

143. Mamada, M.; Pérez-Bolívar, C.; Kumaki, D.; Esipenko, N. A.;
Tokito, S.; Anzenbacher, P., Jr. *Chem. – Eur. J.* **2014,** *20,*
11835–11846. doi:10.1002/chem.201403058

144. Alinezhad, H.; Salehian, F.; Biparva, P. *Synth. Commun.* **2012,** *42,*
102–108. doi:10.1080/00397911.2010.522294

145. Patil, M. R.; Yelamaggad, A.; Keri, R. S. *Lett. Org. Chem.* **2016,** *13,*
474–481. doi:10.2174/2221271780366616072817060

146. Sharma, H.; Singh, N.; Jang, D. O. *Green Chem.* **2014,** *16,*
4922–4930. doi:10.1039/c4gc01142b

147. Park, Y.; Kim, Y.; Chang, S. *Chem. Rev.* **2017,** *117,* 9247–9301.
doi:10.1021/acs.chemrev.6b00644

148. Yang, Y.; Lan, J.; You, J. *Chem. Rev.* **2017,** *117,* 8787–8863.
doi:10.1021/acs.chemrev.6b00567

149. Sharma, H.; Kaur, N.; Singh, N.; Jang, D. O. *Green Chem.* **2015,** *17,*
4263–4270. doi:10.1039/c5gc00536a

150. Chavan, P. V.; Pandit, K. S.; Desai, U. V.; Wadgaonkar, P. P.;
Nawale, L.; Bhansali, S.; Sarkar, D. *Res. Chem. Intermed.* **2017,**
1–16. doi:10.1007/s11164-017-2955-y

151. Panda, S.; Maity, P.; Manna, D. *Org. Lett.* **2017,** *19,* 1534–1537.
doi:10.1021/acs.orglett.7b00313

152. Mukherjee, N.; Ahammed, S.; Bhadra, S.; Ranu, B. C. *Green Chem.*
2013, *15,* 389–397. doi:10.1039/C2GC36521A

153. Tiwari, V. K.; Mishra, B. B.; Mishra, K. B.; Mishra, N.; Singh, A. S.;
Chen, X. *Chem. Rev.* **2016,** *116,* 3086–3240.
doi:10.1021/acs.chemrev.5b00408

154. Gaso-Sokac, D.; Stivojevic, M. *Curr. Org. Chem.* **2016,** *20,*
2211–2221. doi:10.2174/1385272820666160215235852

155. Cook, T. L.; Walker, J. A., Jr.; Mack, J. *Green Chem.* **2013,** *15,*
617–619. doi:10.1039/c3gc36720g

156. Larock, R. C.; Yum, E. K.; Refvik, M. D. *J. Org. Chem.* **1998,** *63,*
7652–7662. doi:10.1021/jo9803277

157. Zille, M.; Stolle, A.; Wild, A.; Schubert, U. S. *RSC Adv.* **2014,** *4,*
13126–13133. doi:10.1039/c4ra00715h

158. Dekamin, M. G.; Eslami, M. *Green Chem.* **2014,** *16,* 4914–4921.
doi:10.1039/c4gc00411f

159. Omachi, H.; Segawa, Y.; Itami, K. *Acc. Chem. Res.* **2012,** *45,*
1378–1389. doi:10.1021/ar300055x

160. Watanabe, M.; Chen, K.-Y.; Chang, Y. J.; Chow, T. J.
Acc. Chem. Res. **2013,** *46,* 1606–1615. doi:10.1021/ar400002y

161. Usta, H.; Facchetti, A.; Marks, T. J. *Acc. Chem. Res.* **2011,** *44,*
501–510. doi:10.1021/ar200006r

162. Jiang, W.; Li, Y.; Wang, Z. *Chem. Soc. Rev.* **2013,** *42,* 6113–6127.
doi:10.1039/c3cs60108k

163. Anthony, J. E. *Chem. Rev.* **2006,** *106,* 5028–5048.
doi:10.1021/cr050966z

164. Mateo-Alonso, A. *Chem. Soc. Rev.* **2014,** *43,* 6311–6324.
doi:10.1039/C4CS00119B

165. Bunz, U. H. F. *Chem. – Eur. J.* **2009,** *15,* 6780–6789.
doi:10.1002/chem.200900990

166. Hsu, D.-T.; Lin, C.-H. *J. Org. Chem.* **2009,** *74,* 9180–9187.
doi:10.1021/jo901754w

167. Hu, J.; Zhang, D.; Harris, F. W. *J. Org. Chem.* **2005,** *70,* 707–708.
doi:10.1021/jo048509q

168. Lin, Y.-C.; Lin, C.-H.; Chen, C.-Y.; Sun, S.-S.; Pal, B.
Org. Biomol. Chem. **2011,** *9,* 4507–4517. doi:10.1039/c0ob00575d

169. Sahoo, P. K.; Giri, C.; Haldar, T. S.; Puttreddy, R.; Rissanen, K.;
Mal, P. *Eur. J. Org. Chem.* **2016,** 1283–1291.
doi:10.1002/ejoc.201690012

170. Li, L.; Wang, J.-J.; Wang, G.-W. *J. Org. Chem.* **2016,** *81,* 5433–5439.
doi:10.1021/acs.joc.6b00786

171. Mukherjee, N.; Chatterjee, T.; Ranu, B. C. *J. Org. Chem.* **2013,** *78,*
11110–11114. doi:10.1021/jo402071b

172. Hernández, J. G.; Bolm, C. *J. Org. Chem.* **2017,** *82,* 4007–4019.
doi:10.1021/acs.joc.6b02887

173. Adeyemi, O. G.; Coville, N. J. *Organometallics* **2003,** *22,* 2284–2290.
doi:10.1021/om0301738

174. Volkov, V. V.; Myakishev, K. G. *Inorg. Chim. Acta* **1999,** *289,* 51–57.
doi:10.1016/S0020-1693(99)00057-2

175. Hernández, J. G.; Macdonald, N. A. J.; Mottillo, C.; Butler, I. S.;
Friščić, T. *Green Chem.* **2014,** *16,* 1087–1092.
doi:10.1039/c3gc42104j

176. Hernández, J. G.; Butler, I. S.; Friščić, T. *Chem. Sci.* **2014,** *5,*
3576–3582. doi:10.1039/C4SC01252F

177. Egbert, J. D.; Slawin, A. M. Z.; Nolan, S. P. *Organometallics* **2013,** *32,*
2271–2274. doi:10.1021/om301187a

178. Juribašić, M.; Užarević, K.; Gracin, D.; Ćurić, M. *Chem. Commun.*
2014, *50,* 10287–10290. doi:10.1039/c4cc04423a

179. Aleksanyan, D. V.; Churusova, S. G.; Aysin, R. R.; Klemenkova, Z. S.;
Nelyubina, Y. V.; Kozlov, V. A. *Inorg. Chem. Commun.* **2017,** *76,*
33–35. doi:10.1016/j.inoche.2016.12.006

180. Rightmire, N. R.; Hanusa, T. P.; Rheingold, A. L. *Organometallics*
2014, *33,* 5952–5955. doi:10.1021/om5009204

181. Do, J.-L.; Mottillo, C.; Tan, D.; Štrukil, V.; Friščić, T.
J. Am. Chem. Soc. **2015,** *137,* 2476–2479. doi:10.1021/jacs.5b00151

182. Hermann, G. N.; Becker, P.; Bolm, C. *Angew. Chem., Int. Ed.* **2015,**
54, 7414–7417. doi:10.1002/anie.201502536

183. Hermann, G. N.; Becker, P.; Bolm, C. *Angew. Chem., Int. Ed.* **2016,**
55, 3781–3784. doi:10.1002/anie.201511689

184. Hernández, J. G.; Bolm, C. *Chem. Commun.* **2015,** *51,* 12582–12584.
doi:10.1039/c5cc04423e

185. Lou, S.-J.; Mao, Y.-J.; Xu, D.-Q.; He, J.-Q.; Chen, Q.; Xu, Z.-Y.
ACS Catal. **2016,** *6,* 3890–3894. doi:10.1021/acscatal.6b00861

186. Hermann, G. N.; Bolm, C. *ACS Catal.* **2017,** *7,* 4592–4596.
doi:10.1021/acscatal.7b00582

187. Hermann, G. N.; Jung, C. L.; Bolm, C. *Green Chem.* **2017,** *19,*
2520–2523. doi:10.1039/c7gc00499k

188. Ladziata, U.; Zhdankin, V. V. *ARKIVOC* **2006,** 26–58.
doi:10.3998/ark.5550190.0007.903

189. Katritzky, A. R.; Khashab, N. M.; Bobrov, S.; Yoshioka, M.
J. Org. Chem. **2006,** *71,* 6753–6758. doi:10.1021/jo060793t

190. Štrukil, V.; Gracin, D.; Magdysyuk, O. V.; Dinnebier, R. E.; Friščić, T.
Angew. Chem., Int. Ed. **2015,** *54,* 8440–8443.
doi:10.1002/anie.201502026

One-pot multistep mechanochemical synthesis of fluorinated pyrazolones

Joseph L. Howard, William Nicholson, Yerbol Sagatov and Duncan L. Browne[*]

Abstract

Solventless mechanochemical synthesis represents a technique with improved sustainability metrics compared to solvent-based processes. Herein, we describe a methodical process to run one solventless reaction directly into another through multistep mechanochemistry, effectively amplifying the solvent savings. The approach has to consider the solid form of the materials and compatibility of any auxiliary used. This has culminated in the development of a two-step, one-jar protocol for heterocycle formation and subsequent fluorination that has been successfully applied across a range of substrates, resulting in 12 difluorinated pyrazolones in moderate to excellent yields.

Introduction

Mechanochemical methods are emerging as an alternative approach to traditional solvent-based reactions for chemical synthesis. Under mechanochemical conditions reactions are performed between neat reagents and do not require a solvent. Processing chemical reactions in such a manner is desirable as reactions are consequently less wasteful and more environmentally benign than the analogous solution-based approaches, especially if the work-up and purification processes can also be made solventless or solvent minimised [1,2]. As such, there is now a significant number of mechanochemical synthetic transformations reported [3-6]. However, for the synthetic commu-

nity, perhaps the most interesting examples of mechanochemical reactions are not those that are merely solventless but those in which different reactivity or selectivity arises, as well as those that are significantly shorter in reaction time than those conducted in solution. Indeed, there are several examples where reactions are clearly significantly faster under mechanochemical conditions [7,8].

One of several challenges to be overcome for the further development of mechanochemistry as an up to date tool for synthesis is to gain a better insight into the ability to run multistep proce-
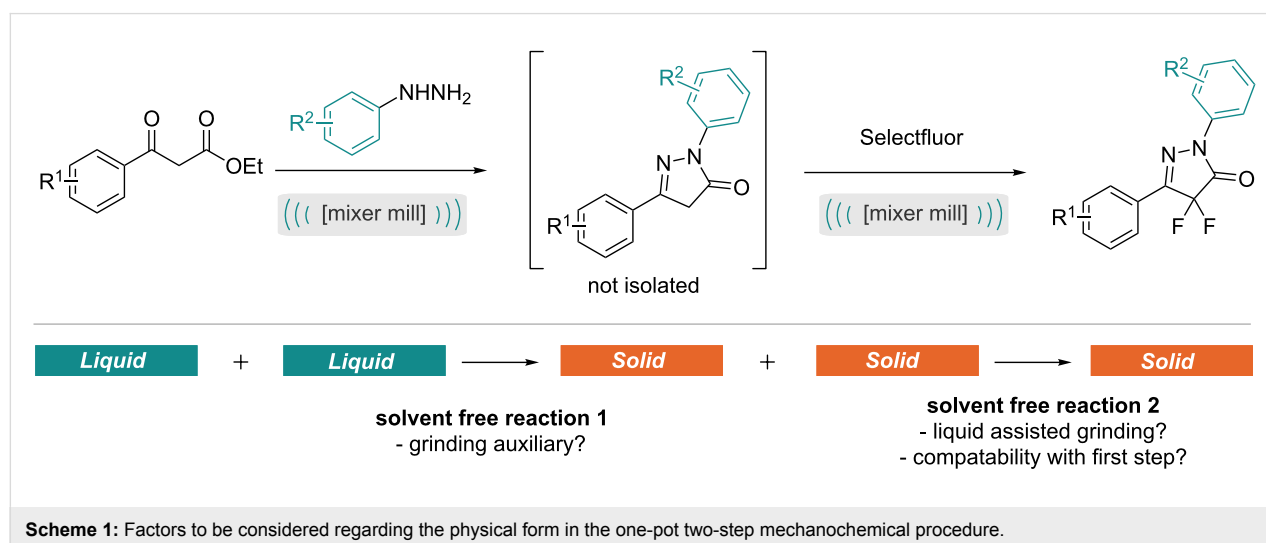
dures. One-pot multistep procedures are particularly efficient, in that the same reaction vessel is used for each step, additional reagents are simply added to the reaction mixture at each stage with no isolation of intermediates or removal of side products [9]. One-pot procedures require the conditions for each step to be compatible with succeeding steps. Typical problems encountered when attempting to multistep reactions include solvent compatibility, or, issues with side products that can inhibit future steps, e.g., by providing access to alternative reaction pathways, poisoning catalysts or altering the pH unfavourably [9]. With regards to mechanochemistry such processing serves to amplify the sustainability metrics by running back-to-back solventless reactions. Multistep mechanochemical procedures have been successfully applied to the synthesis of *O*-glycosides [10], bioactive hydantoins [11], extended iptycenes [12] and organometallics [13] where problems can occur using solution-based synthesis due to limited solubility. Whilst mechanochemical one-pot procedures offer the inherent ability to overcome the issue of identifying a solvent compatible with several consecutive steps, we envisaged alternative hurdles not previously described with regard to compatibility of chemical form. The state of reagents or chemical form is significant to reactions conducted under mechanochemical conditions, where liquids and solids behave differently. For instance, when liquid components are used it may be critical to add a solid auxiliary that helps the transfer of energy and mass (adequate mixing) throughout the mixture. In many cases, leaving out such an auxiliary material can result in a gum or a paste that does not mix well and results in low reaction conversions. Clearly the presence of such a material may have a knock-on effect on any multistep process. Liquid-assisted grinding (LAG) is another phenomenon that can provide enhancement to the reaction outcome and again should be considered for use in a multistep format [14-16].

Having recently begun our research programme in the area of mechanochemistry, we were particularly intrigued by the compatibility of differing chemical forms and additives across a two-step, one-grinding jar solventless process. To investigate this we designed a 2-step reaction related to our recent work on liquid assisted grinding effects of the fluorination of 1,3-dicarbonyl compounds, in which the dicarbonyl will initially form a pyrazolone in the first reaction prior to undergoing difluorination in the second step (Scheme 1) [17].

Notably this approach will likely require a grinding auxiliary in the first step where two liquid phases react and will be catalysed by an acid to afford a solid pyrazolone material. This will then be followed by a difluorination reaction between solid–solid reactants, this reaction may perform better in the presence of base in the second step. In this report, we present a systematic approach to finding the optimal conditions, which are most compatible with both steps. Notably, fluorinated pyrazolones have the potential to be useful pharmaceutical or agrochemical products, given the desirable properties that can be obtained on introduction of fluorine to a molecule [18-25]. However, there have been limited reports on the synthesis of fluorinated pyrazoles, but fluorinated pyrazolones remain poorly studied [26-30].

Results and Discussion

Initially the mechanochemical pyrazolone formation was investigated as the first step of the two step process, we opted to keep the ball size, ball number, jar size and jar and ball material as in our previous studies to reduce the number of variables for this analysis [17]. In the first instance, simply milling the two liquids in the absence of an auxiliary material resulted in a poor yield (Table 1, entry 1). Pleasingly, treatment of ethyl benzoylacetate with one equivalent of phenylhydrazine in the presence

Scheme 1: Factors to be considered regarding the physical form in the one-pot two-step mechanochemical procedure.

of sodium chloride afforded the desired pyrazolone product in 66% yield after milling for 10 minutes (Table 1, entry 2). The addition of a grinding auxiliary could play several roles. We propose that the key benefits are related to improved mixing, and aiding in energy transfer, specifically in mechanochemical reactions where the reaction mixture could be described as a gum, paste or liquid. Notably, the comparable reaction under solvent-based conditions (in toluene, under reflux) required 24 hours to achieve a similar yield (Table 1, entry 3).

Table 1: Optimisation of pyrazolone formation.
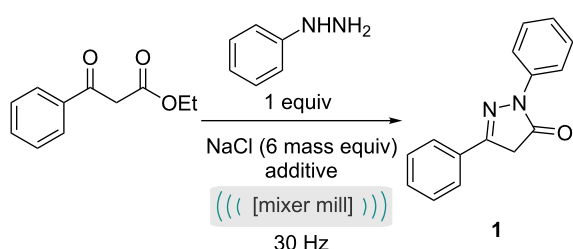
Entry	Additive (equiv)	Time [min]	Yield[a]
1[b]	–	10	20%
2	–	10	66%
3[c]	–	1440	58%
4	HCl (0.5)	10	43%
5	tosic acid (0.5)	10	37%
6	oxalic acid (0.5)	10	22%
7	citric acid (0.5)	10	38%
8	benzoic acid (0.5)	10	88%
9	acetic acid (0.5, 30 µL)	10	88%
10	acetic acid (0.08, 5 µL)	10	75%
11	acetic acid (1.7, 100 µL)	10	97%
12	acetic acid (4.2, 250 µL)	10	73%
13	acetic acid (0.5)	20	86%
14	**acetic acid (0.5)**	**40**	**97% (92%[d])**
15	acetic acid (0.5)	60	97%
16	acetic acid (0.5)	120	97%
17[b]	acetic acid (0.5)	1440	80%

[a]Determined by ^{1}H NMR using mesitylene as an internal standard. [b]Mechanochemical reaction with no NaCl. [c]Solvent based reaction: heating under reflux in toluene, no NaCl. [d]Isolated yield.

As pyrazolone formation can be catalysed by acid, a screen of both solid and liquid acids was next performed (Table 1, entries 4–9). In general, the weaker carboxylate acids performed better than mineral acids, with the highest yield obtained using acetic acid (Table 1, entry 9). The quantity of acid used was then varied. In general, the yield increased with an increase in the amount of acid used (Table 1, entries 9–12), this was with the exception of 250 µL or 4.2 equivalents (Table 1, entry 12), where the yield dropped. The latter observation may be due to

the larger amount of liquid altering the texture of the reaction mixture and thus reducing effective mixing. An alternative justification is that at higher acid equivalents in the solid state the 'on–off' protonation of the hydrazine is slow, meaning that the nucleophilicity is greatly retarded compared to lower acid loadings. Nonetheless, considering that the subsequent fluorination step should proceed optimally under basic conditions [17], the lowest amount of acid which also provided a good yield was thus chosen; 30 µL (Table 1, entry 9). Finally, the reaction time with this quantity of acid was then optimised, whereupon the reaction was found to be complete after 40 minutes producing 92% isolated yield of pyrazolone **1** (Table 1, entry 14). For comparison, these optimal conditions have been applied to a solution-based reaction, resulting in a poorer yield after 24 hours at reflux in toluene (Table 1, entry 17). Having achieved optimal conditions for the first step of the reaction, our attention turned to the second step.

Initial investigation of the fluorination of the pyrazolone focused on finding the optimum reaction time for the isolated step rather than two-step, i.e., the pyrazolone material was isolated from step one and purified before subjecting to this second reaction optimisation. With no additives, the fluorination was complete after 2 hours (Table 2, entry 4), notably an extra hour returned no further improvement (Table 2, entry 5). The fluorination reaction studied here proceeds via an enolate which is aromatic and therefore is relatively facile (compared to the fluorination of other heterocyclic systems). Introduction of a mild base, such as sodium carbonate to the reaction vessel

Table 2: Optimisation of pyrazolone fluorination.
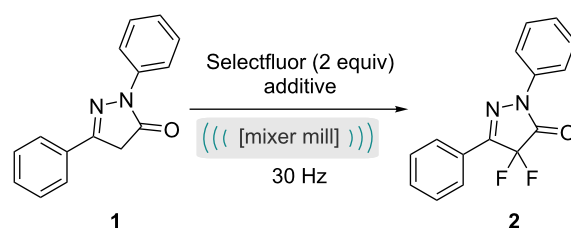
Entry	Additive (equiv)	Time [min]	Yield[a]
1	–	10	11%
2	–	30	41%
3	–	60	83%
4	–	120	95%
5	–	180	94%
6	Na$_2$CO$_3$ (1.0)	60	100%
7	NaCl (6.0)[b]	120	68%
8	acetic acid (0.5)	120	75%
9	NaCl (6.0)[b], Na$_2$CO$_3$ (1.0)	60	100%

[a]Determined by ^{19}F NMR. [b]Mass equivalents NaCl.

served to enhance the rate of reaction, providing complete conversion after 1 hour (Table 2, entry 6).

With an understanding of the second step we then assessed the reaction whilst mimicking aspects of the first reaction in order to look for compatibility of a two-step one-jar process. The most important difference between the two steps is the physical state of the reactants. For the first step (Table 1), both reagents are liquids, and a grinding auxiliary was required to aid mixing and energy transfer. However, for the second step (Table 2), the reagents are solids, and the presence of a grinding agent could have a diluting effect. Indeed, addition of sodium chloride does slow down the fluorination, giving a poorer yield (Table 2, entry 7). Another factor to be explored was the effect of acetic acid on the second step. Again, this resulted in a decrease in yield of the fluorination reaction achievable within a two hour reaction time (Table 2, entry 8).

Pleasingly a combination of sodium carbonate with the sodium chloride grinding auxiliary resulted in complete reaction after one hour (Table 2, entry 9). The only compatibility issue remaining was the acid present from the first step. However, as a base improved the reactivity of the fluorination, the final conditions make use of enough sodium carbonate both to neutralise the remaining acid and accelerate the second step. By applying these compatible conditions to the one-pot procedure, the desired fluorinated pyrazolone was isolated in 75% yield (Scheme 2). Scheme 2 also shows the physical state descriptors and photographs of the practical experiment.

With suitable conditions in hand, the scope of this one-pot mechanochemical process was explored (Scheme 3). Initially, the scope of β-ketoesters was assessed and the procedure was found to be compatible with both the electron-withdrawing and electron-donating groups. However, a poorer yield was ob-

Scheme 2: Optimised conditions for the one-pot synthesis.

Scheme 3: Substrate scope of the one-pot, 2 step mechanochemical synthesis (isolated yields). [a]1 equiv Selectfluor used.
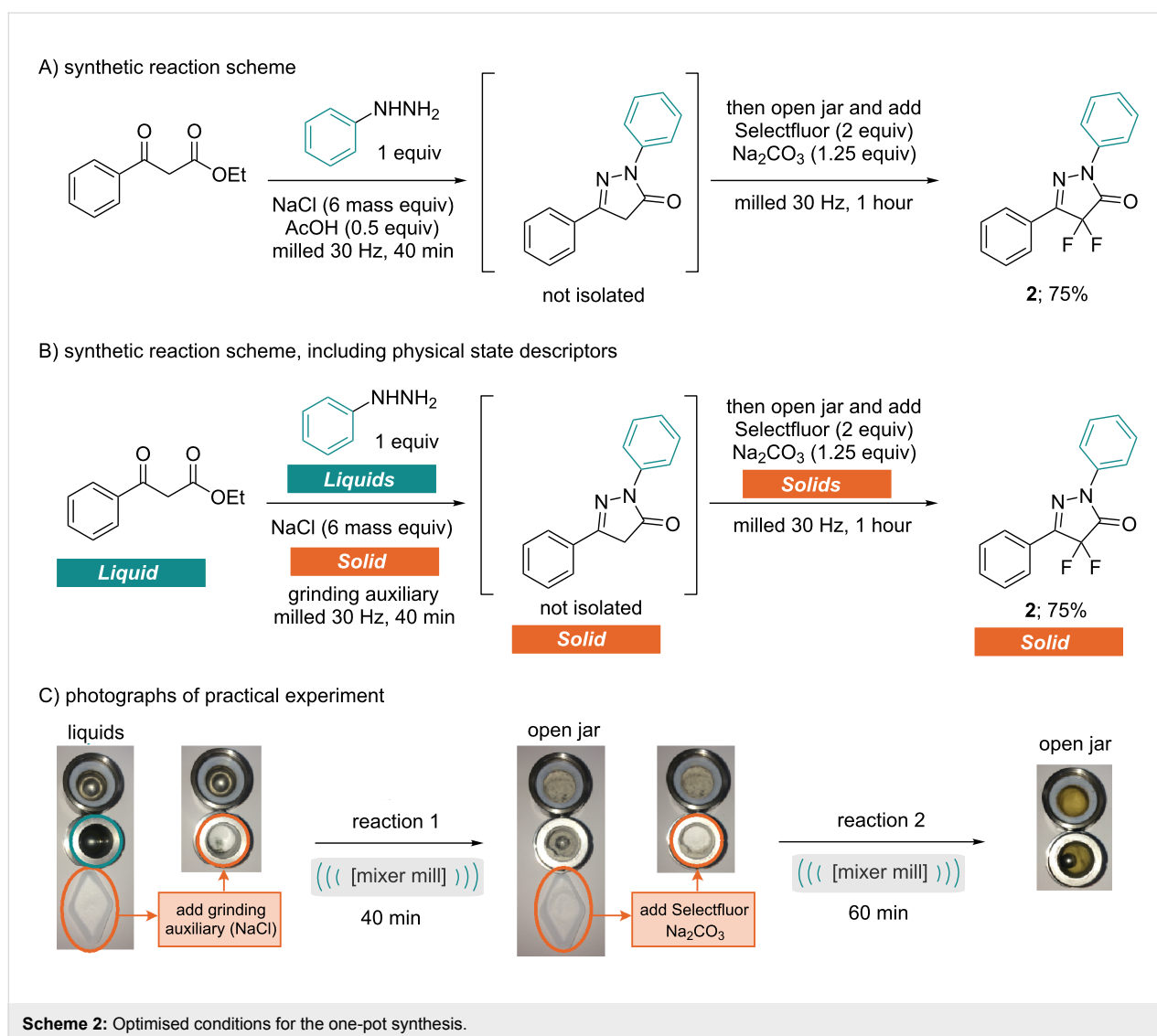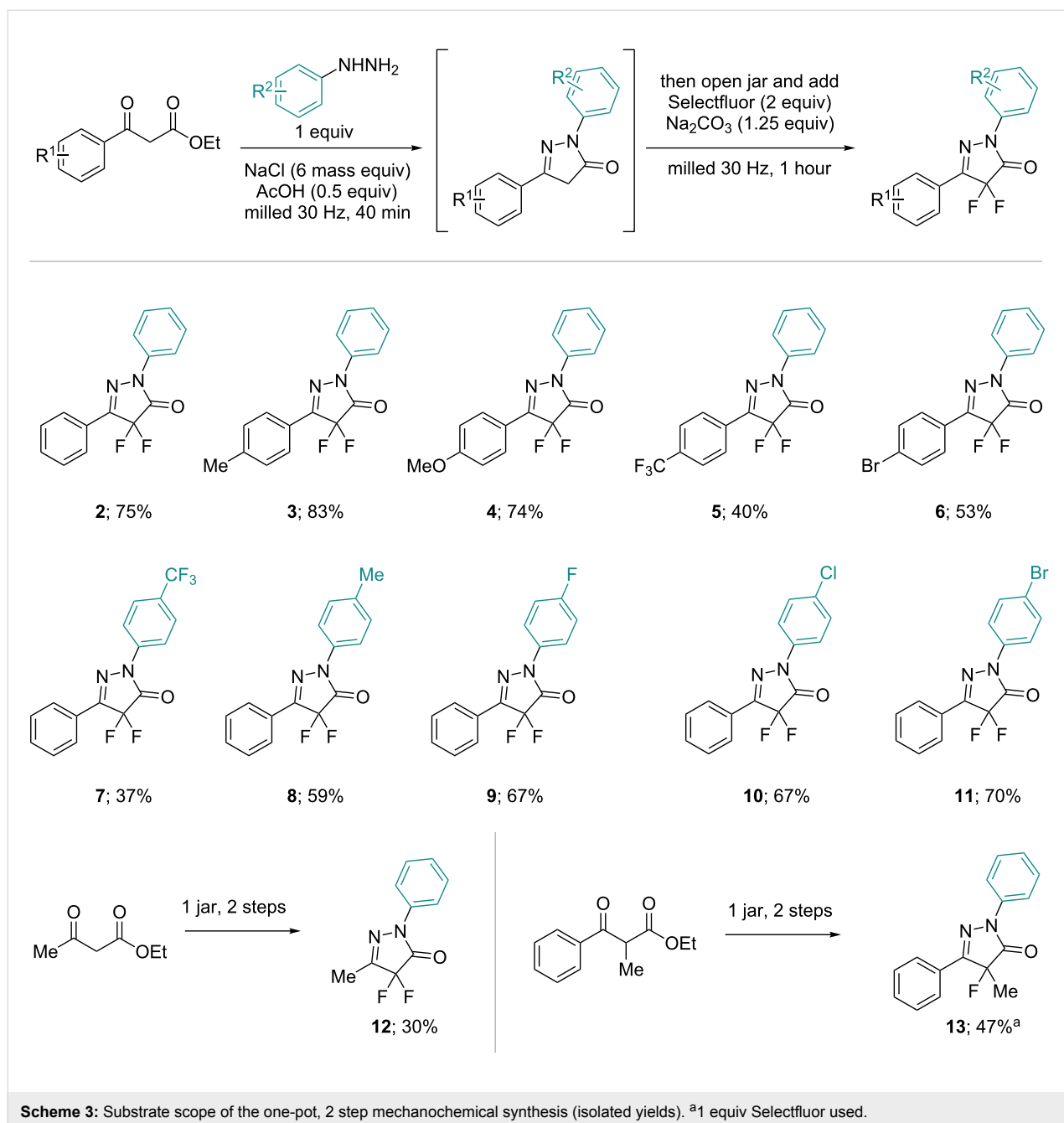
tained for the electron-withdrawing trifluoromethyl substituent (**5**). The scope of phenylhydrazines was also briefly investigated, with several examples demonstrating good isolated yields, again an electron-withdrawing trifluoromethyl substituent was an exception to this (**7**) [31]. For this case, crude ^{19}F NMR after the first step shows a 41% conversion, suggesting that the pyrazolone formation is the limiting factor in this example. An alkyl β-ketoester (ethyl acetoacetate) was also used, affording methyl substituted difluoropyrazolone **12** in modest yield. Finally, an α-substituted β-ketoester was successfully converted to the pyrazolone before monofluorination using one equivalent of

Selectfluor to prepare pyrazolone **13**, also in moderate yield. In general the optimised approach seems to apply to a small range of compounds.

Conclusion

In summary, we have developed a one-pot, two-step mechanochemical synthesis of fluorinated pyrazolones. The experiments provide a logical approach to multistep solventless synthesis under milling conditions and more broadly will assist in the conversion of other processes to such a system. After careful consideration of physical form and additive compatibility the

final protocol has been successfully applied to the preparation of a small library of 12 difluorinated pyrazolones, several of which are hitherto unreported.

Supporting Information

Information about the data that underpins the results presented in this article, including how to access them, can be found in the Cardiff University data catalogue at doi.org/10.17035/d.2017.0038572887.

Supporting Information File 1

Experimental part.
[http://www.beilstein-journals.org/bjoc/content/supplementary/1860-5397-13-189-S1.pdf]

Acknowledgements

References

1. Ranu, B.; Stolle, A., Eds. *Ball Milling Towards Green Synthesis: Applications, Projects, Challenges;* Royal Society of Chemistry: Cambridge, U.K., 2014. doi:10.1039/9781782621980
2. Kaupp, G. *CrystEngComm* **2011,** *13,* 3108–3121. doi:10.1039/c1ce05085k
3. James, S. L.; Adams, C. J.; Bolm, C.; Braga, D.; Collier, P.; Friščić, T.; Grepioni, F.; Harris, K. D. M.; Hyett, G.; Jones, W.; Krebs, A.; Mack, J.; Maini, L.; Orpen, A. G.; Parkin, I. P.; Shearouse, W. C.; Steed, J. W.; Waddell, D. C. *Chem. Soc. Rev.* **2012,** *41,* 413–447. doi:10.1039/C1CS15171A
4. Wang, G.-W. *Chem. Soc. Rev.* **2013,** *42,* 7668–7700. doi:10.1039/c3cs35526h
5. Rodríguez, B.; Bruckmann, A.; Rantanen, T.; Bolm, C. *Adv. Synth. Catal.* **2007,** *349,* 2213–2233. doi:10.1002/adsc.200700252
6. Stolle, A.; Szuppa, T.; Leonhardt, S. E. S.; Ondruschka, B. *Chem. Soc. Rev.* **2011,** *40,* 2317–2329. doi:10.1039/c0cs00195c
7. Do, J.-L.; Friščić, T. *ACS Cent. Sci.* **2017,** *3,* 13–19. doi:10.1021/acscentsci.6b00277
8. Hernández, J. G.; Bolm, C. *J. Org. Chem.* **2017,** *82,* 4007–4019. doi:10.1021/acs.joc.6b02887
9. Hayashi, Y. *Chem. Sci.* **2016,** *7,* 866–880. doi:10.1039/C5SC02913A
10. Tyagi, M.; Khurana, D.; Kartha, K. P. R. *Carbohydr. Res.* **2013,** *379,* 55–59. doi:10.1016/j.carres.2013.06.018
11. Konnert, L.; Dimassi, M.; Gonnet, L.; Lamaty, F.; Martinez, J.; Colacino, E. *RSC Adv.* **2016,** *6,* 36978–36986. doi:10.1039/C6RA03222B
12. Zhao, Y.; Rocha, S. V.; Swager, T. M. *J. Am. Chem. Soc.* **2016,** *138,* 13834–13837. doi:10.1021/jacs.6b09011
13. Hernández, J. G.; Butler, I. S.; Friščić, T. *Chem. Sci.* **2014,** *5,* 3576–3582. doi:10.1039/C4SC01252F
14. Friščić, T.; Childs, S. L.; Rizvi, S. A. A.; Jones, W. *CrystEngComm* **2009,** *11,* 418–426. doi:10.1039/B815174A
15. Hasa, D.; Miniussi, E.; Jones, W. *Cryst. Growth Des.* **2016,** *16,* 4582–4588. doi:10.1021/acs.cgd.6b00682
16. Do, J.-L.; Mottillo, C.; Tan, D.; Štrukil, V.; Friščić, T. *J. Am. Chem. Soc.* **2015,** *137,* 2476–2479. doi:10.1021/jacs.5b00151
17. Howard, J. L.; Sagatov, Y.; Repusseau, L.; Schotten, C.; Browne, D. L. *Green Chem.* **2017,** *19,* 2798–2802. doi:10.1039/C6GC03139K
18. Bégué, J.-P.; Bonnet-Delpon, D. *J. Fluorine Chem.* **2006,** *127,* 992–1012. doi:10.1016/j.jfluchem.2006.05.006
19. Müller, K.; Faeh, C.; Diederich, F. *Science* **2007,** *317,* 1881–1886. doi:10.1126/science.1131943
20. Purser, S.; Moore, P. R.; Swallow, S.; Gouverneur, V. *Chem. Soc. Rev.* **2008,** *37,* 320–330. doi:10.1039/B610213C
21. O'Hagan, D. *J. Fluorine Chem.* **2010,** *131,* 1071–1081. doi:10.1016/j.jfluchem.2010.03.003
22. Jeschke, P. *ChemBioChem* **2004,** *5,* 570–589. doi:10.1002/cbic.200300833
23. Howard, J. L.; Schotten, C.; Alston, S. T.; Browne, D. L. *Chem. Commun.* **2016,** *52,* 8448–8451. doi:10.1039/C6CC02693A
24. Browne, D. L.; Richardson, P. Fluorination Approaches. In *Synthetic Methods in Drug Discovery;* Blakemore, D. C.; Doyle, P. M.; Fobian, Y. M., Eds.; Royal Society of Chemistry: Cambridge, U.K., 2016; Vol. 2, pp 263–370. doi:10.1039/9781782627913-00263
25. Browne, D. L. *Synlett* **2015,** *26,* 33–35. doi:10.1055/s-0034-1379721
26. Surmont, R.; Verniest, G.; De Kimpe, N. *Org. Lett.* **2010,** *12,* 4648–4651. doi:10.1021/ol1019713
27. Skinner, P. J.; Cherrier, M. C.; Webb, P. J.; Shin, Y.-J.; Gharbaoui, T.; Lindstrom, A.; Hong, V.; Tamura, S. Y.; Dang, H. T.; Pride, C. C.; Chen, R.; Richman, J. G.; Connolly, D. T.; Semple, G. *Bioorg. Med. Chem. Lett.* **2007,** *17,* 5620–5623. doi:10.1016/j.bmcl.2007.07.101
28. Dressen, D.; Garofalo, A. W.; Hawkinson, J.; Hom, D.; Jagodzinski, J.; Marugg, J. L.; Neitzel, M. L.; Pleiss, M. A.; Szoke, B.; Tung, J. S.; Wone, D. W. G.; Wu, J.; Zhang, H. *J. Med. Chem.* **2007,** *50,* 5161–5167. doi:10.1021/jm051292n
29. Sloop, J. C.; Jackson, J. L.; Schmidt, R. D. *Heteroat. Chem.* **2009,** *20,* 341–345. doi:10.1002/hc.20556
30. Breen, J. R.; Sandford, G.; Patel, B.; Fray, J. *Synlett* **2015,** *26,* 51–54. doi:10.1055/s-0034-1378915
31. It should be noted that not all of the arylhydrazines investigated had a liquid form.

License and Terms

High-speed vibration-milling-promoted synthesis of symmetrical frameworks containing two or three pyrrole units

Marco Leonardi, Mercedes Villacampa and J. Carlos Menéndez[*]

Abstract

The pseudo-five-component reaction between β-dicarbonyl compounds (2 molecules), diamines and α-iodoketones (2 molecules), prepared in situ from aryl ketones, was performed efficiently under mechanochemical conditions involving high-speed vibration milling with a single zirconium oxide ball. This reaction afforded symmetrical frameworks containing two pyrrole or fused pyrrole units joined by a spacer, which are of interest in the exploration of chemical space for drug discovery purposes. The method was also extended to the synthesis of one compound containing three identical pyrrole fragments via a pseudo-seven-component reaction. Access to compounds having a double bond in their spacer chain was achieved by a different approach involving the homodimerization of 1-allyl- or 1-homoallylpyrroles by application of cross-metathesis chemistry.

Introduction

Symmetrical molecules formed by two or more pharmacophoric units joined by a spacer are very important in drug discovery because many drug targets are symmetrical, the reason most often being that they are composed by two or more identical subunits. Some examples of therapeutic targets in which symmetrical bivalent ligands have proved to be useful include the protease of the human immunodeficiency virus HIV [1], cellular prion protein, PrP[c] [2], and the transient receptor potential melastatin 8 (TRPM8) channel receptor [3]. The synthesis of these symmetrical molecules normally relies on multistep sequences. Due to the special relevance of nitrogen heterocycles in the generation of bioactive molecules, medicinal chemists would greatly benefit from the ability to build two heterocyclic systems at both ends of the spacer chain in a single maneuver. Further advantages in terms of synthetic efficiency would be gained if the key operations leading to the buildup of the heterocyclic frameworks could be performed using multicomponent reactions. However, the simultaneous construction

of two heterocycles in a single operation by means of such reactions has very little precedent in the literature and has never been achieved under mechanochemical conditions.

In this context, we present here our results on the development of pseudo-five-component reactions allowing the construction of bispyrrolic systems **1** starting from β-dicarbonyl compounds **2**, diamine derivatives **3** and aryl ketones **4**, together with some related additional methodology. The disconnection employed and the structural diversity introduced at the three reaction components is summarized in Scheme 1.

Our procedure involves the use of mechanochemistry, which deals with reactions promoted by mechanical energy and is emerging in recent years as a versatile tool that allows solvent-free approaches to organic and inorganic synthesis [4-13]. Indeed, the protocol reported here can be viewed as a generalization of our previously published pyrrole synthesis based on the reaction between primary amines, β-dicarbonyl compounds and ketones, promoted by high-speed vibration milling (HSVM) [14,15]. The importance of pyrrole frameworks stems from the status of this heterocycle as a privileged structure in drug discovery due to its presence as a structural core in molecules that are able to bind various receptors [16].

Results and Discussion

Our route to the target bispyrrole systems is summarized in Scheme 2. Treatment of aromatic ketones **4** with *N*-iodosuccin-

imide (NIS) in the presence of toluenesulfonic acid under high-speed vibration milling for 1 h afforded α-iodoketones **6**, which were not isolated. The suitable β-dicarbonyl compound **2** and α,ω-diamine **3** plus a catalytic amount of Ce(IV) ammonium nitrate (CAN) [17], which had been previously pre-mixed for 30–60 min to ensure the complete generation of the intermediate bis-β-enaminones **5**, were added to the reaction vessel, together with silver nitrate, and the mixture was again submitted to milling for an additional hour. The reactions were routinely performed from 1 mmol of the starting materials, but two of them (leading to compounds **1a** and **1n**) were also carried out at a 10 mmol scale without any significant loss in yield.

This solvent-free protocol combines the initial α-iodination of the starting ketone **4** with a three-component pyrrole synthesis related to the classical Hantzsch reaction. The intermediacy of species **5** and **6** was proved by the following experimental observations:

1. They could be isolated by suitably interrupting our process. As a representative example, the bis-β-enaminone arising from methyl acetoacetate and 1,4-butanediamine was isolated in quantitative yield after mixing the starting materials in the presence of 5% CAN. The isolation and characterization of the intermediate α–iodoketones has been reported previously [15].
2. The isolated intermediates reacted under our usual conditions to give pyrrole derivatives **1**.
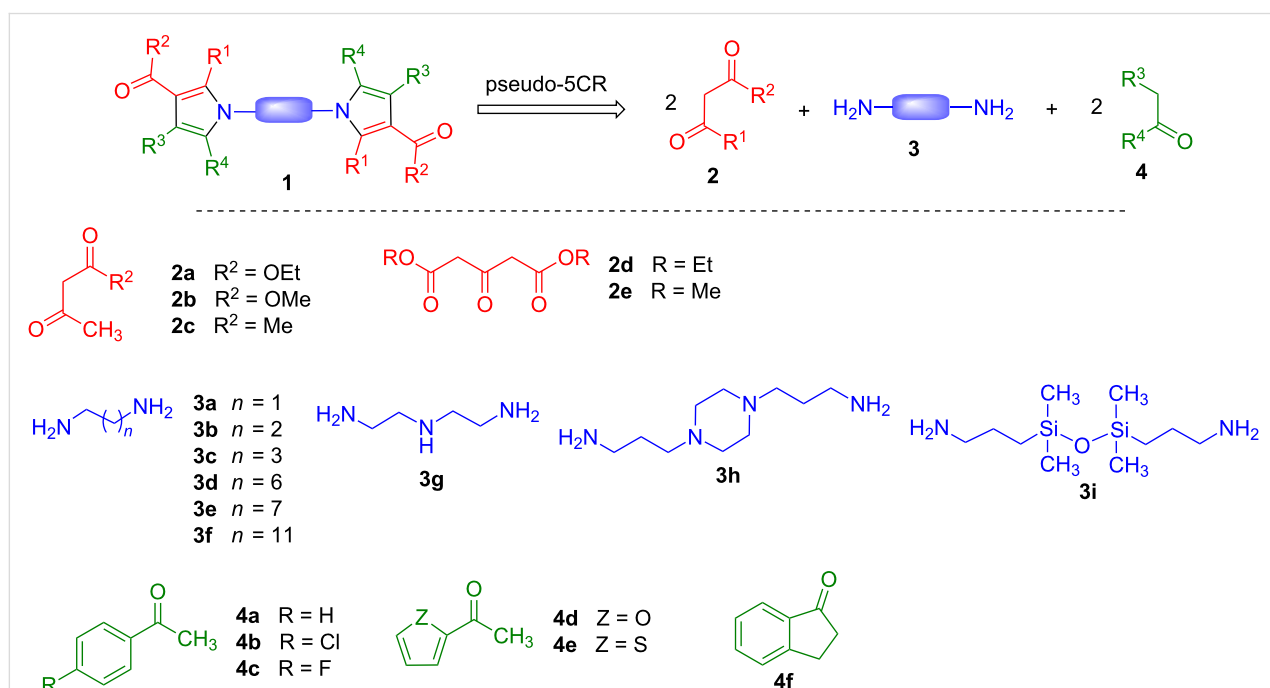
Scheme 1: Our synthetic planning and structural diversity of starting materials employed in our work.

Scheme 2: Pseudo five-component reactions affording symmetrical bispyrrole derivatives joined by a spacer.
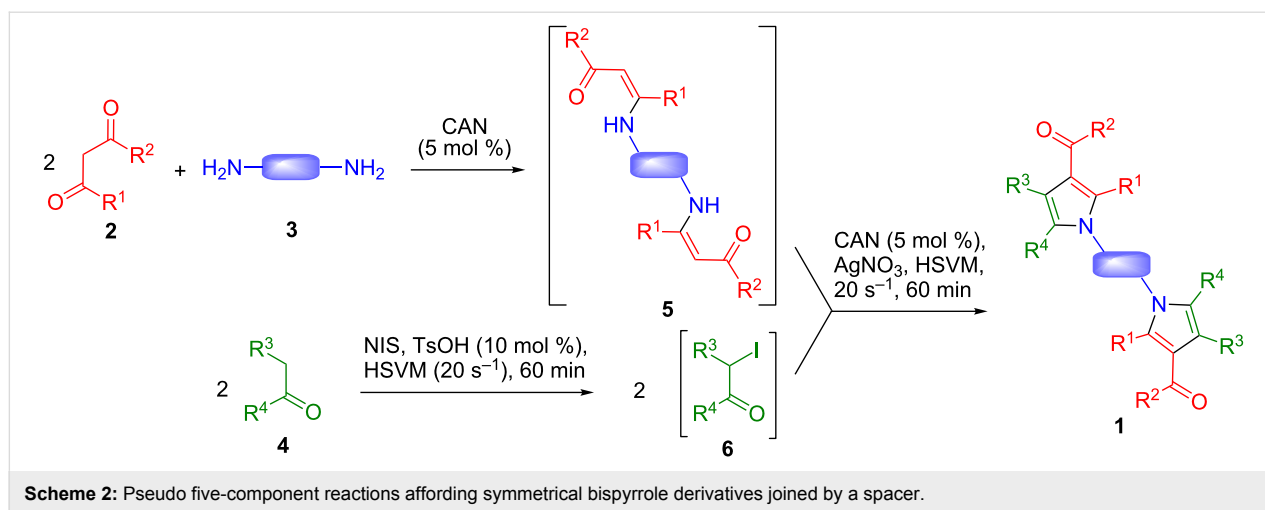
In some cases (compounds **1d**, **1g**, **1j**, **1l**, **1m**, **1o**), the ball milling-promoted iodination step failed and it was necessary to obtain the α-iodoketones **6** in a separate step by treatment of **4** with I_2 and CuO in methanol. The iodination of 1-indanone (eventually leading to **1o**) may be hampered by steric hindrance, since this is the only case where R^3 is different from H. In the cases of 2-furyl methyl ketone and 2-thienyl methyl ketone, the reason for the lower reactivity under solvent-free conditions may be the stabilization of the intermediate enol via intramolecular hydrogen bonding, which would be disrupted in the alternative conditions involving the use of methanol as solvent.

The scope of the method is summarized in Figure 1. In some cases (compounds **1a–g**) the spacer was simply a polymethylene chain, but the inclusion of spacer chains containing an amino group (**1h**), piperazine (**1i**,**j**) or tetramethyldisiloxane (**1k–o**) fragments, was also feasible. Interestingly, the use of N^1-(2-aminoethyl)ethane-1,2-diamine as the starting material was also possible, without interference from the secondary amino group in spite of its nucleophilicity, to give compound **1h**. This kind of functionalized spacers is interesting in that they may allow additional interactions with biological targets. Furthermore, the tetramethyldisiloxane derivatives are of relevance in view of the current interest in silicon-containing compounds for drug discovery applications, which has led to the "silicon switch" approach to the design of bioactive molecules [18-20]. Regarding the pyrrole rings, they were generally methyl-substituted at C-2, but the attachment of functional groups to the methyl substituent was also possible, as shown by the preparation of compounds **1g** and **1n**. Ketone (compounds **1f** and **1j–l**) and ester functions (compounds **1a–e**, **1g–i** and **1m–o**) could be present at C-3, although an attempt to introduce an amide was unsuccessful. A variety of aromatic and heteroaromatic rings could be present at the C-5 position, and the synthesis of compound **1o** from 1-indanone proved the pos-

sibility to prepare systems containing two linked fused pyrrole moieties.

The advantages of the mechanochemical Hantzsch protocol over the conventional one in solution in terms of yield, reaction time and, in most cases, the possibility to telescope the formation of the α-iodide and the pyrrole synthesis in a single process have been previously established [15]. Nevertheless, in order to achieve a more reliable extension of this conclusion to the pseudo-5CR reactions described in the present article, we have performed a control experiment with the reaction leading to **1c** and observed a significantly lower yield (47% vs 62%) and a longer reaction time (5 h vs 2 h) in solution.

The use of triamine **7** as the starting material allowed the preparation of compound **8** via a pseudo-seven-component reaction (Scheme 3). While the overall yield was only moderate, it has to be taken into account that the preparation of **8** involves 12 individual steps, with a linear sequence comprising 9, and thus the average yield is 89% per step. In view of its functionalization, compound **7** can be regarded as a good precursor to heterocyclic dendrimeric structures.

As an additional entry into symmetrical systems containing two pyrrole structural fragments, we briefly examined the homodimerization reactions of 2-allyl- and 2-homoallylpyrroles via cross-metathesis, which should give access to spacers not easily accessible by the previously described route. The starting materials for this study (compounds **11**) were readily prepared under the conditions for single-ring pyrrole derivatives [14,15] and, as shown in Scheme 4, they were uneventfully transformed into the target compounds **12** in the presence of the second-generation Hoveyda–Grubbs catalyst and copper(I) iodide. Interestingly, the reactions starting from 1-allylpyrroles gave a single stereoisomer at the central double bond, which was assumed to
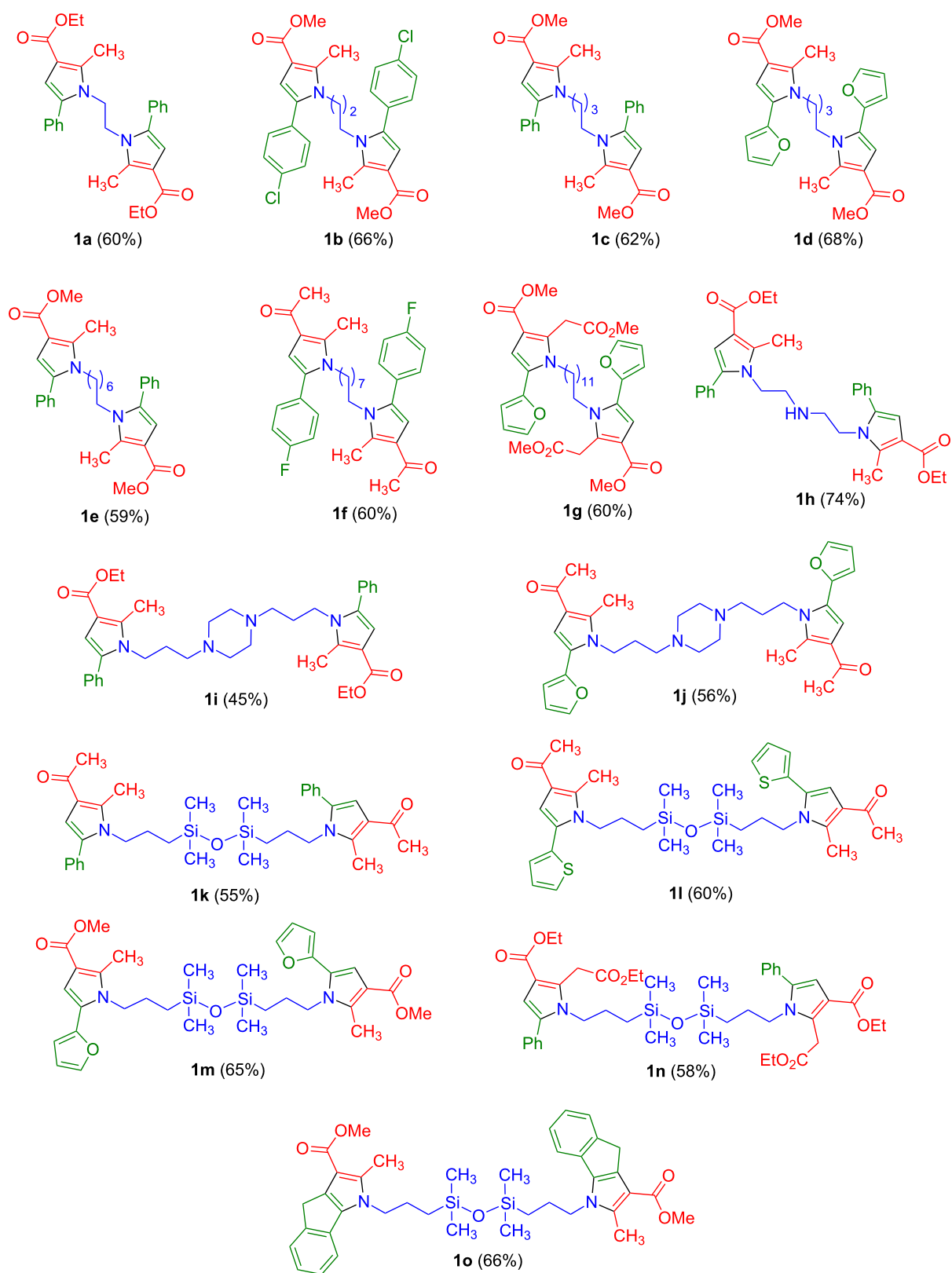
Figure 1: Scope of the synthesis of symmetrical bispyrrole derivatives.
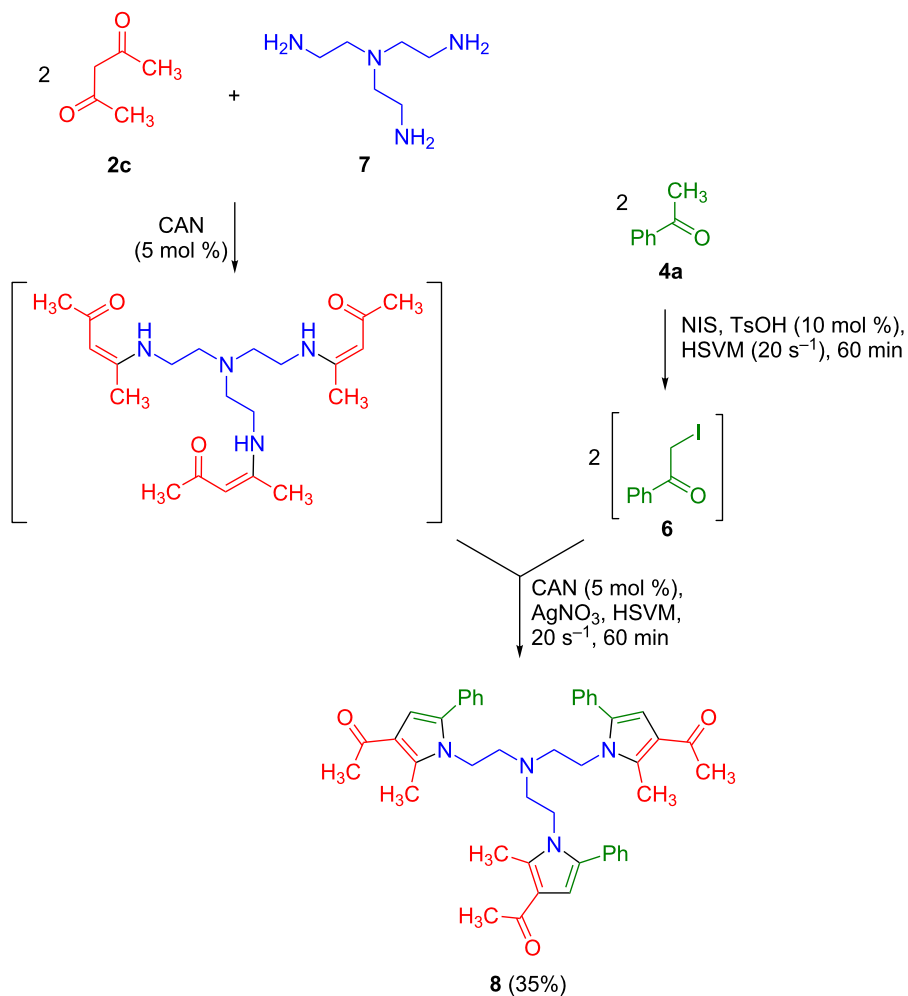
Scheme 3: A pseudo-seven-component reaction that affords a terpyrrole derivative with a functionalized spacer.
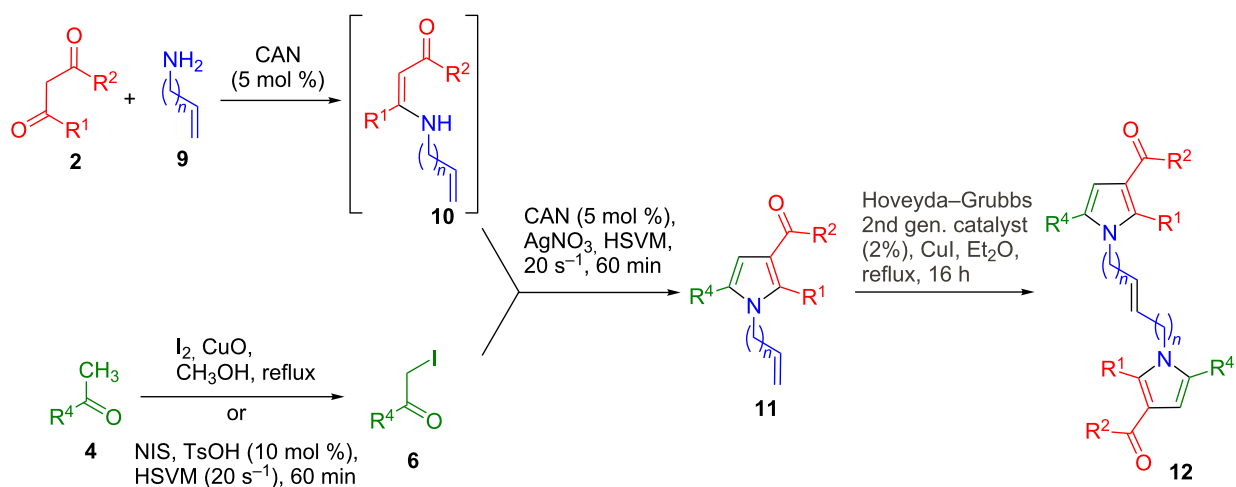
Scheme 4: Homodimerization of 2-allyl- and 2-homoallylpyrroles via cross-metathesis reactions.

be *E*, while compound **12c**, obtained from a 1-homoallyl deriva-tive, was isolated as a 1:1 *E/Z* mixture (Table 1).

Table 1: Yields of the cross-metathesis reactions.

Cmpd	R^1	R^2	R^4	*n*	**11**, %	**12**, %
a	CH$_3$	OMe	2-furyl	1	87	88
b	CH$_3$	Me	C(CH$_3$)$_3$	1	60	70[a]
c	CH$_3$	OMe	2-thienyl	2	71	80[b]
d	CH$_2$-CO$_2$Et	OEt	2-furyl	1	80	88

[a]The reaction time was 48 h in this case. [b]As a 1:1 *E/Z* mixture.

Conclusion

Symmetrical compounds containing two or three pyrrole or fused pyrrole units joined by a spacer are of interest in the exploration of heterocyclic chemical space. Such compounds were readily accessible in a single operation via the construc-tion of their pyrrole fragments by means of mechanochemical multicomponent reactions that were performed starting from very simple starting materials and catalysts. Related com-pounds having a double bond in their spacer chain were ob-tained by a different approach involving the homodimerization of 1-allyl- or 1-homoallylpyrroles by cross-metathesis.

Supporting Information

Supporting Information File 1

Experimental details and NMR spectra.
[http://www.beilstein-journals.org/bjoc/content/
supplementary/1860-5397-13-190-S1.pdf]

Acknowledgements

References

1. Lv, Z.; Chu, Y.; Wang, Y. *HIV/AIDS* **2015,** *7,* 95–104.
doi:10.2147/HIV.S79956
2. Staderini, M.; Legname, G.; Bolognesi, M. L.; Menéndez, J. C.
Curr. Top. Med. Chem. **2013,** *13,* 2491–2503.
doi:10.2174/15680266113136660176
3. De Petrocellis, L.; Arroyo, F. J.; Orlando, P.; Schiano Moriello, A.;
Vitale, R. M.; Amodeo, P.; Sánchez, A.; Roncero, C.; Bianchini, G.;
Martín, M. A.; López-Alvarado, P.; Menéndez, J. C. *J. Med. Chem.*
2016, *59,* 5661–5683. doi:10.1021/acs.jmedchem.5b01448
4. Stolle, A.; Szuppa, T.; Leonhardt, S. E. S.; Ondruschka, B.
Chem. Soc. Rev. **2011,** *40,* 2317–2329. doi:10.1039/c0cs00195c
5. James, S. L.; Adams, C. J.; Bolm, C.; Braga, D.; Collier, P.; Friščić, T.;
Grepioni, F.; Harris, K. D. M.; Hyett, G.; Jones, W.; Krebs, A.; Mack, J.;
Maini, L.; Orpen, A. G.; Parkin, I. P.; Shearouse, W. C.; Steed, J. W.;
Waddell, D. C. *Chem. Soc. Rev.* **2012,** *41,* 413–447.
doi:10.1039/C1CS15171A
6. Bowmaker, G. A. *Chem. Commun.* **2013,** *49,* 334–348.
doi:10.1039/C2CC35694E
7. Wang, G.-W. *Chem. Soc. Rev.* **2013,** *42,* 7688–7700.
doi:10.1039/C3CS35526H
8. Claramunt, R. M.; López, C.; Sanz, D.; Elguero, J.
Adv. Heterocycl. Chem. **2014,** *112,* 117–143.
doi:10.1016/B978-0-12-800171-4.00003-2
9. Hernández, J. G.; Avila-Ortiz, C. G.; Juaristi, E. Useful Chemical
Activation Alternatives in Solvent-Free Organic Reactions. In
Comprehensive Organic Synthesis, 2nd ed.; Molander, G. A.;
Knochel, P., Eds.; Elsevier: Oxford, 2014; Vol. 9, pp 287–314.
doi:10.1016/B978-0-08-097742-3.00935-6
10. Hernández, J. G.; Friščić, T. *Tetrahedron Lett.* **2015,** *56,* 4253–4265.
doi:10.1016/j.tetlet.2015.03.135
11. Do, J.-L.; Friščić, T. *ACS Cent. Sci.* **2017,** *3,* 13–19.
doi:10.1021/acscentsci.6b00277
12. Hernández, J. G.; Bolm, C. *J. Org. Chem.* **2017,** *82,* 4007–4019.
doi:10.1021/acs.joc.6b02887
13. Davor, M.; Štrukil, V., Eds. *Mechanochemical Organic Synthesis;*
Elsevier, 2016.
14. Estévez, V.; Villacampa, M.; Menéndez, J. C. *Chem. Commun.* **2013,**
49, 591–593. doi:10.1039/C2CC38099D
15. Estévez, V.; Sridharan, V.; Sabaté, S.; Villacampa, M.;
Menéndez, J. C. *Asian J. Org. Chem.* **2016,** *5,* 652–662.
doi:10.1002/ajoc.201600061
16. Zhao, H.; Dietrich, J. *Expert Opin. Drug Discovery* **2015,** *10,* 781–790.
doi:10.1517/17460441.2015.1041496
17. Sridharan, V.; Menéndez, J. C. *Chem. Rev.* **2010,** *110,* 3805–3849.
doi:10.1021/cr100004p
18. Mills, J. S.; Showell, G. A. *Expert Opin. Invest. Drugs* **2004,** *13,*
1149–1157. doi:10.1517/13543784.13.9.1149
19. Gately, S.; West, R. *Drug Dev. Res.* **2007,** *68,* 156–163.
doi:10.1002/ddr.20177
20. Franz, A. K.; Wilson, S. O. *J. Med. Chem.* **2013,** *56,* 388–405.
doi:10.1021/jm3010114

Solid-state mechanochemical ω-functionalization of poly(ethylene glycol)

Michael Y. Malca, Pierre-Olivier Ferko, Tomislav Friščić and Audrey Moores[*]

Abstract

Poly(ethylene glycol) (PEG) is a linear polymer with a wide range of applications in chemical manufacturing, drug development and nanotechnology. PEG derivatives are being increasingly used to covalently modify small molecule and peptide drugs, as well as bioactive nanomaterials in order to improve solubility in biological serum, reduce immunogenicity, and enhance pharmacokinetic profiles. Herein we present the development of mechanochemical procedures for PEG functionalization without the need for bulk solvents, offering a cleaner and more sustainable alternative to existing solution-based PEG procedures. The herein presented mechanochemical procedures enable rapid and solvent-free derivatization of PEG with tosyl, bromide, thiol, carboxylic acid or amine functionalities in good to quantitative yields and with no polymer chain oligomerization, proving the versatility of the method.

Introduction

Poly(ethylene glycol) (PEG) is a linear polyether polymer with highly hydrophilic properties. Whereas PEG functionalization is restricted to its terminal functionalities, derivatization of these sites is essential for its use in pharmaceutical and material design. Specifically, modification of bioactive substrates with PEG is well established in drug development, and is also becoming important in the purification of proteins and nucleic acids [1]. Since the first demonstration of PEGylated proteins with altered immunogenicity [2,3], PEG has been heavily inves-

tigated for affording biologically active molecules with superior pharmacokinetic profiles and increased solubility in aqueous media [4-6]. A wide variety of modern PEGylated drugs take advantages of these properties: Mucagen (2004), Cimzia (2008) and Puricase (2010) are but a few examples [7]. On the other end, PEG is also being used to stabilize nanomaterials, allow their stable suspension in aqueous media, and interface them with biological systems [8-10]. Besides for its effects on solubility, PEG also creates a hydrodynamic barrier around the

functionalized nanomaterial, allowing for reduced immunogenicity [11], leading to significant improvements in blood circulation half-lives, decrease in clearance rates, and prolonged pharmacological effects [12-14]. Derivatives of PEG are often used to perform conjugation reactions on small molecule drugs, proteins, or bioactive nanomaterials [15]. Other methods include chelation or ligand-exchange reactions at metal-based nanomaterials with ω-functionalized PEG polymers [16-18].

The two most common methods for accessing ω-functionalized PEG derivatives are solution-based through either ring-opening polymerization of ethylene oxide unites or modification of commercially available, parent hydroxy-terminated PEG [19]. The latter route is milder, more accessible and offers finer control over the polymer molecular weight. However, in both cases, the methods for PEG ω-functionalization raise concerns in terms of environmental impact, given that these reactions typically require dilute conditions under inert atmosphere, warranting large amounts of solvents and time [1,19,20]. High dilution during derivatization is a requirement of solvent-based syntheses to avoid unwanted chain lengthening caused by intermolecular reactions [21]. Having in mind the vocal demands of pharmaceutical industry for the development of cleaner, more efficient synthetic techniques [22], we now explore the possibility of accessing PEG derivatives in the solid-state. The use of mechanochemistry to achieve both supramolecular [23] and covalent [24] synthesis and modification of active pharmaceutical ingredients (APIs) is an emergent area that was recently reviewed [25]. In particular, solvent-free polymerization methods have been recently developed to access polyimines [26], polylactides [27], poly(phenylene vinylene) [28] and polyolefins [29]. There has been, however, limited effort towards the functionalization of premade polymers. Recently, Yan and co-workers used ball milling to deacetylate chitin to afford chitosan [30].

We now provide a proof-of-principle demonstration of mechanochemical ω-functionalization of α-protected methoxy-PEG (mPEG) with –COOH, –OTs, –NH$_2$, –Br, and –SH functionalities, leading to rapid and cost-effective synthesis of these important derivatives in good to quantitative yields under aerobic conditions, using methoxypoly(ethylene glycol) of average molecular weights M_n = 750 Da and M_n = 2000 Da (mPEG$_{750}$ and mPEG$_{2000}$, respectively). We chose these derivatives because of their versatile applicability to covalent conjugation onto various substrates and metal-based nanomaterials.

Results and Discussion

For this study, we focused on the functionalization of mPEG, which allows the simple mono-functionalization of the polymer,

for useful applications to drug development or nanomaterials (Scheme 1). To establish the generality of the method, we used mPEGs of two different, commercially available molecular weights, M_n = 750 and 2000 Da (mPEG$_n$). In all the examples we explored in this study, reaction progress was determined by ^{1}H NMR yields, where yields were determined by integration of peaks attributed to the methylene hydrogens geminal to the ω-functionality of mPEG, namely hydroxy, for the starting material, and the functionality introduced in the reaction explained below, for the products. *p*-Xylene was used as an internal standard for ^{1}H NMR analysis, and the methoxy end of mPEG (singlet at 3.38 ppm) served to confirm conversions. Prudence was given to confirming interchain reactions did not occur by confirming mass balance in all cases.

We first explored the possibility of introducing a *p*-methylsulfonato (tosyl) moiety at the termination of mPEG by ball-milling. Namely, the tosyl moieties are known as excellent leaving groups, making tosylated mPEG (mPEG$_x$–OTs) useful synthons for accessing further PEG derivatives. For this, we conducted a two-step one-pot reaction involving milling first the mPEG reactant with a base, followed by addition of *p*-toluenesulfonyl chloride (TsCl) and further milling (Scheme 1a, Table 1). mPEG$_{750}$ was used to survey and optimize the tosylation reaction conditions. Milling of only mPEG with TsCl led to a poor conversion of 6% (Table 1, entry 1). However, addition of 1 equivalent of weak base, such as K$_2$CO$_3$ or *N*,*N*-diisopropylethylamine (DIPEA) led to ^{1}H NMR yields of 21% and 17%, respectively (Table 1, entries 2 and 3). Switching to NaOH as the base led to a sharp increase of mPEG conversion to 81%. The highest conversions were obtained by using mPEG, NaOH and TsCl in respective stoichiometric ratios of 1:1.2:1.5 (Table 1, entry 4). These conditions functioned similarly with higher molecular weight mPEG$_{2000}$ (Table 1, entry 5). In the ^{1}H NMR spectra of these samples, the triplet of the terminal methylene moieties in the mPEG starting material at 3.72 ppm is replaced by one at 4.15 ppm, consistent with tosylation of the terminal group (Figure 1) [20]. The functionalization of mPEG was also corroborated by the observed shift in the ^{1}H NMR signals of the tosylate group protons from 7.92 (2H) and 7.49 (2H) in TsCl to 7.79 and 7.34 ppm, in mPEG–OTs (Figure S1, Supporting Information File 1) [20].

Employing NaOH as a base yielded the best results with both molecular weight (M_w) mPEGs. NaOH is a strong base, thus favoring deprotonation of mPEG over weaker bases to facilitate subsequent tosylation. The deprotonation step (Scheme 1a) also generates water locally, which may have led to liquid-assisted grinding (LAG) conditions and facilitated the interaction and mobility of substrates [31-33], and allowed the substrates to better interact in situ. Given that DIPEA did not afford
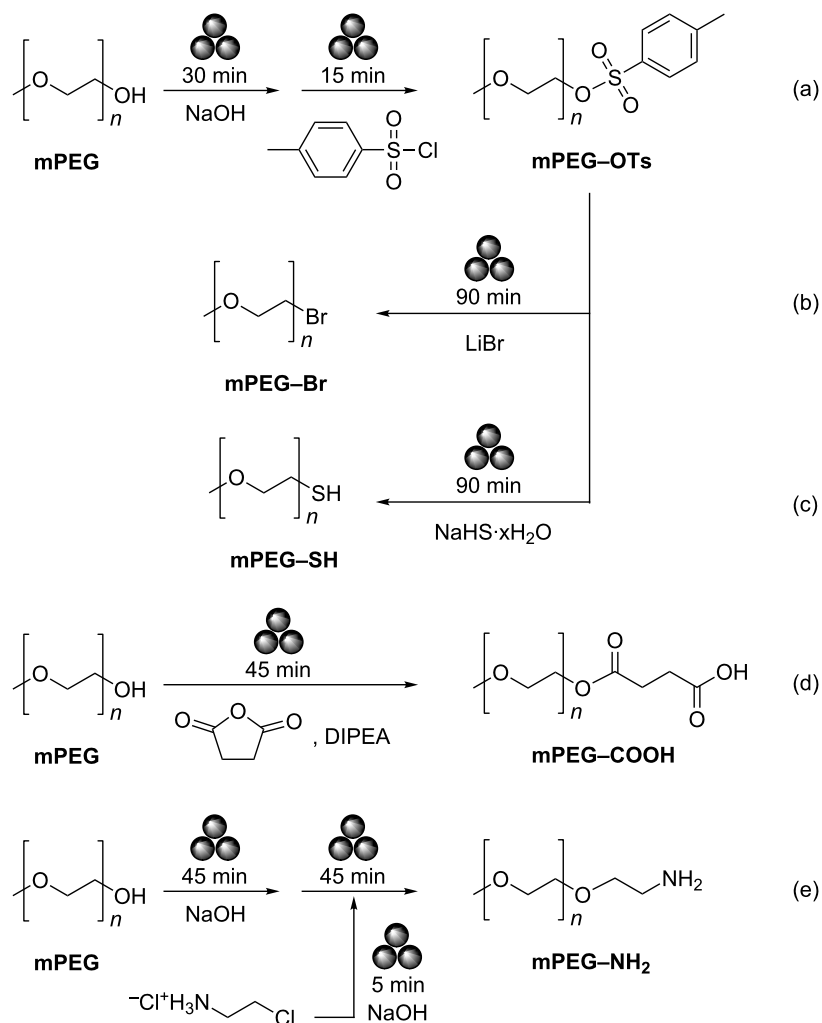
Scheme 1: Developed syntheses for accessing by mechanochemistry: (a) mPEG–OTs, (b) mPEG–Br, (c) mPEG–SH, (d) mPEG–COOH, and (e) mPEG$_x$–NH$_2$. mPEG of M_n = 750 and 2000 Da were investigated as precursors. All milling reactions were performed at an operating frequency of 30 Hz.

Table 1: Surveyed reactions for mechanochemical derivatization of mPEG with tosylate functionality. TsCl = *p*-toluenesulfonyl chloride; CEA = chloroethylamine·HCl; M_w = molecular weight. All reactions were ball-milled at an operating frequency of 30 Hz.

Entry	mPEG M_w	base (equiv)	TsCl (equiv)	Time (min)	^{1}H NMR yield
1	750	–	1.2	45	6%
2	750	K$_2$CO$_3$ (1.0)	1.2	45	21%
3	750	DIPEA (1.0)	1.2	45	17%
4	750	NaOH (1.2)	1.5	15	81%
5	2000	NaOH (1.2)	1.5	15	80%

high yields albeit being liquid and having a pK_a of 3.02, smaller than the one of mPEG (pK_a = 4.5–4.8), it suggests that solvation may play a role in promoting the reaction. Interestingly TsCl is prone to hydrolysis in the presence of water, yet it did not seem to affect the high reactivity observed with NaOH,

likely because the generated, strongly nucleophilic, alkoxide would react even faster.

Progress of reactions in entries 4 and 5 in Table 1 was probed every 15 minutes at the second step (Scheme 1a). After
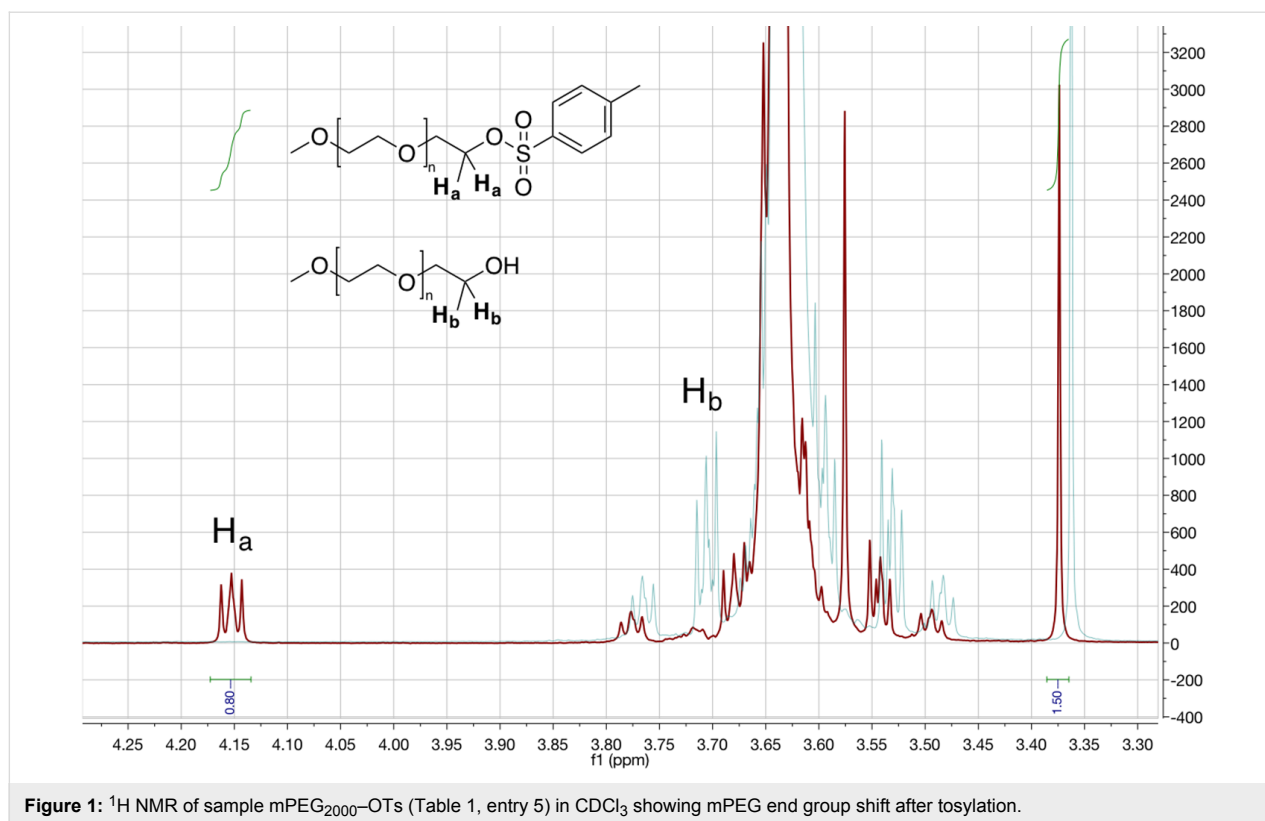
Figure 1: ^{1}H NMR of sample mPEG$_{2000}$–OTs (Table 1, entry 5) in CDCl$_3$ showing mPEG end group shift after tosylation.

15 minutes milling, the reaction was complete, as almost identical ^{1}H NMR yields were obtained for up to 75 min milling for both mPEG$_{750}$ and mPEG$_{2000}$.

The mechanochemically prepared tosylated polymers provided an entry into the synthesis of other mPEG derivatives by mechanochemistry, through ball-milling reaction with additional nucleophiles. The synthesis of terminally brominated mPEG (mPEG–Br) derivatives was achieved by milling of mPEG–OTs with LiBr (Scheme 1b). Analysis of the milled reaction mixture

by ^{1}H NMR revealed the appearance of a new triplet resonance centered at about 3.45 ppm in CDCl$_3$, consistent with the methylene germinal to Br in mPEG–CH_2-Br (Figure S2, Supporting Information File 1) [34,35]. ^{1}H NMR yields of 58% and 65% were obtained for reactants mPEG$_{750}$ and mPEG$_{2000}$, respectively (Table 2, entries 1 and 2). 2D-HSQC was performed to validate terminal bromo functionality showing a cross-peak at ^{1}H, [13]C = 3.45 ppm, 30.10 ppm (Figure S3, Supporting Information File 1). These results are exciting given that PEG bromination is often performed under harsh conditions either via

Table 2: Surveyed reactions of mechanochemical derivatization to afford mPEG–Br, –SH, –COOH and –NH$_2$ derivatives.

Entry	Product	Time of milling (min)	^{1}H NMR yield
1	mPEG$_{750}$-Br	90	58%
2	mPEG$_{2000}$-Br	90	65%
3	mPEG$_{750}$-SH	90	48%[a]
4	mPEG$_{2000}$-SH	90	69%[a]
5	mPEG$_{750}$-COOH	45	99%
6	mPEG$_{2000}$-COOH	45	90%
7	mPEG$_{750}$-NH$_2$	45	42%
8	mPEG$_{2000}$-NH$_2$	45	63%

Reaction conditions for entries 6 and 7: mPEG–OTs, LiBr (3 equiv); for entries 8 and 9: mPEG–OTs, NaHS·xH$_2$O (2 equiv assuming 3 H$_2$O); for entries 10 and 11: mPEG, DIPEA (0.2 equiv), succinic anhydride (1.2 equiv); for entries 12 and 13: mPEG, NaOH (1.2 equiv), CEA·HCl/NaOH (1.2 equiv). All reactions were ball-milled at an operating frequency of 30 Hz. [a]Corresponding disulfides were also observed as minor side product.

radical intermediates or using bromoacyl halides, which introduces unnecessary ester groups instead of direct bromine substitution onto the polymer chain [34,36,37].

Next, we explored the thiolation by milling the mPEG–OTs with NaHS·xH$_2$O for 90 min (Table 2, entries 3 and 4) as reagent, which afforded ^{1}H NMR conversions of 55% and 78% for M_n = 750 and 2000 Da, respectively. In this reaction, thiol was obtained as major product, with a small portion of disulfide as byproduct. Yield of 48% −SH + 7% –S–S– and 69% –SH + 9% –S–S– were measured for M_n = 750 and 2000 Da, respectively. In the ^{1}H NMR spectra, the mPEG–SH was clearly identified by a triplet at 2.86 ppm, characteristic of methylene hydrogens germinal to thiol, while the corresponding peak of mPEG–S–S–mPEG appeared at 2.72 ppm (Figure S4, Supporting Information File 1) [20]. The formation of the disulfide derivatives is explained by the reaction being performed under aerobic conditions [20].

To access mPEG–carboxylate (mPEG–COOH) under milling conditions, native mPEG was reacted directly with succinic anhydride in the presence of catalytic amounts of DIPEA (Scheme 1d; Table 2, entries 5 and 6). Quantitative yields (>99%) of the mPEG$_{750}$–COOH were obtained after only 45 min of milling (Figure S5, Supporting Information File 1) [38]. The end hydroxy group of mPEG at 3.72 disappeared and was replaced by a peak at 4.23 ppm after carboxy functionalization, further proving that the reaction was successful. The starting material succinic anhydride featured a singlet at 3.01 ppm, while the open structure resulting from the reaction with mPEG is characterized by two triplets centered at 2.54 and 2.62 ppm (Figure S6, Supporting Information File 1) [38]. The reaction was readily adaptable to the mPEG$_{2000}$ reactant, in 90% yield according to ^{1}H NMR spectroscopy.

Finally, we explored the possibility of accessing mPEG–NH$_2$ polymers by using chloroethylamine hydrochloride (CEA·HCl) as an aminating agent (Scheme 1e). For this purpose, both mPEG and CEA·HCl were reacted separately mechanochemically with NaOH to afford the deprotonated mPEG and CEA free base, respectively. CEA·HCl was milled with NaOH briefly for only 5 min to avoid polymerization of the free base before reaction with mPEG. The milled products were then mixed and milled for 45 minutes, leading to a yield of 42% and 63% (for M_n = 750 and 2000 Da, respectively), according to ^{1}H NMR spectroscopy (Table 2, entries 7 and 8). Analysis by ^{1}H NMR revealed a new triplet at 2.98 ppm, characteristic of the methylene hydrogens germinal to NH$_2$ (Figure S7, Supporting Information File 1) [20,39]. A 2D-HSQC measurement was performed to validate the addition of this functionality at the terminus of mPEG, showing a cross-peak at (^{1}H, ^{13}C) =

(3.98 ppm, 43.63 ppm) (Figure S8, Supporting Information File 1) [20,39].

Importantly, in all the samples studied for this reaction, complete mass balance was obtained, using an external standard and the ^{1}H NMR signal of the terminal methoxy group of mPEG. This allowed to establish that unfunctionalized polymers were all recovered after reaction as unreacted mPEG and not as mPEG dimers resulting from the intermolecular coupling of two chains. Interestingly, in solvent-based synthesis, dilute conditions are typically required to avoid intermolecular reactions between chains leading to unwanted chain lengthening during the derivatization process. Under mechanochemical conditions, diffusion limitation may favor the reactivity of small molecule reagents over the intermolecular reaction between two polymers to afford the kinetically-favorable end-products, in contrast to solvent-based conditions [21].

Conclusion
We have demonstrated the rapid, efficient and selective synthesis of various PEG derivatives under mechanochemical conditions, without using any bulk solvent. The short times required to achieve reaction completion (45–90 minutes) contrast with the often several hour-long solvent-based reaction conditions [19,40]. Our results also show that solvent-free conditions for the post-functionalization of native PEG is a good avenue to prevent chain lengthening, a known limitation of solvent-based techniques. Finally, our method is advantageous over solvent-based ones, as it eliminates the need for inert atmosphere. Overall, the excellent reactivity and selectivity in the absence of bulk solvent is, to the best of our knowledge, unprecedented.

Supporting Information

Supporting Information File 1
Experimental part and NMR spectra.
[http://www.beilstein-journals.org/bjoc/content/supplementary/1860-5397-13-191-S1.pdf]

References
1. Li, J.; Kao, W. J. *Biomacromolecules* **2003,** *4,* 1055–1067. doi:10.1021/bm034069l
2. Abuchowski, A.; Mccoy, J. R.; Palczuk, N. C.; Es, T. V. A. N.; Davis, F. F. *J. Biol. Chem.* **1976,** *252,* 3582–3586.
3. Abuchowski, A.; Es, T. V.; Palczuk, N. C.; Davis, F. F. *J. Biol. Chem.* **1977,** *252,* 3578–3581.
4. Gref, R.; Minamitake, Y.; Peracchia, M. T.; Trubetskoy, V.; Torchilin, V.; Langer, R. *Science* **1994,** *263,* 1600–1603. doi:10.1126/science.8128245

5. Gref, R.; Domb, A.; Quellec, P.; Blunk, T.; Müller, R. H.; Verbavatz, J. M.; Langer, R. *Adv. Drug Delivery Rev.* **1995,** *16,* 215–233. doi:10.1016/0169-409X(95)00026-4

6. Gref, R.; Lück, M.; Quellec, P.; Marchand, M.; Dellacherie, E.; Harnisch, S.; Blunk, T.; Müller, R. H. *Colloids Surf., B* **2000,** *18,* 301–313. doi:10.1016/S0927-7765(99)00156-3

7. Li, W.; Zhan, P.; De Clercq, E.; Lou, H.; Liu, X. *Prog. Polym. Sci.* **2013,** *38,* 421–444. doi:10.1016/j.progpolymsci.2012.07.006

8. Juliano, R. L. *Adv. Drug Delivery Rev.* **1988,** *2,* 31–54. doi:10.1016/0169-409X(88)90004-X

9. Stolnik, S.; Illum, L.; Davis, S. S. *Adv. Drug Delivery Rev.* **1995,** *16,* 195–214. doi:10.1016/0169-409X(95)00025-3

10. Leroux, J.-C.; Allémann, E.; De Jaeghere, F.; Doelker, E.; Gurny, R. *J. Controlled Release* **1996,** *39,* 339–350. doi:10.1016/0168-3659(95)00164-6

11. Moghimi, M. S.; Hunter, C. A.; Murray, J. C. *Pharmacol. Rev.* **2001,** *53,* 283–318.

12. Hrkach, J. S.; Peracchia, M. T.; Bomb, A.; Lotan, N.; Langer, R. *Biomaterials* **1997,** *18,* 27–30. doi:10.1016/S0142-9612(96)00077-4

13. Klibanov, A. L.; Maruyama, K.; Beckerleg, A. M.; Torchilin, V. P.; Huang, L. *Biochim. Biophys. Acta, Biomembr.* **1991,** *1062,* 142–148. doi:10.1016/0005-2736(91)90385-L

14. Gombotz, W. R.; Guanghui, W.; Horbett, T. A.; Hoffman, A. S. *J. Biomed. Mater. Res.* **1991,** *25,* 1547–1562. doi:10.1002/jbm.820251211

15. Veronese, F. M.; Pasut, G. *Drug Discovery Today* **2005,** *10,* 1451–1458. doi:10.1016/S1359-6446(05)03575-0

16. Na, H. B.; Lee, I. S.; Seo, H.; Park, Y. I.; Lee, J. H.; Kim, S.-W.; Hyeon, T. *Chem. Commun.* **2007,** 5167–5169. doi:10.1039/b712721a

17. Gentili, D.; Ori, G.; Comes Franchini, M. *Chem. Commun.* **2009,** 5874–5876. doi:10.1039/b911582j

18. Smolensky, E. D.; Park, H.-Y. E.; Berquó, T. S.; Pierre, V. C. *Contrast Media Mol. Imaging* **2011,** *6,* 189–199. doi:10.1002/cmmi.417

19. Thompson, M. S.; Vadala, T. P.; Vadala, M. L.; Lin, Y.; Riffle, J. S. *Polymer* **2008,** *49,* 345–373. doi:10.1016/j.polymer.2007.10.029

20. Mahou, R.; Wandrey, C. *Polymer* **2012,** *4,* 561–589. doi:10.3390/polym4010561

21. Loiseau, F. A.; Hii, K. K.; Hill, A. M. *J. Org. Chem.* **2004,** *69,* 639–647. doi:10.1021/jo035042v

22. Dunn, P. J. *Chem. Soc. Rev.* **2012,** *41,* 1452–1461. doi:10.1039/C1CS15041C

23. Delori, A.; Friščić, T.; Jones, W. *CrystEngComm* **2012,** *14,* 2350–2362. doi:10.1039/c2ce06582g

24. Bonnamour, J.; Métro, T.-X.; Martinez, J.; Lamaty, F. *Green Chem.* **2013,** *15,* 1116–1120. doi:10.1039/c3gc40302e

25. Tan, D.; Loots, L.; Friščić, T. *Chem. Commun.* **2016,** *52,* 7760–7781. doi:10.1039/C6CC02015A

26. Klok, H.-A.; Genzer, J. *ACS Macro Lett.* **2015,** *4,* 636–639. doi:10.1021/acsmacrolett.5b00295

27. Ohn, N.; Shin, J.; Kim, S. S.; Kim, J. G. *ChemSusChem* **2017,** *10.* doi:10.1002/cssc.201700873

28. Ravnsbæk, J. B.; Swager, T. M. *ACS Macro Lett.* **2014,** *3,* 305–309. doi:10.1021/mz500098r

29. Jakobs, R. T. M.; Ma, S.; Sijbesma, R. P. *ACS Macro Lett.* **2013,** *2,* 613–616. doi:10.1021/mz400201c

30. Chen, X.; Yang, H.; Zhong, Z.; Yan, N. *Green Chem.* **2017,** *19,* 2783–2792. doi:10.1039/C7GC00089H

31. Friščić, T.; Jones, W. *Cryst. Growth Des.* **2009,** *9,* 1621–1637. doi:10.1021/cg800764n

32. Michalchuk, A. A. L.; Tumanov, I. A.; Konar, S.; Kimber, S. A. J.; Pulham, C. R.; Boldyreva, E. V. *Adv. Sci.* **2017.** doi:10.1002/advs.201700132

33. Karki, S.; Friščić, T.; Jones, W.; Motherwell, W. D. S. *Mol. Pharmaceutics* **2007,** *4,* 347–354. doi:10.1021/mp0700054

34. Zhou, H.; Chen, Y.; Plummer, C. M.; Huang, H.; Chen, Y. *Polym. Chem.* **2017,** *8,* 2189–2196. doi:10.1039/C7PY00283A

35. Wang, J.; Sun, P.; Zheng, Z.; Wang, F.; Wang, X. *Polym. Degrad. Stab.* **2012,** *97,* 2294–2300. doi:10.1016/j.polymdegradstab.2012.07.041

36. Xie, C.; Yang, C.; Zhang, P.; Zhang, J.; Wu, W.; Jiang, X. *Polym. Chem.* **2015,** *6,* 1703–1713. doi:10.1039/C4PY01722F

37. Liu, L.; Zhang, M.; Zhao, H. *Macromol. Rapid Commun.* **2007,** *28,* 1051–1056. doi:10.1002/marc.200700007

38. Ishii, T.; Yamada, M.; Hirase, T.; Nagasaki, Y. *Polym. J.* **2005,** *37,* 221–228. doi:10.1295/polymj.37.221

39. Goswami, L. N.; Houston, Z. H.; Sarma, S. J.; Jalisatgi, S. S.; Hawthorne, M. F. *Org. Biomol. Chem.* **2013,** *11,* 1116–1126. doi:10.1039/c2ob26968f

40. Harris, J. M.; Struck, E. C.; Case, M. G.; Paley, M. S.; Yalpani, M.; Van Alstine, J. M.; Brooks, D. E. *J. Polym. Sci., Polym. Chem. Ed.* **1984,** *22,* 341–352. doi:10.1002/pol.1984.170220207

License and Terms

New bio-nanocomposites based on iron oxides and polysaccharides applied to oxidation and alkylation reactions

Daily Rodríguez-Padrón, Alina M. Balu, Antonio A. Romero and Rafael Luque[*]

Abstract

Polysaccharides from natural sources and iron precursors were applied to develop new bio-nanocomposites by mechanochemical milling processes. The proposed methodology was demonstrated to be advantageous in comparison with other protocols for the synthesis of iron oxide based nanostructures. Additionally, mechanochemistry has enormous potential from an environmental point-of-view since it is able to reduce solvent issues in chemical syntheses. The catalytic activity of the obtained nanocatalysts was investigated in both the oxidation of benzyl alcohol to benzaldehyde and in the alkylation of toluene with benzyl chloride. The microwave-assisted oxidation of benzyl alcohol reached 45% conversion after 10 min. The conversion of the alkylation of toluene in both microwave-assisted and conventional heating methods was higher than 99% after 3 min and 30 min, respectively. The transformation of benzyl alcohol and toluene into valuable product in both the oxidation and alkylation reaction reveals a potential method for the valorization of lignocellulosic biomass.

Introduction

Heterogeneous catalysis has played a crucial role in the development of the chemical industry. It has allowed the design of more efficient processes, both in an economical and environmental way, thanks to the higher activity and selectivity of heterogeneous catalysts [1-3]. These systems, in particular, are preferred over the use of catalysts in a homogeneous phase due to the difficulty in separation and recovery of the latter. Heterogeneous catalytic systems, as a priority of research activity in the field of green chemistry, open up new possibilities for further development of environmentally friendly, catalyzed processes [4]. In this sense, metal oxide nanoparticles have been extensively studied in recent decades because of their high ac-

tivity, specificity of interaction and advantageous properties including a high surface/volume ratio combined with their small size [5-7]. Moreover, metal oxide nanoparticles have the additional advantage of easy recycling and reuse, which is an essential and desired property in many applications such as catalysis, sensors and even medicine [2,6,8,9]. Our research group has recently prepared different types of metal and metal oxide nanoparticles which have several applications in heterogeneous catalysis [10-14]. Transition metal and metal oxide nanoparticles have been reported to be highly active and selective in several processes, such as redox [15-17], C–C and C–heteroatom couplings [18,19]. In particular, iron oxide nanoparticles have been the object of most research from our group over the past years [10,20-22].

One of the main challenges in the field of catalysis is the preparation of new materials to replace the traditional catalysts quickly, cheaply and efficiently [5]. In this regard, mechanochemical synthesis has become one of the most advantageous and environmentally friendly alternatives compared to the traditional routes [5,23]. This novel approach offers the possibility of a solvent-free process, avoiding environmental problems related to toxicity and the use thereof [24,25]. Moreover, the mechanochemical protocols have potential applicability due to the extreme simplicity, cleanliness, reproducibility and versatility, haven been already demonstrated to be highly useful for the development of a range of advanced nanomaterials including metal-organic frameworks (MOFs), supported metal and metal oxide nanoparticles and nanocomposites with diverse applications in catalysis, sensing, drug delivery and adsorption [25-28]. In addition, mechanochemical protocols have also been employed to functionalize the surfaces of magnetic nanoparticles (MNPs) with monosaccharides [29] and to obtain bio-nanocomposites based on proteins and dopamine (DA)-coated metal oxide MNPs [30,31].

On the other hand, nature has inspired many scientists to innovate and design new materials. The miniaturization and efficiency achieved by entities in nature for energy production, biometabolite, photo-processing and resource maximization has always been an attractive option to imitate based on a fundamental and rational understanding [28,32]. In that sense, polysaccharides extracted from fungal organisms can be used both as nanoparticle carriers and sacrificial templates due to their highly functionalized structure. Although such carbohydrates have been widely reported for the preparation of nanocomposites with a great range of applications, due to their low cytotoxicity and notable biocompatibility and stability [33-37], their catalytic application is still lacking. In addition, these natural products are easily and inexpensively produced by microbes, plants, and animals, and constitute a green alternative to synthe-

tic polymers in the preparation of nanomaterials, in order to ameliorate environmental issues [34]. Therefore, one of the objectives of this work was to investigate the catalytic behavior of nanocomposites based on iron oxide and the polysaccharide S4, obtained from *Lentinus Tigrinus* (PS4).

The most promising feature of such nanoentities based on iron oxide and polysaccharides is the bifunctional, oxidative [20] and acidic nature [21], which in turn can be fine-tuned to design highly active materials for both oxidation and acid catalyzed processes.

Among all the known oxidative transformations, the oxidation of alcohols to ketones and aldehydes have gained a lot of attention for the research community due to its broad range of industrial applications [38,39]. Nonetheless, the scale up of the oxidation reactions has been very restricted due to the use of heavy metals, the limited selectivity for highly functionalized compounds, and the thermal hazards posed [40]. Consequently, catalytic reactions should be further investigated in order to find new alternatives to conventional oxidation methods that require stoichiometric amounts of inorganic oxidants, which are highly toxic and polluting. Aiming to minimize chemical waste in these catalytic processes, the scientific community is moving towards the use of clean oxidants ("green oxidants"), such as molecular oxygen or H_2O_2 [39]. Thus, the use of clean oxidants with heterogeneous catalysts such as Fe_2O_3 nanoparticles, Ag nanoparticles supported on hydrotalcites, Au nanoparticles supported on metal oxides, and Pd nanoparticles supported on SBA-15 has been developed [41-44]. In this regard, both unsupported "free" iron oxide nanoparticles [45] and supported iron oxide based catalytic systems [46] have been extensity reported to be active, stable and selective catalysts for the oxidation of alcohols with hydrogen peroxide. Specifically, the oxidation of benzyl alcohol to benzaldehyde has generated great interest in order to study the oxidation of substituted benzyl alcohols. Although benzyl alcohol is industrially produced by reduction of benzaldehyde, this aldehyde is considered as the second most important flavoring molecule after vanillin, due to its variety of applications in cosmetics, perfumes, food, dyes, agrochemicals and pharmaceuticals [41]. Regarding the acid-catalyzed processes, aromatic alkylation reactions are among the most versatile and widely investigated reactions which can grant access to a wide range of compounds as important intermediates, fragrances, agrochemicals and pharmaceuticals [47-49]. In this sense, the benzylation of benzene or other aromatic substrates is well-known to be an important step in the preparation of relevant building blocks in organic synthesis, such as diphenylmethane and substituted diphenylmethanes [50]. Therefore, many studies have been focus on the preparation of novel Lewis

acid catalysts, such as mesostructured zeolitic materials. In particular, in this study, our research group has focused attention on the alkylation of toluene with benzyl chloride, since is promoted by the presence of Lewis acids such as iron oxides [49].

These two reactions in particular (oxidation and alkylation of benzyl alcohol and toluene, respectively) could find current application in the valorization of lignocellulosic biomass with heterogeneous catalysis.

However, the use of heterogeneous catalysts in the aforementioned reactions usually requires a filtration or centrifugation step to recover the catalyst. In order to simplify the recovery and reuse of the catalytic system, a magnetically separable nanocomposite could represent a breakthrough in the scientific community [51]. Therefore, our research group has focused on the investigation of the aforementioned oxidation and alkylation reactions, using heterogeneous catalysts with magnetic properties.

Results and Discussion

In the present study, we prepared and analyzed three different catalysts based on iron oxides and polysaccharides, in particular: iron oxide–polysaccharide 4 magnetic nanoparticles (Fe_2O_3-PS4-MNP), iron oxide–polysaccharide 4 (Fe_2O_3-PS4) and titanium oxide–iron oxide–polysaccharide 4 (TiO_2-Fe_2O_3-PS4) nanocomposites. The materials were successfully obtained using the proposed solvent-free methodology, which is depicted in Figure 1. The materials were characterized by the techniques presented below. The catalytic activity of these systems has been assessed in the alkylation reaction of toluene with benzyl chloride and the selective oxidation of benzyl alcohol to benzaldehyde.

X-ray diffraction

The structure and arrangement of the synthesized materials were analyzed by X-ray diffraction. The XRD pattern of the Fe_2O_3-PS4 nanomaterial exhibited a series of distinctive diffraction lines that could be correlated to the hematite diffraction pattern. A characteristic broad band in the 20° to 40° range,

a) $FeCl_2 \cdot 4H_2O$

b) $Fe(NO_3)_3 \cdot 4H_2O$, propionic acid

c) $FeCl_2 \cdot 4H_2O$, titanium isopropoxide

metal oxide-polysaccharide nanocomposites

a) Fe_2O_3-PS4   b) Fe_2O_3-PS4-MNP   c) TiO_2-Fe_2O_3-PS4
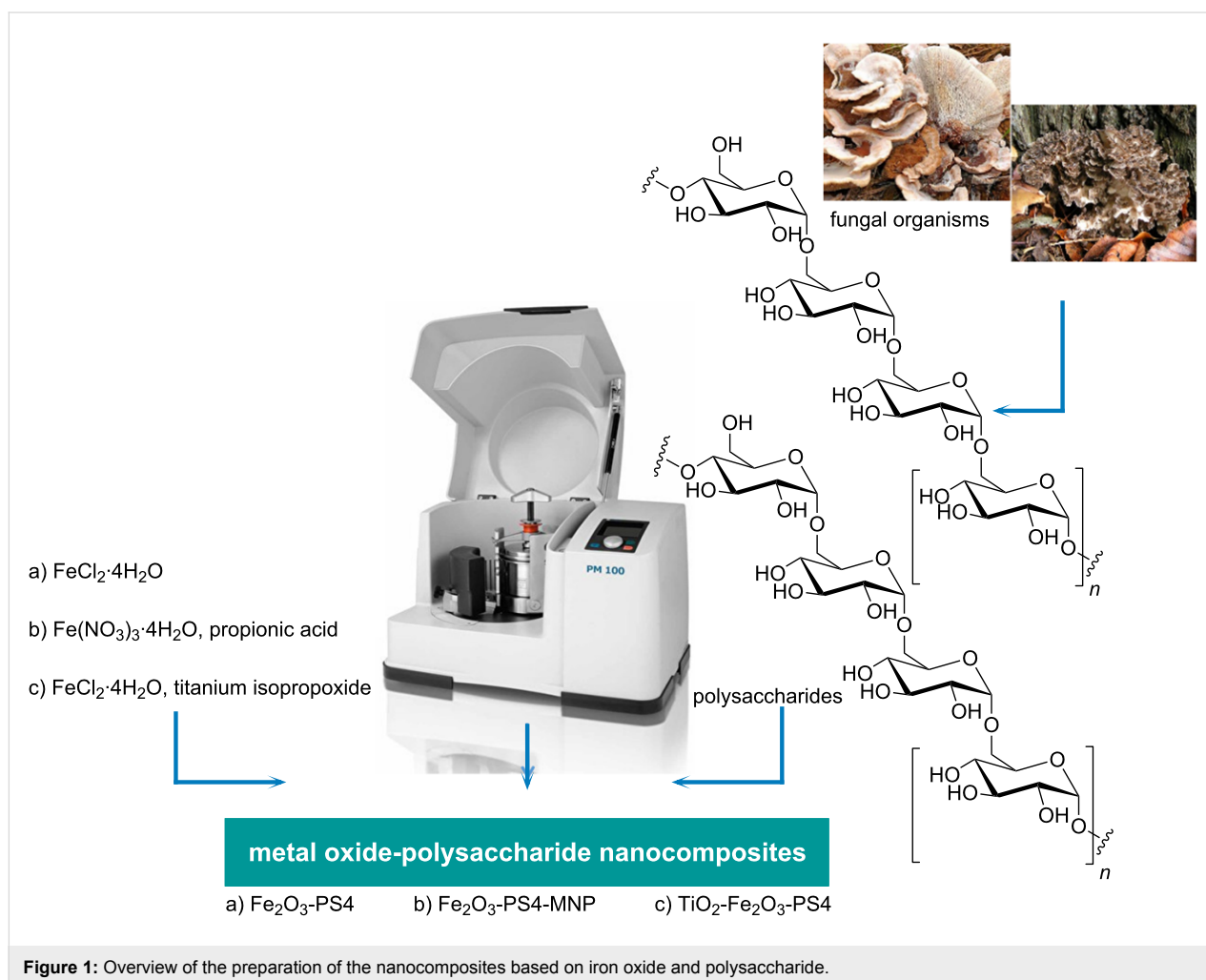
Figure 1: Overview of the preparation of the nanocomposites based on iron oxide and polysaccharide.

typical of amorphous materials, was observed in the Fe_2O_3-PS4 nanomaterial (Supporting Information File 1, Figure S1A). The X-ray diffraction patterns of the magnetic material showed a mixture of maghemite and hematite phases. In this case, a similar XRD pattern could be in principle associated to magnetite (Fe_3O_4) over the maghemite phase, since these two phases are difficult to clearly distinguish by XRD analysis. However, the absence of Fe^{2+} species (see the following XPS analysis) and the reddish color are consistent with a maghemite magnetic phase (Supporting Information File 1, Figure S1B) [51,52]. On the other hand, the crystal structure of the material TiO_2-Fe_2O_3-PS4 turned out to be a mixture of ilmenite and pseudobrookite phases (Supporting Information File 1, Figure S1C).

X-ray photoelectron spectroscopy

X-ray photoelectron spectroscopy (XPS) measurements were consistent with XRD data, where the main peaks were found to correspond to Fe_2O_3 species. In the three nanocomposites, the presence of Fe^{3+} species could be also inferred from the Fe $2p_{3/2}$ and Fe $2p_{1/2}$ peaks around 710 eV and 725 eV, respectively (Figure 2). These results are in good agreement with previous studies and did not show the characteristic peak associated with the presence of Fe(II) or Fe(0) species in the materials [51,52]. Concerning the TiO_2-Fe_2O_3-PS4 nanocatalyst, the XPS experiments results revealed a band at 462 eV (Ti $2p_{3/2}$), which confirmed the presence of TiO_2 on the surface of the nanocomposite (Figure 2C). Additionally, the deconvoluted

C 1s XPS spectra of the obtained materials exhibited two different contributions associated to the presence of C–C/C=C and C–O bonds. Also, the O 1s XPS spectra for the Fe_2O_3-PS4 and Fe_2O_3-PS4-MNP nanomaterials displayed two different peaks attributed to O–C and O–Fe, while for the TiO_2-Fe_2O_3-PS4 nanocomposite contained three contributions related to O–C, O–Ti and O–Fe (see also Supporting Information File 1, Figures S2–S4 for the XPS spectra).

Nitrogen physisorption

The textural properties of the materials have been studied with N_2 absorption–desorption isotherms analysis. The TiO_2-Fe_2O_3-PS4 nanomaterial presents a mesoporous structure with a pore size of 20 nm and a surface area of 58 m^2/g. However, in the other two catalysts, a particular macroporosity was found at $p/p_0 > 0.98$ (isotherms of type III), which are clearly dissimilar to those of conventionally ordered mesoporous materials [53] having a sharp increase in p/p_0 from 0.85 to 0.90 (see Supporting Information File 1, Figure S5 for all adsorption–desorption isotherms). Thus, the Fe_2O_3-PS4 and the Fe_2O_3-PS4-MNP material are macroporous solids with interparticle pores. The surface area was found to be 33 and 6 m^2/g for Fe_2O_3-PS4-MNP and for Fe_2O_3-PS4 nanomaterials, respectively. The pore volumes were found to be in the range of 0.30–0.40 mL/g for the three materials (Table 1). The materials exhibited, in general, satisfying surface areas and pore volumes, particularly taking into account their preparation methodology.
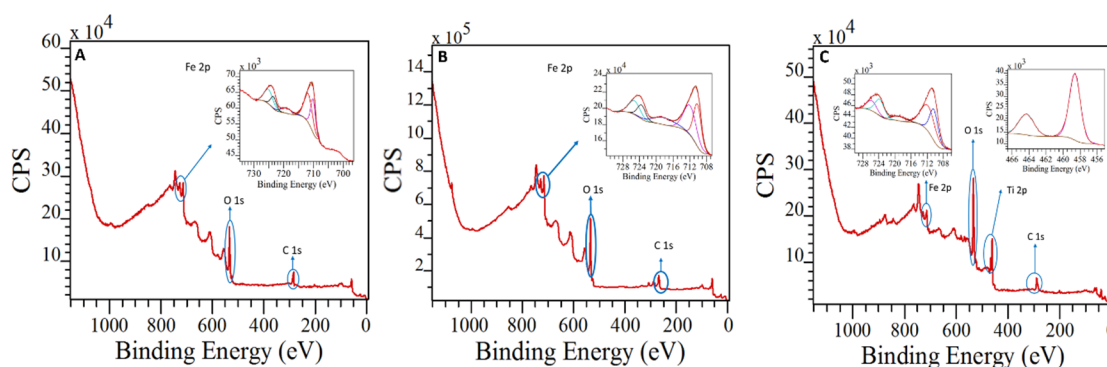
Figure 2: XPS spectra of A: Fe_2O_3-PS4, B: Fe_2O_3-PS4-MNP and C: TiO_2-Fe_2O_3-PS4 nanohybrids.

Table 1: Textural properties of iron oxide/polysaccharide nanohybrids.

Catalyst	TiO_2-Fe_2O_3-PS4	Fe_2O_3-PS4-MNP	Fe_2O_3-PS4
S_{BET} (m^2/g)	58	33	6
D_{BJH} (nm)	20.9	41.2	171.2
V_{BJH} (mL/g)	0.32	0.36	0.40

Electron microscopy

The morphology of the nanomaterials was determined by scanning electron microscopy (SEM) and transmission electron microscopy (TEM). The micrographs show a homogeneous distribution of iron oxide nanoparticles for the three catalysts (Figure 3A,C,E). The analysis of the SEM images reveals the tendency of the constituent particles of the magnetic material to form agglomerates due to their nanometer size (Figure 3E). When these agglomerates are observed at higher magnification, they can be seen as independent particles. The three materials displayed a similar particle-size distribution average of around 9 nm, 12 nm and 10 nm for the TiO_2-

Fe_2O_3-PS4, Fe_2O_3-PS4 and Fe_2O_3-PS4-MNP, respectively (Figure 3B,D,F).

Diffuse reflectance infrared Fourier transform spectroscopy

The acidic properties of the Fe_2O_3-PS4-MNP and TiO_2-Fe_2O_3-PS4 materials were studied by diffuse reflectance infrared Fourier transform spectroscopy (DRIFT) experiments. The TiO_2-Fe_2O_3-PS4 nanocomposite has well-marked acidic characteristics. This can be deduced from the intense and well-defined bands observed at 1449 and 1600 cm^{-1}, which can be attributed to Lewis acid centers (Figure 4A). Additionally, in
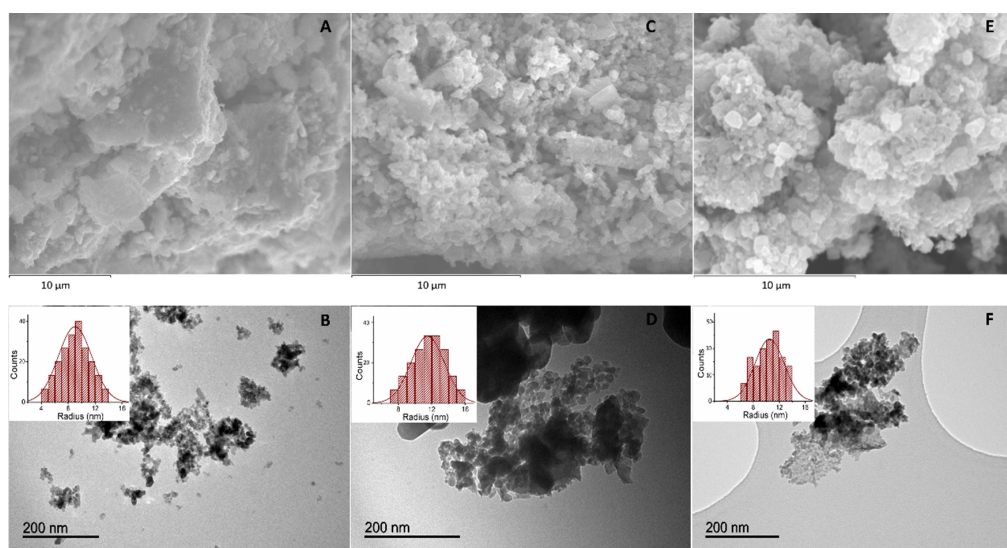
Figure 3: A and B: SEM and TEM images of TiO_2-Fe_2O_3-PS4; C and D: SEM and TEM images of Fe_2O_3-PS4. E and F: SEM and TEM images of Fe_2O_3-PS4-MNP. Inset: Particle-size distribution of the obtained nanohybrids.
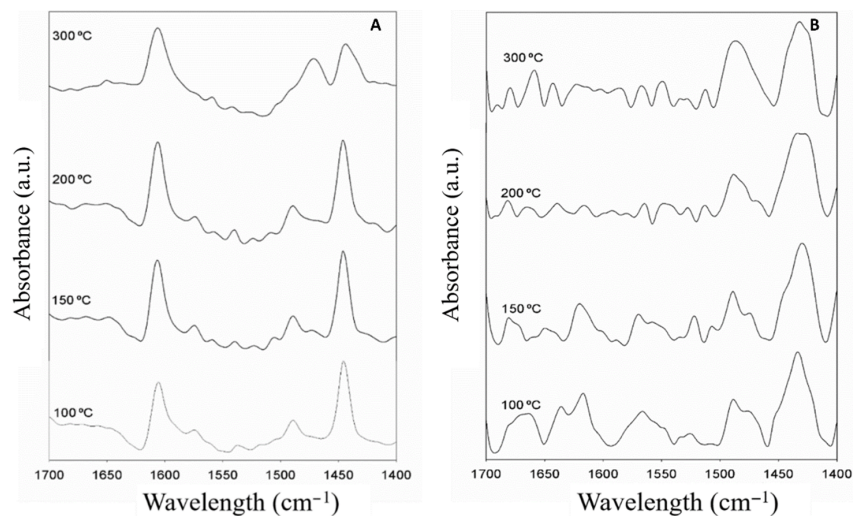
Figure 4: DRIFT spectra of A: TiO_2-Fe_2O_3-PS4 and B: Fe_2O_3-PS4-MNP nanohybrids.

the spectrum of Fe$_2$O$_3$-PS4-MNP, having bands at 1440 and 1618 cm^{-1}, indicates the peculiar Lewis acidity of this material (Figure 4B). Furthermore, in both materials, a band of lesser intensity can be seen around 1490 cm^{-1}, which is due to the presence of both Brønsted and Lewis centers.

These materials maintained a remarkable acidity, even at high temperatures (200 and 300 °C) with visible acid centers distinguishable from noise. This behavior has a high value for acid-catalyzed processes such as alkylation. Furthermore, the Fe$_2$O$_3$-PS4 sample does not show appreciable acidity [43].

Pyridine (PY) and 2,6-dimethylpyridine (DMPY) titration

The acidic properties of these materials have also been determined by the chromatographic method of pulses. Pyridine, due to low steric hindrance, adsorbs nonspecifically in both types of centers, while dimethylpyridine adsorbs specifically on Brønsted acid centers, due to the high steric hindrance of the methyl groups [54]. It is noticeable that the TiO$_2$-Fe$_2$O$_3$-PS4 catalyst possesses both Lewis and Brønsted acid sites with a more marked Lewis acidity. The Fe$_2$O$_3$-PS4-MNP material presents instead only Lewis acid sites, while the Fe$_2$O$_3$-PS4 does not show appreciable acidity to be quantized (Table 2).

Acidity measurements from both methodologies (PY DRIFT, PY and DMPY pulse chromatography titration data) were generally in good agreement, supporting the validity of our assumption on DMPY adsorbing selectively on Brønsted acid sites.

Inductively coupled plasma–mass spectrometry (ICP–MS)

The elemental composition of the TiO$_2$-Fe$_2$O$_3$-PS4 material was determined by ICP–MS. The content of iron and titanium was 38 and 12 wt %, respectively (Table 3). These values corroborate the incorporation of titanium in the material and confirm the results obtained by XPS.

Magnetic susceptibility

The magnetic susceptibility of Fe$_2$O$_3$-PS4-MNP is consistent with the XRD data and confirms the magnetic characteristics of the material. Such values make this a material with attractive feature for magnetic separation (Table 4) [40].

Table 3: Elemental composition of the TiO$_2$-Fe$_2$O$_3$-PS4 nanohybrid material.

Element	ICP–MS (wt %)
Ti	12.8
Fe	38.3

Table 4: Magnetic susceptibility of the Fe$_2$O$_3$-PS4-MNP nanohybrid material.

Catalyst	Milling time (min)	Magnetic susceptibility (10^{-6} m^3 kg^{-1})
Fe$_2$O$_3$-PS4-MNP	15	420
	30	337

Catalytic activity

The catalytic activity of these materials has been investigated in two reactions: 1) the oxidation of benzyl alcohol to benzaldehyde and the 2) alkylation of toluene with benzyl chloride.

The oxidation reaction of benzyl alcohol was carried out using the three nanomaterials as heterogeneous catalysts (Scheme 1). The results of conversion and selectivity are reported in Table 5 and Figure 5. After 10 min, the conversions were 32 and 45% for TiO$_2$-Fe$_2$O$_3$-PS4 and Fe$_2$O$_3$-PS4 nanomaterials, respectively, while for the Fe$_2$O$_3$-PS4-MNP catalyst the conversion reaches just 10%. Remarkably, the selectivity to benzaldehyde, employing Fe$_2$O$_3$-PS4 nanocatalysts, was higher than 90% for a reaction time of 5 and 10 min. Since the best results were obtained with the Fe$_2$O$_3$-PS4 nanocomposite, the latter was employed to carry out the reaction for 30 min in order to improve the obtained results. However, the conversion increased only to

Scheme 1: Oxidation of benzyl alcohol to benzaldehyde.
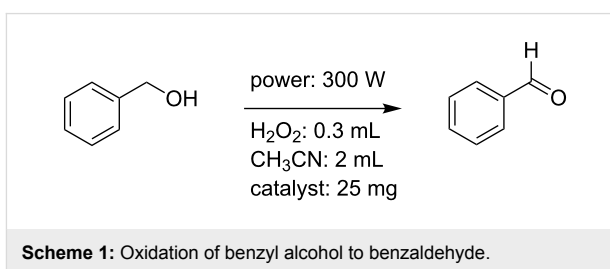
Table 2: Surface acidity of iron oxide/polysaccharide nanohybrids.

Catalyst	Total acidity PY (μM/g)	Brønsted acidity DMPY (μM/g)	Lewis acidity (μM/g)
TiO$_2$-Fe$_2$O$_3$-PS4	81	25	56
Fe$_2$O$_3$-PS4-MNP	14	–	14

Table 5: Conversion and selectivity of the oxidation reaction of benzyl alcohol.

Catalyst	TiO_2-Fe_2O_3-PS4		Fe_2O_3-PS4		Fe_2O_3-PS4-MNP	
Time (min)	C^a (%)	S^b (%)	C^a (%)	S^b (%)	C^a (%)	S^b (%)
5	30	76.6	18	94.4	10	24.4
10	32	78.1	45	97.7	10	24.7

[a]Conversion (%); [b]selectivity (%) to benzaldehyde.
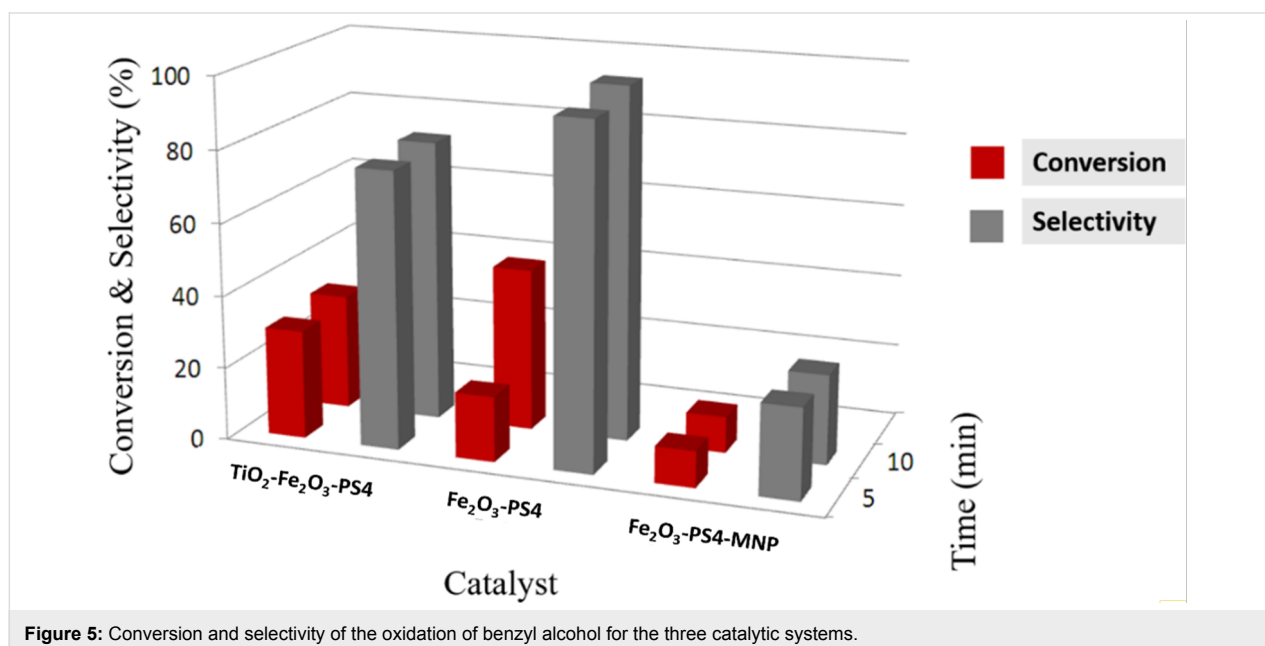
Figure 5: Conversion and selectivity of the oxidation of benzyl alcohol for the three catalytic systems.

47%, which does not compensate the energy consumption by extending the reaction time from 10 to 30 min.

The three synthesized catalysts showed high activity in the alkylation of toluene with benzyl chloride, either via microwave-assisted or with conventional heating (60 °C). For the microwave-assisted reaction (Scheme 2), after three minutes, the conversion was higher than 99% for all of the three materials (Figure 6). For the Fe_2O_3-PS4-MNP nanocatalyst, even after just 1 min, the reaction showed a conversion higher than 99%. In this reaction, the three corresponding isomers (*ortho*, *meta* and *para* substituted) were obtained. In particular, the synthesis of the *para*-isomer can be achieved with high selectivity, employing the TiO_2-Fe_2O_3-PS4 and Fe_2O_3-PS4 nanomaterials for 1 and 2 min, respectively (Table 6).

The alkylation reaction with conventional heating (Scheme 3) was followed by gas chromatography. After 30 min, the conversion was greater than 99% for all of the three materials and the selectivity values were slightly higher compared with the microwave-assisted reaction during 3 min (Table 7, Figure 7).

Scheme 2: Microwave-assisted alkylation of toluene with benzyl chloride.
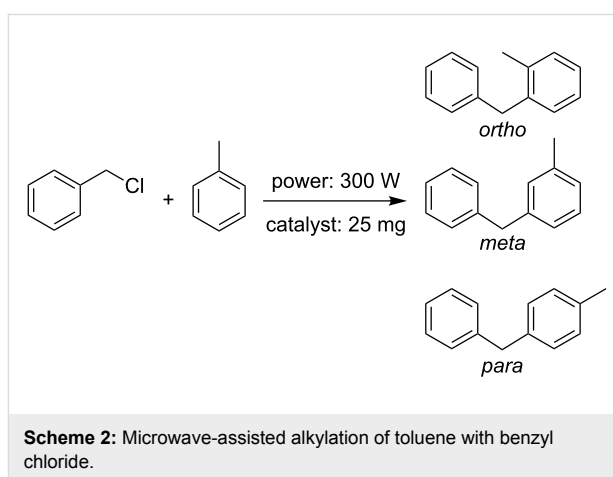
Reusability studies prove the high inherent stability and activity of Fe_2O_3-PS4-MNP and TiO_2-Fe_2O_3-PS4 nanomaterials (Figure 8). However, the Fe_2O_3-PS4 nanocatalyst loses its activity after the first use, which can be due to the loss of residual acidity, which might happen to the material after the synthesis process.
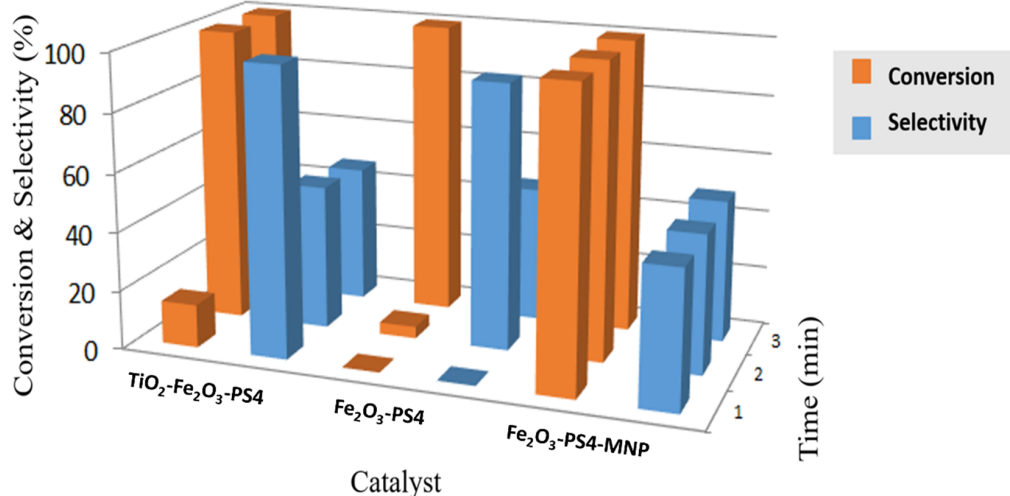
Figure 6: Conversion and selectivity of the microwave-assisted alkylation of toluene for the three catalytic systems.

Table 6: Conversion and selectivity of the microwave-assisted alkylation of toluene for the three catalytic systems.

Catalyst	TiO_2-Fe_2O_3-PS4		Fe_2O_3-PS4		Fe_2O_3-PS4-MNP	
Time (min)	C[a] (%)	S-p[b] (%)	C[a] (%)	S-p[b] (%)	C[a] (%)	S-p[b] (%)
1	14.6	97.9	–	–	>99	46.3
2	>99	49.1	4	90.1	>99	46.9
3	>99	46.8	>99	46	>99	48.4

[a]Conversion (%); [b]selectivity (%) with respect to the *para*-isomer.
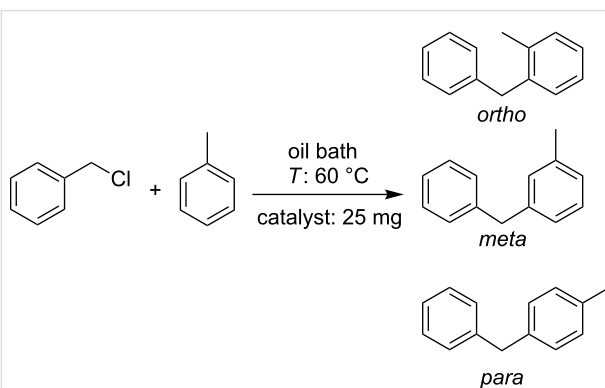
Scheme 3: Alkylation of toluene with benzyl chloride with conventional heating.

Reference experiments for the two investigated reactions were carried out in the absence of catalyst, demonstrating that the nanocomposites play a crucial role in order to accelerate the reaction rates (Supporting Information File 1, Table S1). It can be concluded that for the oxidation of benzyl alcohol, the Fe_2O_3-PS4 presents a better employability outlook, whereas for the alkylation reaction, the Fe_2O_3-PS4-MNP showed promising conversion and selectivity values.

Conclusion

The three bio-nanocomposites TiO_2-Fe_2O_3-PS4, Fe_2O_3-PS4 and Fe_2O_3-PS4-MNP, based on iron oxide and polysaccharide S4 were synthesized by mechanochemical processes. The magnetic susceptibility measurements show attractive magnetic

Table 7: Conversion and selectivity of the alkylation of toluene with conventional heating.

Catalyst	TiO_2-Fe_2O_3-PS4		Fe_2O_3-PS4		Fe_2O_3-PS4-MNP	
Time (min)	C[a] (%)	S-p[b] (%)	C[a] (%)	S-p[b] (%)	C[a] (%)	S-p[b] (%)
30	>99	51.6	>99	50.5	>99	49.5

[a]Conversion (%), [b]selectivity (%) with respect to the *para*-isomer.
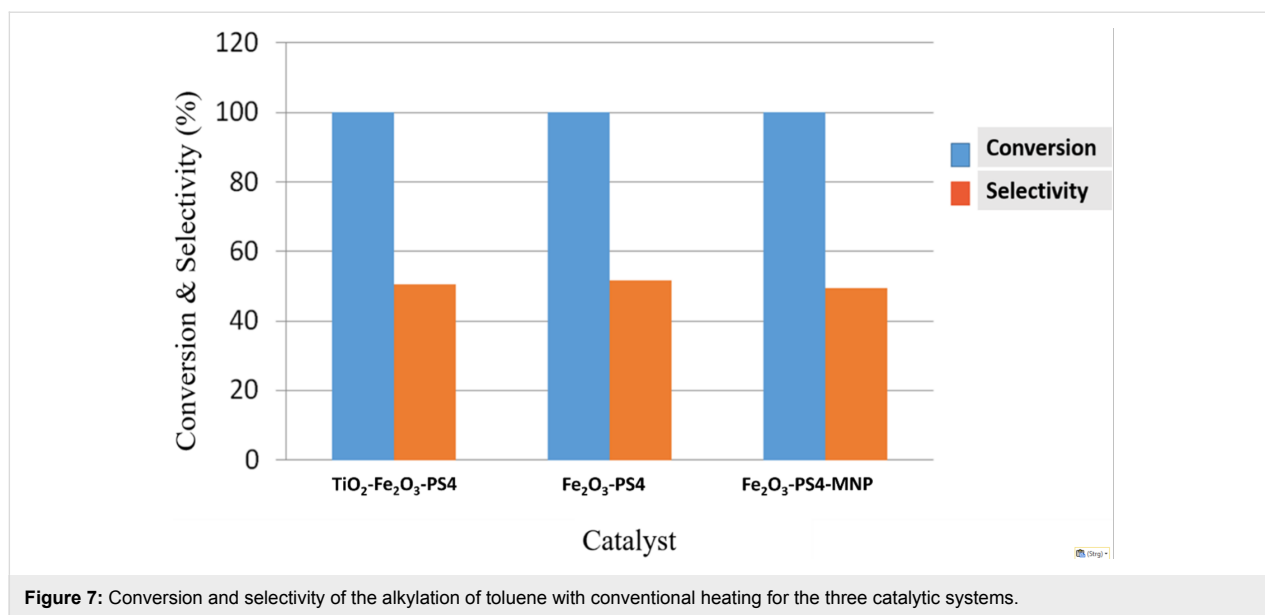
Figure 7: Conversion and selectivity of the alkylation of toluene with conventional heating for the three catalytic systems.
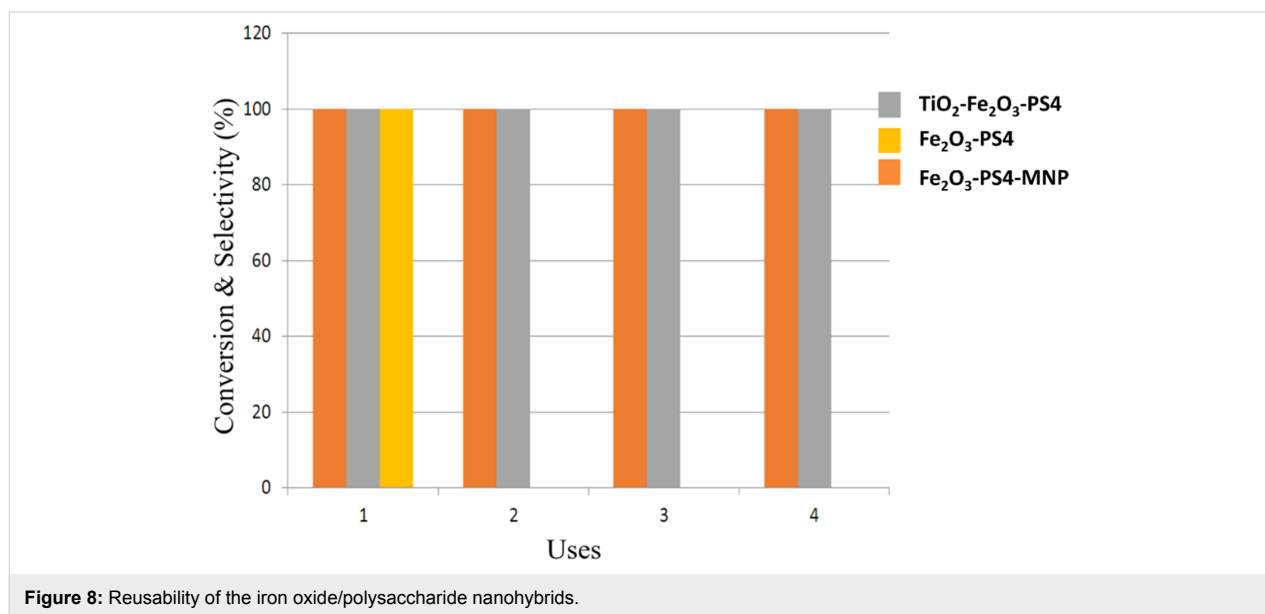
Figure 8: Reusability of the iron oxide/polysaccharide nanohybrids.

characteristics for recovery and reusability of the Fe_2O_3-PS4-MNP nanocomposite. Furthermore, the nanomaterials showed promising activity in the oxidation reaction of benzyl alcohol to benzaldehyde, with conversions of 32–45%. The three synthesized nanocomposites have proved to be highly active and selective catalysts in the alkylation reaction of toluene with benzyl chloride, due to the exceptional surface acidic properties of the nanoparticles. Both microwave irradiation and conventional heating exhibited high conversion and selectivity to the main product of the reaction in extremely short reaction times. Moreover, reusability studies showed high stability and activity of the nanohybrids TiO_2-Fe_2O_3-PS4 and Fe_2O_3-PS4-MNP, establishing these catalysts as potential candidates in both the

selective oxidation of benzyl alcohol and alkylation of toluene with benzyl chloride.

Experimental
Synthesis of bio-nanocomposites based on iron oxide and polysaccharide S4

A simple, reproducible and environmentally friendly protocol has been developed for the synthesis of the three catalysts Fe_2O_3-PS4, Fe_2O_3-PS4-MNP, and TiO_2-Fe_2O_3-PS4. The three materials were synthesized using a 2:1 metal precursor/polysaccharide ratio (2 g of polysaccharide S4, 4 g of $FeCl_2 \cdot 4H_2O$), in a ball mill (Retsch PM100 ball mill model), at 350 rpm for 30 min, using a 125 mL reaction chamber and 18 10 mm stain-

less steel balls. Additionally, in the case of the TiO_2-Fe_2O_3-PS4, 4.08 mL of titanium isopropoxide was added to obtain the desired nanomaterial. Subsequently, the materials were oven-dried at 100 °C for 24 h, and finally calcined at 600 °C for 3 h in air atmosphere.

The Fe_2O_3-PS4-MNP catalyst was obtained using 2 g of polysaccharide S4, 4 g of $Fe(NO_3)_3 \cdot 9H_2O$ and 1.5 mL of propionic acid. The milling process was carried out at 350 rpm for 15 and 30 min, respectively. The resulting material was oven-dried at 100 °C for 24 h and slowly heated up (1 °C/min) to 300 °C under air and kept at that temperature for 30 min.

Material characterization
In order to characterize the synthesized materials, several techniques have been employed, including XRD, XPS, absorption–desorption of N_2, SEM, TEM, DRIFT and titrations with pyridine and dimethylpyridine. In addition, the magnetic susceptibility of Fe_2O_3-PS4-MNP was measured and the elemental composition of TiO_2-Fe_2O_3-PS4 was determined by ICP–MS.

X-ray diffraction
X-ray diffraction has been used for the structural study of the synthesized nanocatalysts. The diffraction patterns were obtained on a Bruker D8 Discover diffractometer, equipped with a goniometer Bragg Brentano θ/θ of high precision, and with a Cu X-ray tube. Scans were performed in the 0.5 to 80° range at a step size of 0.02° with a counting time per step of 20 s.

X-ray photoelectron spectroscopy
XPS measurements were performed at the Central Service of Research Support (SCAI) of the University of Cordoba, in an ultrahigh vacuum (UHV) multipurpose surface analysis system (SpecsTM model, Germany), operating at pressures of $<10^{-10}$ mbar, using a conventional X-ray source (XR-50, Specs, Mg Kα, $h\nu = 1253.6$ eV, 1 eV = 1.603×10^{-19} J) in a "stop and go" mode. Powdered samples were deposited on a sample holder using double-sided adhesive tape and subsequently evacuated overnight under vacuum ($<10^{-6}$ Torr). The spectra were taken at room temperature (pass energy: 25 and 10 eV, step size: 1 and 0.1 eV, respectively) with a Phoibos 150-MCD energy detector. For the deconvolution of the obtained curves, the XPS software CASA was used.

N_2 physisorption
The Brunauer–Emmett–Teller (BET) surface area and pore volume measurements were obtained from N_2 adsorption–desorption isotherms at liquid nitrogen temperature (77 K) in a Micromeritics ASAP 2000 instrument. The weight of the samples ranged between 0.15–0.20 g. Prior to the analysis, the samples were degassed for 24 h at 140 °C under vacuum ($p < 10^{-2}$ Pa). The surface areas were calculated according to the linear equation of BET in the $0.05 < p_0 < 0.22$ range. The pore size distributions (PSDs) were obtained from the N_2 desorption branch.

Electron microscopy
SEM images and the elemental composition were recorder using the JEOL JSM-6490 LV microscope. The samples were Au/Pd-coated on a high-resolution sputter SC7640 at a sputtering rate of 1.5 kV per minute, up to 7 nm thickness. TEM micrographs were obtained in the FEI Tecnai G^2 system, equipped with a charge coupling device camera. Prior to analysis, the samples were suspended in ethanol and directly deposited on a copper grid.

Diffuse reflectance infrared Fourier transform spectroscopy
The DRIFT spectra of the materials were recorder on an infrared spectrophotometer (ABB MB3000 with Horizon MBTM software), equipped with an ATR PIKE MIRacleTM sampler, with a ZnSe window using 256 scans at a resolution of 8 cm^{-1}. During the measurements, the sample was purged with a nitrogen flow (20 mL min^{-1}, dehydrated and deoxygenated). The spectra were recorded at room temperature in the 4000–600 cm^{-1} wavenumber range. The materials were heated at 300 °C for 3 h prior to acquiring the reference spectra. Thus, the temperature was decreased to 200 °C, and after 10 min the reference spectrum was again recorded. Similarly, the reference spectra at 150 and 100 °C were acquired. Once the references were obtained, the acquisition of the spectra was carried out starting with the lowest temperature.

Pyridine (PY) and 2,6-dimethylpyridine (DMPY) titration
Pyridine (PY) and 2,6-dimethylpyridine (DMPY) titration experiments were carried out at 300 °C, via gas phase adsorption of the basic probe molecules applying a pulse chromatographic titration methodology. The catalyst used (≈0.025 g) was fixed inside a tubular stainless steel microreactor (4 mm internal diameter) by Pyrex glass wool. A cyclohexane solution of titrant (0.989 M in PY and 0.686 M in DMPY, respectively) was injected into a gas chromatograph through a microreactor in which the catalyst was previously sited. The injected base was analyzed by gas chromatography with a flame ionization detector and using an analytical column of 0.5 m length, containing 5 wt % of polyphenylether in the Chromosorb AW-DMCS in 80/100. The quantity of probe molecule adsorbed by the solid acid catalyst can subsequently be easily quantified. In order to distinguish between Lewis and Brønsted acidity, it was assumed that all DMPY selectively titrates

Brønsted sites (methyl groups hinder coordination of nitrogen atoms with Lewis acid sites) while PY titrates both Brønsted and Lewis acid sites in the materials. Thus, the difference between the amounts of PY (total acidity) and DMPY (Brønsted acidity) adsorbed should correspond to Lewis acidity in the materials.

ICP–MS

The metal content in the TiO_2-Fe_2O_3-PS4 catalyst was determined by ICP–MS in an Elan DRC-e (PerkinElmer SCIEX) spectrometer. The sample ($\approx$25 mg) was previously digested using an acid mixture of $HF/HNO_3/HCl$ 1:1:1. Dilutions were made with miliQ water (double distilled) up to a maximum of 1% of HF_2^- in acid solution.

Magnetic susceptibility

The magnetic susceptibility was measured at room temperature at low frequency (470 Hz) using a Bartington MS-2 instrument.

Catalytic experiments

The oxidation of benzyl alcohol to benzaldehyde was performed using 25 mg of catalyst, 0.2 mL of benzyl alcohol, 0.3 mL of hydrogen peroxide, and 2 mL of acetonitrile as the solvent, for 5 and 10 min, respectively.

The microwave-assisted alkylation of toluene and oxidation of benzyl alcohol was carried out in a CEM-Discover microwave reactor, equipped with a PC-controlled interface. The alkylation reactions were carried out by the standard "open vessel" method, while for oxidation reactions, the "discover" method was used under pressure, allowing us to control the irradiation power, temperature and pressure.

The alkylation reaction of toluene with benzyl chloride was performed under conventional heating, too. In both alkylation experiments, 2 mL of toluene, 0.2 mL of benzyl chloride and 25 mg of catalyst were used. The microwave-assisted reaction was conducted for 1, 2 and 3 min, while the reaction under conventional heating was carried out for 30 min until the maximum conversion was reached. The temperature in both cases was kept at around 60 °C.

The conversion and selectivity were calculated from the chromatograms by:

$$\text{conversion (\%)} = \left[\frac{c_{\text{initial}} - c_{\text{final}}}{c_{\text{initial}}} \right]$$

$$\text{selectivity (\%)} = \frac{c_{\text{product}}}{\left[c_{\text{initial}} - c_{\text{final}} \right]} \times 100$$

where c_{initial} and c_{final} are the concentrations of the reagents before and after the reaction, respectively, and c_{product} is the concentration of the product, as determined by gas chromatography (GC).

The samples were analyzed with a HP5890 Series II gas chromatograph (60 mL min^{-1} N_2 carrier flow, 20 psi column top head pressure) using a flame ionization detector (FID). A HP-101 capillary column (25 m × 0.2 mm × 0.2 μm) was employed. All calculations were based on the use of benzyl chloride and benzyl alcohol as limiting reagents for the studied alkylation and oxidation reaction, respectively.

Supporting Information

Supporting Information File 1
Additional spectra.
[http://www.beilstein-journals.org/bjoc/content/supplementary/1860-5397-13-194-S1.pdf]

References

1. White, R. J.; Luque, R.; Budarin, V. L.; Clark, J. H.; Macquarrie, D. J. *Chem. Soc. Rev.* **2009,** *38,* 481–494. doi:10.1039/B802654H
2. Astruc, D.; Lu, F.; Aranzaes, J. R. *Angew. Chem., Int. Ed.* **2005,** *44,* 7852–7872. doi:10.1002/anie.200500766
3. Grunes, J.; Zhu, J.; Somorjai, G. A. *Chem. Commun.* **2003,** 2257–2260. doi:10.1039/b305719b
4. Anastas, P. T.; Warner, J. C. *Green Chemistry: Theory and Practice;* Oxford University Press: New York, 1998.
5. Xu, C.; De, S.; Balu, A. M.; Ojeda, M.; Luque, R. *Chem. Commun.* **2015,** *51,* 6698–6713. doi:10.1039/C4CC09876E
6. Astruc, D., Ed. *Nanoparticles and catalysis;* John Wiley & Sons, 2008.
7. Polshettiwar, V.; Luque, R.; Fihri, A.; Zhu, H.; Bouhrara, M.; Basset, J.-M. *Chem. Rev.* **2011,** *111,* 3036–3075. doi:10.1021/cr100230z
8. Cai, D.; Mataraza, J. M.; Qin, Z. H.; Huang, Z.; Huang, J.; Chiles, T. C.; Carnahan, D.; Kempa, K.; Ren, Z. *Nat. Methods* **2005,** *2,* 449–454. doi:10.1038/nmeth761
9. Hu, X.; Dong, S. *J. Mater. Chem.* **2008,** *18,* 1279–1295. doi:10.1039/b713255g
10. Balu, A. M.; Pineda, A.; Yoshida, K.; Campelo, J. M.; Gai, P. L.; Luque, R.; Romero, A. A. *Chem. Commun.* **2010,** *46,* 7825–7827. doi:10.1039/c0cc02015j
11. Garcia-Olmo, A. J.; Yepez, A.; Balu, A. M.; Romero, A. A.; Li, Y.; Luque, R. *Catal. Sci. Technol.* **2016,** *6,* 4705–4711. doi:10.1039/C6CY00249H
12. Ouyang, W.; Kuna, E.; Yepez, A.; Balu, A. M.; Romero, A. A.; Colmenares, J. C.; Luque, R. *Nanomaterials* **2016,** *6,* 93. doi:10.3390/nano6050093
13. Colmenares, J. C.; Ouyang, W.; Ojeda, M.; Kuna, E.; Chernyayeva, O.; Lisovytskiy, D.; De, S.; Luque, R.; Balu, A. M. *Appl. Catal., B: Environ.* **2016,** *183,* 107–112. doi:10.1016/j.apcatb.2015.10.034
14. Yepez, A.; De, S.; Climent, M. S.; Romero, A. A.; Luque, R. *Appl. Sci.* **2015,** *5,* 532–543. doi:10.3390/app5030532

15. Juárez, R.; Parker, S. F.; Concepción, P.; Corma, A.; García, H. *Chem. Sci.* **2010,** *1,* 731–738. doi:10.1039/c0sc00336k
16. Navalon, S.; Martin, R.; Alvaro, M.; Garcia, H. *Angew. Chem., Int. Ed.* **2010,** *49,* 8403–8407. doi:10.1002/anie.201003216
17. Mendes, D.; Garcia, H.; Silva, V. B.; Mendes, A.; Madeira, L. M. *Ind. Eng. Chem. Res.* **2009,** *48,* 430–439. doi:10.1021/ie8010676
18. Gonzalez-Arellano, C.; Luque, R.; Macquarrie, D. J. *Chem. Commun.* **2009,** 1410–1412. doi:10.1039/b818767c
19. Budarin, V. L.; Clark, J. H.; Luque, R.; Macquarrie, D. J.; White, R. J. *Green Chem.* **2008,** *10,* 382–387. doi:10.1039/B715508E
20. Gonzalez-Arellano, C.; Yoshida, K.; Luque, R.; Gai, P. L. *Green Chem.* **2010,** *12,* 1281–1287. doi:10.1039/c003410j
21. Yepez, A.; Lam, F. L. Y.; Romero, A. A.; Kappe, C. O.; Luque, R. *ChemCatChem* **2015,** *7,* 276–282. doi:10.1002/cctc.201402802
22. Ozin, G. A.; Arsenault, A.; Cademartiri, L. *Nanochemistry: A chemical approach to nanomaterials;* Royal Society of Chemistry: Cambridge, UK, 2009.
23. Tsuzuki, T.; McCormick, P. G. *J. Mater. Sci.* **2004,** *39,* 5143–5146. doi:10.1023/B:JMSC.0000039199.56155.f9
24. Mei, K.-C.; Guo, Y.; Bai, J.; Costa, P. M.; Kafa, H.; Protti, A.; Hider, R. C.; Al-Jamal, K. T. *ACS Appl. Mater. Interfaces* **2015,** *7,* 14176–14181. doi:10.1021/acsami.5b03577
25. Ding, J.; Tsuzuki, T.; McCormick, P. G. *J. Mater. Sci.* **1999,** *34,* 5293–5298. doi:10.1023/A:1004736602847
26. Koch, C. C. *Nanostruct. Mater.* **1993,** *2,* 109–129. doi:10.1016/0965-9773(93)90016-5
27. Ding, J.; Shi, Y.; Chen, L. F.; Deng, C. R.; Fuh, S. H.; Li, Y. *J. Magn. Magn. Mater.* **2002,** *247,* 249–256. doi:10.1016/S0304-8853(02)00173-7
28. Xu, C.; Ojeda, M.; Arancon, R. A. D.; Romero, A. A.; Domingo, J. L.; Gómez, M.; Blanco, J.; Luque, R. *ACS Sustainable Chem. Eng.* **2015,** *3,* 2716–2725. doi:10.1021/acssuschemeng.5b00568
29. Herea, D. D.; Chiriac, H.; Lupu, N.; Grigoras, M.; Stoian, G.; Stoica, B. A.; Petreus, T. *Appl. Surf. Sci.* **2015,** *352,* 117–125. doi:10.1016/j.apsusc.2015.03.137
30. Rodriguez-Padrón, D.; Puente-Santiago, A. R.; Balu, A. M.; Romero, A. A.; Luque, R. *Chem. Commun.* **2017,** *53,* 7635–7637. doi:10.1039/C7CC03975A
31. Rodríguez-Padrón, D.; Puente-Santiago, A. R.; Caballero, A.; Benítez, A.; Balu, A. M.; Romero, A. A.; Luque, R. *J. Mater. Chem. A* **2017,** *5,* 16404–16411. doi:10.1039/C7TA04135G
32. Huebsch, N.; Mooney, D. J. *Nature* **2009,** *462,* 426–432. doi:10.1038/nature08601
33. Salgueiriño-Maceira, V.; Correa-Duarte, M. A. *Adv. Mater.* **2007,** *19,* 4131–4144. doi:10.1002/adma.200700418
34. Zheng, Y.; Monty, J.; Linhardt, R. J. *Carbohydr. Res.* **2015,** *405,* 23–32. doi:10.1016/j.carres.2014.07.016
35. Majewski, P.; Thierry, B. *Crit. Rev. Solid State Mater. Sci.* **2007,** *32,* 203–215. doi:10.1080/10408430701776680
36. Tallury, P.; Payton, K.; Santra, S. *Nanomedicine* **2008,** *3,* 579–592. doi:10.2217/17435889.3.4.579
37. Kim, J.; Piao, Y.; Hyeon, T. *Chem. Soc. Rev.* **2009,** *38,* 372–390. doi:10.1039/B709883A
38. Pineda, A.; Balu, A. M.; Campelo, J. M.; Romero, A. A.; Carmona, D.; Balas, F.; Santamaria, J.; Luque, R. *ChemSusChem* **2011,** *4,* 1561–1565. doi:10.1002/cssc.201100265
39. Matsumoto, T.; Ueno, M.; Wang, N.; Kobayashi, S. *Chem. – Asian J.* **2008,** *3,* 196–214. doi:10.1002/asia.200700359
40. Dey, S. K.; Mukherjee, A. *Coord. Chem. Rev.* **2016,** *310,* 80–115. doi:10.1016/j.ccr.2015.11.002
41. Rajabi, F.; Naresian, S.; Primo, A.; Luque, R. *Adv. Synth. Catal.* **2011,** *353,* 2060–2066. doi:10.1002/adsc.201100149
42. Yang, J.-C. E.; Yuan, B.; Cui, H.-J.; Wang, S.; Fu, M.-L. *Appl. Catal., B: Environ.* **2017,** *205,* 327–339. doi:10.1016/j.apcatb.2016.12.046
43. Huang, X.; Wang, X.; Wang, X.; Wang, X.; Tan, M.; Ding, W.; Lu, X. *J. Catal.* **2013,** *301,* 217–226. doi:10.1016/j.jcat.2013.02.011
44. Rak, M. J.; Lerro, M.; Moores, A. *Chem. Commun.* **2014,** *50,* 12482–12485. doi:10.1039/C4CC04749D
45. Shi, F.; Tse, M. K.; Pohl, M.-M.; Brückner, A.; Zhang, S.; Beller, M. *Angew. Chem., Int. Ed.* **2007,** *46,* 8866–8868. doi:10.1002/anie.200703418
46. Campelo, J. M.; Luna, D.; Luque, R.; Marinas, J. M.; Romero, A. A. *ChemSusChem* **2009,** *2,* 18–45. doi:10.1002/cssc.200800227
47. Wilson, K.; Adams, D. J.; Rothenberg, G.; Clark, J. H. *J. Mol. Catal. A* **2000,** *159,* 309–314. doi:10.1016/S1381-1169(00)00185-0
48. Bastock, T. W.; Clark, J. H. *Speciality chemicals;* Elsevier Applied Science: London, New York, 1991; p 383.
49. Pineda, A.; Balu, A. M.; Campelo, J. M.; Luque, R.; Romero, A. A.; Serrano-Ruiz, J. C. *Catal. Today* **2012,** *187,* 65–69. doi:10.1016/j.cattod.2012.02.028
50. Gracia, M. J.; Losada, E.; Luque, R.; Campelo, J. M.; Luna, D.; Marinas, J. M.; Romero, A. A. *Appl. Catal., A* **2008,** *349,* 148–155. doi:10.1016/j.apcata.2008.07.023
51. Ojeda, M.; Balu, A. M.; Barrón, V.; Pineda, A.; Coleto, Á. G.; Romero, A. A.; Luque, R. *J. Mater. Chem. A* **2014,** *2,* 387–393. doi:10.1039/C3TA13564K
52. Bourlinos, A. B.; Simopoulos, A.; Boukos, N.; Petridis, D. *J. Phys. Chem. B* **2001,** *105,* 7432–7437. doi:10.1021/jp010286+
53. Gregg, S. J.; Sing, K. S. W. *Adsorption, Surface Area and Porosity;* Academic Press Inc.: London, 1982.
54. Luque, R.; Campelo, J. M.; Luna, D.; Marinas, J. M.; Romero, A. A. *Microporous Mesoporous Mater.* **2005,** *84,* 11–20. doi:10.1016/j.micromeso.2005.05.013

Mechanochemical Knoevenagel condensation investigated in situ

Sebastian Haferkamp[1,2], Franziska Fischer[1], Werner Kraus[1] and Franziska Emmerling[*1]

Abstract

The mechanochemical Knoevenagel condensation of malononitrile with *p*-nitrobenzaldehyde was studied in situ using a tandem approach. X-ray diffraction and Raman spectroscopy were combined to yield time-resolved information on the milling process. Under solvent-free conditions, the reaction leads to a quantitative conversion to *p*-nitrobenzylidenemalononitrile within 50 minutes. The in situ data indicate that the process is fast and proceeds under a direct conversion. After stopping the milling process, the reaction continues until complete conversion. The continuous and the stopped milling process both result in crystalline products suitable for single crystal X-ray diffraction.

Introduction

Mechanochemical syntheses have gained increasing popularity in different areas such as materials science, chemistry, and pharmacy. Especially for organic syntheses, mechanochemistry is currently implemented as a green, fast, and efficient synthesis approach [1-3]. The syntheses are either solvent-free or require only a minimum amount of solvent. Consequently, solvation and desolvation phenomena can be neglected [4-6]. Mechanochemical syntheses of organic systems provide for example an efficient method for cocrystal screening [7-9], an increased product selectivity [2,10-12], and a pathway to new

products, which are inaccessible via traditional methods [3,13,14]. Often, stoichiometric reactions with quantitative yields of the final product are possible, rendering the use of solvents and work-up procedures unnecessary [3,15]. The mechanochemical synthesis can effect carbon–carbon and carbon–heteroatom covalent bonds, coordinating bonds between metal and ligands, and non-covalent interactions such as hydrogen bonds, halogen bonds, and π···π interactions [16-19]. For example, Toda et al. reported yields of 97% for Aldol condensations in the absence of any solvents [20]. Kaupp et al. described

the first Knoevenagel condensation in a ball mill [21]. Compared to conventional synthesis in which bases or Lewis acids are used as catalysts, Kaupp et al. could reduce the amount of catalysts [21]. The Knoevenagel condensation of *p*-nitrobenzaldehyde with malononitrile was initially only accessible in melts at 150–170 °C or in the presence of a catalyst like calcite or fluorite [21,22]. In an extended study, including different aldehydes, Ondruschka et al. reported a solvent- and catalyst-free Knoevenagel condensation of *p*-nitrobenzaldehyde and malononitrile in a vibrational mill [23]. Here, we report the first direct in situ investigation of a Knoevenagel condensation followed by combined X-ray diffraction and Raman spectroscopy measurements in a tandem approach. Our investigations reveal that the formation of the crystalline product begins after 36 min and is completed after 50 min. The reaction can be described as a melt-mediated reaction since malononitrile melts during the grinding process, whereas *p*-nitrobenzaldehyde remains crystalline until the onset of the product formation. The crystalline product was of sufficient quality for single crystal X-ray structure determination.

Results and Discussion

Scheme 1 illustrates the investigated Knoevenagel condensation of *p*-nitrobenzaldehyde (**1**) with malononitrile (**2**) using a ball mill. The stoichiometric reaction mixture was ball-milled for 60 minutes at 50 Hz in a conventional ball mill with either stainless steel or Perspex grinding jars. For both jar materials, the X-ray diffraction patterns of the product in comparison to those of the reactants reveal a complete and quantitative reaction (see Figure 1). For the in situ investigations, time-resolved

X-ray diffraction patterns and Raman spectra were recorded during the milling reaction. The Raman laser and the X-ray beam were focused on the same spot at the inner wall of a Perspex grinding jar, allowing to monitor the course of the reaction simultaneously. A detailed description of the experimental setup can be found elsewhere [24].

Scheme 1: Knoevenagel condensation of *p*-nitrobenzaldehyde (**1**) with malononitrile (**2**) yielding *p*-nitrobenzylidenemalononitrile (**3**).
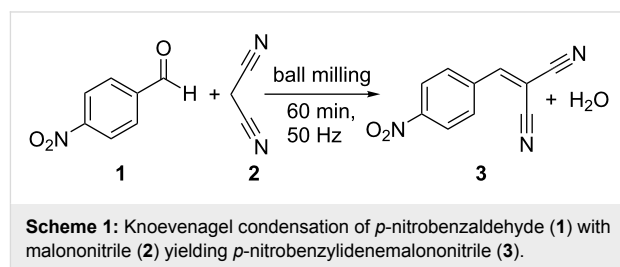
Figure 2 shows the X-ray powder diffraction (XRPD) patterns and the Raman spectra of the in situ investigation, monitored in a time-span of 60 minutes. No reflections of **2** are observed during the reaction. Most probably, **2** melts directly after the start of the reaction. Based on previous thermography investigations [25], we can assume that the temperature in the milling jar rises quickly to 35 °C which is above the melting point of **2** (32 °C). The intensity of the **1** reflections decreases continuously and vanishes after 45 minutes. After 36 minutes, reflections of the products can be detected next to those of **1**. After 45 minutes, only the product reflections can be observed in the time-resolved XRPD patterns (see Supporting Information File 1, Figure S2 for a quantitiative evaluation of the XRPD data). The in situ Raman data show a decreasing signal of the
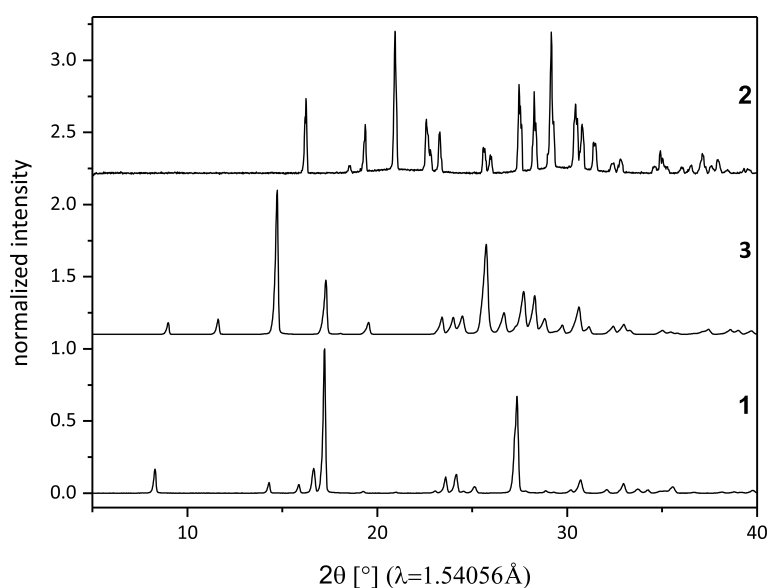
Figure 1: X-ray diffraction patterns of the reactants *p*-nitrobenzaldehyde (**1**) and malononitrile (**2**) and the product *p*-nitrobenzylidenemalononitrile (**3**).
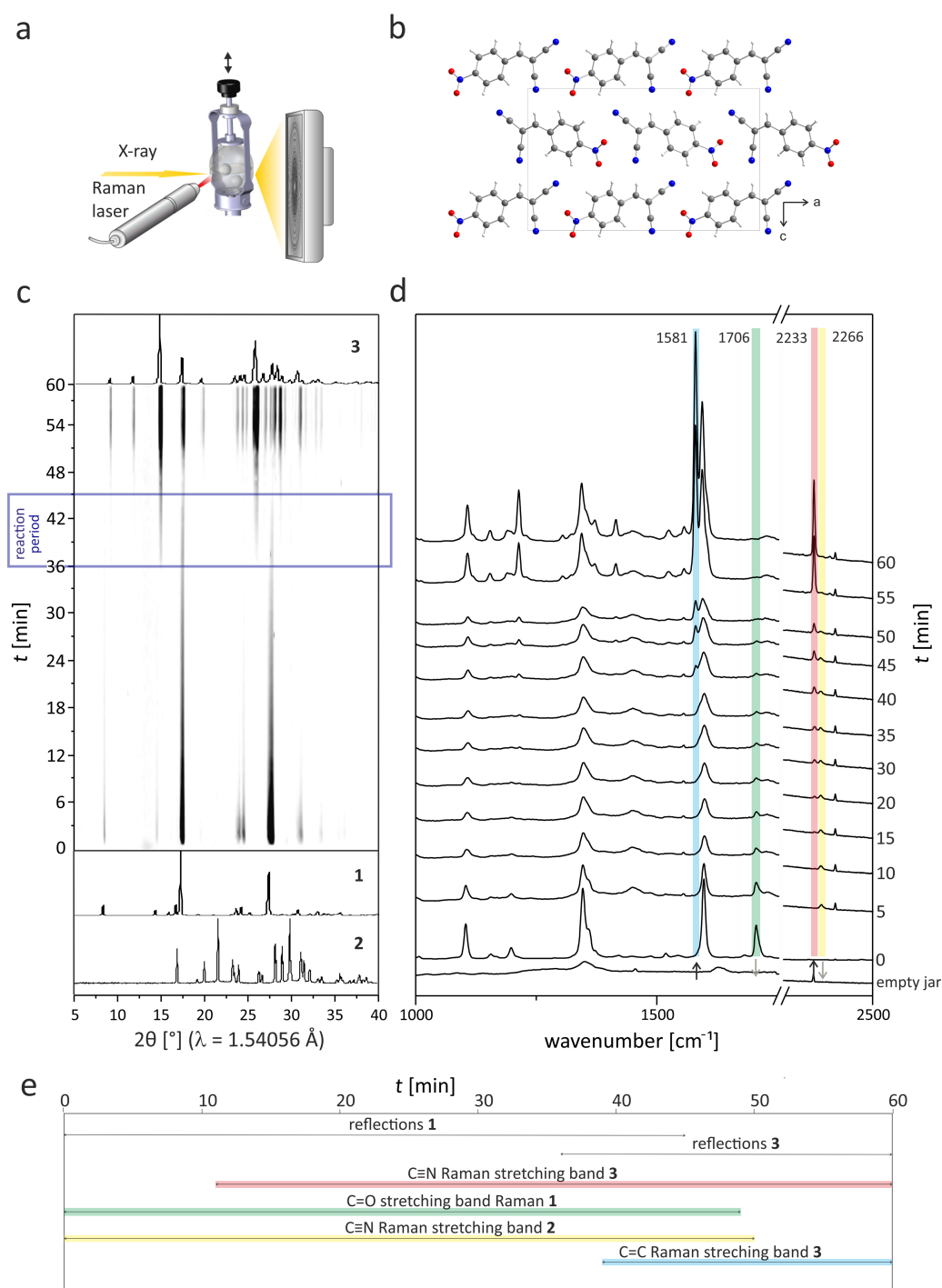
Figure 2: a) Schematic diagram of the in situ setup for investigating mechanochemical reactions in a tandem approach based on synchrotron X-ray powder diffraction and Raman spectroscopy. b) Crystal structure of the final product *p*-nitrobenzylidenemalononitrile (**3**) along the *b*-axis. c) Time-resolved X-ray diffraction patterns recorded during the Knoevenagel condensation of *p*-nitrobenzaldehyde with malononitrile yielding **3**. Three phases can be distinguished based on the XRPD data. During the first 36 minutes, the reflections of the reactant **1** are observed. Within a time-span of nine minutes, the product is formed, evident from two strong reflections at 2θ = 14.6° and 25.7°. d) Time-resolved Raman spectra measured simultaneously (Here, the Raman spectra are shown with a 5 min interval. The complete set of spectra is shown in Supporting Information File 1, Figure S1.) The progress of the reaction can be detected from the decreasing signal of the C=O stretching band of **1** at 1706 cm^{-1} (green) and the increasing signal of the C=C stretching band at 1581 cm^{-1} (blue). The band attributed to the C≡N stretching shifts from 2266 cm^{-1} (yellow) in **2** to 2233 cm^{-1} (red) in the product. The first Raman spectrum shows the contribution of the empty jar. e) Course of the reaction detected by XRPD and Raman spectroscopy.

C=O stretching band at 1706 cm^{-1} (see Figure 2, green box) and an increase of the C=C stretching band at 1581 cm^{-1} (see Figure 2, blue box). The C=C stretching band is shifted to lower wavenumbers due to a higher conjugation of π-electrons. The extended conjugation is also responsible for the shift of the C≡N stretching band from 2266 to 2233 cm^{-1} (see Figure 2, yellow and red box). The signal at 2233 cm^{-1} can be observed after 11 minutes of reaction, indicating that the first *p*-nitrobenzylidenemalononitrile molecules are formed in the condensation reaction. This can be also deduced from the decreasing intensity of the C=O stretching band of **1** at 1706 cm^{-1}. The C=C stretching band of the product at 1581 cm^{-1} is first observed after 39 minutes. In accordance to the diffraction data, the evaluation of the Raman spectra indicates the completion of the reaction after 50 minutes. In the following, the Raman bands become narrower, signifying an increasing crystallinity of the product.

Since the in situ data reveal an onset of the reaction after 36 min, we investigated in further experiments whether ball milling is needed for the completion of the reaction. The ball mill was stopped after 36 minutes and the reaction in the closed jar was monitored with Raman spectroscopy. The data show that under these conditions the reaction to the final product is completed within two hours. Consequently, prolonged milling after the initiation of the reaction is not necessary for a complete conversion to the product, but accelerates the reaction. The XRPD patterns of the product for both types of experiments are comparable and the crystals obtained in the in situ reactions are of sufficient quality for X-ray single crystal determination. The crystal structure could be solved, matching the parameters described in the literature [26].

Conclusion

Using an in situ tandem approach combining synchrotron X-ray powder diffraction and Raman spectroscopy, we investigated the mechanochemical Knoevenagel condensation of malononitrile with *p*-nitrobenzaldehyde in situ. The data show that once the reaction is initiated mechanochemically it proceeds via a direct conversion leading to a highly crystalline material. We could reveal that the activated reaction proceeds also without further milling. The in situ investigation of mechanochemical processes proved to be beneficial for optimizing the milling reactions.

Experimental

Materials: All chemicals were used without further purification.

Syntheses: The milling experiments were performed in a commercial ball mill (Pulverisette 23, Fritsch, Germany). In a typical experiment, equimolar quantities of the reactants *p*-nitrobenzaldehyde (800 mg, 5.29 mmol) and malononitrile 349.67 mg, 5.29 mmol) were weighed in milling jars (10 mL, stainless steel or Perspex). Two milling balls (stainless steel, 4 g, 10 mm diameter) were added to the reaction mixture. The reaction was performed in two different setups: i) The samples were prepared in Perspex grinding jars for the in situ measurements. Either the tandem in situ combination (synchrotron XRPD combined with Raman spectroscopy) or in situ Raman spectroscopy was employed. The reactants were milled at 50 Hz for 60 minutes. ii) Alternatively, the reaction mixture was milled in stainless steel jars at 50 Hz for 45 minutes. The final products were characterized by XRPD.

X-ray powder diffraction: All samples were characterised by XRPD analysis using a Bruker D8 diffractometer: Cu Kα$_1$ radiation (λ = 1.54106 Å), 5.0° ≤ 2 θ ≤ 60°. All data were obtained in transmission mode with an acquisition time of 3 s per step (step size 0.009°)

In situ investigations: The tandem in situ experiments were performed at the μspot beamline (BESSY II, Helmholtz Centre Berlin for Materials and Energy) [27]. For these experiments, a commercial ball mill (Pulverisette 23, Fritsch, Germany) equipped with a Perspex grinding jar was used, providing the necessary strength and transparency for the experiments. The diffraction experiments were performed at an energy of 12.4 keV and a wavelength of 1.0003 Å. The scattered intensities were recorded using a two-dimensional X-ray detector (MarMosaic, CCD 3072 × 3072). The scattering images were processed with FIT2D [28].

A Raman RXN1^{TM} analyzer (Kaiser Optical systems, France) was used for the Raman spectroscopy measurements. A non-contact probe head with a working distance of 6 cm and a spot size of 1 mm. The excitation wavelength was 785 nm. A typical measurement consists of five accumulated recordings for 5 s. A new measurement was started every 30 s.

Single crystal X-ray diffraction: Single crystal XRD measurements were performed on a D8 Venture diffractometer (Bruker AXS, Germany) using Mo Kα radiation (λ = 0.71073 Å) monochromatized by a graphite crystal. The crystals were measured at 150 K. Data reduction was performed with Bruker AXS SAINT and SADABS packages. The structure was solved by direct methods and refined by full-matrix least-squares calculation [29]. Anisotropic thermal parameters were employed for non-hydrogen atoms. The hydrogen atoms were treated isotropically with U$_{iso}$ = 1.2 times the U$_{eq}$ value of the parent atom. Crystal data: chemical formula C$_{10}$H$_5$N$_3$O$_2$, formula weight 199.17, orthorhombic, space group *Pna*2$_1$, *a* = 19.4857(8) Å,

$b = 3.78060(10)$ Å, $c = 11.9120(5)$ Å, $V = 877.53(6)$ Å^3, $Z = 4$, $T = 150(2)$ K, $\mu = 0.110$ mm^{-1}, 25807 reflections measured, 2366 unique reflections, 2222 observed reflections [$I > 2\sigma(I)$], $R_1\text{obs} = 0.0395$, $wR_2\text{obs} = 0.0956$. Crystal size: $0.38 \times 0.28 \times 0.02$ mm.

Supporting Information

Supporting Information File 1

Raman spectra and XRPD data.
[http://www.beilstein-journals.org/bjoc/content/supplementary/1860-5397-13-197-S1.pdf]

References

1. Boldyreva, E. *Chem. Soc. Rev.* **2013,** *42,* 7719–7738. doi:10.1039/c3cs60052a
2. Kaupp, G. *Encyclopedia of Physical Organic Chemistry;* 2005.
3. James, S. L.; Adams, C. J.; Bolm, C.; Braga, D.; Collier, P.; Friščić, T.; Grepioni, F.; Harris, K. D. M.; Hyett, G.; Jones, W.; Krebs, A.; Mack, J.; Maini, L.; Orpen, A. G.; Parkin, I. P.; Shearouse, W. C.; Steed, J. W.; Waddell, D. C. *Chem. Soc. Rev.* **2012,** *41,* 413–447. doi:10.1039/C1CS15171A
4. Sarkar, A.; Santra, S.; Kundu, S. K.; Hajra, A.; Zyryanov, G. V.; Chupakhin, O. N.; Charushin, V. N.; Majee, A. *Green Chem.* **2016,** *18,* 4475–4525. doi:10.1039/C6GC01279E
5. Walsh, P. J.; Li, H.; de Parrodi, C. A. *Chem. Rev.* **2007,** *107,* 2503–2545. doi:10.1021/cr0509556
6. Martins, M. A. P.; Frizzo, C. P.; Moreira, D. N.; Buriol, L.; Machado, P. *Chem. Rev.* **2009,** *109,* 4140–4182. doi:10.1021/cr9001098
7. Wouters, J.; Quéré, L. *Pharmaceutical salts and co-crystals;* Royal Society of Chemistry, 2011. doi:10.1039/9781849733502
8. Trask, A. V.; Motherwell, W. D. S.; Jones, W. *Int. J. Pharm.* **2006,** *320,* 114–123. doi:10.1016/j.ijpharm.2006.04.018
9. Friščić, T.; Jones, W. *Cryst. Growth Des.* **2009,** *9,* 1621–1637. doi:10.1021/cg800764n
10. Karki, S.; Friščić, T.; Jones, W. *CrystEngComm* **2009,** *11,* 470–481. doi:10.1039/B812531G
11. Stolle, A.; Szuppa, T.; Leonhardt, S. E. S.; Ondruschka, B. *Chem. Soc. Rev.* **2011,** *40,* 2317–2329. doi:10.1039/c0cs00195c
12. Zhang, W.; Lu, L.; Cheng, Y.; Xu, N.; Pan, L.; Lin, Q.; Wang, Y. *Green Chem.* **2011,** *13,* 2701–2703. doi:10.1039/c1gc15557a
13. Friščić, T. *Chem. Soc. Rev.* **2012,** *41,* 3493–3510. doi:10.1039/c2cs15332g
14. Trask, A. V.; van de Streek, J.; Motherwell, W. D. S.; Jones, W. *Cryst. Growth Des.* **2005,** *5,* 2233–2241. doi:10.1021/cg0501682
15. Hernández, J. G.; Bolm, C. *J. Org. Chem.* **2017,** *82,* 4007–4019. doi:10.1021/acs.joc.6b02887
16. Tanaka, K.; Kaupp, G. *Solvent-free organic synthesis;* John Wiley & Sons, 2009.
17. Kaupp, G. *CrystEngComm* **2009,** *11,* 388–403. doi:10.1039/B810822F
18. Rodríguez, B.; Bruckmann, A.; Rantanen, T.; Bolm, C. *Adv. Synth. Catal.* **2007,** *349,* 2213–2233. doi:10.1002/adsc.200700252
19. Wang, G.-W. *Chem. Soc. Rev.* **2013,** *42,* 7668–7700. doi:10.1039/c3cs35526h
20. Toda, F.; Tanaka, K.; Hamai, K. *J. Chem. Soc., Perkin Trans. 1* **1990,** 3207–3209. doi:10.1039/P19900003207
21. Kaupp, G.; Reza Naimi-Jamal, M.; Schmeyers, J. *Tetrahedron* **2003,** *59,* 3753–3760. doi:10.1016/S0040-4020(03)00554-4
22. Wada, S.; Suzuki, H. *Tetrahedron Lett.* **2003,** *44,* 399–401. doi:10.1016/S0040-4039(02)02431-0
23. Trotzki, R.; Hoffmann, M. M.; Ondruschka, B. *Green Chem.* **2008,** *10,* 767–772. doi:10.1039/b801661e
24. Batzdorf, L.; Fischer, F.; Wilke, M.; Wenzel, K.-J.; Emmerling, F. *Angew. Chem., Int. Ed.* **2015,** *54,* 1799–1802. doi:10.1002/anie.201409834
25. Kulla, H.; Wilke, M.; Fischer, F.; Röllig, M.; Maierhofer, C.; Emmerling, F. *Chem. Commun.* **2017,** *53,* 1664–1667. doi:10.1039/C6CC08950J
26. Chang, M.-J.; Fang, T.-C.; Tsai, H.-Y.; Luo, M.-H.; Chen, K.-Y. *Acta Crystallogr., Sect. E* **2012,** *68,* o957. doi:10.1107/S1600536812008896
27. Paris, O.; Li, C.; Siegel, S.; Weseloh, G.; Emmerling, F.; Riesemeier, H.; Erko, A.; Fratzl, P. *J. Appl. Crystallogr.* **2007,** *40,* S466–S470. doi:10.1107/S0021889806045444
28. Hammersley, A. P.; Svensson, S. O.; Hanfland, M.; Fitch, A. N.; Hausermann, D. *High Pressure Res.* **1996,** *14,* 235–248. doi:10.1080/08957959608201408
29. Sheldrick, G. M. *Acta Crystallogr., Sect. A: Found. Crystallogr.* **2008,** *64,* 112–122. doi:10.1107/S0108767307043930

License and Terms

Mechanically induced oxidation of alcohols to aldehydes and ketones in ambient air: Revisiting TEMPO-assisted oxidations

Andrea Porcheddu[*1], Evelina Colacino[1,2], Giancarlo Cravotto[3], Francesco Delogu[4] and Lidia De Luca[5]

Abstract

The present work addresses the development of an eco-friendly and cost-efficient protocol for the oxidation of primary and secondary alcohols to the corresponding aldehydes and ketones by mechanical processing under air. Ball milling was shown to promote the quantitative conversion of a broad set of alcohols into carbonyl compounds with no trace of an over-oxidation to carboxylic acids. The mechanochemical reaction exhibited higher yields and rates than the classical, homogeneous, TEMPO-based oxidation.

Introduction

Aldehydes and ketones constitute some of the most powerful and versatile building blocks that are available for a variety of synthetic transformations [1]. The reason for this lies in the capability of the carbonyl group to generate other possible functional groups through more or less complex chemical transformations [2]. The ubiquity of the carbonyl group in biomolecules adds further value to its chemistry, which is crucial for

strategic areas of science related to biochemistry and biotechnology [3,4].

In principle, the oxidation of alcohols represents a convenient option for preparing aldehydes and ketones, as alcohols are among the most abundant naturally occurring organic compounds [5,6]. Although the literature provides a plethora of

generic indications and detailed recipes on this subject [7-10], the selective oxidation of primary alcohols to the corresponding aldehydes is one of the most difficult transformations to control because of the marked propensity towards over-oxidation to the respective carboxylic acid [11,12]. In addition, the appeal of this reaction is reduced by the need to use stoichiometric amounts of strong oxidising agents that are extremely toxic, hazardous, and expensive [13-17]. The use of the stable tetraalkylnitroxyl radical TEMPO (2,2,6,6-tetramethylpiperidine 1-oxyl) as the catalytic oxidising agent (Anelli–Montanari reaction) has been the main driving force behind the successful development of greener oxidation procedures [18,19]. The classic Anelli–Montanari oxidation requires aqueous NaOCl (bleach) as a co-oxidant, and it works in a CH_2Cl_2/H_2O two-phase system buffered at pH 8.5–9.5 [20]. Over the years, bleach has been replaced with an impressively long list of other co-oxidants [21], which are sometimes very expensive, and exhibit a wide spectrum of effectiveness (Scheme 1) [22,23]. Recently, Stahl [24] developed a practical Cu^I/TEMPO-based catalyst for the selective oxidation of primary alcohols to aldehydes under ambient aerobic conditions (Scheme 1) [25,26]. The procedure is operationally simple and extremely effective in terms of both chemoselectivity and reaction yield [27,28]. Gao (2016) further improved this methodology by replacing the bpy/Cu^I/NMI catalyst system with $Fe(NO_3)_3 \cdot 9H_2O$, a cheaper, ligand-free co-oxidant (Scheme 1) [29,30]. This made the oxidative process more appealing for pharmaceutical applications, and specifically beneficial in the preparation of fragrances and food additives [31].

Scheme 1: TEMPO-catalysed aerobic oxidative procedures of alcohols. a) Anelli–Montanari protocol: NaOCl (1.25 mol equiv), TEMPO (1–2 mol %), KBr (10 mol %), $NaHCO_3$ (pH 8.6), CH_2Cl_2/H_2O. b) Stahl protocol: $[Cu(MeCN)_4](OTf)$ (5 mol %), bpy (5 mol %), TEMPO (5 mol %), NMI (10 mol %), CH_3CN, air. c) Gao (2016) protocol: $Fe(NO_3)_3 \cdot 9H_2O$ (10 mol %), 9-azabicyclo[3.3.1]nonane-*N*-oxyl (ABNO, 1–3 mol %), CH_3CN, air.
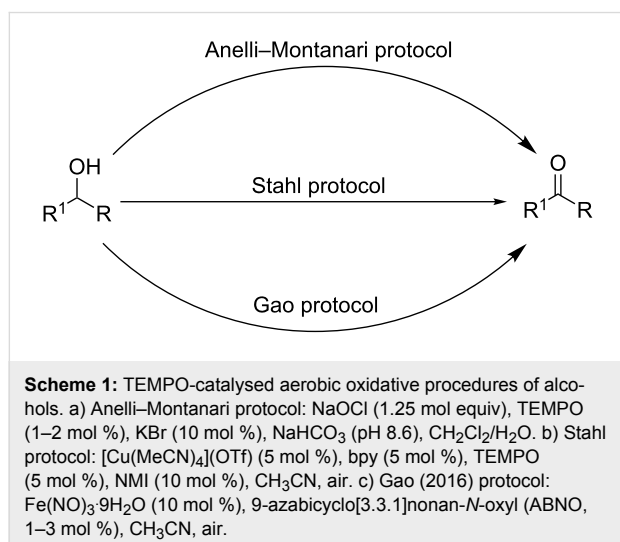
Despite the advances, the choice of solvent for TEMPO-based oxidative procedures remains a crucial issue in the development of greener alternatives to traditional alcohol oxidation reactions [32-34]. In particular, the lack of a green option sig-

nificantly decreases the attractiveness of the proposed synthetic routes, as the solvent is the main component of the reaction system and, thus, the main source of waste in organic synthesis [35]. By far, performing the oxidation of alcohols under solvent-free conditions represents the best strategy to radically eliminate possible drawbacks in regard to waste disposal [36,37]. In this respect, the mechanical activation of solids [38-42], in the absence of solvents [43], or in the presence of catalytic amounts of liquid [44,45], holds significant promise [46-58].

Rooted in ancient practices from the dawn of civilization, a thin historical thread twisting across human history connects powder metallurgy and mineralurgy with science and engineering at the cutting edge of research in the fields of materials science and chemistry [59]. Presently, mechanochemistry is one of the fastest growing areas of investigation that aims to provide alternative methods to traditional syntheses in organic and inorganic chemistry [49,60,61]. Mechanochemistry is also used in supramolecular chemistry [62] and metal-organic chemistry [63].

In this work, we show that mechanical processing by ball milling can represent a viable solution to the selective oxidation of alcohols to aldehydes. Specifically, we investigated the potential of a mechanically activated TEMPO-based oxidative procedure [64].

Results and Discussion

We began our investigation with an attempt to replicate Gao's procedure in a stainless steel reactor of a commercial ball mill in the presence of stainless steel balls and air, and in the absence of solvent. The oxidation of solid 4-nitrobenzyl alcohol (**1a**) to 4-nitrobenzaldehyde (**2a**) was selected as a model reaction. Unfortunately, the alcohol-to-aldehyde conversion was very low (<15%), and the use of larger amounts of the catalyst as well as molecular oxygen instead of air did not result in a significant improvement (Scheme 2, left side). To our great surprise, using Stahl's catalyst, the mechanically activated oxidation of the model substrate **1a** under solvent-free conditions proceed so quickly and selectively that it was complete within just a few minutes. The progress of the reaction was monitored by TLC and GC–MS analysis until the completion of the reaction. The experimental protocol involved two stages, namely the preparation of the catalytic system and the final oxidation reaction. During the first stage $[Cu(MeCN)_4]OTf$ (5 mol %), 2,2′-bipyridine (5 mol %), NMI (10 mol %), and TEMPO (5 mol %) were milled (1 min) in a stainless steel reactor using four stainless steel balls of different sizes. Following the mechanical treatment, the catalyst uniformly covered the reactor walls forming a dark red/brown thin film. Subsequently, solid

Scheme 2: TEMPO-assisted oxidation of 4-nitrobenzylic alcohol under mechanical activation conditions [65].
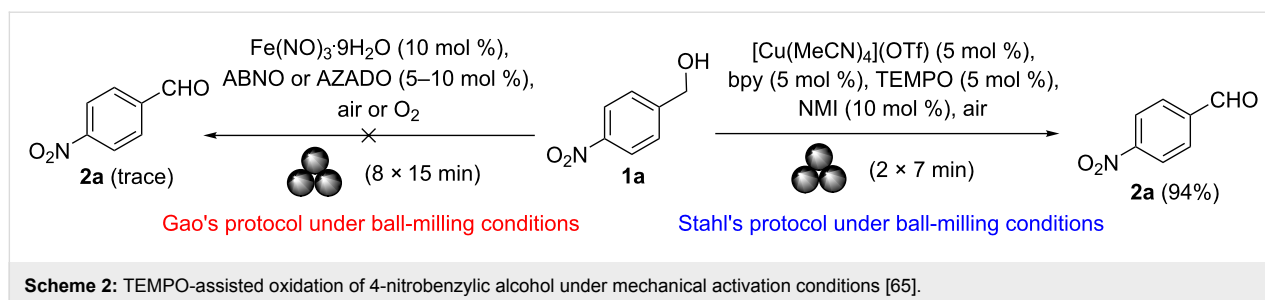
4-nitrobenzyl alcohol (**1a**, 2 mmol) was added together with two more stainless steel balls (12 mm Ø), and the resulting mixture was milled until the starting alcohol was completely oxidized. Despite the poor reactivity of the 4-nitrobenzyl alcohol, the reaction smoothly reached completion in only 14 minutes (two cycles of 7 minutes each). GC–MS analysis of the crude reaction mixture only showed the presence of the desired aromatic aldehyde, indicating that over-oxidation did not occur (Scheme 2, right side). Prolonged milling did not result in the formation of detectable amounts of the carboxylic acid.

Next, we replaced the starting stainless-steel grinding jar and balls with a zirconia jar (45 mL) and six zirconium oxide balls (5 and 12 mm Ø) with the aim of avoiding contamination due to metal release. Under these conditions, it was possible to reduce the loading of [Cu(MeCN)₄]OTf, 2,2′-bipyridine and TEMPO to 3 mol % and NMI loading to 7 mol % without affecting the reaction time or the product yield. Interestingly, the alcohol-to-aldehyde oxidation under ball milling conditions was faster (15 min overall) than that in solution (1 h) [25]. In addition, the absence of a solvent facilitated the purification of the final aldehyde. Specifically, the reaction crude was transferred from the reactor into a beaker containing an aqueous 10% citric acid solution [66,67], and the desired product precipitated as a solid. If necessary, the crude product could be further purified via filtering on a short pad of silica gel to give final aldehyde **2a** with a higher degree of purity (>95% as determined by GC–MS analysis). Since most common alcohols are, unfortunately, liquids at room temperature, their mechanical activation requires using a versatile dispersant. Ideally, a dispersant should not interfere with the oxidation reaction, and should be inexpensive and eco-friendly, if possible. As a first choice, we dispersed benzyl alcohol (**1b**) on alumina and silica gel. However, the reaction did not go to completion. In contrast, it proceeded smoothly (10 min) and in high yields when Na₂SO₄ and NaCl [68] were used as dispersants. Furthermore, the use of sodium chloride (500 mg per mmol of alcohol) facilitated the transfer of the reaction mixture from the reactor to the separating funnel containing the aqueous 10% citric acid solution. On the microscale (2 mmol), the full recovery of benzaldehyde was only achieved after solvent extraction. A minor modifica-

tion to the synthetic protocol, involving the use of additional zirconia balls (four balls × 5 mm Ø, 7 balls × 12 mm Ø) and opening the jar (3 min) to air during the time interval between two consecutive cycles, gave **2b** in 96% overall yield even on the gram scale. On the gram scale, the mechanical activation no longer required an additional solvent to recover the final aldehyde during purification. With the optimized reaction conditions in hand, a series of common benzyl alcohols **1b–n** with different functional groups was then tested in order to examine the scope of the reaction (Scheme 3). To our satisfaction, very high yields (>90%) were obtained with all tested compounds, except **2n** (39%).

Benzyl alcohols containing alkyl or aryl groups on the aromatic ring were all transformed into the desired products in quantitative or nearly quantitative isolated yields (compounds **2c–f** in Scheme 3). The position of the hydrocarbon (–R) on the ring did not significantly affect the aldehyde yield (aldehydes **2c–e** in Scheme 3). Substrates bearing electron-donating and electron-withdrawing functional groups on the aromatic ring of the benzyl alcohol were also viable, giving the corresponding aromatic aldehydes in high yields regardless of the electronic nature of their substituents (aldehydes **2g–k** in Scheme 3). Surprisingly, and contrary to Stahl's original solution procedure [24], the oxidation of 2-hydroxybenzyl alcohol under mechanical activation conditions provided the salicylaldehyde in nearly quantitative yield (compound **2k** in Scheme 3). The reaction was also successfully expanded to heteroaromatic alcohol **1l** (Scheme 3, 2-furylmethanol), giving furfural in a very good yield (90%). The mechanically induced oxidative procedure was also applied to allylic alcohol derivatives. Cinnamyl alcohol (**1m**) was transformed into the corresponding α,β-unsaturated aldehyde in an excellent yield (96%) and with the stereochemical retention of the double bond. Encouraged by these promising results, we attempted to oxidise alkynols to the corresponding propargylic aldehyde derivatives, which were not previously accessible via classical homogeneous phase methods [25]. Contrary to our expectations, the ball milling protocol proved to be an efficient approach for the synthesis of these substrates, giving phenylpropargylaldehyde (**2n**) in a modest yield (39%) after 4 cycles (15 min per cycle). Unfortunately,
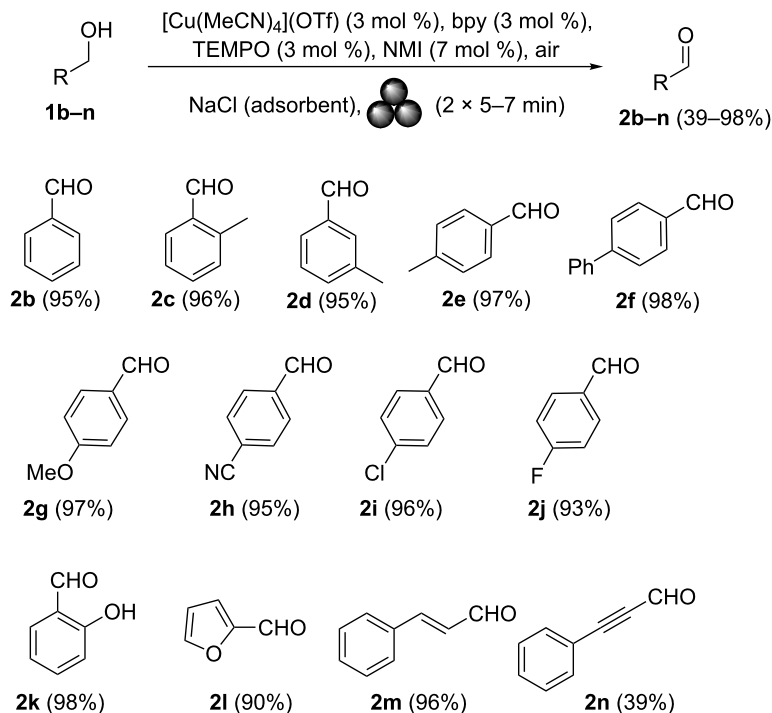
Scheme 3: Scope of primary alcohols in oxidation under ambient air.

prolonged milling times led to the decomposition of the final aldehyde. These promising results prompted us to undertake additional studies on secondary alcohols. The optimised ball milling protocol was applied to alcohols **1o–v**. Excellent yields of the ketones **2o–v** were obtained (Scheme 4). Notably, the product yield was not significantly affected by the position or

electronic nature of the substituents on the aromatic ring of the alcohols.

Encouraged by the facile oxidation of benzyl alcohols, the scope of the reaction was finally extended to the formation of more challenging aliphatic aldehydes. Unfortunately, non-acti-
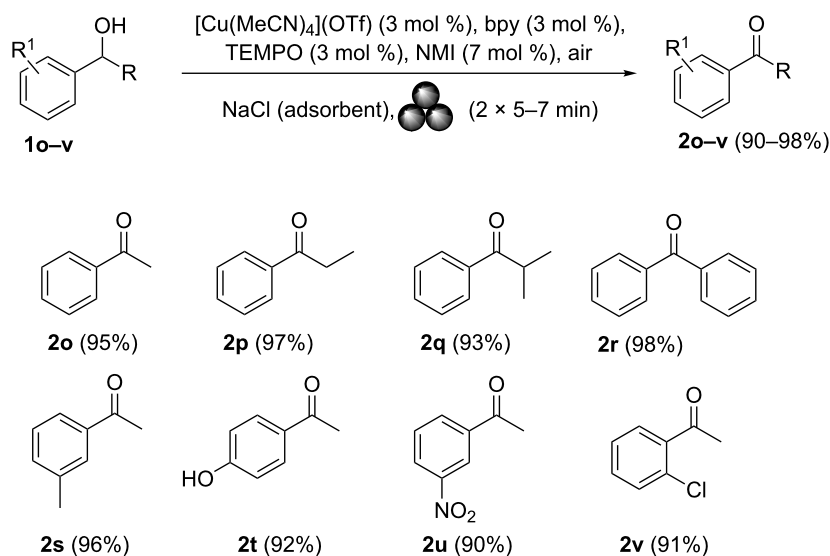
Scheme 4: Scope of secondary alcohols in oxidation under ambient air.

vated aliphatic alcohols did not react efficiently under the reaction conditions, and very low alcohol-to-aldehyde conversions occurred. The extension of milling times to 3 h failed to result in improved yields of all tested substrates: 3-phenyl-1-propanol, cyclohexanol and nonanol. Despite several attempts to improve the alcohol-to-aldehyde conversion, by, for instance, milling under an oxygen atmosphere and the use of more reactive co-oxidant catalysts [69], no significant improvements were observed.

Conclusion

We have developed a TEMPO-based oxidative procedure for the air oxidation of primary and secondary benzyl alcohols to the corresponding aldehydes and ketones under ball milling conditions. A library of common alcohols was efficiently converted into carbonyl compounds with no trace of over-oxidation to the carboxylic acids. The final products could be easily separated/purified from the crude reaction mixture without using toxic organic solvents. Under mechanical activation conditions, the reactions provided better yields and proceeded faster than classical, homogeneous phase TEMPO-based oxidations. Studies are underway to identify more effective TEMPO-based catalysts that are also capable of promoting the oxidation of non-activated alcohols.

Experimental

General procedure to prepare carbonyl compounds **2a–v**. 2,2,6,6-Tetramethylpiperidine 1-oxyl (TEMPO, 9.4 mg, 0.06 mmol, 3 mol %), 2,2′-bipyridyl (9,4 mg, 0.06 mmol, 3 mol %), [Cu(CN)$_4$]OTf (22.6 mg, 0.06 mmol, 3 mol %) and 1-methylimidazole (NMI, 11.5 mg, 11.2 μL, 0.14 mmol, 7 mol %) were placed in a zirconia-milling beaker (45 mL) equipped with four balls (two balls × 5 mm Ø, two balls × 12 mm Ø) of the same material. The jar was sealed and ball-milled for 1 min. Then, benzyl alcohol (216.3 mg, 207 μL, 2.0 mmol), NaCl (1.0 g) together with other two zirconia balls (12 mm Ø) were added and the reaction mixture was subjected to grinding for further 10 minutes overall (two cycles of 5 minutes each). The first milling cycle was followed by a break of 2 min leaving in the meantime the uncovered jar in open air. The progress of the reaction was monitored by TLC analysis (heptane/AcOEt 9:1 v/v) and GC–MS analysis on an aliquot of the crude. Upon completion of the ball milling process, the jar was opened, the milling balls were removed and the resulting crude product (adsorbed on NaCl) was then easily transferred into a separating funnel filled with an aqueous 10% citric acid solution (20 mL). The aqueous phase was extracted with cyclopentyl methyl ether (or alternatively with AcOEt) (3 × 15 mL). The combined organic fractions were washed with H$_2$O (25 mL) and brine (25 mL), then dried over Na$_2$SO$_4$, and concentrated in vacuo to give benzaldehyde in high yield

(195 mg, 92%) and good purity (>93% by GC analysis). Alternatively, after completion of the reaction, the resulting crude product (adsorbed on NaCl) can be also easily purified by a short column chromatography on silica gel using heptane/ethyl acetate (9:1 v/v) as the eluents to afford pure aldehyde **2b** in high yield (202 mg, 95%) as a colourless liquid.

Supporting Information

Supporting Information File 1
Experimental part and NMR spectra.
[http://www.beilstein-journals.org/bjoc/content/supplementary/1860-5397-13-202-S1.pdf]

References

1. Dubrovskiy, A. V.; Kesharwani, T.; Markina, N. A.; Pletnev, A. A.; Raminelli, C.; Yao, T.; Zeni, G.; Zhang, L.; Zhang, X.; Rozhkov, R.; Larock, R. C., Eds. *Comprehensive Organic Transformations: A Guide to Functional Group Preparations,* 3rd ed.; Wiley: New York, 2017.
2. Smith, B. H. *March's Advanced Organic Chemistry: Reactions, Mechanisms, and Structure,* 7th ed.; John Wiley & Sons: New York, 2013.
3. Nicolaou, K. C.; Sorensen, E. J. *Classics in Total Synthesis: Targets, Strategies, Methods;* Wiley-VCH: Weinheim, 1996.
4. Warren, S. *Chemistry of the Carbonyl Group: A Programmed Approach to Organic Reaction Mechanism;* John Wiley & Sons: New York, 1974.
5. Tojo, G.; Fernandez, M. *Oxidations of Alcohols to Aldehydes and Ketones -A Guide to Current Common Practice;* Springer: New York, 2006.
6. Hudlucky, M. *Oxidations in Organic Chemistry;* ACS Monograph Series; American Chemical Society: Washington, DC, 1990.
7. Mancuso, A. J.; Huang, S.-L.; Swern, D. *J. Org. Chem.* **1978,** *43,* 2480–2482. doi:10.1021/jo00406a041
8. Dess, D. B.; Martin, J. C. *J. Org. Chem.* **1983,** *48,* 4155–4156. doi:10.1021/jo00170a070

9. Ley, S. V.; Norman, J.; Griffith, W. P.; Marsden, S. P. *Synthesis* **1994,** 639–666. doi:10.1055/s-1994-25538

10. Baxendale, I. R.; Deeley, J.; Griffiths-Jones, C. M.; Ley, S. V.; Saaby, S.; Tranmer, G. K. *Chem. Commun.* **2006,** 2566–2568. doi:10.1039/B600382F

11. Arends, I. W. C. E.; Sheldon, R. A.; Bäckvall, J. E., Eds. *Modern Oxidation Methods,* 2nd ed.; Wiley-VCH: Weinheim, 2011.

12. Boisvert, L.; Goldberg, K. I. *Acc. Chem. Res.* **2012,** *45,* 899–910. doi:10.1021/ar2003072

13. Luzzio, F. A.; Guziec, F. S., Jr. *Org. Prep. Proced. Int.* **1988,** *20,* 533–584. doi:10.1080/00304948809356301

14. Fatiadi, A. J. *Synthesis* **1976,** 65–104. doi:10.1055/s-1976-23961

15. Tidwell, T. T. *Synthesis* **1990,** 857–870. doi:10.1055/s-1990-27036

16. Sheldon, R. A.; Arends, I. W. C. E.; ten Brink, G.-J.; Dijksman, A. *Acc. Chem. Res.* **2002,** *35,* 774–781. doi:10.1021/ar010075n

17. Tohma, H.; Kita, Y. *Adv. Synth. Catal.* **2004,** *346,* 111–124. doi:10.1002/adsc.200303203

18. Cella, J. A.; Kelley, J. A.; Kenehan, E. F. *J. Org. Chem.* **1975,** *40,* 1860–1862. doi:10.1021/jo00900a049

19. Ganem, B. *J. Org. Chem.* **1975,** *40,* 1998–2000. doi:10.1021/jo00901a030

20. Anelli, P. L.; Biffi, C.; Montanari, F.; Quici, S. *J. Org. Chem.* **1987,** *52,* 2559–2562. doi:10.1021/jo00388a038

21. De Luca, L.; Giacomelli, G.; Porcheddu, A. *Org. Lett.* **2001,** *3,* 3041–3043. doi:10.1021/ol016501m

22. Bolm, C.; Magnus, A. S.; Hildebrand, J. P. *Org. Lett.* **2000,** *2,* 1173–1175. doi:10.1021/ol005792g

23. Markó, I. E.; Giles, P. R.; Tsukazaki, M.; Brown, S. M.; Urch, C. J. *Science* **1996,** *274,* 2044–2046. doi:10.1126/science.274.5295.2044

24. Hoover, J. M.; Steves, J. E.; Stahl, S. S. *Nat. Protoc.* **2012,** *7,* 1161–1167. doi:10.1038/nprot.2012.057

25. Hoover, J. M.; Ryland, B. L.; Stahl, S. S. *J. Am. Chem. Soc.* **2013,** *135,* 2357–2367. doi:10.1021/ja3117203

26. Könning, D.; Olbrisch, T.; Sypaseuth, F. D.; Tzschucke, C. C.; Christmann, M. *Chem. Commun.* **2014,** *50,* 5014–5016. doi:10.1039/C4CC01305K

27. Ryland, B. L.; Stahl, S. S. *Angew. Chem., Int. Ed.* **2014,** *53,* 8824–8838. doi:10.1002/anie.201403110 and references cited therein.

28. Allen, S. E.; Walvoord, R. R.; Padilla-Salinas, R.; Kozlowski, M. C. *Chem. Rev.* **2013,** *113,* 6234–6458. doi:10.1021/cr300527g

29. Wang, L.; Shang, S. S.; Li, G.; Ren, L.; Lv, Y.; Gao, S. *J. Org. Chem.* **2016,** *81,* 2189–2193. doi:10.1021/acs.joc.6b00009

30. Ma, S.; Liu, J.; Li, S.; Chen, B.; Cheng, J.; Kuang, J.; Liu, Y.; Wan, B.; Wang, Y.; Ye, Y.; Yu, Q.; Yuan, W.; Yu, S. *Adv. Synth. Catal.* **2011,** *353,* 1005–1017. doi:10.1002/adsc.201100033

31. Alfonsi, K.; Colberg, J.; Dunn, P. J.; Fevig, T.; Jennings, S.; Johnson, T. A.; Kleine, H. P.; Knight, C.; Nagy, M. A.; Perry, D. A.; Stefaniak, M. *Green Chem.* **2008,** *10,* 31–36. doi:10.1039/B711717E

32. Cao, Q.; Dornan, L. M.; Rogan, L.; Hughes, N. L.; Muldoon, M. J. *Chem. Commun.* **2014,** *50,* 4524–4543. doi:10.1039/C3CC47081D

33. Sheldon, R. A. *Chem. Soc. Rev.* **2012,** *41,* 1437–1451. doi:10.1039/c1cs15219j Acetonitrile is considered by the US Environmental Protection Agency as a hazardous solvent that produces acute systemic and potentially carcinogenic effects.

34. Trost, B. M. *Science* **1991,** *254,* 1471–1477. doi:10.1126/science.1962206

35. Parmeggiani, C.; Cardona, F. *Green Chem.* **2012,** *14,* 547–564. doi:10.1039/C2GC16344F

36. Rothenberg, G.; Downie, A. P.; Raston, C. L.; Scott, J. L. *J. Am. Chem. Soc.* **2001,** *123,* 8701–8708. doi:10.1021/ja0034388

37. Hernández, J. G.; Juaristi, E. *J. Org. Chem.* **2010,** *75,* 7107–7111. doi:10.1021/jo101159a

38. Tabasso, S.; Carnaroglio, D.; Calcio Gaudino, E.; Cravotto, G. *Green Chem.* **2015,** *17,* 684–693. doi:10.1039/C4GC01545B

39. Eagling, R., Ed. *Mechanochemistry: From Functional Solids to Single Molecule;* Faraday Discussions of the Chemical Society, Vol. 170; Royal Society of Chemistry: Cambridge, UK, 2014.

40. Humphry-Baker, S. A.; Garroni, S.; Delogu, F.; Schuh, C. A. *Nat. Mater.* **2016,** *15,* 1280–1286. doi:10.1038/nmat4732

41. Cravotto, G.; Calcio Gaudino, E. Oxidation and reduction by solid oxidants and reducing agents using ball milling. In *Ball Milling Towards Green Synthesis: Applications, Projects, Challenges;* Ranu, B. C.; Stolle, A., Eds.; Royal Society of Chemistry: Cambridge, UK, 2014.

42. James, S. L.; Adams, C. J.; Bolm, C.; Braga, D.; Collier, P.; Friščić, T.; Grepioni, F.; Harris, K. D. M.; Hyett, G.; Jones, W.; Krebs, A.; Mack, J.; Maini, L.; Orpen, A. G.; Parkin, I. P.; Shearouse, W. C.; Steed, J. W.; Waddell, D. C. *Chem. Soc. Rev.* **2012,** *41,* 413–447. doi:10.1039/C1CS15171A

43. Margetic, D.; Štrukil, V. *Mechanochemical Organic Synthesis;* Elselvier: Amsterdam, 2016.

44. Friščić, T.; Childs, S. L.; Rizvi, S. A. A.; Jones, W. *CrystEngComm* **2009,** *11,* 418–426. doi:10.1039/B815174A

45. Hasa, D.; Miniussi, E.; Jones, W. *Cryst. Growth Des.* **2016,** *16,* 4582–4588. doi:10.1021/acs.cgd.6b00682

46. Rodriguez, B.; Bruckmann, A.; Rantanen, T.; Bolm, C. *Adv. Synth. Catal.* **2007,** *349,* 2213–2233. doi:10.1002/adsc.200700252

47. Stolle, A.; Szuppa, T.; Leonhardt, S. E. S.; Ondruschka, B. *Chem. Soc. Rev.* **2011,** *40,* 2317–2329. doi:10.1039/c0cs00195c

48. Tan, D.; Loots, L.; Friščić, T. *Chem. Commun.* **2016,** *52,* 7760–7781. doi:10.1039/C6CC02015A

49. Wang, G.-W. *Chem. Soc. Rev.* **2013,** *42,* 7668–7700. doi:10.1039/C3CS35526H

50. Cravotto, G.; Garella, D.; Carnaroglio, D.; Calcio Gaudino, E.; Rosati, O. *Chem. Commun.* **2012,** *48,* 11632–11634. doi:10.1039/c2cc36365h

51. Stolle, A.; Ranu, B., Eds. *Ball Milling Towards Green Synthesis: Applications, Projects, Challenges;* The Royal Society of Chemistry: Cambridge, 2015.

52. Hernández, J. G.; Friščić, T. *Tetrahedron Lett.* **2015,** *56,* 4253–4265. doi:10.1016/j.tetlet.2015.03.135

53. Machuca, E.; Juaristi, E.; Brindaban, R.; Stolle, A. *Asymmetric Organocatalytic Reactions Under Ball Milling. Ball Milling Towards Green Synthesis: Applications, Projects, Challenges;* Royal Society of Chemistry: Cambridge, UK, 2015; pp 81–95.

54. Hernández, J. G.; Frings, M.; Bolm, C. *ChemCatChem* **2016,** *8,* 1769–1772. doi:10.1002/cctc.201600455

55. Mocci, R.; De Luca, L.; Delogu, F.; Porcheddu, A. *Adv. Synth. Catal.* **2016,** *358,* 3135–3144. doi:10.1002/adsc.201600350

56. Gaspa, S.; Porcheddu, A.; Valentoni, A.; Garroni, S.; Enzo, S.; De Luca, L. *Eur. J. Org. Chem.* **2017.** doi:10.1002/ejoc.201700689

57. Hernández, J. G.; Bolm, C. *J. Org. Chem.* **2017,** *82,* 4007–4019. doi:10.1021/acs.joc.6b02887

58. Do, J.-L.; Friščić, T. *ACS Cent. Sci.* **2017,** *3,* 13–19. doi:10.1021/acscentsci.6b00277

59. Takacs, L. *Chem. Soc. Rev.* **2013,** *42,* 7649–7659. doi:10.1039/c2cs35442j

60. Boldyreva, E. *Chem. Soc. Rev.* **2013,** *42,* 7719–7738.
    doi:10.1039/C3CS60052A
61. Baláž, P.; Achimovičová, M.; Baláž, M.; Billik, P.;
    Cherkezova-Zheleva, Z.; Criado, J. M.; Delogu, F.; Dutková, E.;
    Gaffet, E.; Gotor, F. J.; Kumar, R.; Mitov, I.; Rojac, T.; Senna, M.;
    Streletskii, A.; Wieczorek-Ciurowa, K. *Chem. Soc. Rev.* **2013,** *42,*
    7571–7637. doi:10.1039/c3cs35468g
62. Friščić, T.; Jones, W. *Cryst. Growth Des.* **2009,** *9,* 1621–1637.
    doi:10.1021/cg800764n
63. Friščić, T. *Chem. Soc. Rev.* **2012,** *41,* 3493–3510.
    doi:10.1039/c2cs15332g
64. Sahoo, P. K.; Bose, A.; Mal, P. *Eur. J. Org. Chem.* **2015,** 6994–6998.
    doi:10.1002/ejoc.201501039
    In 2015, Mal et al. reported the first example of a very interesting
    solvent free ball-milling oxidation of activated primary alcohols to
    aldehyde using NBS (1.5 equiv) or oxone (0.6 equiv) as co-oxidising
    agents. This paper has laid the foundation for further studies on this
    topic.
65. Rightmire, N. R.; Hanusa, T. P. *Dalton Trans.* **2016,** *45,* 2352–2362.
    doi:10.1039/C5DT03866A
    The formalism for mechanochemically activated reactions was
    proposed here.
66. Lanzillotto, M.; Konnert, L.; Lamaty, F.; Martinez, J.; Colacino, E.
    ACS Sustainable Chem. Eng. **2015,** *3,* 2882–2889.
    doi:10.1021/acssuschemeng.5b00819
67. Konnert, L.; Lamaty, F.; Martinez, J.; Colacino, E. *J. Org. Chem.* **2014,**
    79, 4008–4017. doi:10.1021/jo500463y
68. Konnert, L.; Gauliard, A.; Lamaty, F.; Martinez, J.; Colacino, E.
    ACS Sustainable Chem. Eng. **2013,** *1,* 1186–1191.
    doi:10.1021/sc4001115
69. Rogan, L.; Hughes, N. L.; Cao, Q.; Dornan, L. M.; Muldoon, M. J.
    Catal. Sci. Technol. **2014,** *4,* 1720–1725. doi:10.1039/C4CY00219A

License and Terms

Main group mechanochemistry

Agota A. Gečiauskaitė and Felipe García[*]

Review

Abstract

Over the past decade, mechanochemistry has emerged as a powerful methodology in the search for sustainable alternatives to conventional solvent-based synthetic routes. Mechanochemistry has already been successfully applied to the synthesis of active pharmaceutical ingredients (APIs), organic compounds, metal oxides, coordination compounds and organometallic complexes. In the main group arena, examples of synthetic mechanochemical methodologies, whilst still relatively sporadic, are on the rise. This short review provides an overview of recent advances and achievements in this area that further validate mechanochemistry as a credible alternative to solution-based methods for the synthesis of main group compounds and frameworks.

Introduction

The original mainspring for the current expansion of solid state methodologies is the need for cleaner, safer and sustainable chemical transformations – particularly since raw materials are becoming ever scarcer. A straightforward strategy to addressing the above is to simply remove or minimise solvent usage throughout any designated synthetic routes. One way to achieve a solvent-free, or nearly solvent-free, synthetic route is via the use of solid-state mechanochemical methodologies. Mechanochemistry [1-10] is an emerging solid state methodology involving the use of little or no solvent, with the potential to challenge the current dominance of 'wet' chemical synthesis [11-15]. From a purely synthetic point of view, it is clear that complete eradication of solvents might not be entirely beneficial.

Solvents ameliorate reactant interactions, control reaction rates, and aid heat dispersion in exothermic reactions inter alia. Needless to say, solvents are necessary for the extraction, separation, and purification of the final products and/or reaction intermediates [16], which are not always attainable by solvent-free methods [17]. However, the benefits associated with solvent-free or nearly solvent-free synthetic routes are becoming increasingly difficult to deny [11-13], even in the eyes of the most sceptical synthetic chemist.

Mechanochemistry is defined as the field of reactions caused by mechanochemical forces (e.g., compression, shear or friction) [18,19]. Examples of mechanochemical methods are manual

and ball-milling grinding techniques [20-22]. Traditional manual mortar and pestle grinding methods are susceptible to variable factors, both human and environmental [23]. In contrast, modern milling technologies address these issues through the use of enclosed solvent-free reaction environments and well-defined experimental conditions throughout the mechanochemical process [24,25]. Amongst the commercially available ball milling designs [23,24], shaker and planetary mills are the most common mechanochemical apparatuses employed in synthetic laboratories [7,16,26,27].

The energy input may be adjusted by modifying parameters including milling time and frequency. Of equal importance in the reaction design is the choice of milling media (i.e., the milling jar loaded with one or more ball bearings). For example, milling balls made from denser materials (e.g., 2.3 g·cm^{-3} vs 15.6 g·cm^{-3} for Teflon and tungsten carbide, respectively) carry greater kinetic energy during the milling progress. The potential for metal leaching [28], rates of wearing [25], and/or promoting chemical reactions [9,29-33] must also be taken into account when selecting appropriate milling media. In addition to variable mechanical and milling media parameters, an alternative approach to controlling the mechanochemical process is via the use of small amounts of liquid and/or solid additives, termed ion- and liquid-assisted (ILAG) or liquid-assisted grinding (LAG), respectively [34,35]. These techniques, in contrast to "dry" milling, often offer advantages such as shorter reaction times and/or greater product selectivity [36].

In traditional solution-based methods, appropriate selection of solvent, temperature and reaction time will determine whether an intended chemical reaction proceeds, to what extent, and the rate at which it does so. In approaching the same chemical reaction by a mechanochemical route, an alternative set of parameters is fine-tuned to optimise reaction conditions (see Scheme 1). Such differences may have the capacity to create unique reactivity patterns and/or access to otherwise unattainable products [11-15].

Although often considered novel, in its broadest terms, mechanochemistry dates back two millennia [20,37,38]. However, it was not until the 19th century that associations between mechanical forces and chemical reactivity were drawn [39-45], and a century later the currently accepted definition of mechanochemistry was proposed [46]. Since then, and during the last 25 years, mechanochemical methods have been applied to various fields, including catalysis [47], organic synthesis [5,7,48,49], metal-organic frameworks (MOFs) [50,51], coordination [52], organometallic [11], supramolecular [53], environmental [54,55], APIs [56], medicinal [57], nanoscience [15], polymer [58-60] and enzymatic chemistry [61]. The recent advances made in mechanochemistry provide an exciting platform for synthetic chemists in the search of novel outcomes and optimal synthetic routes (see Scheme 2).

Review
Main group mechanochemistry
Whilst mechanochemical studies have become increasingly popular (with recent reviews on mechanochemical synthesis by Rightmire and Hanusa [11], Do and Friščić [12], Hernández and Bolm [13], Wang [14], and James et al. [2]) there are relatively few studies concerning main group elements.

Scheme 1: Variables associated with ball-milling (left) and solvent-based methodologies (right).

Scheme 2: Examples of mechanochemically produced species (a [48], b [62], c [63], d [64], e [65], f [66], g [67], h [68]). The symbol for mechano-chemical reactivity proposed by Hanusa et al. [11] is shown centrally.
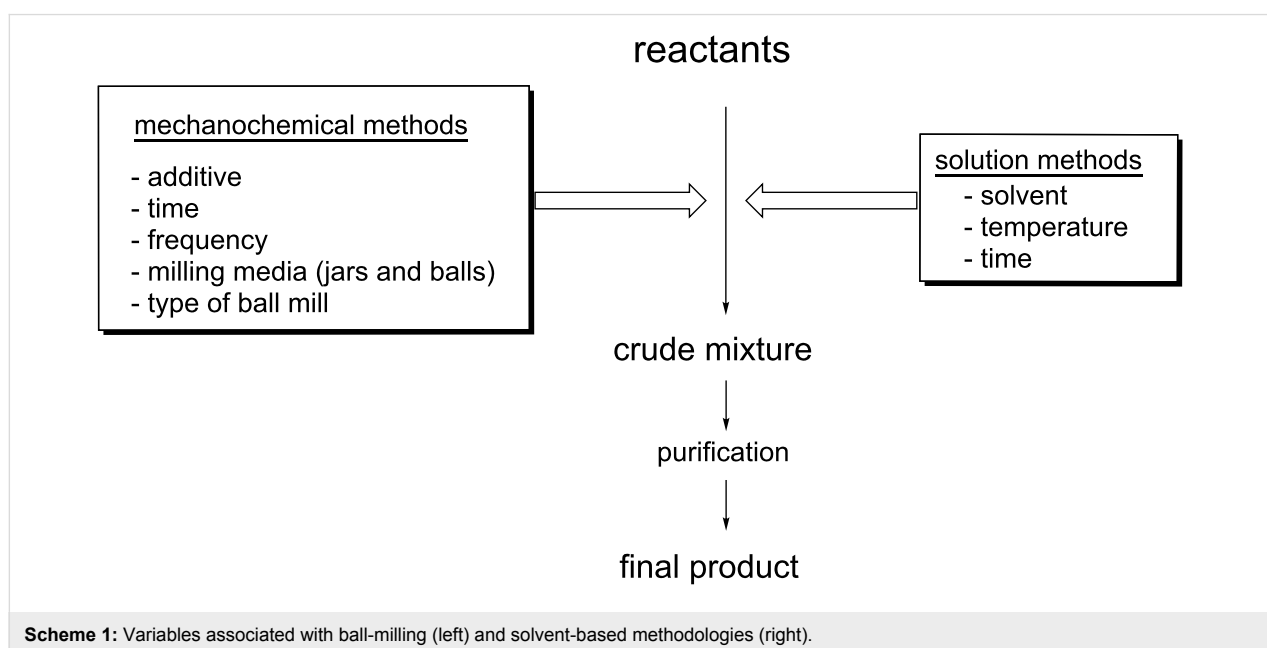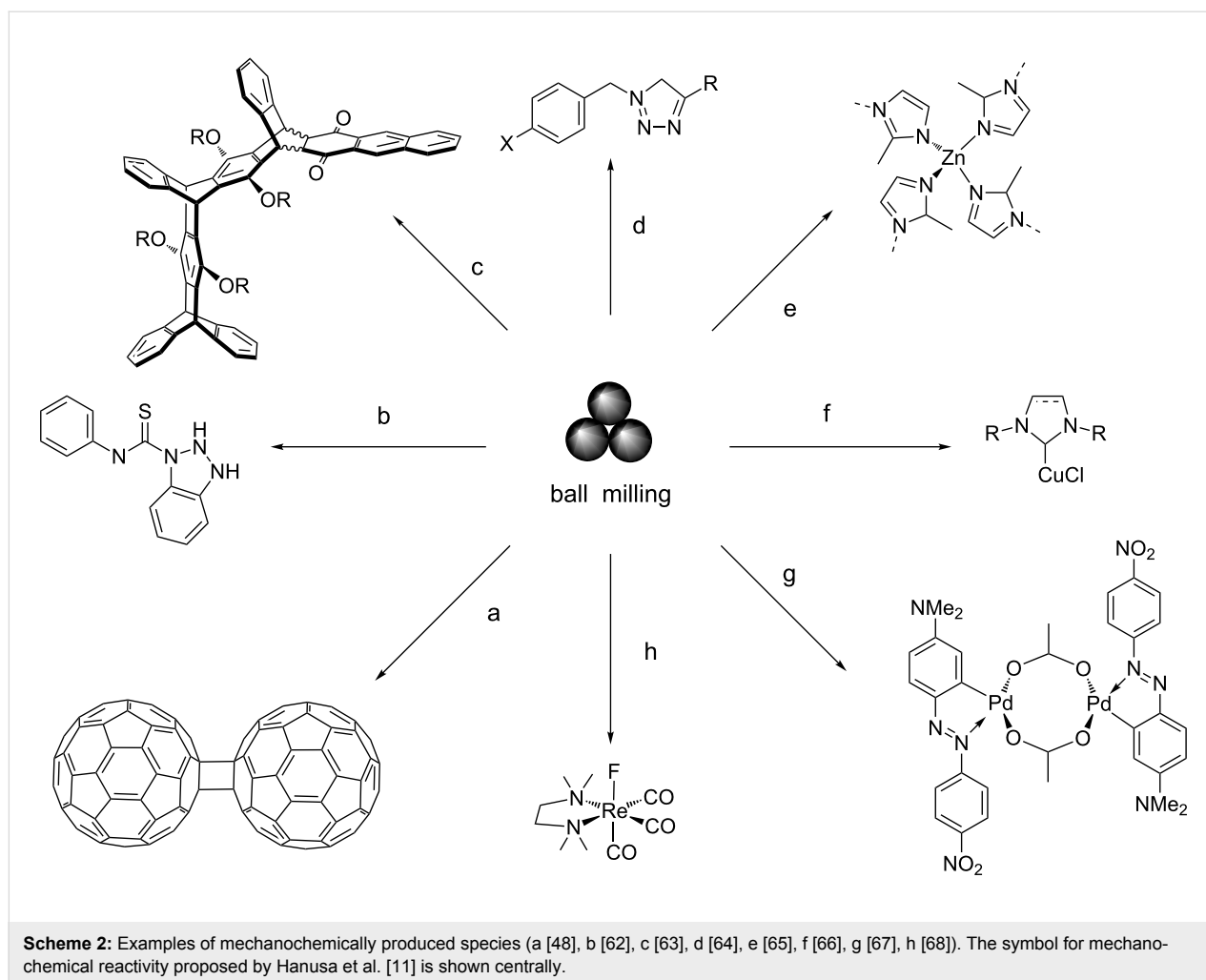
The development of new and novel main group frameworks and compounds is pivotal to shaping chemistry as a discipline, in addition to advancing neighbouring fields such as biomedical, materials and engineering sciences [69]. Moreover, main group compounds represent a large proportion of all commercial inorganic chemicals (ammonia, silicones, etc.) [70], and recent advances continue to propel the importance of this field in the 21st century [71]. For instance, developments in fundamental main group chemistry are pivotal in providing the necessary knowledge and tools for the more sustainable chemical processes, from "blue-skies" to applied research and, eventually, integration into industrial processes.

Herein, we aim to provide an overview of recent advances in this area and an outlook on future directions within the realm of main group molecular systems.

Developments in the area of materials science have already demonstrated benefits of implementing mechanochemical methods [72]. In the context of main group compounds, recent studies have highlighted efficient routes to: (i) alkaline earth carbides and their intercalation compounds, including the first successful synthesis of Mg_2C_3 from its elements [73,74]; (ii) nanomaterials, where main group elements act either as a matrix or a dopant, for catalytic applications [75,76]; and (iii) MOFS containing alkaline earth metals [77,78].

Of particular note are the high yielding syntheses of non-solvated AlH_3 from $LiAlH_4$ and $AlCl_3$ under mild conditions, and kinetic studies on the synthesis of alkaline-earth metal amides. These compounds – promising candidates for fuel-cell technologies based on chemically stored hydrogen – highlight the potential of such syntheses in the development of clean energy solutions [79,80].

Within the area of molecular synthesis, the handful of reported examples fall into two general categories, those that provide enhanced synthetic routes, and those that provide novel synthetic outcomes [81].

Mechanochemical enhanced synthesis

Optimising the route to a desired reaction product is a principle priority of synthetic chemists, and ball milling often offers attractive opportunities to do so.

In the field of organometallic chemistry, we highlight the large-scale synthesis of SrCp′$_2$(OEt$_2$) (Cp′ = C$_5$Me$_4$(*n*-Pr)) (**1**) [82], an ideal precursor for the chemical vapour deposition (CVD) of strontium-based semiconductors – a key material in memory devices [83]. Previously, this compound could only be obtained in small-scale via salt metathesis reactions due to poor starting material (SrI$_2$ and K[Cp′]) solubility in ether solution. LAG provides a high yielding synthetic methodology circumventing the scalability issues associated with the inefficient diffusion of reactants in large-scale solution-based methods (see Scheme 3).·

Scheme 3: Mechanochemical synthesis of SrCp′$_2$(OEt$_2$) (Cp′ = C$_5$Me$_4$(*n*-Pr)).
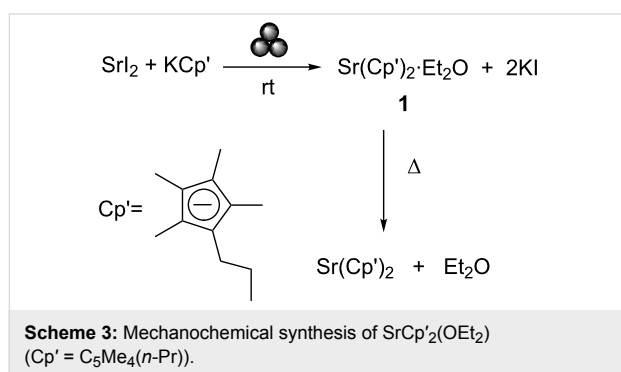
Also noteworthy is the multistep solvent-free mechanochemical route to indium(III) complexes featuring aryl bis(imino)acenaphthene (Ar-BIAN) ligands [84]. Ar-BIAN ligands are versatile π-acceptors and have been widely em-

ployed for catalysis. These ligands are typically synthesised by condensation reactions between acenaphthoquinone and the corresponding aniline derivative under acidic conditions, involving the use of transition-metal templates [85]. The acid-catalysed ball-milling of acenaphthoquinone with aniline derivatives in the presence of an organic catalyst was able to produce the desired Ar-BIAN ligands **2** and **3**, respectively, in good yields (see Scheme 4). Here, mechanochemistry bypasses the use of templating agent transition metals, shortening the synthetic route and reducing its environmental impact. Their respective indium(III) BIAN complexes **4** and **5** were also obtained by further milling equimolar quantities of the relevant BIAN ligand (**2** and **3**, respectively) and InCl$_3$. Performing both reactions at 180 °C in the same reaction vessel without milling lead to thermal decomposition, illustrating the requirement of mechanochemical forces for successful reaction completion. A rare example of a one-pot multistep ball milling reaction is the case of an electron-rich aniline derivative that produced **4** in good yield without the need for ligand isolation. Previously reported examples typically employ "preformed" ligands and metal complexes [68,86], raising the orthogonality of multistep mechanochemical synthesis and widening its applicability.

A significant example of the transformative potential of mechanochemistry is its ability to produce metal complexes directly from bulk metal or metal oxides [66]. Within this context, the LAG synthesis of germanes (GeR$_4$) directly from germanium metal or germanium dioxide (GeO$_2$) was recently reported [87]. Milling of germanium powder or GeO$_2$ with quinone or catechol, respectively, in the presence of a Lewis base under LAG conditions, produced a series of germanium complexes (see Scheme 5). These complexes are inherently

Scheme 4: Mechanochemical synthesis of the Ar-BIAN ligands and indium(III) complexes (top). One-pot synthesis of an indium complex (bottom).

Scheme 5: Synthesis of germanes from germanium (Ge) or germanium oxide (GeO$_2$).
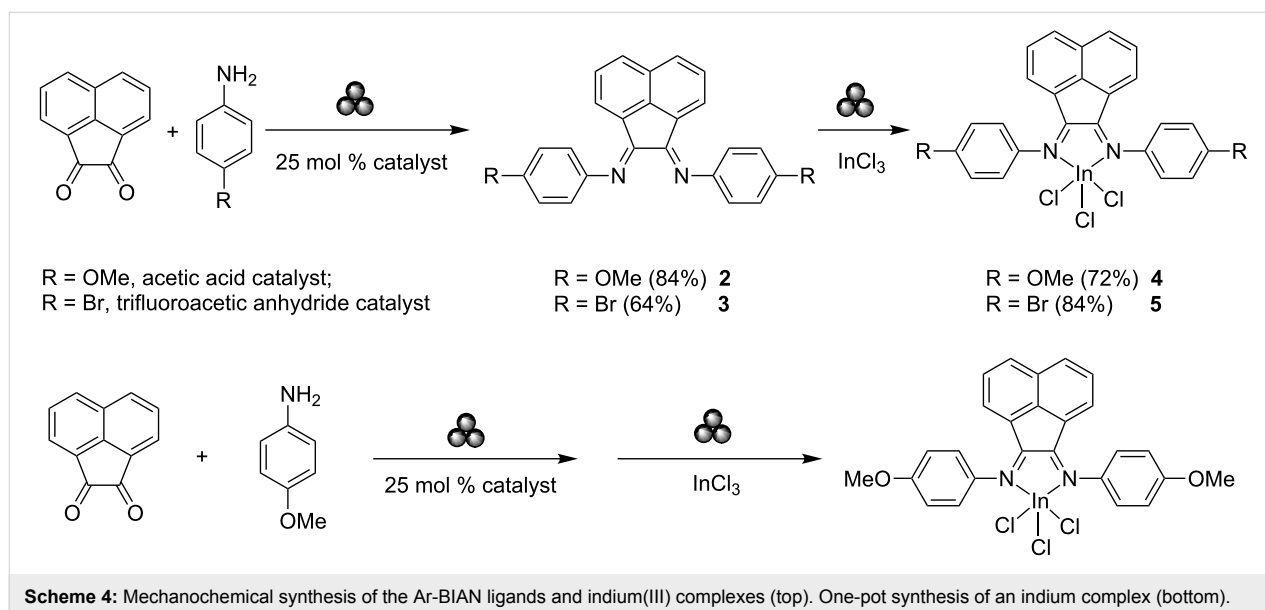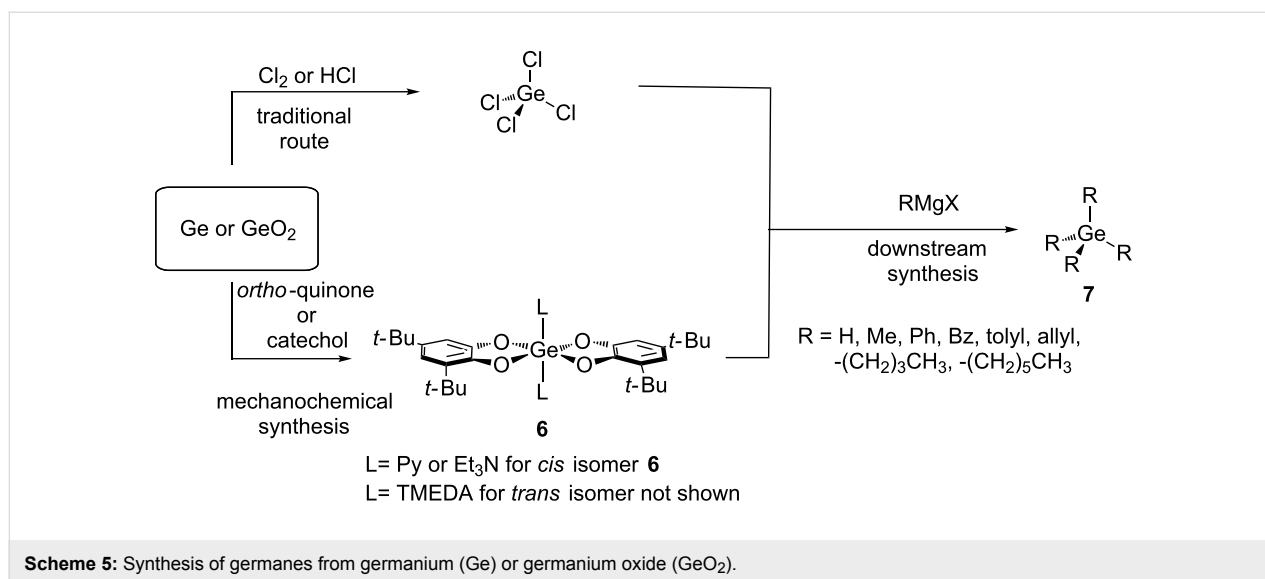
versatile, capable of acting as chemical intermediates for the downstream synthesis of germanes **7**, thus providing a sustainable alternative to the use of GeCl$_4$. Notably, this method can generate highly pure GeH$_4$ for CVD applications under room temperature conditions [88,89].

In addition to organometallics, mechanochemistry has emerged as a technique with great promise for the construction of frameworks based on non-carbon backbones [90], such as those of the phosphazane family [91]. The unique chemical versatility of

these P–N frameworks – provided by the diversity of their topological arrangements – provides potential in numerous applications [92]. However, these species remain typically arduous to synthesize and isolate, since phosphazane arrangements are generally highly air- and moisture-sensitive [93,94], and their halogenated precursors are incompatible with protic solvents. Mechanochemistry therefore offers an elegant synthetic route by circumventing solvent compatibility issues, the tedious processes associated with the use of strict anhydrous solvents, and by minimizing unwanted side-products (see Scheme 6) [95].

Scheme 6: Ball-milling nucleophilic substitution reactions to produce acyclic and cyclic cyclodiphosphazanes.
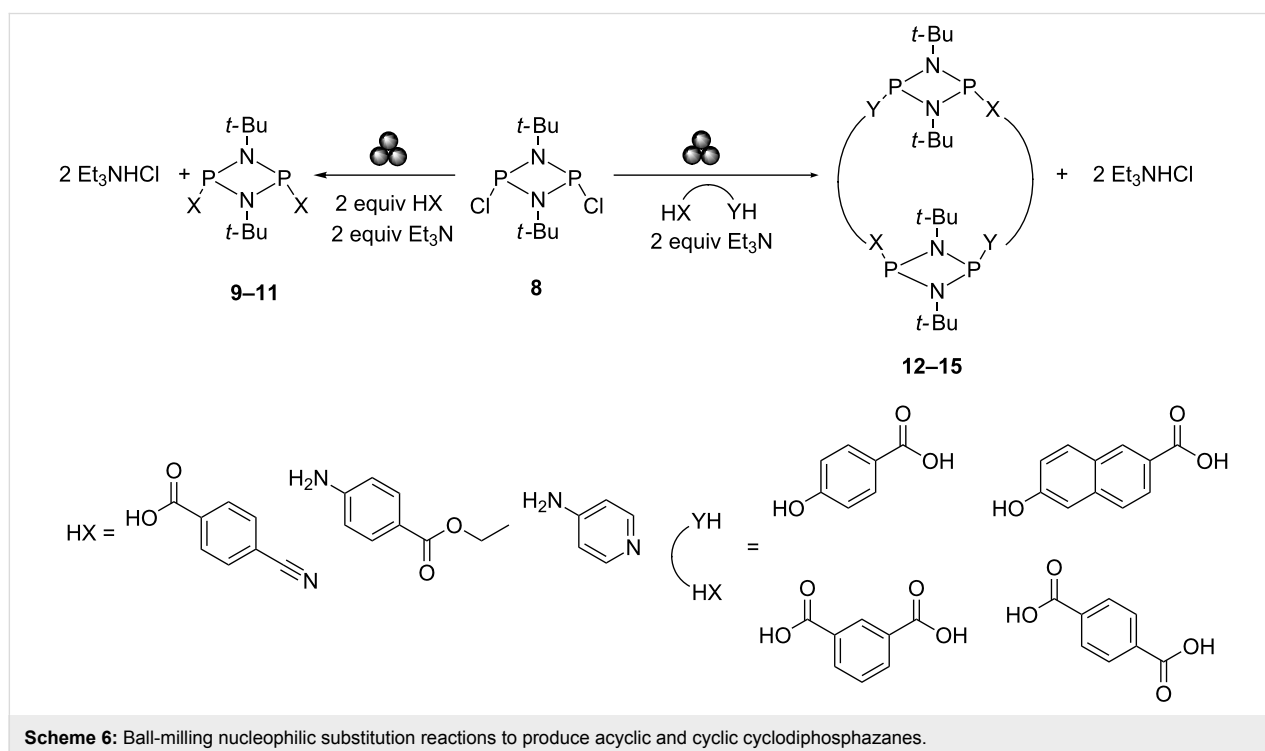
Mechanochemistry picks the lock

The capacity of mechanochemistry to produce unique reaction outcomes and/or product distributions, compared to those obtained by solution-based methods, is an exciting feat [62,96].

Hanusa et al. reported the successful application of ball-milling for the synthesis of an elusive [97] unsolvated tris(allyl)aluminium complex [98]. Grinding 1,3-bis(trimethylsilyl)allylpotassium salt with AlX_3 (X = Cl, Br, I) produced the desired unsolvated product **16** in high yields and on multigram scales. Remarkably, the synthesis of this long sought-after compound was carried out in a simple set-up, consisting of a round bottom flask loaded with steel ball bearings, connected to a rotatory evaporator as a milling device [99]. Compound **16** displays a higher reactivity than its solvated counterparts, attributed to the coordinatively unsaturated Al centre (i.e., three-coordinate Al). Only in the absence of solvents can this be achieved.

Similar studies using group 15 halides (AsI_3 and $SbCl_3$) have shown that selection of solution or mechanochemical conditions influence product stereoisomer distributions. In this case, the mechanochemical route increases the C_1:C_3 stereoisomer ratio in complexes **17** and **18** for As and Sb, respectively (see Scheme 7) [100]. The ability to manipulate isomeric distribution outcomes offers obvious advantages in the application of synthetic mechanochemistry to pharmaceutical and catalysis industries.

Returning to phosphazane chemistry, the structure of the P–N backbone is controlled by steric factors, a textbook example of which being the adamantoid $P_4(NR)_6$ frameworks. These species are synthesised by direct reaction of PCl_3 with steri-

cally unhindered amines RNH_2 (R= Me, Et, iPr, Bz) [101] or by isomerization of their less thermodynamically-stable macrocyclic $[\{P(\mu\text{-}NR)\}_2(\mu\text{-}NR)]_2$ counterparts. In the latter, the isopropyl (iPr) substituted macrocycle $[\{P(\mu\text{-}NiPr)_2\}_2(\mu\text{-}NiPr)]_2$ **19** readily isomerises into the adamantoid framework, $P_4(NiPr)_6$ **20**, upon heating [102]. The non-viability of the *tert*-butyl (*t*-Bu) substituted adamantoid framework [103] has been rationalised on steric grounds, due to its highly sterically-encumbered nature [103-105]. ILAG milling of $[\{P(\mu\text{-}Nt\text{-}Bu)_2\}_2(\mu\text{-}Nt\text{-}Bu)]_2$ **21** in the presence of LiCl readily yielded the adamantoid $P_4(Nt\text{-}Bu)_6$ **22** after 90 min, in strong contrast to previous efforts involving prolonged heating (24 days at 150 °C) or under reflux in a range of solvents with identical amounts of salt additive (see Scheme 8). The ease of this transformation by ball milling illustrates the potential of such approaches towards established chemical syntheses [106].

Conclusion

The use and study of mechanochemical methods have expanded rapidly over the last two decades, and continues to progress as a well-established area of research within chemical and materials sciences. Whilst the synthetic potential of the ball-milling concept has, in our opinion, become indisputable, advancing from representing an anecdotic alternative to solution-based methods, towards becoming a universally adopted methodology by the main group community remains a considerable challenge [69]. Advancement of our current mechanistic understanding of mechanochemical methods is essential if we are to incorporate it as a mainstream tool for synthetic and materials chemists alike [77,107-111]. Theoretical and systematic studies that elucidate the kinetic and thermodynamic driving forces of mechanochemical reactions are undergoing and will be impera-

compound	solution C_1:C_3	ball-milling C_1:C_3
17	71:29	60:40
18	68:32	24:76

Scheme 7: Mechanochemical reactions of potassium 1,3-bis(trimethylsillylallyl) with group 13 (top) and 15 (bottom) halides.
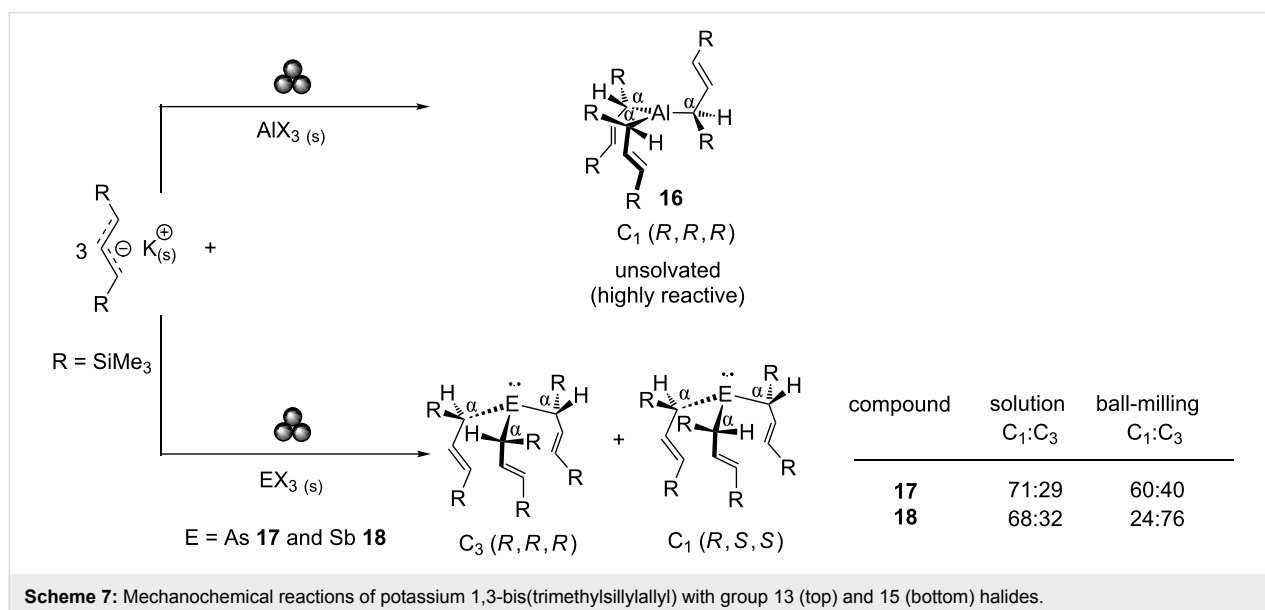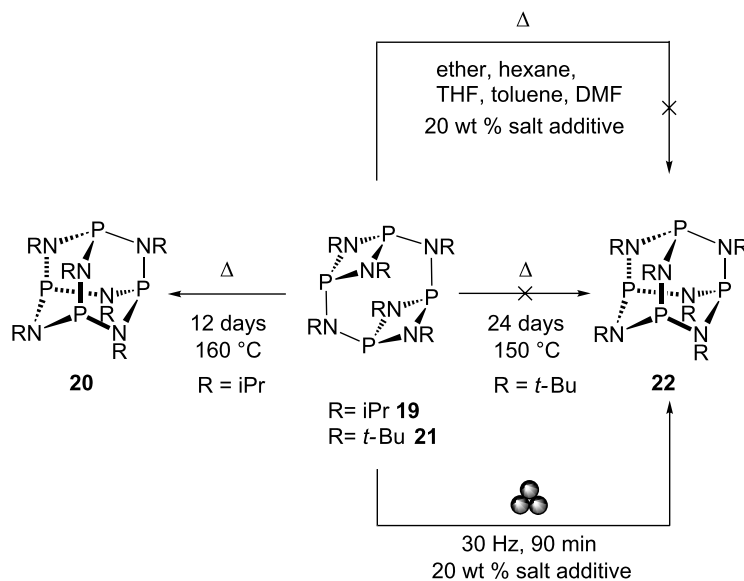
Scheme 8: Synthesis of adamantoid phosphazane framework from its double-decker isomer for R = iPr and *t*-Bu (left and right, respectively).

tive to achieving this goal [106,112-114]. Areas in which we anticipate mechanochemistry will show particular strength in: (i) the synthesis of highly air- and moisture-sensitive compounds, since many are incompatible with a wide range of protic solvents [95]; and (ii) the synthesis of unsolvated species, where chemical reactivity might be hindered by the presence of strongly bound solvent molecules within their coordination sphere [98].

In this short review, we have presented basic underlying concepts followed by recent advances and highlights of mechanochemistry in the context of main group synthesis with the hope of encouraging and accelerating the endorsement of mechanochemistry by the main group and wider synthetic communities.

Acknowledgements

References

1. Mechanochemistry is herein considered within the context of transformations conducted by bulk milling or grinding. This area of mechanochemical research is distinct from the popular use of ultrasonic irradiation for transformations of mechanophores embedded in polymer chains or studies of individual molecules using atomic force spectroscopy.

2. James, S. L.; Adams, C. J.; Bolm, C.; Braga, D.; Collier, P.; Friščić, T.; Grepioni, F.; Harris, K. D. M.; Hyett, G.; Jones, W.; Krebs, A.; Mack, J.; Maini, L.; Orpen, A. G.; Parkin, I. P.; Shearouse, W. C.; Steed, J. W.; Waddell, D. C. *Chem. Soc. Rev.* **2012,** *41,* 413–447. doi:10.1039/C1CS15171A

3. Boldyreva, E. *Chem. Soc. Rev.* **2013,** *42,* 7719–7738. doi:10.1039/c3cs60052a

4. Braga, D.; Maini, L.; Grepioni, F. *Chem. Soc. Rev.* **2013,** *42,* 7638–7648. doi:10.1039/c3cs60014a

5. Stolle, A.; Szuppa, T.; Leonhardt, S. E. S.; Ondruschka, B. *Chem. Soc. Rev.* **2011,** *40,* 2317–2329. doi:10.1039/c0cs00195c

6. Friščić, T. *Chem. Soc. Rev.* **2012,** *41,* 3493–3510. doi:10.1039/c2cs15332g

7. Rodríguez, B.; Bruckmann, A.; Rantanen, T.; Bolm, C. *Adv. Synth. Catal.* **2007,** *349,* 2213–2233. doi:10.1002/adsc.200700252

8. Zhu, S.-E.; Li, F.; Wang, G.-W. *Chem. Soc. Rev.* **2013,** *42,* 7535–7570. doi:10.1039/c3cs35494f

9. Chen, L.; Lemma, B. E.; Rich, J. S.; Mack, J. *Green Chem.* **2014,** *16,* 1101–1103. doi:10.1039/C3GC41847B

10. Mottillo, C.; Friščić, T. *Molecules* **2017,** *22,* 144. doi:10.3390/molecules22010144

11. Rightmire, N. R.; Hanusa, T. P. *Dalton Trans.* **2016,** *45,* 2352–2362. doi:10.1039/C5DT03866A

12. Do, J.-L.; Friščić, T. *ACS Cent. Sci.* **2017,** *3,* 13–19. doi:10.1021/acscentsci.6b00277

13. Hernández, J. G.; Bolm, C. *J. Org. Chem.* **2017,** *82,* 4007–4019. doi:10.1021/acs.joc.6b02887

14. Wang, G.-W. *Chem. Soc. Rev.* **2013,** *42,* 7668–7700. doi:10.1039/c3cs35526h

15. Baláž, P.; Achimovičová, M.; Baláž, M.; Billik, P.; Cherkezova-Zheleva, Z.; Criado, J. M.; Delogu, F.; Dutková, E.; Gaffet, E.; Gotor, F. J.; Kumar, R.; Mitov, I.; Rojac, T.; Senna, M.; Streletskii, A.; Wieczorek-Ciurowa, K. *Chem. Soc. Rev.* **2013,** *42,* 7571–7637. doi:10.1039/c3cs35468g

16. Tanaka, K. *Solvent-free Organic Synthesis,* 2nd ed.; Wiley-VCH: Weinheim, 2009.

17. Friščić, T.; Julien, P. A.; Mottillo, C. Environmentally-Friendly Designs and Syntheses of Metal-Organic Frameworks (MOFs). *Green Technologies for the Environment; ACS Symposium Series*, Vol. 1186; American Chemical Society, 2014; pp 161–183.

18. Horie, K.; Barón, M.; Fox, R. B.; He, J.; Hess, M.; Kahovec, J.; Kitayama, T.; Kubisa, P.; Maréchal, E.; Mormann, W.; Stepto, R. F. T.; Tabak, D.; Vohlídal, J.; Wilks, E. S.; Work, W. J. *Pure Appl. Chem.* **2004,** *76,* 889–906. doi:10.1351/pac200476040889

19. Fernández-Bertran, J. F. *Pure Appl. Chem.* **1999,** *71,* 581–586. doi:10.1351/pac199971040581

20. Takacs, L. *Chem. Soc. Rev.* **2013,** *42,* 7649–7659. doi:10.1039/c2cs35442j

21. Kipp, S.; Šepelák, V.; Becker, K. D. *Chem. Unserer Zeit* **2005,** *39,* 384–392. doi:10.1002/ciuz.200500355

22. Stolle, A.; Schmidt, R.; Jacob, K. *Faraday Discuss.* **2014,** *170,* 267–286. doi:10.1039/C3FD00144J

23. Schmidt, R.; Burmeister, C. F.; Baláž, M.; Kwade, A.; Stolle, A. *Org. Process Res. Dev.* **2015,** *19,* 427–436. doi:10.1021/op5003787

24. Baláž, P. *Mechanochemistry in Nanoscience and Minerals Engineering;* Springer-Verlag: Berlin, 2008.

25. Burmeister, C. F.; Kwade, A. *Chem. Soc. Rev.* **2013,** *42,* 7660–7667. doi:10.1039/c3cs35455e

26. Gorrasi, G.; Sorrentino, A. *Green Chem.* **2015,** *17,* 2610–2625. doi:10.1039/C5GC00029G

27. Martins, M. A. P.; Frizzo, C. P.; Moreira, D. N.; Buriol, L.; Machado, P. *Chem. Rev.* **2009,** *109,* 4140–4182. doi:10.1021/cr9001098

28. Štefanić, G.; Krehula, S.; Štefanić, I. *Chem. Commun.* **2013,** *49,* 9245–9247. doi:10.1039/c3cc44803g

29. Rak, M. J.; Saadé, N. K.; Friščić, T.; Moores, A. *Green Chem.* **2014,** *16,* 86–89. doi:10.1039/C3GC41827H

30. Fulmer, D. A.; Shearouse, W. C.; Medonza, S. T.; Mack, J. *Green Chem.* **2009,** *11,* 1821–1825. doi:10.1039/b915669k

31. Cook, T. L.; Walker, J. A., Jr.; Mack, J. *Green Chem.* **2013,** *15,* 617–619. doi:10.1039/c3gc36720g

32. Tan, D.; Štrukil, V.; Mottillo, C.; Friščić, T. *Chem. Commun.* **2014,** *50,* 5248–5250. doi:10.1039/C3CC47905F

33. Sawama, Y.; Kawajiri, T.; Niikawa, M.; Goto, R.; Yabe, Y.; Takahashi, T.; Marumoto, T.; Itoh, M.; Kimura, Y.; Monguchi, Y.; Kondo, S.-i.; Sajiki, H. *ChemSusChem* **2015,** *8,* 3773–3776. doi:10.1002/cssc.201501019

34. Friščić, T.; Childs, S. L.; Rizvi, S. A. A.; Jones, W. *CrystEngComm* **2009,** *11,* 418–426. doi:10.1039/B815174A

35. Friščić, T.; Reid, D. G.; Halasz, I.; Stein, R. S.; Dinnebier, R. E.; Duer, M. J. *Angew. Chem., Int. Ed.* **2010,** *49,* 712–715. doi:10.1002/anie.200906583

36. Bowmaker, G. A. *Chem. Commun.* **2013,** *49,* 334–348. doi:10.1039/C2CC35694E

37. Theophrastus wrote „On Stones" ca. 315 B.C. This book contains references to the reduction of cinnabar (a mercury ore) to mercury metal by grinding the ore in a copper mortar and pestle.

38. Takacs, L. *JOM* **2000,** *52,* 12–13. doi:10.1007/s11837-000-0106-0

39. Faraday, M. *Q. J. Sci., Lit., Arts* **1820,** *8,* 374–376.

40. Lea, M. C. *Br. J. Photogr.* **1866,** *13,* 84.

41. Lea, M. C. *Am. J. Sci.* **1893,** *46,* 413–420. doi:10.2475/ajs.s3-46.276.413

42. Ling, A. R.; Baker, J. L. *J. Chem. Soc., Trans.* **1893,** *63,* 1314. doi:10.1039/CT8936301314

43. Takacs, L. *J. Therm. Anal. Calorim.* **2007,** *90,* 81–84. doi:10.1007/s10973-007-8479-8

44. The term "mechanochemistry" was first introduced by Wilhelm Ostwald in the Textbook of General Chemistry in 1891, where mechanochemistry was considered as a part of physical chemistry such as thermochemistry, electrochemistry.

45. Ostwald, W. *Handbuch der Allgemeinen Chemie;* Akademische Verlagsgesellschaft mbH: Leipzig, 1919; Vol. 1.

46. Heinicke, G. *Tribochemistry;* Akademie Verlag: Berlin, 1984.

47. Bruckmann, A.; Krebs, A.; Bolm, C. *Green Chem.* **2008,** *10,* 1131–1141. doi:10.1039/b812536h

48. Wang, G.-W.; Komatsu, K.; Murata, Y.; Shiro, M. *Nature* **1997,** *387,* 583–586. doi:10.1038/42439

49. Hernández, J. G.; Friščić, T. *Tetrahedron Lett.* **2015,** *56,* 4253–4265. doi:10.1016/j.tetlet.2015.03.135

50. Friščić, T. Metal-Organic Frameworks: Mechanochemical Synthesis Strategies. *Encyclopedia of Inorganic and Bioinorganic Chemistry;* Wiley: Chichester, 2014; pp 1–19. doi:10.1002/9781119951438.eibc2202

51. Lazuen-Garay, A.; Pichon, A.; James, S. L. *Chem. Soc. Rev.* **2007,** *36,* 846–855. doi:10.1039/b600363j

52. Thabet, S. K.; Tayim, H. A.; Karkanawi, M. U. *Inorg. Nucl. Chem. Lett.* **1972,** *8,* 211–213. doi:10.1016/0020-1650(72)80114-4

53. Hsu, C.-C.; Chen, N.-C.; Lai, C.-C.; Liu, Y.-H.; Peng, S.-M.; Chiu, S.-H. *Angew. Chem., Int. Ed.* **2008,** *47,* 7475–7478. doi:10.1002/anie.200803056

54. Rowlands, S. A.; Hall, A. K.; McCormick, P. G.; Street, R.; Hart, R. J.; Ebell, G. F.; Donecker, P. *Nature* **1994,** *367,* 223. doi:10.1038/367223a0

55. Nomura, Y.; Nakai, S.; Hosomi, M. *Environ. Sci. Technol.* **2005,** *39,* 3799–3804. doi:10.1021/es049446w

56. Jones, W.; Eddleston, M. D. *Faraday Discuss.* **2014,** *170,* 9–34. doi:10.1039/C4FD00162A

57. Tan, D.; Loots, L.; Friščić, T. *Chem. Commun.* **2016,** *52,* 7760–7781. doi:10.1039/C6CC02015A

58. Ravnsbæk, J. B.; Swager, T. M. *ACS Macro Lett.* **2014,** *3,* 305–309. doi:10.1021/mz500098r

59. Grätz, S.; Borchardt, L. *RSC Adv.* **2016,** *6,* 64799–64802. doi:10.1039/C6RA15677K

60. Ohn, N.; Shin, J.; Kim, S. S.; Kim, J. G. *ChemSusChem* **2017,** in press. doi:10.1002/cssc.201700873

61. Hernández, J. G.; Ardila-Fierro, K. J.; Crawford, D.; James, S. L.; Bolm, C. *Green Chem.* **2017,** *19,* 2620–2625. doi:10.1039/C7GC00615B

62. Štrukil, V.; Gracin, D.; Magdysyuk, O. V.; Dinnebier, R. E.; Friščić, T. *Angew. Chem., Int. Ed.* **2015,** *54,* 8440–8443. doi:10.1002/anie.201502026

63. Zhao, Y.; Rocha, S. V.; Swager, T. M. *J. Am. Chem. Soc.* **2016,** *138,* 13834–13837. doi:10.1021/jacs.6b09011

64. Chen, L.; Bovee, M. O.; Lemma, B. E.; Keithley, K. S. M.; Pilson, S. L.; Coleman, M. G.; Mack, J. *Angew. Chem., Int. Ed.* **2015,** *54,* 11084–11087. doi:10.1002/anie.201504236

65. Katsenis, A. D.; Puškarić, A.; Štrukil, V.; Mottillo, C.; Julien, P. A.; Užarević, K.; Pham, M.-H.; Do, T.-O.; Kimber, S. A. J.; Lazić, P.; Magdysyuk, V. O.; Dinnebier, R. E.; Halasz, I.; Friščić, T. *Nat. Commun.* **2015,** *6,* No. 6662. doi:10.1038/ncomms7662

66. Beillard, A.; Metro, T.-X.; Bantreil, X.; Martinez, J.; Lamaty, F. *Chem. Sci.* **2017,** *8,* 1086–1089. doi:10.1039/C6SC03182J

67. Juribašić, M.; Užarević, K.; Gracin, D.; Ćurić, M. *Chem. Commun.* **2014,** *50,* 10287–10290. doi:10.1039/C4CC04423A

68. Hernández, J. G.; Butler, I. S.; Friščić, T. *Chem. Sci.* **2014,** *5,* 3576–3582. doi:10.1039/C4SC01252F

69. Chivers, T. *Comments Inorg. Chem.* **2009,** *30,* 131–176. doi:10.1080/02603590903385752

70. Thomson, R., Ed. *Industrial Inorganic Chemicals: Production and Uses;* The Royal Society of Chemistry: Cambridge, 1995.

71. Aldridge, S.; Jones, C. *Chem. Soc. Rev.* **2016,** *45,* 763–764. doi:10.1039/C6CS90014C

72. Xu, C.; De, S.; Balu, A. M.; Ojeda, M.; Luque, R. *Chem. Commun.* **2015,** *51,* 6698–6713. doi:10.1039/C4CC09876E

73. The alkaline earth carbide CaC$_2$ is an industrial source of acetylene, however, non-mechanochemical methods of its production were unsuitable on a commercial scale due to the requirement of maintaining a very high temperature, oxygen-free atmosphere, and use of hydrogen cyanide gas as reagent. Hence ball milling provides a more efficient and green route to these molecular species.

74. Hick, S. M.; Griebel, C.; Blair, R. G. *Inorg. Chem.* **2009,** *48,* 2333–2338. doi:10.1021/ic8022437

75. Sun, J.; Zheng, G.; Lee, H.-W.; Liu, N.; Wang, H.; Yao, H.; Yang, W.; Cui, Y. *Nano Lett.* **2014,** *14,* 4573–4580. doi:10.1021/nl501617j

76. Kim, M.-J.; Jeon, I.-Y.; Seo, J.-M.; Dai, L.; Baek, J.-B. *ACS Nano* **2014,** *8,* 2820–2825. doi:10.1021/nn4066395

77. Al-Terkawi, A.-A.; Scholz, G.; Emmerling, F.; Kemnitz, E. *Cryst. Growth Des.* **2016,** *16,* 1923–1933. doi:10.1021/acs.cgd.5b01457

78. Al-Terkawi, A.-A.; Scholz, G.; Buzanich, A. G.; Reinsch, S.; Emmerling, F.; Kemnitz, E. *Dalton Trans.* **2017,** *46,* 6003–6012. doi:10.1039/C7DT00734E

79. Gupta, S.; Kobayashi, T.; Hlova, I. Z.; Goldston, J. F.; Pruski, M.; Pecharsky, V. K. *Green Chem.* **2014,** *16,* 4378–4388. doi:10.1039/C4GC00998C

80. Garroni, S.; Takacs, L.; Leng, H.; Delogu, F. *Chem. Phys. Lett.* **2014,** *608,* 80–83. doi:10.1016/j.cplett.2014.05.071

81. To the best of our knowledge, there are no published reports of solvent removal being detrimental throughout main group molecular synthesis. For published results in the area of organometallic synthesis please see section 3.2 in ref [11].

82. Peters, D. W.; Blair, R. G. *Faraday Discuss.* **2014,** *170,* 83–91. doi:10.1039/C3FD00157A

83. Warusawithana, M. P.; Cen, C.; Sleasman, C. R.; Woicik, J. C.; Li, Y.; Kourkoutis, L. F.; Klug, J. A.; Li, H.; Ryan, P.; Wang, L.-P.; Bedzyk, M.; Muller, D. A.; Chen, L.-Q.; Levy, J.; Schlom, D. G. *Science* **2009,** *324,* 367–370. doi:10.1126/science.1169678

84. Wang, J.; Ganguly, R.; Yongxin, L.; Díaz, J.; Soo, H. S.; García, F. *Dalton Trans.* **2016,** *45,* 7941–7946. doi:10.1039/C6DT00978F

85. Ragaini, F.; Cenini, S.; Tollari, S.; Tummololillo, G.; Beltrami, R. *Organometallics* **1999,** *18,* 928–942. doi:10.1021/om980843n

86. Chow, E. H. H.; Strobridge, F. C.; Friščić, T. *Chem. Commun.* **2010,** *46,* 6368–6370. doi:10.1039/c0cc01337d

87. Glavinović, M.; Krause,, M.; Yang,, L.; McLeod, J. A.; Liu, L.; Baines, K. M.; Friščić, T.; Lumb, J.-P. *Sci. Adv.* **2017,** *3,* e1700149. doi:10.1126/sciadv.1700149

88. Rusotti, R. Methods of synthesis of gaseous germane. U.S. Patent US 4,668,502, May 26, 1987.

89. Amadoruge, M. L.; Weinert, C. S. *Chem. Rev.* **2008,** *108,* 4253–4294. doi:10.1021/cr800197r

90. Hardacre, C.; Huang, H.; James, S. L.; Migaud, M. E.; Norman, S. E.; Pitner, W. R. *Chem. Commun.* **2011,** *47,* 5846–5848. doi:10.1039/c1cc11025j

91. In this context, the term 'phosphazane' refers to phosphorus(III) derivatives unless otherwise stated.

92. Balakrishna, M. S. *Dalton Trans.* **2016,** *45,* 12252–12282. doi:10.1039/C6DT01121G

93. Scherer, O. J.; Anselmann, R.; Paine, R. T.; Karthikeyan, S. Tervalent Phosphorus–Nitrogen Ring Compounds. *Inorganic Syntheses;* John Wiley & Sons, Inc., 2007; Vol. 25, pp 7–12.

94. Shi, X. Y.; Liang, R. Z.; Martin, K. A.; Weston, N.; Gonzalez-Calera, S.; Ganguly, R.; Li, Y.; Lu, Y.; Ribeiro, A. J. M.; Ramos, M. J.; Fernandes, P. A.; García, F. *Inorg. Chem.* **2015,** *54,* 6423–6432. doi:10.1021/acs.inorgchem.5b00735

95. Sim, Y.; Shi, Y. X.; Ganguly, R.; Li, Y.; García, F. *Chem. – Eur. J.* **2017,** *23,* 11279–11285. doi:10.1002/chem.201701619

96. Katritzky, A. R.; Witek, R. M.; Rodriguez-Garcia, V.; Mohapatra, P. P.; Rogers, J. W.; Cusido, J.; Abdel-Fattah, A. A. A.; Steel, P. J. *J. Org. Chem.* **2005,** *70,* 7866–7881. doi:10.1021/jo050670t

97. Grignard, V.; Jenkins, R. L. *Bull. Soc. Chim. Fr.* **1925,** *37,* 1376–1385.

98. Rightmire, N. R.; Hanusa, T. P.; Rheingold, A. L. *Organometallics* **2014,** *33,* 5952–5955. doi:10.1021/om5009204

99. Higher yielding and higher scales were also possible using an IKKA tube dispenser (15 min reaction time with 85% yield) and planetary ball mill (5 min at 600 rpm with 88% yield) on a multigram scale.

100. Rightmire, N. R.; Bruns, D. L.; Hanusa, T. P.; Brennessel, W. W. *Organometallics* **2016,** *35,* 1698–1706. doi:10.1021/acs.organomet.6b00151

101. Hill, T. G.; Haltiwanger, R. C.; Thompson, M. L.; Katz, S. A.; Norman, A. D. *Inorg. Chem.* **1994,** *33,* 1770–1777. doi:10.1021/ic00087a009

102. Scherer, O. J.; Andres, K.; Krüger, C.; Tsay, Y.-H.; Wolmerhäser, G. *Angew. Chem., Int. Ed. Engl.* **1980,** *19,* 571–572. doi:10.1002/anie.198005711

103. Brask, J. K.; Chivers, T.; Krahn, M. L.; Parvez, M. *Inorg. Chem.* **1999,** *38,* 290–295. doi:10.1021/ic980117c

104. Bashall, A.; Doyle, E. L.; Garcia, F.; Lawson, G. T.; Linton, D. J.; Moncrieff, D.; McPartlin, M.; Woods, A. D.; Wright, D. S. *Chem. – Eur. J.* **2002,** *8,* 5723–5731. doi:10.1002/1521-3765(20021216)8:24<5723::AID-CHEM5723>3.0.CO;2-D

105. Shi, Y. X.; Liang, R. Z.; Martin, K. A.; Star, D. G.; Díaz, J.; Li, X. Y.; Ganguly, R.; García, F. *Chem. Commun.* **2015,** *51,* 16468–16471. doi:10.1039/C5CC06034F

106. Shi, Y. X.; Xu, K.; Clegg, J. K.; Ganguly, R.; Hirao, H.; Friščić, T.; García, F. *Angew. Chem., Int. Ed.* **2016,** *55,* 12736–12740. doi:10.1002/anie.201605936

107. Michalchuk, A. A. L.; Tumanov, I. A.; Drebushchak, V. A.; Boldyreva, E. V. *Faraday Discuss.* **2014,** *170,* 311–335. doi:10.1039/C3FD00150D

108. Boldyreva, E. *Curr. Pharm. Des.* **2016,** *22,* 4981–5000. doi:10.2174/1381612822666160804093120

109. Tumanov, I. A.; Michalchuk, A. A. L.; Politov, A. A.; Boldyreva, E. V.; Boldyrev, V. V. *CrystEngComm* **2017,** *19,* 2830–2835. doi:10.1039/C7CE00517B

110. Michalchuk, A. A. L.; Tumanov, I. A.; Sumit, K.; Kimber, S. A. J.; Pulham, C. R.; Boldireva, E. V. *Adv. Sci.* **2017,** 1700132. doi:10.1002/advs.201700132

111. Andersen, J. M.; Mack,, J. *Chem. Sci.* **2017,** *8,* 5447–5453. doi:10.1039/C7SC00538E

112. Belenguer, A. M.; Friščić, T.; Day, G. M.; Sanders, J. K. M. *Chem. Sci.* **2011,** *2,* 696–700. doi:10.1039/c0sc00533a

113. Bygrave, P. J.; Case, D. H.; Day, G. M. *Faraday Discuss.* **2014,** *170,* 41–57. doi:10.1039/C3FD00162H

114. Belenguer, A. M.; Lampronti, G. I.; Cruz-Cabeza, A. J.; Hunter, C. A.; Sanders, J. K. M. *Chem. Sci.* **2016,** *7,* 6617–6627. doi:10.1039/C6SC03457H

License and Terms

Peptide synthesis: ball-milling, in solution, or on solid support, what is the best strategy?

Ophélie Maurin, Pascal Verdié, Gilles Subra, Frédéric Lamaty[*], Jean Martinez and Thomas-Xavier Métro[*§]

Abstract

While presenting particularly interesting advantages, peptide synthesis by ball-milling was never compared to the two traditional strategies, namely peptide syntheses in solution and on solid support (solid-phase peptide synthesis, SPPS). In this study, the challenging VVIA tetrapeptide was synthesized by ball-milling, in solution, and on solid support. The three strategies were then compared in terms of yield, purity, reaction time and environmental impact. The results obtained enabled to draw some strengths and weaknesses of each strategy, and to foresee what will have to be implemented to build more efficient and sustainable peptide syntheses in the near future.

Introduction

Peptides play a central role both in biological mechanisms and in therapeutic solutions of the future [1,2]. Pharmaceutical companies are showing a renewed interest for this type of therapeutics. A recent study showed that 140 peptides are currently evaluated in clinical trials and more than 500 are in preclinical development [3]. In the recent years, much progress has been made in the administration modes and in the strategies to improve their in vivo bioavailability and stability. This progresses empowered the potential of therapeutic peptides, suggesting a production surge in the future. Besides this high potential, actual peptide production techniques suffer from major environmental issues [4-6]. Indeed, large amounts of organic solvents (DMF, NMP, 1,4-dioxane, DCM), coupling agents (uroniums, phosphoniums, carbodiimides and auxiliary nucleophiles) and bases (Et_3N, DIPEA, piperidine) are required for their synthesis and purification [4,7]. Unfortunately, these chemicals present highly undesirable safety profiles (flammable, corrosive and/or toxic), and industrial manufacturers are making great efforts to reduce their use [8]. All these problematic chemicals have been widely used because they furnish

liquid reaction mixtures perfectly adapted to the two prevalent peptide synthesis strategies utilized in research laboratories and for industrial production: synthesis in solution and synthesis on a solid support (also known as solid-phase peptide synthesis, SPPS). Indeed, liquid reaction mixtures enable efficient agitation when using a conventional batch reactor equipped with either magnetic stirring bar or impeller, and automated handling such as pumping and filtration. Since Lamaty and co-workers have shown in their seminal work that peptide synthesis could be performed in a ball-mill (BM) [9], various solvent-free or solvent-less peptide synthesis strategies have been developed [10-17]. While these approaches enable to circumvent the use of toxic solvents and bases [18-20], no comparison between ball-milling and conventional approaches was performed, discussed and communicated. Therefore, we performed this comparison by applying three different peptide synthesis strategies (BM, solution and solid support) to the production of the VVIA peptide sequence, protected or not, depending on the strategy (all amino acids bearing L absolute configuration, Figure 1). The sequence has been chosen as it corresponds to the Aβ (39–42) tetrapeptide, a promising small therapeutic peptide that inhibits Aβ42-induced neurotoxicity [21,22], and that is known to be difficult to produce due to high hydrophobicity and steric hindrance [23].
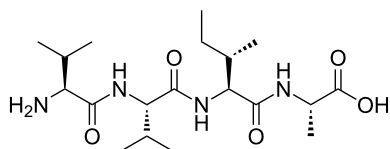
Figure 1: Structure of the VVIA peptide.

Results and Discussion
Synthesis by using a ball-mill (BM)

The Boc-VVIA-OBn tetrapeptide was first synthesized by using the ball-milling strategy, based on our recent developments [14]. Thus, the coupling steps were realized by ball-milling the

amino ester salts (*p*-toluenesulfonate or hydrochloride) with Boc-AA-OH (1.2 equiv) in the presence of the coupling additive ethyl cyano(hydroxyimino)acetate (also known as Oxyma, 1.2 equiv), the base NaH_2PO_4 (4.0 equiv) and the coupling agent *N*-(3-dimethylaminopropyl)-*N′*-ethylcarbodiimide (EDC, 1.2 equiv) in the presence of small amounts of EtOAc as the liquid grinding assistant (Scheme 1). Conventional post-treatments based on acid/base extractions and washings were sufficient to furnish the desired coupling products in satisfying purity and in isolated yields ranging from 78 to 89%. Of note, it was observed previously under similar reaction conditions that the absence of EtOAc as liquid grinding assistant (neat grinding) could lead to inhomogeneity of the reagents distribution inside the ball-mill, thereby leading to a lower overall conversion [14]. The removal of the protecting groups was performed by treatment of the Boc-protected peptides with gaseous HCl in the absence of solvents, providing the amino esters as hydrochlorides in high yield and purity (Scheme 1). Alternatively, removal of the Boc group under mechanochemical conditions was realized. While ball-milling Boc-IA-OBn with 37% aqueous HCl furnished HCl·H-IA-OBn contaminated with products arising from hydrolysis of the benzyl ester group, pure TFA·H-IA-OBn was obtained in quantitative yield by ball-milling Boc-IA-OBn with TFA (5.0 equiv) [24]. Overall, the Boc-VVIA-OBn peptide was obtained in 5 steps with 59% yield and 88% purity (Scheme 1).

Synthesis in solution

In parallel, the Boc-VVIA-OBn tetrapeptide was produced using the conventional synthesis in solution. For this, the amino ester salts (*p*-toluenesulfonate or hydrochloride), Boc-AA-OH (1.2 equiv), the coupling additive Oxyma (1.2 equiv) and the base *N,N*-diisopropylethylamine (DIPEA, 1.2 equiv) were dissolved in the minimal amount of DMF at room temperature, and then reacted with the coupling agent EDC (1.2 equiv) (Scheme 2). As described for the ball-milling approach, post-treatments based on extractions and washings furnished the desired coupling products in good purity and in isolated yields

Scheme 1: Synthesis of Boc-VVIA-OBn by the ball-milling approach.

1) Coupling steps
Boc-AA-OH (1.2 equiv)
Oxyma (1.2 equiv)
DIPEA (4.0 equiv)
EDC (1.2 equiv), DMF
magnetic stirring
64–88% yield

2) Deprotection steps
TFA/CH$_2$Cl$_2$ 50:50 (v/v)
>99% yield

p-TsOH·H-A-OBn

Boc-VVIA-OBn
5 steps
43% overall yield
85% purity

Scheme 2: Synthesis of tetrapeptide Boc-VVIA-OBn in solution.
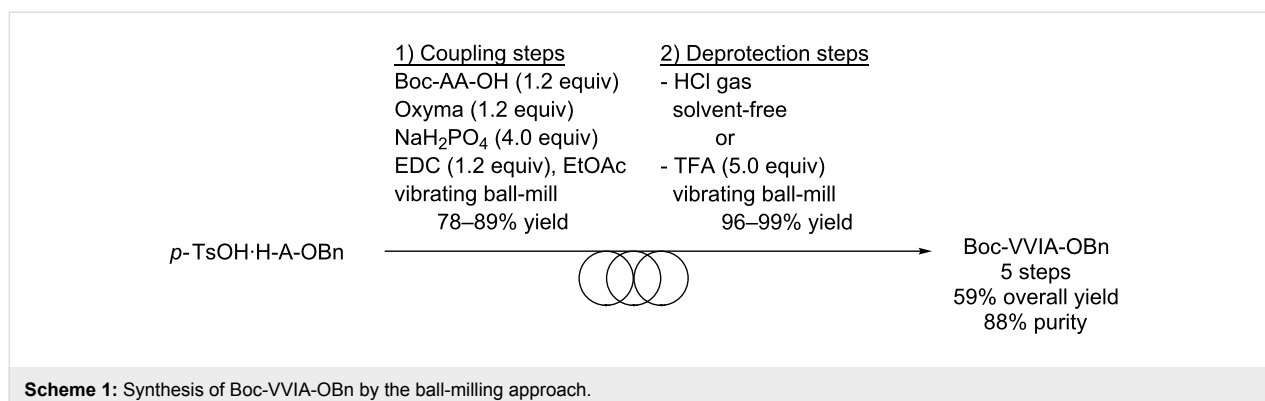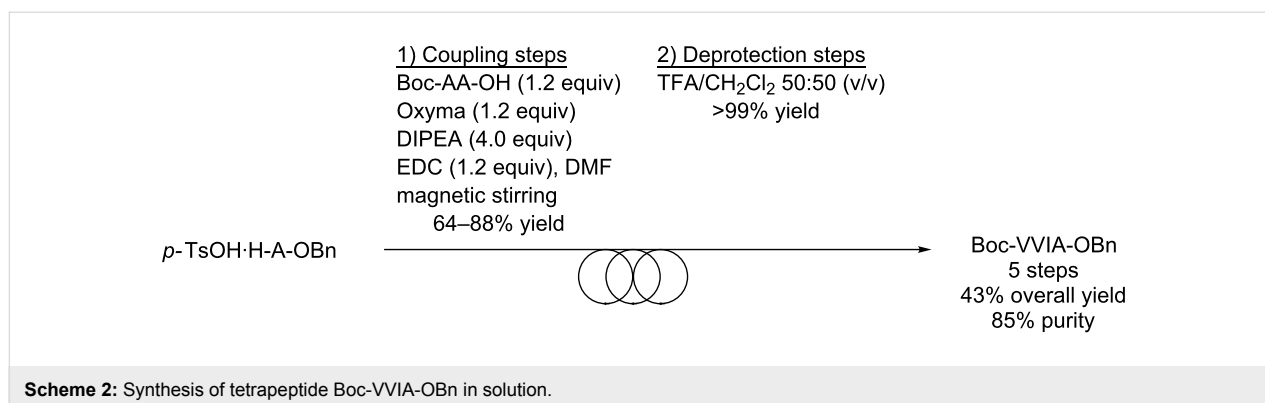
ranging from 64% to 88%. The deprotection steps were performed by dissolving the Boc-protected peptides in TFA/ CH$_2$Cl$_2$ 50:50 (v/v) furnishing the amino esters as TFA salts in high purity and quantitative yields (Scheme 2). Overall, the Boc-VVIA-OBn peptide was obtained in 5 steps with 43% yield and 85% purity.

Synthesis on solid support

For the strategy involving a solid support, the chemistry was slightly different from the one used for BM or in solution, as the standard Fmoc chemistry commonly utilized in laboratories was employed [25,26]. It has to be noted that in this case the fully deprotected TFA·H-VVIA-OH peptide was obtained. Practically, the peptide chain was elongated by means of a peptide synthesizer employing the standard Fmoc chemistry (Scheme 3). The synthesis was conducted on an Fmoc-A-Wang resin on a 0.1 mmol scale with a 5-fold excess of Fmoc-protected amino acids solubilized in DMF (0.2 M), 0.5 M *N,N′*-diisopropylcarbodiimide in DMF (DIC, 5.0 equiv) as coupling reagent and 1 M Oxyma in DMF (5.0 equiv) as the coupling additive. Except for the coupling of Fmoc-V-OH with H-IA-resin and for the deprotection of Fmoc-IA-resin that were performed during 90 min at room temperature, the coupling steps were performed at 70 °C for 7 min under microwave irradiation. The

deprotection steps were carried out with piperidine/DMF 1:4 for 3 min at 70 °C. After the assembly was completed, the peptide-resin was washed with CH$_2$Cl$_2$ and the cleavage was performed with TFA/TIS/H$_2$O 94:3:3 for 2 h at room temperature. Before lyophilization, the peptide was precipitated by the addition of Et$_2$O. Overall, the TFA·H-VVIA-OH peptide was obtained in 8 steps in 54% isolated yield and in 96% purity (Scheme 3).

Comparison of the three different strategies

Having these results in hands, a comparison of the three strategies was realised. Of note, BM and solution strategies employed a Boc/Bn scenario while SPPS was based on the more conventional Fmoc/*t*-Bu scheme. Although one could point out that differences could arise from these chemical divergences, the global aim of this study was to establish a comparison based on a practical point of view. Thus, the comparison was based on the isolated yield and purity of intermediates and the final products, on the reaction time, and on the environmental impact.

Comparison based on the yields and purities of intermediates and final products

Contrary to SPPS where the peptide of interest is isolated at the very end of the process, syntheses performed by BM and in

1) Coupling steps
Fmoc-AA-OH (5.0 equiv)
DIC (5.0 equiv)
Oxyma (5.0 equiv)
DMF, MW or rt

2) Deprotection steps
piperidine/DMF 1:4
MW or rt

3) Resin deprotection
TFA/TIS/H$_2$O 94:3:3
2 h, rt

Fmoc-A-Wang resin

TFA·H-VVIA-OH
8 steps
54% overall yield
96% purity

Scheme 3: Synthesis of TFA·H-VVIA-OH by SPPS.
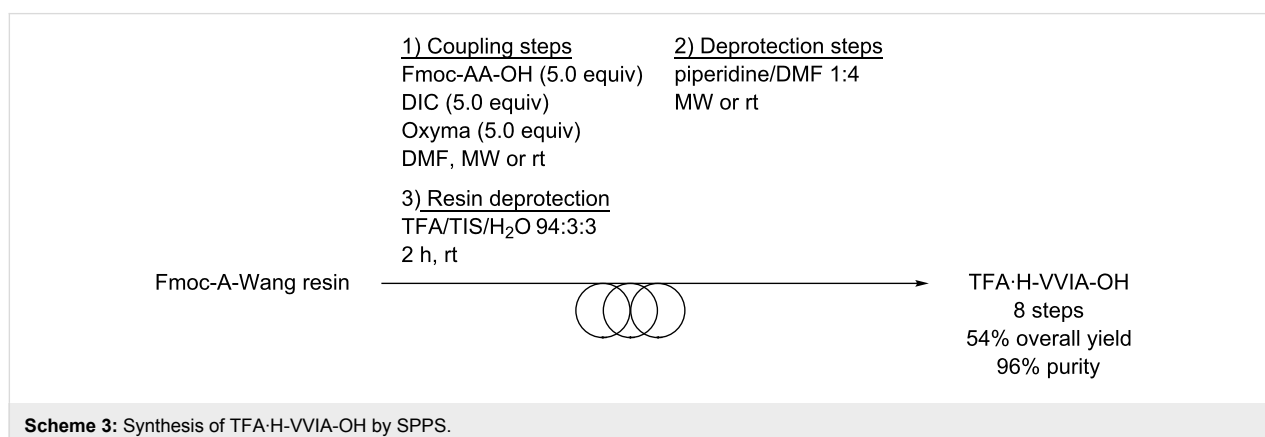
solution allows for a step by step comparison. Thus, for each coupling and deprotection step, the synthesis efficiency in the BM and in solution was compared based both on the isolated yields and on the purity of the peptides that were assessed by HPLC analysis (Table 1).

For all coupling reactions without exception, the yields obtained under BM conditions were higher than that obtained in solution (89% vs 88% for the dipeptide, 89% vs 77% for the tripeptide and 78% vs 64% for the tetrapeptide) (Table 1, entries 1, 3 and 5). Besides, the deprotection steps always furnished the amino ester salts in excellent yields, either by using TFA/CH$_2$Cl$_2$ (solvent strategy) or gaseous HCl without solvent (BM strategy). On the other hand, the dipeptides were obtained with higher purity when synthesized using the conventional solution strategy compared to the BM approach (Table 1, entries 1 and 2). Yet, for all tripeptides and tetrapeptides, the BM strategy furnished the products with higher purities by 3 to 9 percentage points when compared with the solution-based approach (Table 1, entries 3–5). Overall, the 59% yield obtained with BM (Table 1, entry 6) was comparable to the one obtained with the SPPS strategy (54% yield), even more that the tetrapeptide pro-

duced by SPPS was isolated fully deprotected and with the highest purity (96%), giving additional advantage to SPPS. Yet, both in terms of overall yield and purity, the BM strategy is superior to the solution strategy (59% vs 43% overall yield and 88% vs 85% purity).

Comparison based on the reaction time

During the course of the coupling reactions performed in the BM and in solution, aliquots were regularly sampled, quenched and analyzed by HPLC to determine the conversion. Considering the coupling steps realized in solution, the reaction mixture was dissolved in the minimal amount of DMF to ensure maximal speed of reaction while securing proper agitation. On the contrary to the solution synthesis, aliquots sampling from the milling jars implied stopping the milling process for 1–2 minutes. As one could suggest that coupling reactions could be continuing even without milling [27-30], these short pauses were considered as reaction time. As a consequence, the effective milling time was shorter than the reaction time (see Supporting Information File 1 for details). All conversions values were plotted against reaction time and the results are shown in Figure 2 below.

Table 1: Yields and purities for the three strategies (for each entry, the best result is indicated in bold).

Entry	Peptide	Ball-milling		Solution		SPPS	
		Yield[a]	Purity	Yield[a]	Purity	Yield[a]	Purity
1	Boc-IA-OBn	**89%**	93%	88%	**96%**	–	–
2	AH·H-IA-OBn	>99%[b] (>99%)[c]	97%[b] (100%)[c]	>99%[d]	99%[d]	–	–
3	Boc-VIA-OBn	**89%**	**99%**	77%	90%	–	–
4	AH·H-VIA-OBn	96%[b]	97%[b]	**>99%**[d]	92%[d]	–	–
5	Boc-VVIA-OBn	**78%**	**88%**	64%	85%	–	–
6	Overall	**59%**	88%	43%	85%	**54%**[e]	**96%**[e]

[a]Isolated yield. [b]HCl salt. [c]Obtained as TFA salt by ball-milling with 5.0 equiv TFA. [d]TFA salt. [e]Obtained as TFA·H-VVIA-OH.
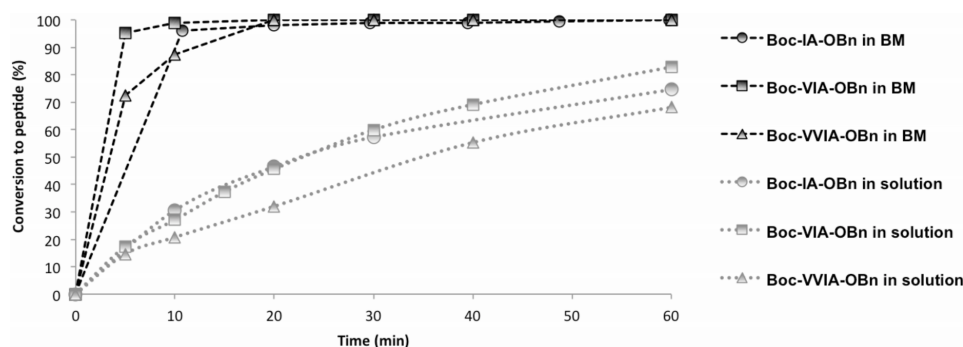
Figure 2: Comparison of the reaction time of the coupling steps performed in the BM and in solution.

After 20 minutes reaction, conversions were >98% for all three coupling steps performed in the BM (Figure 2). Conversely, after the same time, none of the reaction steps done in solution reached 50% conversion. On average, coupling reactions in solution required 3 hours to reach >98% conversion, which is nine times longer than when using the BM (see Supporting Information File 1 for details). Considering the reaction time, coupling steps were considerably more efficient in BM than in solution. Whereas aliquots could be easily taken from reaction mixtures of the coupling steps, no reproducible samples could be taken for the deprotection steps using gaseous HCl. Therefore, for the deprotection no comparison of the reaction times between the two strategies (BM and solution) was possible. Similarly, the speed of reaction was not measured for SPPS, as automation of the coupling and deprotection steps enabled to save a considerable amount of time compared to ball-milling and conventional synthesis in solution. Indeed, post-treatments in BM and in solution strategies were performed by hand. Thus, a few days were necessary to complete the synthesis when using the BM or solution strategies. For comparison, half a day was sufficient to produce the VVIA sequence when using SPPS.

Comparison based on the environmental impact

Finally, the three different strategies were compared in terms of environmental impact. The widely used E-factor [31-33], which is defined as follows:

$$\text{E-factor} = \left(\frac{\sum (\text{mass of waste})}{\text{mass of product}} \right) \times 100$$

was calculated for the coupling and deprotection steps of each strategy (Table 2). Of note, the amount of reactants used in all three strategies were either based on previously optimized reaction conditions or reduced as much as possible without hampering the success of the reaction. This was realized to ensure relevant comparison between the different strategies. For all coupling steps, the E-factor obtained with the BM strategy outperformed the two other strategies, SPPS producing from

seven to twenty times more waste than the BM strategy (Table 2, entries 1, 3 and 4). Unfortunately, the experimental set-up for the removal of the Boc protection group with gaseous HCl prevented the measurement and the optimization of gaseous HCl quantities required complete the reaction. Consequently, the E-factor corresponding to the Boc deprotection steps using gaseous HCl could not be calculated. Yet, deprotection of Boc-IA-OBn by ball-milling in the presence of TFA enabled to calculate the E-factor, which was five times less than in solution and more than thousand times less than SPPS (Table 2, entry 2).

Table 2: Comparison of the E-factor between the three strategies (for each entry, the best result is indicated in bold).

Entry	Peptide	E-factor		
		Ball-milling	Solution	SPPS
1	P-IA-OR	**4.9**	7.3	95.5
2	TFA·H-IA-OR	**1.3**	5.9	1406.6
3	P-VIA-OR	**5.0**	7.1	81.0
4	P-VVIA-OR	**9.4**	17.8	68.1

While providing an interesting insight into the amount of waste produced in each strategy, the E-factor does not provide any information concerning the toxicity of the reactants used. Pursuing an initiative we started previously [34], we calculated the cumulative Number of the Hazard Phrases (cNHP) indicated in the safety data sheets (SDS) of the reactants used in each strategy (Table 3).

As expected, the ball-milling strategy was the one for which this number was the lowest for each of the coupling and deprotection steps, corresponding to the safest approach in terms of toxicity. Of note, various research groups have screened greener solvents for SPPS [35-38]. The results issuing from these studies indicate that a reduction of the cumulative Number of Hazard Phrases in both the coupling and deprotection steps may be accessible by choosing more appropriate solvents than DMF.

Table 3: Comparison of the cumulative Number of Hazard Phrases (for each entry, the best result is indicated in bold).

Entry	Reaction	Cumulative Number of Hazard Phrases		
		Ball-milling	Solution	SPPS
1	coupling	**4**	11	12
2	deprotection with HCl(g)	**3**	–	–
3	deprotection with TFA	**3**	9	–
4	deprotection with Pip/DMF	–	–	11

While this is highly positive information for the development of greener peptide syntheses, these strategies are yet inefficient in reducing the total amount of waste, which is one of the main drawbacks of SPPS.

Conclusion

Overall, both in terms of yield and purity, the efficiency of the three strategies can be ranked as follows: BM ≈ SPPS > solution. Of note, the solution strategy gave the dipeptides with higher purity than the ball-milling approach. Although SPPS is the strategy of choice towards long peptides so far, this study showed that ball-milling was superior to the solution synthesis when considering long peptides. Similarly, ball-milling proved far more efficient than the synthesis in solution when considering the reaction time of the coupling steps. Although producing the peptide of interest with the highest purity, SPPS also presents by far the worst environmental impact. The production of waste can range from seven to thousand times more than BM. Regarding the environmental impact, the three strategies can be ranked as follows: BM > solution >> SPPS. With the increasing implementation of REACH regulations [39], one can easily foresee that the extremely low environmental impact of BM will be a determining advantage in the future. Time and money saved by automation of coupling and deprotection steps in SPPS could be transformed into a crippling burden when considering costs and environmental impact related to the use of large excesses of chemicals associated with SPPS. While SPPS has benefited from more than 50 years of research and development, and is still the method of choice for very long peptides, peptide synthesis by ball-milling is still in its infancy. Further optimization of the deprotection steps, demonstration of the feasibility to synthesize longer peptides, as well as automation of the coupling and deprotection steps would undoubtedly bring peptide synthesis by ball-milling to be the method of choice for peptide synthesis in laboratories, as well as for industrial production.

Supporting Information

Supporting Information File 1

Experimental procedures and characterization data of peptides.
[http://www.beilstein-journals.org/bjoc/content/supplementary/1860-5397-13-206-S1.pdf]

Acknowledgements

References

1. Vlieghe, P.; Lisowski, V.; Martinez, J.; Khrestchatisky, M. *Drug Discovery Today* **2010,** *15,* 40–56. doi:10.1016/j.drudis.2009.10.009
2. Albericio, F.; Kruger, H. G. *Future Med. Chem.* **2012,** *4,* 1527–1531. doi:10.4155/fmc.12.94
3. Fosgerau, K.; Hoffmann, T. *Drug Discovery Today* **2015,** *20,* 122–128. doi:10.1016/j.drudis.2014.10.003
4. Bray, B. L. *Nat. Rev. Drug Discovery* **2003,** *2,* 587–593. doi:10.1038/nrd1133
5. Constable, D. J. C.; Dunn, P. J.; Hayler, J. D.; Humphrey, G. R.; Leazer, J. L., Jr.; Linderman, R. J.; Lorenz, K.; Manley, J.; Pearlman, B. A.; Wells, A.; Zaks, A.; Zhang, T. Y. *Green Chem.* **2007,** *9,* 411–420. doi:10.1039/B703488C
6. Thayer, A. M. *Chem. Eng. News* **2011,** *89,* 21–25.
7. Pattabiraman, V. R.; Bode, J. W. *Nature* **2011,** *480,* 471–479. doi:10.1038/nature10702
8. Patel, P. *Chem. Eng. News* **2017,** *95,* 27–28.
9. Declerck, V.; Nun, P.; Martinez, J.; Lamaty, F. *Angew. Chem., Int. Ed.* **2009,** *48,* 9318–9321. doi:10.1002/anie.200903510
10. Hernández, J. G.; Juaristi, E. *J. Org. Chem.* **2010,** *75,* 7107–7111. doi:10.1021/jo101159a
11. Štrukil, V.; Bartolec, B.; Portada, T.; Đilović, I.; Halasz, I.; Margetić, D. *Chem. Commun.* **2012,** *48,* 12100–12102. doi:10.1039/c2cc36613d
12. Bonnamour, J.; Métro, T.-X.; Martinez, J.; Lamaty, F. *Green Chem.* **2013,** *15,* 1116–1120. doi:10.1039/c3gc40302e
13. Duangkamol, C.; Jaita, S.; Wangngae, S.; Phakhodee, W.; Pattarawarapan, M. *RSC Adv.* **2015,** *5,* 52624–52628. doi:10.1039/C5RA10127A
14. Porte, V.; Thioloy, M.; Pigoux, T.; Métro, T.-X.; Martinez, J.; Lamaty, F. *Eur. J. Org. Chem.* **2016,** 3505–3508. doi:10.1002/ejoc.201600617
15. Gonnet, L.; Tintillier, T.; Venturini, N.; Konnert, L.; Hernandez, J.-F.; Lamaty, F.; Laconde, G.; Martinez, J.; Colacino, E. *ACS Sustainable Chem. Eng.* **2017,** *5,* 2936–2941. doi:10.1021/acssuschemeng.6b02439
16. Landeros, J. M.; Juaristi, E. *Eur. J. Org. Chem.* **2017,** 687–694. doi:10.1002/ejoc.201601276
17. Hernández, J. G.; Ardila-Fierro, K. J.; Crawford, D.; James, S. L.; Bolm, C. *Green Chem.* **2017,** *19,* 2620–2625. doi:10.1039/C7GC00615B
18. Datta, S.; Sood, A.; Török, M. *Curr. Org. Synth.* **2011,** *8,* 262–280. doi:10.2174/157017911794697330
19. Métro, T.-X.; Colacino, E.; Martinez, J.; Lamaty, F. Amino Acids and Peptides in Ball Milling. *Ball Milling Towards Green Synthesis: Applications, Projects;* The Royal Society of Chemistry, 2015; pp 114–150. doi:10.1039/9781782621980-00114
20. Margetić, D.; Štrukil, V. Carbon–Nitrogen Bond-Formation Reactions. *Mechanochemical Organic Synthesis;* Elsevier, 2016; pp 141–233. doi:10.1016/B978-0-12-802184-2.00003-0
21. Li, H.; Du, Z.; Lopes, D. H. J.; Fradinger, E. A.; Wang, C.; Bitan, G. *J. Med. Chem.* **2011,** *54,* 8451–8460. doi:10.1021/jm200982p
22. Zheng, X.; Wu, C.; Liu, D.; Li, H.; Bitan, G.; Shea, J.-E.; Bowers, M. T. *J. Phys. Chem. B* **2016,** *120,* 1615–1623. doi:10.1021/acs.jpcb.5b08177
23. Dev, D.; Palakurthy, N. B.; Thalluri, K.; Chandra, J.; Mandal, B. *J. Org. Chem.* **2014,** *79,* 5420–5431. doi:10.1021/jo500292m
24. Đud, M.; Margetić, D. *Int. J. Org. Chem.* **2017,** *7,* 140–144. doi:10.4236/ijoc.2017.72011

25. Amblard, M.; Fehrentz, J.-A.; Martinez, J.; Subra, G. Fundamentals of Modern Peptide Synthesis. *Peptide Synthesis and Applications;* Humana Press, 2005; Vol. 298, pp 3–24. doi:10.1385/1-59259-877-3:003

26. Jad, Y. E.; Khattab, S. N.; de la Torre, B. G.; Govender, T.; Kruger, H. G.; El-Faham, A.; Albericio, F. *Eur. J. Org. Chem.* **2015,** 3116–3120. doi:10.1002/ejoc.201500142

27. Cliffe, M. J.; Mottillo, C.; Stein, R. S.; Bučar, D.-K.; Friščić, T. *Chem. Sci.* **2012,** *3,* 2495–2500. doi:10.1039/c2sc20344h

28. Cinčić, D.; Brekalo, I.; Kaitner, B. *Chem. Commun.* **2012,** *48,* 11683–11685. doi:10.1039/c2cc36357g

29. Lim, X. *Nature* **2015,** *524,* 20–21. doi:10.1038/524020a

30. Đud, M.; Magdysyuk, O. V.; Margetić, D.; Štrukil, V. *Green Chem.* **2016,** *18,* 2666–2674. doi:10.1039/C6GC00089D

31. Sheldon, R. A. *Chem. Ind. (London)* **1992,** 903–906.

32. Sheldon, R. A. *Green Chem.* **2007,** *9,* 1273–1283. doi:10.1039/b713736m

33. Sheldon, R. A. *Green Chem.* **2017,** *19,* 18–43. doi:10.1039/C6GC02157C

34. Métro, T.-X.; Bonnamour, J.; Reidon, T.; Duprez, A.; Sarpoulet, J.; Martinez, J.; Lamaty, F. *Chem. – Eur. J.* **2015,** *21,* 12787–12796. doi:10.1002/chem.201501325

35. Kumar, A.; Jad, Y. E.; El-Faham, A.; de la Torre, B. G.; Albericio, F. *Tetrahedron Lett.* **2017,** *58,* 2986–2988. doi:10.1016/j.tetlet.2017.06.058

36. Jad, Y. E.; Govender, T.; Kruger, H. G.; El-Faham, A.; de la Torre, B. G.; Albericio, F. *Org. Process Res. Dev.* **2017,** *21,* 365–369. doi:10.1021/acs.oprd.6b00439

37. Lawrenson, S.; North, M.; Peigneguy, F.; Routledge, A. *Green Chem.* **2017,** *19,* 952–962. doi:10.1039/C6GC03147A

38. Lawrenson, S. B.; Arav, R.; North, M. *Green Chem.* **2017,** *19,* 1685–1691. doi:10.1039/C7GC00247E

39. Erickson, B. E. *Chem. Eng. News* **2015,** *93,* 30.

The effect of milling frequency on a mechanochemical organic reaction monitored by in situ Raman spectroscopy

Patrick A. Julien[1], Ivani Malvestiti[1,2] and Tomislav Friščić[*1]

Abstract

We provide the first in situ and real-time study of the effect of milling frequency on the course of a mechanochemical organic reaction conducted using a vibratory shaker (mixer) ball mill. The use of in situ Raman spectroscopy for real-time monitoring of the mechanochemical synthesis of a 2,3-diphenylquinoxaline derivative revealed a pronounced dependence of chemical reactivity on small variations in milling frequency. In particular, in situ measurements revealed the establishment of two different regimes of reaction kinetics at different frequencies, providing tentative insight into processes of mechanical activation in organic mechanochemical synthesis.

Introduction

Over the past decade, mechanochemical reactions [1-4], i.e., chemical transformations induced or sustained through the application of mechanical force in the form of grinding, milling and shearing, have emerged as a highly versatile and general route to conduct chemical reactions in the absence of bulk solvents [2]. Indeed, the demonstrated versatility in organic [5-8], organometallic [9,10], pharmaceutical [11,12], supramolecular [13], metal-organic [14,15], and materials synthesis [16] has rendered mechanochemical reactions by ball milling or grinding as viable, highly environmentally-friendly alternatives to solution-based chemistry. Importantly, mechanochemistry provides not only a means to conduct chemical transformations of poorly soluble reagents [17], but also enables access to reactions that

are difficult or even impossible to achieve in solution [18-20], and allows the synthesis of molecular targets that have so far been considered impossible to synthesize [21] or isolate [22].

However, in contrast to rapid expansion of applications of mechanochemistry, the mechanistic understanding of the underlying physicochemical process remains poor. It was only recently that significant effort was invested in understanding how fundamental environmental parameters, such as temperature, milling frequency, or sample-to-volume ratio [23-26] affect the course of organic mechanochemical reactions. A significant recent advance in mechanistic studies of mechanochemical reaction mechanisms was the introduction of tech-

niques for in situ, real-time monitoring of ball milling processes [27], first through synchrotron X-ray powder diffraction (XRPD) [28,29], and later by Raman spectroscopy [30] or by a tandem technique combining these two techniques [31]. Whereas valuable mechanistic information on the course of a milling reaction can be obtained through stepwise, ex situ monitoring [32] based on periodically interrupting the milling process followed by sample extraction and analysis [33,34] such techniques can also lead to misleading results due to the sample either relaxing rapidly after milling [35] or reacting with surrounding atmosphere during preparation for analysis [36]. Such problems are additionally exacerbated in mechanochemistry of organic or metal-organic materials, readily activated through milling into transient, reactive amorphous phases. In contrast, real-time monitoring provides the opportunity to investigate the reaction course with time resolution in seconds, and without disrupting the milling process [31]. So far, the majority of real-time monitoring studies have focused on reactions of inorganic substances converting into metal-organic frameworks (MOFs) [17,28,37] or supramolecular reactions of cocrystallisation [38]. Real-time monitoring of an organic mechanochemical reaction was only recently reported by Tireli and co-workers, who utilized Raman spectroscopy to investigate how the choice of base influences the course of a base-catalysed nucleophilic substitution reaction [39].

Raman spectroscopy is particularly well-suited for monitoring and tracking organic reactions. It is a generally accessible and inexpensive, with an output based on changes to molecular structure rather than its crystallinity, offering a powerful tool for in situ studies of mechanochemical organic reactions that often proceed through amorphous or eutectic intermediates. We now report a Raman spectroscopy study of the effect of ball milling frequency on the course of a model organic transformation, the previously reported mechanochemical condensation of a diketone and a diamine to form an *N*-heteroacene [40]. We have utilized an in-house built setup for real-time Raman spectroscopy monitoring of the synthesis of 2,3-diphenylquinoxaline from benzil and *o*-phenylenediamine (Scheme 1). As the Raman signals of both reactants and the quinoxaline product can readily be distinguished, and the product can be obtained in high yield and purity by brief milling (less than an hour), we
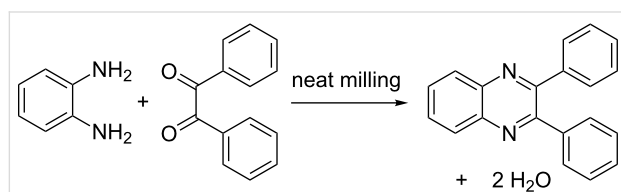
found this model system to be particularly appealing for mechanistic studies.

The milling frequency is one of the fundamental parameters of mechanochemical reactions conducted by ball milling, and for a vibratory shaker (mixer) ball mill it represents the number of full oscillations of the milling vessel (milling jar) per unit time along a curved path (Scheme 2). It is often used as a simple, primary assessment of the intensity of the milling process, and it affects the overall impact force, number and rate of impacts of milling media, as well as associated frictional heating.
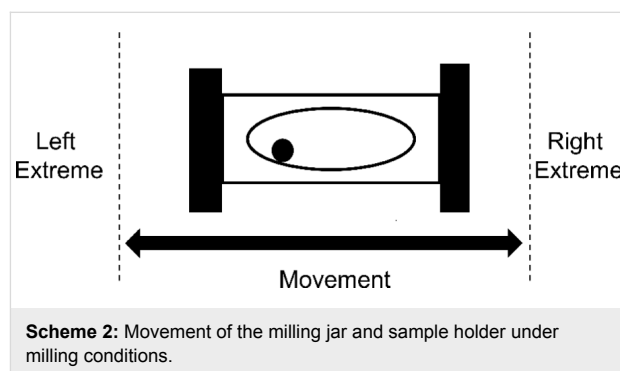
Scheme 2: Movement of the milling jar and sample holder under milling conditions.

Raman spectroscopy was recently utilized for a stepwise, ex situ assessment of the effect of milling frequency on the mechanochemical synthesis of a MOF from ZnO and imidazole in the presence of a small amount of *N,N*-dimethylformamide [41]. This study revealed reaction kinetics consistent with a 2nd order reaction rate law, rationalized through a "pseudo-fluid" reaction model in which the rate-determining factor is the frequency of reactive encounters between the particles. In contrast, ex situ gas chromatography studies of the Knoevenagel condensation between vanillin and barbituric acid in a planetary mill revealed a sigmoidal dependence of reaction yield with time [22]. Similarly, sigmoidal dynamics were detected by in situ XRPD monitoring of the formation of glycinium oxalate salts from γ-glycine and oxalic acid dihydrate [42]. Other examples of explorations of the effect of milling frequency on mechanochemical reactivity include aromatic substitution reactions [43] and the synthesis of nitrogen-doped titania [44], which have all revealed a non-linear relationship between milling frequency and reaction conversion.

Results and Discussion
In situ monitoring of the model condensation reaction
A preliminary investigation of the model condensation reaction was conducted by milling of *o*-phenylenediamine (108 mg, 1.0 mmol) with benzil (210 mg, 1.0 mmol) using a Retsch MM400 mixer mill operating at 30 Hz. The reaction

Scheme 1: Milling synthesis of 2,3-diphenylquinoxaline from benzil and *ortho*-phenylenediamine [40].

mixture was placed in a 15 mL volume optically transparent poly(methyl metacrylate) (PMMA) jar, along with one zirconia ball of 10 mm diameter (ca. 3 grams weight). After 30 minutes milling, the analysis of the crude reaction product by ^{1}H nuclear magnetic resonance (NMR) spectroscopy (see Supporting Information File 1) suggested quantitative conversion, with the presence of only trace impurities. Importantly, as the melting points of the starting materials and the product are considerably above room temperature (benzil: 94–96 °C; *o*-phenylenediamine: 100–102 °C; 2,3-diphenylquinoxaline: 125–127 °C) and no melting was observed upon grinding together of the two reactants, the formation of 2,3-diphenylquinoxaline is a good example of a solid-state reaction. Moreover, XRPD analysis of the crude reaction mixture after milling indicated that the product was crystalline (see Supporting Information File 1). Monitoring of the reaction in situ by Raman spectroscopy revealed the clear disappearance of reactant signals, as well as the emergence of strong signals of the product (Figure 1). Complete disappearance of reactant signals was observed in situ after ≈20 minutes milling, a timescale that is well suited for our study. Due to the

significant scattering associated with collecting data through the 3 mm thick PMMA jar wall, all data were baseline corrected as described in the experimental section.

Circumventing PMMA interference

The milling jar wall produces a strong PMMA Raman signal which creates a strong background and interferes with in situ measurements of our reaction components. To minimize this effect, we focused our study on the spectral region between 1510 cm^{-1} and 1710 cm^{-1}, where both starting materials and the product exhibit characteristic signals, and the PMMA spectrum is featureless (Figure 2).

Fitting the dataset

A principal challenge associated with in situ monitoring of a milling reaction is the variation of the amount of sample in the beam due to the motion of the milling assembly. The resulting variations in the Raman signals of the sample and the scattering background affect the ability to monitor reaction progress, leading us to estimate the ratio of each component within the
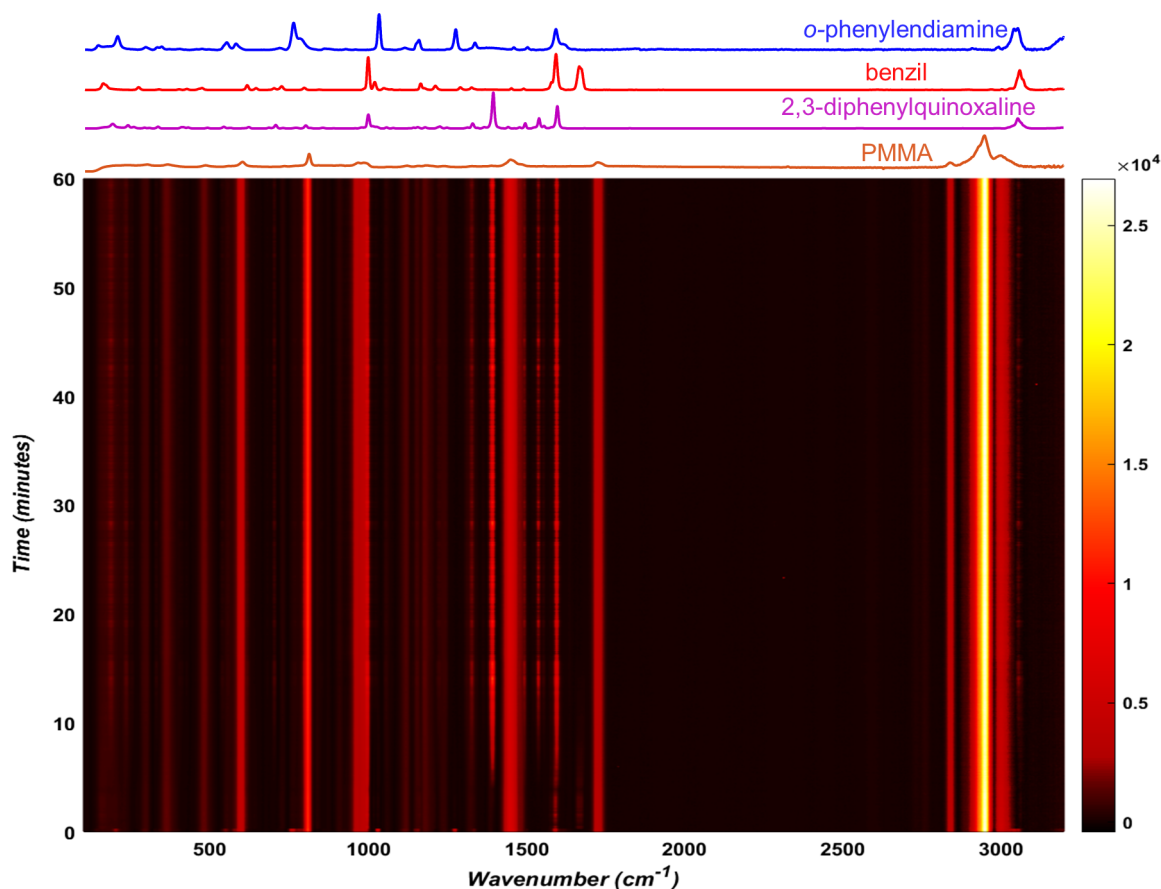
Figure 1: Time-resolved Raman spectrum for the double condensation of *o*-phenylenediamine and benzil to form 2,3-diphenylquinoxaline by milling at 30 Hz, with relevant spectra of reaction components and the PMMA milling jar shown above.

Figure 2: Section of the time-resolved Raman spectrum for the model mechanochemical reaction conducted at 30 Hz, that was selected for least-squares fitting. Normalized and baseline-corrected spectra for pure *o*-phenylenediamine (blue), benzil (red), 2,3-diphenylquinoxaline (purple) and an empty PMMA milling jar (yellow, offset for clarity) are shown above the time-resolved plot.

reaction mixture by a direct classical least-squares (CLS) approach based on experimentally obtained spectra of all scattering materials [45]. As the PMMA signal in the characteristic region between 1510–1700 cm^{-1} is sufficiently low to be neglected, this was limited to the spectra of the two starting materials, *o*-phenylenediamine and benzil, as well as the product 2,3-diphenylquinoxaline (Figure 2, top). The critical assumption in this approach is that all components are known and all spectral signals can be assigned to either the product or any of the reactants. Therefore, the calculated spectrum (C) can be described as a sum of pure component spectra $x_n A_n$, where x_n is the contribution of each spectrum and A_n is the spectrum of each pure component, with all components being known (Equation 1).

$$C = \sum_n x_n A_n = x_1 A_1 + x_2 A_2 + x_3 A_3 \qquad (1)$$

At the same time, the total sum of spectral contributions of all three reaction components must be equal to one, enabling the ratio of components to be calculated for each spectrum (Equation 2).

$$\sum_n x_n = x_1 + x_2 + x_3 = 1 \qquad (2)$$

Variations in background scattering between all in situ collected spectra and the spectra of individual reaction components were accounted for by using the Sonneveld–Visser baseline correction algorithm [46]. In situ collected spectra were fitted as a sum of the normalized component spectra using a non-negative linear least squares algorithm ("lsqnonneg" in Matlab) which solves the fitting problem [47] of Equation 3:

$$\min_x \| A * x - E \|_2^2 \qquad (3)$$

where *A* is a matrix containing the pure components spectra, *E* is the in situ obtained experimental spectrum, and *x* is a matrix of the mole fraction of each component, which satisfies $x \geq 0$. Equation 3 provides the best values of *x* that minimize the difference between $A * x$ and *E*.

The described linear least-squares fitting procedure was applied to every spectrum in the in situ dataset and, following

Equation 1 and Equation 2, enabled us to evaluate the relative spectral contribution of each reaction component x_n (Figure 3).

It is important to note that the herein presented approach to data analysis assumes that the Raman spectra of individual reactants or products are not significantly affected by the degree of crystallinity or changes in the composition of the reaction mixture. While Raman scattering is expected to be directly proportional to the concentration of a particular molecular species [45], which suggests that the spectral contribution of a reaction component should also be directly proportional to its mole fraction, we have not yet calibrated this relationship. Accurate quantitative methods for analysing in situ Raman milling reactions are currently under development in our laboratory.

The effect of milling frequency on the model reactions

Having identified a suitable model reaction and an approach for the analysis of in situ reaction data, we were able to systematically explore the effect of milling frequency on the reaction rate. The systematic studies were conducted by measuring Raman spectra for chemical reactions that were, to the best of our ability, identical in all respects except the choice of milling frequency, i.e., the choice of milling media, the jar volume and material, the ball-to-sample weight ratio, and reactant batches were all kept constant. Specifically, we investigated the reaction behavior upon milling at 20 Hz, 22.5 Hz, 25 Hz, 27.5 Hz, and 30 Hz. For each of the frequencies, the measurements were performed in triplicate, and on the same day, in order to maxi-

mize reproducibility and minimize the variations in the reaction behaviour due to daily variation of ambient temperature or humidity. The final conversion for each experiment was verified by ^{1}H NMR spectroscopy in solution (see Table S1 in Supporting Information File 1) and was found to be consistent with the in situ Raman spectroscopy data. Averaging the triplicate measurements of the time-dependent variation of product spectral contribution for each frequency (Figure 4) reveals remarkable sensitivity of the reaction rate on small changes in milling frequency.

The in situ monitoring data indicates that the reaction progress adopts a sigmoidal profile at milling frequencies higher than 25 Hz, which is consistent with the results of earlier ex situ studies of a Knoevenagel condensation reaction [22]. At milling frequencies below 25 Hz, however, the reaction appears to exhibits linear behavior. Further insight into the frequency-dependent behavior of our model reaction is obtained from the consistency of measurements within each set of triplicate in situ Raman scattering datasets for a given milling frequency (Figure 5). The individual datasets before averaging reveal that all measurements for a particular frequency are mutually consistent when milling at 30 Hz, 27.5 Hz, 22.5 Hz and 20 Hz.

At 25 Hz, however, the behavior of the reaction for each of the triplicate measurements was highly erratic and generally irreproducible. Overall, there is a clear difference in the kinetics of product formation when ball milling at 27.5 Hz and 30 Hz, compared to milling at frequencies of 20 Hz and 22.5 Hz, while
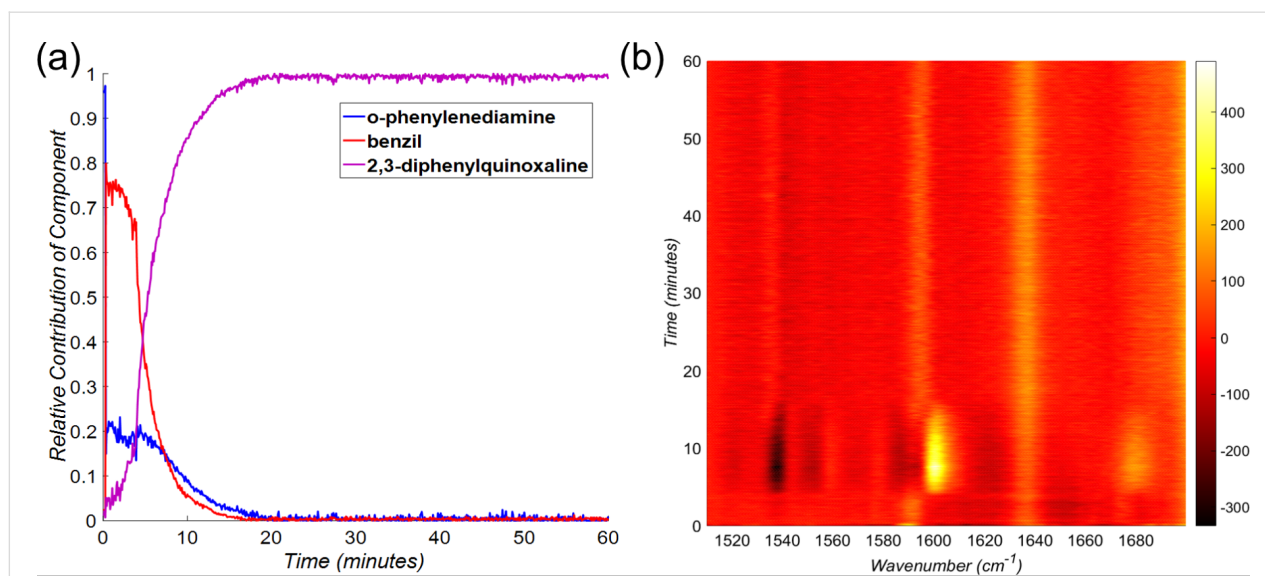
Figure 3: (Left) Estimated contribution of each component for each Raman spectrum over time of the synthesis of 2,3-diphenylquinoxaline at 30 Hz. (Right) Residual plot of the difference between experimental and estimated Raman spectra. In this case, this plot suggests an overestimation of 2,3-diphenylquinoxaline and an underestimation of *o*-phenylenediamine between ≈5 and ≈15 minutes. More information on the fitting can be found in Supporting Information File 1.
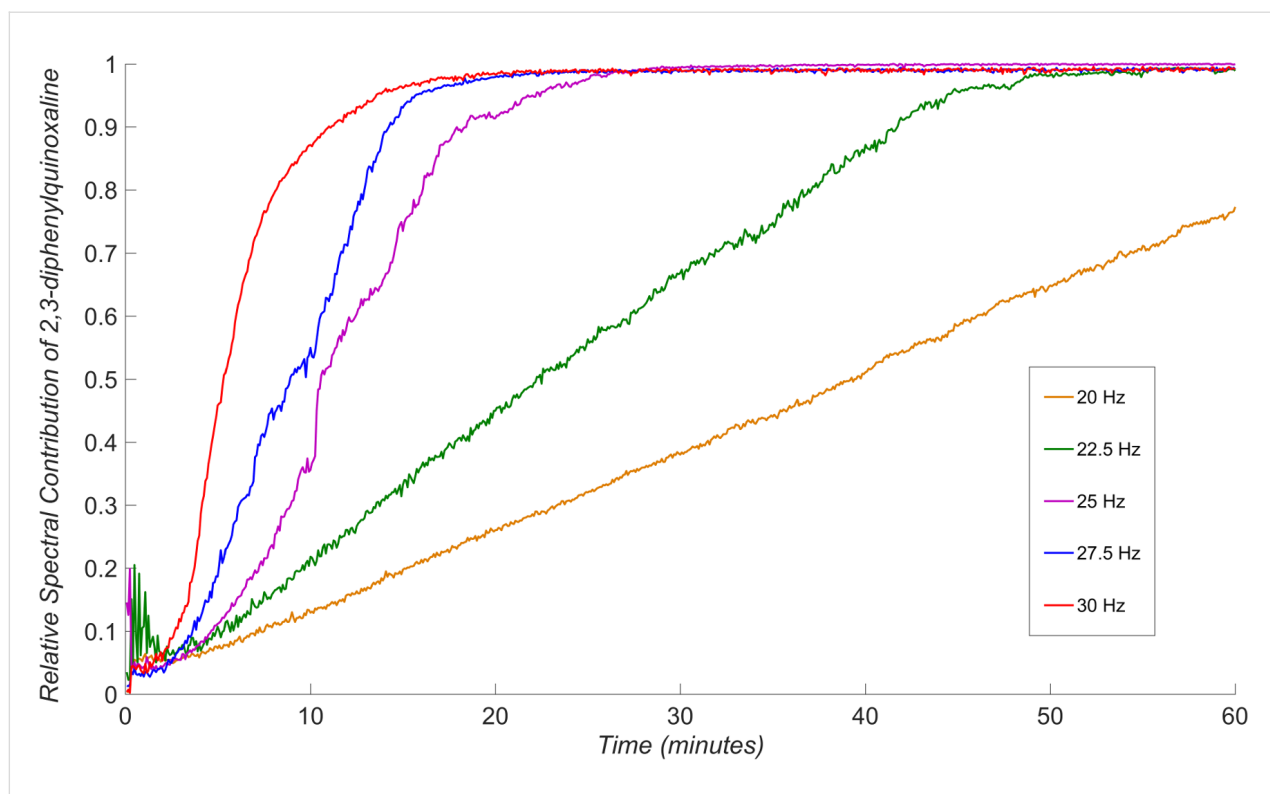
Figure 4: The effect of milling frequency on the milling condensation of benzil and *o*-phenylenediamine to form 2,3-diphenylquinoxaline, with data for each milling frequency averaged from a set of triplicate measurements. Variation close to the onset of milling may be due to poor initial homogeneity of the sample.
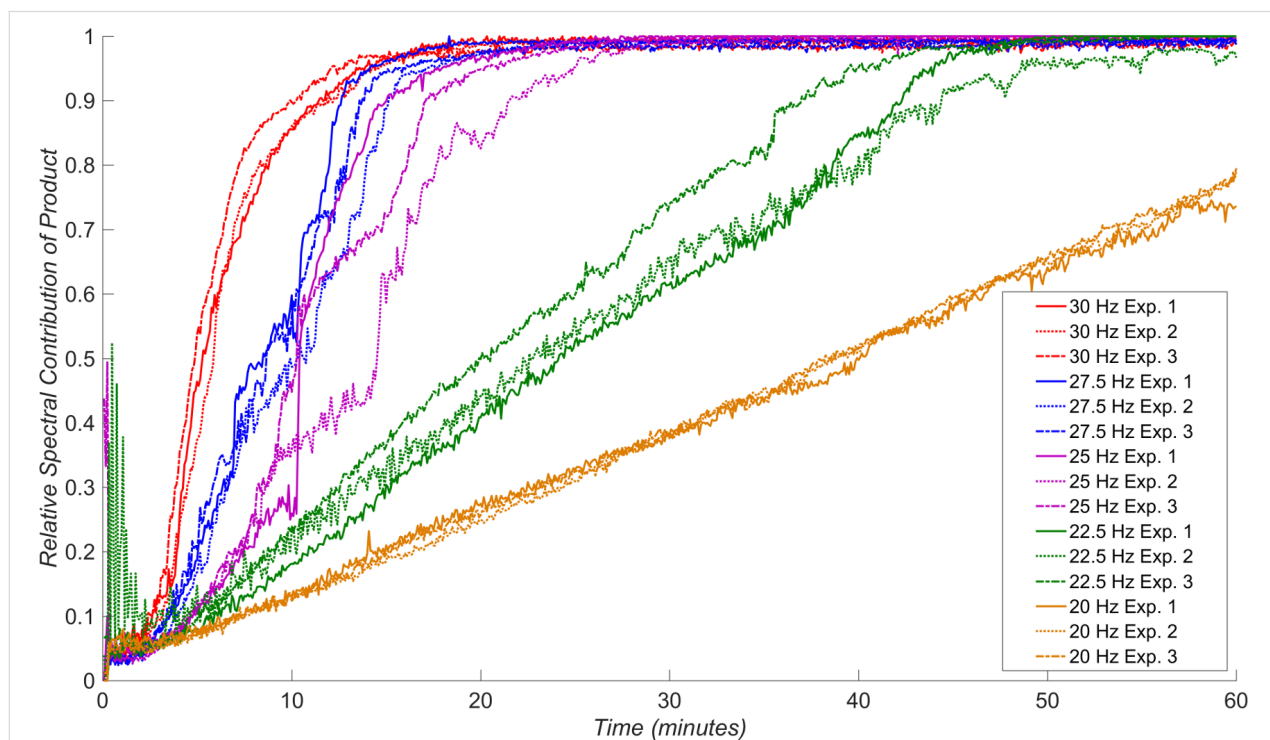
Figure 5: The reproducibility of varying milling frequency on the neat mechanochemical condensation of benzil and *o*-phenylenediamine, as measured by triplicate experiments.

milling at an intermediate frequency of 25 Hz led to irreproducible behavior. Tentatively, we interpret such switching between reactivity profiles by adopting the assumption that mechanochemical reactions proceed through the introduction of mechanically activated sites at which the reactions are facilitated, such as stacking faults and structural defects in general [48]. In such a scenario, different frequencies of milling are expected to lead to different levels of mechanical activation: at lower frequencies (i.e., 20 Hz or 22.5 Hz), the extent of mechanical activation is expected to be lower and product formation can progress at a similar rate to creation of novel activated sites. In contrast, at higher milling frequencies the rate of mechanical activation is much higher and product formation takes place in a highly activated environment, leading to a sigmoidal dependence of product formation with time. The above tentative explanation of our observations suggests that real-time Raman spectroscopy studies could offer an opportunity to directly probe the nature of mechanical activation underlying mechanochemical reactivity. Importantly, the proposed explanation is also consistent with different modes of ball motion during milling, as lower frequencies are known to favor rolling and shearing motion, whereas higher ones should lead to a greater number of more energetic mechanical impacts [25,49].
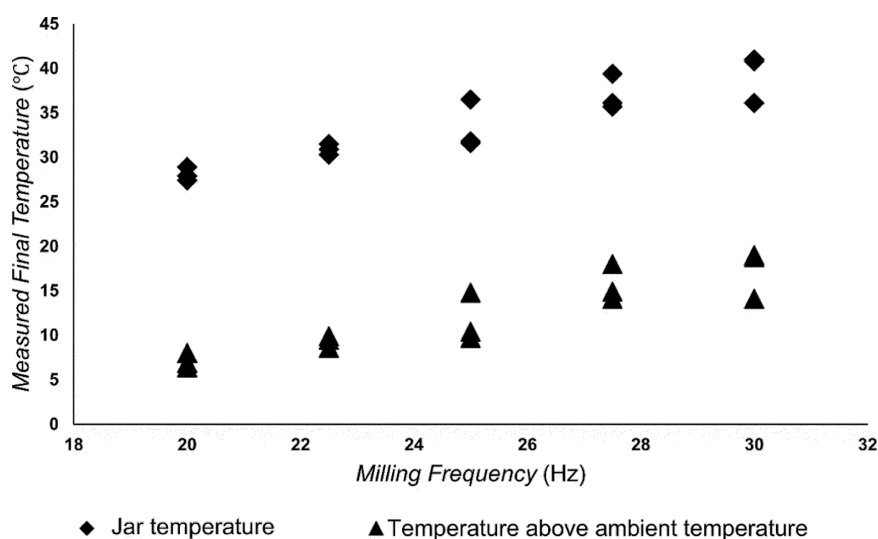
Milling frequency vs temperature

One of the challenges in exploring the effects of milling frequency on mechanochemical reactivity is the increase in temperature of milling jars due to frictional heating [50,51]. Due to such heating effects, an increase in milling frequency should lead not only to greater mechanical activation, e.g., through impact and structure deformation, but also to an increase in reaction rate [52]. In order to evaluate the thermal effect associated with each of herein explored ball milling frequencies, we have also measured the temperature of the internal jar wall immediately after milling, revealing a potentially linear relationship between milling frequency and jar temperature (Figure 6). Importantly, the measured temperature never exceeded 45 °C, and was never higher than 19 °C above the ambient temperature. Although the observed temperature increases are generally not very large, they might be relevant for the observed variation of reaction kinetics with milling frequency, especially as a recent variable-temperature in situ PXRD study has demonstrated that mechanochemical reaction rates can be highly sensitive to temperature [52].

Conclusion

In conclusion, we have utilized an in-house Raman spectroscopy setup to conduct real-time, in situ monitoring of the progress of a model mechanochemical organic reaction at different ball milling frequencies. The methodologies for real-time monitoring of mechanochemistry by ball milling have only recently been introduced and have so far been employed largely in studies of metal-organic or organic materials (e.g., model pharmaceutical cocrystals). The herein presented proof-of-principle study is the first to investigate in real time how the milling frequency, which is one of the fundamental parameters of mechanochemical reactivity, affects an organic transformation. Our results reveal high sensitivity of a carefully selected model mechanochemical reaction to the milling frequency, and establishment of clearly different regimes of reaction kinetics depending on the frequency. At lower frequencies, the model reaction exhibits a largely linear profile, resembling pseudo-zero order reaction kinetics, whereas increasing the frequency lead to a switch to apparently sigmoidal behavior. While these

Figure 6: The effect of milling frequency on the internal jar temperature measured immediately after reaction completion.

observations can tentatively be rationalized by different levels of mechanical activation of the reaction mixture at different frequencies, validating such an explanation requires further and quantitative studies. Nevertheless, we believe that the apparent ability of a mechanochemical reaction to switch between different regimes of chemical kinetics in response to minor changes in milling frequency is an important observation not only in the context of organic mechanochemistry, and may even be of importance in reconciling differences in recently reported in situ and ex situ studies of mechanochemical reactivity [22,41,42,53].

Experimental
Chemicals
Benzil (98%) was purchased from Aldrich Chemical. *o*-Phenylenediamine (98%) was purchased from Alfa Aesar. Both were used without further purification.

Milling reactions and characterization
The double condensation was conducted by milling 210 mg of benzil (1.0 mmol) and 108 mg of *o*-phenylenediamine (1.0 mmol) with a single zirconia ball of 10 mm diameter (ca. 3 grams weight) in a 15 mL poly(methyl methacrylate) (PMMA) optically transparent milling jar, using a Retsch® MM400 mixer mill. For all real-time reaction monitoring, reactions were monitored using a RamanRxn1™ analyzer by Kaiser Optical Systems Inc. every 5 seconds using a 785 nm laser. Spectra were dark and intensity corrected using the Holograms® software package before being processed. The products of these reactions were analyzed without purification. The identity of the final product was confirmed through ^{1}H and ^{13}C NMR in CDCl$_3$ using a 500 MHz AVIIIHD 500 Bruker spectrometer. Infrared spectra were collected on a Bruker Vertex 70 FT-IR Platinum ATR, while X-ray powder diffraction patterns were collected on a Proto Manufacturing AXRD Benchtop Powder Diffractometer using Ni-filtered Cu K$_\alpha$ radiation. The conversion for each solid-state reaction was evaluated after milling using ^{1}H NMR spectroscopy conducted in CDCl$_3$ on a 300 MHz Varian Mercury spectrometer. The ambient temperature was measured using a digital thermometer by VWR and the internal jar temperature was acquired immediately after milling finished using a Mastercraft Temperature Reader with Digital Display and Laser Pointer (accuracy ±2 °C).

Supporting Information

Supporting Information File 1
Experimental part.
[http://www.beilstein-journals.org/bjoc/content/supplementary/1860-5397-13-216-S1.pdf]

References
1. Hernández, J. G.; Friščić, T. *Tetrahedron Lett.* **2015,** *56,* 4253–4265. doi:10.1016/j.tetlet.2015.03.135
2. James, S. L.; Adams, C. J.; Bolm, C.; Braga, D.; Collier, P.; Friščić, T.; Grepioni, F.; Harris, K. D. M.; Hyett, G.; Jones, W.; Krebs, A.; Mack, J.; Maini, L.; Orpen, A. G.; Parkin, I. P.; Shearouse, W. C.; Steed, J. W.; Waddell, D. C. *Chem. Soc. Rev.* **2012,** *41,* 413–447. doi:10.1039/C1CS15171A
3. Ostwald, W. *The fundamental principles of chemistry: an introduction to all text-books of chemistry;* Longmans, Green, and Company: New York, 1909.
4. Takacs, L. *Chem. Soc. Rev.* **2013,** *42,* 7649–7659. doi:10.1039/c2cs35442j
5. Wang, G.-W. *Chem. Soc. Rev.* **2013,** *42,* 7668–7700. doi:10.1039/c3cs35526h
6. Stolle, A.; Szuppa, T.; Leonhardt, S. E. S.; Ondruschka, B. *Chem. Soc. Rev.* **2011,** *40,* 2317–2329. doi:10.1039/c0cs00195c
7. Rodríguez, B.; Bruckmann, A.; Rantanen, T.; Bolm, C. *Adv. Synth. Catal.* **2007,** *349,* 2213–2233. doi:10.1002/adsc.200700252
8. Stolle, A.; Ondruschka, B. *Pure Appl. Chem.* **2011,** *83,* 1343–1349. doi:10.1351/PAC-CON-10-09-26
9. Juribašić, M.; Užarević, K.; Gracin, D.; Ćurić, M. *Chem. Commun.* **2014,** *50,* 10287–10290. doi:10.1039/C4CC04423A
10. Rightmire, N. R.; Hanusa, T. P. *Dalton Trans.* **2016,** *45,* 2352–2362. doi:10.1039/C5DT03866A
11. Tan, D.; Loots, L.; Friščić, T. *Chem. Commun.* **2016,** *52,* 7760–7781. doi:10.1039/C6CC02015A
12. Delori, A.; Friščić, T.; Jones, W. *CrystEngComm* **2012,** *14,* 2350–2362. doi:10.1039/c2ce06582g
13. Friščić, T. *Chem. Soc. Rev.* **2012,** *41,* 3493–3510. doi:10.1039/c2cs15332g
14. Friščić, T. *J. Mater. Chem.* **2010,** *20,* 7599–7605. doi:10.1039/c0jm00872a
15. Braga, D.; Giaffreda, S. L.; Grepioni, F.; Pettersen, A.; Maini, L.; Curzi, M.; Polito, M. *Dalton Trans.* **2006,** 1249–1263. doi:10.1039/b516165g
16. Ralphs, K.; Hardacre, C.; James, S. L. *Chem. Soc. Rev.* **2013,** *42,* 7701–7718. doi:10.1039/c3cs60066a
17. Julien, P. A.; Užarević, K.; Katsenis, A. D.; Kimber, S. A. J.; Wang, T.; Farha, O. K.; Zhang, Y.; Casaban, J.; Germann, L. S.; Etter, M.; Dinnebier, R. E.; James, S. L.; Halasz, I.; Friščić, T. *J. Am. Chem. Soc.* **2016,** *138,* 2929–2932. doi:10.1021/jacs.5b13038
18. Tan, D.; Mottillo, C.; Katsenis, A. D.; Štrukil, V.; Friščić, T. *Angew. Chem., Int. Ed.* **2014,** *53,* 9321–9324. doi:10.1002/anie.201404120
19. Wang, G.-W.; Komatsu, K.; Murata, Y.; Shiro, M. *Nature* **1997,** *387,* 583–586. doi:10.1038/42439

20. Hernández, J. G.; Bolm, C. *J. Org. Chem.* **2017,** *82,* 4007–4019. doi:10.1021/acs.joc.6b02887
21. Shi, Y. X.; Xu, K.; Clegg, J. K.; Ganguly, R.; Hirao, H.; Friščić, T.; García, F. *Angew. Chem., Int. Ed.* **2016,** *55,* 12736–12740. doi:10.1002/anie.201605936
22. Štrukil, V.; Gracin, D.; Magdysyuk, O. V.; Dinnebier, R. E.; Friščić, T. *Angew. Chem., Int. Ed.* **2015,** *54,* 8440–8443. doi:10.1002/anie.201502026
23. Stolle, A.; Schmidt, R.; Jacob, K. *Faraday Discuss.* **2014,** *170,* 267–286. doi:10.1039/C3FD00144J
24. Schmidt, R.; Burmeister, C. F.; Baláž, M.; Kwade, A.; Stolle, A. *Org. Process Res. Dev.* **2015,** *19,* 427–436. doi:10.1021/op5003787
25. McKissic, K. S.; Caruso, J. T.; Blair, R. G.; Mack, J. *Green Chem.* **2014,** *16,* 1628–1632. doi:10.1039/c3gc41496e
26. Michalchuk, A. A. L.; Tumanov, I. A.; Drebushchak, V. A.; Boldyreva, E. V. *Faraday Discuss.* **2014,** *170,* 311–335. doi:10.1039/C3FD00150D
27. Užarević, K.; Halasz, I.; Friščić, T. *J. Phys. Chem. Lett.* **2015,** *6,* 4129–4140. doi:10.1021/acs.jpclett.5b01837
28. Halasz, I.; Kimber, S. A. J.; Beldon, P. J.; Belenguer, A. M.; Adams, F.; Honkimäki, V.; Nightingale, R. C.; Dinnebier, R. E.; Friščić, T. *Nat. Protoc.* **2013,** *8,* 1718–1729. doi:10.1038/nprot.2013.100
29. Friščić, T.; Halasz, I.; Beldon, P. J.; Belenguer, A. M.; Adams, F.; Kimber, S. A. J.; Honkimäki, V.; Dinnebier, R. E. *Nat. Chem.* **2013,** *5,* 66–73. doi:10.1038/nchem.1505
30. Gracin, D.; Štrukil, V.; Friščić, T.; Halasz, I.; Užarević, K. *Angew. Chem., Int. Ed.* **2014,** *53,* 6193–6197. doi:10.1002/anie.201402334
31. Batzdorf, L.; Fischer, F.; Wilke, M.; Wenzel, K.-J.; Emmerling, F. *Angew. Chem., Int. Ed.* **2015,** *54,* 1799–1802. doi:10.1002/anie.201409834
32. Tumanov, I. A.; Achkasov, A. F.; Boldyreva, E. V.; Boldyrev, V. V. *CrystEngComm* **2011,** *13,* 2213–2216. doi:10.1039/c0ce00869a
33. Cinčić, D.; Friščić, T.; Jones, W. *J. Am. Chem. Soc.* **2008,** *130,* 7524–7525. doi:10.1021/ja801164v
34. Karki, S.; Friščić, T.; Jones, W. *CrystEngComm* **2009,** *11,* 470–481. doi:10.1039/B812531G
35. Štrukil, V.; Fábián, L.; Reid, D. G.; Duer, M. J.; Jackson, G. J.; Eckert-Maksić, M.; Friščić, T. *Chem. Commun.* **2010,** *46,* 9191–9193. doi:10.1039/c0cc03822a
36. Braga, D.; Giaffreda, S. L.; Grepioni, F.; Polito, M. *CrystEngComm* **2004,** *6,* 459–462. doi:10.1039/B406375A
37. Katsenis, A. D.; Puškarić, A.; Štrukil, V.; Mottillo, C.; Julien, P. A.; Užarević, K.; Pham, M.-H.; Do, T.-O.; Kimber, S. A. J.; Lazić, P.; Magdysyuk, O.; Dinnebier, R. E.; Halasz, I.; Friščić, T. *Nat. Commun.* **2015,** *6,* No. 6662. doi:10.1038/ncomms7662
38. Halasz, I.; Puškarić, A.; Kimber, S. A. J.; Beldon, P. J.; Belenguer, A. M.; Adams, F.; Honkimäki, V.; Dinnebier, R. E.; Patel, B.; Jones, W.; Štrukil, V.; Friščić, T. *Angew. Chem., Int. Ed.* **2013,** *52,* 11538–11541. doi:10.1002/anie.201305928
39. Tireli, M.; Juribašić Kulcsar, M.; Cindro, N.; Gracin, D.; Biliškov, N.; Borovina, M.; Ćurić, M.; Halasz, I.; Užarević, K. *Chem. Commun.* **2015,** *51,* 8058–8061. doi:10.1039/C5CC01915J
40. Sahoo, P. K.; Giri, C.; Haldar, T. S.; Puttreddy, R.; Rissanen, K.; Mal, P. *Eur. J. Org. Chem.* **2016,** 1283–1291. doi:10.1002/ejoc.201600005
41. Ma, X.; Yuan, W.; Bell, S. E. J.; James, S. L. *Chem. Commun.* **2014,** *50,* 1585–1587. doi:10.1039/c3cc47898j
42. Michalchuk, A. A. L.; Tumanov, I. A.; Konar, S.; Kimber, S. A. J.; Pulham, C. R.; Boldyreva, E. V. *Adv. Sci.* **2017,** *4,* 1700132. doi:10.1002/advs.201700132
43. Schmidt, R.; Stolle, A.; Ondruschka, B. *Green Chem.* **2012,** *14,* 1673–1679. doi:10.1039/c2gc16508b
44. Yin, S.; Yamaki, H.; Komatsu, M.; Zhang, Q.; Wang, J.; Tang, Q.; Saito, F.; Sato, T. *J. Mater. Chem.* **2003,** *13,* 2996–3001. doi:10.1039/b309217h
45. Strachan, C. J.; Rades, T.; Gordon, K. C.; Rantanen, J. *J. Pharm. Pharmacol.* **2007,** *59,* 179–192. doi:10.1211/jpp.59.2.0005
46. Sonneveld, E. J.; Visser, J. W. *J. Appl. Crystallogr.* **1975,** *8,* 1–7. doi:10.1107/S0021889875009417
47. Lawson, C.; Hanson, R. *Solving Least Squares Problems;* Prentice-Hall: Upper Saddle River, New Jersey, 1974; pp 161 ff.
48. Baláž, P.; Achimovičová, M.; Baláž, M.; Billik, P.; Cherkezova-Zheleva, Z.; Criado, J. M.; Delogu, F.; Dutková, E.; Gaffet, E.; Gotor, F. J.; Kumar, R.; Mitov, I.; Rojac, T.; Senna, M.; Streletskii, A.; Wieczorek-Ciurowa, K. *Chem. Soc. Rev.* **2013,** *42,* 7571–7637. doi:10.1039/c3cs35468g
49. Michalchuk, A. A. L.; Tumanov, I. A.; Boldyreva, E. V. *CrystEngComm* **2013,** *15,* 6403–6412. doi:10.1039/c3ce40907d
50. Kulla, H.; Wilke, M.; Fischer, F.; Röllig, M.; Maierhofer, C.; Emmerling, F. *Chem. Commun.* **2017,** *53,* 1664–1667. doi:10.1039/C6CC08950J
51. Fang, Y.; Salamé, N.; Woo, S.; Bohle, D. S.; Friščić, T.; Cuccia, L. A. *CrystEngComm* **2014,** *16,* 7180–7185. doi:10.1039/C4CE00328D
52. Užarević, K.; Štrukil, V.; Mottillo, C.; Julien, P. A.; Puškarić, A.; Friščić, T.; Halasz, I. *Cryst. Growth Des.* **2016,** *16,* 2342–2347. doi:10.1021/acs.cgd.6b00137
53. Halasz, I.; Friščić, T.; Kimber, S. A. J.; Užarević, K.; Puškarić, A.; Mottillo, C.; Julien, P.; Štrukil, V.; Honkimäki, V.; Dinnebier, R. E. *Faraday Discuss.* **2014,** *170,* 203–221. doi:10.1039/C4FD00013G

License and Terms

A mechanochemical approach to access the proline–proline diketopiperazine framework

Nicolas Pétry[1], Hafid Benakki[1,2], Eric Clot[3], Pascal Retailleau[4], Farhate Guenoun[2], Fatima Asserar[2], Chakib Sekkat[2], Thomas-Xavier Métro[*1], Jean Martinez[1] and Frédéric Lamaty[*1]

Address:
[1]Institut des Biomolécules Max Mousseron (IBMM), UMR 5247, CNRS, Université de Montpellier, ENSCM, Campus Triolet, Place Eugène Bataillon, 34095 Montpellier Cedex 5, France, [2]Laboratory of Chemistry Biology Applied to the Environment, Faculty of Sciences, Moulay Ismail University BP: 11201 Zitoune Meknès, Morocco, [3]Institut Charles Gerhardt, UMR 5253 CNRS-UM-ENSCM, Université de Montpellier, Place Eugène Bataillon, cc 1501, 34095 Montpellier Cedex 5, France and [4]Institut de Chimie des Substances Naturelles, CNRS UPR 2301, Université Paris-Saclay, 1 Avenue de la Terrasse, 91198 Gif-sur-Yvette, France

Email:
Thomas-Xavier Métro[*] - thomas-xavier.metro@umontpellier.fr;
Frédéric Lamaty[*] - frederic.lamaty@umontpellier.fr

* Corresponding author

Abstract

Ball milling was exploited to prepare a substituted proline building block by mechanochemical nucleophilic substitution. Subsequently, the mechanocoupling of hindered proline amino acid derivatives was developed to provide proline–proline dipeptides under solvent-free conditions. A deprotection–cyclization sequence yielded the corresponding diketopiperazines that were obtained with a high stereoselectivity which could be explained by DFT calculations. Using this method, an enantiopure disubstituted Pro–Pro diketopiperazine was synthesized in 4 steps, making 5 new bonds using a ball mill.

Introduction

2,5-Diketopiperazines (DKPs) are heterocyclic structures, usually derived from dipeptides, which find many applications in chemistry and biology, and have attracted attention in the last years [1,2]. The diketopiperazine backbone can be found in many natural products exhibiting various biological activities [3]. Consequently, medicinal chemists have used DKPs extensively as a synthetic platform, easily synthesized and stereochemically controlled, for the preparation of small bioactive molecules [4,5]. DKPs have also been considered as chiral auxiliaries in asymmetric synthesis [6]. Furthermore, the

rigidity of the DKPs is a unique feature, used for the preparation of biologically active peptides and peptidomimetics [7], for applications in organocatalysis [8-10], and for the preparation of novel materials [11,12].

An interesting sub-family of these compounds are DKPs derived from the amino acid proline and its analogues, which provide a useful rigid structure. During the course of our project on the exploitation of dimethyl dibromoadipate as a synthon to access original molecules [13,14], we thought that it could provide an original access to the DKP Pro–Pro framework. More specifically, this type of framework has been used as a scaffold for the preparation of small compound libraries [15].

The Pro–Pro diketopiperazine can be prepared directly by dimerization of unprotected proline in a one-pot transformation, generally under harsh conditions [16]. Good results were indeed reported, although this procedure gives access only to symmetrical products and can be detrimental for more fragile molecules such as substituted enantiomerically pure compounds. As shown by a retrosynthetic analysis (Scheme 1), a classical milder approach would consist in preparing first the dipeptide, followed by an intramolecular ester aminolysis. This strategy

has been extensively used [1], involving milder conditions and provides access to unsymmetrical dipeptides and DKPs. Furthermore, substituted prolines could be obtained by nucleophilic substitution of benzylamine from dimethyl dibromoadipate, allowing the addition of functional groups on the Pro–Pro-based framework [17]. Recently, mechanochemistry has become a powerful synthetic technique for making new organic molecules [18,19]. In the course of this project, we applied mechanochemistry to a nucleophilic substitution and the efficient coupling of two proline residues.

Results and Discussion

First we studied the preparation of simple Pro–Pro DKP as a model compound. The use of ball milling in peptide synthesis has drawn some attention in the recent years [20-28]. We took advantage of our extensive experience in peptide mechanosynthesis [20,23-25,27] to prepare the Pro–Pro dipeptide from the corresponding amino acid derivatives. We investigated the coupling of proline *N*-hydroxysuccinimide ester with proline methyl ester in a vibrating ball mill (vbm, Scheme 2) [23].

Surprisingly, while the coupling of various other amino acids previously used yielded the corresponding dipeptides [23], no
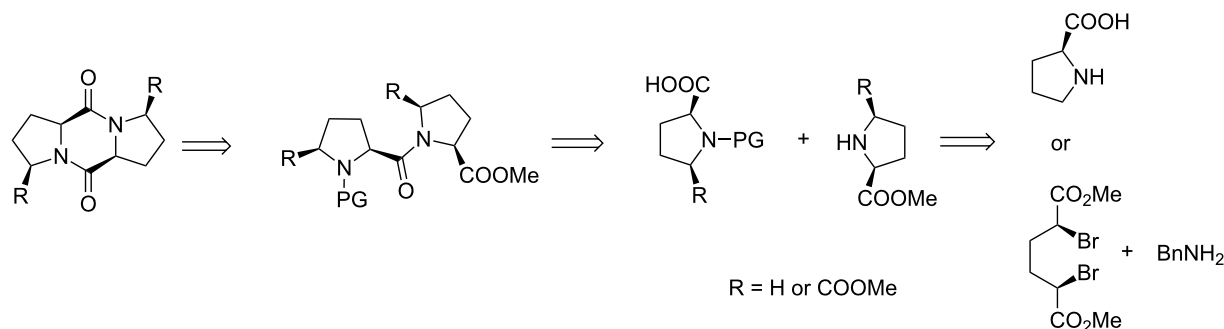
Scheme 1: Retrosynthesis of the Pro–Pro DKP framework.
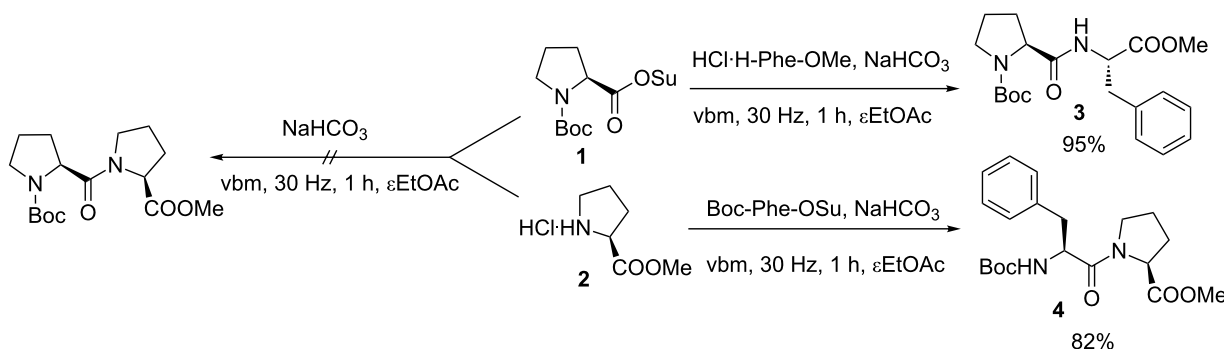
Scheme 2: Coupling with *N*-hydroxysuccinimide-activated amino acids.

reaction occurred in the case of the two prolines **1** and **2**, even by varying the reaction conditions. To verify the reactivity of either Boc–Pro–OSu (**1**) or H–Pro–OMe (**2**) in the mechanocoupling, we reacted HCl·H–Phe–OMe or Boc–Phe–OSu with respectively Boc–Pro–OSu and HCl·H–Pro–OMe. In both cases, the reaction proceeded smoothly to give good yields of dipeptides **3** and **4** (95% of Boc–Pro–Phe–OMe and 82% of Boc–Phe–Pro–OMe, respectively). Most probably, this method was less adapted to hindered amino acid derivatives such as proline.

As an alternative approach, we tested the optimal conditions developed previously for peptide mechanosynthesis [25], starting with unactivated amino acids together with a coupling agent. We had indeed reported two successful examples of couplings involving proline amino esters. The initial conditions, using 1-ethyl-3-(3-dimethylaminopropyl)carbodiimide (EDC), ethyl cyano(hydroxyimino)acetate (oxyma) in the presence of a base and a liquid additive, were adapted to the preparation of Z–Pro–Pro–OMe (**7**) and Boc–Pro–Pro–OMe (**8**, Table 1). It consisted in ball milling the two amino acid derivatives **5** or **6** with **2** in the presence of EDC (coupling agent), a base and a small amount [29] of EtOAc as liquid grinding assistant. The role of oxyma was mainly to suppress amino acid epimerization during the coupling, a limited problem in the case of proline. Consequently, our first experiments did not involve this reagent (Table 1, entries 1–3). Gratifyingly, the initial results showed that this method was adequate to prepare the Pro–Pro dipeptide **7** albeit in fair yield (Table 1, entry 1). Adding more starting material **6** (Table 1, entry 2) and changing the base

(Table 1, entry 3) did not provide much improvement. Finally supplementing the reaction mixture with oxyma (Table 1, entries 4–7) increased the yield up to 85–90% depending on the protection on the proline nitrogen (Boc or Z). Both of the bases gave similar yields (Table 1, entry 5 vs 7 and entry 4 vs 6). Eventually, as proposed before [25], NaH_2PO_4 was preferred since it would avoid a potential pressure build-up (release of CO_2) which could occur with $NaHCO_3$. Noteworthy, no epimerization could be detected by NMR or HPLC analyses.

Both peptides **7** and **8** were then deprotected and cyclized into the corresponding diketopiperazine **9**. Palladium-catalyzed hydrogenolysis of the Z group of **7**, in the presence of $NaHCO_3$, in MeOH, provided the DKP **9** in 83% yield. Compound **8** was deprotected with gaseous HCl, and the resulting dipeptide was cyclized in the presence of $NaHCO_3$, in MeOH, yielding 70% of **9** (Scheme 3).

Then, as proposed above, we expanded this method to the preparation of substituted Pro–Pro DKPs. For this purpose, we considered using dimethyl (2*R*,5*S*)-pyrrolidine-2,5-dicarboxylate (*cis*-**11**) as a building block in the synthesis of dipeptides and diketopiperazines. This building block was used in a very limited number of cases for the formation of DKP in combination with an amino acid derivative [30,31]. Original preparative conditions of the protected compound **11** consisted in performing a nucleophilic substitution of benzylamine with meso dimethyl-2,5-dibromohexanedioate (**10**) in benzene or toluene as solvent, yielding two diastereomers *cis*-**11** (meso) and *trans*-**11** (racemic), which could be separated by crystallization or

Table 1: Optimization of the Pro-Pro coupling[a].
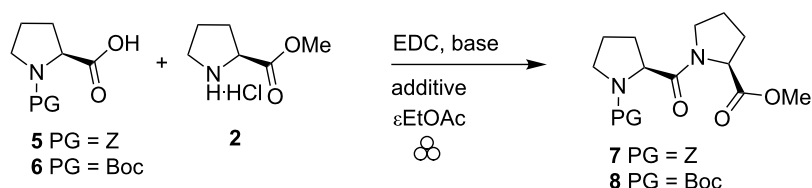
Entry	PG	equiv of **5** or **6**	Base (equiv)	Activating agent (equiv)	Reaction time	Yield (%)
1	Boc	1.2	$NaHCO_3$ (3)	EDC (1.2)	1 h	65
2	Boc	1.2 + 0.5	$NaHCO_3$ (3)	EDC (1.5)	2 × 45 min	68
3	Boc	1.2 + 0.5	NaH_2PO_4 (3)	EDC (1.5)	2 × 45 min	66
4	Boc	1.2	$NaHCO_3$ (4)	EDC/oxyma (1.2)	1 h	78
5	Z	1.2	$NaHCO_3$ (4)	EDC/oxyma (1.2)	1 h	90
6	Boc	1.2	NaH_2PO_4 (4)	EDC/oxyma (1.2)	1 h	85
7	Z	1.2	NaH_2PO_4 (4)	EDC/oxyma (1.2)	1 h	88

[a]Reactions performed under air, in a vibrating ball mill (vbm) at 30 Hz with EtOAc (as a liquid grinding assistant).
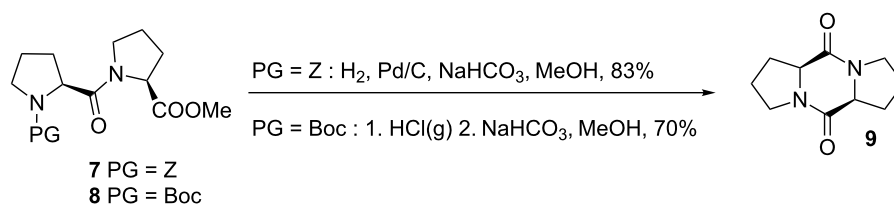
Scheme 3: Synthesis of Pro–Pro DKP.

column chromatography [17,32,33]. Trying to avoid as much as possible the use of (toxic) solvents, we considered extending the known nucleophilic substitution in a ball mill [34-41] to this reaction system (Table 2).

For sake of comparison, we first performed the reaction between *meso*-**10** and benzylamine in toluene (Table 2, entry 1) providing a full conversion into the expected product **11** with a 78:22 *cis/trans* ratio. Then we studied the mechanosynthesis of these compounds (Table 2, entries 2–8), starting by mixing an equimolar amount of the starting materials together with a base (K₂CO₃) in a vibratory ball mill at 25 Hz (Table 2, entry 2). This resulted in a lower conversion compared to that obtained in solution. Using an excess of base increased the conversion to 62% (Table 2, entry 3). Switching to Cs₂CO₃ resulted in an increased conversion of 74% (Table 2, entry 4), further improved to 82% when the milling frequency was adjusted to 30 Hz (Table 2, entry 5). Adding EtOAc as liquid grinding assistant did not improve the conversion, with either K₂CO₃ or Cs₂CO₃ (Table 2, entries 6 and 7). Finally, we tested the planetary ball

mill (pbm) with the advantage of its capacity to produce more material. In this case (Table 2, entry 8), using cheaper K₂CO₃, full conversion was obtained and *cis*-**11** was isolated in 75% yield and a larger amount of *cis*-**11** could be prepared. Interestingly the *cis/trans* ratio (*cis*-**11**/*trans*-**11**) was different when the reaction was performed in solution (Table 2, entry 1) or in the ball mill (Table 2, entries 2–9) with a higher selectivity in the latter case [42].

With this building block in hands, the preparation of a variety of DKPs could be envisaged (Scheme 4).

Pyrrolidine *cis*-**11** is an *N*-protected amino ester, which can be used in the synthesis of diketopiperazines by deprotecting either the amino group or the ester function. Hydrogenolysis of the benzyl group of *cis*-**11** provided the nitrogen-free pyrrolidine derivative **12** in excellent yield and purity after filtration of the catalytic system. **12** was engaged without further purification in a coupling reaction with Z-proline (**5**) and Boc-proline (**6**), in the solvent-free conditions described above. In both cases, the

Table 2: Optimization of the substitution reaction.

Entry	equiv BnNH₂	Base (equiv)	Conditions	Conversion[a]	*cis/trans*-**11** ratio
1	3	–	toluene, 16 h, reflux	100	78:22
2	1	K₂CO₃ (1.2)	vbm, 1 h, 25 Hz	40	96:04
3	1	K₂CO₃ (3)	vbm, 1 h, 25 Hz	62	98:02
4	1.1	Cs₂CO₃ (3)	vbm, 1 h, 25 Hz	74	91:09
5	1.1	Cs₂CO₃ (3)	vbm, 1 h, 30 Hz	82	94:06
6	1.1	K₂CO₃ (3)	vbm, 1 h, 30 Hz[b]	49	98:02
7	1.1	Cs₂CO₃ (3)	vbm, 1 h, 30 Hz[b]	59	87:13
8	1.3	K₂CO₃ (2.2)	pbm, 2 h, 500 rpm[b]	97	97:03

[a]Measured by ¹H NMR [b]EtOAc was used as liquid grinding assistant.
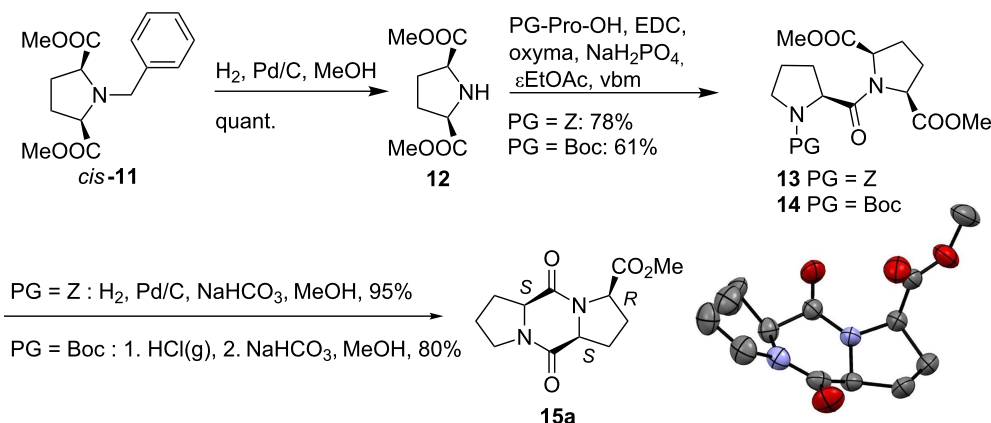
Scheme 4: Synthesis of substituted Pro–Pro DKP **15a**.

dipeptides **13** and **14** were obtained in good yields (78 and 61%, respectively). Deprotection followed by cyclization provided the corresponding diketopiperazine **15a** in 95% yield (from **13**) or 80% yield (from **14**). In this case, two carboxymethyl groups could participate in the cyclization providing two possible diastereomers **15a** and **15b** (Scheme 5).

To our delight, this stereodivergent cyclization was selective and only one diastereomer was obtained, as supported by analytical data. X-ray analysis of the product confirmed the stereochemistry of the three chiral centres and the structure of **15a**.

To shed more light on the origin of the selectivity observed in the deprotection–cyclization transformation, DFT calculations

of the reaction mechanism have been carried out. DFT calculations were applied to the various pathways starting from the deprotected amine **16** and reaction pathways leading to either product **15a**, resulting from nucleophilic attack of the amine on C_a, or to product **15b** resulting from attack on C_b, were considered (Scheme 5).

The first step was to study if there was any preferential interaction between the free nitrogen atom and either C_a or C_b before the C–N bond formation. Both optimized structures are shown in Figure 1, and compound **16a** is computed to be less stable than **16b** by $\Delta G = 2.7$ kcal mol^{-1}. The C···N bond distance is slightly shorter in **16b** (2.673 Å) than in **16a** (2.682 Å). Many attempts to locate a transition state structure for the C–N bond
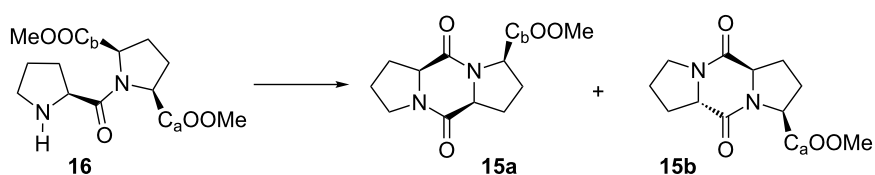
Scheme 5: Potential isomers yielded by cyclization of **16**.
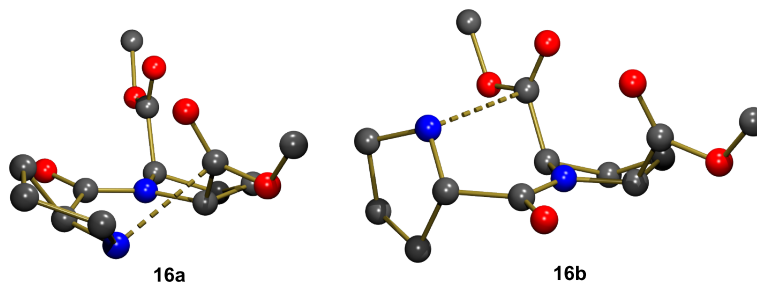
Figure 1: Optimized geometries for the two conformers presenting interactions with either C_a (**16a**) or C_b (**16b**). H atoms were omitted for clarity.

formation starting from either **16a** or **16b** failed. Even though the geometry optimizations were performed with implicit inclusion of the solvent influence (SMD model with methanol), the zwitterionic character developing in the C–N bond formation could not be stabilized. However, the protic methanol solvent could act both as a base to abstract the proton from the nitrogen atom, and as an acid to facilitate the C–OMe bond cleavage. Transition state structures with combined implicit (SMD model) and explicit inclusion of the solvent were thus searched for.

The geometry of **16a** allowed the creation of a network of stabilizing interactions between an explicit methanol solvent molecule and both the N–H proton and the OMe group (N–H···O = 2.153 Å, H···OMe = 1.925 Å; see **16a-solv** in Figure 2). **16a-solv** was computed to be less stable than **16a** by $\Delta G = 9.3$ kcal mol^{-1}. This higher Gibbs free energy was due only to entropic factors as **16a-solv** was computed to be more stable than **16a** by $\Delta E = -4.0$ kcal mol^{-1}. Interestingly, upon interaction with an explicit methanol molecule the C···N distance in **16a-solv** had been reduced to 2.464 Å compared to a value of 2.682 Å in **16a**. A transition state structure, **TS-16a-solv**, corresponding to a concerted C–N bond formation and a C–OMe bond cleavage could be located (Figure 2). Table 3 collects selected bond distances associated to the transformation. In the transition state, the C–OMe bond cleavage was well advanced and the C–N bond formation was also almost complete. This indicated that the transformation was concerted and that the explicit methanol molecule only acted as a relay to accept the proton from the amine and to facilitate the departing of the methoxy group by transferring a proton. The activation energy from **16a-solv** was computed to be $\Delta G^{\#} = 22.8$ kcal mol^{-1}, in good agreement with an easy reaction at room temperature. The reaction was strongly exoergic

with $\Delta G = -17.3$ kcal mol^{-1} and the geometry of **15a-solv** (Figure 2) had the stereochemistry expected for **15a** (Scheme 5).

Table 3: Selected bond distances (Å) for the structures optimized along the transformation **16a-solv→15a-solv**.

Bond	16a-solv	TS-16a-solv	15a-solv
N–H	1.077	1.167	2.310
NH···O	2.153	1.341	0.965
MeO–H	0.970	1.226	1.761
H···OMe	1.925	1.117	0.979
C–OMe	1.340	1.935	3.784
N–C	2.464	1.500	1.343

The geometry of **16b** did not allow creating a similar network of H-bonding interactions when one explicit molecule of methanol was considered. The N–H bond is pointed in a direction of space remote from the methoxy group of the ester functionality. Rotation by 180° around the C–C bond of the ester led to a geometry in which a methanol molecule could interact with both groups as illustrated in **16b-solv** (Figure 3). This structure was computed to be more stable than **16a-solv** by $\Delta G = -3.8$ kcal mol^{-1}, probably because in addition to the expected H-bonds between N–H and O (N–H···O = 2.123 Å), and between O–H and OMe (H···OMe = 2.488 Å), there existed an additional H-bond with the other ester functionality (H···OC = 1.873 Å). However, despite the greater stability of **16b-solv**, the concerted formation of C–N and cleavage of the C–OMe bond through **TS-16b-solv** was associated to a higher activation barrier with $\Delta G^{\#} = 30.0$ kcal mol^{-1} and a less exoergic reaction

16a-solv   TS-16a-solv   15a-solv
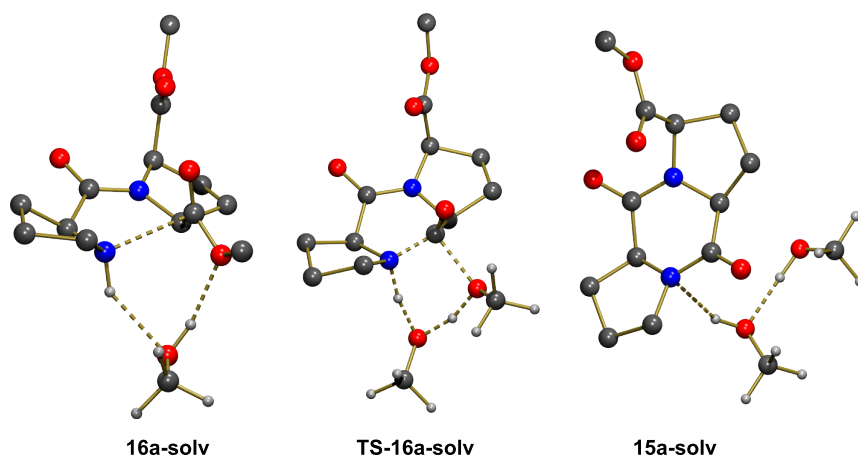
Figure 2: Optimized geometries of the extrema located along the pathway for formation of **15a** with explicit participation of one solvent molecule. Most H atoms were omitted for clarity.
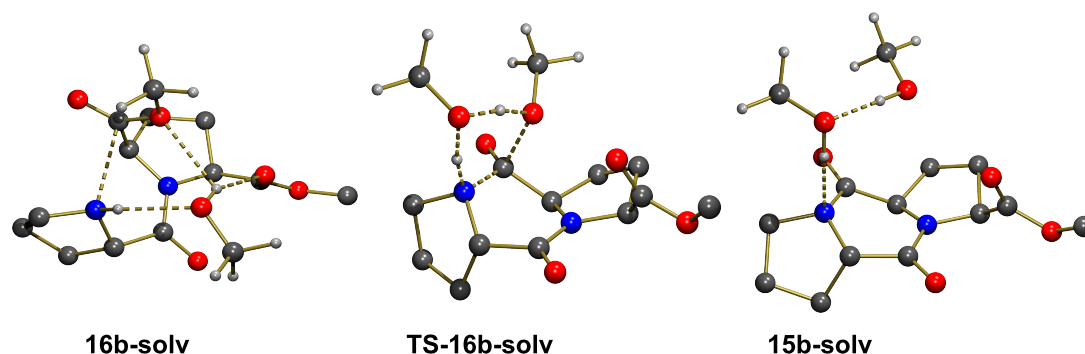
Figure 3: Optimized geometries of the extrema located along the pathway for formation of **15b** with explicit participation of one solvent molecule. Most H atoms were omitted for clarity.

($\Delta G = -2.6$ kcal mol^{-1}). Selected bond distances in Table 4 clearly show that the formation of C–N and cleavage of C–O are both well advanced in **TS-16b-solv**, similarly to the situation observed in **TS-16a-solv**. The essential difference was the significant longer C⋯N distance in **16b-solv** (2.625 Å vs 2.464 Å in **16a-solv**), and the longer H-bond between the methanol molecule and the methoxy group in **16b-solv** (2.488 Å) compared to that observed in **16a-solv** (1.925 Å). The origin of these differences lied in the presence of an H-bond between the methanol molecule and the carbonyl group of the other ester functionality. This interaction stabilized a geometry with a longer C⋯N distance, and destabilized the transition state structure as it needed to be lost in **TS-16b-solv** (H⋯OC = 3.326 Å vs 1.873 Å in **16b-solv**).

There was thus a significant energetic preference for the formation of **15a** with respect to **15b** with a $\Delta\Delta G^{\#} = 7.3$ kcal mol^{-1}. However, the positions of the methanol molecule in

Table 4: Selected bond distances (Å) for the structures optimized along the transformation **16b-solv→15b-solv**.

Bond	16b-solv	TS-16b-solv	15b-solv
N–H	1.018	1.165	2.014
NH⋯O	2.123	1.342	0.971
MeO–H	0.973	1.212	1.751
H⋯OMe	2.488	1.182	0.979
C–OMe	1.326	1.940	3.333
N–C	2.625	1.521	1.365

TS-16a-solv and **TS-16b-solv** were significantly different, and this could be the origin of the stability of the former. Therefore a transition state structure leading to **15b** with the methanol molecule in an "exo" position was optimized (**TSbis-16b-solv**, Figure 4). This transition state was less stable than **TS-16b-solv** by 2.9 kcal mol^{-1}. Alternatively, a transition state structure
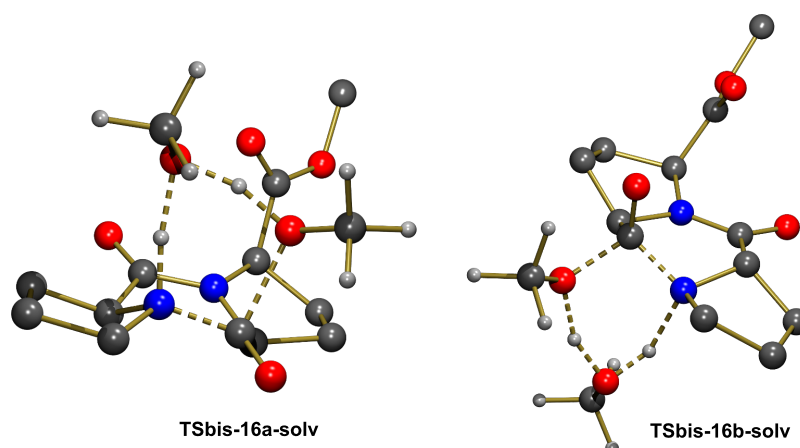
Figure 4: Optimized geometries for the transition states associated to alternate position of the methanol molecule. Most H atoms were omitted for clarity.

leading to **15a** with a methanol molecule in an "endo" position was located (**TSbis-16a-solv**, Figure 4). This structure was computed to be less stable than **TS-16a-solv** by 3.9 kcal mol^{-1}. The calculations thus clearly indicated that there was a low lying pathway for the formation of **15a** consisting in a concerted C–N bond formation and C–OMe bond cleavage mediated by a solvent methanol molecule acting as both a proton acceptor from N–H and a proton donor to OMe. All the alternative pathways were associated to transition states lying at significantly higher energy not to be observed experimentally. This was in agreement with the experimental formation of only **15a**.

As mentioned above, another possibility to exploit *meso* pyrrolidine *cis*-**11** would be to desymmetrize [43] the ester functions by selective hydrolysis. The corresponding carboxylic acid could then be engaged in a peptide coupling. Pig liver esterase (PLE)-catalyzed enzymatic hydrolysis of meso *cis*-**11** provided selectively the *N*-protected amino acid **17** as one enantiomer [33,44,45]. Mechanocoupling of **17** with pyrrolidine **12** provided the dipeptide **18** in excellent yield. Removal of the benzyl group by hydrogenation in the presence of Pd(OH)$_2$/C followed by cyclization provided unprecedented DKP **19** in 52% yield. In this case again, spectral data and X-ray analysis showed the selective formation of diketopiperazine **19** as only one isomer (Scheme 6).

Conclusion

In summary, we have developed an efficient synthesis of two enantiopure substituted diketopiperazines based on the proline–proline framework. The synthetic schemes included two key reactions, which were performed under mechanochemical conditions, including a peptide coupling leading to the formation of Pro–Pro dipeptides, and a nucleophilic substitution furnishing substituted proline derivatives. The diastereoselec-

tive cyclization, which was clearly supported by DFT calculations is noteworthy. Further developments and applications of these scaffolds are currently underway.

Supporting Information

Experimental procedures and characterization of new compounds, X-ray data including CCDC numbers and CIF files.

Supporting Information File 1
Experimental part.
[http://www.beilstein-journals.org/bjoc/content/supplementary/1860-5397-13-217-S1.pdf]

Supporting Information File 2
Crystallographic data.
[http://www.beilstein-journals.org/bjoc/content/supplementary/1860-5397-13-217-S2.pdf]

Supporting Information File 3
X-ray of meso-**10**.
[http://www.beilstein-journals.org/bjoc/content/supplementary/1860-5397-13-217-S3.cif]
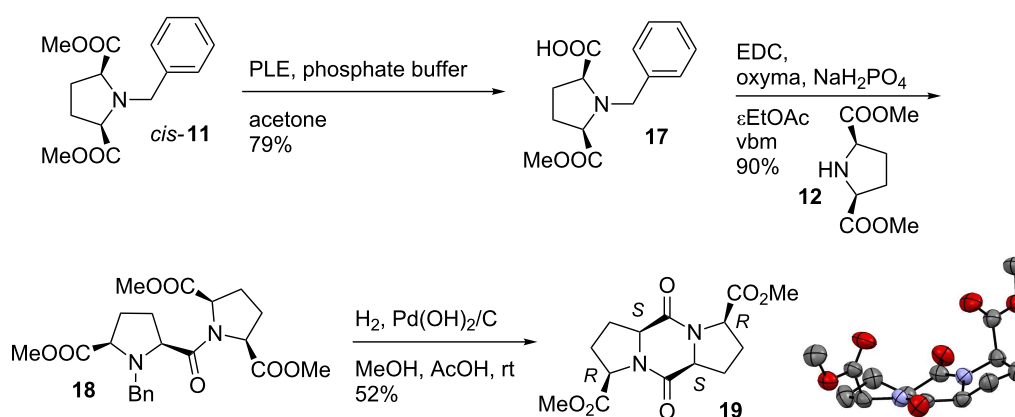
Supporting Information File 4
X-ray of **15a**.
[http://www.beilstein-journals.org/bjoc/content/supplementary/1860-5397-13-217-S4.cif]

Supporting Information File 5
X-ray of **19**.
[http://www.beilstein-journals.org/bjoc/content/supplementary/1860-5397-13-217-S5.cif]

Scheme 6: Synthesis of diketopiperazine **19**.

Acknowledgements

References

1. Borthwick, A. D. *Chem. Rev.* **2012,** *112,* 3641–3716. doi:10.1021/cr200398y
2. Martins, M. B.; Carvalho, I. *Tetrahedron* **2007,** *63,* 9923–9932. doi:10.1016/j.tet.2007.04.105
3. Huang, R.-M.; Yi, X.-X.; Zhou, Y.; Su, X.; Peng, Y.; Gao, C.-H. *Mar. Drugs* **2014,** *12,* 6213–6235. doi:10.3390/md12126213
4. González, J. F.; Ortin, I.; de la Cuesta, E.; Menéndez, J. C. *Chem. Soc. Rev.* **2012,** *41,* 6902–6915. doi:10.1039/c2cs35158g
5. Cornacchia, C.; Cacciatore, I.; Baldassarre, L.; Mollica, A.; Feliciani, F.; Pinnen, F. *Mini-Rev. Med. Chem.* **2012,** *12,* 2–12. doi:10.2174/138955712798868959
6. Sano, S.; Nakao, M. *Heterocycles* **2015,** *91,* 1349–1375. doi:10.3987/REV-15-820
7. Ressurreição, A. S. M.; Delatouche, R.; Gennari, C.; Piarulli, U. *Eur. J. Org. Chem.* **2011,** 217–228. doi:10.1002/ejoc.201001330
8. Durini, M.; Sahr, F. A.; Kuhn, M.; Civera, M.; Gennari, C.; Piarulli, U. *Eur. J. Org. Chem.* **2011,** 5599–5607. doi:10.1002/ejoc.201100794
9. Becker, C.; Hoben, C.; Schollmeyer, D.; Scherr, G.; Kunz, H. *Eur. J. Org. Chem.* **2005,** 1497–1499. doi:10.1002/ejoc.200500044
10. Iyer, M. S.; Gigstad, K. M.; Namdev, N. D.; Lipton, M. *J. Am. Chem. Soc.* **1996,** *118,* 4910–4911. doi:10.1021/ja952686e
11. Kleinsmann, A. J.; Nachtsheim, B. J. *Chem. Commun.* **2013,** *49,* 7818–7820. doi:10.1039/c3cc44110e
12. Xie, Z.; Zhang, A.; Ye, L.; Feng, Z.-g. *Soft Matter* **2009,** *5,* 1474–1482. doi:10.1039/b816664a
13. Lenda, F.; Guenoun, F.; Tazi, B.; Ben Iarbi, N.; Allouchi, H.; Martinez, J.; Lamaty, F. *Eur. J. Org. Chem.* **2005,** 326–333. doi:10.1002/ejoc.200400328
14. Lenda, F.; Crouzin, N.; Cavalier, M.; Guiramand, J.; Lanté, F.; Barbanel, G.; Cohen-Solal, C.; Martinez, J.; Guenoun, F.; Lamaty, F.; Vignes, M. *Amino Acids* **2011,** *40,* 913–922. doi:10.1007/s00726-010-0713-1
15. Deppermann, N.; Prenzel, A. H. G. P.; Beitat, A.; Maison, W. *J. Org. Chem.* **2009,** *74,* 4267–4271. doi:10.1021/jo9004876
16. Nakamura, D.; Kakiuchi, K.; Koga, K.; Shirai, R. *Org. Lett.* **2006,** *8,* 6139–6142. doi:10.1021/ol0626387
17. Cignarella, G.; Nathansohn, G. *J. Org. Chem.* **1961,** *26,* 1500–1504. doi:10.1021/jo01064a046
18. James, S. L.; Adams, C. J.; Bolm, C.; Braga, D.; Collier, P.; Friščić, T.; Grepioni, F.; Harris, K. D. M.; Hyett, G.; Jones, W.; Krebs, A.; Mack, J.; Maini, L.; Orpen, A. G.; Parkin, I. P.; Shearouse, W. C.; Steed, J. W.; Waddell, D. C. *Chem. Soc. Rev.* **2012,** *41,* 413–447. doi:10.1039/C1CS15171A
19. Wang, G.-W. *Chem. Soc. Rev.* **2013,** *42,* 7668–7700. doi:10.1039/c3cs35526h
20. Declerck, V.; Nun, P.; Martinez, J.; Lamaty, F. *Angew. Chem., Int. Ed.* **2009,** *48,* 9318–9321. doi:10.1002/anie.200903510
21. Hernández, J. G.; Juaristi, E. *J. Org. Chem.* **2010,** *75,* 7107–7111. doi:10.1021/jo101159a
22. Štrukil, V.; Bartolec, B.; Portada, T.; Đilović, I.; Halasz, I.; Margetić, D. *Chem. Commun.* **2012,** *48,* 12100–12102. doi:10.1039/c2cc36613d
23. Bonnamour, J.; Métro, T.-X.; Martinez, J.; Lamaty, F. *Green Chem.* **2013,** *15,* 1116–1120. doi:10.1039/c3gc40302e
24. Métro, T.-X.; Colacino, E.; Martinez, J.; Lamaty, F. Amino Acids and Peptides in Ball Milling. In *Ball Milling Towards Green Synthesis: Applications, Projects, Challenges;* Stolle, A.; Ranu, B., Eds.; *RSC Green Chem. Ser.*, Vol. 31; Royal Society of Chemistry: Cambridge, UK, 2015; pp 114–150. doi:10.1039/9781782621980-00114
25. Porte, V.; Thioloy, M.; Pigoux, T.; Métro, T.-X.; Martinez, J.; Lamaty, F. *Eur. J. Org. Chem.* **2016,** 3505–3508. doi:10.1002/ejoc.201600617
26. Landeros, J. M.; Juaristi, E. *Eur. J. Org. Chem.* **2017,** 687–694. doi:10.1002/ejoc.201601276
27. Gonnet, L.; Tintillier, T.; Venturini, N.; Konnert, L.; Hernandez, J.-F.; Lamaty, F.; Laconde, G.; Martinez, J.; Colacino, E. *ACS Sustainable Chem. Eng.* **2017,** *5,* 2936–2941. doi:10.1021/acssuschemeng.6b02439
28. Hernández, J. G.; Ardila-Fierro, K. J.; Crawford, D.; James, S. L.; Bolm, C. *Green Chem.* **2017,** in press.
29. Bowmaker, G. A. *Chem. Commun.* **2013,** *49,* 334–348. doi:10.1039/C2CC35694E
30. Guenoun, F.; Zair, T.; Lamaty, F.; Pierrot, M.; Lazaro, R.; Viallefont, P. *Tetrahedron Lett.* **1997,** *38,* 1563–1566. doi:10.1016/S0040-4039(97)00130-5
31. Yu, W.; Vibulbhan, B.; Rosenblum, S. B.; Martin, G. S.; Vellekoop, A. S.; Holst, C. L.; Coburn, C. A.; Wong, M.; Selyutin, O.; Ji, T.; Zhong, B.; Hu, B.; Chen, L.; Dwyer, M. P.; Jiang, Y.; Nair, A. G.; Tong, L.; Zeng, Q.; Agrawal, S.; Carr, D.; Rokosz, L.; Liu, R.; Curry, S.; McMonagle, P.; Ingravallo, P.; Lahser, F.; Asante-Appiah, E.; Fells, J.; Kozlowski, J. A. *Bioorg. Med. Chem. Lett.* **2016,** *26,* 3793–3799. doi:10.1016/j.bmcl.2016.05.042
32. Kubyshkin, V. S.; Mykhailiuk, P. K.; Ulrich, A. S.; Komarov, I. *Synthesis* **2009,** 3327–3331. doi:10.1055/s-0029-1216963
33. Chiaroni, A.; Riche, C.; Zair, T.; Guenoun, F.; Lazaro, R.; Viallefont, P. *Acta Crystallogr., Sect. C: Cryst. Struct. Commun.* **1997,** *53,* 459–461. doi:10.1107/S0108270196014606
34. Nun, P.; Martin, C.; Martinez, J.; Lamaty, F. *Tetrahedron* **2011,** *67,* 8187–8194. doi:10.1016/j.tet.2011.07.056
35. Nun, P.; Pérez, V.; Calmès, M.; Martinez, J.; Lamaty, F. *Chem. – Eur. J.* **2012,** *18,* 3773–3779. doi:10.1002/chem.201102885
36. Beillard, A.; Golliard, E.; Gillet, V.; Bantreil, X.; Métro, T.-X.; Martinez, J.; Lamaty, F. *Chem. – Eur. J.* **2015,** *21,* 17614–17617. doi:10.1002/chem.201503472
37. Jörres, M.; Aceña, J. L.; Soloshonok, V. A.; Bolm, C. *ChemCatChem* **2015,** *7,* 1265–1269. doi:10.1002/cctc.201500102
38. Abdulwahaab, B. H.; Burke, B. P.; Domarkas, J.; Silversides, J. D.; Prior, T. J.; Archibald, S. J. *J. Org. Chem.* **2016,** *81,* 890–898. doi:10.1021/acs.joc.5b02464
39. Hernández, J. G.; Turberg, M.; Schiffers, I.; Bolm, C. *Chem. – Eur. J.* **2016,** *22,* 14513–14517. doi:10.1002/chem.201603057
40. Sethi, K. P.; Kartha, K. P. R. *Trends Carbohydr. Res.* **2016,** *8,* 29–32.
41. Métro, T.-X.; Salom-Roig, X. J.; Reverte, M.; Martinez, J.; Lamaty, F. *Green Chem.* **2015,** *17,* 204–208. doi:10.1039/C4GC01416B
42. Hernández, J. G.; Bolm, C. *J. Org. Chem.* **2017,** *82,* 4007–4019. doi:10.1021/acs.joc.6b02887
43. Merad, J.; Candy, M.; Pons, J.-M.; Bressy, C. *Synthesis* **2017,** *49,* 1938–1954. doi:10.1055/s-0036-1589493
44. Morimoto, Y.; Terao, Y.; Achiwa, K. *Chem. Pharm. Bull.* **1987,** *35,* 2266–2271. doi:10.1248/cpb.35.2266
45. Chênevert, R.; Jacques, F.; Giguère, P.; Dasser, M. *Tetrahedron: Asymmetry* **2008,** *19,* 1333–1338. doi:10.1016/j.tetasy.2008.05.022

Solvent-free copper-catalyzed click chemistry for the synthesis of *N*-heterocyclic hybrids based on quinoline and 1,2,3-triazole

Martina Tireli[‡1], Silvija Maračić[‡2], Stipe Lukin[1], Marina Juribašić Kulcsár[1], Dijana Žilić[1], Mario Cetina[3], Ivan Halasz[1], Silvana Raić-Malić[*2] and Krunoslav Užarević[*1]

Abstract

Copper-catalyzed mechanochemical click reactions using Cu(II), Cu(I) and Cu(0) catalysts have been successfully implemented to provide novel 6-phenyl-2-(trifluoromethyl)quinolines with a phenyl-1,2,3-triazole moiety at O-4 of the quinoline core. Milling procedures proved to be significantly more efficient than the corresponding solution reactions, with up to a 15-fold gain in yield. Efficiency of both solution and milling procedures depended on the *p*-substituent in the azide reactant, resulting in H < Cl < Br < I reactivity bias. Solid-state catalysis using Cu(II) and Cu(I) catalysts entailed the direct involvement of the copper species in the reaction and generation of highly luminescent compounds which hindered in situ monitoring by Raman spectroscopy. However, in situ monitoring of the milling processes was enabled by using Cu(0) catalysts in the form of brass milling media which offered a direct insight into the reaction pathway of mechanochemical CuAAC reactions, indicating that the catalysis is most likely conducted on the surface of milling balls. Electron spin resonance spectroscopy was used to determine the oxidation and spin states of the respective copper catalysts in bulk products obtained by milling procedures.

Introduction

The copper-catalyzed azide–alkyne cycloaddition (CuAAC) represents a prime example of click chemistry. Click chemistry describes "a set of near-perfect" reactions [1] for an efficient regioselective generation of 1,4-disubstituted 1,2,3-triazoles [1-3]. After their discovery [1], click reactions affording 1,2,3-triazoles rapidly became important for simple and robust binding of versatile molecules and for the building of stable polymer structures [4]. At the same time, the 1,2,3-triazoles be-

came the heterocycle of choice in drug discovery, due to their favourable pharmacokinetic and safety profiles, hydrogen-bonding capability, moderate dipole moment, rigidity and stability under in vivo conditions [5,6]. Also, the ability of 1,2,3-triazoles to act as amide bond bioisosteres made the click reaction a valuable synthetic methodology for conjugation of bioactive molecules [7-9] aiming to improve their biological activities [4,10,11]. Discovery of copper(I) ion catalysis in azide–alkyne cycloadditions was decisive for applications of this reaction, as it increases reaction rates and yields and directs the azide–alkyne cycloaddition exclusively towards 1,4-substituted regioisomers, whereas the non-catalyzed process results in a non-stoichiometric mixture of 1,4- and 1,5-regioisomers. Even though CuAAC reactions are efficiently performed in solution, there is a persistent incentive to find greener alternatives, which would reduce time and energy requirements as well as waste generated by these reactions. Among other non-conventional approaches such as microwave and ultrasound irradiation [7,12,13], mechanochemistry has emerged as a viable approach for CuAAC. In a broader sense, mechanochemistry, i.e., chemical transformations induced by mechanical force [14], has been rapidly advancing in various fields of synthesis and materials sciences, including inorganic [15], organic [16,17] and supramolecular materials [18,19], intermetallic compounds [20], nanoparticles [15,21], and with a wide application in the synthesis of pharmaceutical solids [22]. Furthermore, medicinal mechanochemistry, a new research discipline that provides an access to the active pharmaceutical ingredients, is anticipated to have a strong impact on the future development of medicinal chemistry and demands of the pharmaceutical industry for greener and more efficient approaches to chemical synthesis [23-25]. In accordance with the progress of mechanochemistry in organic syntheses [26], ball milling has been successfully implemented for solvent-free CuAAC reactions [27-30]. Significantly shortened reaction time and reduced energy requirements, along with clear benefits in yields revealed a wide potential of the mechanochemical approach for CuAAC. The initial report showed applications of standard catalyst systems, copper(II) salts and ascorbic acid [27], but it was soon demonstrated that the application of mechanochemistry allowed for the use of heterogeneous copper(0) catalysts, either as copper milling vessels [28] or copper powder [30] for performing CuAAC rapidly and efficiently. The use of a copper(0) catalyst for CuAAC is also known in solution, but these reactions are usually much slower [31]. Also, click polymerization was applied using a ball-milling process with no significant influence on the integrity of the polymer chain [27,32].

Herein we have studied the efficiency of copper catalysts with Cu(0), Cu(I) and Cu(II) oxidation states for the mechanochemical CuAAC reaction of target quinoline derivatives and

p-substituted phenyl azides. We have also investigated the effect of the *p*-substituent in the azide on the reaction progress and yields. Direct monitoring by in situ Raman spectroscopy was used to gain an insight into the milling CuAAC reaction pathway when using different catalysts. The electronic structure of Cu catalysts after the reaction completion was assayed by electron spin resonance (ESR) spectroscopy. All milling reactions, except the one using copper(0) as catalyst, were compared to solution procedures to establish the benefits of each synthetic method. The structures of all products were determined by single-crystal X-ray diffraction, and the products were additionally characterized by NMR, Raman and FTIR–ATR spectroscopic methods.

Results and Discussion
Conventional solution-based click reactions for the synthesis of **5–8**

Based on the recently obtained 1,2,3-triazole-appended *N*-heterocycles, as promising lead compounds with efficient and selective cytostatic activities [8,9], our research groups share an interest in derivatization of target compounds by a triazole bridge [33]. Quinoline is an important constituent of compounds with diverse applications, some of which display potent cytostatic activity through different mechanisms of action such as DNA intercalation, apoptosis, abrogation of cell migration, inhibition of angiogenesis and disregulation of nuclear receptor signaling [34,35]. Moreover, it was found that halogenated compounds have an important role in therapeutic application increasing their lipophilicity, metabolic stability and improving interactions of protein–ligand complexes [36]. Taking into consideration the aforementioned, we have designed and synthesized 6-phenylquinoline derivatives containing a trifluoromethyl group at C-2 and a *p*-halogen-substituted and non-substituted phenyl-1,2,3-triazole moieties. The synthesis of 2-(trifluoromethyl)-6-phenylquinolone was achieved by Conrad–Limpach reaction of a primary aromatic amine with a β-ketoester [37,38]. Namely, thermal condensation of 4-aminobiphenyl (**1**) with ethyl 4,4,4-trifluoro-3-oxobutanoate in polyphosphoric acid (PPA) followed by the cyclization of the Schiff base intermediate afforded the 2-(trifluoromethyl)-6-phenylquinolone **3** (Scheme 1).

O-Alkynylquinoline derivative **4** required for the click synthesis of target triazoles was obtained in the second step using propargyl bromide in the presence of K_2CO_3, as a base, to afford exclusively the *O*-substituted quinoline, with no traces of the *N*-substituted analog. The formation of the *O*-propargyl regioisomer was confirmed by NMR spectroscopy using the connectivity between *O*-methylene and methine C-3 protons displayed in a $^1H,^1H$-NOESY spectrum of **4** (Figure S10 in Supporting Information File 1). Compound **4** was then

Scheme 1: Synthetic procedures for preparation of *p*-halogen-substituted and non-substituted phenyl-1,2,3-triazole 6-phenyl-2-(trifluoromethyl)quinolines.
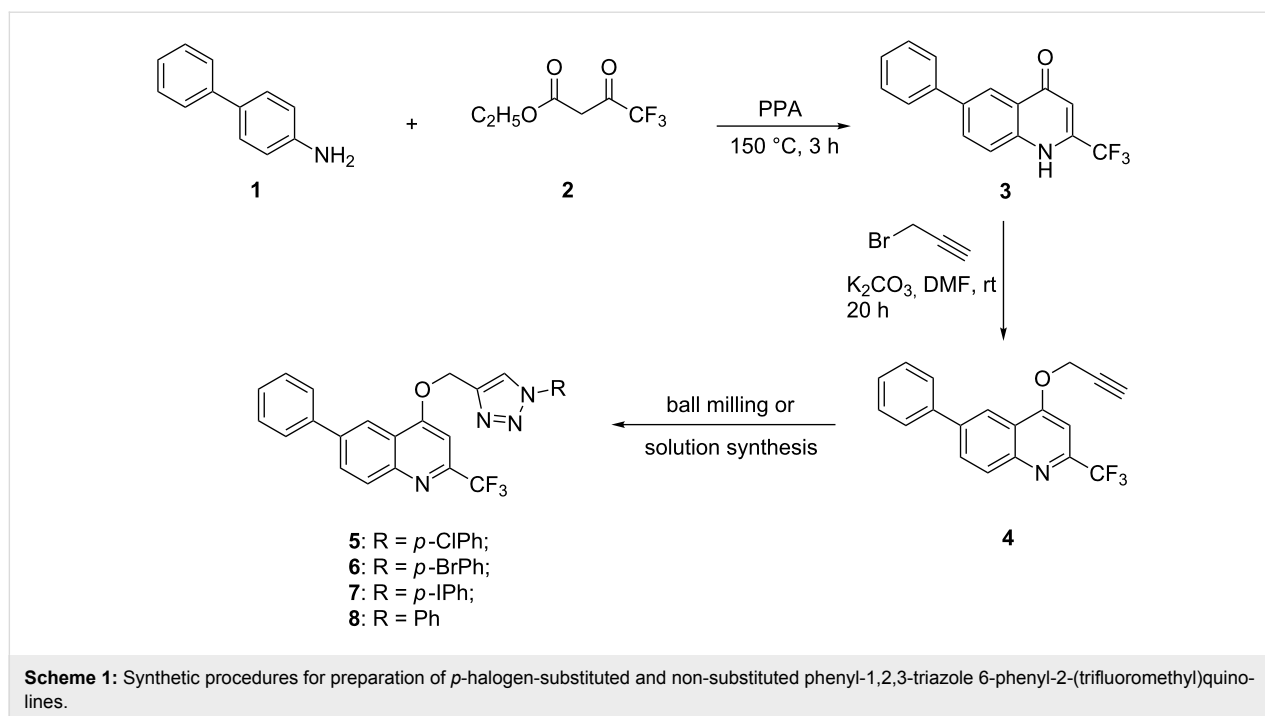
submitted to Cu(I)-catalyzed 1,3-dipolar cycloaddition with selected halogen-substituted and non-substituted aromatic azides to yield target *N*-heterocyclic hybrids **5–8** containing quinoline and 1,2,3-triazole scaffolds. Based on the known protocols for click conjugation [39] that include direct utilization of a Cu(I) source as well as alternative creation of Cu(I) from a Cu(II) source or elemental copper, initially we have examined the most common CuAAC reaction procedure using in situ generated Cu(I) through the reduction of Cu(II).

Conventional solution-based CuAAC reaction using copper(II) acetate monohydrate was applied to provide triazoles **5–8**. Two modes of heating the reaction mixture were used in order to test the reactivity of the azide reactants: heating at 60 °C for 3.5 h (method 1a) and heating at 60 °C overnight (method 1a*). Reaction with *p*-iodophenyl azide, which furnished the target compound **7**, was the most efficient giving the same high yield (89%) performed either by method 1a or method 1a*, Table 1, entry 3.

However, the isolated yields were significantly raised by application of method 1a* for the *p*-chloro- (from 21 to 77%, Table 1, entry 1) and *p*-bromophenyl azides (from 45 to 76%, Table 1, entry 2). On the other hand, the reaction with the non-substituted azide in all solution procedures, even by method 1a*, gave compound **8** in low yield (5–21%, Table 1, entry 4). Solution-based method 1b using CuI, *N,N'*-diisopropylethylamine (DIPEA) and acetic acid afforded compounds **5–7** in 5–52% isolated yield and was thus less successful for the syn-

thesis of **5–8** derivatives than methods 1a and 1a*, which include copper(II) acetate monohydrate as catalyst. Methods 1a and 1a*, however, include heating of reaction mixture to 60 °C, so the methods 1a and 1b are not readily comparable.
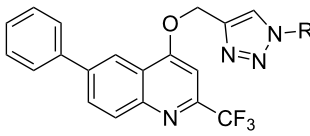
The efficiency of triazole formation using the method 1b steadily grows from a yield of 5% for the non-substituted azide (entry 4, Table 1) to ca. 50% for the *p*-iodo-substituted azide (entry 3, Table 1), resulting in the following order of reactivity: H < Cl < Br < I. These results are somewhat contrary to common CuAAC which are considered to be insensitive to electronic properties of both the alkyne and the azide [40]. It is evident here that the solution reaction with the azide bearing the iodo substituent resulted in almost 10-fold better yield in comparison to that of the unsubstituted azide (Table 1). When considering the proposed mechanism for CuAAC [3,41], such an influence of the electronic structure of the azide reactant could be tentatively ascribed to a reaction step where the azide is coordinated to the copper–alkyne complex via the most negative nitrogen (the one closest to the phenyl ring), before proceeding to the cyclization step with the coordinated alkyne.

Mechanochemical click reactions for the synthesis of **5–8**

In order to investigate the eficiency of different copper species for the solvent-free mechanochemical CuAAC in a ball mill, we conducted a number of milling experiments where we assayed catalytic action of most commonly used copper(0), copper(I) and copper(II) catalysts. Mechanochemical reactions were com-

Table 1: Reaction conditions and yields for the solvent-free mechanochemical and solvent-based conventional click reactions to afford 1,4-disubstituted 1,2,3-triazole **5–8**.

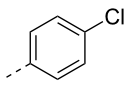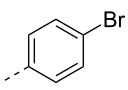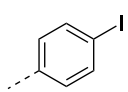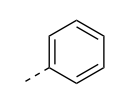| Entry	Compound	R	Conventional click reaction	Yield [%][a]	Mechanochemical click reaction	Yield [%][a]
1	**5**	(4-Cl-phenyl)	method 1a	21	method 2a	57
			method 1b	5	method 2b	85
			method 1a[*]	77	method 2c	77
2	**6**	(4-Br-phenyl)	method 1a	45	method 2a	60
			method 1b	40	method 2b	87
			method 1a[*]	76	method 2c	80
3	**7**	(4-I-phenyl)	method 1a	89	method 2a	77
			method 1b	52	method 2b	92
			method 1a[*]	89	method 2c	87
4	**8**	(phenyl)	method 1a	10	method 2a	72
			method 1b	5	method 2b	79
			method 1a[*]	21	method 2c	76

[a]Yields were determined after isolation of product using column chromatography. Conventional click reaction. Method 1a: Cu(OAc)$_2$·H$_2$O, CH$_3$OH, 60 °C, stirring for 3.5 h; method 1a[*]: Cu(OAc)$_2$·H$_2$O, CH$_3$OH, 60 °C, stirring overnight; method 1b: CuI, DIPEA, acetic acid, CH$_2$Cl$_2$, rt, 3.5 h stirring. Mechanochemical click reaction. Method 2a: Cu(OAc)$_2$·H$_2$O, two stainless-steel milling balls (7 mm), PTFE vessel, 3.5 h, rt, 30 Hz; method 2b: CuI, DIPEA, acetic acid, two stainless-steel milling balls (7 mm), PTFE vessel, 3.5 h, rt, 30 Hz; method 2c: DIPEA, acetic acid, PTFE vessel, two brass balls (7 mm), rt, 3.5 h.

pared to traditional solvent-based procedures, except for CuAAC with the Cu(0) catalyst, which was reported to be very slow in solution [31]. Various synthetic approaches used here are described in detail in the Experimental section and briefly in Table 1, where a comparison between solution-based and milling syntheses using different copper catalysts is given.

Milling using copper(II) acetate monohydrate (method 2a) was performed without a reducing agent. The Cu(II) catalyst proved effective for mechanochemical CuAAC, affording pure **5–8** in 60–80% isolated yield. Using copper(I) iodide as the catalyst in the presence of *N,N*-diisopropylethylamine (DIPEA) (method 2b) significantly increased yields for each respective CuAAC process, yielding up to 92% of the isolated triazole product (entry 3, Table 1), with the ^{1}H NMR spectra of the reaction mixture showing complete conversion of the reactants. Method 2b was additionally tested in the absence of DIPEA, which lowered the yield of the reactions by 10–20% points. It is well documented that the presence of DIPEA increases the yield of CuI-catalyzed CuAAC in solution [42], due to its role in the deprotonation of the alkyne substrate and easier formation of the reactive Cu(I) acetylide intermediate [3,42]. We continued to study mechanochemical CuAAC reactions by introducing copper(0) to the reaction mixture using copper milling vessels.

Leaching and wearing of milling vessels or balls during the milling process was an object of several studies [43,44], and Mack and co-workers found how to exploit it for catalytic purposes. They manufactured copper milling equipment as catalysts for mechanochemical CuAAC [28], resulting in good to excelent yields of the studied CuAAC reactions. It was recently shown how even the addition of simple copper powder to the reaction mixture can be successfully used for the mechanochemical CuAAC process [30]. In our case, however, using copper milling vessels did not result in good reaction yields (less than 20%), and the product was littered with copper microparticles. As an alternative to copper vessels, we have tested vessels made from brass, an alloy of copper and zinc, which is much harder and mechanically more resistant than pure copper. We tested two approaches, one using a completely brass milling assembly (brass milling vessels and balls), while the other combined brass milling balls with polytetrafluoroethylene (PTFE, Teflon) vessels. Surprisingly, using brass milling equipment did not increase the yields of the studied click rections, which still remained bellow 25%. In an attempt to activate the brass, as a catalyst, we added DIPEA and a small amount of acetic acid to the reaction mixture. Such an improvement of the synthetic procedure resulted in complete conversions of reactants to the triazole products with the isolated

yields ranging from 80–90%. After the isolation and purification, copper-sensitive ESR spectroscopy showed no traces of copper in the products (Materials and methods within the Experimental section).

Compared to solution procedures, CuAAC reactions proved to be more efficient under solvent-free ball-milling conditions, with ca. 15-fold increase in yields of products **5** and **8**. Tested mechanochemical methods showed the same dependence of reactivity to the *p*-substituent as reactions in solution, H < Cl < Br < I, but the difference in yields was significantly less pronounced.

In situ Raman monitoring of mechanochemical click reactions

In an attempt to gain a direct insight into reaction pathways of mechanochemical CuAAC reactions we repeated milling experiments 2a–2c in the preparation of the chloro-substituted product **5** while monitoring the reaction course by in situ Raman spectroscopy [45]. While this methodology was already successfully applied for establishing mechanistic and kinetic details in the formation of cocrystals [46], coordination and organometallic compounds [47], it proved to be especially valuable for the organic solid-state synthesis, revealing the base-catalysis in an amide formation reaction [48], and detecting intermediate phases not available from solution [49].

Raman spectra (Figure 1) were assigned combining literature data [50] and DFT calculations.

Calculated spectra are shown in Figures S15–S19 in Supporting Information File 1. Raman spectra of all studied compounds, the alkyne **4** and the isolated products **5**–**8**, are characterized by strong bands assigned to various vibrations of aromatic rings (Figure 1 and Supporting Information File 1, Table S1). Dried aryl azides were excluded from measuring due to their explosive nature (Materials and methods within the Experimental section). According to calculations, vibrations of all rings contribute to two bands at about 1600 cm⁻¹ as well as bands at 1000 and 730 cm⁻¹, whereas stretching vibrations including the quinoline C(9)–C(10) bond dominantly contributes to a strong band about 1360 cm⁻¹. Raman spectrum of the alkyne reactant contains a fingerprint medium intensity band at 2133 cm⁻¹ assigned to stretching of the triple C≡C bond.

Solid triazole products have mutually similar Raman spectra as the only significant structural difference is a *p*-substituent on the phenyl ring originating from the azide reactant. Apart from the phenyl and quinolinyl vibrations, a strong band observed at 1258 cm⁻¹ is attributed mostly to stretching of the N₃ group in the triazole ring. Structural diversity in products is supported by
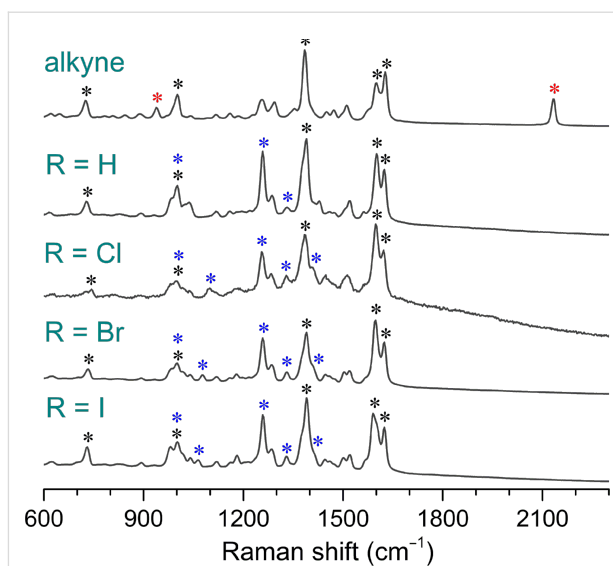
Figure 1: Experimental Raman spectra of the alkyne **4** and triazole products **5**–**8**. Bands attributed to the vibrational modes common to all compounds are marked with a black asterisk (*). Bands assigned to the alkyne and triazole products are marked with red and blue asterisks, respectively. For detailed vibrational analysis of these compounds please refer to Table S1, Supporting Information File 1.

observations of weak bands at 1099 (Cl), 1077 (Br) and 1064 (I) cm⁻¹ which are assigned to vibration of the phenyl ring that contains the carbon–halogen bond. Characteristic C≡C alkyne band at 2133 cm⁻¹ along with the band at 1258 cm⁻¹ of the triazole products are appropriate for monitoring of the reaction progress.

In situ Raman monitoring of formation of the triazole **5** using copper(II) acetate monohydrate (5 mol %, method 2a) revealed strong luminescence of the reaction mixture indicating the direct involvement of the catalyst in the milling process and the formation of luminescent copper species, which hindered a detailed insight into the reaction pathway. Nevertheless, the starting Raman spectrum had a clearly visible alkyne signal, which was, however, after a couple of minutes milling, covered by two broad luminescent "humps", Figure 2a.

After 13 minutes milling no pronounced Raman bands could be unambiguously detected. The luminescence of the reaction mixture gradually changed during milling and the final spectrum after 213 minutes milling exhibited a single luminescent maximum centered at around 1500 cm⁻¹ (Figure 2a) possibly due the formation of different copper complexes as milling progressed. Milling by method 2b, where the catalyst CuI was added in concentrations of 2 mol %, showed strong luminescence similar to the one observed in milling by method 2a, starting after ca. 3 minutes milling and covering most of Raman signals already after 10 minutes milling. In this case, however,

Figure 2: In situ Raman monitoring of a) mechanochemical formation of triazole **5** using copper(II) acetate monohydrate as catalyst (method 2a); and b) mechanochemical formation of triazole **5** by method 2b using CuI/DIPEA catalyst.
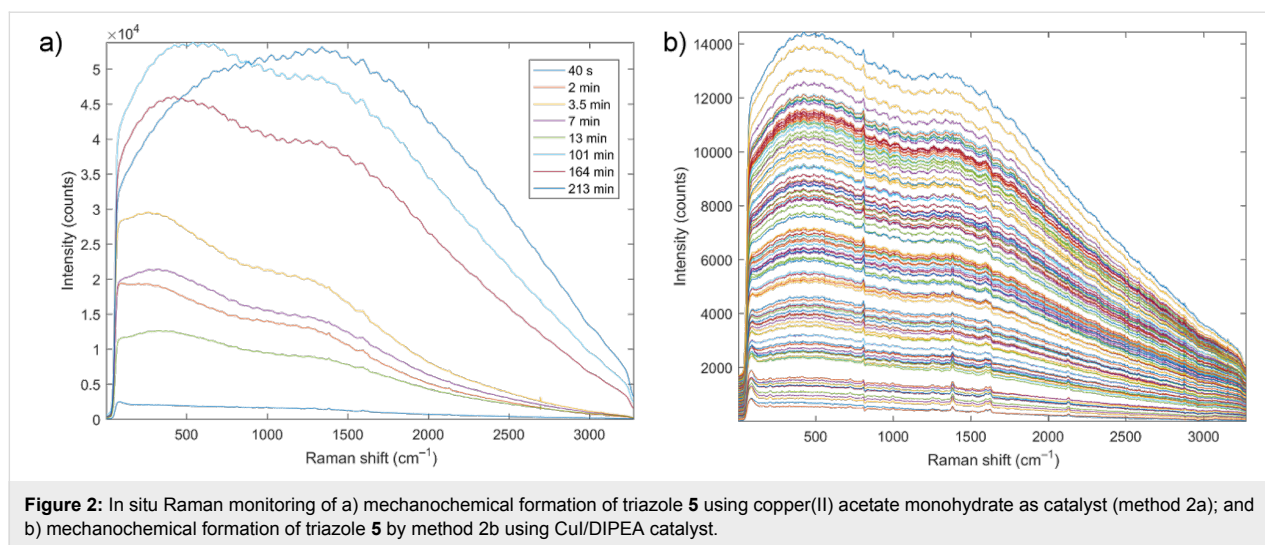
luminescence grew steadily but the positions of the two luminescent peaks did not change until the end of milling (Figure 2b). While milling using CuI alone did not result in raise of luminescence (Figure S20a in Supporting Information File 1), growth of the luminescent peak was observed when the CuI was milled with the purified triazole product **5**, indicating the interaction between CuI and **5** that occurred during the milling process (Figure S20b in Supporting Information File 1). Here, the two broad luminescent "humps" with position similar to those observed with method 2b prevented clear detection of Raman vibrations even after 15 minutes milling.

Surprisingly, monitoring the mechanochemical formation of **5** by milling with brass balls (method 2c) enabled a clear insight into the evolution of the reaction mixture (Figure 3a). The luminescent peak remained weak throughout the experiment, leaving the Raman signals of the reaction participants clearly visible.

Analysis of time-resolved Raman monitoring data showed a direct formation of the product **5**, without any detectable intermediates. The C≡C band was very weak but still visible at the end of the milling, indicating that 210 minutes milling was not enough to complete this reaction, which was further corroborated by ex situ analyses. The fact that we were able to monitor milling by method 2c, as opposed to methods 2a and 2b where copper catalyst was directly added to reaction mixture in catalytic quantity of 2–5 mol %, could tentatively be explained by even a lower content of copper compounds in the reaction mixture. This strongly indicates that during mechanochemical reactions with milling balls containing copper(0), the catalytic process is mostly happening on the surface of milling balls, and diffusion of copper ions to reaction mixture is minute. This could further explain the absence of other intermediate species in the spectra of solid reaction mixture, such as copper–alkyne

Figure 3: a) In situ Raman monitoring for mechanochemical synthesis of **5** using brass balls and PMMA reaction vessel. b) Selected Raman spectra from panel a) highlighting the slow transformation of the alkyne to the triazole product. The characteristic C≡C alkyne band at 2133 cm⁻¹ along with the triazole band at 1258 cm⁻¹ of the triazole product (Supporting Information File 1, Table S1) are suitable to evaluate the reaction progress. The C≡C band is still visible after 210 minutes milling, indicating that the reaction was not complete.

complexes, which are commonly considered as a part of the solution catalytic cycle [51]. We anticipate that monitoring these highly luminescent CuAAC reactions by using advanced Raman techniques such as shifted-excitation Raman difference spectroscopy (SERDS) could be possible [52]. In this way, mechanistic details of these reactions and the behavior of all studied copper catalysts may be more visible, opening the path towards elucidation of mechanism(s) for the solvent-free click reactions.

Electron spin resonance (ESR) spectroscopy

ESR is an ideal technique for validating the oxidation and spin state of copper cations. Elemental copper and copper(I) are ESR silent, whereas the copper(II) shows strong and characteristic lines revealing local properties of this ion. Here we were interested to establish how the milling procedures 2a–2c for the synthesis of **5** would affect the oxidation state and coordination modes of all three evaluated catalysts when the milling was performed in air. Analyzing the reaction mixture after milling with brass balls (method 2c, DIPEA and acetic acid added) showed that there are no copper(II) cations present in the final mixture (Figure 4). The ESR spectrum reveals only the presence of free radicals, characterized by sharp signal with g-value $g \approx 2.01$.

Figure 4: ESR spectra of samples obtained after milling by methods 2a (black), 2b (red) and 2c (blue). The inset shows the spectrum of [Cu(OAc)$_2$(H$_2$O)]$_2$ [53]. All spectra are recorded at room temperature.
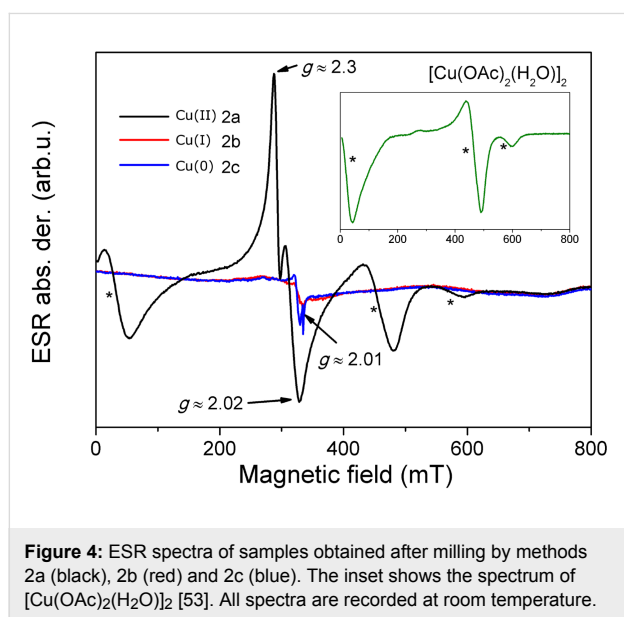
Milling the azide and alkyne with copper(I) catalytic system (CuI/DIPEA/acetic acid, method 2b) resulted in an ESR silent yellow product, revealing that the oxidation did not occur and no copper(II) was present in the reaction mixture. To test the sensitivity of CuI to milling in air, we conducted two additional experiments. When the sole CuI was milled for 30 minutes in air, no Cu(II) was detected in the mixture. However, milling the CuI/DIPEA/acetic acid catalytic system as used in method 2b,

only without the azide and alkyne reactants, results in oxidation of Cu(I) to Cu(II), with the final product showing ESR lines characteristic for copper(II) acetate. Thus, it seems that the presence of alkyne and azide in the reaction mixture stabilizes the copper(I) ion in its catalytically active state.
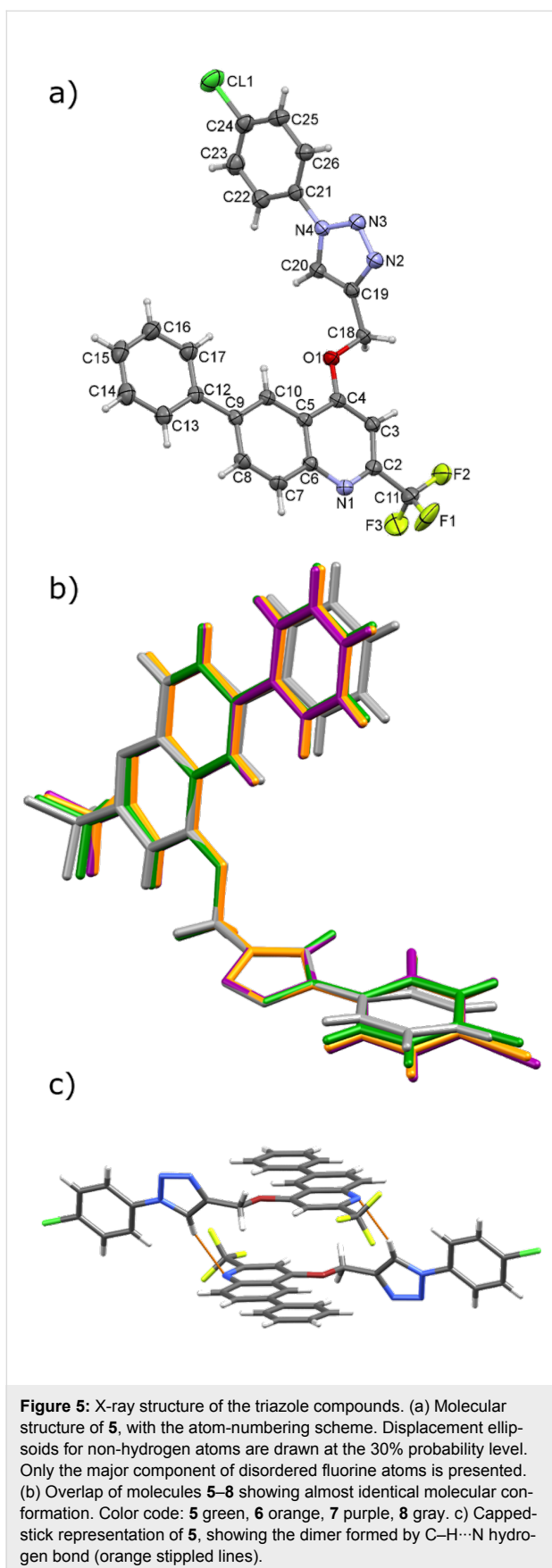
The product yielded by method 2a, where copper(II) acetate monohydrate was added as catalyst in 5 mol % quantity, shows a complex ESR spectrum (Figure 4). Three lines marked by asterisks are characteristic for copper(II) acetate monohydrate [53]. These lines reveal the presence of two strongly antiferromagnetically coupled copper ions with spin $S = 1/2$. In the spectrum of the product obtained by method 2a, an additional strong signal is detected (peaks at $g = 2.02$ and $g = 2.3$) that could be assigned to the presence of non-coupled paramagnetic Cu(II) ions in the sample, suggesting that beside the copper(II) acetate paddlewheel complex at least one other copper(II) coordination complex with monomeric core is present in the reaction mixture. Thus, it seems that reacting copper(II) with vast excess of alkyne and azide reactants does not result in the total reduction of copper(II) to the catalytically active form, which can possibly explain the lower efficiency of method 2a in comparison to the other used mechanochemical methods. It should be noted here that the same product after purification by column chromatography shows no traces of copper in the ESR spectrum (Supporting Information File 1, Figure S21).

X-ray crystal structure analysis

Single-crystal X-ray structure analysis was performed for all products. It provided clear identification of the novel triazole derivatives and it was largely helpful for calculating the Raman spectra for monitoring purposes. It corroborated the substitution of the phenyl-1-(1,2,3-triazolyl)methyl unit at O-4 position of the quinolone heterocycle and formation of the 1,2,3-triazole ring in compounds **5–8** (Figure 5 and Supporting Information File 1, Figure S22). Thus, the molecular structures differ in the substituent bonded to the C24 atom of the C21–C26 phenyl ring, which is chlorine in **5**, bromine in **6**, iodine in **7**, and hydrogen in **8**. The corresponding bond lengths in these structures are similar, as well as the conformations of the molecules (Figure 5b and Supporting Information File 1, section 7).

Compound **5** may serve as a model for the crystal structure description. The molecules of **5** are linked by one C–H···N hydrogen bond, so forming a dimer via eighteen-membered ring (e.g., see Figure 5c for **5**) which can be described by graph-set notation as R$_2^2$(18) [54]. Although the same motif formed by the analogous hydrogen bond is observed in other three structures (Table S3, Supporting Information File 1), the final supramolecular structures of **5–8** differ, from one-dimensional chains to three-dimensional network. It should be mentioned that the

Figure 5: X-ray structure of the triazole compounds. (a) Molecular structure of **5**, with the atom-numbering scheme. Displacement ellipsoids for non-hydrogen atoms are drawn at the 30% probability level. Only the major component of disordered fluorine atoms is presented. (b) Overlap of molecules **5**–**8** showing almost identical molecular conformation. Color code: **5** green, **6** orange, **7** purple, **8** gray. c) Capped-stick representation of **5**, showing the dimer formed by C–H···N hydrogen bond (orange stippled lines).

interactions between the present halogen atoms were not observed. For more detailed description of crystal structures of **5**–**8** please refer to the section 7 of Supporting Information File 1 and Figures S23–S28 therein.

Conclusion

In conclusion, mechanochemistry was successfully applied in CuAAC click reaction to provide the target 6-phenyl-2-(trifluoromethyl)quinolines containing *p*-halogen-substituted and non-substituted phenyl-1,2,3-triazole unit attached at the O-4 position of the quinoline fragment. All triazole products have almost identical conformations in the solid state, with no halogen bonding observed in their crystal structures. Milling procedures using Cu(II), Cu(I) and Cu(0) catalysts proved to be significantly more efficient than the corresponding solution reactions, with up to 15-fold gain in yield. Both procedures showed the same reactivity trend, resulting in the H < Cl < Br < I bias, but the differences in yields for solution procedures were much more pronounced. In situ Raman monitoring of the milling processes using Cu(I) and Cu(II) catalysts revealed active involvement of copper catalysts through coordination and occurrence of strongly luminescent copper compounds which, despite the fact they were present in mere 2–5 mol %, completely covered vibrational Raman bands. On the contrary, using copper(0) in the form of brass milling balls resulted in a mild luminescence of the reaction mixture and enabled a direct insight into the reaction pathway, which showed direct transformation of reactants to products. Thus, we propose that the catalytic reaction for the method 2c is most likely occurring on the surface of brass milling balls, with minute diffusion of the copper ions to the reaction mixture. During the milling reactions, copper(0) and copper(I) catalysts do not oxidize to Cu(II) when the alkyne and azide are present in the reaction mixture, while in the product obtained after the milling with copper(II) catalyst (5 mol %) a significant amount of copper(II) ions are still present. In future, we will be focused on elucidating the solid-state mechanisms for this important class of organic reactions by applying advanced in situ Raman monitoring techniques. Screening of cytostatic and antibacterial activities of novel compounds **5**–**8** and their structural analogs will be reported in due course.

Experimental

Materials and methods. Compounds **5**–**8** were synthesized from corresponding aryl azides (0.5 M in *tert*-butyl methyl ether, ≥95.0%) that were obtained commercially from Sigma-Aldrich. To ensure solvent-free milling conditions, *tert*-butyl methyl ether was evaporated under vacuo immediatelly before the milling was commenced. The progress of reactions was monitored using thin-layer chromatography (TLC) on pre-coated Merck silica gel 60F-254 plates with an appropriate sol-

vent system and the spots were detected under UV light (254 nm). Column chromatography was performed using silica gel (Fluka, 0.063–0.2 mm). In order to scavenge the copper residues from the click reactions, one additional column chromatography using aluminium oxide (Fluka, 0.063–0.2 mm) was performed. Melting points (uncorrected) were determined with a Kofler micro hot-stage (Reichert, Wien) apparatus.

NMR spectra were acquired on a Bruker 300 and 600 MHz NMR spectrometer. Spectra were recorded in DMSO-d_6 at 298 K. Chemical shifts were referenced to the residual solvent signal of DMSO at δ 2.50 ppm for ^{1}H and δ 39.50 ppm for ^{13}C. Individual resonances were assigned on the basis of their chemical shifts, signal intensities, multiplicity of resonances and H–H coupling constants (Supporting Information File 1, Figures S1–S5, S10).

High-resolution mass spectra of the final compounds were recorded on Applied Biosystems 4800 Maldi TOF/TOF Analyzer (Supporting Information File 1, Figures S6–S9).

Mechanochemical reactions were carried out using an IST500 (InSolido Tehnologies, Croatia) mixer mill operating at 30 Hz in PTFE reaction vessels using stainless steel or brass balls.

Fourier-transform infrared attenuated total reflectance spectroscopy (FTIR–ATR) was performed using a Perkin-Elmer SpectrumTwo spectrometer, from 4400 cm^{-1} to 500 cm^{-1}, with resolution 4 cm^{-1} (Supporting Information File 1, Figures S11–S14).

Computational details. Calculations were carried out using the B3LYP hybrid functional combined with an empirical Grimme's D3 dispersion correction [55] (B3LYP-D3) implemented in Gaussian 09 [56]. The standard 6-311+G(2d,p) basis set with the ultrafine method was used for C, H, N, F, Cl and Br atoms. Iodine atoms were modeled by the Stuttgart−Dresden (SDD) pseudopotential and the accompanying SDD basis set [57]. Full geometry optimization in the gas phase was followed by vibrational frequency calculations that identified calculated stationary points as minima. Calculated Raman spectra were scaled by 0.98 (Supporting Information File 1, Figures S15–S19, Table S1).

In situ Raman monitoring of mechanochemical reactions was performed in translucent and amorphous reaction vessels made from poly(methyl metacrylate) (PMMA) using a portable Raman system with a PD-LD (now Necsel) BlueBox laser source (excitation wavelength 785 nm) equipped with B&W-Tek fiber optic Raman BAC102 probe, and coupled with Maya2000Pro (OceanOptics) spectrometer. The probe was

positioned under the milling vessel using a movable stand, so to place a focus of the laser ≈1 mm inside of the vessel.

ESR spectroscopy was performed on a Varian E-9 spectrometer, at room temperature. The measurements were obtained at the microwave frequency around 9.3 GHz with the magnetic field modulation amplitude of 0.5 mT. For detecting copper in the final products, ESR spectra were recorded by an X-band Bruker Elexsys 580 FT/CW spectrometer with a microwave frequency around 9.7 GHz. The measurements were performed at a modulation frequency of 100 kHz and a magnetic field modulation amplitude of 0.5 mT. The results are shown in Supporting Information File 1, Figure S21.

X-ray crystal structure analysis. Single crystals of **5**–**8** suitable for single crystal X-ray structure analysis were obtained at room temperature by partial evaporation of the solvent from the mixture of dichloromethane and methanol. Data for **5**–**7** were collected at 295 K on a Oxford Diffraction Xcalibur2 diffractometer with a Sapphire 3 CCD detector using graphite-monochromatized Mo K$_\alpha$ radiation (λ = 0.71073 Å). Data for **8** were collected at the same temperature on Oxford Diffraction Xcalibur Nova R diffractometer with Ruby detector using mirror-monochromatized Cu K$_\alpha$ radiation (λ = 1.54184 Å). The *CrysAlisPro* program [58] was used for the data collection and processing. The intensities were corrected for absorption using the multi-scan absorption correction method (**5**, **7** and **8**) and gaussian absorption correction method (**6**) [58]. All structures were solved using direct methods with SIR–2004 [59] and refined by full-matrix least-squares calculations based on F^2 using SHELXL–2016 [60] integrated in the WinGX program package [61]. All hydrogen atoms were included in calculated positions, with SHELXL–2016 defaults. Fluorine atoms of trifloromethyl groups in **5**–**8** were disordered and have been refined with fixed occupancy ratio of 0.60/0.40 in **5** and **8**, 0.70/0.30 in **6**, and 0.68/0.32 in **7**. Geometric restraint on some of the C–F distances and restraint on anisotropic displacement parameters of some fluorine atoms in **5**–**8** were applied in the refinement. The PLATON [62] and Mercury [63] programs were used for structure analysis and molecular and crystal structure drawings preparation. The CCDC 1549136-1549139 contain the supplementary crystallographic data for this paper. These data can be obtained free of charge from The Cambridge Crystallographic Data Centre via http://www.ccdc.cam.ac.uk/data_request/cif.

Crystal data for **5**: 0.763 × 0.424 × 0.155 mm^3; $C_{25}H_{16}ClF_3N_4O$, M_r = 480.87, triclinic, space group *P*-1 (No. 2); a = 8.0775(4) Å, b = 10.3530(5) Å, c = 13.7751(6) Å, α = 82.383(4)°, β = 74.062(4)°, γ = 84.946(4)°, V = 1096.29(9) Å^3; Z = 2; ρ = 1.457 g cm^{-3}, μ(Mo K$_\alpha$) = 0.226 mm^{-1}; θ$_{max}$ =

27.999°, 19408 reflections measured, 5276 unique reflections and 3932 with $I \geq 2\sigma(I)$, $R_{int} = 0.0337$; Final R indices [($I > 2\sigma(I)$)]: $R = 0.0538$, $wR = 0.1453$, [all data]: $R = 0.0729$, $wR = 0.1603$, $S = 1.180$ for 334 parameters and 23 restraints, largest diff. peak and hole $0.335/−0.403$ e Å^{-3}.

Crystal data for **6**: $0.774 \times 0.563 \times 0.335$ mm^3; C$_{25}$H$_{16}$BrF$_3$N$_4$O, $M_r = 525.33$, triclinic, space group P-1 (No. 2); $a = 8.0114(7)$ Å, $b = 10.5132(8)$ Å, $c = 13.8073(11)$ Å, $\alpha = 93.316(6)°$, $\beta = 105.865(7)°$, $\gamma = 94.002(6)°$, $V = 1112.31(16)$ Å^3; $Z = 2$; $\rho = 1.568$ g cm^{-3}, μ(Mo K$_\alpha$) = 1.899 mm^{-1}; $\theta_{max} = 27.999°$, 13486 reflections measured, 5351 unique reflections and 2785 with $I \geq 2\sigma(I)$, $R_{int} = 0.0622$; Final R indices [($I > 2\sigma(I)$)]: $R = 0.0614$, $wR = 0.1418$, [all data]: $R = 0.1300$, $wR = 0.1778$, $S = 1.056$ for 334 parameters and 35 restraints, largest diff. peak and hole $0.408/−0.733$ e Å^{-3}.

Crystal data for **7**: $0.871 \times 0.660 \times 0.330$ mm^3; C$_{25}$H$_{16}$F$_3$IN$_4$O, $M_r = 572.32$, triclinic, space group P-1 (No. 2); $a = 7.9657(5)$ Å, $b = 10.7068(5)$ Å, $c = 13.7205(8)$ Å, $\alpha = 91.683(4)°$, $\beta = 104.718(5)°$, $\gamma = 93.136(5)°$, $V = 1128.96(11)$ Å^3; $Z = 2$; $\rho = 1.684$ g cm^{-3}, μ(Mo K$_\alpha$) = 1.469 mm^{-1}; $\theta_{max} = 28.000°$, 20218 reflections measured, 5425 unique reflections and 3995 with $I \geq 2\sigma(I)$, $R_{int} = 0.0346$; Final R indices [($I > 2\sigma(I)$)]: $R = 0.0411$, $wR = 0.1027$, [all data]: $R = 0.0614$, $wR = 0.1133$, $S = 1.123$ for 334 parameters and 36 restraints, largest diff. peak and hole $0.511/−0.658$ e Å^{-3}.

Crystal data for **8**: $0.386 \times 0.194 \times 0.131$ mm^3; C$_{25}$H$_{17}$F$_3$N$_4$O, $M_r = 446.42$, triclinic, space group P-1 (No. 2); $a = 8.2427(3)$ Å, $b = 10.1166(4)$Å, $c = 13.1179(6)$ Å, $\alpha = 78.396(3)°$, $\beta = 78.370(3)°$, $\gamma = 83.739(3)°$, $V = 1046.84(8)$ Å^3; $Z = 2$; $\rho = 1.416$ g cm^{-3}, μ(Cu K$_\alpha$) = 0.907 mm^{-1}; $\theta_{max} = 69.999°$, 9006 reflections measured, 3939 unique reflections and 3494 with $I \geq 2\sigma(I)$, $R_{int} = 0.0288$; Final R indices [($I > 2\sigma(I)$)]: $R = 0.0595$, $wR = 0.0641$, [all data]: $R = 0.1664$, $wR = 0.1727$, $S = 1.320$ for 325 parameters and 35 restraints, largest diff. peak and hole $0.426/−0.307$ e Å^{-3}. For detailed description of crystal structures for compounds **5–8** please check Supporting Information File 1, Figures S22–S28 and Tables S2–S4.

General procedure for the conventional click reactions of 1,2,3-triazole–quinoline derivatives 5–8

Method 1a: Compound **4** (80 mg, 0.24 mmol) and the corresponding aryl azide (0.49 mL, 0.24 mmol) were dissolved in methanol (8 mL) and Cu(OAc)$_2$ (2.24 mg, 0.05 equiv) was added. The reaction mixture was stirred for 3.5 h at 60 °C. The solvent was removed under reduced pressure and residue was purified by column chromatography on silica gel and Al$_2$O$_3$ with dichloromethane as eluent. We used here dichloromethane

as an eluent as it is commonly used in similar systems, but it was shown that other mixtures, such as *n*-hexane/ethyl acetate (50:1) could also be efficient for the purification purposes. ESR spectroscopy showed no traces of copper in the purified product.

Method 1a*: Procedure as described in method 1a using compound **4** (1 equiv), the corresponding aryl azide (1 equiv) and Cu(OAc)$_2$ (0.05 equiv) in methanol. The reaction mixture was stirred overnight at 60 °C.

Method 1b: To a mixture of CuI (1 mg, 4.9 mmol, 0.02 equiv), DIPEA (4.3 µL, 0.1 equiv) and HOAc (1.5 µL, 0.1 equiv) in dichlorometane (1.0 mL) 6-phenyl-4-(prop-2-ynyloxy)-2-(trifluoromethyl)quinoline (**4**, 80 mg, 0.24 mmol) and the corresponding azide (0.49 mL, 0.24 mmol) were added at room temperature. The reaction mixture was stirred for 3.5 h. The solvent was removed under reduced pressure and the residue was purified by column chromatography on silica gel and Al$_2$O$_3$ with dichloromethane as eluent.

General procedure for the mechanochemical click reactions of 1,2,3-triazole–quinoline derivatives 5–8

Method 2a: Compound **4** (80 mg, 0.24 mmol) and the corresponding aryl azide (0.49 mL, 0.24 mmol) were weighed in one half of the reaction vessel and the other half was filled with Cu(OAc)$_2$ (2.24 mg, 0.05 equiv) and two 7 mm diameter stainless steel balls. The aryl azide solution was evaporated to dryness under vacuo, and the closed vessel was positioned in the IST500 mill. The mixture was ground for 3.5 h at 30 Hz and then purified by column chromatography on silica gel and Al$_2$O$_3$ with dichloromethane as eluent.

Method 2b: In one half of the reaction vessel we weighed azide (0.49 mL, 0.24 mmol), DIPEA (4.3 µL, 0.1 equiv) and acetic acid (1.5 µL, 0.1 equiv); the other half was filled with compound **4** (80 mg, 0.24 mmol) and CuI (1 mg, 4.9 mmol, 0.02 equiv), and two 7 mm diameter stainless steel balls (ball weight 1.3 g). The aryl azide solution was evaporated to dryness under vacuo, and the vessel was sealed and positioned in IST500 mill. The mixture was ground for 3.5 h at 30 Hz and then purified by column chromatography on silica gel and Al$_2$O$_3$ with dichloromethane as eluent.

Method 2c: In one half of the reaction vessel were weighed azide (0.49 mL, 0.24 mmol), DIPEA (4.3 µL, 0.1 equiv) and acetic acid (1.5 µL, 0.1 equiv) the other half was filled with compound **4** (80 mg, 0.24 mmol) and two brass balls each weighing 1.1 g. The aryl azide solution was evaporated to dryness under vacuo, and the vessel was sealed and positioned

in IST500 mill. The mixture was ground for 3.5 h at 30 Hz and then purified by column chromatography on silica gel and Al_2O_3 with dichloromethane as eluent.

Supporting Information

Supporting Information File 1
Solution synthetic procedures, characterization data, ^{1}H, ^{13}C NMR spectra of **4–8**, NOESY spectrum of **4**, high-resolution mass spectra of **5–8**, crystallographic data, FTIR–ATR, and Raman data.
[http://www.beilstein-journals.org/bjoc/content/supplementary/1860-5397-13-232-S1.pdf]

Acknowledgments

References

1. Kolb, H. C.; Finn, M. G.; Sharpless, K. B. *Angew. Chem., Int. Ed.* **2001,** *40,* 2004–2021. doi:10.1002/1521-3773(20010601)40:11<2004::AID-ANIE2004>3.0.CO;2-5

2. Tornøe, C. W.; Christensen, C.; Meldal, M. *J. Org. Chem.* **2002,** *67,* 3057–3064. doi:10.1021/jo011148j

3. Hein, J. E.; Fokin, V. V. *Chem. Soc. Rev.* **2010,** *39,* 1302–1315. doi:10.1039/b904091a

4. Moses, J. E.; Moorhouse, A. D. *Chem. Soc. Rev.* **2007,** *36,* 1249–1262. doi:10.1039/B613014N

5. Hou, J.; Liu, X.; Shen, J.; Zhao, G.; Wang, P. G. *Expert Opin. Drug Discovery* **2012,** *7,* 489–501. doi:10.1517/17460441.2012.682725

6. Raić-Malić, S.; Meščić, A. *Curr. Med. Chem.* **2015,** *22,* 1462–1499. doi:10.2174/0929867322666150227150127

7. Kappe, C. O.; Van der Eycken, E. *Chem. Soc. Rev.* **2010,** *39,* 1280–1290. doi:10.1039/B901973C

8. Gregorić, T.; Sedić, M.; Grbčić, P.; Tomljenović Paravić, A.; Kraljević Pavelić, S.; Cetina, M.; Vianello, R.; Raić-Malić, S. *Eur. J. Med. Chem.* **2017,** *125,* 1247–1267. doi:10.1016/j.ejmech.2016.11.028

9. Gazivoda Kraljević, T.; Harej, A.; Sedić, M.; Kraljević Pavelić, S.; Stepanić, V.; Drenjančević, D.; Talapko, J.; Raić-Malić, S. *Eur. J. Med. Chem.* **2016,** *124,* 794–808. doi:10.1016/j.ejmech.2016.08.062

10. Ötvös, S. B.; Mándity, I. M.; Kiss, L.; Fülöp, F. *Chem. – Asian J.* **2013,** *8,* 800–808. doi:10.1002/asia.201201125

11. Tiwari, V. K.; Mishra, B. B.; Mishra, K. B.; Mishra, N.; Singh, A. S.; Chen, X. *Chem. Rev.* **2016,** *116,* 3086–3240. doi:10.1021/acs.chemrev.5b00408

12. Ötvös, S. B.; Fülöp, F. *Catal. Sci. Technol.* **2015,** *5,* 4926–4941. doi:10.1039/C5CY00523J

13. Meščić, A.; Šalić, A.; Gregorić, T.; Zelić, B.; Raić-Malić, S. *RSC Adv.* **2017,** *7,* 791–800. doi:10.1039/C6RA25244C

14. James, S. L.; Adams, C. J.; Bolm, C.; Braga, D.; Collier, P.; Friščić, T.; Grepioni, F.; Harris, K. D. M.; Hyett, G.; Jones, W.; Krebs, A.; Mack, J.; Maini, L.; Orpen, A. G.; Parkin, I. P.; Shearouse, W. C.; Steed, J. W.; Waddell, D. C. *Chem. Soc. Rev.* **2012,** *41,* 413–447. doi:10.1039/C1CS15171A

15. Balaž, P.; Achimovičová, M.; Baláž, M.; Billik, P.; Cherkezova-Zheleva, Z.; Criado, J. M.; Delogu, F.; Dutková, E.; Gaffet, E.; Gotor, F. J.; Kumar, R.; Mitov, I.; Rojac, T.; Senna, M.; Streletskii, A.; Wieczorek-Ciurowa, K. *Chem. Soc. Rev.* **2013,** *42,* 7571–7637. doi:10.1039/c3cs35468g

16. Stolle, A.; Szuppa, T.; Leonhardt, S. E. S.; Ondruschka, B. *Chem. Soc. Rev.* **2011,** *40,* 2317–2329. doi:10.1039/c0cs00195c

17. Wang, G.-W. *Chem. Soc. Rev.* **2013,** *42,* 7668–7700. doi:10.1039/c3cs35526h

18. Friščić, T. *Chem. Soc. Rev.* **2012,** *41,* 3493–3510. doi:10.1039/c2cs15332g

19. Sokolov, A. N.; Bučar, D.-K.; Baltrusaitis, J.; Gu, S. X.; MacGillivray, L. R. *Angew. Chem., Int. Ed.* **2010,** *49,* 4273–4277. doi:10.1002/anie.201000874

20. Koch, C. C.; Whittenberger, J. D. *Intermetallics* **1996,** *4,* 339–355. doi:10.1016/0966-9795(96)00001-5

21. Sopicka-Lizer, M., Ed. *High-Energy Ball Milling, Mechanochemical Processing of Nanopowders;* Woodhead Publishing: Cambridge, UK, 2010. doi:10.1533/9781845699444

22. Tan, D.; Loots, L.; Friščić, T. *Chem. Commun.* **2016,** *52,* 7760–7781. doi:10.1039/C6CC02015A

23. Watson, W. J. W. *Green Chem.* **2012,** *14,* 251–259. doi:10.1039/C1GC15904F

24. Rantanennand, J.; Khinast, J. *J. Pharm. Sci.* **2015,** *104,* 3612–3638. doi:10.1002/jps.24594

25. Constable, D. J. C.; Curzons, A. D.; Freitas dos Santos, L. M.; Geen, G. R.; Hannah, R. E.; Hayler, J. D.; Kitteringham, J.; McGuire, M. A.; Richardson, J. E.; Smith, P.; Webb, R. L.; Yu, M. *Green Chem.* **2001,** *3,* 7–9. doi:10.1039/b007875l

26. Hernández, J. G.; Bolm, C. *J. Org. Chem.* **2017,** *82,* 4007–4019. doi:10.1021/acs.joc.6b02887

27. Thorwirth, R.; Stolle, A.; Ondruschka, B.; Wild, A.; Schubert, U. S. *Chem. Commun.* **2011,** *47,* 4370–4372. doi:10.1039/c0cc05657j

28. Cook, T. L.; Walker, J. A., Jr.; Mack, J. *Green Chem.* **2013,** *15,* 617–619. doi:10.1039/c3gc36720g

29. Cummings, A. J.; Ravalico, F.; McColgan-Bannon, K. I. S.; Eguaogie, O.; Elliott, P. A.; Shannon, M. R.; Bermejo, I. A.; Dwyer, A.; Maginty, A. B.; Mack, J.; Vyle, J. S. *Nucleosides, Nucleotides Nucleic Acids* **2015,** *34,* 361–370. doi:10.1080/15257770.2014.1001855

30. Rinaldi, L.; Martina, K.; Baricco, F.; Rotolo, L.; Cravotto, G. *Molecules* **2015,** *20,* 2837–2849. doi:10.3390/molecules20022837

31. Chassaing, S.; Bénéteau, V.; Pale, P. *Catal. Sci. Technol.* **2016,** *6,* 923–957. doi:10.1039/C5CY01847A

32. Brantley, S.; Konda, S. S. M.; Makarov, D. E.; Bielawski, C. W. *J. Am. Chem. Soc.* **2012,** *134,* 9882–9885. doi:10.1021/ja303147a

33. Afzal, O.; Kumar, S.; Haider, M. R.; Ali, M. R.; Kumar, R.; Jaggi, M.; Bawa, S. *Eur. J. Med. Chem.* **2015,** *97,* 871–910. doi:10.1016/j.ejmech.2014.07.044

34. Cheng, G.; Hao, H.; Dai, M.; Liu, Z.; Yuan, Z. *Eur. J. Med. Chem.* **2013,** *66,* 555–562. doi:10.1016/j.ejmech.2013.01.057

35. de O. Freitas, L. B.; Borgati, T. F.; de Freitas, R. P.; Ruiz, A. L. T. G.; Marchetti, G. M.; de Carvalho, J. E.; da Cunha, E. F. F.; Ramalho, T. C.; Alves, R. B. *Eur. J. Med. Chem.* **2014,** *84,* 595–604. doi:10.1016/j.ejmech.2014.07.061

36. Auffinger, P.; Hays, F. A.; Westhof, E.; Ho, P. S.
Proc. Natl. Acad. Sci. U. S. A. **2004,** *101,* 16789–16794.
doi:10.1073/pnas.0407607101

37. Conrad, M.; Limpach, L. *Ber. Dtsch. Chem. Ges.* **1887,** *20,* 944–948.
doi:10.1002/cber.188702001215

38. Marull, M.; Schlosser, M. *Eur. J. Org. Chem.* **2003,** 1576–1588.
doi:10.1002/ejoc.200390217

39. Berg, R.; Straub, B. F. *Beilstein J. Org. Chem.* **2013,** *9,* 2715–2750.
doi:10.3762/bjoc.9.308

40. Meldal, M.; Tornøe, C. W. *Chem. Rev.* **2008,** *108,* 2952–3015.
doi:10.1021/cr0783479

41. Bock, V. D.; Hiemstra, H.; van Maarseveen, J. H. *Eur. J. Org. Chem.*
2006, 51–68. doi:10.1002/ejoc.200500483

42. Shao, C.; Wang, X.; Zhang, Q.; Luo, S.; Zhao, J.; Hu, Y. *J. Org. Chem.*
2011, *76,* 6832–6836. doi:10.1021/jo200869a

43. Métro, T.-X.; Bonnamour, J.; Reidon, T.; Duprez, A.; Sarpoulet, J.;
Martinez, J.; Lamaty, F. *Chem. – Eur. J.* **2015,** *21,* 12787–12796.
doi:10.1002/chem.201501325

44. Štefanić, G.; Krehula, S.; Štefanić, I. *Chem. Commun.* **2013,** *49,*
9245–9247. doi:10.1039/c3cc44803g

45. Gracin, D.; Štrukil, V.; Friščić, T.; Halasz, I.; Užarević, K.
Angew. Chem., Int. Ed. **2014,** *53,* 6193–6197.
doi:10.1002/anie.201402334

46. Lukin, S.; Stolar, T.; Tireli, M.; Blanco, M. V.; Babić, D.; Friščić, T.;
Užarević, K.; Halasz, I. *Chem. – Eur. J.* **2017,** *23,* 13941–13949.
doi:10.1002/chem.201702489

47. Juribašić, M.; Užarević, K.; Gracin, D.; Ćurić, M. *Chem. Commun.*
2014, *50,* 10287–10290. doi:10.1039/C4CC04423A

48. Tireli, M.; Juribašić-Kulcsár, M.; Cindro, N.; Gracin, D.; Biliškov, N.;
Borovina, M.; Ćurić, M.; Halasz, I.; Užarević, K. *Chem. Commun.* **2015,**
51, 8058–8061. doi:10.1039/C5CC01915J

49. Štrukil, V.; Gracin, D.; Magdysyuk, O. V.; Dinnebier, R. E.; Friščić, T.
Angew. Chem., Int. Ed. **2015,** *54,* 8440–8443.
doi:10.1002/anie.201502026

50. Silverstein, R. M.; Webster, F. X.; Kiemle, D. J. *Spectrometric
identification of organic compounds,* 7th ed.; John Wiley & Sons:
Hoboken, NJ, 2005.

51. Sun, S.; Wu, P. *J. Phys. Chem. A* **2010,** *114,* 8331–8336.
doi:10.1021/jp105034m

52. Gebrekidan, M. T.; Knipfer, C.; Stelzle, F.; Popp, J.; Will, S.;
Braeuer, A. *J. Raman Spectrosc.* **2016,** *47,* 198–209.
doi:10.1002/jrs.4775

53. Stolar, T.; Batzdorf, L.; Lukin, S.; Žilić, D.; Mottillo, C.; Friščić, T.;
Emmerling, F.; Halasz, I.; Užarević, K. *Inorg. Chem.* **2017,** *56,*
6599–6608. doi:10.1021/acs.inorgchem.7b00707

54. Bernstein, J.; Davis, R. E.; Shimoni, L.; Chang, N.-L.
Angew. Chem., Int. Ed. Engl. **1995,** *34,* 1555–1573.
doi:10.1002/anie.199515551

55. Grimme, S.; Antony, J.; Ehrlich, S.; Krieg, H. *J. Chem. Phys.* **2010,**
132, 154104. doi:10.1063/1.3382344

56. *Gaussian 09,* Revision D.01; Gaussian, Inc.: Wallingford CT, 2009.

57. Andrae, D.; Häußermann, U.; Dolg, M.; Stoll, H.; Preuss, H.
Theor. Chim. Acta **1990,** *77,* 123–141. doi:10.1007/BF01114537

58. Oxford Diffraction, Xcalibur CCD System, CrysAlisPro, Agilent
Technologies, Abingdon, England, 2012.

59. Burla, M. C.; Caliandro, R.; Camalli, M.; Carrozzini, B.;
Cascarano, G. L.; De Caro, L.; Giacovazzo, C.; Polidori, G.;
Spagna, R. *J. Appl. Crystallogr.* **2005,** *38,* 381–388.
doi:10.1107/S002188980403225X

60. Sheldrick, G. M. *Acta Crystallogr., Sect. C: Struct. Chem.* **2015,** *71,*
3–8. doi:10.1107/S2053229614024218

61. Farrugia, L. J. *J. Appl. Crystallogr.* **2012,** *45,* 849–854.
doi:10.1107/S0021889812029111

62. Spek, A. L. *Acta Crystallogr., Sect. D: Biol. Crystallogr.* **2009,** *65,*
148–155. doi:10.1107/S090744490804362X

63. Macrae, C. F.; Bruno, I. J.; Chisholm, J. A.; Edgington, P. R.;
McCabe, P.; Pidcock, E.; Rodriguez-Monge, L.; Taylor, R.;
van de Streek, J.; Wood, P. A. *J. Appl. Crystallogr.* **2008,** *41,* 466–470.
doi:10.1107/S0021889807067908

Exploring mechanochemistry to turn organic bio-relevant molecules into metal-organic frameworks: a short review

Vânia André[*], Sílvia Quaresma, João Luís Ferreira da Silva and M. Teresa Duarte

Abstract

Mechanochemistry is a powerful and environmentally friendly synthetic technique successfully employed in different fields of synthetic chemistry. Application spans from organic to inorganic chemistry including the synthesis of coordination compounds. Metal-organic frameworks (MOFs) are a class of compounds with numerous applications, from which we highlight herein their application in the pharmaceutical field (BioMOFs), whose importance has been growing and is now assuming a relevant and promising domain. The need to find cleaner, greener and more energy and material-efficient synthetic procedures led to the use of mechanochemistry into the synthesis of BioMOFs.

Introduction

Mechanochemistry is a straightforward and clean technique by which the desired products are obtained in high purity and high or quantitative yield. It combines high reaction efficiency with a minimum input of energy and solvent. It is an approach to green chemistry, an area devoted to the discovery of environmentally friendly synthetic pathways, eliminating or drastically reducing the amount of solvent necessary to catalytically promote reactions. Mechanochemistry consists of grinding together two or more compounds to promote a reaction, by inducing the breaking/forming of covalent or supramolecular bonds [1,2].

There are different approaches towards mechanochemistry. The most direct is neat grinding (NG), in which the reagents are ground together without the addition of any solvent or other ad-

ditive [3]. NG evolved into liquid-assisted grinding (LAG), also known as solvent-drop grinding or kneading, which includes the addition of catalytic amounts of solvent to facilitate the reaction. This technique proved to be useful for the synthesis of new compounds that could not be obtained by solution or NG techniques, while still avoiding excessive use of solvent [3-7]. The addition of catalytic amounts of an inorganic salt together with catalytic amounts of solvent, resulted in another mechanochemical approach, the ion and liquid-assisted grinding (ILAG), a technique that was also very successful in promoting solid-state reactions [8-11]. Polymer-assisted grinding (POLAG) is another variation of mechanochemistry, very recently disclosed and making use of polymers to stimulate the reaction [6,12].

Concerning the synthesis of molecular compounds and molecular crystals [2,13-15] mechanochemistry has been known for a long time [16-23] as a viable synthetic route and early works date back to the pioneer investigations by Etter [17,18,24], Rastogi [19,22,23] and Curtin and Paul [16,25,26]. Nowadays it is still a method of choice in different areas of chemistry and materials sciences, including organic solids [2] with pharmaceutical, luminescence- and thermoactive properties; studies of biomolecular recognition, asymmetric catalysis, interlocked systems and racemic resolution [2]. More recently mechanochemical methods were again successfully applied to the field of supramolecular chemistry [27-29], for solvent-free preparation of co-crystals, and adducts [30-38], polymorphs [12], supramolecular aggregates [4,30,39-42], host–guest complexes [5,43-45], metal-organic frameworks (MOFs) [8,28,44,46-50], and coordination networks [46-48,51].

All these applications comprise the formation of intermolecular interactions, the basis of supramolecular chemistry. This discipline was fully recognized internationally with the attribution of the Nobel Prize of Chemistry in 1987 to Donald J. Cram and Jean-Marie Lehn [52-55]. The energetics involved in supramolecular chemical reactions are not very severe, making mechanochemistry an excellent technique to be used in these processes.

In this short review, we particularly focused on the application of mechanochemistry to the synthesis of MOFs, especially on BioMOFs. MOFs are among the most exciting structures and their range of applications is rather vast, including, but is not limited to ion exchange, adsorption and gas storage [56-61], separation processes [62], catalysis [63,64], polymerization reactions [65,66], luminescence [67], non-linear optics [68] and magnetism [69], as well as contrast agents for magnetic resonance imaging (MRI) [70] and as drug carriers in systems for controlled drug delivery and release [64,71-80]. Also under development are new systems with potential use in further biomedical/pharmaceutical applications [71], such as cancer therapy [81-83].

MOFs combine coordination and supramolecular chemistry. Coordination chemistry is present in the coordination of organic molecules (linkers) to metal ions or clusters (coordination centers), while supramolecular chemistry relies on the formation of intermolecular interactions between linker molecules. This combination results in 1D, 2D or 3D porous frameworks. The pore size can be adjusted by varying the size of the linkers, a modification that can be associated to the change in functional groups in the organic moieties. These functional groups can form intermolecular interactions with potential pore incorporated molecules [72,84-86]. Their characteristics led

researchers to explore the potential of MOFs as incarceration and/or delivery systems [70,79,83-87].

In BioMOFs, endogenous molecules, active pharmaceutical ingredients (APIs) or other bioactive organic molecules are used as building blocks for the framework [8]. Besides the advantages of MOFs as controlled delivery systems, BioMOFs have additional benefits, such as: i) porosity is no longer an issue as the release of the APIs or bioactive molecules is achieved by degradation of the framework, ii) no multistep synthesis is required as the molecules are part of the matrix itself, iii) synergetic effects between the active molecule and the metal may be explored, and iv) co-delivery of drugs is possible if a porous network is built with one ingredient and an incorporation of another is feasible [88]. BioMOFs are promising candidates for the development of more effective therapies with reduced side effects.

Two families of MOFs, MILs (materials of Institute Lavoisier) and CPOs (coordination polymers from Oslo), were the first to be studied for their potential medicinal applications. Here, the main focus was their use as drug-delivery systems [71,72,89], with particular attention to the toxicity of the metal centers [84]. Toxicity is a concern not only for the safe use of these compounds for humans but also for environmental reasons. These issues also led to the quest for biodegradable MOFs, the first being prepared in 2010 by Miller et al. [77].

Another family of MOFs, ZIFs (zeolitic imidazolate frameworks), that involves organic imidazoles as linkers, has been explored for medicinal purposes as a result of the enhancement of MOF structural and stability properties [90,91]. Bioactive molecules like caffeine [92,93] and anticancer drugs [94-98] were incorporated in ZIF-8 and tests proved that these systems allowed for a controlled drug release. Further studies involving ZIF-8 with encapsulated anticancer drugs have also shown that these have potential to be used in fluorescence imaging.

The number of reports on MOFs synthesized by mechanochemistry [8,28,50,99-101] has been increasing and some in situ studies on the mechanosynthesis of MOFs and coordination polymers are already being carried out with success. These studies show the propensity for stepwise mechanisms, especially in case of ZIFs, with a low density or a highly solvated product often formed first which is then transformed into increasingly dense, less solvated materials, resembling Ostwald's rule of stages [8,102-107].

Many reviews on mechanochemistry [10,28,29,50,101,107,108] and MOFs [76,78,79,88,90,109] have been published due to the increasing relevance of both the technique and the type of com-

pounds. We have recently published two reviews, one focused on the use of mechanochemical processes towards attaining metallopharmaceuticals, metallodrugs and MOFs synthesized within our group [49], and another on the design, screening, and characterization of BioMOFs in general [110]. To the best of our knowledge, this is the first short review targeting on the mechanochemical synthesis of BioMOFs.

Review
BioMOFs prepared by mechanochemistry and their main features

BioMOFs can be divided into two major classes: i) BioMOFs in which the APIs are the building blocks of the framework, thus excluding the need for large pores and ii) BioMOFs in which the API is incorporated (encapsulated) as a guest within the pores of the MOF. In the second situation, the choice of the linker is crucial, as it needs to be an organic molecule listed of the generally regarded as safe (GRAS) compounds, an endogenous compound or a bioactive molecule. In both classes, the judicious choice of the metals to be used in these systems is of great importance. Several metal species are known to display important biological activities that are applied for the treatment or diagnosis of several diseases. So, BioMOFs should contain either endogenous metal cations essential for life or exogenous metals that display a specific bioactive function in appropriate dosages, allowing to take benefits of possible synergetic effects between the metal and the APIs. Nevertheless, toxicity is also dependent on many other factors such as speciation, chemical nature, administration route, exposition time and accumulation/ elimination from the body [88]. The examples given here will be separated according to the function of the APIs in the BioMOF: linker or guest.

BioMOFs with active pharmaceutical ingredients (APIs) as linkers

Several BioMOFs with APIs as building blocks have been synthesized recurring to mechanochemistry and we will just present a few examples herein. It is common that these compounds are reported as coordination networks, or metallopharmaceuticals. One example we would like to mention has been proposed by Braga et al. [111], in which gabapentin was used as linker to build two new coordination complexes with $ZnCl_2$ and $CuCl_2 \cdot 2H_2O$ by manually grinding both solids. Gabapentin is a neuroleptic drug used for the prevention of seizures, the treatment of mood disorders, anxiety, tardive dyskinesia [111-119], and neuropathic pain [120]. The synthesis of these coordination compounds with gabapentin was based on studies concerning the understanding of the physiological and pathophysiological roles played by Zn^{2+} and Cu^{2+} in various biological systems [121-123], and therefore the use of such coordination complexes was envisaged a new route for the delivery of those

drugs. Gabapentin was also used by Quaresma et al. [124] in the synthesis by manual grinding of seventeen new metal coordination networks with Y(III), Mn(II) and several lanthanide chlorides ($LnCl_3$), Ln = La^{3+}, Ce^{3+}, Nd^{3+}, and Er^{3+}. Ten out of these compounds were structurally characterized and represent the first coordination networks of pharmaceuticals involving lanthanides, showing different types of architectures based on mono-, di-, tri- and hexametallic centers and 1D polymeric chains. These new compounds proved to be unstable under shelf conditions. With regard to their thermal stability these compounds lose water at approximately 80 °C and melt/decompose above 200–250 °C [124]. This type of BioMOFs enclosing lanthanides and cations with potential luminescence properties can be explored for theranostic applications. Figure 1 shows some examples of the networks obtained.

Braga et al. synthesized new BioMOFs using 4-aminosalicylic acid and piracetam. 4-Aminosalicylic acid is an antibiotic that has been used in the treatment of tuberculosis, inflammatory bowel diseases, namely distal ulcerative colitis [125,126] and Crohn's disease [127], while piracetam is a nootropic drug used to improve cognitive abilities. A 1D framework was synthesized which is stable up to 130 °C. The new compound resulting from the reaction between piracetam and $Ni(NO_3)_2 \cdot 6H_2O$ consists of a polymeric chain based on a tetrameric repeating unit comprising a pair of piracetam molecules and two metal atoms and proved to be stable up to approximately 80 °C. Both BioMOFs were obtained recurring to manual mechanochemistry. Due to the possibility of synergic effects with Ag^+, a known antimicrobial agent, the new network with 4-aminosalicylic acid and silver is highly interesting, as it represents a promising candidate to future biomedical applications [128].

Having in mind the synthesis of BioMOFs involving the excipient magnesium oxide initially proposed by Byrn et al. [129], Chow et al. and Friščić et al. developed new BioMOFs by LAG, grinding together MgO with the non-steroidal anti-inflammatory drugs (NSAIDS) ibuprofen (*S* and *RS*-forms), salicylic acid [130] and naproxen using water as the grinding liquid [7]. With naproxen, LAG was also used to screen for hydrated forms of magnesium–naproxen by systematically varying the fraction of water in the LAG experiments [7]. Low, intermediate and high amounts of water as grinding liquid led to the formation of a 1D coordination polymer monohydrate, a tetrahydrate complex and an octahydrate, respectively (Figure 2) [7,29].

BioMOFs based on generally regarded as safe (GRAS), bioactive or endogenous linkers for the encapsulation of APIs

Another approach to build a BioMOF consists of the use of generally regarded as safe (GRAS), bioactive or endogenous
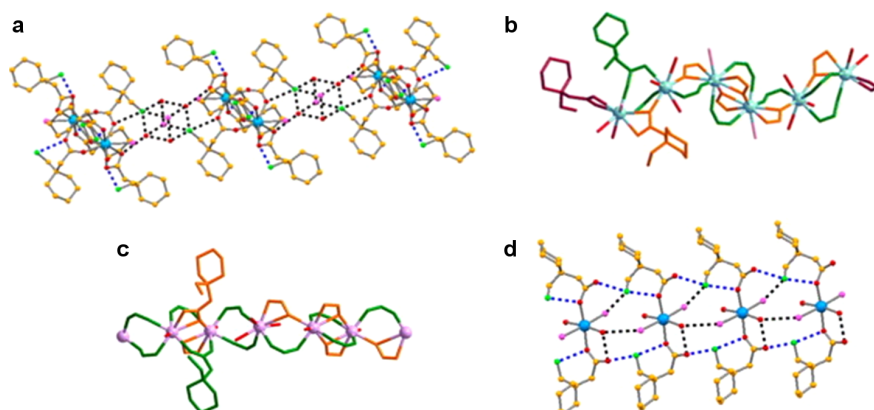
Figure 1: a) Detailed supramolecular packing of a gabapentin–Er network; b) view along the *b*-axis of the supramolecular packing of a gabapentin–Ce network; c) view of a GBP–Y network showing an infinite 1D chain; d) simplified packing of a gabapentin–Mn network. H atoms were omitted for clarity. Reprinted with permission from [49], copyright 2017 Elsevier.
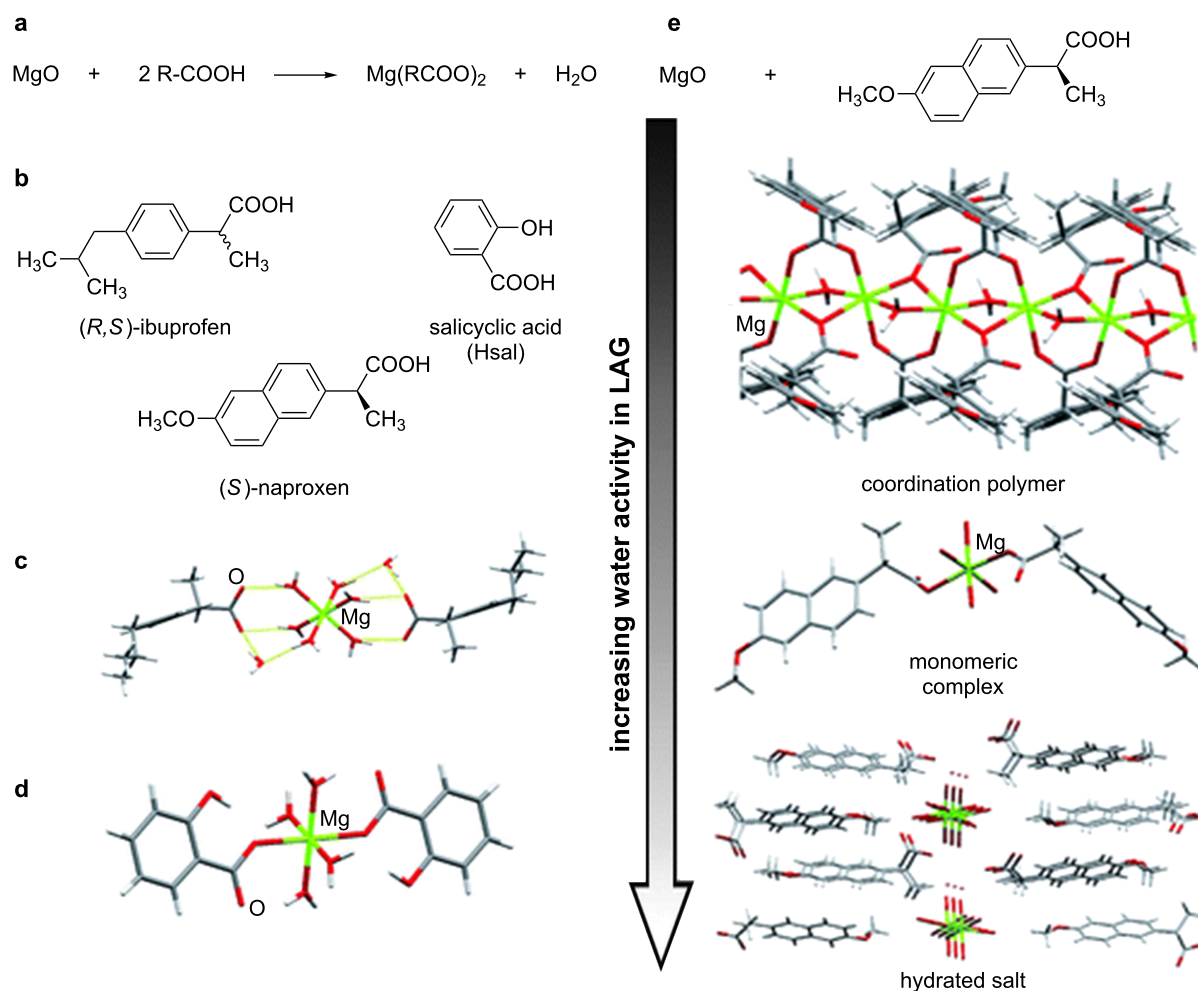
Figure 2: a) Mechanochemical reactivity between the excipient MgO and carboxylic acid NSAID molecules; b) NSAID molecules explored in mechanochemical reactions with MgO; c) fragment of the crystal structure of a mechanochemically obtained magnesium–ibuprofen complex; d) fragment of the crystal structure of a mechanochemically obtained magnesium–salicylate complex; e) screening for different hydrated forms of magnesium–naproxen BioMOFs by systematically varying the quantity of water in LAG reactions of MgO and (*S*)-naproxen. Reprinted with permission from [29], copyright 2012 the Royal Society of Chemistry.

linkers to form the 3D framework followed by the encapsulation of the APIs in the BioMOF. In these cases, the 3D frameworks may be synthesized by mechanochemistry, but the encapsulation of the drug is usually carried out by soaking methods. However, a significant number of these frameworks obtained by mechanochemistry with potential to be used as drug delivery systems have not yet been fully tested for the loading of drugs.
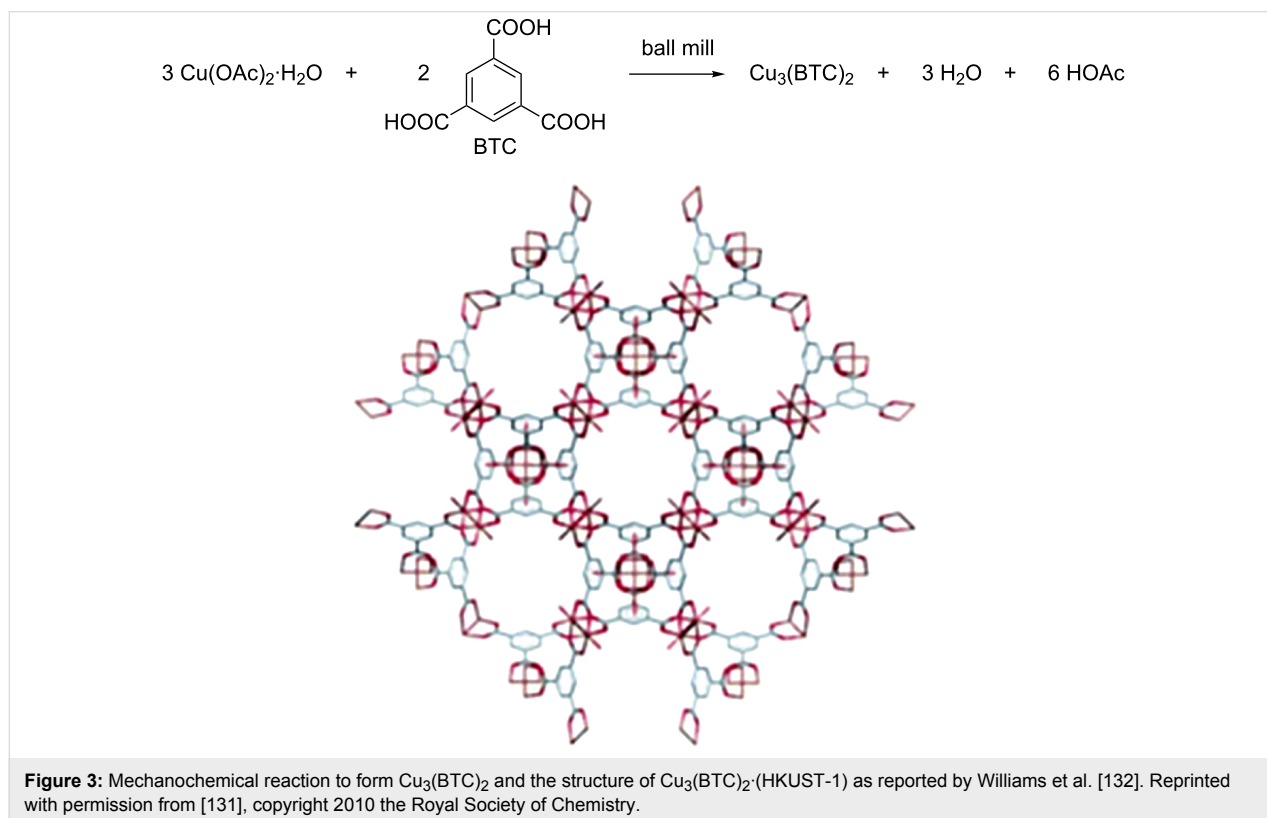
Pichon et al. proposed the first BioMOF synthesized by mechanochemistry using copper acetate and isonicotinic acid [46]. This type of compounds is useful for gas separation applications, but they haven't been tested for biological applications yet. The solvothermal methods that were previously reported for the synthesis of this compound required high temperatures (150 °C), a 48 hours reaction and the use of solvents. With mechanochemistry, the same compound is obtained in high yield within 10 minutes at room temperature and without the use of solvents. Thus, this work revealed a fast, convenient, less expensive and effective preparative method for the synthesis of robust and stable 3D BioMOFs and rapidly inspired other groups to follow this methodology.

This has been proved by the work of Wenbing Yuan et al., in which a very important 3D BioMOF, known as HKUST-1, was synthesized by grinding together copper acetate with 1,3,5-b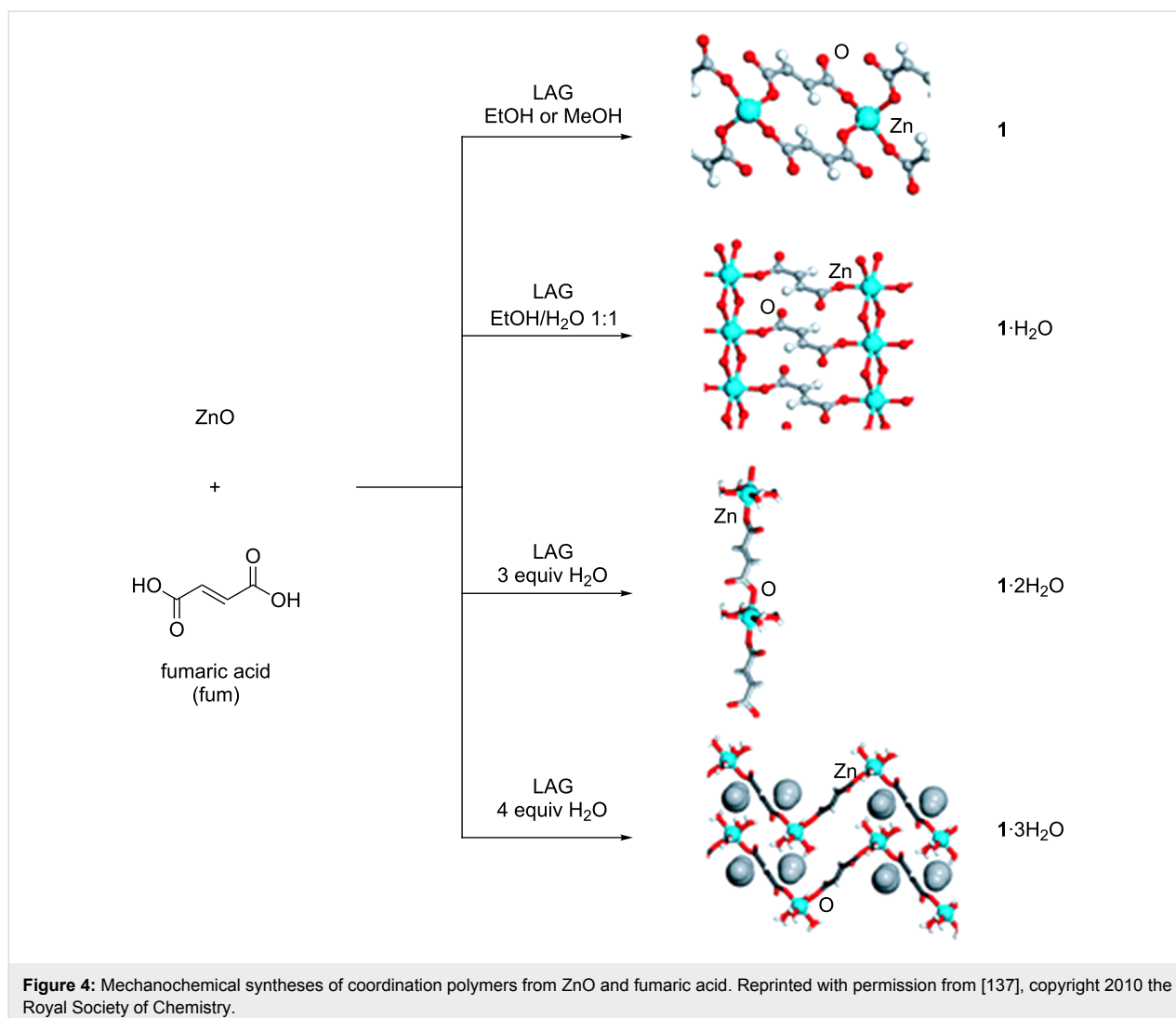enzenetricarboxylic acid (BTC, Figure 3) in a ball mill for 15 minutes without solvent. This procedure delivered HKUST-1 with some improved properties, including higher microporosity and surface area, when compared to those made in solution and by other techniques [131].

The presence of unsaturated open metal sites turns this compound into a potential adsorption/desorption material. Gravimetric tests with nitric oxide (NO), a gas with medicinal applications, demonstrated that HKUST-1, despite showing a reasonable aptitude to absorb this gas, displays very low rates of desorption when compared to others MOFs [56,84,133,134]. Furthermore, HKUST-1 is reported as a mean to achieve a controlled release of biologically active copper ions and it has shown to be an effective antifungal agent against representative yeast and mold [135].

Friščić et al. also reported the synthesis of coordination polymers and BioMOFs using LAG by grinding together zinc oxide and fumaric acid. In this work, they initially obtained four different coordination polymers, depending on the choice of the grinding liquid: anhydrous zinc fumarate (**1**) when grinding with ethanol or methanol; a dihydrate (**1**·2H$_2$O) when using a mixture of water and ethanol; a tetrahydrate (**1**·4H$_2$O) and a pentahydrate (**1**·5H$_2$O) when grinding with three or four equiv of water, respectively (Figure 4) [136,137].

Figure 3: Mechanochemical reaction to form Cu$_3$(BTC)$_2$ and the structure of Cu$_3$(BTC)$_2$·(HKUST-1) as reported by Williams et al. [132]. Reprinted with permission from [131], copyright 2010 the Royal Society of Chemistry.

Figure 4: Mechanochemical syntheses of coordination polymers from ZnO and fumaric acid. Reprinted with permission from [137], copyright 2010 the Royal Society of Chemistry.
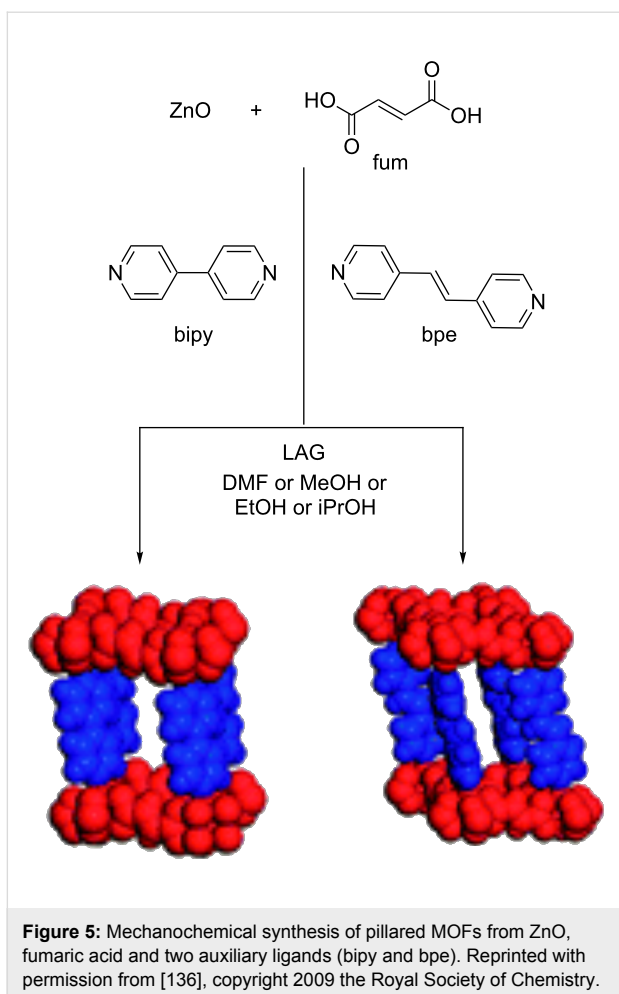
This method was further applied to the mechanochemical synthesis of porous materials with introduced auxiliary ligands. These would allow for coordination to zinc in order to generate pillared MOFs, that could be used to incorporate APIs as a guest. Indeed, they synthesized two BioMOFs by grinding together zinc, fumaric acid and 4,4'-bipyridyl (bipy) or *trans*-1,2-di(4-pyridyl)ethylene (bpe) as ligands in the presence of a space-filling liquid agent (*N,N*-dimethylformamide, DMF). This synthesis also proceeded when using environmentally more friendly solvents, such as methanol, ethanol or 2-propanol, making these BioMOFs acceptable for biological and pharmaceuticals applications (Figure 5) [136,138]. However, studies supporting this goal have not been reported so far.

In 2015, Prochowicz et al. reported a new mechanochemical approach called "SMART" (secondary basic units-based mechanochemical approach for precursor transformation), in which pre-assembled secondary building units were explored.

This method led to the successful synthesis of MOF-5 by mechanochemistry starting from Zn$_4$O and 1,4-benzenodicarboxylic acid, without the need for bulky solvents, external bases or acids and high temperatures, all required in the conventional synthetic procedure [139].
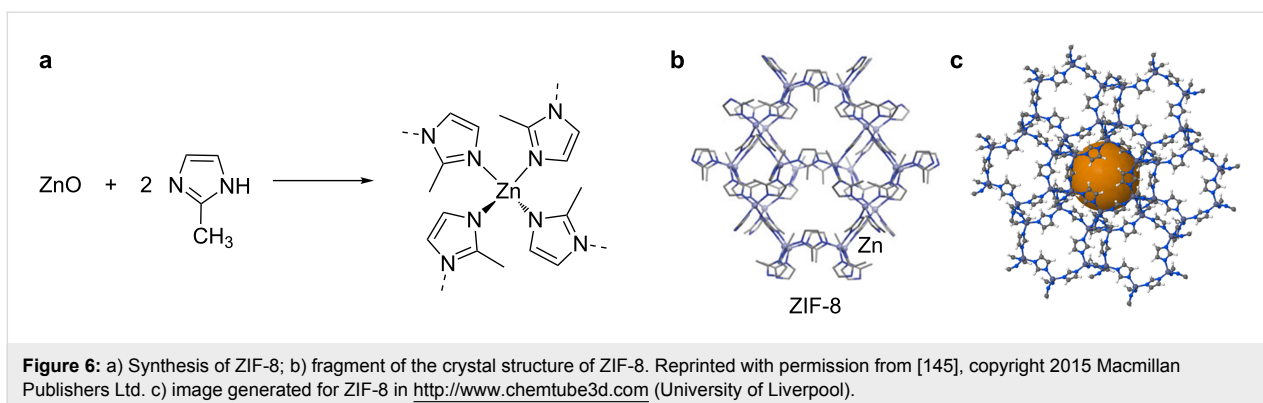
Even though MOF-5 has not yet been tested for the incorporation of drugs, using the same linker, Xu et al. unveiled in 2016 the mechanochemical synthesis of MIL-101(Cr) involving heating which was successfully tested for the incorporation of ibuprofen. In this case, mechanochemistry proved once again to be a much faster process than the traditional hydrothermal synthesis that was used to obtain this compound involving solvents and often also hydrofluoric acid [140]. The linker used to build MIL-101 is 1,4-benzenedicarboxylic acid. Different applications of MIL-101 have been reported, from which we highlight the delivery of ibuprofen. MIL-101 exhibits a very high capacity of ibuprofen and therefore only very little quantities of

Figure 5: Mechanochemical synthesis of pillared MOFs from ZnO, fumaric acid and two auxiliary ligands (bipy and bpe). Reprinted with permission from [136], copyright 2009 the Royal Society of Chemistry.

MIL-101 are necessary for the administration of a high dosage of ibuprofen [141].

The mechanochemical synthesis was expanded by Beldon et al. to the synthesis of a very different family of metal-organic materials, the zeolitic imidazolate frameworks (ZIFs) [8]. ZIFs exploit a combination of metal ions and imidazolate linkers to build the 3D framework and have simultaneously the character-

istics of MOFs and zeolites, making them very promising for biomedical applications [90,91]. In their work, Beldon et al. explored the synthesis of new ZIFs using imidazole (HIm), 2-methylimidazole (HMeIm) and 2-ethylimidazole (HEtIm) as ligands. Initially, they used LAG with ZnO and the previous imidazole ligands in the presence of DMF as a space-filling liquid. However, this method only partially succeeded: with HIm the quantitative formation of ZIF-4 was obtained after 60 min, whereas with HMeIm only partial formation of ZIF-8 was achieved and with HEtIm no reaction was observed at all [8]. As ILAG had already shown to accelerate and direct the formation of large-pore pillared MOFs [9], it was applied to these systems. A variety of ZIFs with defined topologies was obtained quantitatively by this method using ammonium nitrate, methanesulfonate or sulfate. Topology control could be achieved by either the solvent chosen for grinding or the choice of the salt additive. The most impressive result was the persistent formation of ZIF-8 (Figure 6) as it was obtained in all the reactions, showing the notable stability of this framework and making it a promising candidate to biomedical applications [8]. Indeed, ZIF-8 has been largely used to encapsulate APIs such as doxorubicin, an anticancer drug [96,142] or even as an efficient pH-sensitive drug-delivery system [92,95,143,144]. Usually, the encapsulation of small molecules into MOFs involves two steps: i) the synthesis of the framework and ii) the encapsulation of the small molecule by soaking and diffusion methods under mild conditions [96]. However, there are some one-pot syntheses reported for the encapsulation of small molecules into ZIF-8. Liédana et al. disclosed the in situ encapsulation of caffeine into ZIF-8 [98] and Zhuang et al. proposed a method to synthesize nanosized ZIF-8 spheres with encapsulation of small molecules into the framework during synthesis [95]. Also, Zheng et al. proposed a fast, single step synthesis of ZIF-8 with direct incorporation of small molecules, including doxorubicin [142]. The controlled drug release is due to the small pore size of ZIF-8 that prevents premature release and its pH sensitivity. At pH 5–6 there dissociation of the framework takes place with consequent drug release ideal to target cancer cells [95].

Figure 6: a) Synthesis of ZIF-8; b) fragment of the crystal structure of ZIF-8. Reprinted with permission from [145], copyright 2015 Macmillan Publishers Ltd. c) image generated for ZIF-8 in http://www.chemtube3d.com (University of Liverpool).

Mechanochemistry in the synthesis of a metallodrug, another metal-organic target

The study of the chemical reactivity of bismuth and carboxylic acids, in particular salicylic acid, is quite relevant for the pharmaceutical industry, because of the large production of bismuth subsalicylate (Pepto-Bismol), an anti-acid used in the treatment of stomach and intestine disorders. So far, this product was synthesized exclusively in solution involving harsh reaction conditions. André et al. [11] used ILAG [146,147] to prepare it directly from Bi_2O_3 (Bi) and salicylic acid (SA) in a 1:1 (Bi·SA) stoichiometry. This method proved not only to be more efficient but also very selective [11]. Changing the stoichiometric ratio of the reactants to 1:2 and 1:3 allowed the syntheses of another two bismuth–salicylate compounds, namely the disalicylate and the trisalicylate, respectively. The only previously known crystal structure obtained for bismuth salicylates was a Bi_{38} cluster isolated by recrystallization of the trisalicylate from acetone [148] and this was then considered a possible model for the structure of bismuth subsalicylate [11]. In 2011, André et al. performed a similar recrystallization of the disalicylate and obtained a similar Bi_{38} cluster with coordinated *N,N*-dimethylformamide (DMF) molecules instead of acetone, showing the structural robustness of this core in solution. The crystal structure solution from powder X-ray diffraction data of the disalicylate revealed the first crystal structure of a bismuth salicylate without coordinated solvent molecules (Figure 7). This indicates that bismuth salicylates form extended structures without the presence of other ligands [11].

Conclusion

All examples presented herein and collected in Table 1 show the advantages of combining pharmaceutically relevant organic molecules with metal centers, in order to obtain compounds with enhanced biological properties.

New metal-organic frameworks, BioMOFs, for the use of controlled drug delivery and/or release or other biological applications, were successfully synthesized either by direct incorporation of the bioactive molecule in the framework (linker), or by encapsulation (guest). Mechanochemistry has proved to be an efficient, high performance, environmentally friendly, cleaner, and faster synthetic procedure, leading to significantly lower costs of production.

There is still much to explore in the combination of BioMOFs with mechanochemistry and this is certainly an expanding area in the field of organic coordination chemistry.
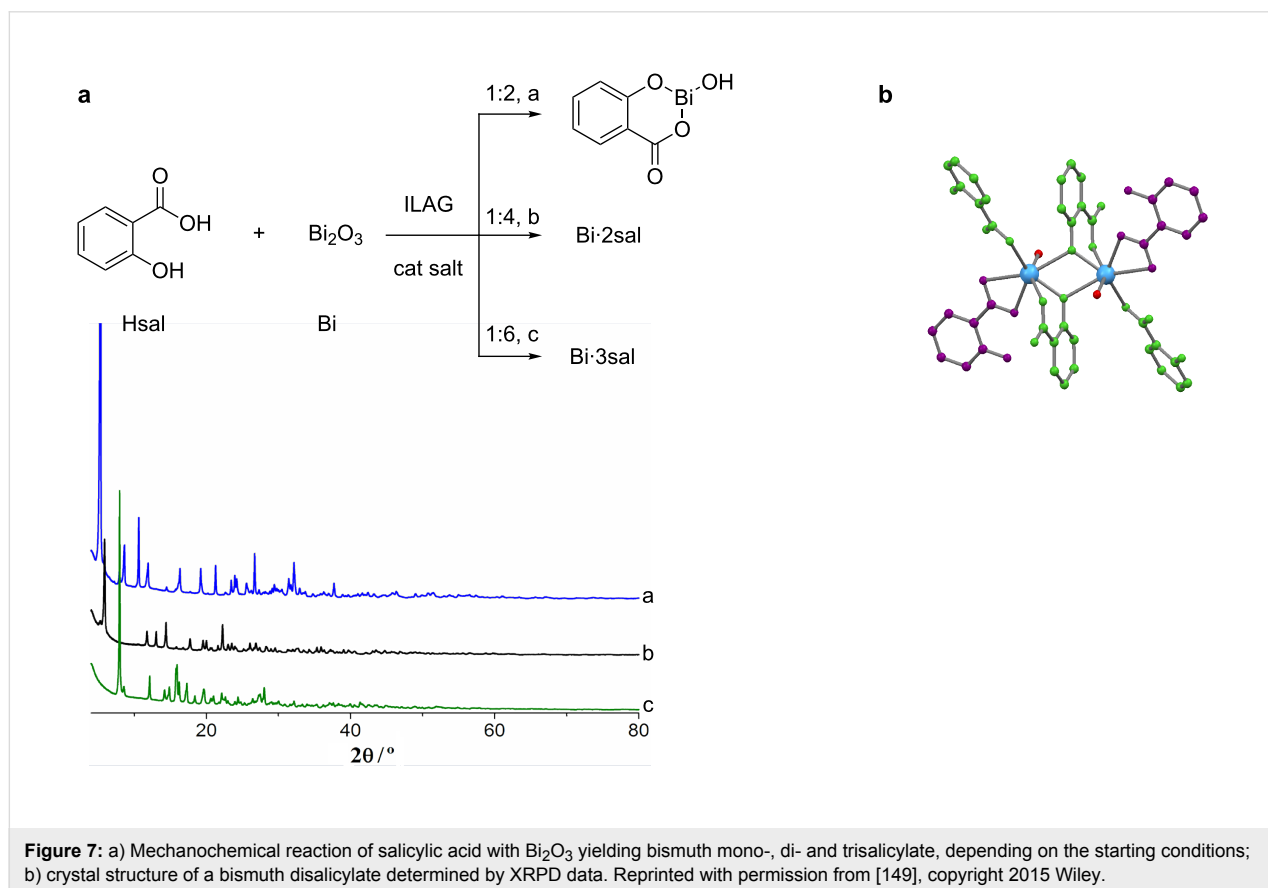
Figure 7: a) Mechanochemical reaction of salicylic acid with Bi_2O_3 yielding bismuth mono-, di- and trisalicylate, depending on the starting conditions; b) crystal structure of a bismuth disalicylate determined by XRPD data. Reprinted with permission from [149], copyright 2015 Wiley.

Table 1: Summary of the BioMOFs synthesized by mechanochemistry presented herein.

Metal	Linker	Ref.
Zn^{2+}, Cu^{2+}	gabapentin	[111]
La^{3+}, Ce^{3+}, Nd^{3+},Er^{3+}, y^{3+}, Mn^{2+}	gabapentin	[124]
Ag^+	4-aminosalicylic acid	[128]
Ni^{2+}	piracetam	[128]
Mg^{2+}	ibuprofen, naproxen, salicylic acid	[7]
Cu^{2+}	isonicotinic acid	[46]
Cu^{2+}	1,3,5-benzenetricarboxylic acid	[131]
Zn^{2+}	fumaric acid	[136]
Zn^{2+}	fumaric acid + 4,4'-bipyridine	[138]
Zn^{2+}	fumaric acid + 1,2-di(4-pyridyl)ethylene	[138]
Zn_4O	1,4-benzenedicarboxylic acid	[139]
Cr^{3+}	1,4-benzenedicarboxylic acid	[140]
Zn^{2+}	2-methylimidazole	[8]
Zn^{2+}	2-ethylimidazole	[8]
Bi^{3+}	salicylic acid	[11]

Acknowledgements

References

1. Chadwick, K.; Davey, R.; Cross, W. *CrystEngComm* **2007,** *9,* 732–734. doi:10.1039/b709411f
2. Tanaka, K.; Toda, F. *Chem. Rev.* **2000,** *100,* 1025–1074. doi:10.1021/cr940089p
3. Karki, S.; Friščić, T.; Jones, W.; Motherwell, W. D. S. *Mol. Pharmaceutics* **2007,** *4,* 347–354. doi:10.1021/mp0700054
4. Trask, A. V.; Motherwell, W. D. S.; Jones, W. *Chem. Commun.* **2004,** 890–891. doi:10.1039/b400978a
5. Friščić, T.; Trask, A. V.; Jones, W.; Motherwell, W. D. S. *Angew. Chem., Int. Ed.* **2006,** *45,* 7546–7550. doi:10.1002/anie.200603235
6. Hasa, D.; Rauber, G. S.; Voinovich, D.; Jones, W. *Angew. Chem., Int. Ed.* **2015,** *54,* 7371–7375. doi:10.1002/anie.201501638
7. Friščić, T.; Halasz, I.; Strobridge, F. C.; Dinnebier, R. E.; Stein, R. S.; Fábián, L.; Curfs, C. *CrystEngComm* **2011,** *13,* 3125–3129. doi:10.1039/c0ce00894j
8. Beldon, P. J.; Fábián, L.; Stein, R. S.; Thirumurugan, A.; Cheetham, A. K.; Friščić, T. *Angew. Chem., Int. Ed.* **2010,** *49,* 9640–9643. doi:10.1002/anie.201005547
9. Friščić, T.; Reid, D. G.; Halasz, I.; Stein, R. S.; Dinnebier, R. E.; Duer, M. J. *Angew. Chem., Int. Ed.* **2010,** *49,* 712–715. doi:10.1002/anie.200906583
10. Friščić, T. *J. Mater. Chem.* **2010,** *20,* 7599–7605. doi:10.1039/c0jm00872a
11. André, V.; Hardeman, A.; Halasz, I.; Stein, R. S.; Jackson, G. J.; Reid, D. G.; Duer, M. J.; Curfs, C.; Duarte, M. T.; Friščić, T. *Angew. Chem., Int. Ed.* **2011,** *50,* 7858–7861. doi:10.1002/anie.201103171

12. Hasa, D.; Carlino, E.; Jones, W. *Cryst. Growth Des.* **2016,** *16,* 1772–1779. doi:10.1021/acs.cgd.6b00084
13. Cave, G. W. V.; Raston, C. L.; Scott, J. L. *Chem. Commun.* **2001,** 2159–2169. doi:10.1039/b106677n
14. Rothenberg, G.; Downie, A. P.; Raston, C. L.; Scott, J. L. *J. Am. Chem. Soc.* **2001,** *123,* 8701–8708. doi:10.1021/ja0034388
15. Kaupp, G. *CrystEngComm* **2003,** 117–133. doi:10.1039/b303432a
16. Patil, A. O.; Curtin, D. Y.; Paul, I. C. *J. Am. Chem. Soc.* **1984,** *106,* 348–353. doi:10.1021/ja00314a017
17. Ojala, W. H.; Etter, M. C. *J. Am. Chem. Soc.* **1992,** *114,* 10288–10293. doi:10.1021/ja00052a026
18. Etter, M. C.; Reutzel, S. M.; Choo, C. G. *J. Am. Chem. Soc.* **1993,** *115,* 4411–4412. doi:10.1021/ja00063a089
19. Rastogi, R. P.; Bassi, P. S.; Chadha, S. L. *J. Phys. Chem.* **1962,** *66,* 2707–2708. doi:10.1021/j100818a503
20. Rastogi, R. P.; Singh, N. B. *J. Phys. Chem.* **1968,** *72,* 4446–4449. doi:10.1021/j100859a013
21. Rastogi, R. P.; Dubey, B. L. *J. Am. Chem. Soc.* **1967,** *89,* 200–209. doi:10.1021/ja00978a003
22. Rastogi, R. P.; Singh, N. B. *J. Phys. Chem.* **1966,** *70,* 3315–3324. doi:10.1021/j100882a047
23. Rastogi, R. P.; Bassi, P. S.; Chadha, S. L. *J. Phys. Chem.* **1963,** *67,* 2569–2573. doi:10.1021/j100806a016
24. Etter, M. C. *J. Phys. Chem.* **1991,** *95,* 4601–4610. doi:10.1021/j100165a007
25. Chiang, C. C.; Lin, C. T.; Wang, A. H. J.; Curtin, D. Y.; Paul, I. C. *J. Am. Chem. Soc.* **1977,** *99,* 6303–6308. doi:10.1021/ja00461a020
26. Paul, I. C.; Curtin, D. Y. *Acc. Chem. Res.* **1973,** *6,* 217–225. doi:10.1021/ar50067a001
27. Braga, D. *Chem. Commun.* **2003,** 2751–2754. doi:10.1039/b306269b
28. Friščić, T. *Chem. Soc. Rev.* **2012,** *41,* 3493–3510. doi:10.1039/c2cs15332g
29. Delori, A.; Friščić, T.; Jones, W. *CrystEngComm* **2012,** *14,* 2350–2362. doi:10.1039/c2ce06582g
30. Kuroda, R.; Imai, Y.; Tajima, N. *Chem. Commun.* **2002,** 2848–2849. doi:10.1039/b207417f

31. Cinčić, D.; Friščić, T.; Jones, W. *Chem. – Eur. J.* **2008,** *14,* 747–753. doi:10.1002/chem.200701184

32. Cinčić, D.; Friščić, T.; Jones, W. *J. Am. Chem. Soc.* **2008,** *130,* 7524–7525. doi:10.1021/ja801164v

33. Trivedi, D. R.; Fujiki, Y.; Goto, Y.; Fujita, N.; Shinkai, S.; Sada, K. *Chem. Lett.* **2008,** *37,* 550–551. doi:10.1246/cl.2008.550

34. Yoshida, J.; Nishikiori, S.-i.; Kuroda, R. *Chem. – Eur. J.* **2008,** *14,* 10570–10578. doi:10.1002/chem.200801627

35. Braga, D.; Maini, L.; de Sanctis, G.; Rubini, K.; Grepioni, F.; Chierotti, M. R.; Gobetto, R. *Chem. – Eur. J.* **2003,** *9,* 5538–5548. doi:10.1002/chem.200304940

36. Cheung, E. Y.; Kitchin, S. J.; Harris, K. D. M.; Imai, Y.; Tajima, N.; Kuroda, R. *J. Am. Chem. Soc.* **2003,** *125,* 14658–14659. doi:10.1021/ja030506s

37. Imai, Y.; Tajima, N.; Sato, T.; Kuroda, R. *Chirality* **2002,** *14,* 604–609. doi:10.1002/chir.10098

38. Kuroda, R.; Higashiguchi, K.; Hasebe, S.; Imai, Y. *CrystEngComm* **2004,** *6,* 464–468. doi:10.1039/b408971e

39. Pedireddi, V. R.; Jones, W.; Chorlton, A. P.; Docherty, R. *Chem. Commun.* **1996,** 987–988. doi:10.1039/cc9960000987

40. Balema, V. P.; Wiench, J. W.; Pruski, M.; Pecharsky, V. K. *Chem. Commun.* **2002,** 724–725. doi:10.1039/b111515d

41. Balema, V. P.; Wiench, J. W.; Pruski, M.; Pecharsky, V. K. *Chem. Commun.* **2002,** 1606–1607. doi:10.1039/b203694k

42. Orita, A.; Jiang, L.; Nakano, T.; Ma, N.; Otera, J. *Chem. Commun.* **2002,** 1362–1363. doi:10.1039/B203651G

43. Friščić, T.; Trask, A. V.; Motherwell, W. D. S.; Jones, W. *Cryst. Growth Des.* **2008,** *8,* 1605–1609. doi:10.1021/cg700929e

44. Braga, D.; Curzi, M.; Johansson, A.; Polito, M.; Rubini, K.; Grepioni, F. *Angew. Chem., Int. Ed.* **2006,** *45,* 142–146. doi:10.1002/anie.200502597

45. Braga, D.; Maini, L.; Giaffreda, S. L.; Grepioni, F.; Chierotti, M. R.; Gobetto, R. *Chem. – Eur. J.* **2004,** *10,* 3261–3269. doi:10.1002/chem.200305751

46. Pichon, A.; Lazuen-Garay, A.; James, S. L. *CrystEngComm* **2006,** *8,* 211–214. doi:10.1039/b513750k

47. Belcher, W. J.; Longstaff, C. A.; Neckenig, M. R.; Steed, J. W. *Chem. Commun.* **2002,** 1602–1603. doi:10.1039/b202652j

48. Nichols, P. J.; Raston, C. L.; Steed, J. W. *Chem. Commun.* **2001,** 1062–1063. doi:10.1039/b103411c

49. Quaresma, S.; André, V.; Fernandes, A.; Duarte, M. T. *Inorg. Chim. Acta* **2017,** *455,* 309–318. doi:10.1016/j.ica.2016.09.033

50. Craig, S. L. *Nature* **2012,** *487,* 176–177. doi:10.1038/487176a

51. Garay, A. L.; Pichon, A.; James, S. L. *Chem. Soc. Rev.* **2007,** *36,* 846–855. doi:10.1039/b600363j

52. Lehn, J. M. *Pure Appl. Chem.* **1978,** *50,* 871–892. doi:10.1351/pac197850090871

53. Lehn, J.-M. *Angew. Chem., Int. Ed. Engl.* **1988,** *27,* 89–112. doi:10.1002/anie.198800891

54. Lehn, J.-M.; Rigault, A. *Angew. Chem., Int. Ed. Engl.* **1988,** *27,* 1095–1097. doi:10.1002/anie.198810951

55. Dunitz, J. D. *Pure Appl. Chem.* **1991,** *63,* 177–185. doi:10.1351/pac199163020177

56. Xiao, B.; Wheatley, P. S.; Zhao, X.; Fletcher, A. J.; Fox, S.; Rossi, A. G.; Megson, I. L.; Bordiga, S.; Regli, L.; Thomas, K. M.; Morris, R. E. *J. Am. Chem. Soc.* **2007,** *129,* 1203–1209. doi:10.1021/ja066098k

57. Graetz, J. *Chem. Soc. Rev.* **2009,** *38,* 73–82. doi:10.1039/B718842K

58. Müller, M.; Zhang, X.; Wang, Y.; Fischer, R. A. *Chem. Commun.* **2009,** 119–121. doi:10.1039/B814241F

59. Suh, M. P.; Cheon, Y. E.; Lee, E. Y. *Coord. Chem. Rev.* **2008,** *252,* 1007–1026. doi:10.1016/j.ccr.2008.01.032

60. Han, S. S.; Mendoza-Cortés, J. L.; Goddard, W. A., III. *Chem. Soc. Rev.* **2009,** *38,* 1460–1476. doi:10.1039/b802430h

61. Düren, T.; Bae, Y.-S.; Snurr, R. Q. *Chem. Soc. Rev.* **2009,** *38,* 1237–1247. doi:10.1039/b803498m

62. Ma, S.; Sun, D.; Ambrogio, M.; Fillinger, J. A.; Parkin, S.; Zhou, H.-C. *J. Am. Chem. Soc.* **2007,** *129,* 1858–1859. doi:10.1021/ja067435s

63. Farrusseng, D.; Aguado, S.; Pinel, C. *Angew. Chem., Int. Ed.* **2009,** *48,* 7502–7513. doi:10.1002/anie.200806063

64. Lee, J.; Farha, O. K.; Roberts, J.; Scheidt, K. A.; Nguyen, S. T.; Hupp, J. T. *Chem. Soc. Rev.* **2009,** *38,* 1450–1459. doi:10.1039/b807080f

65. Uemura, T.; Yanai, N.; Kitagawa, S. *Chem. Soc. Rev.* **2009,** *38,* 1228–1236. doi:10.1039/b802583p

66. Uemura, T.; Ono, Y.; Kitagawa, K.; Kitagawa, S. *Macromolecules* **2008,** *41,* 87–94. doi:10.1021/ma7022217

67. Allendorf, M. D.; Bauer, C. A.; Bhakta, R. K.; Houk, R. J. T. *Chem. Soc. Rev.* **2009,** *38,* 1330–1352. doi:10.1039/b802352m

68. Evans, O. R.; Lin, W. *Acc. Chem. Res.* **2002,** *35,* 511–522. doi:10.1021/ar0001012

69. Kurmoo, M. *Chem. Soc. Rev.* **2009,** *38,* 1353–1379. doi:10.1039/b804757j

70. Della Rocca, J.; Liu, D.; Lin, W. *Acc. Chem. Res.* **2011,** *44,* 957–968. doi:10.1021/ar200028a

71. Horcajada, P.; Serre, C.; Vallet-Regí, M.; Sebban, M.; Taulelle, F.; Férey, G. *Angew. Chem., Int. Ed.* **2006,** *45,* 5974–5978. doi:10.1002/anie.200601878

72. Horcajada, P.; Serre, C.; Maurin, G.; Ramsahye, N. A.; Balas, F.; Vallet-Regi, M.; Sebban, M.; Taulelle, F.; Férey, G. *J. Am. Chem. Soc.* **2008,** *130,* 6774–6780. doi:10.1021/ja710973k

73. Férey, G. *Chem. Soc. Rev.* **2008,** *37,* 191–214. doi:10.1039/B618320B

74. Millange, F.; Guillou, N.; Walton, R. I.; Grenèche, J.-M.; Margiolaki, I.; Férey, G. *Chem. Commun.* **2008,** 4732–4734. doi:10.1039/b809419e

75. Eddaoudi, M.; Moler, D. B.; Li, H.; Chen, B.; Reineke, T. M.; O'Keeffe, M.; Yaghi, O. M. *Acc. Chem. Res.* **2001,** *34,* 319–330. doi:10.1021/ar000034b

76. Eddaoudi, M.; Sava, D. F.; Eubank, J. F.; Adil, K.; Guillerm, V. *Chem. Soc. Rev.* **2015,** *44,* 228–249. doi:10.1039/C4CS00230J

77. Miller, S. R.; Heurtaux, D.; Baati, T.; Horcajada, P.; Grenèche, J.-M.; Serre, C. *Chem. Commun.* **2010,** *46,* 4526–4528. doi:10.1039/c001181a

78. Li, S.; Huo, F. *Nanoscale* **2015,** *7,* 7482–7501. doi:10.1039/C5NR00518C

79. Sun, C.-Y.; Qin, C.; Wang, X.-L.; Su, Z.-M. *Expert Opin. Drug Delivery* **2013,** *10,* 89–101. doi:10.1517/17425247.2013.741583

80. Wang, S.; Wang, X. *Small* **2015,** *11,* 3097–3112. doi:10.1002/smll.201500084

81. Wuttke, S.; Braig, S.; Preiß, T.; Zimpel, A.; Sicklinger, J.; Bellomo, C.; Rädler, J. O.; Vollmar, A. M.; Bein, T. *Chem. Commun.* **2015,** *51,* 15752–15755. doi:10.1039/C5CC06767G

82. Wang, X.-G.; Dong, Z.-Y.; Cheng, H.; Wan, S.-S.; Chen, W.-H.; Zou, M.-Z.; Huo, J.-W.; Deng, H.-X.; Zhang, X.-Z. *Nanoscale* **2015,** *7,* 16061–16070. doi:10.1039/C5NR04045K

83. Férey, G.; Serre, C. *Chem. Soc. Rev.* **2009,** *38,* 1380–1399. doi:10.1039/b804302g

84. Keskin, S.; Kızılel, S. *Ind. Eng. Chem. Res.* **2011,** *50,* 1799–1812. doi:10.1021/ie101312k

85. Janiak, C.; Vieth, J. K. *New J. Chem.* **2010,** *34,* 2366–2388. doi:10.1039/c0nj00275e

86. McKinlay, A. C.; Morris, R. E.; Horcajada, P.; Férey, G.; Gref, R.; Couvreur, P.; Serre, C. *Angew. Chem., Int. Ed.* **2010,** *49,* 6260–6266. doi:10.1002/anie.201000048

87. Imaz, I.; Rubio-Martínez, M.; An, J.; Solé-Font, I.; Rosi, N. L.; Maspoch, D. *Chem. Commun.* **2011,** *47,* 7287–7302. doi:10.1039/c1cc11202c

88. Rojas, S.; Devic, T.; Horcajada, P. *J. Mater. Chem. B* **2017,** *5,* 2560–2573. doi:10.1039/C6TB03217F

89. Dietzel, P. D. C.; Blom, R.; Fjellvåg, H. *Eur. J. Inorg. Chem.* **2008,** 3624–3632. doi:10.1002/ejic.200701284

90. Chen, B.; Yang, Z.; Zhu, Y.; Xia, Y. *J. Mater. Chem. A* **2014,** *2,* 16811–16831. doi:10.1039/C4TA02984D

91. Li, R.; Ren, X.; Zhao, J.; Feng, X.; Jiang, X.; Fan, X.; Lin, Z.; Li, X.; Hu, C.; Wang, B. *J. Mater. Chem. A* **2014,** *2,* 2168–2173. doi:10.1039/C3TA14267A

92. Ren, H.; Zhang, L.; An, J.; Wang, T.; Li, L.; Si, X.; He, L.; Wu, X.; Wang, C.; Su, Z. *Chem. Commun.* **2014,** *50,* 1000–1002. doi:10.1039/C3CC47666A

93. Sun, C.-Y.; Qin, C.; Wang, X.-L.; Yang, G.-S.; Shao, K.-Z.; Lan, Y.-Z.; Su, Z.-M.; Huang, P.; Wang, C.-G.; Wang, E.-B. *Dalton Trans.* **2012,** *41,* 6906–6909. doi:10.1039/c2dt30357d

94. He, L.; Wang, T.; An, J.; Li, X.; Zhang, L.; Li, L.; Li, G.; Wu, X.; Su, Z.; Wang, C. *CrystEngComm* **2014,** *16,* 3259–3263. doi:10.1039/c3ce42506a

95. Zhuang, J.; Kuo, C.-H.; Chou, L.-Y.; Liu, D.-Y.; Weerapana, E.; Tsung, C.-K. *ACS Nano* **2014,** *8,* 2812–2819. doi:10.1021/nn406590q

96. Vasconcelos, I. B.; da Silva, T. G.; Militão, G. C. G.; Soares, T. A.; Rodrigues, N. M.; Rodrigues, M. O.; da Costa, N. B., Jr.; Freire, R. O.; Junior, S. A. *RSC Adv.* **2012,** *2,* 9437–9442. doi:10.1039/c2ra21087h

97. Paseta, L.; Potier, G.; Abbott, S.; Coronas, J. *Org. Biomol. Chem.* **2015,** *13,* 1724–1731. doi:10.1039/C4OB01898B

98. Liédana, N.; Galve, A.; Rubio, C.; Téllez, C.; Coronas, J. *ACS Appl. Mater. Interfaces* **2012,** *4,* 5016–5021. doi:10.1021/am301365h

99. Klimakow, M.; Klobes, P.; Thünemann, A. F.; Rademann, K.; Emmerling, F. *Chem. Mater.* **2010,** *22,* 5216–5221. doi:10.1021/cm1012119

100. Zhang, P.; Li, H.; Veith, G. M.; Dai, S. *Adv. Mater.* **2015,** *27,* 234–239. doi:10.1002/adma.201403299

101. Stojaković, J.; Farris, B. S.; MacGillivray, L. R. *Chem. Commun.* **2012,** *48,* 7958–7960. doi:10.1039/c2cc33227b

102. Julien, P. A.; Užarević, K.; Katsenis, A. D.; Kimber, S. A. J.; Wang, T.; Farha, O. K.; Zhang, Y.; Casaban, J.; Germann, L. S.; Etter, M.; Dinnebier, R. E.; James, S. L.; Halasz, I.; Friščić, T. *J. Am. Chem. Soc.* **2016,** *138,* 2929–2932. doi:10.1021/jacs.5b13038

103. Tireli, M.; Kulcsár, M. J.; Cindro, N.; Gracin, D.; Biliškov, N.; Borovina, M.; Ćurić, M.; Halasz, I.; Užarević, K. *Chem. Commun.* **2015,** *51,* 8058–8061. doi:10.1039/C5CC01915J

104. Desiraju, G. R. *J. Mol. Struct.* **2003,** *656,* 5–15. doi:10.1016/S0022-2860(03)00354-5

105. Novoa, J. J.; Braga, D.; Addadi, L. *Engineering of crystalline materials properties*; State of the Art in Modeling, Design and Applications. Erice International School of Crystallography, 39th crystallographic meeting at Erice; June, 7 – to June 17th, 2007.

106. Friščić, T.; Halasz, I.; Beldon, P. J.; Belenguer, A. M.; Adams, F.; Kimber, S. A. J.; Honkimäki, V.; Dinnebier, R. E. *Nat. Chem.* **2013,** *5,* 66–73. doi:10.1038/nchem.1505

107. Do, J.-L.; Friščić, T. *ACS Cent. Sci.* **2017,** *3,* 13–19. doi:10.1021/acscentsci.6b00277

108. Mottillo, C.; Friščić, T. *Molecules* **2017,** *22,* 144. doi:10.3390/molecules22010144

109. Ryder, M. R.; Tan, J.-C. *Mater. Sci. Technol.* **2014,** *30,* 1598–1612. doi:10.1179/1743284714Y.0000000550

110. André, V.; Quaresma, S. Bio-inspired Metal-Organic Frameworks in the Pharmaceutical World: a brief review. In *Metal-Organic Frameworks;* Zafar, F., Ed.; InTech: Croatia, 2016; pp 135–156. doi:10.5772/64027

111. Braga, D.; Grepioni, F.; Maini, L.; Brescello, R.; Cotarca, L. *CrystEngComm* **2008,** *10,* 469–471. doi:10.1039/b719451j

112. Jensen, A. A.; Mosbacher, J.; Elg, S.; Lingenhoehl, K.; Lohmann, T.; Johansen, T. N.; Abrahamsen, B.; Mattsson, J. P.; Lehmann, A.; Bettler, B.; Bräuner-Osborne, H. *Mol. Pharmacol.* **2002,** *61,* 1377–1384. doi:10.1124/mol.61.6.1377

113. Taylor, C. P. *Neurology* **1994,** *44,* S10–S13. doi:10.1212/WNL.44.12_Suppl_10.S10

114. Taylor, C. P.; Gee, N. S.; Su, T.-Z.; Kocsis, J. D.; Welty, D. F.; Brown, J. P.; Dooley, D. J.; Boden, P.; Singh, L. *Epilepsy Res.* **1998,** *29,* 233–249. doi:10.1016/S0920-1211(97)00084-3

115. Santi, C. M.; Cayabyab, F. S.; Sutton, K. G.; McRory, J. E.; Mezeyova, J.; Hamming, K. S.; Parker, D.; Stea, A.; Snutch, T. P. *J. Neurosci.* **2002,** *22,* 396–403.

116. Errington, A. C.; Stohr, T.; Lees, G. *Curr. Top. Med. Chem.* **2005,** *5,* 15–30. doi:10.2174/1568026053386872

117. Ettinger, A. B.; Argoff, C. E. *Neurotherapeutics* **2007,** *4,* 75–83. doi:10.1016/j.nurt.2006.10.003

118. Kato, A. S.; Bredt, D. S. *Curr. Opin. Drug Discovery Dev.* **2007,** *10,* 565–572.

119. Eisenberg, E.; River, Y.; Shifrin, A.; Krivoy, N. *Drugs* **2007,** *67,* 1265–1289. doi:10.2165/00003495-200767090-00003

120. Ananda, K.; Aravinda, S.; Vasudev, P. G.; Raja, K. M. P.; Sivaramakrishnan, H.; Nagarajan, K.; Shamala, N.; Balaram, P. *Curr. Sci.* **2003,** *85,* 1002–1011.

121. Besag, F. M. C.; Berry, D. *Drug Saf.* **2006,** *29,* 95–118. doi:10.2165/00002018-200629020-00001

122. Thompson, R. B. *Curr. Opin. Chem. Biol.* **2005,** *9,* 526–532. doi:10.1016/j.cbpa.2005.08.020

123. Henkel, G.; Krebs, B. *Chem. Rev.* **2004,** *104,* 801–824. doi:10.1021/cr020620d

124. Quaresma, S.; André, V.; Antunes, A. M. M.; Cunha-Silva, L.; Duarte, M. T. *Cryst. Growth Des.* **2013,** *13,* 5007–5017. doi:10.1021/cg401187x

125. O'Donnell, L. J.; Arvind, A. S.; Hoang, P.; Cameron, D.; Talbot, I. C.; Jewell, D. P.; Lennard-Jones, J. E.; Farthing, M. J. *Gut* **1992,** *33,* 947–949. doi:10.1136/gut.33.7.947

126. Schreiber, S.; Howaldt, S.; Raedler, A. *Gut* **1994,** *35,* 1081–1085. doi:10.1136/gut.35.8.1081

127. Bailey, M. A.; Ingram, M. J.; Naughton, D. P.; Rutt, K. J.; Dodd, H. T. *Transition Met. Chem.* **2008,** *33,* 195–202. doi:10.1007/s11243-007-9031-1

128. Braga, D.; Grepioni, F.; André, V.; Duarte, M. T. *CrystEngComm* **2009,** *11,* 2618–2621. doi:10.1039/b913433f

129. Byrn, S. R.; Xu, W.; Newman, A. W. *Adv. Drug Delivery Rev.* **2001,** *48,* 115–136. doi:10.1016/S0169-409X(01)00102-8

130. Chow, E. H. H.; Strobridge, F. C.; Friščić, T. *Chem. Commun.* **2010,** *46,* 6368–6370. doi:10.1039/c0cc01337d

131. Yuan, W.; Garay, A. L.; Pichon, A.; Clowes, R.; Wood, C. D.; Cooper, A. I.; James, S. L. *CrystEngComm* **2010,** *12,* 4063–4065. doi:10.1039/c0ce00486c

132. Chui, S. S.-Y.; Lo, S. M.-F.; Charmant, J. P. H.; Orpen, A. G.; Williams, I. D. *Science* **1999,** *283,* 1148–1150. doi:10.1126/science.283.5405.1148

133. Boës, A.-K.; Xiao, B.; Megson, I. L.; Morris, R. E. *Top. Catal.* **2009,** *52,* 35–41. doi:10.1007/s11244-008-9137-5

134. Hinks, N. J.; McKinlay, A. C.; Xiao, B.; Wheatley, P. S.; Morris, R. E. *Microporous Mesoporous Mater.* **2010,** *129,* 330–334. doi:10.1016/j.micromeso.2009.04.031

135. Chiericatti, C.; Basilico, J. C.; Basilico, M. L. Z.; Zamaro, J. M. *Microporous Mesoporous Mater.* **2012,** *162,* 60–63. doi:10.1016/j.micromeso.2012.06.012

136. Friščić, T.; Fábián, L. *CrystEngComm* **2009,** *11,* 743–745. doi:10.1039/b822934c

137. Strobridge, F. C.; Judaš, N.; Friščić, T. *CrystEngComm* **2010,** *12,* 2409–2418. doi:10.1039/c003521a

138. Friščić, T.; Halasz, I.; Štrukil, V.; Eckert-Maksić, M.; Dinnebier, R. E. *Croat. Chem. Acta* **2012,** *85,* 367–378. doi:10.5562/cca2014

139. Prochowicz, D.; Sokołowski, K.; Justyniak, I.; Kornowicz, A.; Fairen-Jimenez, D.; Friščić, T.; Lewiński, J. *Chem. Commun.* **2015,** *51,* 4032–4035. doi:10.1039/C4CC09917F

140. Leng, K.; Sun, Y.; Li, X.; Sun, S.; Xu, W. *Cryst. Growth Des.* **2016,** *16,* 1168–1171. doi:10.1021/acs.cgd.5b01696

141. Babarao, R.; Jiang, J. *J. Phys. Chem. C* **2009,** *113,* 18287–18291. doi:10.1021/jp906429s

142. Zheng, H.; Zhang, Y.; Liu, L.; Wan, W.; Guo, P.; Nystrom, A. M.; Zou, X. *J. Am. Chem. Soc.* **2016,** *138,* 962–968. doi:10.1021/jacs.5b11720

143. Engin, K.; Leeper, D. B.; Cater, J. R.; Thistlethwaite, A. J.; Tupchong, L.; McFarlane, J. D. *Int. J. Hyperthermia* **1995,** *11,* 211–216. doi:10.3109/02656739509022457

144. Stubbs, M.; McSheehy, P. M. J.; Griffiths, J. R.; Bashford, C. L. *Mol. Med. Today* **2000,** *6,* 15–19. doi:10.1016/S1357-4310(99)01615-9

145. Katsenis, A. D.; Puškarić, A.; Štrukil, V.; Mottillo, C.; Julien, P. A.; Užarević, K.; Pham, M.-H.; Do, T.-O.; Kimber, S. A. J.; Lazić, P.; Magdysyuk, O.; Dinnebier, R. E.; Halasz, I.; Friščić, T. *Nat. Commun.* **2015,** *6,* 6662. doi:10.1038/ncomms7662

146. Ge, R.; Sun, H. *Acc. Chem. Res.* **2007,** *40,* 267–274. doi:10.1021/ar600001b

147. Briand, G. G.; Burford, N. *Chem. Rev.* **1999,** *99,* 2601–2658. doi:10.1021/cr980425s

148. Andrews, P. C.; Deacon, G. B.; Forsyth, C. M.; Junk, P. C.; Kumar, I.; Maguire, M. *Angew. Chem., Int. Ed.* **2006,** *45,* 5638–5642. doi:10.1002/anie.200600469

149. André, V.; Gomes, C. B. G.; Duarte, M. T. Mechanochemistry: a tool in the synthesis of catalysts, metallodrugs and metallophamaceuticals. In *Advances in Organometallic Chemistry and Catalysis: The Silver/Gold Jubilee International Conference on Organometallic Chemistry Celebratory Book;* Pombeiro, A. J. L., Ed.; John Wiley & Sons, 2014; pp 493–500.

Palladium-catalyzed *ortho*-halogenations of acetanilides with *N*-halosuccinimides via direct sp^2 C–H bond activation in ball mills

Zi Liu[1], Hui Xu[1] and Guan-Wu Wang[*1,2]

Abstract

A solvent-free palladium-catalyzed *ortho*-iodination of acetanilides using *N*-iodosuccinimide as the iodine source has been developed under ball-milling conditions. This present method avoids the use of hazardous organic solvents, high reaction temperature, and long reaction time and provides a highly efficient methodology to realize the regioselective functionalization of acetanilides in yields up to 94% in a ball mill. Furthermore, the current methodology can be extended to the synthesis of *ortho*-brominated and *ortho*-chlorinated products in good yields by using the corresponding *N*-halosuccinimides.

Introduction

Aryl halides have been widely utilized in organic syntheses, which give access to a range of complex natural products [1,2]. However, traditional halogenations of aromatic compounds by direct electrophilic halogenation [3] and Sandmeyer reaction [4] have several drawbacks such as low regioselectivities, complicated reaction procedures and even a risk of danger. Thus, it is necessary to discover new approaches to the regioselective construction of C–X bonds. With the development of transition-metal-catalyzed cross-coupling reactions, a series of halogenations at the *ortho*-position of the directing groups have been disclosed [5-18]. Nevertheless, from the viewpoint of green chemistry, the reduction or even elimination of organic solvents, shorter reaction times, simplification of work-up procedures and improvement of product yields are highly demanding. In recent years, the application of mechanochemical techniques in organic syntheses has attracted increasing attention [19-28].
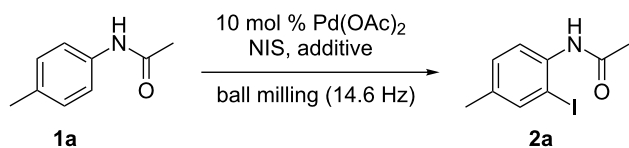
A few mechanochemical *ortho*-C–H bond activation reactions under the catalysis of rhodium and palladium salts have been reported [29-38]. Hernández and Bolm reported the rhodium-catalyzed bromination and iodination of 2-phenylpyridine using *N*-bromosuccinimide (NBS) and *N*-iodosuccinimide (NIS), respectively, as the halogen source [30]. However, the mechanochemical *ortho*-halogenation using the cheaper palladium catalysts has not been reported yet. In continuing our interest in mechanochemistry [21,22,39-41] and C–H activation reactions [42-44], we have independently investigated the solvent-free *ortho*-iodination of acetanilides under ball-milling conditions [45]. In addition, the current reaction can be extended to *ortho*-bromination and *ortho*-chlorination by using the corresponding *N*-halosuccinimides. Herein, we report these regioselective *ortho*-halogenations in detail.

Results and Discussion

To begin our study, *N*-(*p*-tolyl)acetamide (**1a**) was chosen as the model substrate to react with NIS using Pd(OAc)$_2$ as the catalyst to optimize reaction parameters such as additive, reaction time and reagent ratio. The reaction of **1a** (0.4 mmol) with NIS (0.4 mmol) was initially performed under the catalysis of Pd(OAc)$_2$ (10 mol %) in a Spex SamplePrep 8000 mixer mill at a frequency of 875 cycles per minute at room temperature for

3 h. Unfortunately, the desired iodinated product was not detected (Table 1, entry 1). Then, various acids were examined because the addition of acids into the reaction system could promote the C–H bond halogenation according to the previous literature [46]. As desired, compound **2a** was isolated in 87% yield when *p*-toluenesulfonic acid (PTSA) was employed (Table 1, entry 2). A control experiment was conducted for the reaction of **1a** with NIS in the absence of Pd(OAc)$_2$, yet still with PTSA as the promoter, and no iodinated product was furnished (Table 1, entry 3). The use of D-camphorsulfonic acid (D-CSA) or mesitylenesulfonic acid dihydrate provided inferior results than that obtained in the presence of PTSA (Table 1, entries 4 and 5 vs entry 2). Furthermore, no desired product was obtained when pyridine-2-sulfonic acid, 2-nitrobenzoic acid, 2-aminoethanesulfonic acid or tungstophosphoric acid hydrate (HPA) was used in the reaction (Table 1, entries 6–9). Thus, the combination of Pd(OAc)$_2$ with PTSA was essential for the reaction to take place effectively. Subsequently, the ratio of substrates was investigated, and the results demonstrated that the amount of both NIS and PTSA affected the product yield. Decreasing or increasing the amount of PTSA was not beneficial to the reaction (Table 1, entries 10 and 11). When the amount of NIS was increased from 1.0 equiv to 1.5 equiv and 2.0 equiv, the yield of the iodinated product did not further go up (Table 1,

Table 1: Optimization of the reaction conditions.[a]

entry	ratio of reagents[b]	additive	time (h)	yield[c] (%)
1	1:0.1:1:0	–	3 h	N.R.
2	**1:0.1:1:2**	**PTSA**	**3 h**	**87**
3	1:0:1:2	PTSA	3 h	N.R.
4	1:0.1:1:2	D-CSA	3 h	62
5	1:0.1:1:2	mesitylenesulfonic acid dihydrate	3 h	56
6	1:0.1:1:2	pyridine-2-sulfonic acid	3 h	N.R.
7	1:0.1:1:2	2-nitrobenzoic acid	3 h	N.R.
8	1:0.1:1:2	2-aminoethanesulfonic acid	3 h	N.R.
9	1:0.1:1:2	HPA	3 h	N.R.
10	1:0.1:1:1.5	PTSA	3 h	81
11	1:0.1:1:2.5	PTSA	3 h	86
12	1:0.1:1.5:2	PTSA	3 h	88
13	1:0.1:2:2	PTSA	3 h	86
14	1:0.1:1:2	PTSA	2 h	80
15	1:0.1:1:2	PTSA	4 h	87

[a]Unless otherwise specified, all the reactions were carried out in a Spex SamplePrep 8000 mixer mill using **1a** (0.4 mmol). [b]The reagent ratio referred to **1a**:Pd(OAc)$_2$:NIS:additive. [c]Isolated yield. N.R. = no reaction.

entries 12 and 13). The iodination was slightly less efficient for a shorter time of 2 h (Table 1, entry 14), and prolongation of the reaction time from 3 h to 4 h did not lead to a superior result (Table 1, entry 15).

To demonstrate the generality of this protocol, the regioselective iodination of a series of acetanilides was then examined in the presence of Pd(OAc)$_2$ and PTSA under the ball-milling conditions (Table 2). Gratifyingly, the *ortho*-iodinated acetanilides were obtained in moderate to good isolated yields. Both *p*-Me and *m*-Me-substituted acetanilides provided products **2a** and **2b** in excellent yields of 87% and 80%, respectively (Table 2, entries 1 and 2). As expected, 3,4-dimethylacetanilide underwent iodination successfully at the less sterically hindered *ortho*-position and gave product **2c** in 85% yield (Table 2, entry 3). The unsubstituted acetanilide provided the desired product **2d** in 77% yield (Table 2, entry 4). It is worth mentioning that the presence of a potentially reactive group, such as fluoro, chloro, and bromo substituents in the
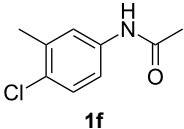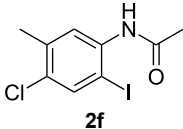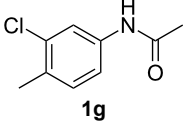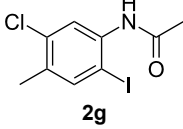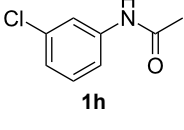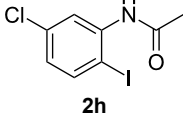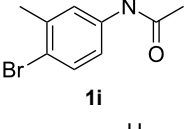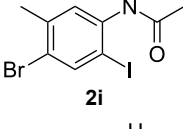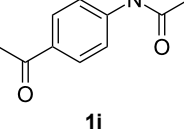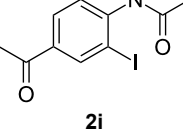
acetanilides was tolerable, and products **2e–i** were isolated in 51–94% yields (Table 2, entries 5–9), highlighting the functional group compatibility of the current protocol. The presence of an acetyl group at the *para*-position of the phenyl ring of acetanilide **1j** decreased the yield of the corresponding product **2j** to 11% (Table 2, entry 10). Unfortunately, substrates bearing a strong electron-donating methoxy group and a strong electron-withdrawing nitro group could not afford any desired products, and the reason is not quite clear right now.

In an aim to investigate the influence of the milling frequency, the model reaction of **1a** with NIS was conducted by employing different types of mixer mills with different milling frequencies. *Ortho*-iodized acetanilide **2a** was furnished in 90% yield after milling for 2 h by using a Retsch MM 200 mixer mill (30 Hz, Scheme 1a). At a milling frequency of 50 Hz in a Spex SamplePrep 5100 mixer mill, the iodination was accomplished within 1.5 h to afford the corresponding product **2a** in 92% yield (Scheme 1b). According to the above experimental results,

Table 2: Substrate scope.[a]

entry	substrate **1**	product **2**[b]	yield[c] (%)
1	**1a**	**2a**	87
2	**1b**	**2b**	80
3	**1c**	**2c**	85
4	**1d**	**2d**	77
5	**1e**	**2e**	94

Table 2: Substrate scope.[a] (continued)

6	**1f**	**2f**	71
7	**1g**	**2g**	74
8	**1h**	**2h**	51
9	**1i**	**2i**	70
10	**1j**	**2j**	11

[a]All the reactions were carried out in a Spex SamplePrep 8000 mixer mill using **1** (0.4 mmol), NIS (0.4 mmol), Pd(OAc)$_2$ (10 mol %) and PTSA (0.8 mmol) for 3 h. [b]Properly characterized by ^{1}H NMR, ^{13}C NMR, and HRMS spectral data. [c]Isolated yield.

it could be concluded that the higher milling frequency had a beneficial effect on the reaction efficiency in terms of product yield and reaction time.

Scheme 1: The influence of the milling frequency on the reaction of **1a** with NIS.

To illustrate the superiority of the ball-milling technique, the reaction was also investigated in an organic solvent. The reaction of **1a** with NIS conducted in toluene at room temperature

for 3 h provided the desired product **2a** in only 49% yield, which was inferior to those obtained by our mechanochemical approaches (Scheme 2).
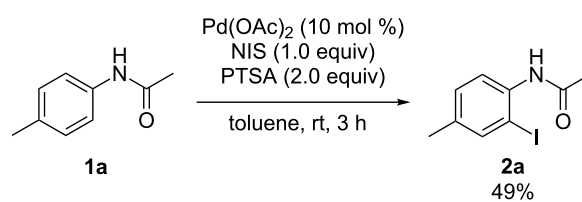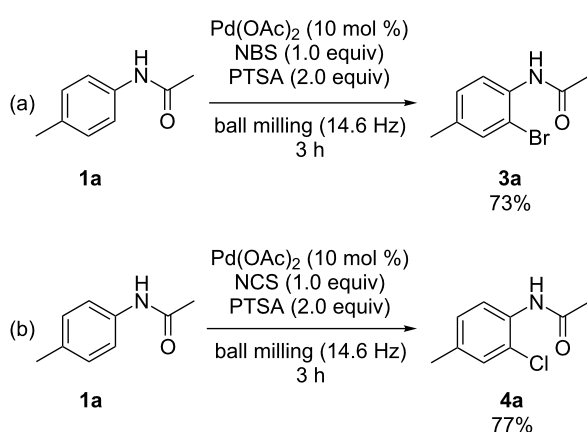

Scheme 2: Palladium-catalyzed *ortho*-iodination of **1a** in toluene.

The plausible mechanism is proposed and depicted in Scheme 3. The addition of PTSA was essential for the present reaction. It is believed the more active Pd(OTs)$_2$ is formed in situ from Pd(OAc)$_2$ and TsOH [46,47]. The formed Pd(OTs)$_2$ inserts into the *ortho* C–H bond of the anilides after coordination to the oxygen atom of the amide moiety, affording the species **A**. Oxidative addition of the species **A** with NIS generates the Pd(IV) complex **B**. Finally, the iodinated product is provided by reductive elimination along with regeneration of Pd(OTs)$_2$ in the presence of TsOH.
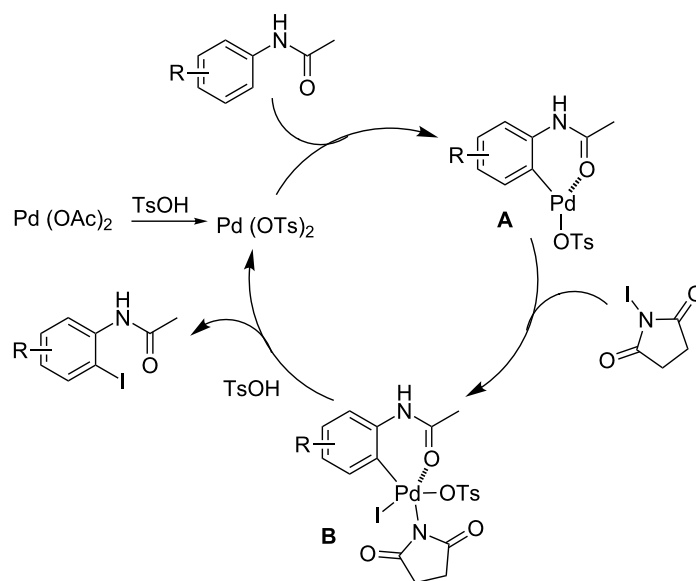
Scheme 3: Plausible mechanism.

It was intriguing to find that *N*-bromosuccinimide (NBS) and *N*-chlorosuccinimide (NCS) could also be used as reaction partners to react with the representative acetanilide **1a** under identical ball-milling conditions. The corresponding *ortho*-brominated and *ortho*-chlorinated products **3a** and **4a** were obtained in 73% and 77% yields, respectively (Scheme 4).

Scheme 4: Palladium-catalyzed *ortho*-bromination and chlorination of **1a** in a ball mill.

Conclusion

In summary, we have developed a solvent-free and efficient protocol to synthesize *ortho*-iodinated acetanilide derivatives with Pd(OAc)$_2$ as the catalyst and *N*-iodosuccinimide as the halogen source under mechanical milling conditions. This protocol shows its advantages in terms of high regioselectivity,

simple operation and environmentally friendliness. In addition, the present protocol can be extended to the synthesis of *ortho*-brominated and chlorinated acetanilides delivering good yields by using the corresponding *N*-halosuccinimides.

Supporting Information

Supporting Information File 1
Experimental, analytical data and NMR spectra of **2a–j**, **3a** and **4a**.
[https://www.beilstein-journals.org/bjoc/content/supplementary/1860-5397-14-31-S1.pdf]

Acknowledgements

ORCID® iDs

Guan-Wu Wang - https://orcid.org/0000-0001-9287-532X

References

1. Evans, D. A.; Katz, J. L.; Peterson, G. S.; Hintermann, T. *J. Am. Chem. Soc.* **2001,** *123,* 12411–12413. doi:10.1021/ja011943e
2. Pelletier, J. C.; Youssefyeh, R. D.; Campbell, H. F. Substituted Saturated and Unsaturated Indole Quinoline and Benzazepine Carboxamides and Their Use as Pharmacological Agents. U.S. Patent 4920219 A, April 24, 1990.
3. de la Mare, P. B. D., Ed. *Electrophilic Halogenation;* Cambridge University Press: New York, 1976.

4. Hodgson, H. H. *Chem. Rev.* **1947,** *40,* 251–277. doi:10.1021/cr60126a003

5. Kalyani, D.; Dick, A. R.; Anani, W. Q.; Sanford, M. S. *Org. Lett.* **2006,** *8,* 2523–2526. doi:10.1021/ol060747f

6. Bedford, R. B.; Haddow, M. F.; Mitchell, C. J.; Webster, R. L. *Angew. Chem., Int. Ed.* **2011,** *50,* 5524–5527. doi:10.1002/anie.201101606

7. Dubost, E.; Fossey, C.; Cailly, T.; Rault, S.; Fabis, F. *J. Org. Chem.* **2011,** *76,* 6414–6420. doi:10.1021/jo200853j

8. Schröder, N.; Wencel-Delord, J.; Glorius, F. *J. Am. Chem. Soc.* **2012,** *134,* 8298–8301. doi:10.1021/ja302631j

9. John, A.; Nicholas, K. M. *J. Org. Chem.* **2012,** *77,* 5600–5605. doi:10.1021/jo300713h

10. Ma, X.-T.; Tian, S.-K. *Adv. Synth. Catal.* **2013,** *355,* 337–340. doi:10.1002/adsc.201200902

11. Zhao, X.; Dimitrijević, E.; Dong, V. M. *J. Am. Chem. Soc.* **2009,** *131,* 3466–3467. doi:10.1021/ja900200g

12. Wang, W.; Pan, C.; Chen, F.; Cheng, J. *Chem. Commun.* **2011,** *47,* 3978–3980. doi:10.1039/c0cc05557c

13. Mei, T.-S.; Giri, R.; Maugel, N.; Yu, J.-Q. *Angew. Chem., Int. Ed.* **2008,** *47,* 5215–5219. doi:10.1002/anie.200705613

14. Mei, T.-S.; Wang, D.-H.; Yu, J.-Q. *Org. Lett.* **2010,** *12,* 3140–3143. doi:10.1021/ol1010483

15. Li, J.-J.; Mei, T.-S.; Yu, J.-Q. *Angew. Chem., Int. Ed.* **2008,** *47,* 6452–6455. doi:10.1002/anie.200802187

16. Wan, X.; Ma, Z.; Li, B.; Zhang, K.; Cao, S.; Zhang, S.; Shi, Z. *J. Am. Chem. Soc.* **2006,** *128,* 7416–7417. doi:10.1021/ja060232j

17. Bedford, R. B.; Engelhart, J. U.; Haddow, M. F.; Mitchell, C. J.; Webster, R. L. *Dalton Trans.* **2010,** *39,* 10464–10472. doi:10.1039/c0dt00385a

18. Song, B.; Zheng, X.; Mo, J.; Xu, B. *Adv. Synth. Catal.* **2010,** *352,* 329–335. doi:10.1002/adsc.200900778

19. Stolle, A.; Szuppa, T.; Leonhardt, S. E. S.; Ondruschka, B. *Chem. Soc. Rev.* **2011,** *40,* 2317–2329. doi:10.1039/c0cs00195c

20. James, S. L.; Adams, C. J.; Bolm, C.; Braga, D.; Collier, P.; Friščić, T.; Grepioni, F.; Harris, K. D. M.; Hyett, G.; Jones, W.; Krebs, A.; Mack, J.; Maini, L.; Orpen, A. G.; Parkin, I. P.; Shearouse, W. C.; Steed, J. W.; Waddell, D. C. *Chem. Soc. Rev.* **2012,** *41,* 413–447. doi:10.1039/C1CS15171A

21. Zhu, S.-E.; Li, F.; Wang, G.-W. *Chem. Soc. Rev.* **2013,** *42,* 7535–7570. doi:10.1039/c3cs35494f

22. Wang, G.-W. *Chem. Soc. Rev.* **2013,** *42,* 7668–7700. doi:10.1039/c3cs35526h

23. Do, J.-L.; Friščić, T. *ACS Cent. Sci.* **2017,** *3,* 13–19. doi:10.1021/acscentsci.6b00277

24. Hernández, J. G.; Bolm, C. *J. Org. Chem.* **2017,** *82,* 4007–4019. doi:10.1021/acs.joc.6b02887

25. Achar, T. K.; Bose, A.; Mal, P. *Beilstein J. Org. Chem.* **2017,** *13,* 1907–1931. doi:10.3762/bjoc.13.186

26. Hernández, J. G. *Chem. – Eur. J.* **2017,** *23,* in press. doi:10.1002/chem.201786861

27. Bose, A.; Mal, P. *Tetrahedron Lett.* **2014,** *55,* 2154–2156. doi:10.1016/j.tetlet.2014.02.064

28. Maiti, S.; Mal, P. *Synth. Commun.* **2014,** *44,* 3461–3469. doi:10.1080/00397911.2014.946995

29. Juribašić, M.; Užarević, K.; Gracin, D.; Ćurić, M. *Chem. Commun.* **2014,** *50,* 10287–10290. doi:10.1039/C4CC04423A

30. Hernández, J. G.; Bolm, C. *Chem. Commun.* **2015,** *51,* 12582–12584. doi:10.1039/C5CC04423E

31. Hermann, G. N.; Becker, P.; Bolm, C. *Angew. Chem., Int. Ed.* **2015,** *54,* 7414–7417. doi:10.1002/anie.201502536

32. Hermann, G. N.; Becker, P.; Bolm, C. *Angew. Chem., Int. Ed.* **2016,** *55,* 3781–3784. doi:10.1002/anie.201511689

33. Lou, S.-J.; Mao, Y.-J.; Xu, D.-Q.; He, J.-Q.; Chen, Q.; Xu, Z.-Y. *ACS Catal.* **2016,** *6,* 3890–3894. doi:10.1021/acscatal.6b00861

34. Hermann, G. N.; Bolm, C. *ACS Catal.* **2017,** *7,* 4592–4596. doi:10.1021/acscatal.7b00582

35. Hermann, G. N.; Jung, C. L.; Bolm, C. *Green Chem.* **2017,** *19,* 2520–2523. doi:10.1039/C7GC00499K

36. Jia, K.-Y.; Yu, J.-B.; Jiang, Z.-J.; Su, W.-K. *J. Org. Chem.* **2016,** *81,* 6049–6055. doi:10.1021/acs.joc.6b01138

37. Jiang, X.; Chen, J.; Zhu, W.; Cheng, K.; Liu, Y.; Su, W.-K.; Yu, C. *J. Org. Chem.* **2017,** *82,* 10665–10672. doi:10.1021/acs.joc.7b01695

38. Cheng, H.; Hernández, J. G.; Bolm, C. *Org. Lett.* **2017,** *19,* 6284–6287. doi:10.1021/acs.orglett.7b02973

39. Li, L.; Wang, J.-J.; Wang, G.-W. *J. Org. Chem.* **2016,** *81,* 5433–5439. doi:10.1021/acs.joc.6b00786

40. Li, H.-G.; Wang, G.-W. *J. Org. Chem.* **2017,** *82,* 6341–6348. doi:10.1021/acs.joc.7b00912

41. Xu, H.; Liu, H.-W.; Lin, H.-S.; Wang, G.-W. *Chem. Commun.* **2017,** *53,* 12477–12480. doi:10.1039/C7CC08306H

42. Wang, G.-W. *Top. Organomet. Chem.* **2016,** *55,* 119–136. doi:10.1007/3418_2015_128

43. Wang, G.-W.; Yuan, T.-T.; Li, D.-D. *Angew. Chem., Int. Ed.* **2011,** *50,* 1380–1383. doi:10.1002/anie.201005874

44. Li, Z.-Y.; Li, L.; Li, Q.-L.; Jing, K.; Xu, H.; Wang, G.-W. *Chem. – Eur. J.* **2017,** *23,* 3285–3290. doi:10.1002/chem.201700354

45. Liu, Z., *Two Organic Reactions under Mechanochemical Conditions,* Master thesis, University of Science and Technology of China, 2013.

46. Zhu, B.; Wang, G.-W. *Org. Lett.* **2009,** *11,* 4334–4337 and references cited therein. doi:10.1021/ol901675t

47. Boele, M. D. K.; van Strijdonck, G. P. F.; de Vries, A. H. M.; Kamer, P. C. J.; de Vries, J. G.; van Leeuwen, P. W. N. M. *J. Am. Chem. Soc.* **2002,** *124,* 1586–1587. doi:10.1021/ja0176907

License and Terms

Liquid-assisted grinding and ion pairing regulates percentage conversion and diastereoselectivity of the Wittig reaction under mechanochemical conditions

Kendra Leahy Denlinger, Lianna Ortiz-Trankina, Preston Carr, Kingsley Benson, Daniel C. Waddell and James Mack[*]

Abstract

Mechanochemistry is maturing as a discipline and continuing to grow, so it is important to continue understanding the rules governing the system. In a mechanochemical reaction, the reactants are added into a vessel along with one or more grinding balls and the vessel is shaken at high speeds to facilitate a chemical reaction. The dielectric constant of the solvent used in liquid-assisted grinding (LAG) and properly chosen counter-ion pairing increases the percentage conversion of stilbenes in a mechanochemical Wittig reaction. Utilizing stepwise addition/evaporation of ethanol in liquid-assisted grinding also allows for the tuning of the diastereoselectivity in the Wittig reaction.

Introduction

Mechanochemistry is maturing as a discipline and continuing to develop and grow [1-16]. Thus it is important to continue studying and understanding the rules governing the system. Under mechanochemical conditions, the reactants are added into a vessel along with one or more grinding balls, and the vessel is shaken at high speeds to generate the product. Several years ago, Balema and Percharsky first demonstrated the success of the Wittig reaction under mechanochemical conditions [17,18]. The Wittig reaction is one of the most useful reactions for the synthesis of olefins [19-23]. Aside from its synthetic utility, its unique reaction mechanism (shown in Figure 1) and inherent diastereoselectivity has led to a vast amount of intrigue by the chemical community [24-26].

Our research group has continued the study of the Wittig reaction under mechanochemical conditions with the use of a functionalized polymer resin. During these studies, we discovered a few exciting differences between our results and the ones ob-
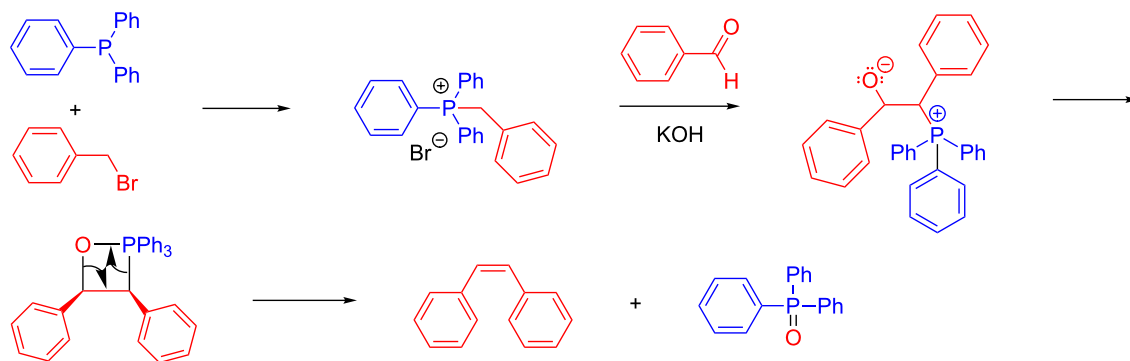
Figure 1: Solution-based Wittig reaction mechanism.

tained under traditional solution-based conditions. First, we observed that using functionalized resins allowed us to isolate the desired product in an easy and environmentally benign manner. Second, we observed that the incorporation of liquid-assisted grinding (LAG) increased the rate of the reaction in comparison to completely solvent-free conditions. Finally, we observed that there was an effect of the dielectric constant of the solvent used in LAG on the stereochemistry of the product [27]. Although previously we were able to generate high yields of Wittig products under liquid-assisted grinding conditions, we did not truly understand the influence of the reaction medium on the reaction. Therefore, we were interested in better understanding these observations, with the goal of increasing the overall conversion and having better control over the stereoselectivity of the product.

Results and Discussion
Liquid-assisted grinding
To focus the study, benzaldehyde, benzyl bromide, polymer-supported triphenylphosphine (PS-C$_6$H$_4$-PPh$_2$) and potassium

carbonate were ball-milled in a stainless steel vial with two LAG solvents at opposite ends of the dielectric spectrum, as well as a control without any solvent (Table 1).

In general, we noticed that more polar solvents (high dielectric constants) favour *Z* selectivity and a higher overall conversion, whereas the use of less polar or no solvent (lower dielectric constants) favour *E* selectivity and a lower overall conversion.

As shown in Table 1, a side product (benzyl benzoate) is also generated during the reaction. ^{1}H NMR spectroscopy was used to determine the *E*:*Z* ratio of the product as well as the percentage of the side product formation. Figure 2 shows the particular peaks for each compound integrated to determine product ratios.

It is important to note that under traditional solution-based conditions, benzyl benzoate has never been reported as a product in the Wittig reaction. Under mechanochemical conditions, the side-product formation appears to be hindered when

Table 1: LAG solvent effect on the mechanochemical Wittig reaction.

LAG solvent	dielectric constant [17]	% conversion to stilbene	*E*:*Z* ratio	stilbene/side product ratio
none	–	30	67:33	1/0.83
toluene	2.38	25	61:39	1/0.44
ethanol	24.5	95	40:60	1/0.03
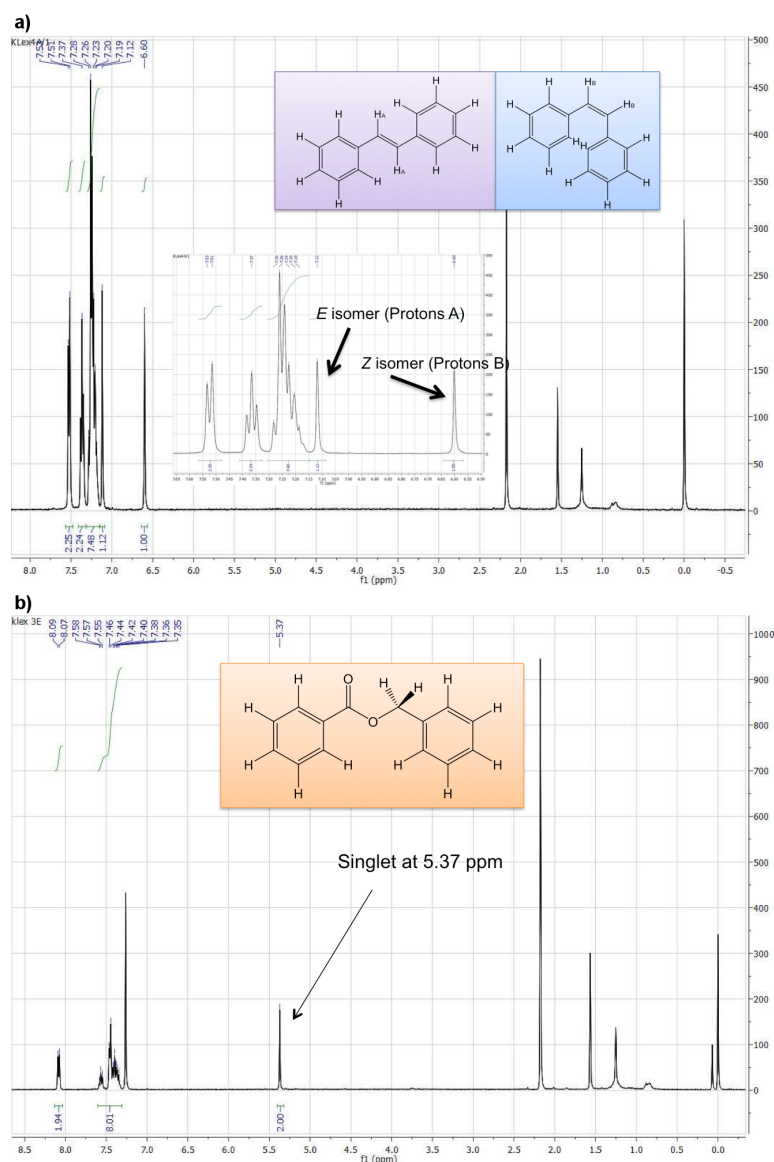
Figure 2: ^{1}H NMR spectra of stilbene mixture (a) and benzyl benzoate (b).

utilizing a LAG solvent with a high dielectric constant. These results were used to probe the ability to tune the Wittig reaction under mechanochemical conditions.

To determine the origin of benzyl benzoate, we performed a number of control reactions to determine if all reactants are necessary to form the side product (Table 2). Benzyl bromide was absent in each control reaction, and a "√" in the table indicates reactants that were present in each control trial.

Interestingly, it was found that all four components of the reaction (benzyl bromide, benzaldehyde, base, and PS-C$_6$H$_4$-PPh$_2$) are necessary for the production of benzyl benzoate. Based on this evidence, we propose a mechanism for the formation of this
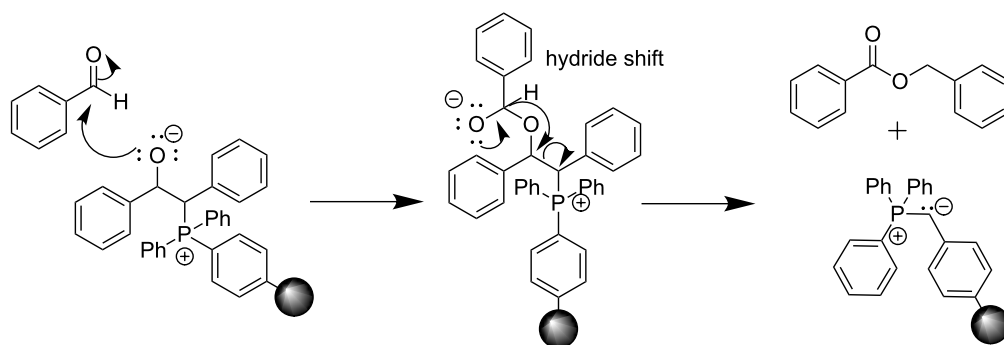
side product, which involves the addition of benzaldehyde to the traditional betaine intermediate of the Wittig reaction. This addition step occurs before the rotation and formation of the oxaphosphetane (Scheme 1). In the presence of very small amounts of solvent (LAG) or no solvent at all, the concentration of reactants is very high. This could cause the additional benzaldehyde to be close enough to the intermediate to react before the rotation occurs. To bolster further this argument, the highest amount of side product is observed in the absence of solvent, i.e., at highest reactant concentration (Table 1).

Further, our results show that the *E* selectivity and benzyl benzoate formation are observed together (when the dielectric constant of the LAG solvent is low). Therefore, if the benzyl

Table 2: Control reactions to determine the origin of the side product benzyl benzoate.

| control trial	benzaldehyde	K_2CO_3	PS-C$_6$H$_4$-PPh$_2$	result
1	√			No reaction
2	√	√		No reaction
3	√		√	No reaction
4	√	√	√	No reaction

**Scheme 1:** Possible mechanism of benzyl benzoate formation.

benzoate formation follows the path presented in Scheme 1, perhaps the mechanism of the *E* selectivity is similar. The intermediate (Scheme 1) allows for a reaction pathway involving the formation of a six-membered ring instead of the traditional four-membered oxaphosphetane ring of the Wittig reaction. This six-membered ring may account for the higher *E* selectivity due to the preference for larger groups to be in equatorial positions in cyclohexane rings (Scheme 2).

The *E* selectivity is driven by both the high concentrations of reactants and a low dielectric constant of the LAG solvent (or no solvent). To evaluate which might be playing a more critical role in the selectivity, the reaction was run with an excess of

benzaldehyde (Scheme 3) to increase the concentration of reactants. At the same time, benzaldehyde can be considered a LAG solvent with a high dielectric constant (benzaldehyde has a dielectric constant of 17.8 [28]). The increased concentration should favour *E* selectivity, but the high dielectric constant should favour *Z* selectivity.

Compared to the original reaction (*E:Z* ratio 67:33, Table 1, entry 1), the reaction with excess benzaldehyde resulted in an increase in *Z* selectivity with an *E:Z* ratio of 52:48. Therefore, it can be concluded that, if a LAG solvent is present, its dielectric constant will be the determining factor in diastereoselectivity, consistent with our previous observations.
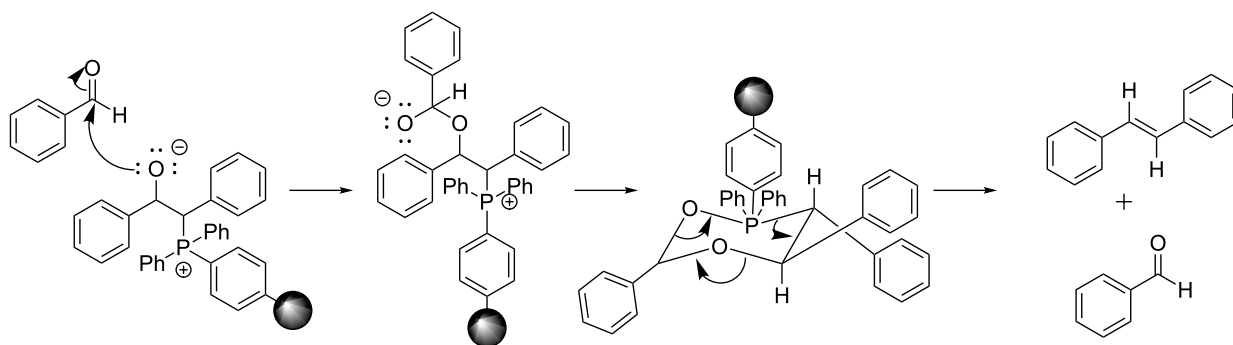
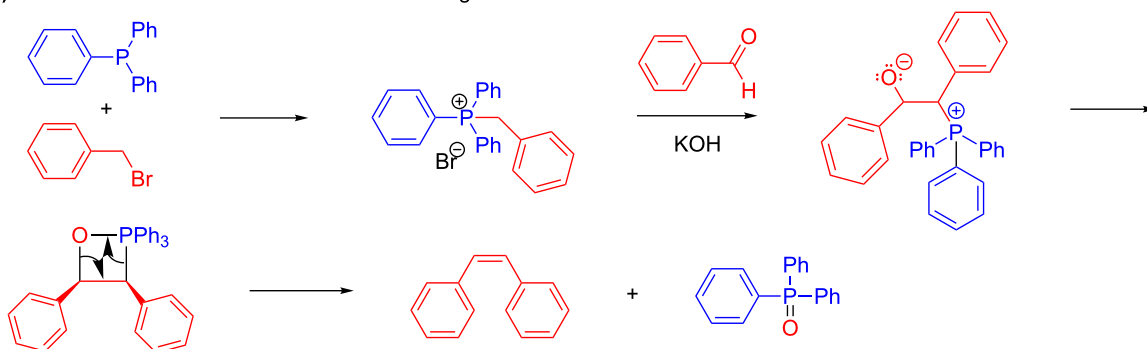**Scheme 2:** A possible mechanistic explanation for the *E* selectivity.
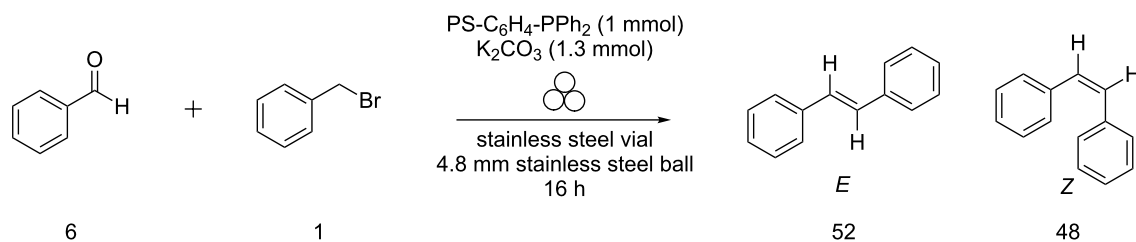
Scheme 3: Ball-milled Wittig reaction using excess benzaldehyde.
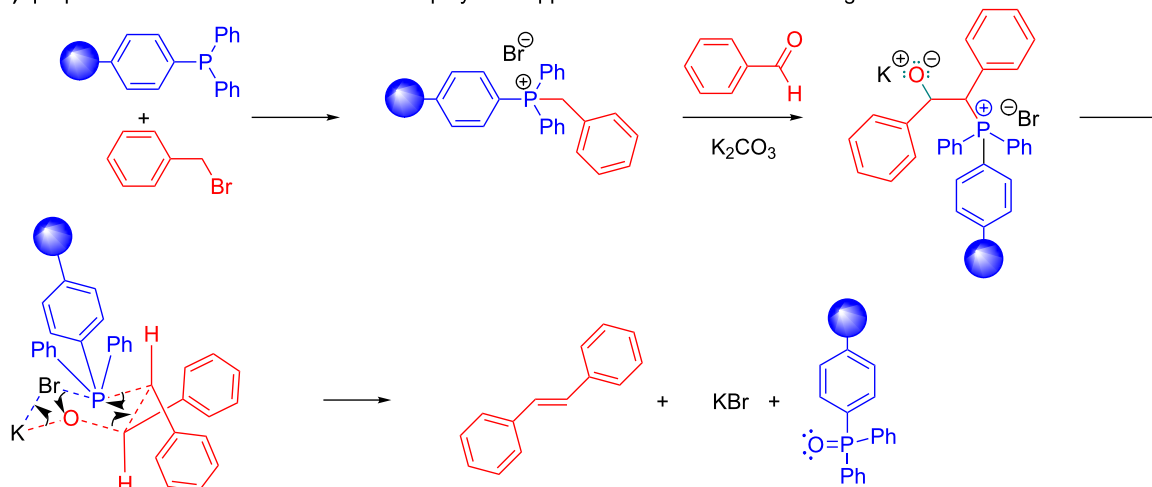
Counter-ion pairing

We further hypothesized that, if the benzyl benzoate is formed through a six-membered ring intermediate to give (*E*)-stilbene as the major product, then the same rationale could be used in the case of our solvent-free conditions. In solution, ions are separated and stabilized by solvent molecules. Mechanistically we envision ions to start out as contact ion pairs, then solvent separated ion pairs (i.e., loose ion pairs) followed by free ion pairs.

However, this pathway is shut down under solvent-free conditions, making everything in the system a contact ion pair. The traditional solution-based mechanism of the Wittig reaction proceeds via a four-membered oxaphosphetane intermediate. However, by incorporating the halide anion and the alkali metal cation into the mechanism, a six-membered ring, similar to that proposed in Scheme 2, would result (Figure 3).

Figure 3: Comparison of solution based Wittig reaction (a) with polymer-supported mechanochemical Wittig reaction (b).

Table 3: Counter-ion partnerships.

Ion	Pearson HSAB concept	Jones–Dole viscosity B coefficient [31]	Ionic radius (pm)
Li^+	hard	0.150	76
Na^+	hard	0.086	102
K^+	hard	−0.007	138
Rb^+	borderline	−0.030	152
Cs^+	soft	−0.045	167
Cl^-	hard	−0.007	181
Br^-	borderline	−0.032	196

Based on this hypothesis, in addition to the oxygen and phosphorous forming a stable bond, the alkali metal and halide must form a stable contact ion pair as well. These interactions and the formation of this bond may have a large influence under mechanochemical conditions because there is not a solvent reservoir to accept the dispersion of these ions. Using Pearson's hard and soft acid and base (HSAB) theory [29] and the Jones–Dole viscosity B coefficient [30] (Table 3), we can predict which alkali metal and halide pairs would be most favourable. For example, bromide is a borderline soft anion, so based on the proposed mechanism we would expect more product to form if the counter ion is Cs^+(soft) than if it was Li^+ (hard). Using the Jones–Dole viscosity B coefficient, we could also predict that Cs^+ and Br^- would be a good pair, since their values are similar. We would expect Rb^+ to pair well with Br^- for the same reason. To test this idea and to understand the effect of the interaction, we conducted the solvent-free polymer-supported Wittig reaction with various carbonate salts and alkyl halides (Table 4).

Pairing of a hard acid (Li^+ or Na^+) with a moderately soft base (Br^-) leads to no or poor conversion to stilbene products. Conversely, the best conversion resulted when combining Cs^+ (soft acid) with Br^- (borderline soft base). The benzyl benzoate side-product observed in trials 1, 2, and 5 indicates that the carbonate bases deprotonated the phosphonium salt to form the ylide which then subsequently added to the benzaldehyde. However, the oxygen anion could not bind to the phosphorus cation to produce the stilbene product, presumably due to the mismatched counter ion pair. After identifying the caesium–bromine pair was optimal for the conversion, caesium carbonate was the base of choice for the described stepwise study with ethanol.
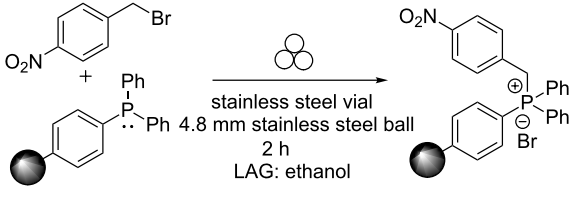
Table 4: Counter-ion partnerships in the solvent-free mechanochemical Wittig reaction.

trial	cation (M^+)	anion (X^-)	*E:Z* ratio	conversion to stilbene	conversion to benzyl benzoate
1	Li	Br	–	0%	6%
2	Na	Br	–	0%	29%
3	K	Br	67:33	30%	45%
4	Cs	Br	78:22	72%	9%
5	Li	Cl	–	0%	10%
6	Na	Cl	72:28	11%	13%
7	K	Cl	69:31	37%	24%
8	Cs	Cl	74:26	36%	28%

Tuning liquid-assisted grinding with ethanol

Because using ethanol (high dielectric constant) as the LAG solvent afforded the highest conversion to stilbene and the least amount of benzyl benzoate, we began our study on the yield and diastereoselectivity using this solvent. First, we were interested in the influence of ethanol on the mechanochemical reaction of the alkyl halide and the polymer-supported triphenylphosphine. For this purpose, $PS-C_6H_4-PPh_2$ and 4-nitrobenzyl bromide were ball-milled for two hours with and without ethanol as the LAG solvent. Afterwards, the reaction mixture was filtered with ethanol to determine the amount of 4-nitrobenzyl bromide in solution: the higher the amount recovered means that less 4-nitrobenzyl bromide reacted and is bound to the polymer and thus less production of the desired phosphonium salt. As expected, only 8.5% unreacted 4-nitrobenzyl bromide was recovered when ethanol was used as a LAG solvent, demonstrating that ethanol is an effective LAG solvent for the production of the phosphonium salt (Table 5).

Table 5: How much 4-nitrobenzyl bromide adds to the polymer-supported triphenylphosphine, $PS-C_6H_4-PPh_2$?

ethanol as LAG solvent?	percent mass recovery[a]
no	79.5 %
yes (1 mL)	8.5%

[a]Average of two trials.

Because the formation of the phosphonium salt is the first step of the Wittig reaction, the question arose whether performing the reaction stepwise could influence our ability to select for both percent conversion and diastereoselectivity. Using a stepwise reaction approach with ethanol as the LAG solvent (no work-up performed between the steps), a 98% conversion to stilbene was observed with an *E*:*Z* ratio of 43:57 (Scheme 4).

As can be seen from the scheme, the reaction proceeded with high conversion and *Z* selectivity, which was ascribed to the high dielectric constant of ethanol. However, if ethanol was allowed to evaporate from the vial before the addition of benzaldehyde, thus creating a non-LAG condition, then *E* selectivity should be favoured for the Wittig reaction. Indeed, it turned out that a 98% conversion to the product along with an *E*:*Z* ratio of 78:22 (Scheme 5) occurred.

As shown, the dielectric constant of the solvent used in LAG can affect both the percent conversion of the reaction as well as the diastereoselectivity. By running the reaction stepwise, we can tune the reaction to proceed with high percent conversion while changing the diastereoselectivity of the product.

Conclusion

Both a high dielectric constant of the solvent used in liquid-assisted grinding (LAG) and proper ion pairing were found to increase the percent conversion to stilbenes under mechanochemical conditions. Choosing appropriate ion pairs when LAG is utilized in the system also allowed tuning the diastereoselectivity. Specifically, this selectivity could be achieved by combining the Cs^+/Br^- pair with the LAG solvent as follows: if one millilitre of ethanol was present in both reaction steps a higher *Z* selectivity was obtained. If one millilitre of ethanol was present only in the first step of the experiment, a higher *E* selectivity was obtained. The high concentration of reactants under mechanochemical conditions allows for unique and potentially selective reactions that may not be achievable by traditional synthetic means. Further studies on the influence of
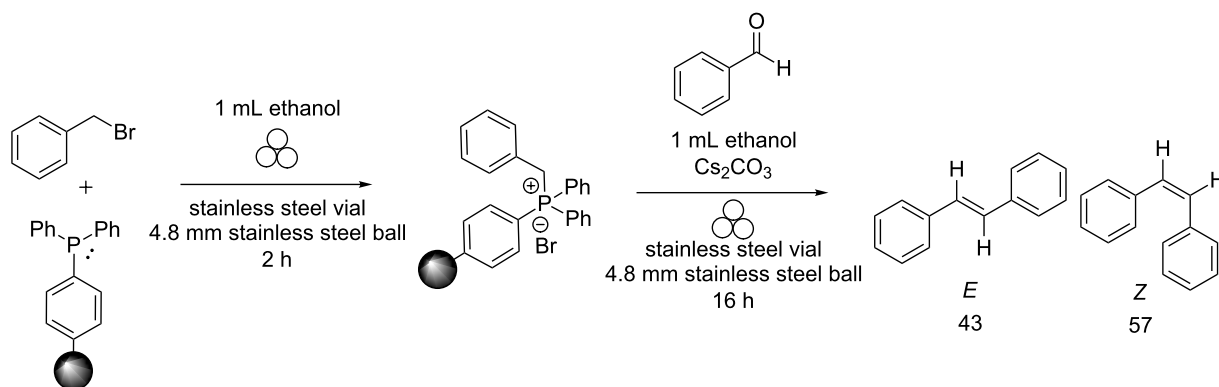
Scheme 4: Stepwise ball-milled Wittig reaction with ethanol as the LAG solvent.

Scheme 5: Stepwise ball-milled Wittig reaction with ethanol evaporation between the steps.
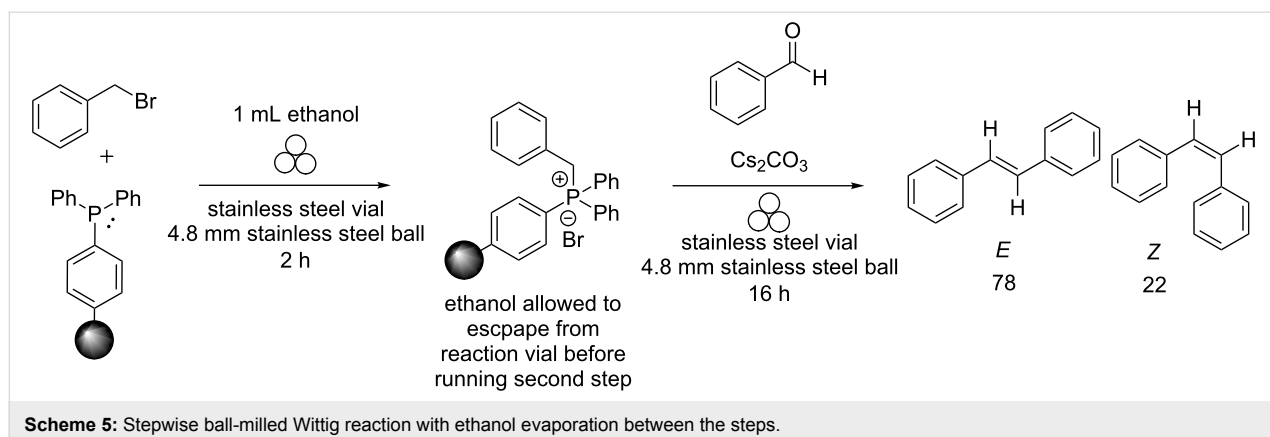
HSAB theory and the Jones–Dole viscosity B coefficient under mechanochemical conditions are ongoing.

Experimental

NMR spectra were obtained using a Bruker Avance 400 MHz spectrometer. Deuterated chloroform was obtained from Cambridge Isotope Laboratories Inc., Addover, MA, and used without further purification. Triphenylphosphine-functionalized polystyrene, 2% cross-linked with divinylbenzene (PS-C_6H_4-PPh$_2$) was obtained from Biotage® and used without further purification. Benzaldehyde was obtained from Sigma Aldrich and used without further purification. Alkyl halides and carbonate bases were obtained from Fisher Scientific and used without further purification.

Mechanochemical Wittig reaction

To a customized stainless steel vial (3.0 mL volume) was added 1 mmol (500 mg) of PS-C_6H_4-PPh$_2$, 0.998 mmol alkyl halide, 0.58 mmol aldehyde, and 1.3 mmol carbonate base. This mixture was ball-milled for 16 h. For liquid-assisted grinding experiments, also 1 mL solvent was added. For stepwise reactions, PS-C_6H_4-PPh$_2$, the alkyl halide, and the LAG solvent were ball-milled for 2 h. Afterwards, the aldehyde and carbonate bases were added, and the reaction mixture was ball-milled for further 16 h. A 4.8 mm (3/16") stainless steel ball was added to the vial for all steps. The vial was shaken at 18 Hz in a Spex8000M Mixer/Mill. To work up the reaction after the reaction was complete, 2 mL of ethyl acetate were added to the vial, and the vial was returned to the mill for 5 min. The resulting mixture was gravity filtered with ethyl acetate. The solvent was removed under reduced pressure. ^{1}H NMR spectroscopy was performed to assess the composition of the filtrate.

Acknowledgements

ORCID® iDs

Daniel C. Waddell - https://orcid.org/0000-0001-7318-7687

References

1. Do, J.-L.; Friščić, T. *ACS Cent. Sci.* **2017**, *3*, 13–19. doi:10.1021/acscentsci.6b00277
2. James, S.; Adams, C.; Bolm, C.; Braga, D.; Collier, P.; Friščić, T.; Grepioni, F.; Harris, K.; Hyett, G.; Jones, W.; Krebs, A.; Mack, J.; Maini, L.; Orpen, A.; Parkin, I.; Shearouse, W.; Steed, J.; Waddell, D. *Chem. Soc. Rev.* **2012**, *41*, 413–447. doi:10.1039/C1CS15171A
3. Wang, G.-W. *Chem. Soc. Rev.* **2013**, *42*, 7668–7700. doi:10.1039/c3cs35526h
4. Takacs, L. *Chem. Soc. Rev.* **2013**, *42*, 7649–7659. doi:10.1039/c2cs35442j
5. Boldyreva, E. *Chem. Soc. Rev.* **2013**, *42*, 7719–7738. doi:10.1039/c3cs60052a
6. Strukil, V. *Beilstein J. Org. Chem.* **2017**, *13*, 1828–1849. doi:10.3762/bjoc.13.178
7. Metro, T.-X. M.; Martinez, J.; Lamaty, F. *ACS Sustainable Chem. Eng.* **2017**, *5*, 9599–9602. doi:10.1021/acssuschemeng.7b03260
8. Do, J.-L.; Friščić, T. *Synlett* **2017**, *28*, 2066–2092. doi:10.1055/s-0036-1590854
9. Achar, T. K.; Bose, A.; Mal, P. *Beilstein J. Org. Chem.* **2017**, *13*, 1907–1931. doi:10.3762/bjoc.13.186
10. Zhao, S.; Li, Y.; Liu, C.; Zhao, Y. *Tetrahedron Lett.* **2018**, *59*, 317–324. doi:10.1016/j.tetlet.2017.12.021
11. Tan, D.; Friščić, T. *Eur. J. Org. Chem.* **2018**, *2018*, 18–33. doi:10.1002/ejoc.201700961
12. Strukil, V. *Synlett* **2018**, in press. doi:10.1055/s-0036-1591868
13. Intasa-ard, S. G.; Imwiset, K.; Bureekaew, S.; Ogawa, M. *Dalton Trans.* **2018**, *47*, 2896–2916. doi:10.1039/c7dt03736h
14. Hernandez, J. G. *Chem. – Eur. J.* **2017**, *23*, 17157–17165. doi:10.1002/chem.201703605
15. Geciauskaite, A. A.; Garcia, F. *Beilstein J. Org. Chem.* **2017**, *13*, 2068–2077. doi:10.3762/bjoc.13.204
16. Andre, V.; Quaresma, S.; Ferreira da Silva, J. L.; Duarte, M. T. *Beilstein J. Org. Chem.* **2017**, *13*, 2416–2427. doi:10.3762/bjoc.13.239
17. Balema, V.; Wiench, J.; Pruski, M.; Pecharsky, V. *J. Am. Chem. Soc.* **2002**, *124*, 6244–6245. doi:10.1021/ja017908p
18. Balema, V.; Wiench, J.; Pruski, M.; Pecharsky, V. *Chem. Commun.* **2002**, 724–725. doi:10.1039/b111515d
19. Cristau, H.-J. *Chem. Rev.* **1994**, *94*, 1299–1313. doi:10.1021/cr00029a006

20. Murphy, P.; Lee, S. *J. Chem. Soc., Perkin Trans. 1* **1999,** 3049–3066. doi:10.1039/a803560a

21. Hajos, G.; Nagy, I. *Curr. Org. Chem.* **2008,** *12,* 39–58. doi:10.2174/138527208783330082

22. Fairlamb, I. *ChemSusChem* **2009,** *2,* 1021–1024. doi:10.1002/cssc.200900208

23. Marsden, S. *Nat. Chem.* **2009,** *1,* 685–687. doi:10.1038/nchem.458

24. Schlosser, M. *Top. Stereochem.* **1970,** *5,* 1–30. doi:10.1002/9780470147146.ch1

25. Vedejs, E.; Peterson, M. *Top. Stereochem.* **1994,** *21,* 1–157. doi:10.1002/9780470147306.ch1

26. Vedejs, E.; Peterson, M. *Adv. Carbanion Chem.* **1996,** *2,* 1–85.

27. Shearouse, W.; Mack, J. *Green Chem.* **2012,** *14,* 2771–2775. doi:10.1039/c2gc35669d

28. El-Anwnr, I. M.; Foad, I. Z. S. A. A. *J. Mater. Sci. Technol.* **1995,** *11,* 222–228.

29. Pearson, R. G. *J. Am. Chem. Soc.* **1963,** *85,* 3533–3539. doi:10.1021/ja00905a001

30. Jones, G.; Dole, M. *J. Am. Chem. Soc.* **1929,** *51,* 2950–2964. doi:10.1021/ja01385a012

31. Jenkins, H. D. B.; Marcus, Y. *Chem. Rev.* **1995,** *95,* 2695–2724. doi:10.1021/cr00040a004